CLIMATE CHANGE AND LIGHT IN AQUATIC ECOSYSTEMS: VARIABILITY & ECOLOGICAL CONSEQUENCES

EDITED BY: Patrick J. Neale, Oliver Zielinski, Rebecca L. North, Maren Striebel and Jochen Wollschläger

PUBLISHED IN: Frontiers in Marine Science and Frontiers in Envrionmental Science

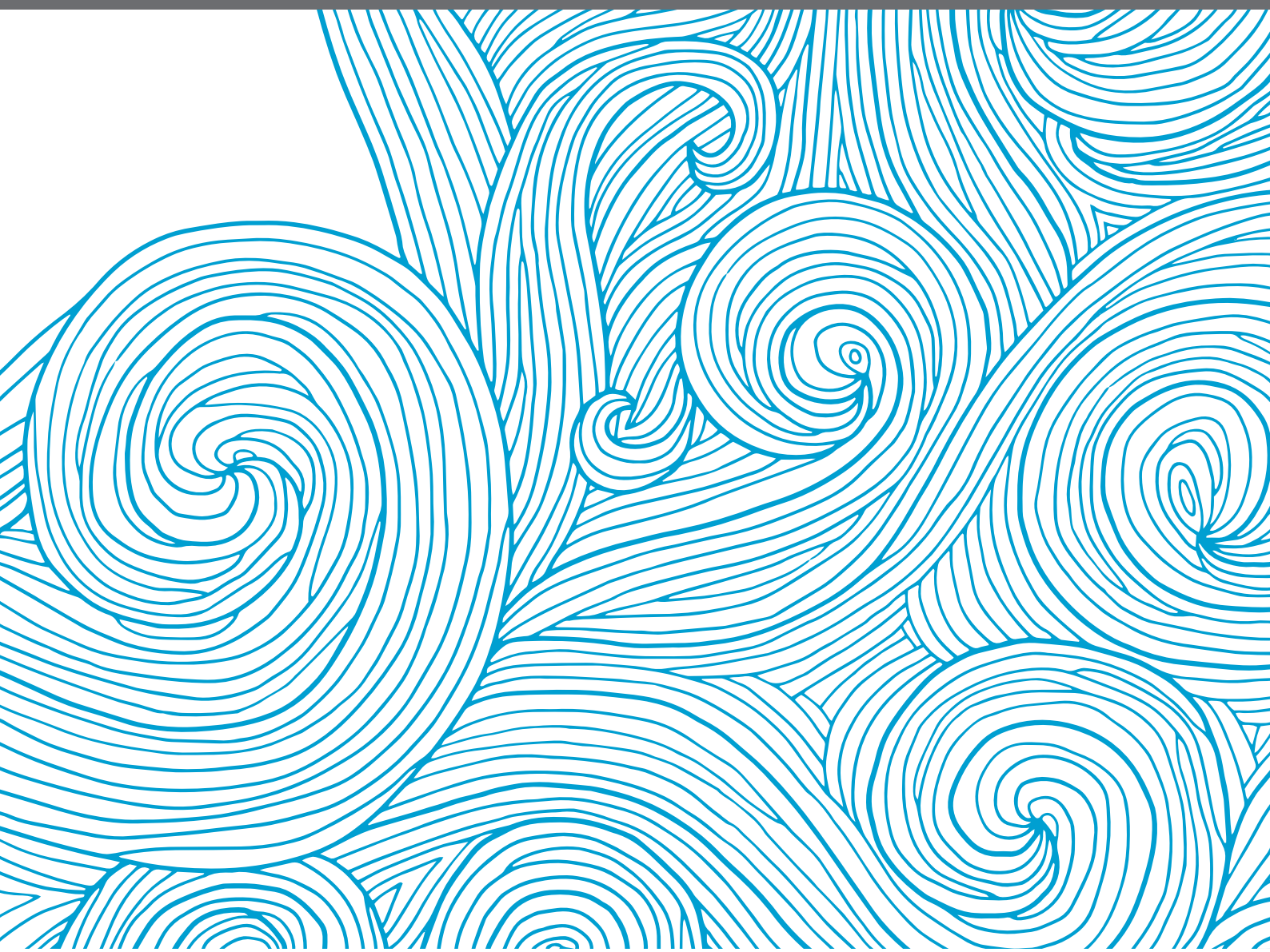

frontiers Research Topics

frontiers

ISSN 1664-8714
ISBN 978-2-88966-980-6
DOI 10.3389/978-2-88966-980-6

About Frontiers

Frontiers is more than just an open-access publisher of scholarly articles: it is a pioneering approach to the world of academia, radically improving the way scholarly research is managed. The grand vision of Frontiers is a world where all people have an equal opportunity to seek, share and generate knowledge. Frontiers provides immediate and permanent online open access to all its publications, but this alone is not enough to realize our grand goals.

Frontiers Journal Series

The Frontiers Journal Series is a multi-tier and interdisciplinary set of open-access, online journals, promising a paradigm shift from the current review, selection and dissemination processes in academic publishing. All Frontiers journals are driven by researchers for researchers; therefore, they constitute a service to the scholarly community. At the same time, the Frontiers Journal Series operates on a revolutionary invention, the tiered publishing system, initially addressing specific communities of scholars, and gradually climbing up to broader public understanding, thus serving the interests of the lay society, too.

Dedication to Quality

Each Frontiers article is a landmark of the highest quality, thanks to genuinely collaborative interactions between authors and review editors, who include some of the world's best academicians. Research must be certified by peers before entering a stream of knowledge that may eventually reach the public - and shape society; therefore, Frontiers only applies the most rigorous and unbiased reviews.
Frontiers revolutionizes research publishing by freely delivering the most outstanding research, evaluated with no bias from both the academic and social point of view. By applying the most advanced information technologies, Frontiers is catapulting scholarly publishing into a new generation.

What are Frontiers Research Topics?

Frontiers Research Topics are very popular trademarks of the Frontiers Journals Series: they are collections of at least ten articles, all centered on a particular subject. With their unique mix of varied contributions from Original Research to Review Articles, Frontiers Research Topics unify the most influential researchers, the latest key findings and historical advances in a hot research area! Find out more on how to host your own Frontiers Research Topic or contribute to one as an author by contacting the Frontiers Editorial Office: frontiersin.org/about/contact

CLIMATE CHANGE AND LIGHT IN AQUATIC ECOSYSTEMS: VARIABILITY & ECOLOGICAL CONSEQUENCES

Topic Editors:
Patrick J. Neale, Smithsonian Environmental Research Center (SI), United States
Oliver Zielinski, University of Oldenburg, Germany
Rebecca L. North, University of Missouri, United States
Maren Striebel, University of Oldenburg, Germany
Jochen Wollschläger, University of Oldenburg, Germany

Citation: Neale, P. J., Zielinski, O., North, R. L., Striebel, M., Wollschläger, J., eds. (2021). Climate Change and Light in Aquatic Ecosystems: Variability & Ecological Consequences. Lausanne: Frontiers Media SA. doi: 10.3389/978-2-88966-980-6

Table of Contents

frontiers in Marine Science

EDITORIAL
published: 11 May 2021
doi: 10.3389/fmars.2021.688712

Editorial: Climate Change and Light in Aquatic Ecosystems: Variability & Ecological Consequences

Jochen Wollschläger[1], Patrick J. Neale[2], Rebecca L. North[3], Maren Striebel[1] and Oliver Zielinski[1,4]*

[1] Institute for Chemistry and Biology of the Marine Environment, University of Oldenburg, Oldenburg, Germany, [2] Smithsonian Environmental Research Center (SI), Edgewater, NJ, United States, [3] School of Natural Resources, University of Missouri, Columbia, MO, United States, [4] German Research Center for Artificial Intelligence (DFKI), Oldenburg, Germany

Keywords: light, marine, freshwater, bio-optics, ecosystems, climate change

Editorial on the Research Topic

Climate Change and Light in Aquatic Ecosystems: Variability & Ecological Consequences

Light is a key variable in nearly all ecosystems on Earth, both in the terrestrial and the aquatic domain. It shapes the ecological niche of organisms in various ways, either by providing visual information for orientation, predation, and reproduction (McFarland, 1986), or–most importantly–providing the energy for photosynthesis and thus primary production, which is eventually transferred to higher trophic levels. With the nine articles in this Research Topic, we aim to raise awareness on the importance of light for aquatic ecosystems, both freshwater and marine, as well as on present and future changes of light availability induced by climate change. As an introduction to the Research Topic, we provide herewith some background on how climate change affects the aquatic light environment and describe the specific themes covered in these articles.

In aquatic habitats, light propagation is more complex than on land, as the water itself–in contrast to air–is a strong attenuator of light, especially in the red part of the visible light spectrum (Kirk, 2011). The consequence is a decrease in light intensity with water depth and a simultaneous shift in wavelength composition toward a higher proportion of shorter wavelengths, one of the reasons why very clear water appears blue. In addition to this general principle, the presence of substances with their specific optical properties further modify the underwater light field, causing greenish, yellowish, or brownish waters. The most relevant of these optically active substances (OAS) are phytoplankton, that have different photosynthetic and photoprotective pigments, colored dissolved organic matter (CDOM), as well as non-living organic and inorganic particles (e.g., detritus and suspended mineral particles). They determine the inherent optical properties (IOP; e.g., absorption and scattering) of the water which, together with the ambient light conditions, govern the apparent optical properties (AOP; e.g., diffuse attenuation or water color). Analytically, AOP and IOP are related by the radiative transfer equations (Mobley, 1994), however, as their solution is rather complex and computationally expensive, for certain applications less complex empirical or semi-analytical models can be sufficient as shown by Gonçalves-Araujo and Markager.

The interplay of the optical properties of the water and the OAS creates highly characteristic underwater light climates to which the organisms living within are adapted. Changes in these conditions propose a challenge to these organisms and might induce alterations of community structures and, eventually, ecosystem functioning. A number of studies have observed a trend toward reduced light availability, thus "darker" waters in aquatic ecosystems. In freshwater systems,

OPEN ACCESS

Edited and reviewed by:
Angel Borja,
Technological Center Expert in Marine and Food Innovation (AZTI), Spain

****Correspondence:***
Jochen Wollschläger
jochen.wollschlaeger@uni-oldenburg.de

Specialty section:
This article was submitted to Marine Ecosystem Ecology, a section of the journal Frontiers in Marine Science

Received: *31 March 2021*
Accepted: *14 April 2021*
Published: *11 May 2021*

Citation:
Wollschläger J, Neale PJ, North RL, Striebel M and Zielinski O (2021) Editorial: Climate Change and Light in Aquatic Ecosystems: Variability & Ecological Consequences. Front. Mar. Sci. 8:688712. doi: 10.3389/fmars.2021.688712

this phenomenon is well-studied and known as brownification, since there, the reduced light availability is mainly caused by increased input of terrestrial CDOM (Pace and Cole, 2002; Graneli, 2012 and references therein). A "coastal darkening" has also been observed in certain marine environments, such as fjord systems or shallow shelf seas (Aksnes et al., 2009; Dupont and Aksnes, 2013; Capuzzo et al., 2015). Mustaffa et al. report that input of terrestrial CDOM to coastal waters can also negatively impact phytoplankton growth due to reduced light availability, with consequences possibly propagating to the next trophic level. Nevertheless, the effects of such temporally and/or spatially variable terrestrial CDOM input might differ between freshwater and marine systems. In addition to CDOM input, increased particle loads have also been considered as drivers of darker coastal waters. This includes both increased resuspension of available sediments and input of new particulate material by glacial melting and increased erosion on land (Walling, 2009). Besides these climate change-related impacts, there are also direct human activities like trawling, sand extraction, and coastal engineering measures that can contribute to reduced light availability (Palanques et al., 2001). However, other effects of altered light climate on higher trophic levels occur besides those indirectly mediated via phytoplankton. Williamson et al. show that the light attenuation attributed to darker waters can directly shape the ecological niche of higher trophic levels such as zooplankton by altering other environmental factors like temperature, oxygen, and UV radiation regimes, while showing minor impact on the phytoplankton.

Eventually, it is the interplay of (variable) light conditions on different scales with other factors such as nutrients that controls phytoplankton responses such as photosynthetic adjustments, adaptations in pigments, biomass production, and taxonomical composition. The interplay of these factors are considered in Marzetz et al. and Petty et al.. Knowledge about these interactions is important to (i) understand ecosystem functioning in general and (ii) make predictions regarding the consequences of ongoing changes induced by climate change and eutrophication, which has implications in the management of freshwaters and the prevention of increasingly widespread cyanobacterial harmful algal blooms. Manipulation of the light regime via artificial "darkening" is explored by Gaskill et al. as an alternative or complementary strategy to achieve a decrease in cyanobacterial biomass or a change in community structure toward non-toxin producing phytoplankton.

Increased light, although in general favorable for primary production, is, however, not always beneficial for aquatic organisms. Short wave radiation such as UV-A and UV-B can damage genetic material, thus acting as a stressor by putting the intracellular repair mechanisms under pressure. Overmans and Agustí. consider the relevance of UV exposure for non-motile organisms living in shallow areas (e.g., corals) that are also being stressed from rising temperatures due to climate change.

To assess the long-term effects of changing underwater light levels on a broad spatial scale, numerical models are a powerful tool, provided that the propagation of light is reasonably well-represented. The majority of models use a parameterization of light attenuation based on the distribution of phytoplankton, which is a suitable approach for open ocean environments. Models that account for inorganic particulate matter, however, are shown by Thewes et al. to perform considerably better in optically complex coastal waters. To further improve model performance, Wollschläger et al. have developed light parameterizations that account for all OAS and their spectrally variable optical properties, while being computationally affordable.

As it can be seen by the variety of research fields that are addressed by the contributions to this Research Topic, the issue of light variability in aquatic ecosystems is certainly a complex one. It becomes clear that light availability as well as light quality are key parameters for aquatic organisms across different scales and that their effects on the ecosystems have to be considered in interaction with multiple environmental variables. The presented studies highlight that we need a better grasp of the implications that climate change and human activities pose on both the timing and the magnitude of altered light conditions on our aquatic ecosystems on local, regional, and global scales. The papers collected here give an overview about the several important aspects of this topic and show the current state of research.

AUTHOR CONTRIBUTIONS

JW provided the first draft of the manuscript. All authors contributed equally to its finalization.

REFERENCES

Aksnes, D. L., Dupont, N., Staby, A., Fiksen, O., Kaartvedt, S., and Aure, J. (2009). Coastal water darkening and implications for mesopelagic regime shifts in Norwegian fjords. *Mar. Ecol. Prog. Ser.* 387, 39–49. doi: 10.3354/meps08120

Capuzzo, E., Stephens, D., Silva, T., Barry, J., and Forster, R. M. (2015). Decrease in water clarity of the southern and central North Sea during the 20th century. *Glob. Chang. Biol.* 21, 2206–2214. doi: 10.1111/gcb.12854

Dupont, N., and Aksnes, D. L. (2013). Centennial changes in water clarity of the baltic sea and the north sea. *Estuar. Coast. Shelf Sci.* 131, 282–289. doi: 10.1016/j.ecss.2013.08.010

Graneli, W. (2012). "Brownification of lakes," in *Encyclopedia of Lakes and Reservoirs: Encyclopedia of Earth Sciences Series*, eds L. Bengtsson, R. W. Herschy, R. W. Fairbridge (Dordrecht: Springer).

Kirk, J. T. O. (2011). *Light & Photosynthesis in Aquatic Ecosystems, 3rd Edn*. New York, NY: Cambridge University Press.

McFarland, W. N. (1986). Light in the sea - correlations with behaviors of fishes and invertebrates. *Integr. Comp. Biol.* 26, 389–401. doi: 10.1093/icb/26.2.389

Mobley, C. D. (1994). *Light and Water: Radiative Transfer in Natural Waters*. London: Academic Press.

Pace, M. L., and Cole, J. J. (2002). Synchronous variation of dissolved organic carbon and color in lakes. *Limnol. Oceanogr.* 47, 333–342. doi: 10.4319/lo.2002.47.2.0333

Palanques, A., Guillén, J., and Puig, P. (2001). Impact of bottom trawling on water turbidity and muddy sediment of an unfished continental shelf. *Limnol. Oceanogr.* 46, 1100–1110. doi: 10.4319/lo.2001.46.5.1100

Walling, D. E. (2009). *The Impact of Global Change on Erosion and Sediment Transport by Rivers: Current Progress and Future Challenges*. Paris: UNESCO

Conflict of Interest: The authors declare that the research was conducted in the absence of any commercial or financial relationships that could be construed as a potential conflict of interest.

frontiers in Marine Science

ORIGINAL RESEARCH
published: 23 January 2020
doi: 10.3389/fmars.2019.00816

Sensitivity of a 3D Shelf Sea Ecosystem Model to Parameterizations of the Underwater Light Field

Daniel Thewes[1]*, *Emil V. Stanev*[1,2] *and Oliver Zielinski*[3,4]

[1] Coastal Research, Institute for Chemistry and Biology of the Marine Environment, University of Oldenburg, Oldenburg, Germany, [2] Helmholtz Centre for Materials and Coastal Research (HZG), Geesthacht, Germany, [3] Marine Sensor Systems, Institute for Chemistry and Biology of the Marine Environment, University of Oldenburg, Oldenburg, Germany, [4] Marine Perception Research Group, German Research Center for Artificial Intelligence (DFKI), Oldenburg, Germany

The inherent optical properties of water in the North Sea vary widely in space and time. Their impact on the performance of a 3D-ecosystem-model of the North Sea needs to be critically evaluated, which is the major research issue in the present paper, specifically the horizontal variability of turbidity. We have performed a sensitivity analysis to a modification of a common approach of light treatment that is both valid for the North Sea, as well as computationally efficient to implement within a 3D-ecosystem-model. Using a coupled hydrodynamical model (Regional Ocean Modeling System, ROMS) and biological model (Carbon Silicate and Nitrogen Ecosystem model, CoSiNE), we found that simple changes to the original parameterization can yield significant improvements. ROMS-CoSiNE is shown to be suitable for use in a coupled ecosystem model of the North Sea. The model accurately reproduces the seasonal cycle of primary production in terms of timing and magnitude, while still being more affordable in comparison to full hyperspectral treatment or solving the radiative transfer equation. The modification introduces vertically increasing attenuation that is stronger in shallow domains, in a way that is similar to attenuation due to sediment. The resulting reduction of light availability leads to strongly reduced phytoplankton growth in shallow areas with high turbidity and weak nutrient limitation. Areas of depths between 50 and 100 m show greatest relative change with respect to their total ranges, while the deepest areas remain largely unchanged. We found that the consideration of spacial variability of light attenuation is necessary when modeling a heterogeneous domain, such as the North Sea.

Keywords: SPM, ROMS, CoSiNE, ecosystem model, chlorophyll, light availability, light attenuation, North Sea

OPEN ACCESS

Edited by:
Michael Arthur St. John, Technical University of Denmark, Denmark

Reviewed by:
Hernan G. Arango, Rutgers, The State University of New Jersey, United States
Christian Lindemann, University of Bergen, Norway

***Correspondence:**
Daniel Thewes
daniel.thewes@uni-oldenburg.de

Specialty section:
This article was submitted to Marine Ecosystem Ecology, a section of the journal Frontiers in Marine Science

Received: *15 July 2019*
Accepted: *17 December 2019*
Published: *23 January 2020*

Citation:
Thewes D, Stanev EV and Zielinski O (2020) Sensitivity of a 3D Shelf Sea Ecosystem Model to Parameterizations of the Underwater Light Field. Front. Mar. Sci. 6:816. doi: 10.3389/fmars.2019.00816

1. INTRODUCTION

A common class of biological models are the Nutrient, Zooplankton, Phytoplankton and Detritus (NPZD) models, which are usually simple four component models. Other models are immensely more complex with several, in some cases uncoupled nutrient cycles, functional groups of phyto- and zooplankton, bacteria, etc. (e.g., Fasham et al., 1990; Baretta et al., 1995; Kühn and Radach, 1997; Moll, 1997, 1998; Bissett et al., 1999, 2001; Chai et al., 2002; Schrum et al., 2006a,b; Daewel and Schrum, 2013). What all of these models have in common, however, is that for phytoplankton growth, specifically for photosynthesis, light is required.

There are various approaches to treat light in biological models. Especially in the early years of ecosystem modeling, simplifications had to be made due to the limitations in affordable computational power. Common approximations that are found in literature are spacially averaging the physics (Baretta et al., 1995; Lenhart et al., 1995; Chai et al., 2002), or using spectrally integrated irradiance or photosynthetically available radiation (PAR) instead of a spectral approach (Baretta et al., 1995; Chai et al., 2002; Schrum et al., 2006a; Daewel and Schrum, 2013). For some purposes, a simple approach may well be appropriate. However, Mobley et al. (2015) have shown that both a spectral light treatment and the inclusion of a daily cycle can significantly change the results of a biological model, while technological advances have made these approaches more affordable. Thus, for quantitatively more correct, complex and precise applications, it is advisable to use fewer approximations. In our case, the sparsity of available spectral data, the greater effort in evaluating a spectral model, justify the use of spectrally integrated irradiance.

In many biological models, attenuation due to suspended particulate matter (SPM) is sometimes considered indirectly by increasing the attenuation coefficient of water, which is often assumed constant in space and time. Hence, such approaches only show spacial or temporal variability of light attenuation due to chlorophyll, yet not due to SPM. However, many areas of the North Sea are rich in SPM and independently so of chlorophyll, with rather high horizontal variability (e.g., van der Molen et al., 2009). An online coupling between the optical components of a biogeochemical and the physical model is rare, however, it has been shown that optically active water constituents can influence the physics significantly (Cahill et al., 2008; Mobley et al., 2015). Cahill et al. (2008) found feedback mechanisms between light attenuation and the resulting mixed layer depth. They concluded that stronger stratification leads to higher concentrations of optically active water components in the upper water column, causing the stratification to become even stronger. This indicates the importance of considering vertical variability of attenuation. However, many models do not consider horizontally or vertically varying turbidity.

The light climate in the North Sea has been subject to change over the past decades. Recent studies on Secchi-depth data have found centennial negative trends, indicating an increase in turbidity and a subsequent decrease in light availability for photosynthesis (Dupont and Aksnes, 2013; Capuzzo et al., 2015). Capuzzo et al. (2015) defined distinct areas through their hydrodynamic properties as permanently mixed, seasonally stratified, intermediate, regions of fresh water influence and the East Anglia plume. They attributed significant decreases in mean Secchi-depths from the first to the second half of the twentieth century to SPM (e.g., due to increased dredging) and chlorophyll (Capuzzo et al., 2015) or colored dissolved organic matter (CDOM) (Dupont and Aksnes, 2013). Both SPM and CDOM have been found to have a stronger effect on light attenuation than chlorophyll has (Harvey et al., 2019). Opdal et al. (2019) support the hypothesis that the coastal darkening is not impacted by changes in chlorophyll, but rather non-planktonic substances, i.e., SPM and CDOM. The darkening has been shown to delay the spring bloom of phytoplankton (Opdal et al., 2019). Wilson and Heath (2019) indicate that over the past 20 years, due to climate change and a subsequent change in the wind regime, the trends of increasing SPM over the twentieth century might have reversed in several areas of the North Sea. The above mentioned works motivate investigations into how changes to the light climate affect the ecosystem in the North Sea, given the apparent trend in reduced light availability and increased turbidity, especially in the southern North Sea.

We aim to analyse the underwater light field numerically, and specifically the effects of introducing heterogeneous, bathymetry dependent turbidity. For this purpose, we set up a three-dimensional (3D) hydrodynamic model (ROMS), coupled with a one-dimensional (1D) biological model (CoSiNE) of the North Sea. We modified the classic light treatment in CoSiNE, making the attenuation effectively bathymetry dependent and vertically increasing, independently of phytoplankton. This is to accommodate for the greater turbidity in shallow coastal waters, while being virtually no more expensive in terms of computational effort than the original formulation. We test the capability of the modified light treatment as a functioning proxy for attenuation due to horizontally varying inorganic SPM. For reasons of simplicity, we exclude both the effects of CDOM and temporal changes in SPM in this work.

Through sensitivity studies, the impact of reduced light availability is determined. The model results are compared to the Atlantic Margin Model with 7 km horizontal resolution of the MetOffice, UK, and the European Regional Seas Ecosystem Model (ERSEM, Baretta et al., 1995; Blackford et al., 2004), to which AMM7 is coupled, using the reanalyzed data as provided by the Copernicus Marine Environment Monitoring Service (CMEMS, http://marine.copernicus.eu), Chlorophyll Color Index (CCI, https://esa-oceancolour-cci.org) satellite data, as well as bottle and FerryBox data, provided by the International Council for Exploration of the Sea (ICES, https://ices.dk) and the Coastal Observing System for Northern and Arctic Seas (COSYNA, https://www.hzg.de/institutes_platforms/cosyna/index.php.de, Baschek et al., 2017), respectively. The models, the used data and the experiments are described in section 2. The results are described and discussed in section 3, and the conclusions we draw from them are found in section 4. A brief overview of the model's physical performance can be found in the supplement.

2. DATA AND METHODS

2.1. Physical Model

The physical model is the regional ocean modeling system (ROMS) (Haidvogel et al., 2000). It solves the primitive equations, using a split-explicit time-stepping scheme. In the vertical, it utilizes a terrain-following s-coordinate (Song and Haidvogel, 1994), and in the horizontal a curvilinear structured grid. Turbulence closure is achieved with a generic length scale (GLS) approach in a k-kl configuration (Umlauf and Burchard, 2003; Warner et al., 2005).

The horizontal grid is taken from the MetOffice's AMM7 model, as is available from the COPERNICUS web portal, extended from 5°W to 13°E and 48°N to 60°N. The horizontal

resolution is 7 km. In the vertical, the domain is divided into 35 s-layers, stretched to increase the resolution at the surface. The initial and boundary conditions (IC and BC) were taken from AMM7 as well. We applied a Champman type BC for the free surface, which is tidally filtered and averaged daily and the ROMS tidal constituent model using Finite Element Solution (FES, the 2014 model as provided by AVISO) tides, contributing the tidal signal. A Flather type BC was chosen for 2D-momentum, and radiation with nudging BC for 3D-momentum and tracers. The atmospheric forcing is taken from NCEP/NCAR and is of a quarter daily temporal and 21 km horizontal resolution. The river input is climatological, and is taken from the pan-European Hydrological Predictions for the Environment (E-HYPE) model of the Swedish Meteorological and Hydrological Institute (SMHI), which gives freshwater fluxes from 34 rivers discharging into the Baltic Sea and North Sea. For reasons of simplicity, we have used only the rivers Trent, Thames, Seinne, Maas, Rhine, Schelde, Ems, Weser, Elbe, and Glomma, as well as the combined outflow of the Baltic Sea in the Kattegat.

The vertical coordinate in ROMS can be configured in such a way that all surface layers are at the same approximate geopotential depth. This is beneficial for reducing pressure gradient error and other density related issues that s-coordinates typically have. Our model has strong horizontal density gradients in several areas of the domain, e.g., the German Bight or the Skagerrak. While the German Bight is relatively shallow and has comparably smooth bathymetry gradients, the same cannot be said about the Skagerrak. The errors resulting from using conventional s-coordinates, where the surface layers are not at approximately the same geopotential depths, are thus expected to be relatively small in the German Bight, and larger in the Skagerrak. Therefore, a detailed comparison to the output of AMM7 has been performed. Our simulations are satisfactorily similar to that of AMM7 (not shown). We describe in section 2.3.2 that our light parameterization benefits from our model's surface layers not being equally distributed.

2.2. Biological Model

The biological model is the CoSiNE model, as developed by Chai et al. (2002). In the used version, it consists of 11 state variables, including the four nutrients nitrate (NO3), ammonium (NH4), silicate (SiOH4), and phosphate (PO4), two phytoplankton groups (small phytoplankton, S1 and diatoms, S2), two zooplankton groups (microzooplankton, Z1 and mesozooplankton, Z2), as well as detrital nitrogen (dN) and silicate (dS), as well as oxygen (O2). All plankton groups are expressed in units of $mmol\,N\,m^{-3}$. The details may be found e.g., in Chai et al. (2002) and Liu et al. (2018). Nitrate uptake by phytoplankton may be inhibited, if ammonium is more abundant than nitrate (Liu et al., 2018), however, we do not make use of this function. The biological IC and BC (in the 3D-model) are taken from AMM7-ERSEM, as available from CMEMS (described in section 2.4). In the case of those variables that arent available, typical ratios are assumed, e.g., ammonium is assumed to be of about a tenth the abundance of nitrate. Plankton BC are of Neumann type. River input of nutrients is taken from E-HYPE.

2.3. Light Parameterization

2.3.1. Classic Formulation

The exponential decay of irradiance (e.g., Evans and Parslow, 1985; Zielinski et al., 2002) is perhaps the most frequently used formulation of light in biological models. The basis of this scheme can be found in the description of CoSiNE (Chai et al., 2002), with additions regarding SPM made in recent works (Liu et al., 2018).

$$I(z) = I_0 \cdot \exp(cff1)) \tag{1}$$

$$cff1 = a_w \cdot (\zeta - z) + a_p \int_z^\zeta (P1 + P2)\,\mathrm{d}z' + \int_z^\zeta a_{SPM} SPM\,\mathrm{d}z', \tag{2}$$

with ζ being the free surface height, and $a_w = 0.036\ 1/m$, $a_p = 0.03\ m^2/mmol\,N$ and a_{SPM} being the attenuation coefficients, specifically for water, phytoplankton and inorganic SPM. $P1$ and $P2$ are the phytoplankton biomass of small phytoplankton and diatoms, respectively, in units of $mmol\,N/m^3$, taken from CoSiNE. Because there is a technical possibility to compute SPM, it is included in Equation (2). It is, however, excluded in the experiment, because SPM content is not known, so that it cannot be explicitly prescribed and we do not couple our model to a sediment and wind wave module. A homogeneous approach is not valid for the entire domain, due to the large horizontal variability, and a vertical distribution function would need to be found and validated first.

2.3.2. Index Scheme

The index (IND) scheme was designed as a cost efficient way to estimate the effects of SPM on light attenuation, by multiplying the right hand side of Equation (2) with a factor k/N, where $k \in [1, 2, 3, \ldots, N]$ is the layer index and N is the total number of layers, $k = 1$ being the bottom most layer and $k = N$ being the top layer. This way, the attenuation is strongest at the bottom. While in the classic scheme, the 1%-depth is exactly twice the 10%-depth, in the IND scheme, this is not the case. **Figure B.1A** shows the ratio of 1%-depth over 10%-depth in the default state (without chlorophyll specific attenuation). Note that it is slightly larger than 2 in the deeper areas, but slightly smaller than 2 elsewhere. This is due to the stretching of the vertical coordinate (see section 2.1). The full modified version of Equations (1) and (2) then reads

$$I_{IND}(z) = I_0 \cdot k/N \cdot \exp\left(-a_w z - a_p \int_z^\zeta (P1 + P2)\,\mathrm{d}z\right) = I_{classic}(z) \cdot k/N, \tag{3}$$

with k/N taking the role of $\exp\left(-a_{SPM} \int_z^\zeta SMP\mathrm{d}z\right)$. Because $k/N \leq 1$, downwelling irradiance is always lower in the IND scheme below the top most layer.

There are mathematical and physical inconsistencies in this formulation. Taking the factor k/N into the exponential, and

discretizing yields

$$I(z_k) = I_0 \cdot k/N \cdot \exp\left(-a_w z - a_p \sum_{i=k}^{N} (P1_i + P2_i) \cdot \Delta z_i\right) = I_0 \cdot \exp\left(-a_w z - a_p \sum_{i=k}^{N} (P1_i + P2_i) \cdot \Delta z_i + \ln\left(\frac{k}{N}\right)\right), \quad (4)$$

where $1 \leq k \leq N \in \mathbb{N}$, and Δz_i is the distance between the depth of a cell center z_i and that of the cell above z_{i+1}, except when $i = N$, where $\Delta z_i = z_i$. The first and most obvious flaw with this approach is that the natural logarithm is not bounded, and thus for $k = 1$,

$$N \to \infty : \ \ln(k/N) \to -\infty. \quad (5)$$

While this is theoretically undesirable, this is not problematic in practice, as the natural logarithm does not occur in the coding, k/N and $exp(-\ln(k/N))$ converge to zero, and N is bounded by numerical and practical constraints. Nevertheless, in this formulation, the strength of the attenuation at depth is dependent on the number of layers (**Figure 1**). The curve for $N = 10$ is less attenuated by about 1.8% at -0.5 m, and 2.4% at -9.5 m depth than that for $N = 20$. The dependency of the attenuation on N at the same depth vanishes as $N \to \infty$. The number of layers thus affects the hypothesized SPM content, which is clearly unrealistic. Furthermore, consider a water column of 10 m depth. In the classic formulation, the lowest layers would always be above 70% of the surface radiation for a water attenuation coefficient of $a_w = 0.036$ 1/m. For $N = 10$, the remaining irradiance at the center of the bottom layer would then be

$$I_{IND,N=10}(k = 1) = I_{classic}(k = 1) \cdot 1/10 \approx 0.071 \cdot I_0,$$

and for $N = 20$

$$I_{IND,N=20}(k = 1) = I_{classic}(k = 1) \cdot 1/20 \approx 0.036 \cdot I_0.$$

Physically, this means that for $N \geq 10$, the irradiance at the bottom is always lower than 10% of its surface value. For high values of N, it vanishes entirely. This is obviously false, since there is no physical basis to assume that downwelling shortwave radiation must always vanish toward the bottom. For many areas of application, also in the North Sea (Capuzzo et al., 2015), the sea floor is within the photic zone. In our model, using 35 layers and a minimum depth of 10 m, the bottom layer can have a maximum of 19% of the surface irradiance. In applying this method, we thus accept a physical inconsistency, for the benefit of efficiency over online coupling to a full 3D sediment module, which in turn would require a wind wave module to simulate the wave component of the bottom stress, which is needed to compute erosion and deposition.

Another inconsistency arises from the assumption that $\ln(k/N)$ is analogous to the attenuation due to SPM $a_{SPM} \int_{z_k}^{\zeta} SPM dz$, as it implies that every layer has a homogeneous concentration of SPM over the entire horizontal domain, i.e., a specific layer carries the same amount of sediment in the Sakgerrak as it does in the German Bight, even though the Skagerrak has more than ten times the depth of the German Bight, and a layer that is close to the surface is unlikely to carry the same content of SPM in both regions. Additionally, as the s-layers are thicker in deeper regions, integrating sediment over depth would imply that deeper regions contain more sediment within the water column. It is thus important to understand that k/N is in fact not a proxy for SPM. However, for layers below the photic zone, where photosynthesis is impossible, the error is biggest, but also least important. The modification can thus serve as a proxy for attenuation due to SPM in the photic zone, yet not as a proxy for actual SPM distribution.

Keeping in mind that the classic scheme assumes constant attenuation over the entire domain when neglecting the influence of phytoplankton, it is helpful to visualize what that implies. While it is impossible to display the sea floor illumination in the IND scheme, due to the noted physical inconsistency, it is possible to compare the 1%- and 10%-depths, as shown in **Figure 2**. In the classic scheme, if disregarding phytoplankton, the 10%- and 1%-depths are analytically found at $z_{10\%} = \frac{1}{a_w} \cdot \ln(0.1) = -64$ m and $z_{1\%} = \frac{1}{a_w} \cdot \ln(0.01) = -128$ m, respectively, for $a_w = 0.036$ 1/m. As shown above, the 1%-depth is always lower in the IND scheme than in the classic scheme and the bottom layer irradiance is always lower than 10% of its surface level. Consequently, in areas shallower than 64 m (i.e., the floor would be illuminated in the classic scheme), the IND scheme often has a 1%-depth that is shallower than the 10%-depth of the classic scheme.

Both methods are somewhat unrealistic and must be applied with caution and knowledge of their respective flaws. Trying to make a model of a conglomerate of several notoriously complex and diverse ecosystems in such an oversimplified way as we do will come with its shortcomings. While a more precise approach is certainly desirable for some applications, especially in a more localized domain, we argue for efficiency over precision when trying to show the effects of reducing light availability globally, but more strongly in shallow areas. Furthermore, we stride to make a simple, qualitative study on the effect of heterogeneous reduction of light availability. The IND method has been shown to improve model performance over a large domain with heterogeneous turbidity, while not requiring the costs of a full 3D sediment model (Zhou et al., 2017). The expected results thus justify the use of the IND method.

2.4. Description of Used Data

All of our set-ups of ROMS-CoSiNE are initialized, and in the case of the 3D set-ups also forced at the open boundaries with data taken from AMM7-ERSEM. The Forecasting Ocean Assimilation Model (FOAM, Bell et al., 2003) was applied to the Atlantic Margin Region (40 deg N, 20 deg W to 65 deg N, 13 deg E) with 1/15 deg latitudinal and 1/9 deg latitudinal resolution (∼7 km-square, hence the acronym AMM7), giving reanalyzed hydrodynamic data. The physical core of AMM7 is the Nucleus for European Modeling of the Ocean (NEMO,

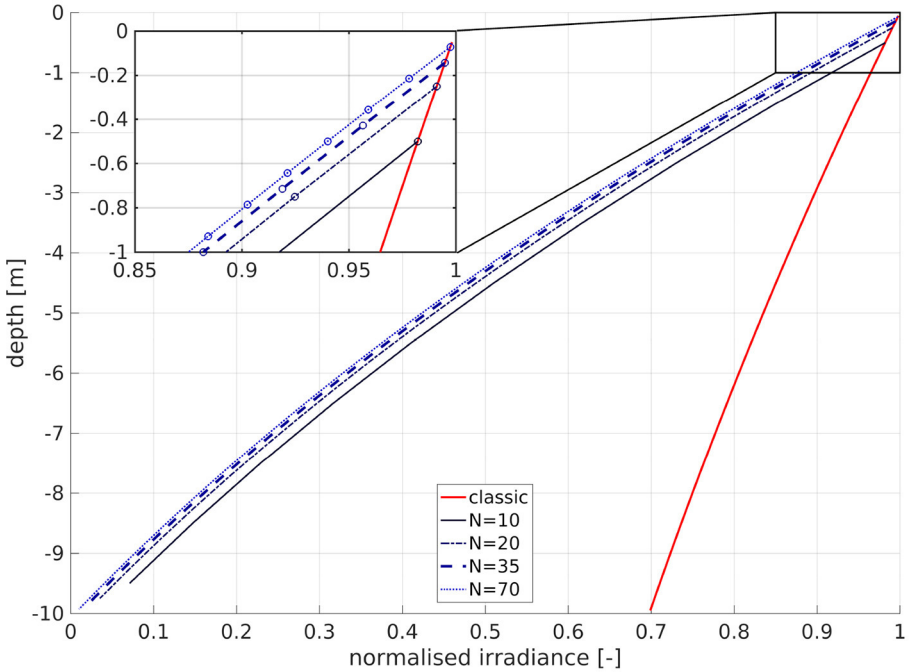

FIGURE 1 | Influence of number of layers N on the attenuation of normalized irradiance for a depth of 10 m. The abscissa is normalized irradiance, and the ordinate is depth. The solid red line is the classic scheme, the other lines are for the IND scheme: solid black is for $N = 10$, dark blue dashed is for $N = 20$, bold dashed blue is for $N = 35$ (as in our model), and dotted blue is for $N = 70$. The circles in the magnified inset denote the cell center depths of the respective layers.

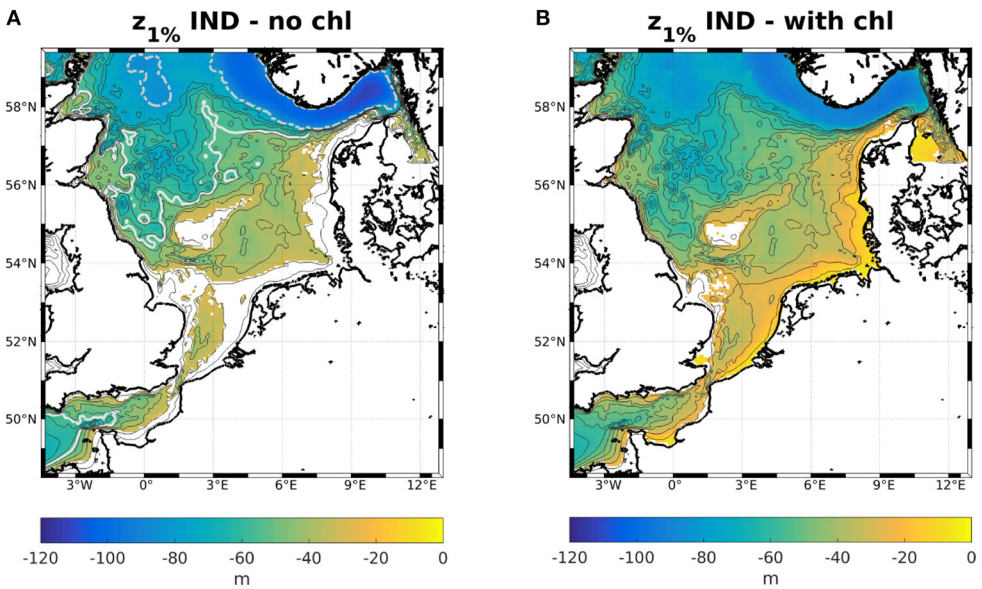

FIGURE 2 | Colors: 1%-depths for the IND scheme **(A)** neglecting chlorophyll and **(B)** considering chlorophyll. The dashed gray isoline in **(A)** is the 1%-, and the white isoline is the 10%-depth of the classic scheme. Blank cells mark areas where the bottom layer irradiance is higher than 1 or 10%, respectively.

Madec, 2008), which uses a structured horizontal Arakawa C-grid, as well as a hybrid s-z-grid in the vertical. The physical model is coupled to ERSEM (Baretta et al., 1995; Radach and Lenhart, 1995). In its original formulation, the biological structure ERSEM is immensely complex, compared to that of CoSiNE (Baretta-Bekker et al., 1995; Baretta et al., 1995; Chai et al., 2002; Zhou et al., 2017; Liu et al., 2018), including both a benthic and a pelagic component for a combined total of 31

state variables with decoupled nutrient cycles[1]. For reasons of simplicity, benthic modules are often omitted—as in the case of AMM7-ERSEM and ROMS-CoSiNE. CoSiNE is based on a nitrogen cycle, to which carbon, phosphate, and silicate cycles are coupled, and mostly act as nutrient limiting factors. It also does not explicitly model dissolved organic matter (DOM), as ERSEM does. The version of ERSEM that was used in AMM7 is one-dimensional along the vertical axes, and is described in Blackford et al. (2004). We compare our model against AMM7-ERSEM, because (a) our model was built on it, and (b), the available amount of *in situ* data is rather poor and AMM7-ERSEM has been reanalyzed using the available data.

Because we aim for a simple, inexpensive model, CoSiNE13 is an optimal choice. We accept several strong restrictions for the benefit of efficiency, yet to test the modification of the light treatment, a model like ERSEM or CoSiNE in its 2014 formulation (Xiu and Chai, 2014) would be too complex. Nevertheless, when aiming for accuracy in prediction of chlorophyll and nutrient dynamics, one might consider or even prefer utilizing a more complete and less restrictive ecosystem model.

2.5. Methods of Analysis

To compare magnitudes of phytoplankton bloom as well as horizontal distribution of surface values to measurements and AMM7-ERSEM, monthly means were computed at the surface over the entire domain. We performed area averages over the ICES boxes (see **Figure 3**, O'Driscoll, 2014). To do so, we first interpolated the ROMS data onto geopotential layers (z-layers). For reasons of comparability, we chose to take the same depth levels as are available for AMM7-ERSEM data via CMEMS (0, 3, 10, 15, 20, 30, 50, 75, 100, 125, 150, 200, 250, 300, 400, and 500 m). To quantify the effect of the modification, the bias and root mean square differences (RMSD) of the area averages, normalized by the total range of chlorophyll for the classic scheme within a box (nbias and nRMSD), were calculated for each z-layer.

Utilizing a method applied to Scanfish data (Zhao et al., 2019b), we sorted chlorophyll profiles in the German Bight into four categories: high content in upper layers (HCU) and lower layers (HCL), well mixed profiles (WM) and subsurface chlorophyll maxima (SCM). Zhao et al. (2019b) distinguished between SCM with HCL, with HCU and otherwise well mixed situations, however, due to the relative scarcity of SCM, we do not make this distinction here.

3. RESULTS AND DISCUSSION

3.1. Evaluation of the Biological Model

The model simulates a realistic seasonal cycle. **Figure 4** shows an example of nitrate, all plankton groups and nitrogenous detritus at depth vs. time in the German Bight (black cross in **Figure 1**) for the IND scheme. The spring bloom for diatoms occurs earlier than that for small phytoplankton. The microzooplankton

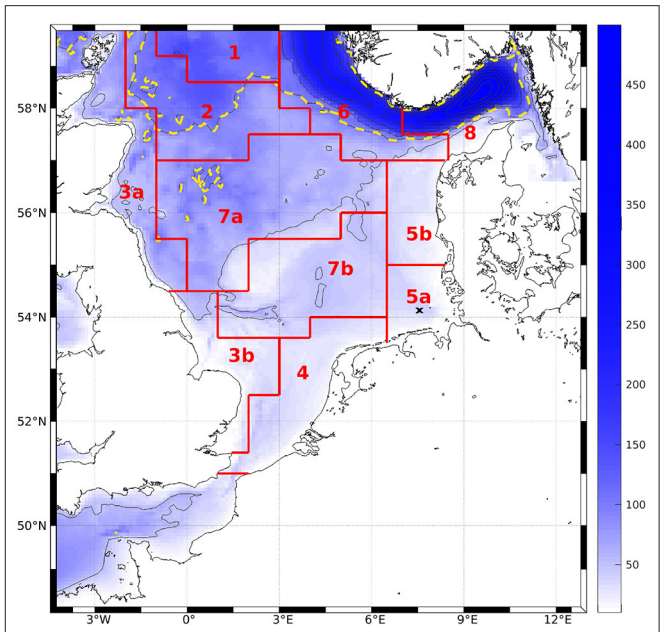

FIGURE 3 | Bathymetry of the model area. Contour intervals are 50 m, dashed line denotes 100 m. Red lines and tags show ICES boxes after O'Driscoll (2014). The black cross marks the station to which **Figures 4** and **7** refer.

feeds on small phytoplankton exclusively, and as the latter is outcompeted by the diatoms, the microzooplankton is also of low concentration. Because the diatoms are more abundant in the second year, the small phytoplankton is almost entirely absent, and subsequently, so is the microzooplankton, not occurring at all in 2013. The year 2012 was slightly colder than 2013, which is why primary production in 2013 was stronger. This also shows in AMM7. The mesozooplankton feeds of diatoms, small phytoplankton, microzooplankton and detritus, for which reason it is present throughout the entire runtime, usually with a phase lag of a few weeks, respective to phytoplankton and detritus. Both diatoms and detritus sink to the floor. This leads the diatoms to accumulate below the surface, where light availability is still high enough.

A comparison with AMM7-ERSEM data for the same nutrients showed no obvious or critical mismatch. All nutrients recover in the winter of 2012 and 2013 to about the same value they had in the IC. Note that **Figure 4** shows output at one particular station in the German Bight, which is a region of strong horizontal turbulence. Thus, no single station is representative of the entire region. Area averages reveal that all nutrients do indeed recover (not shown). Given the immense complexity of ERSEM and AMM7, relative to our model, and the fact that we are comparing to reanalyzed data, could explain some of the quantitative differences. The comparisons to AMM7 and CCI data (**Figure 5**) show that ROMS-CoSiNE matches the spacial distribution patterns of the chlorophyll dynamics in the North Sea, and in some cases even better than AMM7-ERSEM does. ROMS-CoSiNE shows an overestimation of chlorophyll along the south western shore, and an underestimation in the deeper, northern North Sea, as well as the East Anglia Plume. However,

[1]Note, that we are comparing ERSEM to a version of CoSiNE with 13 state variables (CoSiNE13). There exists a version of CoSiNE with 31 pelagic state variables (CoSiNE31), utilizing a spectral treatment of light, which is applied to the Pacific ocean, hence not requiring a benthic module (Xiu and Chai, 2014).

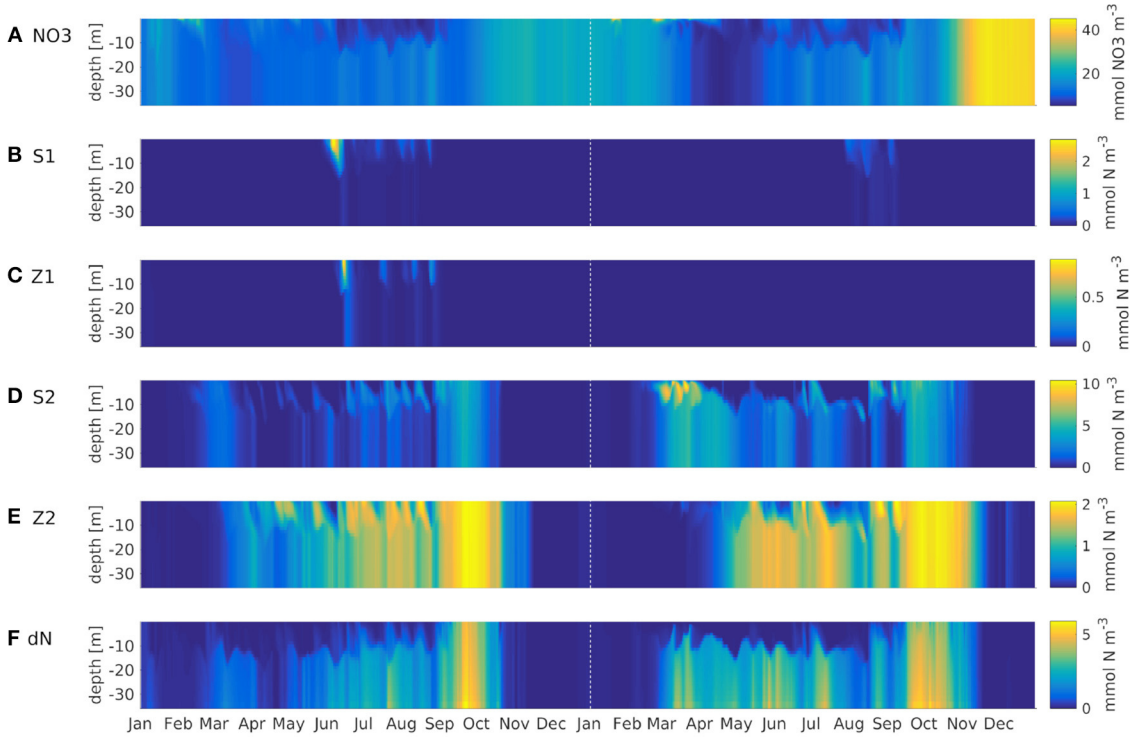

FIGURE 4 | Hovmöller diagrams of ROMS-CoSiNE simulations using the IND scheme at the station marked by the black cross in **Figure 1**. In top down order, the panels are NO3 ($mmol\,NO3m^{-3}$) **(A)**, small phytoplankton **(B)**, microzooplankton **(C)**, diatoms **(D)**, mesozooplankton **(E)** and nitrogenous detritus **(F)** (all $mmol\,Nm^{-3}$). The dashed vertical line marks the first of January 2013.

the horizontal distribution patterns of ROMS-CoSiNE (both schemes) and CCI are very alike.

The area averages of both schemes and AMM7 at 3 m depth, as well as ICES bottle data and FerryBox data of chlorophyll-a is shown in **Figure 6**. In the north western boxes, the data availability is rather scarce, however there, the CCI data (**Figure 5**) can be taken as a good point of reference. The agreement between models and measurements are of varying degree, both locally and temporarily. Many of the differences between the models and data are found for both models. Furthermore, the *in situ* data consists of subsampled data from a large domain that shows significant horizontal variability. We have filtered the bottle and FerryBox data points so that only regions of salinity greater than $30PSU$ were considered. This was done to exclude data points taken in river mouths or very close to the shore (e.g., the Wadden Sea), where processes which we cannot resolve might influence the phytoplankton growth. Furthermore, we have taken daily averages, in case there were multiple data points per day. The comparison shows that our simulations are realistic, qualitatively speaking. Pätsch and Kühn (2008) have performed a study using a 3D ecosystem model (ECOHAM) in the North Sea for the years 1993 to 1996. Simulated nitrate and chlorophyll values in the upper layers (their Figure 6) were found to largely agree with our simulations, patternwise. Magnitudes were lower in ROMS-CoSiNE for box 1 and 7 (compare **Figure 6** to Pätsch and Kühn, 2008, their Figures 6D,E—note that AMM7 is overestimating here), and higher for box 5a (Pätsch and Kühn, 2008, their Figure 6F). Another reason for differences could be that we are comparing different time periods with 17 years between their study and ours. Note also that while we are comparing area averages, the areas we average over are of different size than those (Pätsch and Kühn, 2008) average over.

3.2. Comparison of the Two Light Schemes

The coupling of CoSiNE in the classic formulation to ROMS increases the total amount of parallel computation time by 226% with respect to a physical run. The inclusion of the IND scheme does not influence the runtime, relative to the classic formulation by any significant number (0.57%).

The effect of the IND scheme is visualized in **Figure 7**, which shows normalized irradiance attenuated with depth, taking phytoplankton absorption into account. Without phytoplankton present (i.e., winter months), the normalized irradiance in the classic scheme is well above 10% at the bottom, while the 10%-depth in the IND scheme is at around 21 m by default. While the chlorophyll attenuation coefficient is the same in both set-ups, the factor k/N has a strong effect in lower layers, causing the 10%-depth to be reduced by half in times of high chlorophyll-a abundance. In the classic scheme, the remaining light never reaches a value of 1% or lower, while it does in the IND scheme.

Floeter et al. (2017) have performed measurements in the German Bight in similar positions as station used in

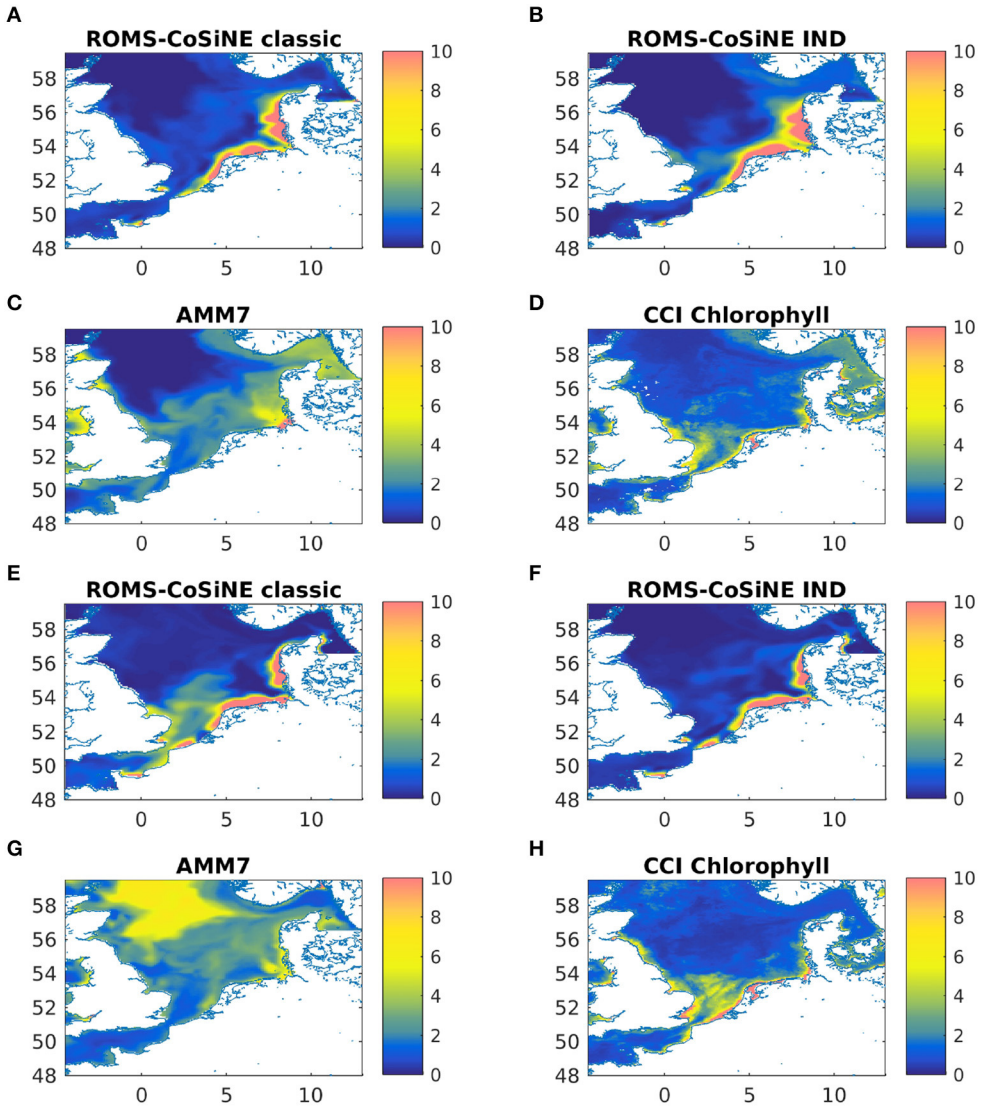

FIGURE 5 | Monthly means of chlorophyll-a [$mgChl - am^{-3}$] for ROMS-CoSine in the classic formulation **(A,E)**, and the IND formulation **(B,F)**, as well as AMM7 **(C,G)**, and CCI data **(D,H)** for March 2013 **(A–D)** and May 2013 **(E–H)**.

Figures 1, **4**, **7**. Using a hyperspectral TriOS Ramses-ACC irradiance sensor, they calculated the 1%-depths along transects through wind farms. The measured depths ranged between 26 and 21 m in July 2014 (see Floeter et al., 2017, their Figure 11). As can be seen in **Figure 7**, the IND scheme is thus more realistic here, showing similar (if slightly too great) 1%-depths in the summer months of 2012 and 2013. Note that we neglect the effects of CDOM, which are potentially significant at this particular station in the German Bight (compare to e.g., Painter et al., 2018).

The nRMSD and nbias are shown in **Figure 8**. While the patterns of both quantities are largely similar, there is often times a pronounced nRMSD at the surface, while there is no or only a small nbias there. This is explained by a difference in timing with no or little difference in magnitude (as can be seen in **Figure 6**). Note that the maxima of nRMSD and nbias are not found in the bottom layers but around the boxes' average depths. Over large areas along the southern shore, the North Sea is shallower than 10 m, yet, our model has no dryfalling and a minimum depth is prescribed as 10 m. Around a third of box 5a is shallower than 15 m (compare **Figure 1**), which explains why the largest nRMSD and nbias are found there at 10 m depth (**Figure 8**), as we are comparing the area averages that have been interpolated onto a z-grid. The two boxes where the largest nRMSD and nbias do not occur at the boxes' respective average depths (boxes 6 and 8) are so deep that in both schemes, the lowest layers are outside of the photic zone. Accordingly, there is neither significant nbias nor nRMSD in the bottom layers of these boxes. The least pronounced effects on both nRMSD and nbias are found in boxes 1 and 6, where there is mostly a shift in timing (see also **Figure 6**). The largest values for nRMSD and nbias are found in the lower layers of box 7a (central North Sea), a box

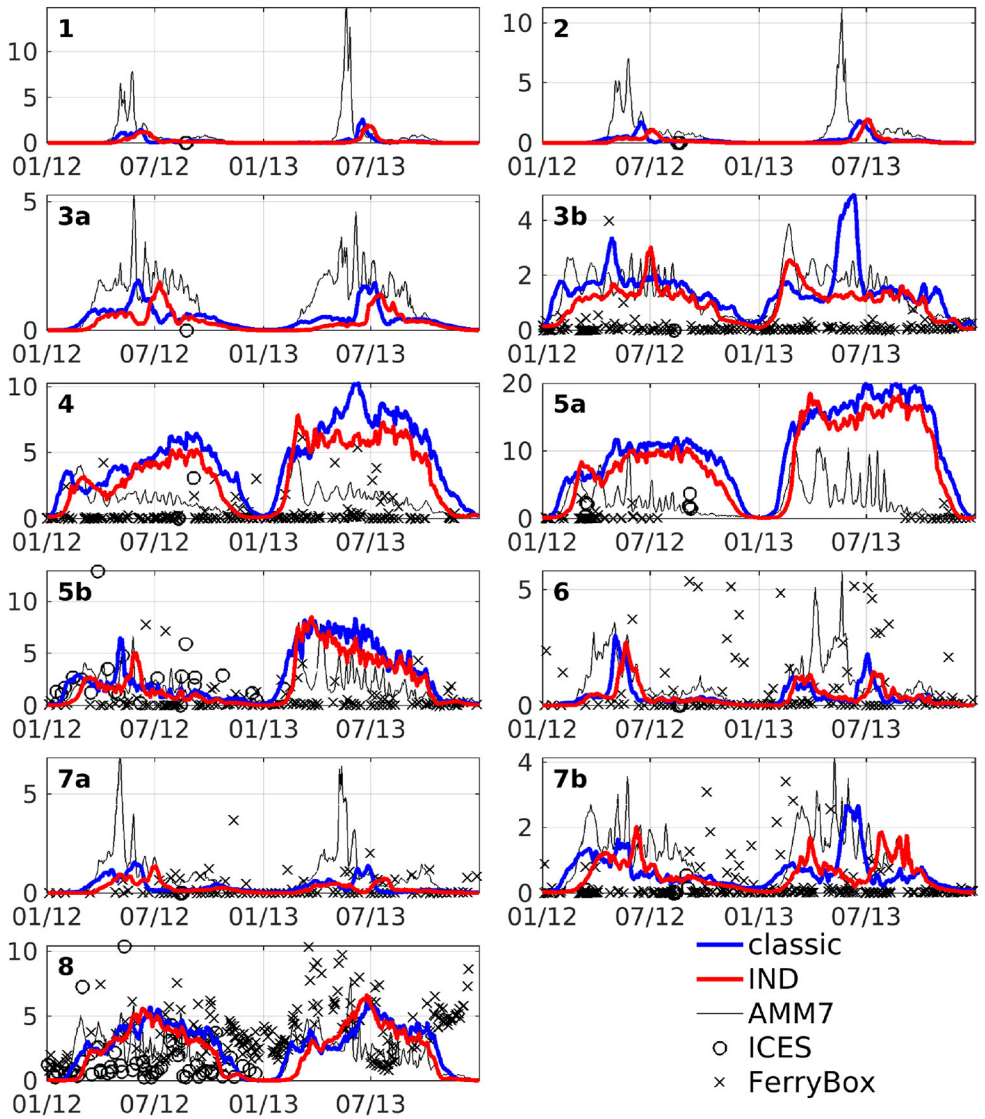

FIGURE 6 | Area averages of chlorophyll at 3 m depth in units of *mg Chl* m^{-3}. Blue line is the classic scheme, red is the IND scheme, black is AMM7, black crosses is FerryBox data and black circles is ICES bottle data.

that is remote from any river influx and has an average depth of 62 ± 5 m (which is close to the 10%-depth of 64 m in the classic scheme). This largely falls into a domain which Capuzzo et al. (2015) described as seasonally stratified and for which they found average Secchi depths between $z_{SD} = 4.11 \pm 1.3$ m in winter and $z_{SD} = 10.61 \pm 3.56$ m in summer. According to Lee et al. (2015), the Secchi depth is approximately the inverse of the downwelling attenuation coefficient k_d, and given that $k_d = -z_{1\%}^{-1} \ln(\frac{I(z_{1\%})}{I_0})$, it follows that $z_{SD} \approx 0.22 z_{1\%}$. **Figure 3B** shows that the IND scheme is close to this, with $z_{1\%}$-values ranging between roughly 20 and 70 m, and thus Secchi depths of roughly 4 to 15 m on average. The classic scheme never reaches values below $z_{SD} \approx 30$ m (not shown).

For the IND scheme, as **Figures 9C,D** show, the largest reductions of both the 1%- and 10%-depths with respect to the total water depth are found in the southern North Sea, along the Dutch, German, and Danish coasts. This is likely due to the overestimation of diatoms there. The same can be seen in the classic scheme (not shown). However, all areas where the relative change in 1%- and 10%-depths are greater than 15% are characterized by large riverine nutrient influxes. In other shallow regions, e.g., at the Oyster grounds (box 7b), the reductions are not as pronounced. The areas of the greatest absolute change are thus areas that are light limited and those with the greatest relative change are nutrient limited (compare e.g., Zhao et al., 2019a, their Figure 3). In absolute terms, the greatest reduction of the 1%- and 10%-depths are found along the Norwegian coast and in the Skagerrak, which is largely due to the greater water depth (**Figures 9A,B**). **Figure B.1** shows the ratios between 1%- and 10%-depths both with and

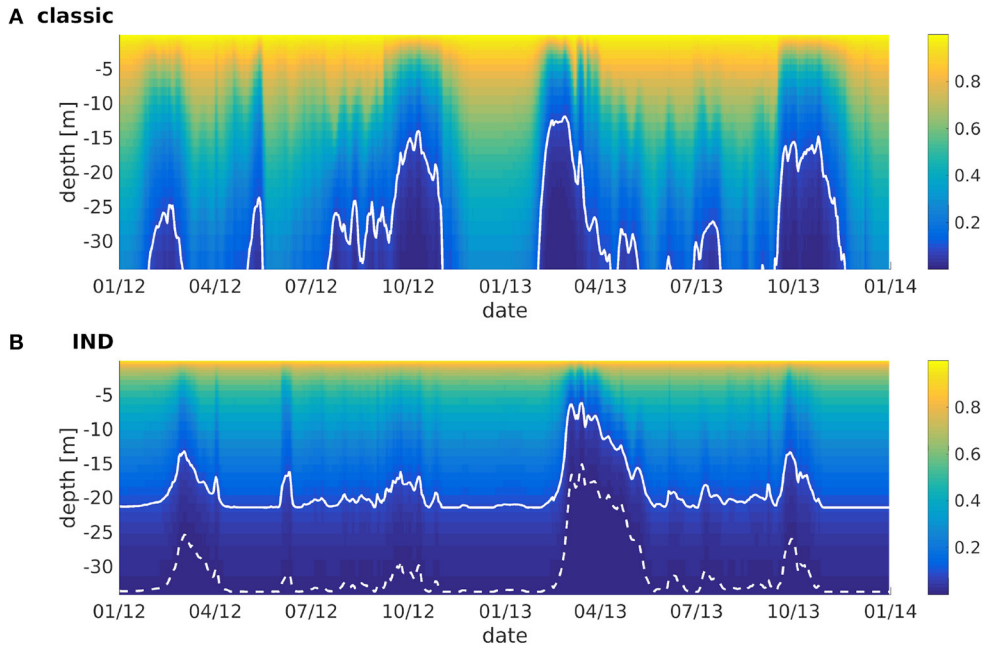

FIGURE 7 | Normalized irradiance at depth vs. time for ROMS-CoSiNE at the station marked by the black cross in **Figure 1** using **(A)** the classic formulation and **(B)** the IND scheme. The solid line denotes the 10%-, and the dashed line the 1%-depth.

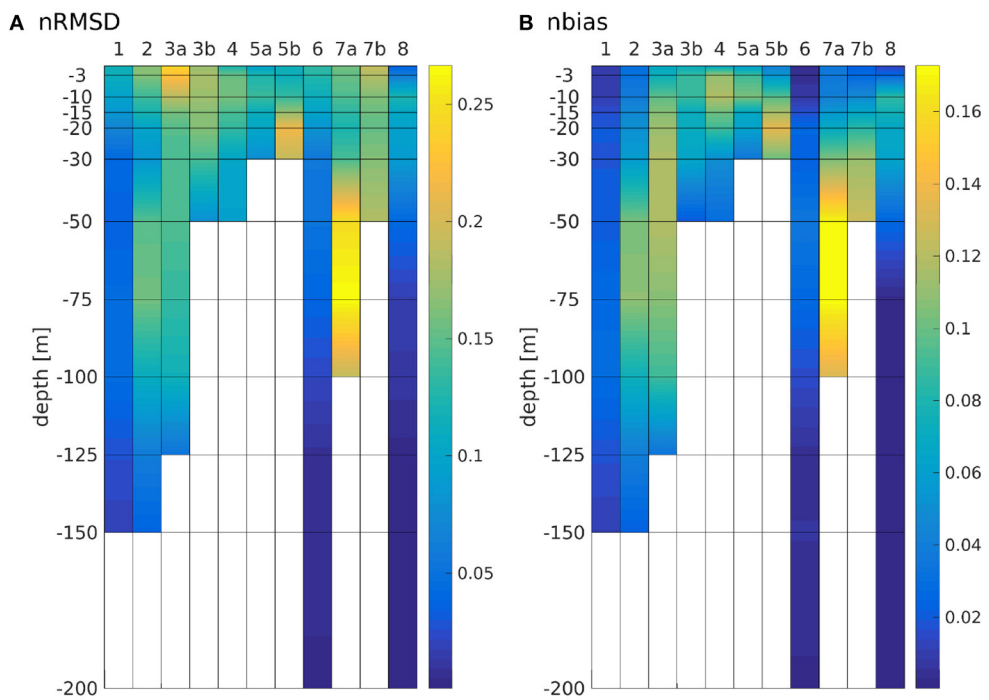

FIGURE 8 | Normalized RMSD **(A)** and bias **(B)** of chlorophyll between classic and IND for all boxes.

without considering chlorophyll specific attenuation. The ratio noticeably increases in the areas where the absolute reductions of the 1%- and 10%-depths are greatest (**Figures 9A,B**), which is due to the self shadowing of phytoplankton. Capuzzo et al. (2015) show a map of sea floor illumination in the area of the East Anglia Plume (their Figure 3), classifying regions that have been illuminated before and after 1950 (dark blue), only were illuminated before 1950 (lighter blue), or were never

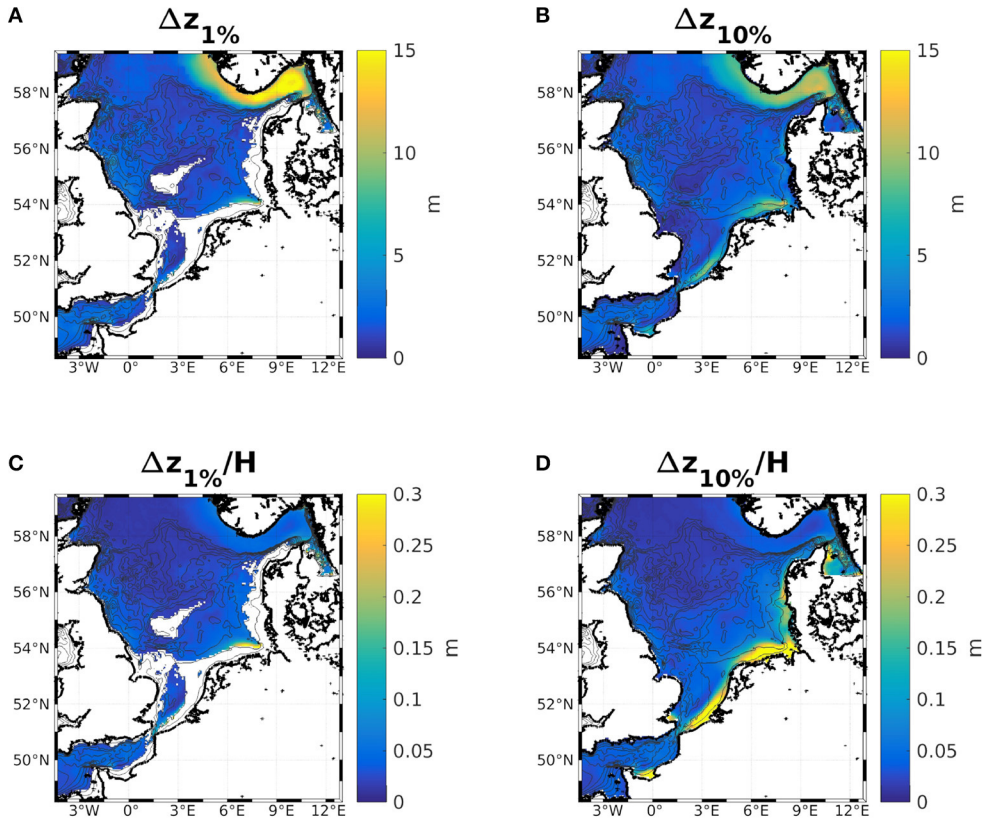

FIGURE 9 | Differences of the 2 year means of the 1%- **(A,C)** and 10%-depths **(B,D)** with chlorophyll specific attenuation minus without. Absolute values are shown in **(A,B)**, and **(C,D)** show the same, normalized by the local water depth.

illuminated (light blue). Noticeably, the areas that are still illuminated today match the areas in our model were the average bottom irradiance is greater than 1% of the surface irradiance (**Figure B.1B**).

The area averaged chlorophyll differences show that there is merely a reduction of magnitude, but no vertical shift of a subsurface maximum between the two schemes. From **Figure 6**, we can see that in box 7b, there is one strong peak of chlorophyll in the summer of 2013 for the classic scheme, but in the IND scheme, there is one peak in spring and one in autumn, both being smaller than the peak in the classic scheme. The biannual mean of the differences are low at the surface, because approximately the same amount of chlorophyll is produced in both schemes, yet the nRMSD responds to the different temporal behavior of the blooms (**Figure 8**). In the Skagerrak, there are biases of $2mg\ Chl\ m^{-}3$, reaching depths of up to 50 m and prevailing for several months (not shown). This is due to the inclusion of parts of the Kattegat in Box 8, which is rather shallow, and heavily influenced by the Baltic outflow. All other deep boxes do show differences, but they are mostly differences in timing and less in magnitude. As **Figure 6** shows, the blooms in these boxes are comparably short.

Comparing our results for the German Bight (box 5a, **Figure 10**) to Zhao et al. (2019b their Figure 4), there are a few differences, but the overall agreement is reasonably good, and more so with the implementation of a modified light regime. There are fewer stratified profiles in the IND case, compared to the classic case, in almost all areas and at almost all times, except areas that are of depths between 15 and 25 m, where the IND scheme shows generally more stratified profiles. In regions deeper than 15 m, there are more HCU situations in the IND scheme than in the classic scheme. There are relatively fewer SCM situations in ROMS-CoSiNE than there are in the scanfish data, analyzed by Zhao et al. (2019b). A likely reason for this is the relatively coarse resolution of 35 layers. Due to the overestimation of winter chlorophyll, there are more stratified profiles in early months in the model than there are in the Scanfish data. SCM tend to occur in shallower regions in the IND scheme, compared to the classic scheme and the Scanfish data. HCL situations are more frequent than HCU, because the diatoms, which are prevalent in the German Bight, sink to the floor.

Figure 11 shows depth integrated chlorophyll for both schemes. Especially in boxes that are shallow and/or have large riverine nutrient influence (3b to 6, 7b, and 8), the spring bloom peaks are of similar, and sometimes higher magnitude than the classic scheme. There is a time shift of up to several months in both years (explaining the presence of nRMSD, yet absence of bias in the upper layers; see above and **Figure 8**). The growth throughout the rest of the year shows no shift in timing, but often

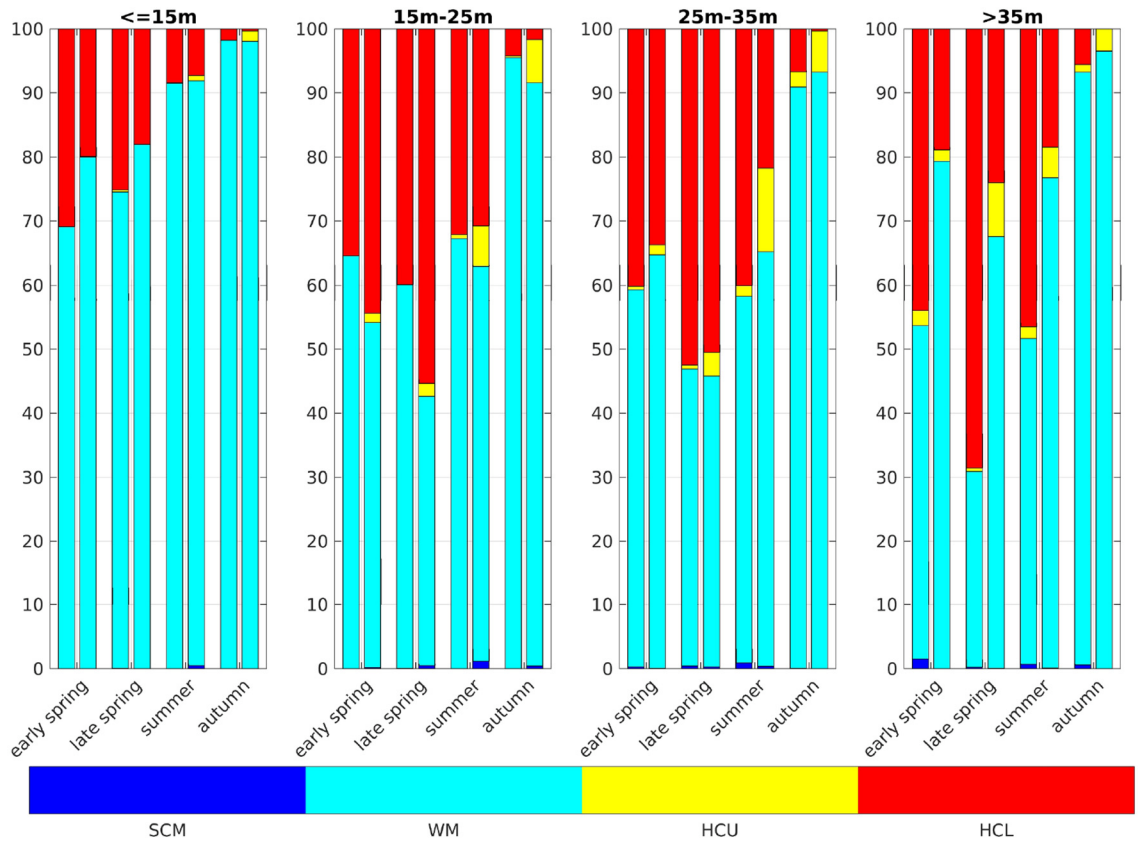

FIGURE 10 | Categories of vertical chlorophyll profiles in the German Bight. Dark blue are subsurface chlorophyll maxima (SCM), turquois are well mixed profiles (WM), yellow are high chlorophyll content in upper layers (HCU), and red are high chlorophyll content in lower layers (HCL). The left bars show the classic scheme and the right the IND. Early spring is March and April, late spring is May, summer is June, July, and August, and autumn is September, following the classification of Zhao et al. (2019b).

significantly lower magnitudes. In the remaining boxes (1 to 4a, and 7a), the growth is generally weaker and slower.

The comparisons of area averages (**Figures 6**, **11**), as well as that of monthly means of surface chlorophyll to CCI and AMM7 data (**Figure 5**) show that for some situations, the classic scheme is closer to the data (more in the deep northern and western areas), and for others the IND does. It can be noted that the agreement between AMM7 and ROMS-CoSiNE is generally good, with some glaring differences (AMM7 chl is higher in the deeper, northern regions, but lower near the Belgian, Dutch, and German coast). The inclusion of the IND scheme helps to bring ROMS-CoSiNE and AMM7 closer together in some areas (e.g., boxes 4, 5a, 5b), but in others, it does the opposite (e.g., boxes 1, 2, 3a, 7a). Incidentally, the deep, northern boxes 1 to 3a are the ones where AMM7 agrees least with CCI data (**Figure 5**).

4. CONCLUSIONS

A functioning ecosystem model was established, which is capable of reproducing a realistic seasonal cycle of nutrients, phyto- and zooplankton, as well as detritus. The horizontal distribution of chlorophyll matches that of measurements. Because the model is relatively cheap to run, it gives a good starting point for further investigations of light climate, although adjustments will need to be made to accommodate the effects of temporal variability and CDOM. To the best of our knowledge, there has not been a published application of ROMS-CoSiNE in the North Sea. We have shown that ROMS is capable of giving reliable numeric simulations of the physical North Sea. CoSiNE is capable of simulating important aspects of its biology. For the purpose of a sensitivity study, the model produces results of sufficient accuracy.

The reduction of light availability leads to weaker total production of chlorophyll-a. Because the modification reduces light availability in the entire domain, this was an expected result. For all boxes, the reduced light availability in the IND scheme expresses itself in three ways: the spring bloom peaks occur later, their magnitudes are weaker, and the magnitude of growth after the spring bloom is weakened. However, these three characteristics need not be present in the same extremity for all boxes. Generally, deep boxes with little terrestrial nutrient input (1, 2, and 3a) show the least change in total magnitude. The far greatest total reductions in growth are found in regions with large

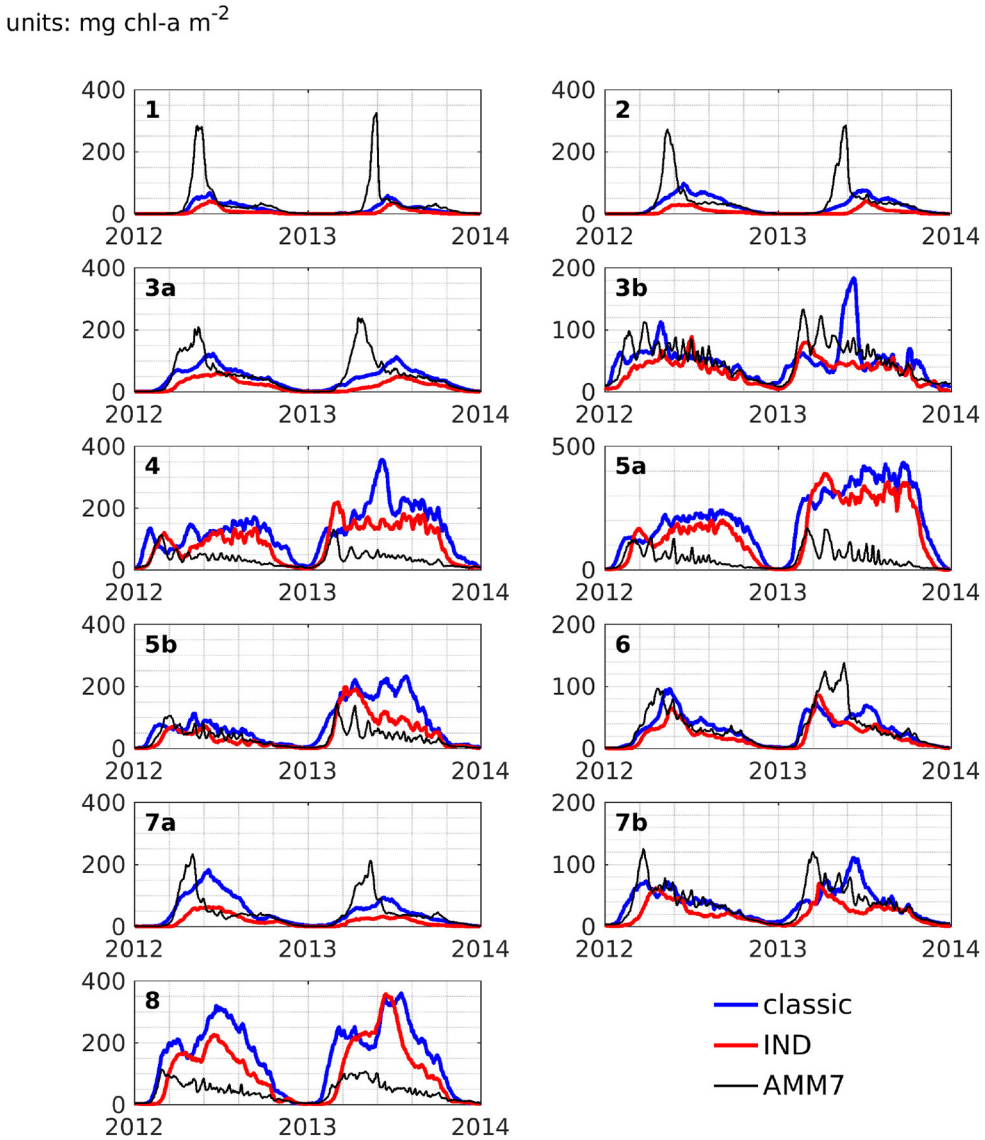

FIGURE 11 | Depth integrated area averages of chlorophyll-a for ROMS-CoSiNE in the classic formulation (blue) and the IND scheme (red), as well as AMM7 (black), for all areas.

river inputs. Because there is no nutrient limitation there, light limitation is dominant. The total magnitudes are also larger there, allowing for greater total reduction. In relative terms, the greatest impact is found in deep areas with low magnitudes and strong nutrient limitation. As regions of high terrestrial water input are typically rich in CDOM (e.g., Painter et al., 2018), the inclusion of CDOM specific attenuation is expected to further increase the total reduction of magnitude in those areas.

The IND scheme thus provides the expected results exactly where they are desired, but also brings undesired results elsewhere. A hybrid scheme could help correct for this, where the IND scheme (or a similar modification) is active in a nearshore environment and inactive in domains that can be seen as case 1 waters, are deep enough for SPM to not play a role, or where there is otherwise naturally little SPM effect on light attenuation. For turbid regions, such as estuaries or specific marginal seas or coastal subbasins (e.g., German Bight, East China Sea, San Francisco Bay, Chesapeake Bay—all areas where CoSiNE has been used), the global use of the IND scheme may be more desirable than coupling to a sediment and wind wave module, for reasons of simplicity, affordability, and qualitatively similar results. The use of a simple weighting function (e.g., activating the IND scheme for all depths below a threshold value, or activation via a prescribed mask) can make the scheme more flexible without defeating the purpose of having a very affordable scheme that is also easy to implement. Furthermore, ROMS has the capability (as do many other models), to distribute the upper layers (almost) equally, along geopotential surfaces, especially in deeper areas. This is generally desirable for physical applications in areas of large bottom slopes and strong stratification, but it

is not ideal for the use of the IND scheme. Again, this may be controlled for by weighting functions.

The SPM attenuation proxy we apply has several important short-comings: (a) we only account for inorganic SPM, while organic SPM is left out [more advanced biological models can account for organic SPM (e.g., Xiu and Chai, 2014)]; (b) the proxy is dependent on bathymetry only, while SPM content in a water column itself has several important influencing factors, such as bottom stress due to wind waves and currents (which is time dependent), grain size and the soil texture of the sea floor (which is horizontally varying, and which can be advected); (c) the vertical distribution of SPM content is approximated by a dependency on bathymetry following s-layers, i.e., a model specific quantity, and not a physical one; (d) the actual SPM content need not be (pseudo) linearly or even monotonously increasing with depth, as we assume it to be; (e) our SPM proxy is, mathematically speaking, unstable, because it contains a singularity (which is numerically speaking outside of our domain). Nevertheless, it is extremely simple to implement and has proven to be effective (Zhou et al., 2017), while being literally no more expensive than the classic approach, without the need to employ an online-coupled sediment and wind wave module, next to the existing configuration. Given that the omission of the modification is equally unphysical, but considerably less realistic, we deem its use justified.

As stated in the introduction, we do not consider CDOM in this work. However, CDOM has been shown in numerous works to be one of the key influences of water clarity (e.g., Dupont and Aksnes, 2013; Urtizberea et al., 2013; Opdal et al., 2019). In the context of coastal ocean darkening over the twentieth century, as it is suggested by multiple studies (e.g., Dupont and Aksnes, 2013; Capuzzo et al., 2015; Opdal et al., 2019), one cannot ignore the role CDOM plays. Future works on the subject of the coastal underwater light field will have to include the effects of CDOM, be it through directly modeling it, as (e.g., Xiu and Chai, 2014) do, or inversely modeling it by applying linear relationships with salinity (e.g., Bowers et al., 2004; Bowers and Brett, 2008; Painter et al., 2018). It is our intention to include CDOM in future works. Furthermore, SPM contents in the North Sea are subject to both seasonal (e.g., van der Molen et al., 2009; Dobrynin et al., 2010; Gohin, 2011) and interannual variability (e.g., van der Molen et al., 2009; Capuzzo et al., 2015; Wilson and Heath, 2019). The IND scheme cannot model temporal effects and is thus unsuitable for use in long term studies. For such purposes, one might use offline data, or directly model SPM.

DATA AVAILABILITY STATEMENT

The datasets generated for this study are available on request to the corresponding author.

AUTHOR CONTRIBUTIONS

The practical work and majority of the writing was carried out by DT in the context of his Ph.D. study, under the supervision of ES, within the Coastal Ocean Darkening project, which is headed by OZ. ES and OZ directed DT, and reviewed and edited the text and figures.

FUNDING

This work was carried out within the project Coastal Ocean Darkening (grant no. ZN3175), funded by the Ministry of Science and Culture of the German federal state of Lower Saxony.

ACKNOWLEDGMENTS

The study has been conducted using E.U. Copernicus Marine Service Information. The code used to compute FES2014, was developed in collaboration between Legos, Noveltis, CLS Space Oceanography Division and CNES, and is available under GNU General Public License. Atmospheric forcing data was provided by the NOAA ESRL Physical Sciences Division, Boulder, Colorado, USA, and taken from their website at http://www.esrl.noaa.gov/psd/.

For their helpful insight, and guidance, we would like to thank Fei Chai, Feng Zhou, Johannes Pein, and Sebastian Grayek.

SUPPLEMENTARY MATERIAL

The Supplementary Material for this article can be found online at: https://www.frontiersin.org/articles/10.3389/fmars.2019.00816/full#supplementary-material

REFERENCES

Baretta, J., Ebenhöh, W., and Ruardij, P. (1995). The European regional seas ecosystem model, a complex marine ecosystem model. *Netherlands J. Sea Res.* 33, 233–246. doi: 10.1016/0077-7579(95)90047-0

Baretta-Bekker, J., Baretta, J., and Koch Rasmussen, E. (1995). The microbial food web in the european regional seas ecosystem model. *Netherlands J. Sea Res.* 33, 363–379. doi: 10.1016/0077-7579(95)90053-5

Baschek, B., Schroeder, F., Brix, H., Riethmüller, R., Badewien, T., Breitbach, G., et al. (2017). The coastal observing system for Northern and Arctic seas (COSYNA). *Ocean Sci.* 13, 379–410. doi: 10.5194/os-13-379-2017

Bell, M., Barciela, R., Hines, A., Martin, M., McCulloch, M., and Storkey, D. (2003). The forecasting ocean assimilation model (FOAM) system. *Elsevier Oceanogr. Ser.* 69, 197–202. doi: 10.1016/S0422-9894(03)80033-8

Bissett, W., Schofield, O., Scott, G., Cullen, J., Miller, W., Plueddemann, A., et al. (2001). Resolving the impacts and feedback of ocean optics on upper ocean ecology. *Oceanography* 14, 30–53. doi: 10.5670/oceanog.2001.22

Bissett, W., Walsh, J., Dieterle, D., and Carder, K. (1999). Carbon cycling in the upper waters of the Sargasso Sea: I. Numerical simulation of differential carbon and nitrogen fluxes. *Deep Sea Res. Part I Oceanogr. Res. Pap.* 42, 205–269. doi: 10.1016/S0967-0637(98)00062-4

Blackford, J., Allen, J., and Gilbert, F. (2004). Ecosystem dynamics at six contrasting sites: a generic modelling study. *J. Mar. Syst.* 52, 191–215. doi: 10.1016/j.jmarsys.2004.02.004

Bowers, D., and Brett, H. (2008). The relationship between CDOM and salinity in estuaries: an analytical and graphical solution. *J. Mar. Syst.* 73, 1–7. doi: 10.1016/j.jmarsys.2007.07.001

Bowers, D., Evans, D., Thomas, D., Ellis, K., and Williams, P. B. (2004). Interpreting the colour of an estuary. *Estuar. Coast. Shelf Sci.* 59, 13–20. doi: 10.1016/j.ecss.2003.06.001

Cahill, B., Schofield, O., Chant, R., Wilkin, J., Hunter, E., Glenn, S., et al. (2008). Dynamics of turbid buoyant plumes and the feedbacks on near-shore biogeochemistry and physics. *Geophys. Res. Lett.* 35. doi: 10.1029/2008GL033595

Capuzzo, E., Stephens, D., Silva, T., Barry, J., and Forster, R. (2015). Decrease in water clarity of the southern and central North Sea during the 20th century. *Glob. Change Biol.* 21, 2206–2214. doi: 10.1111/gcb.12854

Chai, F., Dugdale, R., Peng, T.-H., Wilkerson, F., and Barber, R. (2002). One-dimensional ecosystem model of the equatorial Pacific upwelling system. Part I: model development and silicon and nitrogen cycle. *Deep Sea Res. II Top. Stud. Oceanogr.* 49, 2713–2745. doi: 10.1016/S0967-0645(02)00055-3

Daewel, U., and Schrum, C. (2013). Simulating long-term dynamics of the coupled North Sea and Baltic Sea ecosystem with ECOSMO II: model description and validation. *J. Mar. Syst.* 119–120, 30–49. doi: 10.1016/j.jmarsys.2013.03.008

Dobrynin, M., Gayer, G., Pleskachevsky, A., and Günther, H. (2010). Effect of waves and currents on the dynamics and seasonal variations of suspended particulate matter in the North Sea. *J. Mar. Syst.* 82, 1–20. doi: 10.1016/j.jmarsys.2010.02.012

Dupont, N., and Aksnes, D. (2013). Centennial changes in water clarity of the Baltic Sea and the North Sea. *Estuar. Coast. Shelf Sci.* 131, 282–289. doi: 10.1016/j.ecss.2013.08.010

Evans, G., and Parslow, J. (1985). A model of annual plankton cycles. *Biol. Oceanogr.* 3, 328–347.

Fasham, M., Ducklow, H., and McKelvie, S. (1990). A nitrogen-based model of plankton dynamics in the oceanic mixed layer. *J. Mar. Res.* 48, 591–639. doi: 10.1357/002224090784984678

Floeter, J., Van Beusekom, J., Auch, D., Callies, U., Carpenter, J., Dudeck, T., et al. (2017). Pelagic effects of offshore wind farm foundations in the stratified North Sea. *Prog. Oceanogr.* 156, 154–173. doi: 10.1016/j.pocean.2017.07.003

Gohin, F. (2011). Annual cycles of chlorophyll-a, non-algal suspended particulate matter, and turbidity observed from space and *in-situ* in coastal waters. *Ocean Sci.* 7, 705–732. doi: 10.5194/os-7-705-2011

Haidvogel, D., Arango, H., Hedstrom, K., Beckmann, A., Malanotte-Rizzoli, P., and Shchepetkin, A. (2000). Model evaluation experiments in the North Atlantic Basin: simulations in nonlinear terrain-following coordinates. *Dyn. Atmos. Ocean* 32, 239–281. doi: 10.1016/S0377-0265(00)00049-X

Harvey, E., Walve, J., Andersson, A., Karlson, B., and Kratzer, S. (2019). The effect of optical properties on secchi depth and implications for eutrophication management. *Front. Mar. Sci.* 5:496. doi: 10.3389/fmars.2018.00496

Kühn, W., and Radach, G. (1997). A one-dimensional physical-biological model study of the pelagic nitrogen cycling during the spring bloom in the northern North Sea (FLEX '76). *J. Mar. Res.* 55, 687–734. doi: 10.1357/0022240973224229

Lee, Z., Shang, S., Hu, C., Du, K., Weidemann, A., Hou, W., et al. (2015). Secchi disk depth: a new theory and mechanistic model for underwater visibility. *Remote Sens. Environ.* 169, 139–149. doi: 10.1016/j.rse.2015.08.002

Lenhart, H., Radach, G., Backhaus, J., and Pohlmann, T. (1995). Simulations of the north sea circulation, its variability, and its implementation as hydrodynamical forcing in ERSEM. *Netherlands J. Sea Res.* 33, 271–299. doi: 10.1016/0077-7579(95)90050-0

Liu, Q., Chai, F., Dugdale, R., Chao, Y., Xue, H., Rao, S., et al. (2018). San Francisco Bay nutrients and plankton dynamics as simulated by a coupled hydrodynamic-ecosystem model. *Continent. Shelf Res.* 161, 29–48. doi: 10.1016/j.csr.2018.03.008

Madec, G. (2008). *NEMO Ocean Engine*. Technical report, Institut Pierre-Simon Laplace (IPSL).

Mobley, C., Chai, F., Xiu, P., and Sundman, L. (2015). Impact of improved light calculations on predicted phytoplankton growth and heating in an idealized upwelling-downwelling channel geometry. *J. Geophys. Res.* 120, 875–892. doi: 10.1002/2014JC010588

Moll, A. (1997). Phosphate and plankton dynamics during a drift experiment in the German Bight: simulation of phosphorus-related plankton production . *Mar. Ecol. Prog. Ser.* 156, 289–297. doi: 10.3354/meps156289

Moll, A. (1998). Regional distribution of primary production in the North Sea simulated by a three-dimensional model. *J. Mar. Syst.* 162, 151–170. doi: 10.1016/S0924-7963(97)00104-8

O'Driscoll, K. (2014). Air-sea exchange of legacy POPs in the North Sea based on results of fate and transport, and shelf-sea hydrodynamic ocean models. *Atmosphere* 5, 156–177. doi: 10.3390/atmos5020156

Opdal, A., Lindemann, C., and Aksnes, D. (2019). Centennial decline in North Sea water clarity causes strong delay in phytoplankton bloom timing. *Glob. Change Biol.* 25, 3946–3953. doi: 10.1111/gcb.14810

Painter, S., Lapworth, D., Woodward, E., Kroeger, S., Evans, C., Mayor, D., et al. (2018). Terrestrial dissolved organic matter distribution in the North Sea. *Sci. Total Environ.* 630, 630–647. doi: 10.1016/j.scitotenv.2018.02.237

Pätsch, J., and Kühn, W. (2008). Nitrogen and carbon cycling in the North Sea and exchange with the North Atlantic—A model study. Part I. Nitrogen budget and fluxes. *Continent. Shelf Res.* 28, 767–787. doi: 10.1016/j.csr.2007.12.013

Radach, G., and Lenhart, H. (1995). Nutrient dynamics in the north sea: fluxes and budgets in the water column derived from ESEM . *Netherlands J. Sea Res.* 33, 301–335. doi: 10.1016/0077-7579(95)90051-9

Schrum, C., Alekseeva, I., and St. John, M. (2006a). Development of a coupled physical–biological ecosystem model ECOSMO: Part I: model description and validation for the North Sea. *J. Mar. Syst.* 61, 79–99. doi: 10.1016/j.jmarsys.2006.01.005

Schrum, C., St. John, M., and Alekseeva, I. (2006b). ECOSMO, a coupled ecosystem model of the North Sea and Baltic Sea: Part II. Spatial-seasonal characteristics in the North Sea as revealed by EOF analysis. *J. Mar. Syst.* 61, 100–113. doi: 10.1016/j.jmarsys.2006.01.004

Song, Y., and Haidvogel, D. (1994). A semi-implicit ocean circulation model using a generalized topography-following coordinate system. *J. Comput. Phys.* 115, 228–244. doi: 10.1006/jcph.1994.1189

Umlauf, L., and Burchard, H. (2003). A generic length-scale equation for geophysical turbulence models. *J. Mar. Res.* 61, 235–265. doi: 10.1357/002224003322005087

Urtizberea, A., Dupont, N., Rosland, R., and Aksnes, D. (2013). Sensitivity of euphotic zone properties to CDOM variations in marine ecosystem models. *Ecol. Model.* 256, 16–22. doi: 10.1016/j.ecolmodel.2013.02.010

van der Molen, J., Bolding, K., Greenwood, N., and Mills, D. K. (2009). A 1-D vertical multiple grain size model of suspended particulate matter in combined currents and waves in shelf seas. *J. Geophys. Res.* 114, 148–227. doi: 10.1029/2008JF001150

Warner, J., Sherwood, C., Arango, H., and Signell, R. (2005). Performance of four turbulence closure methods implemented using a generic length scale method. *Ocean Model.* 8, 81–113. doi: 10.1016/j.ocemod.2003.12.003

Wilson, R., and Heath, M. (2019). Increasing turbidity in the North Sea during the 20th century due to changing wave climate. *Ocean Sci.* 15, 1615–1625. doi: 10.5194/os-15-1615-2019

Xiu, P., and Chai, F. (2014). Connections between physical, optical and biogeochemical processes in the Pacific Ocean. *Prog. Oceanogr.* 122, 30–53. doi: 10.1016/j.pocean.2013.11.008

Zhao, C., Daewel, U., and Schrum, C. (2019a). Tidal impacts on primary production in the North Sea. *Earth Syst. Dyn.* 10, 287–317. doi: 10.5194/esd-10-287-2019

Zhao, C., Maerz, J., Hofmeister, R., Roettgers, R., Wirtz, K., Riethmüller, R., et al. (2019b). Characterizing the vertical distribution of chlorophyll a in the German Bight. *Continent. Shelf Res.* 175, 127–146. doi: 10.1016/j.csr.2019.01.012

Zhou, F., Chai, F., Huang, D., Xue, H., Chen, J., Xiu, P., et al. (2017). Investigation of hypoxia off the Changjiang Estuary using a coupled model of ROMS-CoSiNE. *Prog. Oceanogr.* 159, 237–254. doi: 10.1016/j.pocean.2017.10.008

Zielinski, O., Llinas, O., Oschlies, A., and Reuter, R. (2002). Underwater light field and its effect on a one-dimensional ecosystem model at station ESTOC, north of the Canary Islands. *Deep Sea Res. II* 49, 3529–3542. doi: 10.1016/S0967-0645(02)00096-6

Conflict of Interest: The authors declare that the research was conducted in the absence of any commercial or financial relationships that could be construed as a potential conflict of interest.

frontiers in Marine Science

ORIGINAL RESEARCH
published: 28 February 2020
doi: 10.3389/fmars.2020.00111

Unraveling the Seasonality of UV Exposure in Reef Waters of a Rapidly Warming (Sub-)tropical Sea

Sebastian Overmans and Susana Agustí*

Red Sea Research Center, King Abdullah University of Science and Technology, Thuwal, Saudi Arabia

Ultraviolet radiation (UV) is a crucial abiotic stressor that can have severe impacts on biota residing in the upper euphotic zone, especially if UV stress coincides with other stressors such as extreme sea surface temperatures (SSTs). Exposure-dependent effects of UV exposure have been described for a broad range of marine taxa and ecosystems such as coral reefs, yet little is known about the magnitude and seasonality of UV exposure in natural waters. In the present study, we determined how daily exposure of UV-B and UV-A varies seasonally along the water column of a reef system in the central Red Sea, and identified periods when damaging UV levels are likely to coincide with episodes of extreme SST, both presently and in the future. Between July 2016 and September 2018, UV spectroradiometer profiles were recorded fortnightly at a pelagic site adjacent to a mid-shore reef off the Saudi Arabian Red Sea coast, while atmospheric UV-B and UV-A irradiances were measured in 10-min intervals. Additionally, we quantified the concentration of chlorophyll-*a* (Chl-*a*) and absorption by chromophoric dissolved organic matter (aCDOM) in the reef as well as the surrounding waters. Biologically effective optical depths (Z10%) ranged from 6.3–12.9 m (UV-B) and 14.4–27.3 m (UV-A), with the highest UV transparency being observed in late summer when photodegradation of dissolved organic matter (DOM) was most intense and the concentration and molecular weight of CDOM were at their lowest. Incident UV peaked a few weeks prior to this later summer maximum in UV transparency. Consequently, organisms living close to the water surface experienced their most intense UV exposure in May/June, while the timing of maximum UV exposure for biota below ∼2–4 m coincided with the annual peak in water transparency and water temperature, i.e., in July/August. However, SSTs in the Red Sea are increasing at a rapid rate due to climate change, with the consequence that extreme temperatures are occurring earlier in the year and may eventually coincide with extreme UV radiation in shallower areas of the reef. This development could have potentially detrimental effects on highly sensitive, immotile reef biota such as reef-building corals.

Keywords: Red Sea, coral reefs, marine optics, ultraviolet radiation (UV), downwelling diffuse attenuation coefficient (K_d), chlorophyll-*a* (Chl-*a*), chromophoric dissolved organic matter (CDOM), climate change

OPEN ACCESS

Edited by:
Patrick J. Neale, Smithsonian Environmental Research Center (SI), United States

Reviewed by:
Anastazia T. Banaszak, National Autonomous University of Mexico, Mexico
Norman B. Nelson, University of California, Santa Barbara, United States

****Correspondence:***
Sebastian Overmans
sebastian.overmans@kaust.edu.sa

Specialty section:
This article was submitted to Marine Ecosystem Ecology, a section of the journal Frontiers in Marine Science

Received: *03 November 2019*
Accepted: *11 February 2020*
Published: *28 February 2020*

Citation:
Overmans S and Agustí S (2020) Unraveling the Seasonality of UV Exposure in Reef Waters of a Rapidly Warming (Sub-)tropical Sea. Front. Mar. Sci. 7:111. doi: 10.3389/fmars.2020.00111

INTRODUCTION

Ultraviolet radiation (UV: 200–400 nm) is a crucial constituent of solar radiation that is further subdivided into three spectral bands: UV-A (315–400 nm), UV-B (280–315 nm), and UV-C (200–280 nm). Wavelengths of the most damaging spectrum (i.e., UV-C) are entirely absorbed by stratospheric ozone and consequently do not reach the earth's surface, whereas UV-A and UV-B are only partially attenuated in the atmosphere and therefore reach the ocean, where they can impact marine organisms in the euphotic zone (Smith and Baker, 1989; Williamson et al., 2014).

Effects of UV exposure on marine biota include direct changes to metabolism, pigmentation, reproductive output, genetic material and survival, as reported for a wide range of taxa (Helbling and Zagarese, 2003; Banaszak and Lesser, 2009; Llabres et al., 2013), including phytoplankton (Llabres et al., 2010; Nahon et al., 2010; Yadav et al., 2016; Shi et al., 2017; Joshi et al., 2018), macroalgae (van de Poll et al., 2001; Schweikert et al., 2011; Ayres-Ostrock and Plastino, 2014; Xiao et al., 2015), seagrasses (Larkum and Wood, 1993), tunicates (Hirabayashi et al., 2006; Hirose et al., 2006), corals (Gleason et al., 2006; Ferrier-Pages et al., 2007; Torregiani and Lesser, 2007; Torres-Perez and Armstrong, 2012), bivalves (Buck et al., 2002), echinoderms (Shick et al., 1992; Karentz et al., 1997), crustaceans (Kim et al., 2015; Zeni et al., 2015; Carreja et al., 2016), and fish (Kaweewat and Hofer, 1997; Zamzow et al., 2013; Carrasco-Malio et al., 2014). Furthermore, UV radiation can cause damage indirectly through the production of reactive oxygen species (ROS) that subsequently disrupt protein synthesis and the integrity of photosynthetic membranes (Lesser et al., 1990; Lesser, 1996), or by enhancing the toxicity of harmful compounds (e.g., petroleum products) present in the water column (Gomes et al., 2009; Barron, 2017; Overmans et al., 2018).

However, the extent of both direct and indirect UV effects depends on the time of day as well as the exposure, i.e., the intensity and duration of solar UV exposure, which in turn are determined by latitude, season and atmospheric conditions such as cloud cover and pollution (Pfeifer et al., 2006). Due to its proximity to the equator and low cloud cover, the Red Sea region receives intense solar and UV radiation (Khogali and Albar, 1992; McKenzie et al., 2007; Acker et al., 2008; Smyth, 2011). However, aerosols in the atmosphere, such as sea salt, mineral dust or sulfuric acid droplets, can severely reduce the amount of UV reaching the Red Sea surface (Dickerson et al., 1997). In the Sahara and Arabian Peninsula, aerosols are primarily composed of mineral dust originating from the desert (Hsu et al., 2004), with dust storms frequently passing over the Red Sea, causing reduced visibility and high attenuation of UV-B radiation in the atmosphere (Kalenderski et al., 2013; Prakash et al., 2015).

Once in the water column, the magnitude of UV exposure is dependent on multiple factors. The penetration of UV in marine environments is partly dependent on the optical properties of saltwater, but it is primarily dependent on the amount and characteristics of dissolved organic matter (DOM) as well as phytoplankton and other suspended particles (Lee et al., 2005). Of these factors, the two most crucial water constituents known to modulate UV attenuation are chlorophyll *a* (Chl-*a*) and chromophoric dissolved organic matter (CDOM). Whereas water absorbs mostly in the energetically low, red spectrum (>600 nm), Chl-*a* found in planktonic primary producers absorbs most strongly in the blue range (450 nm) and also in the UV spectrum. In contrast, CDOM exhibits an absorption spectrum that increases exponentially from the visible light wavelengths into the UV range, and is therefore commonly referred to as the principal modulator of UV attenuation in marine waters (Bricaud et al., 1981; Coble et al., 2004; Tedetti and Sempere, 2006).

Coastal regions tend to have the highest concentrations of nutrients, Chl-*a* and CDOM, due to riverine inputs of sediments and dissolved nutrients. The Red Sea region, however, is characterized by arid climatic conditions and lacks major river catchments that could transport nutrients of terrigenous origin into the Red Sea. Consequently, the Red Sea is an ultra-oligotrophic sea where concentrations of both Chl-*a* and CDOM are exceptionally low, with Chl-*a* of generally <0.8 mg m^{-3}, reaching its annual minimum of <0.1 mg m^{-3} during the summer when the water column is stratified (Sofianos and Johns, 2002; Raitsos et al., 2013; Kheireddine et al., 2018; López-Sandoval et al., 2019). A study by Overmans and Agusti (2019) reported that this summer minimum coincides with the period when Red Sea waters exhibit their highest transparency to UV radiation, and they concluded that both Chl-*a* and CDOM explained the observed variability in the downwelling diffuse attenuation coefficient (K_d).

Existing studies suggest that the Red Sea has some of the lowest reported K_d values for UV wavelengths among the global oceans and seas (Stambler, 2005; Dishon et al., 2012; Cao et al., 2014; Overmans and Agusti, 2019). However, we still lack long-term data describing the magnitude and seasonality of ambient and underwater UV exposure, which could help to evaluate UV-induced stress on marine organisms residing in oligotrophic, tropical waters (Banaszak and Lesser, 2009). Moreover, unraveling whether periods of intense UV exposure coincide with those of extreme water temperature is critical, as high temperature has been shown to enhance the damaging effects of intense irradiance, or vice versa, on marine organisms (Buck et al., 2002; Ferrier-Pages et al., 2007; Giordanino et al., 2011; Lionard et al., 2012; Bellworthy and Fine, 2017). For some organisms, such as tropical reef corals, temperature and UV radiation have been identified to act synergistically, resulting in negative impacts of multiplicative magnitude (Drohan et al., 2005; Jin et al., 2019). This finding poses several questions regarding the future health status of highly sensitive marine ecosystems such as coral reefs, as current climate predictions suggest a gradual increase of both temperature and UV radiation until the end of this century (Bais et al., 2011; Williamson et al., 2014; IPCC, 2018). This rising trend is of major relevance for environments that already experience extreme conditions such as the Red Sea. Here, sea surface temperatures (SSTs) during the summer can reach close to 34°C in open waters, and even above 35°C in shallow coastal ecosystems, while at the same time the basin exhibits annual SST warming rates that are above the global average (Raitsos et al., 2011; Fine et al., 2013; Chaidez et al., 2017;

Garcias-Bonet and Duarte, 2017; Osman et al., 2018; Genevier et al., 2019; Giomi et al., 2019).

In the present study, we aim to describe the seasonal variability of underwater UV exposure in the rapidly warming Red Sea, and identify the periods when high temperatures and damaging levels of UV radiation co-occur. We quantify the variability in incident UV solar radiation and the attenuation properties of coastal waters in the central Red Sea in order to estimate the daily exposure of UV received by organisms along the water column. Additionally, we analyze time-series data of water temperature, Chl-*a* and CDOM and evaluate the contribution of the latter two parameters to UV attenuation in the central Red Sea. The presented results provide an insight into the present and projected seasonal variability of UV exposure in the water column that can be used to evaluate UV-induced stress and possible interactions with temperature on marine organisms such as reef-building corals, which constitute important ecosystem engineers in the coastal waters of the Red Sea.

MATERIALS AND METHODS

Study Sites and Time-Series Measurements

Between July 2016 and September 2018, we recorded time-series measurements at three study sites near King Abdullah University of Science and Technology (KAUST) in Thuwal, Saudi Arabia (see **Figure 1** for locations). One location was at the end of the pier located at the Coastal and Marine Resources Core Lab (CMOR) at KAUST (22.304639°N, 39.102167°E), while a further two marine sampling locations were located approximately 7 km offshore from KAUST and included a reef station at a shallow area (<2 m depth) of the mid-shore reef called Al Fahal (22.252833°N, 38.961222°E) and a pelagic station (45–50 m depth) adjacent to the reef (22.309333°N, 38.997389°E).

At the CMOR pier, we measured atmospheric UV irradiances with two stationary radiometers (SUV-B UV and SUV-A UV by Kipp & Zonen, Netherlands). Specifically, the radiometers recorded spectrally integrated, unweighted UV-B (280–315 nm) and UV-A (315–400 nm) irradiances in 10-min intervals between February 2017 and September 2018. The sensor lenses were cleaned weekly to minimize dust accumulation. Raw data were downloaded monthly from the stationary radiometers and processed using the software package UVIATOR (Kipp & Zonen, Netherlands). For each UV measurement, the program calculated the solar zenith angle (using location and time) and determined ozone column density using the EPTOMS Ozone plugin (v1.1). This plugin utilizes NASA's Earth Probe Total Ozone Mapping Spectrometer data set to convert measured voltages into corrected, observed UV-B and UV-A irradiances.

At the reef and pelagic stations, we measured SST with a high precision digital thermometer (Catalog # 89369-138; VWR International, United States) approximately every fortnight between 26th July 2016 and 27th September 2018. Additionally, we took water samples from the first meter of the water column for the quantitative analysis of Chl-*a* and CDOM in the lab, following the procedures described by Overmans and Agusti (2019). Briefly, the concentration of Chl-*a* was determined using a Trilogy Fluorometer (Turner Designs, United States) after filtration and pigment extraction. For the CDOM analysis, pre-filtered (0.2 μm) seawater samples were injected into a 2.5 m liquid waveguide capillary cell (LWCC) (Miller et al., 2002), coupled with a miniature fiber-optic spectrometer (USB2000+, preconfigured to 200–850 nm; Ocean Optics Inc.) and dual lamp (tungsten and deuterium) light source (DH-2000, Ocean Optics Inc.). The sample spectrum was compared against that of Milli-Q water after a correction of the refractive index to account for salinity differences, following the method of Babin et al. (2003). CDOM absorption coefficients $a_{CDOM}(\lambda)$ (in m^{-1}) were calculated as shown in equation (1):

$$a_{CDOM}(\lambda) = 2.303 \frac{[OD_{CDOM}(\lambda) - OD_{null,\ CDOM}]}{l} \quad (1)$$

where l is the optical pathlength (m), and 2.303 is the factor to convert base e to base 10 logarithms. We report a_{CDOM} for 305, 313, 320, 340, 380, and 395 nm as a proxy of CDOM abundance. In addition, we calculated the ratio of absorption coefficients at 254 and 365 nm, $a_{CDOM}(254/365)$, the slopes of a_{CDOM} spectra in the regions 275–295 nm [$S_{(275-295)}$] and 350–400 nm [$S_{(350-400)}$], and the ratio of these slopes [$S_{(275-295)}/S_{(350-400)}$], also termed S_R, to identify photobleaching processes and the molecular weight of the CDOM (Dahlen et al., 1996; Helms et al., 2008).

Furthermore, at the pelagic study site, we recorded downwelling irradiance (E_d) depth profiles (n = 51) approximately every fortnight between 26th July 2016 and 27th September 2018. From July 2016 to April 2017, we used a BIC radiometer (Biospherical Instruments, San Diego, CA, United States) with three UV wavebands (305, 313, 320 nm) and PAR (400–700 nm) for the data collection, which was subsequently replaced with a C-OPS (Compact-Optical Profiling System) radiometer (Biospherical Instruments, San Diego, CA, United States) with six UV channels (305, 313, 320, 340, 380, 395 nm) and PAR (400–700 nm) for the remaining data collection period (April 2017 to September 2018). We performed an intercomparison of the two instruments for the four shared wavelength channels to ensure the results obtained with the two spectroradiometer models were highly comparable (error < 3%).

On each sampling day, we deployed the radiometer from a small boat in the late morning (09:30 am–11:15 am) during generally cloud-free and calm sea conditions down to a maximum depth of 30–35 m. We performed a dark-correction of the depth and optical channels before each measurement and recorded profiles on the sunny side of the boat to minimize shading. For the BIC radiometer, we used the free-fall technique (Waters et al., 1990), while the C-OPS was maneuvered approximately 5 m away from the boat at the surface before vertical profiling started at a speed of ∼0.4 m s^{-1}. Both radiometers were equipped with pressure sensors so that irradiances could be recorded continuously (5 Hz) during the profiles.

Calculation of K_d, $Z_{n\%}$ and UV Exposure

We used irradiance versus depth profiles from the spectroradiometer casts to calculate diffuse attenuation

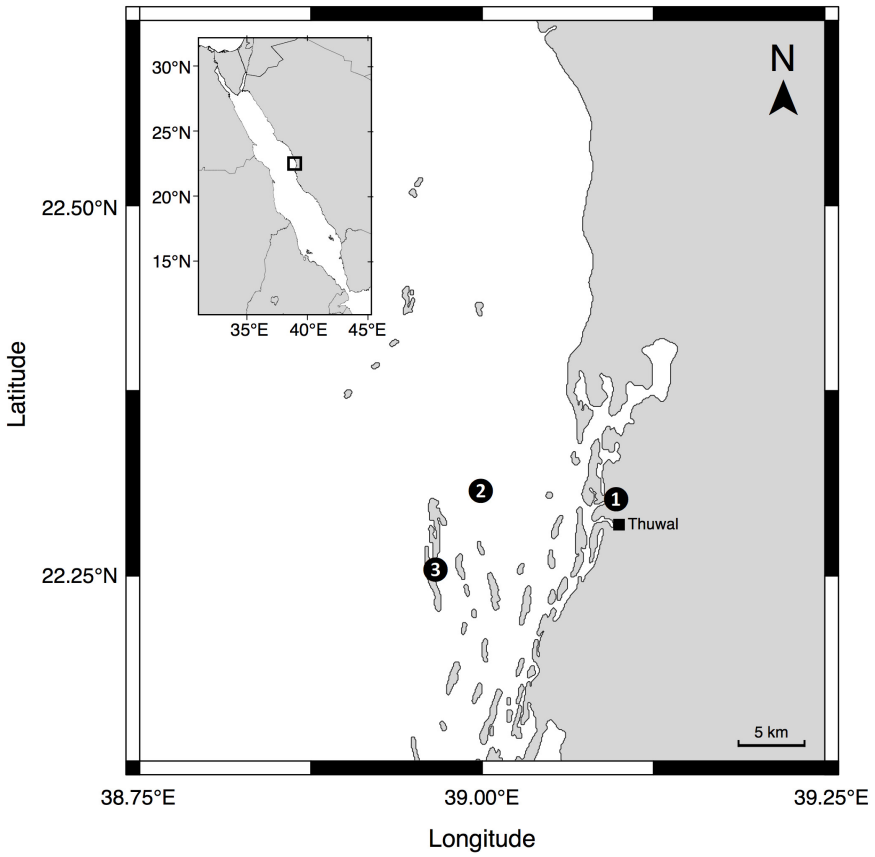

FIGURE 1 | Locations of the sampling sites where time series measurements were taken: (1) The pier of the Coastal and Marine Resources Core Lab (CMOR) at KAUST, (2) the pelagic station, and (3) Al Fahal Reef.

coefficients $K_d(\lambda)$ and the 10 and 1% percent attenuation depths ($Z_{n\%}$), as previously described by Overmans and Agusti (2019).

We determined daily exposures of unweighted atmospheric UV-B and UV-A (I_A; in kJ m^{-2} d^{-1}) by integrating the incident irradiance values for each day using GraphPad Prism 8.0.2 (GraphPad Software Inc., San Diego, CA, United States). Additionally, we calculated incident, erythemally weighted UV (UV-Ery) doses using the relationship between unweighted integrated UV-B irradiance and erythemally weighted UV, as described by McKenzie et al. (2004). Although this relationship is variable depending on total column ozone (TCO) and solar zenith angles (SZA), the authors found that the following conversion for TCO = 300 DU and SZA = 30° can be applied in the range of 250–400 DU with an error of less than ±10% for solar zenith angles ≤60°:

$$\mathrm{UV-B}_{(280-315\mathrm{nm})} = 7.55 \times \mathrm{UV-Ery} \quad (2)$$

Unweighted UV exposure immediately beneath the water surface (I_0) was calculated using the unweighted atmospheric UV exposure (I_A), assuming that downwelling irradiance is attenuated (predominantly reflected) on average by 7% when changing from air to water (Campbell and Aarup, 1989):

$$I_0 = 0.93\ I_A \quad (3)$$

To acquire daily exposures of UV-B and UV-A in the water column, we first determined the downwelling attenuation coefficient (K_d) for each day. Specifically, K_d of UV-B and UV-A wavelengths were directly determined on 42 and 36 days, respectively, when radiometer profiles were recorded *in situ*. For the remaining days when underwater UV attenuation was not directly determined (UV-B: n = 562; UV-A: n = 493), we calculated K_d by linearly extrapolating the K_d values from the preceding and the following sampling event. We calculated the depths (z) at which selected daily UV exposures (I_z) were received, using the sub-surface UV exposure (I_0) and downwelling attenuation coefficient (K_d), as shown in equation (4):

$$z = \frac{\ln(I_0/I_z)}{K_d} \quad (4)$$

We plotted daily UV exposure against date as a contour plot with contour lines smoothed at a level of 0.025 using the software JMP Pro 14.1.0 (SAS Institute Inc., Cary, NC, United States).

Projection of Future SST and UV-B Exposure

To identify periods when extreme SSTs coincide with extreme UV-B exposure at our study site (in 0.5, 1.0, and 2.0 m depth), we

used our existing time-series data set for the years 2017/2018, as well as projected future values for the years 2050 and 2100 based on existing future climate models.

Due to the Red Sea's unusually fast warming rate, which is above the global average, the projected SST values were calculated based on two warming reports of the Red Sea. For example, according to the latest IPCC report, the SST of the ocean is estimated to increase by an additional 0.6–2.0°C before the end of the century (Rhein et al., 2013). In comparison, two recent studies by Chaidez et al. (2017) and Osman et al. (2018) found the SST in the central Red Sea warms at rates of 0.017°C year^{-1} (+ 1.40°C by 2100) and 0.035°C year^{-1} (+ 2.87°C by 2100), respectively. For our future projections, we, therefore, used an intermediate rate of 0.026°C (i.e., an increase of 2.13°C by 2100) to determine potential future SSTs. Specifically, we first calculated the mean temperature for each calendar month using our time series data from 2017/2018 and increased the values by 0.832°C (32 years × 0.026°C year^{-1}) for the 2050 projection or by 2.132°C (82 years × 0.026°C year^{-1}) for the 2100 scenario.

We calculated daily exposures of UV-B in the upcoming decades based on the latest future-UV radiation models, which are in agreement that UV-B exposure is expected to remain unchanged in the tropics until 2050 due to the drastic reduction in the emission of ozone-depleting substances (ODS) and the associated recovery of the total column ozone (Bais et al., 2011, 2019; McKenzie et al., 2011; Watanabe et al., 2011; Meul et al., 2016). The same studies found that by 2100, UV-B exposure will likely have increased by up to 3% as a consequence of continued greenhouse gas (GHG) emissions. Therefore, our projected values for 2050 are identical to those of 2017/2018, whereas, for the 2100 projection, we increased our present UV-B exposure that we calculated for each depth and individual day by 3%.

The damaging UV-B exposure threshold was chosen as 20 kJ m^{-2} d^{-1}, based on a study from southern Taiwan, i.e., at a similar latitude (21°N) to the central Red Sea, where the physiology, development and settlement of the coral *Pocillopora damicornis* were severely impacted at those UV-B exposure levels (Zhou et al., 2016). For the extreme temperature threshold, we selected the climatological maximum monthly mean of the Jeddah region, which has been identified as 31.1°C in a recent report by Osman et al. (2018).

We smoothed each temperature and UV-B data set in GraphPad Prism 8.0.2 (GraphPad Software Inc., San Diego, CA, United States) using a sixth-order polynomial trendline.

Statistical Analysis

To analyze the CDOM slopes and the CDOM ratios, we first tested if the data were normally distributed and whether the variances were equal using the Shapiro–Wilk test and Levene's test, respectively. Subsequently, we performed a multi-comparison of each data pair using Student *t*-tests to identify differences between seasons. Differences were considered to be significant at a level of $p < 0.05$. Furthermore, we explored the relationship between K_d, CDOM and Chl-*a* by performing a set of linear regressions. In addition, we fitted a standard least squares multiple linear model to the a_{CDOM} and Chl-*a* data from the pelagic station in order to predict the K_d of the reef waters. We carried out data analyses and visualizations in either JMP Pro 14.1.0 (SAS Institute Inc., Cary, NC, United States) or GraphPad Prism 8.0.2 (GraphPad Software Inc., San Diego, CA, United States).

RESULTS

Atmospheric UV Exposure and UV-Ery Doses

We recorded atmospheric midday UV-B irradiances as high as 2.59 W m^{-2} in 2017 (May) and 2.66 W m^{-2} in 2018 (May), while maximum midday UV-Ery irradiances were 0.34 (May 2017) and 0.35 W m^{-2} (May 2018) (**Table 1**). For UV-A, we also recorded the maximum atmospheric midday irradiance of 2017 in May (77.5 W m^{-2}), but the 2018 maximum was recorded much earlier in the year, i.e., in February (72.9 W m^{-2}). Whereas maximum midday UV-B and UV-Ery irradiances were recorded in May in both years, the monthly means peaked in June 2017 (UV-B: 2.24 ± 0.18 W m^{-2}; UV-Ery: 0.30 ± 0.02) and in April the following year (UV-B: 2.2 ± 0.16 W m^{-2}; UV-Ery: 0.30±), which was also the same time when we recorded the highest mean values of midday UV-A irradiances in each year: 64.7 ± 3.8 W m^{-2} in June 2017 and 65.0 ± 4.0 W m^{-2} in April 2018 (**Table 1**).

The monthly averaged daily exposure of atmospheric UV varied from 21.6 (December 2017) to 48.3 kJ m^{-2} d^{-1} (June 2017) for UV-B, and from 899 (December 2017) to 1699 kJ m^{-2} d^{-1} (June 2017) for UV-A (**Table 1**). UV-Ery ranged from 2.86 (December 2017) to 6.40 kJ m^{-2} d^{-1} (June 2017). However, daily UV-A exposures reached a maximum of 1952 kJ m^{-2} d^{-1} in 2017 (June) and 1892 kJ m^{-2} d^{-1} in May of the following year (**Table 1** and **Figure 2A**). For UV-B, we detected maximum daily exposures of 56.7 kJ m^{-2} d^{-1} in 2017 (June) and 55.7 kJ m^{-2} d^{-1} in 2018 (May), while UV-Ery doses reached maxima of 7.51 and 7.38 kJ m^{-2} d^{-1} in June 2017 and May 2018, respectively (**Table 1** and **Figure 2B**).

It is conspicuous that in 2017, we identified June as the month when mean daily UV exposure peaked; however, in the following year, daily UV exposure was on average highest in April. The annual maximum incident UV irradiances (in W m^{-2}), on the other hand, were recorded in May, except for the UV-A maximum in 2018, which was detected in February.

Independent of the distinct seasonality of UV-B and UV-A, we observed several days with unusually low UV during dust storm events, suggesting a strong influence of aerosols on UV attenuation in the atmosphere. For example, on 19th March 2017, daily exposures of atmospheric UV-B (12.0 kJ m^{-2} d^{-1}) and UV-A (505 kJ m^{-2} d^{-1}), and daily doses of UV-Ery (1.59 kJ m^{-2} d^{-1}) were minimal due to an intense sand storm (**Figure 2**). Our measurements showed that this dust event continued to influence incident UV radiation until 24th March. A similar, albeit less severe, storm event occurred on 29th May 2017, when the daily exposures of atmospheric UV-B and UV-A were 21.2 and 781 kJ m^{-2} d^{-1}, respectively, and erythemally weighted UV doses were 2.81 kJ m^{-2} d^{-1} (**Figure 2**). In this case, however, atmospheric UV irradiances were noticeably reduced on the day of the event only.

TABLE 1 | Atmospheric UV-B (280–315 nm), UV-A (315–400 nm), and erythemally weighted UV (UV-Ery) conditions at KAUST (22.304639°N, 39.102167°E) between February 2017 and September 2018.

		UV-B (280–315 nm)						**UV-A (315–400 nm)**						**UV-Ery**					
		Midday irradiance ($W\ m^{-2}$)			**Daily exposure ($kJ\ m^{-2}\ d^{-1}$)**			**Midday irradiance ($W\ m^{-2}$)**			**Daily exposure ($kJ\ m^{-2}\ d^{-1}$)**			**Midday irradiance ($W\ m^{-2}$)**			**Daily dose ($kJ\ m^{-2}\ d^{-1}$)**		
Year	**Month**	**Mean**		**Maximum**	**Mean**		**Maximum**	**Mean**		**Maximum**	**Mean**		**Maximum**	**Mean**		**Maximum**	**Mean**		**Maximum**
2017	February	1.58	± 0.26	1.98	26.6	± 6.9	37.9	51.7	± 6.4	60.2	1025	± 248	1375	0.21	± 0.03	0.26	3.52	± 0.91	5.02
	March	1.83	± 0.35	2.16	34.9	± 7.6	43.6	57.3	± 8.2	66.3	1277	± 256	1548	0.24	± 0.05	0.29	4.62	± 1.01	5.78
	April	1.89	± 0.19	2.29	35.8	± 5.4	45.7	57.1	± 4.3	69.0	1295	± 168	1547	0.25	± 0.03	0.30	4.74	± 0.72	6.06
	May	2.15	± 0.31	**2.59**	42.6	± 6.2	50.8	63.9	± 7.0	**77.5**	1512	± 195	1714	0.28	± 0.04	**0.34**	5.64	± 0.82	6.73
	June	**2.24**	**± 0.18**	2.58	**48.3**	**± 4.1**	**56.7**	**64.7**	**± 3.8**	72.3	**1699**	**± 123**	**1952**	**0.30**	**± 0.02**	0.34	**6.40**	**± 0.54**	**7.51**
	July	2.13	± 0.18	2.50	45.2	± 4.4	54.7	62.6	± 4.3	71.5	1609	± 147	1916	0.28	± 0.02	0.33	5.99	± 0.58	7.24
	August	1.91	± 0.22	2.22	38.4	± 5.1	44.7	55.6	± 6.0	65.6	1308	± 166	1533	0.25	± 0.03	0.29	5.09	± 0.68	5.92
	September	1.99	± 0.10	2.22	39.4	± 2.3	44.9	59.5	± 2.4	65.4	1397	± 73	1595	0.26	± 0.01	0.29	5.21	± 0.30	5.95
	October	1.74	± 0.18	2.01	33.5	± 4.2	40.0	55.2	± 3.6	60.3	1260	± 110	1420	0.23	± 0.02	0.27	4.44	± 0.56	5.29
	November	1.41	± 0.12	1.60	25.3	± 2.9	29.4	48.0	± 2.7	52.8	1013	± 105	1141	0.19	± 0.02	0.21	3.36	± 0.38	3.89
	December	1.22	± 0.09	1.36	21.6	± 1.7	23.7	42.7	± 2.8	47.5	899	± 65	989	0.16	± 0.01	0.18	2.86	± 0.23	3.14
2018	January	1.39	± 0.12	1.60	24.5	± 3.0	29.5	48.7	± 3.6	56.1	1016	± 127	1202	0.18	± 0.02	0.21	3.25	± 0.40	3.91
	February	1.62	± 0.21	2.39	28.9	± 4.8	39.1	52.1	± 5.5	**72.9**	1088	± 171	1366	0.21	± 0.03	0.32	3.82	± 0.64	5.17
	March	2.10	± 0.19	2.36	41.5	± 4.7	47.3	62.2	± 4.8	68.1	1463	± 156	1644	0.28	± 0.03	0.31	5.49	± 0.62	6.26
	April	**2.29**	**± 0.16**	2.47	**47.6**	**± 4.2**	52.0	**65.0**	**± 4.0**	69.0	**1610**	**± 144**	1773	**0.30**	**± 0.02**	0.33	**6.31**	**± 0.56**	6.89
	May	2.18	± 0.24	**2.66**	45.8	± 5.5	**55.7**	61.8	± 6.2	72.6	1562	± 187	**1892**	0.29	± 0.03	**0.35**	6.06	± 0.73	**7.38**
	June	2.08	± 0.22	2.40	43.7	± 5.9	51.9	59.9	± 5.1	67.8	1509	± 179	1744	0.28	± 0.03	0.32	5.79	± 0.78	6.87
	July	2.19	± 0.13	2.38	45.6	± 3.0	50.2	63.5	± 3.5	69.1	1610	± 105	1796	0.29	± 0.02	0.32	6.03	± 0.40	6.65
	August	2.07	± 0.08	2.29	41.7	± 2.7	47.2	59.8	± 2.5	65.9	1448	± 102	1637	0.27	± 0.01	0.30	5.53	± 0.36	6.25
	September	1.87	± 0.15	2.11	36.3	± 3.5	41.8	56.2	± 3.9	61.1	1303	± 119	1495	0.25	± 0.02	0.28	4.81	± 0.46	5.54

Values are means (±SD) and maxima of both midday irradiances ($W\ m^{-2}$) and daily exposure ($kJ\ m^{-2}\ d^{-1}$), or daily doses ($kJ\ m^{-2}\ d^{-1}$) in the case of UV-Ery. The highest values per category in each year are highlighted in bold.

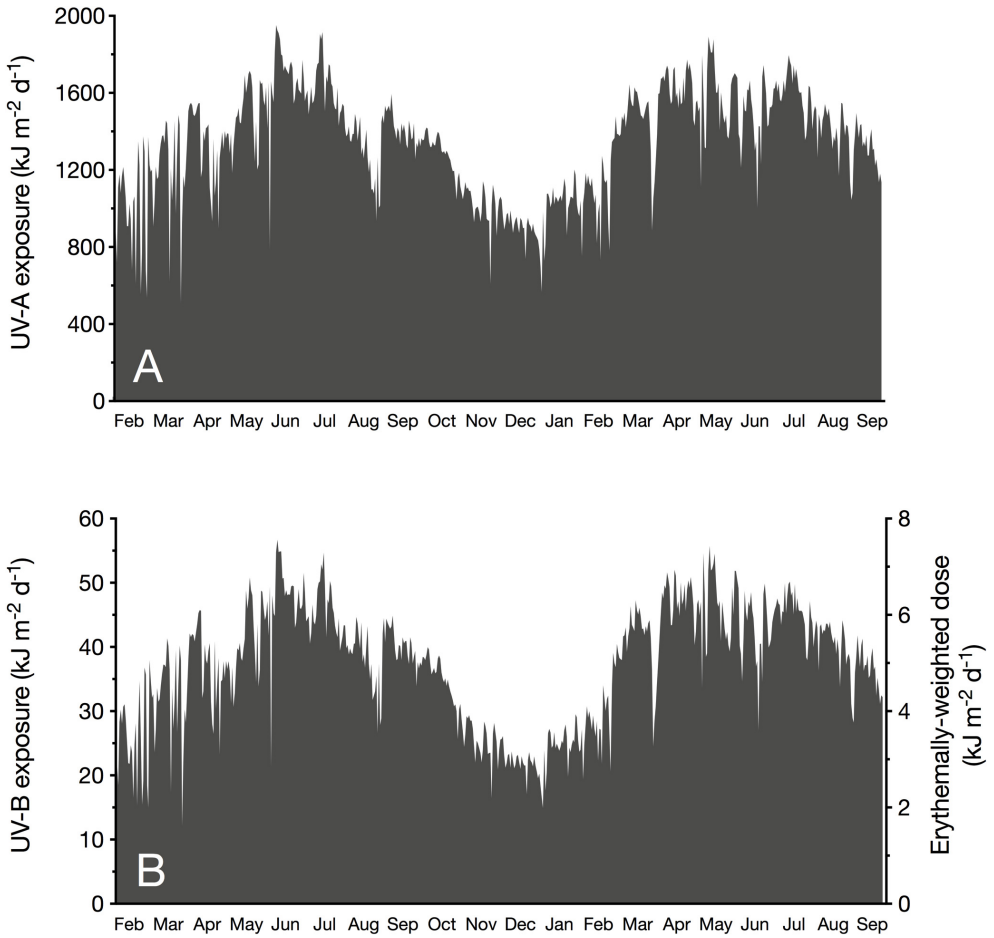

FIGURE 2 | Daily exposure (kJ m^{-2} d^{-1}) of incident unweighted UV-A (315–400 nm; **A**) and UV-B (280–315 nm; **B**, left *y*-axis) radiation, and erythemally weighted UV doses (**B**, right *y*-axis). Values were measured at sea level at the KAUST CMOR pier (22.304639°N, 39.102167°E) between February 2017 and September 2018.

Temperature, Chl-*a* and CDOM

During the study period, the SST at the pelagic site ranged from 24.4°C, recorded in February 2018, to 32.2°C in August 2016 and 2018 (**Figure 3**). Interannual variability between minimum temperatures in winter was negligible, with minimum February temperatures of 24.6 and 24.6°C in 2017 and 2018, respectively. We found an equally low difference for the annual summer temperature extremes, with maximum values of 32.2, 32.1, and 32.2°C in 2016, 2017, and 2018, respectively. In comparison, the SST at the reef site reached the same summer maximum temperature as the pelagic station (i.e., 32.2°C); however, the minimum winter temperature recorded at the reef was considerably lower with values of 23.9°C and 22.8°C in January of 2017 and 2018, respectively. During the three summers of our study, we measured at the reef maximum summer SSTs of 32.2, 31.8, and 32.2°C in 2016, 2017, and 2018, respectively.

Concentrations of Chl-*a* were generally low at the pelagic study site but exhibited a seasonal pattern. The lowest concentrations (<0.14 mg m^{-3}) were measured between July and September, whereas in February, Chl-*a* reached surface concentrations of up to 0.83 mg m^{-3} (**Figure 3**). Although the maximum Chl-*a* concentration was detected in February in both years, we noticed a second, albeit less pronounced, bloom occurring in December and a pronounced interannual variability. Specifically, the two Chl-*a* concentration peaks in December and February in winter 2016/2017 (0.55 and 0.68 mg m^{-3}) were noticeably smaller than in the following winter of 2017/2018 (0.81 and 0.83 mg m^{-3}). At the reef, Chl-*a* concentrations were generally lower than at the pelagic site, which was particularly apparent during spring blooms when concentrations at the reef remained below 0.46 and 0.60 mg m^{-3} in the winters of 2016/2017 and 2017/2018, respectively (**Figure 3**). Furthermore, we measured the annual Chl-*a* concentration peaks at the reef in December, and thereby 6–8 weeks prior to the peaks at the pelagic site. The lowest amount of Chl-*a* in the reef waters was detected in June 2016, when concentrations reached a minimum of 0.09 mg m^{-3}. In the following year, concentrations reached a similar low of 0.11 mg Chl-*a* m^{-3} at the reef.

For CDOM, we found that the magnitude and range of absorption varied considerably between wavelengths and

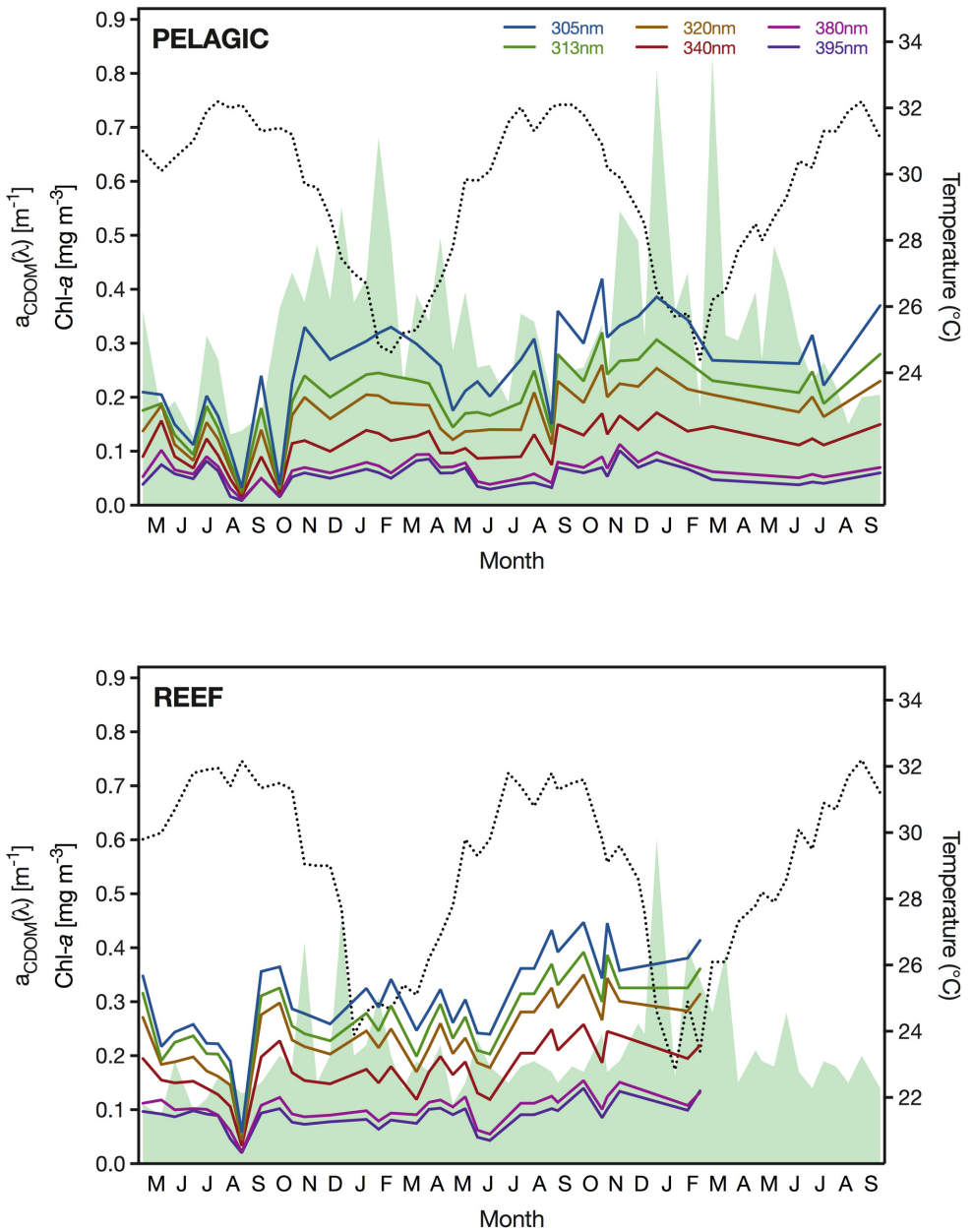

FIGURE 3 | Sea surface temperature (SST) in <1 m depth (dotted black line), surface concentration of Chl-*a* (shaded green area) and absorption coefficient of CDOM (a_{CDOM}) for the wavelengths 305, 313, 320, 340, 380, 395 nm (see figure legend for color coding) between May 2016 and September 2018 at the pelagic sampling station (22.309333°N, 38.997389°E) **(upper panel)** and the reef (22.309333°N, 38.997389°E) **(lower panel)**.

sampling events. Specifically, $a_{CDOM}(305\ nm)$ ranged greatly from 0.032 m^{-1} (September 2016) to 0.420 m^{-1} (October 2017) at the pelagic site and from 0.058 m^{-1} (September 2016) to 0.447 m^{-1} (September 2017) at the reef (**Figure 3**). In comparison, a_{CDOM} (395 nm) only ranged from 0.009 m^{-1} (September 2016) to 0.101 m^{-1} (November 2017) and from 0.020 m^{-1} (September 2016) to 0.140 m^{-1} (September 2017) at the open water station and the reef, respectively. At both locations, we observed abrupt changes in the CDOM absorption coefficient between subsequent sampling events, which was particularly obvious in late summer, when we also observed both the annual minimum and maximum a_{CDOM} values. Despite this large variance, a_{CDOM} exhibited the lowest mean value in summer across all wavelengths at both stations.

The ratio of a_{CDOM} at 254 and 365 nm [i.e., $a_{CDOM}(254/365)$], which is a proxy of CDOM molecular weight, exhibited a distinct seasonality (**Table 2**). Specifically, at the pelagic station, the ratio was significantly higher in summer (14.60 ± 3.36) than in autumn (10.22 ± 2.80) [$t(16.9) = -3.10$, $p < 0.01$] and winter (10.95 ± 2.23) [$t(11.6) = 2.51$, $p < 0.05$]. In comparison, the reef

TABLE 2 | Ratio of absorption coefficients at 254 and 365 nm [$a_{CDOM}(254/365)$], the slopes of the $a_{CDOM}(\lambda)$ spectra in the regions 275–295 nm [$S_{(275-295)}$] and 350–400 nm [($S_{(350-400)}$], and the ratio of these two slopes [$S_{(275-295)}/S_{(350-400)}$], summarized by station and season for the period May 2016 to September 2018.

Station	Season	a_{CDOM} (254/365)			S(275–295) [μm^{-1}]			S(350–400) [μm^{-1}]			S(275–295)/ S(350–400)		
		Min.	Mean	Max.	Min.	Mean	Max.	Min.	Mean	Max.	Min.	Mean	Max.
Pelagic	Winter	7.60	10.95	13.80	26	29	32	11	15	21	1.23	2.08	2.90
	Spring	7.71	13.07	16.04	25	36	42	7	11	18	1.98	3.56	5.32
	Summer	10.23	14.60	21.86	27	41	53	6	12	24	1.44	4.33	7.87
	Autumn	5.45	10.22	14.20	20	28	35	8	11	16	1.71	2.66	4.68
	All seasons	5.45	12.44	21.86	20	34	53	6	12	24	1.23	3.32	7.87
Reef	Winter	7.54	8.84	10.00	26	29	31	10	13	15	1.91	2.28	3.10
	Spring	6.93	8.97	12.29	26	32	39	7	12	18	1.83	3.03	5.54
	Summer	5.77	9.33	12.96	22	34	42	5	11	16	1.36	4.00	8.66
	Autumn	3.88	6.46	8.26	18	26	31	9	12	15	1.58	2.13	2.99
	All seasons	3.88	8.37	12.96	18	31	42	5	12	18	1.36	2.97	8.66

waters had a significantly lower $a_{CDOM}(254/365)$ ratio in autumn (6.46 ± 1.56) than in winter (8.84 ± 1.03) [$t(11.5) = -3.44$, $p < 0.01$], spring (8.97 ± 1.90) [$t(15.4) = -3.06$, $p < 0.01$] and summer (9.33 ± 2.39) [$t(15.6) = -3.12$, $p < 0.01$)]; however, there was no difference between any of the latter three seasons. For the parameter $S_{(275-295)}$, we found significantly higher slope values at the pelagic site during summer (40.8 ± 9.5 μm^{-1}) compared to autumn (28.4 ± 4.9 μm^{-1}) [$t(13.8) = -3.61$, $p < 0.01$] and winter (29.0 ± 2.8 μm^{-1}) [$t(11.6) = 3.62$, $p < 0.01$] (**Table 2**). In contrast, the $S_{(275-295)}$ slope values of the reef water were significantly lower in autumn (25.8 ± 3.6 μm^{-1}) than in spring (32.1 ± 4.0 μm^{-1}) [$t(15.8) = -3.52$, $p < 0.01$] and summer (34.0 ± 8.2 μm^{-1}) [$t(12.6) = -2.88$, $p < 0.05$]. At neither of the stations did we find seasonal differences for the slope $S_{(350-400)}$ (**Table 2**). The slope ratio S_R was consistently above 1 and as high as 7.87 (pelagic) and 8.66 (reef) (**Table 2**). Moreover, at both stations, the ratio was significantly higher in summer than in autumn or winter, all of which suggests that intense photobleaching occurred at both study sites throughout the year but peaked in summer.

Downwelling Attenuation Coefficient (K_d) and Percent Attenuation Depth ($Z_{n\%}$)

Attenuation of UV radiation varied considerably between wavelengths and seasons. Specifically, the downwelling diffuse K_d ranged between 0.054 (minimum K_d of 395 nm) and 0.425 m^{-1} (maximum K_d of 305 nm)(**Figure 4**). K_d values were generally lowest in late summer when Chl-*a* concentrations and absorption by CDOM reached their annual minimum. During our study, UV attenuation was lowest in October 2016, with K_d values of 0.222 m^{-1} (305 nm), 0.171 m^{-1} (313 nm) and 0.148 m^{-1} (320 nm). We observed similarly low UV attenuation in August 2018, when the downwelling K_d of 305, 313, 320, 340, 380, and 395 nm were 0.225, 0.193, 0.166, 0.124, 0.065, and 0.054 m^{-1}, respectively. Generally, we found UV attenuation to be strongest during spring; however, we recorded the highest K_d values in October 2017, when K_d reached 0.425, 0.352 0.312, 0.218, 0.124, and 0.105 m^{-1} for 305, 313, 320, 340, 380, and 395 nm, respectively (**Figure 4**). Attenuation of PAR loosely mirrored the pattern observed for UV wavelengths but with a narrower range of K_d values; the minimum and maximum K_d(PAR) were 0.049 m^{-1} (September 2016) and 0.119 m^{-1} (December 2017), respectively (**Figure 4**).

The midpoint and bottom of the euphotic layer varied between 19.3 and 46.6 m [$Z_{10\%}$(PAR)] and 38.7–93.1 m [$Z_{1\%}$(PAR)] (**Table 3**). Additionally, we found the biologically effective optical depths of UV in 6.3–12.9 m [$Z_{10\%}$(UV-B)] and 14.4–27.3 m [$Z_{1\%}$(UV-A)], while the depths where UV-B and UV-A could still be detected at 1% of the surface irradiance ranged from 12.6–25.7 m [$Z_{1\%}$(UV-B)] and 28.8–54.5 m [$Z_{1\%}$(UV-A)] (**Table 3**).

UV Exposure in the Water Column

In the water column, the calculated UV exposures continued to exhibit a distinct seasonality. For example, in December 2017, when incoming solar UV reached its annual minimum and UV was strongly attenuated in the water column, daily exposure of UV-B and UV-A at 1 m were less than 16 kJ m^{-2} d^{-1} (mean:

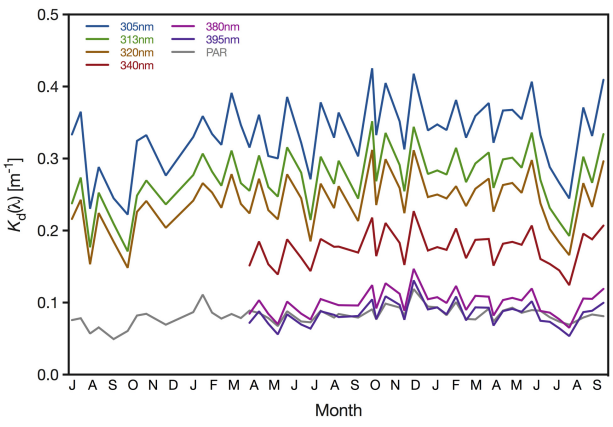

FIGURE 4 | Downwelling attenuation coefficients (K_d) of 305, 313, 320, 340, 380, 395 nm and PAR (400–700 nm) determined for the pelagic sampling station (22.309333°N, 38.997389°E) offshore from KAUST. Measurements of the wavelengths 305, 313, and 320 nm and PAR started in July 2016, whereas the remaining wavebands were included after April 2017.

TABLE 3 | Percent attenuation depths ($Z_{10\%}$ and $Z_{1\%}$) for the UV-B (280–315 nm), UV-A (315–400 nm), and PAR (400–700 nm) spectra.

	$Z_{10\%}$ (m)									$Z_{1\%}$ (m)								
	UV-B			UV-A			PAR			UV-B			UV-A			PAR		
Month	Min.	Mean	Max.	Min.	Mean	Max.	Min.	Mean	Max.	Min.	Mean	Max.	Min.	Mean	Max.	Min.	Mean	Max.
January	7.8	8.0	8.1	19.3	19.4	19.6	24.4	25.2	26.5	15.7	15.9	16.2	38.5	38.8	39.1	48.7	50.3	52.9
February	7.0	7.5	8.0	16.6	18.6	20.6	20.7	24.5	27.8	14.0	15.1	15.9	33.2	37.2	41.1	41.4	49.0	55.6
March	7.0	7.8	8.5	20.0	21.2	22.5	27.3	29.2	30.0	14.0	15.6	16.9	40.0	42.5	45.0	54.6	58.3	60.1
April	7.1	7.9	8.5	19.0	21.6	24.4	25.2	27.5	31.1	14.2	15.8	17.1	38.0	43.1	48.8	50.3	54.9	62.2
May	7.3	8.1	9.1	19.0	22.0	27.3	24.7	28.3	34.0	14.6	16.2	18.1	38.0	43.9	54.5	49.5	56.7	68.0
June	6.5	7.2	8.1	17.4	19.7	22.2	25.7	25.9	26.1	13.1	14.4	16.3	34.7	39.4	44.4	51.3	51.8	52.3
July	7.8	9.3	10.3	23.4	24.5	25.7	28.8	30.6	31.6	15.7	18.6	20.6	46.7	49.0	51.5	57.7	61.3	63.3
August	7.2	8.8	12.3	19.4	21.2	25.9	25.9	30.6	40.2	14.4	17.6	24.6	38.8	42.4	51.9	51.9	61.1	80.4
September	6.6	9.2	12.1	17.4	19.4	21.3	27.6	33.3	46.6	13.2	18.3	24.1	34.8	38.7	42.5	55.1	66.6	93.1
October	6.3	9.0	12.9	16.8	19.4	22.1	25.3	30.3	38.0	12.6	18.0	25.7	33.6	38.9	44.1	50.6	60.6	75.9
November	6.6	7.5	8.3	16.5	17.5	18.5	23.3	25.1	27.2	13.2	15.0	16.6	33.0	35.0	36.9	46.6	50.1	54.4
December	6.5	8.3	9.8	14.4	18.7	23.1	19.3	26.8	33.2	12.9	16.7	19.7	28.8	37.5	46.1	38.7	53.6	66.4

Attenuation depths were measured at the pelagic station (22.309333°N, 38.997389°E) between July 2016 and September 2018.

13.7 kJ m^{-2} d^{-1}) and 820 kJ m^{-2} d^{-1} (mean: 724 kJ m^{-2} d^{-1}), respectively (**Figure 5** and **Table 4**). Below 4 m, daily exposure in December rarely exceeded 5 kJ m^{-2} d^{-1} (UV-B) and 500 kJ m^{-2} d^{-1} (UV-A), while at 10 m, UV-B was barely detectable (<1 kJ m^{-2} d^{-1}) and UV-A generally was less than 300 kJ m^{-2} d^{-1} (**Figure 5**). In contrast, in July 2018, daily UV exposures in 10 m were on average 3.0 kJ m^{-2} d^{-1} (UV-B) and 555 kJ m^{-2} d^{-1} (UV-A), but we recorded exposures as high as 3.6 and 626 kJ m^{-2} d^{-1} for UV-B and UV-A, respectively, during that month (**Table 4**).

Additionally, in 2017, the highest average daily exposures at depths above 1 m (for UV-B) and 4 m (for UV-A) were present in June, but below those depths, average daily exposures reached their peak in July. In 2018, however, the maximum daily exposures at any depth were recorded in July (**Table 4**).

Relationship Between K_d, Chl-*a* and CDOM

We identified that the relationship between aCDOM at the six radiometrically studied UV wavelengths and Chl-*a* was significantly positive; however, both the correlation coefficient and regression slope generally decreased with increasing wavelength: 305 nm ($y = 0.26x + 0.16$, $p < 0.01$, $R^2 = 0.22$), 313 nm ($y = 0.20x + 0.13$, $p < 0.01$, $R^2 = 0.24$), 320 nm ($y = 0.16x + 0.11$, $p < 0.01$, $R^2 = 0.23$), 340 nm ($y = 0.10x + 0.08$, $p < 0.01$, $R^2 = 0.23$), 380 nm ($y = 0.05x + 0.05$, $p < 0.05$, $R^2 = 0.15$) and 395 nm ($y = 0.05x + 0.05$, $p < 0.05$, $R^2 = 0.14$) (**Figure 6A**).

Furthermore, we identified a significant positive linear relationship between the concentration of Chl-*a* and K_d for each of the analyzed wavelengths: 305 nm ($y = 0.14x + 0.29$, $p < 0.01$), 313 nm ($y = 0.12x + 0.23$, $p < 0.01$), 320 nm ($y = 0.11x + 0.21$, $p < 0.01$), 340 nm ($y = 0.07x + 0.15$, $p < 0.01$), 380 nm ($y = 0.07x + 0.08$, $p < 0.001$) and 395 nm ($y = 0.07x + 0.06$, $p < 0.001$) (**Figure 6B**). The correlation between $K_d(\lambda)$ and the pigment concentration was generally low but gradually increased with increasing wavelength, while for the wavelengths 380 nm ($R^2 = 0.36$) and 395 nm ($R^2 = 0.42$) the correlation was even higher than for CDOM (**Figures 6B,C**).

In comparison, the correlation between $K_d(\lambda)$ and $a_{CDOM}(\lambda)$ was moderately strong for 395 nm ($R^2 = 0.28$), but reasonably high for the wavelengths 313 nm ($R^2 = 0.49$), 320 nm ($R^2 = 0.51$), and 340 nm ($R^2 = 0.51$) (**Figure 6C**). Across all wavelengths, we identified a significant, positive linear relationship between a_{CDOM} and K_d: 305 nm ($y = 0.35x + 0.25$, $p < 0.001$), 313 nm ($y = 0.44x + 0.18$, $p < 0.001$), 320 nm ($y = 0.50x + 0.16$, $p < 0.001$), 340 nm ($y = 0.59x + 0.11$, $p < 0.001$), 380 nm ($y = 0.56x + 0.07$, $p < 0.01$) and 395 nm ($y = 0.50x + 0.06$, $p < 0.05$) (**Figure 6C**).

Using a least squares multiple linear regression to predict $K_d(320\text{ nm})$ based on $a_{CDOM}(320)$ and Chl-*a* concentration data from the pelagic station revealed a significant regression equation [$F(2,32) = 16.892$], $p < 0.0001$), with an R^2 of 0.514. However, of these two environmental parameters, only $a_{CDOM}(320)$ was found to be a significant predictor of the attenuation coefficient $K_d(320\text{ nm})$ ($p < 0.001$). The model prediction expression output was as follows:

$$K_d(320\text{ nm}) = 0.47307337 * a_{CDOM}(320) + 0.01652723 * \text{Chl-a conc.} + 0.15587985 \quad (4)$$

After using this model output to calculate the expected $K_d(320\text{ nm})$ for the reef waters, we performed a Student's *t*-test, which identified that the $K_d(320\text{ nm})$ values of the reef (0.271 ± 0.031 m^{-1}) were significantly higher than those of the pelagic site (0.238 ± 0.030 m^{-1}) [$t(64) = 4.34$, $p < 0.0001$].

Variability of Present and Future Extreme Temperature and UV

We identified that during our study period, daily exposure of UV-B close to the surface (0.5 m depth) reached its annual maximum in late May, which was approximately 8 weeks before we observed

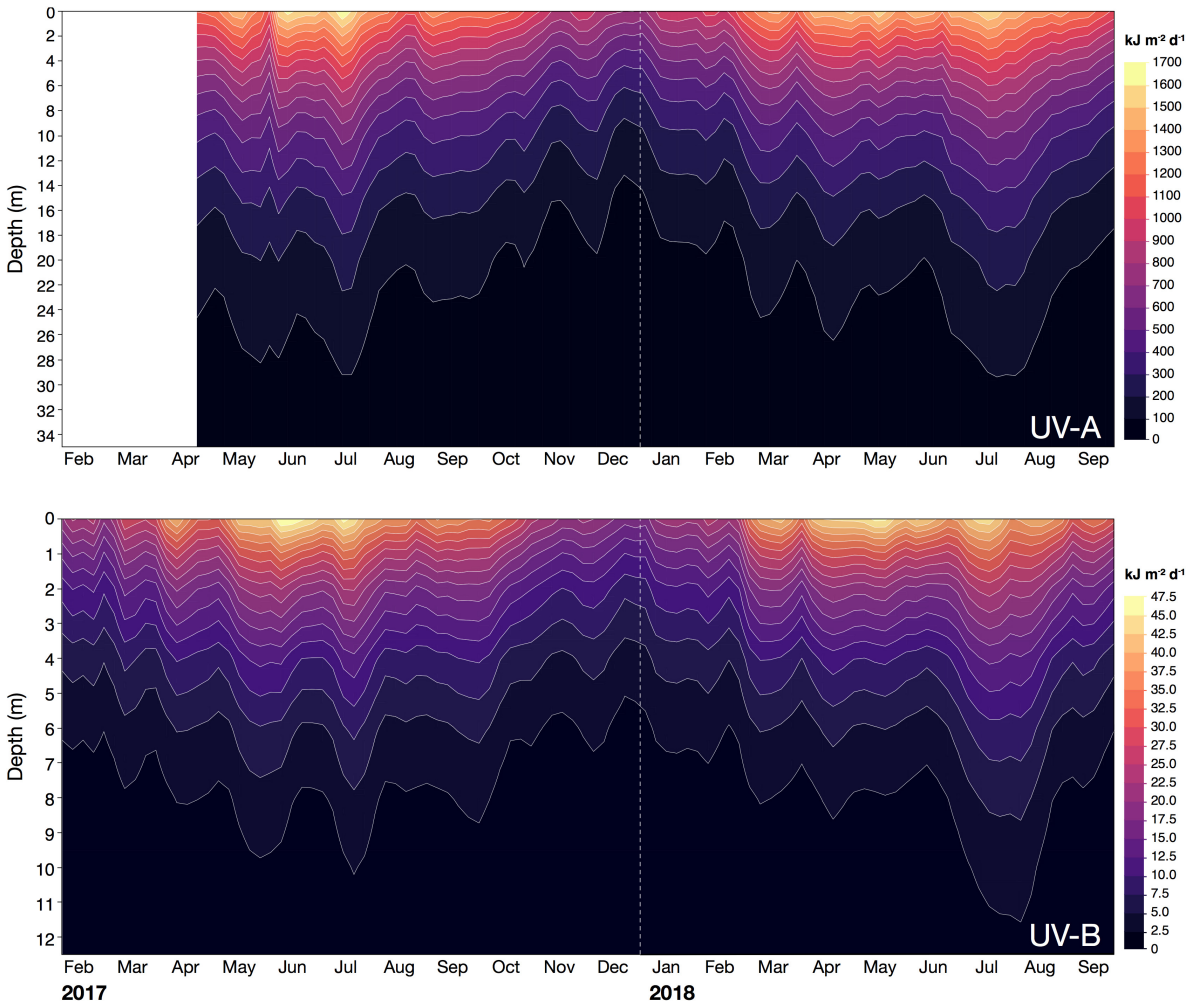

FIGURE 5 | Daily exposure (kJ m^{-2} d^{-1}) of UV-A (315–400 nm; **upper panel**) and UV-B radiation (280–315 nm; **lower panel**) received in the water column at the pelagic station (22.309333°N, 38.997389°E) off KAUST between February 2017 and September 2018. Contour lines were smoothed at a level of 0.025.

the maximum SST (**Figure 7**, left panels). Further down the water column, we detected maximum UV-B exposure slightly later in the year (∼2 weeks later at 2 m depth) because the waters only reached their highest transparency to UV in late summer. Across all depths, extreme UV exposures (>20 kJ m^{-2} d^{-1}) and temperatures (>31.1°C) coincided from the beginning of June. However, the duration of this concurrence was depth-dependent, i.e., lasting for 9 weeks at 0.5 and 1 m and for 6 weeks at 2 m depth (**Figure 7**, left panels).

Using the intermediate Red Sea warming rate of the two rates reported by Chaidez et al. (2017) and Osman et al. (2018), we identified a potential SST increase of 0.8 and 2.1°C by 2050 and 2100, respectively, which means that mean SSTs in August could be as high as 33.0 and 34.3°C by 2050 and 2100, respectively (**Figure 7**, middle and right panels). Based on these projections, the extreme temperature threshold of 31.1°C, i.e., the climatological maximum monthly mean (Osman et al., 2018), would be exceeded earlier in the year. Consequently, extreme SSTs and UV-B exposures would likely start to coincide earlier in the year in the upcoming decades, by an estimated 3 weeks in 2050 and 5–6 weeks in 2100 (see shaded area in **Figure 7**). In addition to an earlier onset, the combination of extreme temperature and UV exposure will also likely terminate later in the year. Specifically, we found that by 2100, those extreme environmental conditions at 0.5, 1, and 2 m depth might cease an estimated 4, 3, and 2 weeks later, respectively, compared to the years 2017/2018. At shallower depths (<1.5 m), the stressor co-occurrence in autumn would end with the sudden decrease in temperature, whereas at 2 m depth, UV-B exposures would fall below damaging threshold levels first, followed by temperature. This stressor co-occurrence is a common feature that we identified for both present and future conditions.

DISCUSSION

Our findings show a seasonal pattern in the attenuation of UV radiation in the Red Sea water column, with the lowest

TABLE 4 | Mean daily exposure of UV-B (280–315 nm) and UV-A (315–400 nm) received in different depths of the water column at the Red Sea pelagic sampling station (22.309333°N, 38.997389°E).

		UV-B exposure (kJ m^{-2} d^{-1})										UV-A exposure (kJ m^{-2} d^{-1})									
Year	**Month**	**0 m**	**0.5 m**	**1 m**	**2 m**	**4 m**	**6 m**	**8 m**	**10 m**	**12 m**	**15 m**	**0 m**	**0.5 m**	**1 m**	**2 m**	**4 m**	**6 m**	**8 m**	**10 m**	**15 m**	**20 m**
2017	February	24.7	20.7	17.3	12.2	6.0	2.9	1.5	0.7	0.4	0.12	N/A	N/A	N/A	N/A	N/A	N/A	N/A	N/A	N/A	N/A
	March	32.4	27.1	22.7	15.9	7.9	3.9	1.9	1.0	0.5	0.17	N/A	N/A	N/A	N/A	N/A	N/A	N/A	N/A	N/A	N/A
	April	33.2	28.1	23.8	17.0	8.7	4.5	2.3	1.2	0.6	0.22	1210	1143	1079	963	766	610	485	386	219	124
	May	39.6	33.9	29.0	21.2	11.4	6.1	3.3	1.8	1.0	0.39	1406	1335	1268	1144	931	758	617	503	302	182
	June	**44.9**	**37.4**	**31.1**	21.6	10.4	5.0	2.4	1.2	0.6	0.19	**1580**	**1492**	**1410**	**1259**	**1003**	800	638	509	289	165
	July	42.1	36.0	30.8	**22.6**	**12.2**	**6.6**	**3.6**	**2.0**	**1.1**	**0.44**	1497	1421	1350	1217	990	**805**	**655**	**533**	**319**	**191**
	August	35.7	29.9	25.0	17.5	8.6	4.2	2.1	1.0	0.5	0.17	1216	1145	1078	955	750	589	462	363	198	108
	September	36.6	31.1	26.4	19.0	9.9	5.2	2.7	1.4	0.7	0.28	1299	1226	1156	1029	815	646	511	405	226	126
	October	31.2	25.7	21.3	14.5	6.8	3.2	1.5	0.7	0.3	0.11	1172	1098	1029	904	697	538	415	320	168	88
	November	23.6	19.4	16.0	10.8	5.0	2.3	1.1	0.5	0.2	0.07	942	879	819	712	539	408	309	234	117	58
	December	20.1	16.6	13.7	9.4	4.4	2.1	1.0	0.5	0.2	0.08	836	778	724	627	472	356	269	203	102	52
2018	January	22.8	19.2	16.1	11.4	5.7	2.8	1.4	0.7	0.4	0.12	945	887	833	733	569	441	342	266	141	75
	February	26.8	22.4	18.6	12.9	6.2	3.0	1.4	0.7	0.3	0.11	1012	947	887	777	597	459	353	271	141	73
	March	38.6	32.3	27.0	18.9	9.3	4.6	2.3	1.1	0.5	0.19	1361	1283	1209	1074	848	669	528	417	231	128
	April	**43.3**	36.2	30.3	21.2	10.4	5.1	2.5	1.2	0.6	0.21	**1498**	1413	1333	1186	939	744	590	468	262	148
	May	42.6	35.4	29.4	20.3	9.7	4.6	2.2	1.0	0.5	0.16	1453	1364	1281	1130	878	683	531	413	220	117
	June	40.6	33.6	27.8	19.1	9.0	4.3	2.0	1.0	0.5	0.16	1403	1318	1237	1091	849	661	515	401	216	116
	July	42.4	**37.1**	**32.4**	**24.8**	**14.5**	**8.5**	**5.0**	**3.0**	**1.7**	**0.79**	1497	**1425**	**1356**	**1228**	**1007**	**826**	**677**	**555**	**339**	**206**
	August	38.8	33.5	29.0	21.7	12.3	7.0	4.0	2.4	1.4	0.63	1347	1276	1210	1087	877	708	572	463	273	161
	September	33.5	27.9	23.2	16.0	7.7	3.7	1.8	0.9	0.4	0.14	1211	1134	1062	931	715	550	423	325	168	87

The highest values for each depth per year are highlighted in bold.

transparency to UV in spring (March/April) and the highest in late summer (August/September) when CDOM photobleaching processes were most active. Furthermore, our results indicate that the intra-annual variability in UV attenuation is larger than previously described and that the date on which organisms experience their annual maximum of daily UV exposure depends on their depth in the water column. Also, the timing and duration when extreme UV exposure and maximum temperatures coincide is strongly depth-dependent.

The coastal Red Sea site studied here was more transparent than expected from recent reports. For example, Overmans and Agusti (2019) calculated K_d(320 nm) values of 0.158 m^{-1} (October 2016) and 0.196 m^{-1} (August 2017) for a nearby sampling site (22.276000°N, 38.787694°E), whereas in the present study, K_d(320 nm) exhibited a much broader range of values (0.148–0.312 m^{-1}), highlighting that the variability in UV attenuation has been underestimated to date. Equally, the same study by Overmans and Agusti (2019) reported that $Z_{1\%}$(320 nm) at this location varied from 23.5 to 29.0 m, whereas in the present study we calculated $Z_{1\%}$(320 nm) ranging from 14.7 to 31.0 m. Red Sea waters in the far north are still the most UV-transparent identified to date, with a $Z_{1\%}$(320 nm) maximum of 41.9 m (Overmans and Agusti, 2019). To put our results in a global context, we found that UV-A [$Z_{10\%}$(340 nm): 18 m] and UV-B [$Z_{10\%}$(305 nm): 10 m] wavelengths in the central Red Sea can reach depths similar to those reported for the highly transparent western Mediterranean Sea [$Z_{10\%}$(340 nm): 15–21 m; $Z_{10\%}$(305 nm): 10–11 m] (Llabres et al., 2010; Sempere et al., 2015), but not as deep as in oceanic waters such as the central subtropical Atlantic Ocean [$Z_{10\%}$(340 nm): 35 m; $Z_{10\%}$(305 nm): 16 m], the Gulf of Mexico [$Z_{10\%}$(340 nm): 37 m; $Z_{10\%}$(305 nm): 13 m] or the exceptionally transparent South Pacific Gyre [$Z_{10\%}$(340 nm): 59.0 m; $Z_{10\%}$(305 nm): 27.7 m] (Weinbauer et al., 1997; Obernosterer et al., 2001; Tedetti and Sempere, 2006; Tedetti et al., 2007).

Regarding UV exposure received in the Red Sea region, our study identified that daily exposure of atmospheric UV reached their maxima in June, with values of 57 and 1952 kJ m^{-2} d^{-1} for UV-B and UV-A, respectively. In comparison, Adam (2015) reported an annual mean UV-B exposure of 57 kJ m^{-2} d^{-1} and a maximum exposure of 84 kJ m^{-2} d^{-1} (June) for the Egyptian city of Qena located 200 km from the central Red Sea coast. Furthermore, maximum daily UV-B and UV-A exposures of approximately 85 and 1540 kJ m^{-2} d^{-1}, respectively, have been reported for the Gulf of Aqaba in the far north of the Red Sea (Dishon et al., 2012). However, Dishon et al. (2012) chose 320 nm as the upper boundary of the UV-B spectrum as compared to 315 nm in the present study, which explains the significant discrepancy between the annual maxima of UV-B exposures. If we compare the annual maxima of daily exposure for the UV spectrum as a whole (280–400 nm), we find that the maximum daily UV exposure during summer in the lower-latitude central Red Sea (2010 kJ m^{-2} d^{-1}) is approximately 24% higher than those observed in the Gulf of Aqaba (1625 kJ m^{-2} d^{-1}).

Regarding *in situ* UV conditions, Dishon et al. (2012) identified that maximum UV (280–400 nm) exposure in the water column occurred in September with daily exposure of

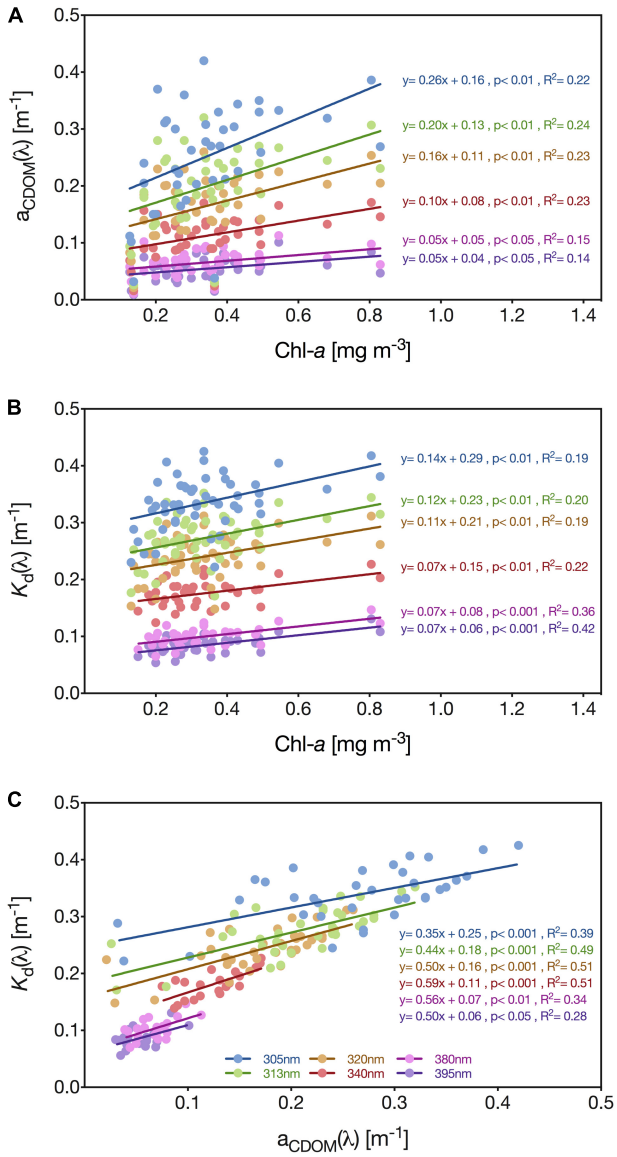

FIGURE 6 | Linear regression analysis of the relationship between $a_{CDOM}(\lambda)$ and the concentration of Chl-*a* **(A)**, the downwelling diffuse attenuation coefficient [$K_d(\lambda)$] and Chl-*a* concentration **(B)**, and $a_{CDOM}(\lambda)$, and $K_d(\lambda)$ and $a_{CDOM}(\lambda)$ **(C)** for the wavelengths 305 (blue circles), 313 (green circles), 320 (brown circles), 340 (red circles), 380 (pink circles), and 395 nm (purple circles). Solid lines represent linear regression lines.

approximately 1080, 640, and 286 kJ m^{-2} d^{-1} in 5, 15, and 30 m depth, respectively. In contrast, we found that daily exposure of total UV was on average highest in July, with mean daily UV exposures of 923, 340, and 77 kJ m^{-2} d^{-1} in 5, 15, and 30 m, respectively. However, UV exposure at the aforementioned depths reached absolute maxima of 1103 (on 3rd June 2017), 407 (10th July 2017) and 106 kJ m^{-2} d^{-1} (28th May 2017), respectively. While the maximum exposure we recorded at 5 m depth slightly exceeds the value reported for the Gulf of Aqaba, the exposures at 10 and 15 m were substantially higher than in our study. In a global context, the UV intensities reported here for the Red Sea are exceptionally high. For example, a study by Downs et al. (2013) investigating UV-B (280–320 nm) exposure in a fringing coral reef in southern Queensland reported that daily exposure at a mean daylight water depth of 1.60 m reached a maximum of approximately 11 kJ m^{-2} d^{-1} during the austral spring in September 2010 (i.e., at the onset of the strong 2010–2012 La Niña event). Since the La Niña event impacted the water turbidity, a further study by the same authors found that UV-B (290–315 nm) exposure in a turbid inshore reef after the event were <21.13 kJ m^{-2} d^{-1} during peak summer exposure conditions (Downs et al., 2016), which represents a drastic increase in UV-B exposure, especially given the different definitions of the UV-B spectrum between the two studies (i.e., 280–320 nm vs. 290–315 nm). However, the reported maximum exposure of 21.13 kJ m^{-2} d^{-1} is still considerably lower than the maximum UV-B exposure of 31.4 kJ m^{-2} d^{-1} at 1.60 m depth at our pelagic study site in the Red Sea. Although we did not directly determine daily UV exposure nor the attenuation of UV radiation at our mid-shore coral reef sampling site, our data evidenced that the inshore side of the reef was characterized by consistently higher absorption by CDOM [e.g., $a_{CDOM}(320)$: 0.236 ± 0.065 m^{-1}] than the open-water station [$a_{CDOM}(320)$: 0.162 ± 0.060 m^{-1}], caused by the greater organic matter production of reef organisms. In contrast, the concentration of Chl-*a* in the reef waters (0.20 ± 0.08 mg m^{-3}) was lower than at the pelagic site (Chl-*a*: 0.35 ± 0.15 mg m^{-3}), likely due to the efficient removal of phytoplankton by benthic filter feeders (Yahel et al., 1998; Richter et al., 2001; van Duyl et al., 2002). Additionally, both sites showed high values of $a_{CDOM}(254/365)$ (Pelagic: 12.4 ± 3.3 m^{-1}; Reef: 8.4 ± 2.2 m^{-1}) and the slope ratio S_R [i.e., $S_{(275-295)}/S_{(350-400)}$] (Pelagic: 3.32 ± 1.83; Reef: 2.97 ± 1.64), evidencing that photobleaching is occurring at high rates throughout the year and that the bulk of CDOM is of low molecular weight (Helms et al., 2008; Berggren et al., 2010). In comparison, Romera-Castillo et al. (2013) reported a higher annual mean $a_{CDOM}(254/365)$ (14.8 ± 0.6 m^{-1}) but a lower S_R (2.02 ± 0.05) for a coastal site in the oligotrophic, north-western Mediterranean Sea. Furthermore, a recent study by Iuculano et al. (2019) investigating the CDOM properties of the oligotrophic oceans found that the $a_{CDOM}(254/365)$ ratio varied considerably among the biogeographic provinces of the ocean, from the lowest mean of 10 (IQR, 6–13) in the North Pacific to the highest mean of 32 (IQR, 24–37) in the North Atlantic tropical gyre, which puts our $a_{CDOM}(254/365)$ values for the Red Sea close to the lower end of the range. The same study by Iuculano et al. (2019) also found that the UV spectral slope $S_{(275-295)}$ ranged from 30.0 μm^{-1} (IQR, 23.5–35.5 μm^{-1}) in the North Pacific to 47.2 μm^{-1} (IQR, 41.3–53.1 μm^{-1}) in the Indian South subtropical gyre. For our Red Sea study sites, we calculated intermediate mean values of 34.4 ± 8.2 μm^{-1} for the pelagic site and 30.5 ± 6.2 μm^{-1} for the reef, suggesting that the CDOM present in the reef waters is of higher molecular weight.

Although we could not directly measure UV attenuation with the profiling radiometer in the Red Sea reef due to the shallow water depth (<2 m), we expect K_d values of the reef waters to be higher than those of the pelagic site

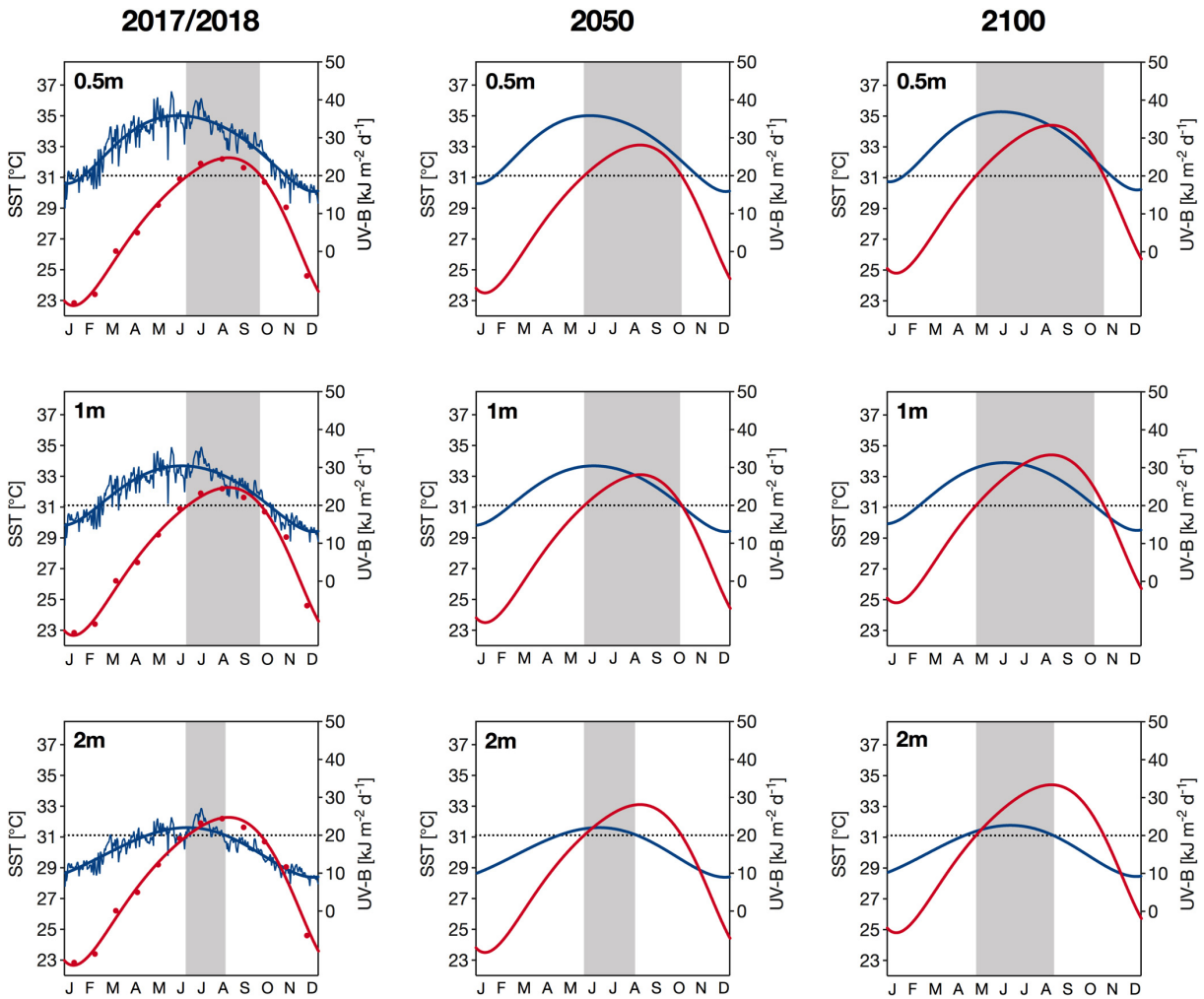

FIGURE 7 | Current (years 2017/2018; **left column**) and projected (year 2050: **middle column**; year 2100: **right column**) sea surface temperatures (SST; in red) and daily UV-B exposure (280–315 nm) (in blue) at Al Fahal reef in 0.5m **(top row)**, 1 m **(middle row)** and 2 m depth **(bottom row)**. Current UV-B exposure are the daily means of exposure received in 2017 and 2018, while current temperature is shown as the monthly mean temperature during the same period. Thick lines represent sixth-order polynomial trendlines. Projected SST values were calculated based on an annual warming rate of 0.026°C, which is the mean of the two warming rates reported for the central Red Sea by Chaidez et al. (2017) and Osman et al. (2018). Daily UV-B exposure in 2050 are identical to current exposure, while exposure in 2100 are 3% higher, representing the projected increase of UV-B radiation in the tropics according to the latest future-UV radiation models (Bais et al., 2019; Meul et al., 2016). The dotted black line indicates (1) the threshold of severely damaging UV-B exposure (i.e., >20 kJ m^{-2} d^{-1}) for corals (Zhou et al., 2016) and (2) the climatological maximum monthly mean (31.1°C) of the Jeddah region (Osman et al., 2018). Shaded areas indicate periods when both parameters exceed the aforementioned thresholds.

for short UV wavelengths because of the higher absorption by CDOM at the reef, while the lower Chl-*a* concentrations in the reef waters would suggest the opposite. The multiple regression of our a_{CDOM} and Chl-*a* data from the pelagic station, using 320 nm as a representative wavelength of the UV spectrum, indeed revealed a higher predicted attenuation of UV wavelengths at the reef [K_d(320 nm): 0.271 ± 0.031 m^{-1})] than at the pelagic site (0.238 ± 0.030 m^{-1}). However, the reef itself and the surrounding area are characterized by a light-colored substrate, which can potentially reflect a large proportion of the downwelling solar radiation (Joyce and Phinn, 2003; Wangpraseurt et al., 2014) and thereby increase UV exposure. Therefore, it is still uncertain how UV exposure at the shallow reef site compares to the exposure conditions in the same depth at the pelagic site.

Nevertheless, the maximum daily UV exposures calculated for the central Red Sea in the present study were substantially higher than those reported by Downs et al. (2013) for the Australian reef. Hence, we can assume that Red Sea organisms living in shallow waters experience high levels of UV-induced stress. Several reports from the Red Sea have confirmed the severe impacts of UV radiation on key Red Sea biota. Al-Aidaroos et al. (2015) found increased mortality rates in ten different zooplankton taxa in response to natural UV-B exposure intensities comparable to those received *in situ* at ∼3.5 m depth, while a study by Boelen et al. (2002) reported UV-induced DNA damage in natural

communities of bacterio- and phytoplankton from the surface down to a depth of 50 m. For Red Sea corallimorpharians, UV exposure induces a reduction in the concentration of chlorophyll pigments as well as the abundance of endosymbionts living in association with *Rhodactis rhodostoma*, while exposure to UV causes *Discosoma unguja* to physically migrate away from exposed locations toward shaded habitats in order to avoid UV damage (Kuguru et al., 2010). For other anthozoans in the Red Sea, such as soft corals, a decreased survival rate in response to combined UV-B (0.8 W m^{-2}) and UV-A (3.0 W m^{-2}) exposure has been reported during the early developmental stages of *Heteroxenia fuscescens* and *Rhytisma fulvum fulvum* (Zeevi Ben-Yosef and Benayahu, 2008).

Despite their importance for the region, no studies to date have investigated the sensitivity of Red Sea scleractinian corals to UV radiation. A study by Bellworthy and Fine (2017) reported that the corals *Stylophora pistillata* and *Acropora eurystoma* from the Gulf of Aqaba exhibited a high sensitivity to intense solar radiation, yet the authors could not distinguish whether the observed photoinhibition and reduction in symbiont density was due to intense PAR, UVR, or a combination of the two. For the central and southern Red Sea where incident UV exposure is higher than in the northern part of the basin, no studies to date have investigated the sensitivity of corals to solar radiation. Further studies on the impact of UV on corals in areas that are already prone to thermally induced coral bleaching events are critical. In contrast, the northern part of the Red Sea basin has been termed a thermal refuge for corals due to the much lower SSTs relative to the rest of the region (Fine et al., 2013; Osman et al., 2018).

The interplay between temperature and UV stress in the context of coral bleaching is not yet fully understood. However, several studies have suggested that intense UV radiation not only has direct detrimental effects on the physiology and molecular compartments of corals but also acts as an interactive factor that further intensifies thermally induced damage and bleaching in corals worldwide (Gleason and Wellington, 1993; Drollet et al., 1995; Ferrier-Pages et al., 2007; Torregiani and Lesser, 2007; Banaszak and Lesser, 2009; Lesser, 2010). Specifically, Lesser and Farrell (2004) identified that the additional stress caused by exposure to intense UV radiation reduces the bleaching threshold temperature and the number of degree heating weeks (DHWs) required to induce coral bleaching. For the region of our study sites (Jeddah region), a recent study reported a bleaching threshold temperature of 32.1°C (Osman et al., 2018), which we found was frequently exceeded in late summer. During late summer, incident UV exposure were still moderately high; however, we detected that the annual peak intensity occurred several weeks prior. Generally, in the upper meters of the water column ($<\sim$1.5 m), the time of maximum UV exposure (May/June) occurred before that of maximum SST (July/August) (**Figure 7**), which may presently provide sessile benthic organisms such as corals a means of protection. Further down the water column, however, maximum water temperatures and peak UV exposure coincided in July/August, since the highest transparency to UV occurred in late summer. However, the UV exposure in those depths was substantially lower and UV-induced damage was not as pronounced as in shallower depths. Alarmingly, we have found that in the future, due to the steady increase in SST as a consequence of global climate change, bleaching threshold temperatures will likely be exceeded earlier in the year. As a consequence, the current time gap between the annual extreme of UV and the time when the bleaching threshold temperature is reached will gradually decrease, and thus the two abiotic stressors are more likely to coincide during early summer in the future. This holds especially true if the Red Sea continues to warm at the rapid rate recently reported for the region (Chaidez et al., 2017; Osman et al., 2018) that could result in a temperature change of $\sim$2°C by 2100 relative to the 1986–2005 period, which is in between the moderate (RCP4.5: ΔT 1.8°C) and high (RCP 6.0: ΔT 2.2°C) IPCC emission scenario (IPCC, 2014). Our predictions are, however, restrained as we did not consider the effect of warming on declining Chl-*a* concentrations (Behrenfeld et al., 2006; Boyce et al., 2014) that could result in future increases in water transparency, thereby enhancing underwater UV exposure.

It should also be noted that different biological processes are differentially affected by changes in K_d or the depletion of total column ozone (TCO) since certain UV wavelengths target specific molecular responses. For example, the action spectra for erythema (McKinlay and Diffey, 1987) and UV-induced DNA damage (Setlow, 1974) are heavily weighted toward short-waved UV-B, while the action spectrum for photosynthesis-related impacts extends far into the UV-A range (Cullen et al., 1992; Lesser and Lewis, 1996). Zepp et al. (2008) have found that a 30% decrease in the K_d of the Florida Keys' water column would result in an equal reduction in the photosynthetic activity in 3 m depth whereas the presence of DNA damage could be enhanced by as much as $\sim$100%. Similarly, while a 5% decrease in stratospheric ozone could cause a 10% increase in DNA-weighted UV doses, photosynthesis-weighted UV doses would be less impacted since ozone depletion does not affect wavelengths $>$ 330 nm (Cutchis, 1974). These findings highlight the importance of applying biological weighting functions when trying to determine the impacts of increased UV-B exposure on a specific organismal compartment or process rather than an organism as a whole.

CONCLUSION

In conclusion, we identified that the central Red Sea coast exhibits exceptionally high transparency to UV radiation compared to other coastal waters due to negligible inputs of terrestrial CDOM. In addition, we observed a seasonal pattern of transparency to UV governed by the seasonality of Chl-*a* (i.e., phytoplankton), and the generation and photodegradation of CDOM present in the water column. The Red Sea region experiences high UV radiation for most of the year. However, we identified that maximum incident irradiance does not co-occur at the same time when waters are at their most transparent and reach maximum temperatures. This implies that Red Sea organisms close to the surface experience extreme UV exposure earlier in the year than organisms living at greater depths in the water column, where two abiotic stresses (i.e., extreme UV and temperature) reach

their maximum in late summer, even though UV radiation is only at moderately high levels. However, if SSTs continue to increase steadily as a consequence of climate change, bleaching threshold temperatures will be reached earlier in the year and hence will coincide with extreme UV radiation in shallower areas of the reef, which could potentially increase the frequency of coral bleaching events in the near future.

DATA AVAILABILITY STATEMENT

The datasets generated as part of this study can be found in the data repository Mendeley Data (http://dx.doi.org/10.17632/9rdfbfctm7.1).

AUTHOR CONTRIBUTIONS

SA conceptualized the study and directed the time series project. SO collected and processed the optical data and water samples, generated the tables and figures. SO and SA analyzed the data. SO wrote the manuscript with a substantial contribution from SA.

FUNDING

The research reported in this publication was supported by baseline funding from KAUST to SA under award number BAS/1/1072-01-01.

ACKNOWLEDGMENTS

We would like to express special thanks to Juan Martinez-Ayala, Cecilia Martin and Katherine Rowe of the Red Sea Research Center (RSRC) at King Abdullah University of Science and Technology (KAUST), and the team of the Coastal and Marine Resources Core Lab (CMOR) at KAUST for their expert support and assistance during the fieldwork.

REFERENCES

Acker, J., Leptoukh, G., Shen, S., Zhu, T., and Kempler, S. (2008). Remotely-sensed chlorophyll a observations of the northern Red Sea indicate seasonal variability and influence of coastal reefs. *J. Mar. Syst.* 69, 191–204. doi: 10.1016/j.jmarsys.2005.12.006

Adam, M. E. (2015). Determination of daily total ultraviolet-B in a subtropical region (Upper Egypt): an empirical approach. *Atmos. Res.* 153, 1–9. doi: 10.1016/j.atmosres.2014.07.025

Al-Aidaroos, A. M., El-Sherbiny, M. M. O., Satheesh, S., Mantha, G., Agusti, S., Carreja, B., et al. (2015). Strong sensitivity of red sea zooplankton to UV-B radiation. *Estuaries Coast.* 38, 846–853. doi: 10.1007/s12237-014-9868-4

Ayres-Ostrock, L. M., and Plastino, E. M. (2014). Effects of UV-B radiation on growth rates, pigment content and ultrastructure of red (wild type), greenish-brown and green strains of *Gracilaria birdiae* (Gracilariales, Rhodophyta). *Eur. J. Phycol.* 49, 197–212. doi: 10.1080/09670262.2014.904931

Babin, M., Stramski, D., Ferrari, G. M., Claustre, H., Bricaud, A., Obolensky, G., et al. (2003). Variations in the light absorption coefficients of phytoplankton, nonalgal particles, and dissolved organic matter in coastal waters around Europe. *J. Geophys. Res. Oceans* 108, 1–18.

Bais, A. F., Bernhard, G., McKenzie, R. L., Aucamp, P. J., Young, P. J., Ilyas, M., et al. (2019). Ozone-climate interactions and effects on solar ultraviolet radiation. *Photochem. Photobiol. Sci.* 18, 602–640. doi: 10.1039/c8pp90059k

Bais, A. F., Tourpali, K., Kazantzidis, A., Akiyoshi, H., Bekki, S., Braesicke, P., et al. (2011). Projections of UV radiation changes in the 21st century: impact of ozone recovery and cloud effects. *Atmos. Chem. Phys.* 11, 7533–7545. doi: 10.5194/acp-11-7533-2011

Banaszak, A. T., and Lesser, M. P. (2009). Effects of solar ultraviolet radiation on coral reef organisms. *Photochem. Photobiol. Sci.* 8, 1276–1294. doi: 10.1039/b902763g

Barron, M. G. (2017). Photoenhanced toxicity of petroleum to aquatic invertebrates and fish. *Arch. Environ. Contam. Toxicol.* 73, 40–46. doi: 10.1007/s00244-016-0360-y

Behrenfeld, M. J., O'Malley, R. T., Siegel, D. A., McClain, C. R., Sarmiento, J. L., Feldman, G. C., et al. (2006). Climate-driven trends in contemporary ocean productivity. *Nature* 444, 752–755. doi: 10.1038/nature05317

Bellworthy, J., and Fine, M. (2017). Beyond peak summer temperatures, branching corals in the Gulf of Aqaba are resilient to thermal stress but sensitive to high light. *Coral Reefs* 36, 1071–1082. doi: 10.1007/s00338-017-1598-1

Berggren, M., Laudon, H., Haei, M., Strom, L., and Jansson, M. (2010). Efficient aquatic bacterial metabolism of dissolved low-molecular-weight compounds from terrestrial sources. *ISME J.* 4, 408–416. doi: 10.1038/ismej.2009.120

Boelen, P., Post, A. F., Veldhuis, M. J., and Buma, A. G. (2002). Diel patterns of UVBR-induced DNA damage in picoplankton size fractions from the Gulf of Aqaba, Red Sea. *Microb. Ecol.* 44, 164–174. doi: 10.1007/s00248-002-1002-7

Boyce, D. G., Dowd, M., Lewis, M. R., and Worm, B. (2014). Estimating global chlorophyll changes over the past century. *Prog. Oceanogr.* 122, 163–173. doi: 10.1016/j.pocean.2014.01.004

Bricaud, A., Morel, A., and Prieur, L. (1981). Absorption by dissolved organic-matter of the sea (Yellow Substance) in the Uv and visible domains. *Limnol. Oceanogr.* 26, 43–53. doi: 10.4319/lo.1981.26.1.0043

Buck, B. H., Rosenthal, H., and Saint-Paul, U. (2002). Effect of increased irradiance and thermal stress on the symbiosis of *Symbiodinium microadriaticum* and *Tridacna gigas*. *Aquat. Living Resour.* 15, 107–117. doi: 10.1016/s0990-7440(02)01159-2

Campbell, J. W., and Aarup, T. (1989). Photosynthetically available radiation at high-latitudes. *Limnol. Oceanogr.* 34, 1490–1499. doi: 10.1364/AO.57.003088

Cao, F., Fichot, C. G., Hooker, S. B., and Miller, W. L. (2014). Improved algorithms for accurate retrieval of UV/visible diffuse attenuation coefficients in optically complex, inshore waters. *Remote Sens. Environ.* 144, 11–27. doi: 10.1016/j.rse.2014.01.003

Carrasco-Malio, A., Diaz, M., Mella, M., Montoya, M. J., Miranda, A., Landaeta, M. F., et al. (2014). Are the intertidal fish highly resistant to UV-B radiation? A study based on oxidative stress in Girella laevifrons (Kyphosidae). *Ecotoxicol. Environ. Saf.* 100, 93–98. doi: 10.1016/j.ecoenv.2013.07.030

Carreja, B., Fernandez, M., and Agusti, S. (2016). Joint additive effects of temperature and UVB radiation on zoeae of the crab Taliepus dentatus. *Mar. Ecol. Prog. Ser.* 550, 135–145. doi: 10.3354/meps11715

Chaidez, V., Dreano, D., Agusti, S., Duarte, C. M., and Hoteit, I. (2017). Decadal trends in Red Sea maximum surface temperature. *Sci. Rep.* 7:8144. doi: 10.1038/s41598-017-08146-z

Coble, P. G., Zepp, R. G., and Zika, R. G. (2004). CDOM in the ocean: transformation processes and their effects on optical properties. *Mar. Chem.* 89, 1–1.

Cullen, J. J., Neale, P. J., and Lesser, M. P. (1992). Biological weighting function for the inhibition of phytoplankton photosynthesis by ultraviolet-radiation. *Science* 258, 646–650. doi: 10.1126/science.258.5082.646

Cutchis, P. (1974). Stratospheric ozone depletion and solar ultraviolet radiation on Earth. *Science* 184, 13–19. doi: 10.1126/science.184.4132.13

Dahlen, J., Bertilsson, S., and Pettersson, C. (1996). Effects of UV-A irradiation on dissolved organic matter in humic surface waters. *Environ. Int.* 22, 501–506. doi: 10.1016/0160-4120(96)00038-4

Dickerson, R. R., Kondragunta, S., Stenchikov, G., Civerolo, K. L., Doddridge, B. G., and Holben, B. N. (1997). The impact of aerosols on solar ultraviolet radiation

and photochemical smog. *Science* 278, 827–830. doi: 10.1126/science.278.5339.827

Dishon, G., Dubinsky, Z., Fine, M., and Iluz, D. (2012). Underwater light field patterns in subtropical coastal waters: a case study from the Gulf of Eilat (Aqaba). *Isr. J. Plant Sci.* 60, 265–275. doi: 10.1560/ijps.60.1-2.265

Downs, N. J., Schouten, P. W., and Parisi, A. V. (2013). Seasonal variations in the subsurface ultraviolet-B on an inshore Pacific coral reef ecosystem. *Photochem. Photobiol.* 89, 1234–1243. doi: 10.1111/php.12101

Downs, N. J., Schouten, P. W., and Parisi, A. V. (2016). "In-situ measurements of solar exposure distribution on a coral reef: preliminary findings relating to reef aspect, water turbidity and dosimeter design," in *Proceedings of the 13th International Coral Reef Symposium: Book of Abstracts*, Honolulu, HI.

Drohan, A. F., Thoney, D. A., and Baker, A. C. (2005). Synergistic effect of high temperature and ultraviolet-B radiation on the gorgonian *Eunicea tourneforti* (Octocorallia : Alcyonacea : Plexauridae). *Bull. Mar. Sci.* 77, 257–266.

Drollet, J. H., Faucon, M., and Martin, P. M. V. (1995). Elevated sea-water temperature and solar UV-B flux associated with two successive coral mass bleaching events in tahiti. *Mar. Freshw. Res.* 46, 1153–1157.

Ferrier-Pages, C., Richard, C., Forcioli, D., Allemand, D., Pichon, M., and Shick, J. M. (2007). Effects of temperature and UV radiation increases on the photosynthetic efficiency in four scleractinian coral species. *Biol. Bull.* 213, 76–87. doi: 10.2307/25066620

Fine, M., Gildor, H., and Genin, A. (2013). A coral reef refuge in the Red Sea. *Glob. Chang. Biol.* 19, 3640–3647. doi: 10.1111/gcb.12356

Garcias-Bonet, N., and Duarte, C. M. (2017). Methane production by seagrass ecosystems in the Red Sea. *Front. Mar. Sci.* 4:340. doi: 10.3389/fmars.2017.00340

Genevier, L. G. C., Jamil, T., Raitsos, D. E., Krokos, G., and Hoteit, I. (2019). Marine heatwaves reveal coral reef zones susceptible to bleaching in the Red Sea. *Glob. Chang. Biol.* 25, 2338–2351. doi: 10.1111/gcb.14652

Giomi, F., Barausse, A., Duarte, C. M., Booth, J., Agusti, S., Saderne, V., et al. (2019). Oxygen supersaturation protects coastal marine fauna from ocean warming. *Sci. Adv.* 5:eaax1814. doi: 10.1126/sciadv.aax1814

Giordanino, M. V., Strauch, S. M., Villafane, V. E., and Helbling, E. W. (2011). Influence of temperature and UVR on photosynthesis and morphology of four species of cyanobacteria. *J. Photochem. Photobiol. B* 103, 68–77. doi: 10.1016/j.jphotobiol.2011.01.013

Gleason, D. F., Edmunds, P. J., and Gates, R. D. (2006). Ultraviolet radiation effects on the behavior and recruitment of larvae from the reef coral Porites astreoides. *Mar. Biol.* 148, 503–512. doi: 10.1007/s00227-005-0098-y

Gleason, D. F., and Wellington, G. M. (1993). Ultraviolet-radiation and coral bleaching. *Nature* 365, 836–838. doi: 10.1038/365836a0

Gomes, V., Passos, M. J. A. C. R., Leme, N. M. P., Santos, T. C. A., Campos, D. Y. F., Hasue, F. M., et al. (2009). Photo-induced toxicity of anthracene in the Antarctic shallow water amphipod, Gondogeneia antarctica. *Polar Biol.* 32, 1009–1021. doi: 10.1007/s00300-009-0600-y

Helbling, E. W., and Zagarese, H. (2003). *UV Effects in Aquatic Organisms and Ecosystems*. Cambridge: The Royal Society of Chemistry.

Helms, J. R., Stubbins, A., Ritchie, J. D., Minor, E. C., Kieber, D. J., and Mopper, K. (2008). Absorption spectral slopes and slope ratios as indicators of molecular weight, source, and photobleaching of chromophoric dissolved organic matter. *Limnol. Oceanogr.* 53, 955–969. doi: 10.4319/lo.2008.53.3.0955

Hirabayashi, S., Kasai, F., Watanabe, M. M., and Hirose, E. (2006). Contents of ultraviolet-absorbing substances in two color morphs of the photosymbiotic ascidian Didemnum molle. *Hydrobiologia* 571, 419–422. doi: 10.1007/s10750-006-0244-7

Hirose, E., Hirabayashi, S., Hori, K., Kasai, F., and Watanabe, M. M. (2006). UV protection in the photosymbiotic ascidian Didemnum molle inhabiting different depths. *Zoolog. Sci* 23, 57–63. doi: 10.2108/zsj.23.57

Hsu, N. C., Tsay, S. C., King, M. D., and Herman, J. R. (2004). Aerosol properties over bright-reflecting source regions. *IEEE Trans. Geosci. Remote* 42, 557–569. doi: 10.1109/tgrs.2004.824067

IPCC, (2014). "Climate change 2014: synthesis report," in *Contribution of Working Groups I, II and III to the Fifth Assessment Report of the Intergovernmental Panel of Climate Change*, eds Core Writing Team, R. K. Pachauri, and L. A. Meyer, (Geneva: IPCC).

IPCC, (2018). "Summary for Policymakers," in *An IPCC Special Report on the Impacts of Global Warming of 1.5°C Above Pre-Industrial Levels and Related Global Greenhouse Gas Emission Pathways, in the Context of Strengthening the Global Response to the Threat of Climate Change, Sustainable Development, and Efforts to Eradicate Poverty* eds V. Masson-Delmotte, P. Zhai, H.-O. Pörtner, D. Roberts, J. Skea, P. R. Shukla, et al. (Geneva: IPCC).

Iuculano, F., Alverez-Salgado, X. A., Otero, J., Catala, T. S., Sobrino, C., Duarte, C. M., et al. (2019). Patterns and drivers of UV absorbing chromophoric dissolved organic matter in the euphotic layer of the open ocean. *Front. Mar. Sci.* 6:320.

Jin, P., Overmans, S., Duarte, C. M., and Agustí, S. (2019). Increasing temperature within thermal limits compensates negative ultraviolet-B radiation effects in terrestrial and aquatic organisms. *Glob. Ecol. Biogeogr.* 28, 1695–1711. doi: 10.1111/geb.12973

Joshi, D., Mohandass, C., and Dhale, M. (2018). Effect of UV-B radiation and desiccation stress on photoprotective compounds accumulation in marine *Leptolyngbya* sp. *Appl. Biochem. Biotechnol.* 184, 35–47. doi: 10.1007/s12010-017-2523-3

Joyce, K. E., and Phinn, S. R. (2003). Hyperspectral analysis of chlorophyll content and photosynthetic capacity of coral reef substrates. *Limnol. Oceanogr.* 48, 489–496. doi: 10.4319/lo.2003.48.1_part_2.0489

Kalenderski, S., Stenchikov, G., and Zhao, C. (2013). Modeling a typical winter-time dust event over the Arabian Peninsula and the Red Sea. *Atmos. Chem. Phys.* 13, 1999–2014. doi: 10.5194/acp-13-1999-2013

Karentz, D., Dunlap, W. C., and Bosch, I. (1997). Temporal and spatial occurrence of UV-absorbing mycosporine-like amino acids in tissues of the Antarctic sea urchin *Sterechinus neumayeri* during springtime ozone-depletion. *Mar. Biol.* 129, 343–353. doi: 10.1007/s002270050174

Kaweewat, K., and Hofer, R. (1997). Effect of UV-B radiation on goblet cells in the skin of different fish species. *J. Photochem. Photobiol. B Biol.* 41, 222–226. doi: 10.1016/s1011-1344(97)00104-8

Kheireddine, M., Ouhssain, M., Calleja, M. L., Moran, X. A. G., Sarma, Y. V. B., Tiwari, S. P., et al. (2018). Characterization of light absorption by chromophoric dissolved organic matter (CDOM) in the upper layer of the Red Sea. *Deep Sea Res. Part I* 133, 72–84. doi: 10.1016/j.dsr.2018.02.001

Khogali, A., and Albar, O. F. (1992). A study of solar ultraviolet-radiation at makkah solar station. *Sol. Energy* 48, 79–87. doi: 10.1016/0038-092x(92)90036-a

Kim, B. M., Rhee, J. S., Lee, K. W., Kim, M. J., Shin, K. H., Lee, S. J., et al. (2015). UV-B radiation-induced oxidative stress and p38 signaling pathway involvement in the benthic copepod *Tigriopus japonicus*. *Comp. Biochem. Physiol. C Toxicol. Pharmacol.* 167, 15–23. doi: 10.1016/j.cbpc.2014.08.003

Kuguru, B., Achituv, Y., Gruber, D. F., and Tchernov, D. (2010). Photoacclimation mechanisms of corallimorpharians on coral reefs: photosynthetic parameters of zooxanthellae and host cellular responses to variation in irradiance. *J. Exp. Mar. Biol. Ecol.* 394, 53–62. doi: 10.1016/j.jembe.2010.07.007

Larkum, A. W., and Wood, W. F. (1993). The effect of UV-B radiation on photosynthesis and respiration of phytoplankton, benthic macroalgae and seagrasses. *Photosynth. Res.* 36, 17–23. doi: 10.1007/BF00018071

Lee, Z. P., Du, K. P., Arnone, R., Liew, S. C., and Penta, B. (2005). Penetration of solar radiation in the upper ocean: a numerical model for oceanic and coastal waters. *J. Geophys. Res. Oceans* 110:C09019.

Lesser, M. P. (1996). Elevated temperatures and ultraviolet radiation cause oxidative stress and inhibit photosynthesis in symbiotic dinoflagellates. *Limnol. Oceanogr.* 41, 271–283. doi: 10.4319/lo.1996.41.2.0271

Lesser, M. P. (2010). Interactions between stressors on coral reefs: analytical approaches, re-analysis of old data, and different conclusions. *Coral Reefs* 29, 615–619. doi: 10.1007/s00338-010-0625-2

Lesser, M. P., and Farrell, J. H. (2004). Exposure to solar radiation increases damage to both host tissues and algal symbionts of corals during thermal stress. *Coral Reefs* 23, 367–377. doi: 10.1007/s00338-004-0392-z

Lesser, M. P., and Lewis, S. (1996). Action spectrum for the effects of UV radiation on photosynthesis in the hermatypic coral *Pocillopora damicornis*. *Mar. Ecol. Prog. Ser.* 134, 171–177. doi: 10.3354/meps134171

Lesser, M. P., Stochaj, W. R., Tapley, D. W., and Shick, J. M. (1990). Bleaching in coral-reef anthozoans - effects of irradiance, ultraviolet-radiation, and temperature on the activities of protective enzymens against active oxygen. *Coral Reefs* 8, 225–232. doi: 10.1007/bf00265015

Lionard, M., Roy, S., Tremblay-Letourneau, M., and Ferreyra, G. A. (2012). Combined effects of increased UV-B and temperature on the pigment-determined marine phytoplankton community of the St Lawrence Estuary. *Mar. Ecol. Prog. Ser.* 445, 219–234. doi: 10.3354/meps09484

Llabres, M., Agusti, S., Alonso-Laita, P., and Herndl, G. J. (2010). Synechococcus and Prochlorococcus cell death induced by UV radiation and the penetration of lethal UVR in the Mediterranean Sea. *Mar. Ecol. Prog. Ser.* 399, 27–37. doi: 10.3354/meps08332

Llabres, M., Agusti, S., Fernandez, M., Canepa, A., Maurin, F., Vidal, F., et al. (2013). Impact of elevated UVB radiation on marine biota: a meta-analysis. *Glob. Ecol. Biogeogr.* 22, 131–144. doi: 10.1111/j.1466-8238.2012.00784.x

López-Sandoval, D. C., Rowe, K., Carillo-de-Albonoz, P., Duarte, C. M., and Agusti, S. (2019). Rates and drivers of Red Sea plankton community metabolism. *Biogeosciences* 16, 2983–2995. doi: 10.5194/bg-16-2983-2019

McKenzie, R., Smale, D., and Kotkamp, M. (2004). Relationship between UVB and erythemally weighted radiation. *Photochem. Photobiol. Sci.* 3, 252–256.

McKenzie, R. L., Aucamp, P. J., Bais, A. F., Bjorn, L. O., and Ilyas, M. (2007). Changes in biologically-active ultraviolet radiation reaching the Earth's surface. *Photochem. Photobiol. Sci.* 6, 218–231. doi: 10.1039/b700017k

McKenzie, R. L., Aucamp, P. J., Bais, A. F., Bjorn, L. O., Ilyas, M., and Madronich, S. (2011). Ozone depletion and climate change: impacts on UV radiation. *Photochem. Photobiol. Sci.* 10, 182–198. doi: 10.1039/c0pp90034f

McKinlay, A. F., and Diffey, B. L. (1987). A reference action spectrum for ultraviolet erythema in human skin. *CIE J.* 6, 17–22.

Meul, S., Dameris, M., Langematz, U., Abalichin, J., Kerschbaumer, A., Kubin, A., et al. (2016). Impact of rising greenhouse gas concentrations on future tropical ozone and UV exposure. *Geophys. Res. Lett.* 43, 2919–2927. doi: 10.1002/2016gl067997

Miller, R. L., Belz, M., Del Castillo, C., and Trzaska, R. (2002). Determining CDOM absorption spectra in diverse coastal environments using a multiple pathlength, liquid core waveguide system. *Cont. Shelf Res.* 22, 1301–1310. doi: 10.1016/s0278-4343(02)00009-2

Nahon, S., Charles, F., Lantoine, F., Vetion, G., Escoubeyrou, K., Desmaladed, M., et al. (2010). Ultraviolet radiation negatively affects growth and food quality of the pelagic diatom *Skeletonema costatum*. *J. Exp. Mar. Biol. Ecol.* 383, 164–170. doi: 10.1016/j.jembe.2009.12.006

Obernosterer, I., Ruardij, P., and Herndl, G. J. (2001). Spatial and diurnal dynamics of dissolved organic matter (DOM) fluorescence and H2O2 and the photochemical oxygen demand of surface water DOM across the subtropical Atlantic Ocean. *Limnol. Oceanogr.* 46, 632–643. doi: 10.4319/lo.2001.46.3.0632

Osman, E. O., Smith, D. J., Ziegler, M., Kurten, B., Conrad, C., El-Haddad, K. M., et al. (2018). Thermal refugia against coral bleaching throughout the northern Red Sea. *Glob. Chang. Biol.* 24, e474–e484. doi: 10.1111/gcb.13895

Overmans, S., and Agusti, S. (2019). Latitudinal gradient of UV attenuation along the highly transparent Red Sea Basin. *Photochem. Photobiol.* 95, 1267–1279. doi: 10.1111/php.13112

Overmans, S., Nordborg, M., Diaz-Rua, R., Brinkman, D. L., Negri, A. P., and Agusti, S. (2018). Phototoxic effects of PAH and UVA exposure on molecular responses and developmental success in coral larvae. *Aquat. Toxicol.* 198, 165–174. doi: 10.1016/j.aquatox.2018.03.008

Pfeifer, M. T., Koepke, P., and Reuder, J. (2006). Effects of altitude and aerosol on UV radiation. *J. Geophys. Res. Atmos.* 111:D01203.

Prakash, P. J., Stenchikov, G., Kalenderski, S., Osipov, S., and Bangalath, H. (2015). The impact of dust storms on the Arabian Peninsula and the Red Sea. *Atmos. Chem. Phys.* 15, 199–222. doi: 10.5194/acp-15-199-2015

Raitsos, D. E., Hoteit, I., Prihartato, P. K., Chronis, T., Triantafyllou, G., and Abualnaja, Y. (2011). Abrupt warming of the Red Sea. *Geophys. Res. Lett.* 38:L14601.

Raitsos, D. E., Pradhan, Y., Brewin, R. J., Stenchikov, G., and Hoteit, I. (2013). Remote sensing the phytoplankton seasonal succession of the Red Sea. *PLoS One* 8:e64909. doi: 10.1371/journal.pone.0064909

Rhein, M., Rintoul, S. R., Aoki, S., Campos, E., Chambers, D., Feely, R. A., et al. (2013). "Observations: ocean," in *Climate Change 2013: The Physical Science Basis. Contribution of Working Group I to the Fifth Assessment Report of the Intergovernmental Panel on Climate Change*, eds T. F. Stocker, D. Qin, G.-K. Plattner, M. Tignor, S. K. Allen, J. Boschung, et al. (Cambridge: Cambridge University Press).

Richter, C., Wunsch, M., Rasheed, M., Kotter, I., and Badran, M. I. (2001). Endoscopic exploration of Red Sea coral reefs reveals dense populations of cavity-dwelling sponges. *Nature* 413, 726–730. doi: 10.1038/35099547

Romera-Castillo, C., Alvarez-Salgado, X. A., Gali, M., Gasol, J. M., and Marrase, C. (2013). Combined effect of light exposure and microbial activity on distinct dissolved organic matter pools. A seasonal field study in an oligotrophic coastal system (Blanes Bay, NW Mediterranean). *Mar. Chem.* 148, 44–51. doi: 10.1016/j.marchem.2012.10.004

Schweikert, K., Sutherland, J. E. S., Hurd, C. L., and Burritt, D. J. (2011). UV-B radiation induces changes in polyamine metabolism in the red seaweed Porphyra cinnamomea. *Plant Growth Regul.* 65, 389–399. doi: 10.1111/jpy.12166

Sempere, R., Para, J., Tedetti, M., Charriere, B., and Mallet, M. (2015). Variability of solar radiation and CDOM in surface coastal waters of the northwestern mediterranean sea. *Photochem. Photobiol.* 91, 851–861. doi: 10.1111/php.12434

Setlow, R. B. (1974). The wavelengths in sunlight effective in producing skin cancer: a theoretical analysis. *Proc. Natl. Acad. Sci. U.S.A.* 71, 3363–3366. doi: 10.1073/pnas.71.9.3363

Shi, K. P., Yu, J., Liu, C. Y., Xu, Z. M., and Tang, X. X. (2017). Impacts of enhanced UVB radiation on photosynthetic characteristics of the marine diatom *Phaeodactylum tricornutum* (Bacillariophyceae, Heterokontophyta). *J. Appl. Phycol.* 29, 1287–1296. doi: 10.1007/s10811-017-1067-9

Shick, J. M., Dunlap, W. C., Chalker, B. E., Banaszak, A. T., and Rosenzweig, T. K. (1992). Survey of ultraviolet radiation-absorbing mycosporine-like amino-acids in organs of coral-reef holothuroids. *Mar. Ecol. Prog. Ser.* 90, 139–148. doi: 10.3354/meps090139

Smith, R. C., and Baker, K. S. (1989). Stratospheric ozone, middle ultraviolet radiation and phytoplankton productivity. *Oceanography* 2, 4–10. doi: 10.5670/oceanog.1989.01

Smyth, T. J. (2011). Penetration of UV irradiance into the global ocean. *J. Geophys. Res. Oceans* 116:C11020.

Sofianos, S. S., and Johns, W. E. (2002). An oceanic general circulation model (OGCM) investigation of the Red Sea circulation, 1. Exchange between the Red Sea and the Indian Ocean. *J. Geophys. Res. Oceans* 107:3196.

Stambler, N. (2005). Bio-optical properties of the northern Red Sea and the Gulf of Eilat (Aqaba) during winter 1999. *J. Sea Res.* 54, 186–203. doi: 10.1016/j.seares.2005.04.006

Tedetti, M., and Sempere, R. (2006). Penetration of ultraviolet radiation in the marine environment. A review. *Photochem. Photobiol.* 82, 389–397.

Tedetti, M., Sempere, R., Vasilkov, A., Charriere, B., Nerini, D., Miller, W. L., et al. (2007). High penetration of ultraviolet radiation in the south east Pacific waters. *Geophys. Res. Lett.* 34:L12610. doi: 10.1029/2007GL029823

Torregiani, J. H., and Lesser, M. P. (2007). The effects of short-term exposures to ultraviolet radiation in the Hawaiian coral Montipora verrucosa. *J. Exp. Mar. Biol. Ecol.* 340, 194–203. doi: 10.1016/j.jembe.2006.09.004

Torres-Perez, J. L., and Armstrong, R. A. (2012). Effects of UV radiation on the growth, photosynthetic and photoprotective components, and reproduction of the Caribbean shallow-water coral Porites furcata. *Coral Reefs* 31, 1077–1091. doi: 10.1007/s00338-012-0927-7

van de Poll, W. H., Eggert, A., Buma, A. G. J., and Breeman, A. M. (2001). Effects of UV-B-induced DNA damage and photoinhibition on growth of temperate marine red macrophytes: habitat-related differences in UV-B tolerance. *J. Phycol.* 37, 30–37.

van Duyl, F., Gast, G., Steinhoff, W., Kloff, S., Veldhuis, M., and Bak, R. (2002). Factors influencing the short-term variation in phytoplankton composition and biomass in coral reef waters. *Coral Reefs* 21, 293–306. doi: 10.1007/s00338-002-0248-3

Wangpraseurt, D., Polerecky, L., Larkum, A. W. D., Ralph, P. J., Nielsen, D. A., Pernice, M., et al. (2014). The in situ light microenvironment of corals. *Limnol. Oceanogr.* 59, 917–926. doi: 10.4319/lo.2014.59.3.0917

Watanabe, S., Sudo, K., Nagashima, T., Takemura, T., Kawase, H., and Nozawa, T. (2011). Future projections of surface UV-B in a changing climate. *J. Geophys. Res. Atmos.* 116:D16118.

Waters, K. J., Smith, R. C., and Lewis, M. R. (1990). Avoiding ship-induced light-field perturbation in the determination of oceanic optical properties. *Oceanography* 3, 18–21.

Weinbauer, M. G., Wilhelm, S. W., Suttle, C. A., and Garza, D. R. (1997). Photoreactivation compensates for UV damage and restores infectivity to

natural marine virus communities. *Appl. Environ. Microbiol.* 63, 2200–2205. doi: 10.1128/aem.63.6.2200-2205.1997

Williamson, C. E., Zepp, R. G., Lucas, R. M., Madronich, S., Austin, A. T., Ballare, C. L., et al. (2014). Solar ultraviolet radiation in a changing climate. *Nat. Clim. Change* 4, 434–441. doi: 10.1039/c8pp90060d

Xiao, X., de Bettignies, T., Olsen, Y. S., Agusti, S., Duarte, C. M., and Wernberg, T. (2015). Sensitivity and acclimation of three canopy-forming seaweeds to UVB radiation and warming. *PLoS One* 10:e0143031. doi: 10.1371/journal.pone.0143031

Yadav, S., Prajapati, R., and Atri, N. (2016). Effects of UV-B and heavy metals on nitrogen and phosphorus metabolism in three cyanobacteria. *J. Basic Microbiol.* 56, 2–13. doi: 10.1002/jobm.201500504

Yahel, G., Post, A. F., Fabricius, K., Marie, D., Vaulot, D., and Genin, A. (1998). Phytoplankton distribution and grazing near coral reefs. *Limnol. Oceanogr.* 43, 551–563. doi: 10.4319/lo.1998.43.4.0551

Zamzow, J. P., Siebeck, U. E., Eckes, M. J., and Grutter, A. S. (2013). Ultraviolet-B wavelengths regulate changes in UV absorption of cleaner fish Labroides dimidiatus mucus. *PLoS One* 8:e78527. doi: 10.1371/journal.pone.0078527

Zeevi Ben-Yosef, D., and Benayahu, Y. (2008). Synergistic effects of UVR and temperature on the survival of azooxanthellate and zooxanthellate early developmental stages of soft corals. *Bull. Mar. Sci.* 83, 401–414.

Zeni, E. C., Ammar, D., Leal, M. L., da Silva, H. S., Allodi, S., Muller, Y. M., et al. (2015). Light-mediated DNA Repair Prevents UVB-induced Cell Cycle Arrest in Embryos of the Crustacean Macrobrachium olfersi. *Photochem. Photobiol.* 91, 869–878. doi: 10.1111/php.12457

Zepp, R. G., Shank, G. C., Stabenau, E., Patterson, K. W., Cyterski, M., Fisher, W., et al. (2008). Spatial and temporal variability of solar ultraviolet exposure of coral assemblages in the Florida Keys: importance of colored dissolved organic matter. *Limnol. Oceanogr.* 53, 1909–1922. doi: 10.4319/lo.2008.53.5.1909

Zhou, J., Fan, T. Y., Beardall, J., and Gao, K. S. (2016). Incident ultraviolet irradiances influence physiology, development and settlement of larva in the coral *Pocillopora damicornis*. *Photochem. Photobiol.* 92, 293–300. doi: 10.1111/php.12567

Conflict of Interest: The authors declare that the research was conducted in the absence of any commercial or financial relationships that could be construed as a potential conflict of interest.

frontiers in Marine Science

ORIGINAL RESEARCH
published: 19 May 2020
doi: 10.3389/fmars.2020.00343

Light in the Dark: Retrieving Underwater Irradiance in Shallow Eutrophic Waters From AC-S Measurements

Rafael Gonçalves-Araujo†* and *Stiig Markager*

Department of Bioscience, Aarhus University, Roskilde, Denmark

OPEN ACCESS

Edited by:
Patrick J. Neale, Smithsonian Environmental Research Center (SI), United States

Reviewed by:
Patrick Biber, University of Southern Mississippi, United States
Jochen Wollschläger, University of Oldenburg, Germany

***Correspondence:**
Rafael Gonçalves-Araujo
rafgo@aqua.dtu.dk; rafaelgoncalvesaraujo@gmail.com

†Present address:
Rafael Gonçalves-Araujo, National Institute of Aquatic Resources, Technical University of Denmark, Lyngby, Denmark

Specialty section:
This article was submitted to Marine Ecosystem Ecology, a section of the journal Frontiers in Marine Science

Received: *08 December 2019*
Accepted: *23 April 2020*
Published: *19 May 2020*

Citation:
Gonçalves-Araujo R and Markager S (2020) Light in the Dark: Retrieving Underwater Irradiance in Shallow Eutrophic Waters From AC-S Measurements. Front. Mar. Sci. 7:343. doi: 10.3389/fmars.2020.00343

Light is essential for primary production and, therefore, its attenuation controls the vertical distribution of plants and phytoplankton over the water column. The diffuse attenuation of irradiance (K) is mainly governed by the attenuation by the water itself and the concentrations of optically active substances (e.g., phytoplankton, inorganic particles and colored dissolved molecules), which makes it an important parameter for eutrophication monitoring. Over the past century, Denmark has had recurrent eutrophication events, with extreme episodic cases where anoxic conditions were observed. Since the 1980's, eutrophication in Danish waters has been monitored with regards to the diffuse attenuation coefficient of scalar irradiance (K_o) of photosynthetically active radiation (PAR, 400–700 nm), K_o(PAR). However, radiometric measurements in Denmark are difficult in winter due to low solar zenith angle and only few light hours. On top of that, radiometric measurements in the first meters of the water column are highly affected by light refraction influenced by waves, compromising the monitoring of shallow turbid waters as in Denmark. Therefore, we developed a semi-analytical model based on data to from a spectral AC instrument (AC-S, Sea-Bird Scientific) that can estimate the underwater light field and the diffuse attenuation coefficient of downwelling irradiance, K_d(PAR). We tested two distinct approaches based on equations from the literature for estimation of K_d(PAR). The results show that modeled PAR profiles follow the overall shape of *in situ* radiometric profiles but with smoother profiles, especially in the surface layer (2–5 m). Along with that, the method provided robust K_d(PAR) estimates, that were strongly correlated to the reference K_o(PAR) values from *in situ* profiles and with low root mean square error (RMSE). Thus, AC-S data can be used to estimate the underwater light field and K_o(PAR). This will make possible to retrieve K_o(PAR) in the absence of daylight and, therefore, allow for environmental monitoring outside the daylight hours, making environmental monitoring more efficient. In addition, the method provides valuable insights into the factors controlling light attenuation.

Keywords: bio-optics, photosynthetically active radiation, diffuse attenuation coefficient, absorption coefficient, beam attenuation, inherent optical properties

INTRODUCTION

Anthropogenic nutrient loadings from land to the marine environments is a worldwide problem (Cloern, 2001). Eutrophication and the associated negative effects for the marine environment, e.g., anoxic events, increase in light attenuation, and loss of underwater vegetation, have been observed not only in Danish marine waters, but in many places around the world (Riemann et al., 2016) and is a calling for political actions as well as systematic monitoring of the marine environment (de Jonge et al., 2006). The highest amounts of nitrogen loadings from Danish land were observed during the 80's. Then a series of political action plans were implemented to mitigate the inputs of nitrogen and phosphorous to the marine environment (Dalgaard et al., 2014; Murray et al., 2019). Eutrophication events alter, among many aspects, the underwater light regime, leading to significant changes in the structure and food web of the ecosystem and in particular the distribution of primary production among types of photo-autotrophs with important implications for the ecosystem (Krause-Jensen et al., 2012). A common pattern is that the primary production is displaced toward the surface both in shallow systems (Krause-Jensen et al., 2012) where the benthic macrophytes are replaced by phytoplankton, and in planktonic systems where production in the pycnocline is replaced by production in the mixed layer (Lyngsgaard et al., 2014). In both cases the driving factor is an increase in light attenuation (Kirk, 1994; Carstensen et al., 2013; Pedersen et al., 2014; Riemann et al., 2016). Moreover, light attenuation governs the vertical distribution of different types of macrophytes in all aquatic ecosystems from lakes (Middelboe and Markager, 1997) to the clearest marine waters (Markager and Sand-Jensen, 1992) as a response to differences in minimum light requirements for different types of plants (Markager and Sand-Jensen, 1992, 1996; Middelboe and Markager, 1997). Hence, an in-depth understanding of light attenuation is essential for our understanding of aquatic ecosystems and the mechanisms in eutrophication.

Since transparency is a key property in aquatic ecosystems, and a consequence of eutrophication is an increase in light attenuation due to increasing amounts of particles and colored dissolved organic matter (CDOM), light attenuation has been an important component of eutrophication monitoring. For instance, Secchi disk depth measurements have been widely used in the Baltic Sea as an eutrophication proxy, water quality assessment and management (Fleming-Lehtinen and Laamanen, 2012; Dupont and Aksnes, 2013; Harvey et al., 2019). The light attenuation is often expressed as Secchi disc readings or as the diffuse attenuation coefficient (K) of scalar (K_o) or downwelling irradiance (K_d) at a given wavelength [$K_o(\lambda)$ or $K_d(\lambda)$] or over the PAR range [K_o(PAR) or K_d(PAR)] (Kirk, 1994). K is an apparent optical property (AOP) and therefore determined by the interactions between the inherent optical properties (IOPs, i.e., absorption and scattering), the solar zenith angle and sky and sea state conditions. K_d and K_o estimations and their partitioning into distinct components (with varying target wavelengths, e.g., 490 nm, PAR and spectrally resolved) have been the subject of several previous studies applying various empirical and semi-analytical approaches to a diversity of input variables: *in situ* IOP measurements (Lund-Hansen, 2004; Pierson et al., 2008; Devlin et al., 2009; Simon and Shanmugam, 2013; Murray et al., 2015; Rose et al., 2019), ocean color remote sensing data (Wang et al., 2009; Zhang et al., 2012a; Barnes et al., 2014; Alikas et al., 2015; Simon and Shanmugam, 2016), Secchi disc depth (Bracchini et al., 2009; Zhang et al., 2012b) and neural network inversion (Jamet et al., 2012). K_d(PAR) is also a key variable for estimating the ocean's heat budget (Lewis et al., 1990; Kowalczuk et al., 2017; Soppa et al., 2019), and is fundamental for assessing water quality, eutrophication and ecosystem function assessment (Krause-Jensen et al., 2012; Carstensen et al., 2013; Murray et al., 2019) and, ultimately, for ecosystem modeling (Maar et al., 2011; Byun et al., 2014; Neumann et al., 2015). For instance, in coastal areas, sensitive species such as the eelgrass (*Z. marina*) has considerable ecological importance and promptly respond to eutrophication pressures, due to light limitation. Therefore, this species has become an important parameter for assessing ecological status of marine systems not only in the Baltic region (Orth et al., 2010; Fertig et al., 2013), as their depth limit is closely related to water transparency and light penetration in the water column (Nielsen et al., 2002; Balsby et al., 2013), which is then related to K_d(PAR). Thus, it is essential to develop alternative methods to estimate K_d(PAR) in temperate areas, given the limitations faced for performing traditional PAR measurements due to the low solar angle and short day length during winter.

The waters surrounding Denmark have been monitored for environmental properties since the 1980's. A national program was launched in 1987 (NOVANA, *National Monitoring and Assessment Programme for the Aquatic and Terrestrial Environment*) as part of the Danish Action Plan on the Aquatic Environment. Its main objective is to follow the status of the aquatic and terrestrial environments and the main pressures upon them (Friberg et al., 2005). The program has established time series for many parameters that have been consistently sampled since its start. The NOVANA program was implemented when nutrient loadings to the marine environment were high and, with the strategies adopted, nutrient input has been reduced over the past decades (Dalgaard et al., 2014; Riemann et al., 2016; Murray et al., 2019). Early Secchi disk measurements date to1905 in the Baltic (Fleming-Lehtinen and Laamanen, 2012) and water transparency from about 1900 has been deduced from old observations of depth limits of eelgrass (*Zostera marina*). Vertical profiles of PAR have been measured in the NOVANA monitoring program since late 1980's. As established in the monitoring program protocol (Markager and Fossing, 2015), PAR measurements and estimation of K_o(PAR) are the standard method for monitoring of the underwater light field within the program. Sampling for bio-optical properties (particularly radiometric measurements) in temperate regions like the Baltic (∼55 to 65°N) is nevertheless challenging, given several factors: (1) due to the high latitude, the solar zenith angle is often low; (2) there is a high frequency of overcast days making the use of satellite observations difficult; (3) the day length is short close to the winter solstice causing low efficiency for ship based sampling; (4) the waters are often shallow and turbid, which affects the

performance of radiometers. Therefore, it is beneficial to develop alternative approaches for estimating light attenuation regardless of sky and weather conditions and in darkness. The light attenuation coefficient is used for two purposes. One is to allow the calculation of PAR at specific depth, e.g., the daily integrated PAR at the sea floor. The other purpose is to use it as an indicator for the environmental state that can be followed over time. This study is part of a general attempt to improve the NOVANA program by employing new technologies for monitoring water quality. We believe that there is a worldwide need to optimize environmental monitoring since eutrophication is a widespread phenomenon and changes in marine environments are linked to other pressure factors such as climate change. Therefore, a first step toward an automated, sensor-based monitoring was the incorporation of an AC-S instrument to the sampling program in 2017. The future perspective in the program is to use the AC-S for monitoring other environmental parameters such as chlorophyll (that can also be derived from the absorption line height), CDOM absorption and to relate scattering to concentrations of particles (e.g., total suspended matter–TSM).

Given the limitations presented above regarding sampling daylight irradiance in Denmark and the interests toward the implementation of state-of-the-art sensor based sampling, the main objective of this study is to develop a semi-analytical model that can retrieve K_d(PAR) from the spectrally resolved underwater light field derived from IOP measurements acquired with an AC-S instrument and assess whether the estimated K_d(PAR) is a good proxy for the K_o(PAR) consistently monitored within the NOVANA program.

MATERIALS AND METHODS

Sampling Strategy and Measurements of Hydrographic Properties, Chlorophyll-a Fluorescence and Underwater Irradiance

86 sampling stations in the waters surrounding the island of Fyn (Denmark) were visited in the autumn 2017 (Oct. 17th –Nov. 1st) and spring 2019 (Apr. 25th–May 6th). However, after data quality control, only 48 sampling stations presented reasonable data with respect to all the considered parameters (**Figure 1**). The sampling comprised a range of stations from very shallow coastal sites with local depth of about 3 m to deeper areas reaching bottom depths of 40 m. At each station, vertical profiles of physico-chemical and bio-optical water properties were acquired by deploying several sensors attached to a CTD frame. The CTD-frame was equipped with sensors for conductivity (AMT, Analysemesstechnik GmbH), temperature (AMT, Analysemesstechnik GmbH), PAR (Biospherical Instruments Inc.) and chlorophyll-*a* (Chl-*a*) fluorescence (ECO, Sea-Bird Scientific). Sensors for conductivity and temperature were calibrated every second week (accuracy of ± 1 and 0.1°C; precision of ± 0.05 and 0.05°C, for salinity and temperature, respectively) and annually on the factory. The signal for chlorophyll fluorescence was converted to a chlorophyll concentration based on water samples from 1, 5, 10, to 15 m from each profile according (Lyngsgaard et al., 2014). The profiles of temperature, salinity and Chl-a were median binned to a 0.2-m vertical resolution. Underwater scalar irradiance profiles (E_o) in the PAR range [E_o(PAR),%] were measured with a spherical PAR sensor (Biospherical Instruments Inc.) placed on the CTD frame and expressed as percentage of the readings of a surface reference sensor on top of the vessel. It will hereafter be referred to as PAR-CTD. The PAR-CTD sensor was placed on the very top of the CTD frame. After processing, profiles for all variables were median binned and presented in the same vertical resolution, i.e., 0.2 m. The PAR profiles were then visually quality controlled, and any noisy profiles were not taken into consideration for this study. An additional sampling survey was conducted on Jun. 13th, 2019 with the purpose of spectral validation of the model for underwater light field based on the AC-S measurements. On that occasion, spectrally resolved radiometric measurements were performed at five stations. Profiles of downwelling irradiance (E_d, W m^{-2} nm^{-1}) were obtained with a Satlantic free-falling optical profiler (Sea-Bird Scientific) equipped with hyperspectral up- and downwelling radiometers (350–800 nm). Another hyperspectral radiometer was placed on top of the vessel and used as reference. PAR-Sat was obtained by integrating the E_d spectra over the PAR wavelength range (400–700 nm). At each station, four to eight profiles were sampled ensuring that the profiler was at least 15 m away from the boat. After visual inspection, the best PAR-Sat profile (i.e., with less noise) was considered. Data was then processed and interpolated at a 0.2 m vertical resolution using the ProSoft software (Sea-Bird Scientific, version 7.7).

AC-S Measurements

A 25 cm-path length AC-S spectrophotometer (Sea-Bird Scientific) was mounted on the CTD frame to measure the hyperspectral absorption [$a(\lambda)$, m^{-1}] and beam attenuation [$c(\lambda)$, m^{-1}] coefficients in the water pumped through the cuvettes with the aid of a pump installed in the frame. Measurements were performed for 83 individual channels over a spectral range of 400–740 nm with ∼4 nm increments. The measurements were recorded with a sampling rate of 4 Hz, with an acquisition of ca. 40–45 measurements per meter. The instrument was cleaned with Milli-Q water daily, after sampling, and calibrated with Milli-Q water daily, prior to the start of the measurements. AC-S data were 0.2-m median binned (set of 9 measurements centered at the target depth) and measurements out of the ± 2 standard deviation-interval were removed. Profiles with sparse data over the water column were not taken into consideration for this study. The absorption and scattering spectra of pure water were accounted while processing the AC-S data (Pope and Fry, 1997; Zhang et al., 2009), and the data was corrected for temperature and salinity dependence by the water itself (Sullivan et al., 2006) as well as for proportional scatter (Zaneveld et al., 1994). $a(\lambda)$ and $c(\lambda)$ were interpolated to common wavelengths and scattering coefficient values [$b(\lambda)$, m^{-1}] were obtained by subtracting $a(\lambda)$ from $c(\lambda)$. In this study, apart from reporting spectra from the analyzed parameters, we also report *a*, *b,* and *c* results at the blue range, 440 nm, given its application to bio-optics and ocean color

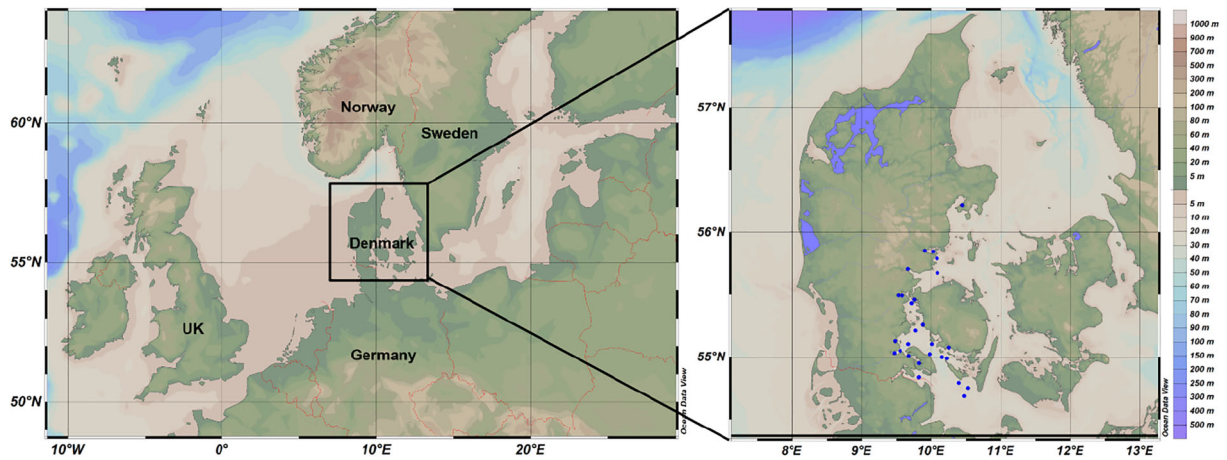

FIGURE 1 | Sampling stations of the NOVANA monitoring program considered in this study (autumn 2017 and spring 2019).

remote sensing (Prieur and Sathyendranath, 1981; IOCCG, 2006; Gonçalves-Araujo et al., 2018, 2019).

Retrieval of Underwater Irradiance From AC-S Measurements

The spectral measurements of $a(\lambda)$ and $b(\lambda)$ were used to estimate the profiles of $K_d(\lambda,z)$ over the layer extended from the surface to the depth where irradiance values measured with the PAR-meter were reduced to 1%. $K_d(\lambda,z)$ (m^{-1}). Two methods were applied. First the equation by Kirk was used (Kirk, 1994, 2003):

$$K_d(\lambda, z) = [a(\lambda, z)^2 + G \times a(\lambda, z) \times b(\lambda, z)]^{1/2} \quad (1)$$

where G is the coefficient representing the relative contribution of scattering to the vertical attenuation of irradiance. In this study we used a constant value of $G = 0.256$ (Kirk, 1994). Secondly, $K_d(\lambda,z)$ was obtained by applying a semi-analytical model of light attenuation based on the radiative transfer equation, where $K_d(\lambda,z)$ is estimated for the depth where the downward irradiance is reduced to 10% of that penetrating the surface (Lee et al., 2005):

$$K_d(\lambda, z) = (1 + 0.005Q_a) \times a_{total}(\lambda, z) + 4.18\times$$
$$(1 - 0.52e^{-10.8a_{total}(\lambda,z)}) \times b_b(\lambda, z) \quad (2)$$

where Q_a is the solar zenith angle (in degrees), a_{total} is the total absorption coefficient ($a + a_{water}$) and b_b is the backscattering. We approximated $b_b(\lambda,z)$ by applying the averaged b_b:b ratio of 0.0138 (Loisel et al., 2007) to $b(\lambda,z)$. Although water also contributes to b_b, it was not incorporated to our calculations since it is often negligible in coastal waters (Morel, 1974).

$K_d(\lambda,z)$ was then used to calculated the light spectra with depth by applying AC-S-derived $K_d(\lambda)$ values to a surface irradiance spectrum representing the averaged surface irradiance [$E_d(\lambda, 0)$ (W m^{-2} nm^{-1})] for Denmark (Markager, unpubl. results). The spectrally resolved underwater irradiance at a given depth [$E_d(\lambda, z)$] was approximated as follows (Kirk, 1994, 2003):

$$E_d(\lambda, z) = E_d(\lambda, 0) \times e^{-z \times k_d(\lambda)} \quad (3)$$

where z is depth. $E_d(\lambda,z)$ spectra were integrated over the PAR range (400–700 nm). In this way we obtain depth profiles of the PAR irradiance based on AC-S measurements, hereafter referred to as PAR-Kirk and PAR-Lee, for the spectra calculated using K_d values generated with (Equations 1and 2), respectively. The profile of these PAR-values with depth contain the same features as those recorded with a PAR sensor, e.g., a spectral narrowing that caused a decrease in K_d with depth. The approach therefore allows a direct comparison of the two methods. **Figure 2** presents a schematic description of the steps in the data analysis and computing routines implemented in this study.

K(PAR) Estimation and Statistical Analyses

The methods described in the section above give us a set of $K_d(\lambda)$ spectra. However, our main purpose is to quantify our ability to predict K_o(PAR) as estimated from depth profiles of PAR irradiance, as this is the standard method in monitoring and biological oceanography. For this, it is usually assumed that K_o(PAR) is constant with depth, despite several factors that can cause K_o(PAR) to change with depth: for instance, that the light spectrum will change with depth toward the wavelengths with low $K(\lambda)$-values (Morel, 1988), and that the average zenith angle for photons varies with depth due to and changes in the balance between scattering and absorption with depth and to changes in concentrations of optically active compounds. K(PAR) (m^{-1}) over the water column was determined from the slope in a linear regression between depth and the natural logarithm transformed PAR values after a visual inspection of each profile. This approach was employed to all PAR profiles analyzed in this study (e.g., PAR-CTD, PAR-ACS and PAR-Sat). Additionally, since in this study we have estimated E_d(PAR) with two methods (Kirk vs. Lee), the subsequent K_d(PAR) estimates will be hereafter referred to as K_d-Kirk and K_d-Lee, respectively.

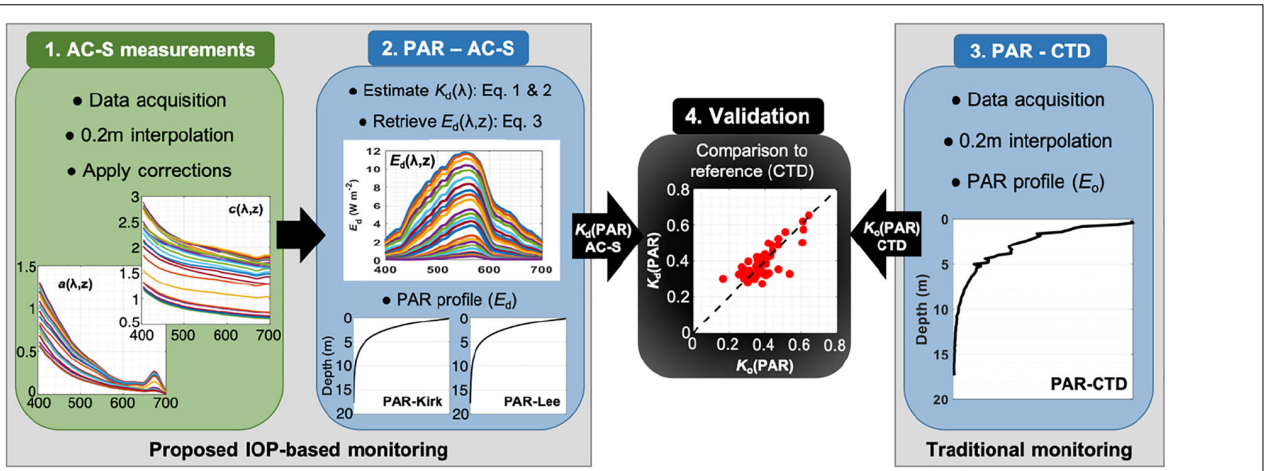

FIGURE 2 | Scheme showing the routine employed in this study. First, we retrieved the underwater light field and the diffuse attenuation coefficient for downwelling irradiance in the PAR range [K_d(PAR), 400–700 nm] from AC-S measurements with a spectrally resolved semi-analytical model. Then we calculate the scalar K_o(PAR) from the light profile (reference observations). Finally, the AC-S based K_d-values were validated against the reference K_o(PAR)-values.

When performing field measurements of E_o(PAR), values close to the surface were sometimes noisy likely due to the light refraction from wave action and movements of the ship. The upper most values (varying from 0 to 2 m) were, therefore, omitted, following the standard protocol for the monitoring program (Markager and Fossing, 2015 [in Danish]). Similarly, at greater depths, the changes with depth would decrease and approach the dark current signal when the sensor reach its detection limit. Thus, the depth interval with a log-linear profile of irradiance was selected from inter-active plots and based on the monitoring program protocol (Markager and Fossing, 2015 [in Danish]) and common practice in biological oceanography and limnology (Kirk, 1994; Markager and Vincent, 2000). Since our objective is to estimate comparable K(PAR) derived from PAR profiles obtained with different methodologies, we have employed the same routine established in the monitoring program. We are aware that more advanced techniques for calculating K_d are available (Murray, 2015; Murray et al., 2015; Holding et al., 2019), but these are more difficult to use and not yet implemented in the monitoring program. In addition to the averaged K(PAR) estimated over the entire water column (excluding the very surface data) and in order to check the variability of K(PAR) over the water column, we have estimated the apparent K(PAR). This parameter was similarly estimated by deriving the slope in a linear regression between depth and the natural logarithm transformed E_o(PAR) and E_d(PAR), considering a 1-m window interval over the water column.

We acknowledge that PAR-CTD and both PAR-Kirk and PAR-Lee do not represent the same quantities, as the former is expressed in quantum units whereas latter is in energy units. The relative depth profiles of these two quantities can be slightly different, which may lead to differences in K_d estimates. Since those differences are generally small (Thimijan and Heins, 1983), here we directly compare K_o(PAR) estimated from the CTD measurements with K_d(PAR), estimated from either measured or modeled irradiance.

The relationship between the modeled K_d(PAR)-values and the measured K_o(PAR)-values were evaluated with orthogonal linear regression to determine the slope (S), intercept, the coefficient of correlation (r) and p-value. The root mean square error (RMSE) was also calculated to assess the performance of modeled K_d(PAR):

$$RMSE = \sqrt{\frac{\sum_{n=1}^{N}[\log_{10} Y - \log_{10} X]^2}{N}} \quad (4)$$

where Y is the modeled K_d(PAR) (i.e., K_d-Kirk and K_d-Lee) and X is the measured K_o. Finally, to compare the variables among themselves or among different groups of samples, two-sample Kolmogorov–Smirnov tests were applied, after performing normality tests.

RESULTS

Water Column Structure and Biogeochemical Parameters

The water column was generally characterized by a shallow mixed layer with the presence of marked pycnocline observed at 3–15 m depth, except for the shallowest stations (bottom depth < 5 m) that presented well-mixed thermohaline profiles. Surface Chl-*a* concentration ranged from 4.1 to 12.1 mg m^{-3}, with the highest values observed within the upper mixed layer, where no marked sub-surface peak was observed.

Surface values of a(440), b(440), and c(440) varied between 0.35–0.91 m^{-1}, 0.26–1.49 m^{-1}, and 0.68–2.38 m^{-1}, respectively. For the three parameters, the highest values occurred at shallow stations with high turbidity, probably due to resuspension. Those parameters were constant over the upper mixed layer and then decreasing from the pycnocline and toward the bottom, with similar behavior as presented by Chl-*a*. However, for some stations a(440), b(440), and c(440) tend to increase near the

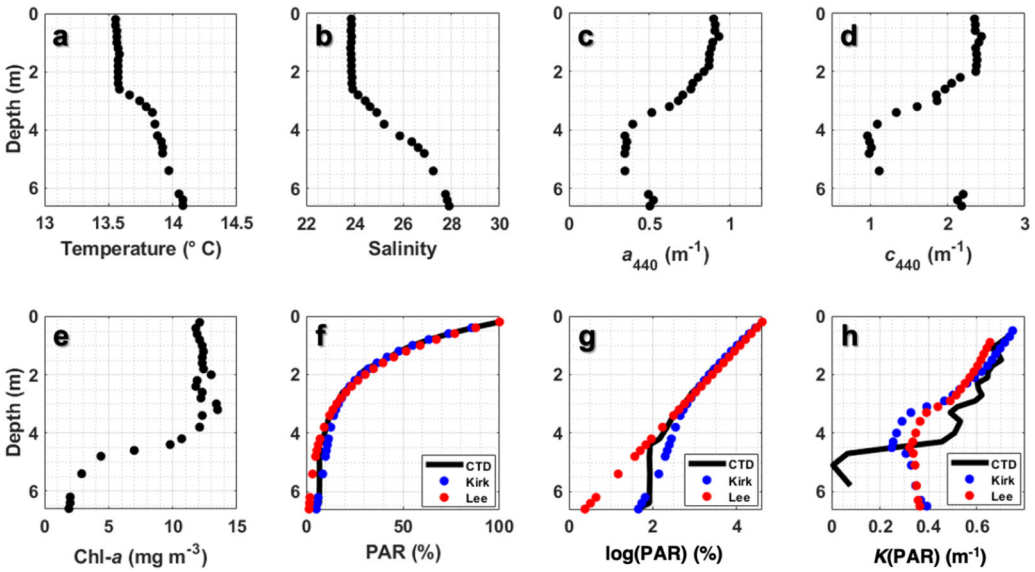

FIGURE 3 | Example of vertical profiles of environmental parameters for a shallow sampling station (number 2) visited on 19 Oct. 2017: **(a)** temperature (°C); **(b)** salinity; **(c)** a_{440} (m^{-1}); **(d)** c_{440} (m^{-1}); **(e)** Chl-a fluorescence (mg m^{-3}); **(f)** PAR (%); **(g)** log(PAR); **(h)** apparent K (m^{-1}) obtained for every 1-m interval.

bottom, most likely due to resuspension of sediments from the seabed (**Figure 3**). $a(440)$ at the surface was directly correlated with surface Chl-*a* ($r = 0.50$; $p < 0.001$).

Representation of Underwater Light Field

We compared the four profiles for PAR (PAR-CTD, PAR-Sat, PAR-Kirk and PAR-Lee). All four methods gave the expected exponential decrease for PAR (**Figures 3**,**4**). The Satlantic and the CTD-PAR measurements were very similar, however, both types were sometimes affected by practical problems close to the surface (**Figure 4**). The PAR-CTD measurements become noisy if the boat is pitching or rocking and these movements are transferred to the CTD-frame (**Figure 4E**). The relative effect of this is highest close to the surface. The Satlantic instrument is free falling and therefore not affected by this problem. However, both types of measurements can be affected by the shadow of the boat close to the surface (**Figures 4A,B**), despite attempts to avoid this, particularly if the sun and wind or current are coming from the same direction. On top of that, the fluctuations of downwelling irradiance observed at near-surface depths may also be due to the focusing of sunlight by wind-driven surface waves, which is a natural phenomenon inherent to *in situ* radiometric measurements (You et al., 2010). However, it is not possible to assure what were the factors driving the variability observed in our study.

At depth, the results show the clear advantages of the AC-S measurements. **Figure 3f** and particularly **Figure 3g** show that the CTD-PAR data become noisy at 3.5 m depth and stop working at 4 m as the irradiance falls below the sensitivity of the sensor. On the other hand, the estimates based on the AC-S measurements continue to provide results for K_d, albeit the two methods begin to deviate. Similar limitations for CTD-PAR measurements at seen at **Figures 5d–f**. Thus, the AC-S measurements were capable of recoding the increase in K_d close to the bottom based on the increase in both *a* and *c* values. That increase in suspended material content has direct impact on the underwater light attenuation, should there be light available, and that was not detected by the PAR-CTD measurements (**Figure 3g**).

Another aspect of the underwater light field is the spectral shape, which was validated here by comparing the AC-S data with data from the Satlantic profiler in June 2019. Overall, the spectra are similar with high attenuation for high and low wavelengths within the PAR-spectrum and a minimum $K_d(\lambda)$-value at ca. 570 nm. For these five profiles the two models, AC-S Kirk and AC-S Lee, gave very similar results. The most notable difference was between the modeled spectra and the data from the Satlantic profiler in both ends of the spectrum. Here the Satlantic profiler gave $K_d(\lambda)$-values that were systematically lower than the models (**Figures 6e,f**).

K_d(PAR) Estimations

Our estimations of K_o(PAR), K_d(PAR)-Kirk and K_d(PAR)-Lee ranged from 0.21–0.62 m^{-1}, 0.20–0.52 m^{-1}, to 0.27–0.65 m^{-1}, respectively (**Table 1** and **Figure 7**). K(PAR) values were significantly higher at shallow stations ($p < 0.01$) with the highest $a(\lambda)$ and $c(\lambda)$ values and, therefore, indicating the highest turbidity. The AC-S derived K_d(PAR) estimates (K_d-Kirk and K_d-Lee) were strongly, significantly correlated to the reference, K_o (**Table 1** and **Figure 7**), thus denoting the efficiency of the approach to retrieve underwater light conditions. Additionally, K_d-Kirk and K_d-Lee could detect increase in K_d at close to the bottom due to sediment resuspension, which was not observed in K_o (**Figure 3h**). Although both K_d-Kirk and K_d-Lee were in good agreement with K_o estimates, there were differences in their

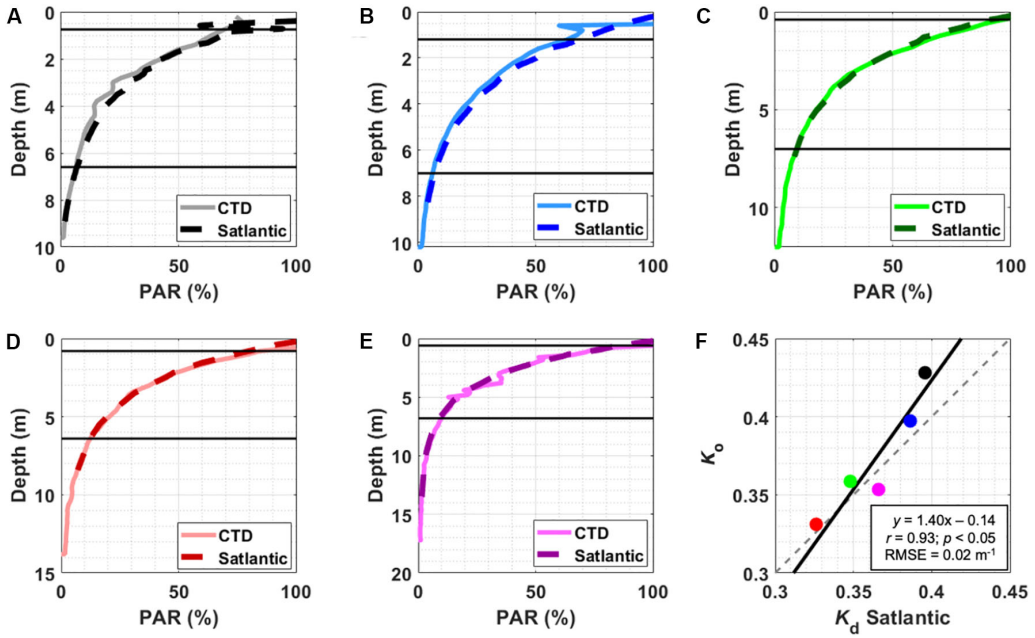

FIGURE 4 | (A–E) Profiles of PAR (%) acquired with the PAR-meter (CTD) and a free-falling optical profiler (Satlantic) for the 5 stations visited during the calibration exercise on Jun. 13th, 2019. Black horizontal lines indicate the depth limits considered for estimating K_d(PAR) for each station. **(F)** Scatter plot of K_d(PAR)-Sat vs. K_o(PAR)-CTD (m^{-1}); solid black line shows the orthogonal linear regression fit and the dashed gray line indicates the 1:1 line.

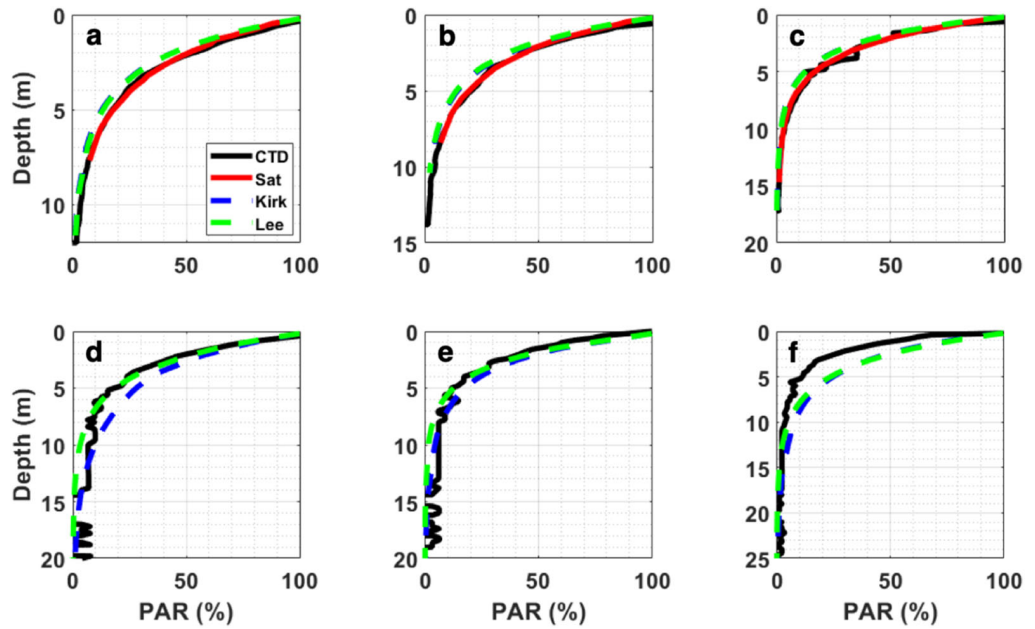

FIGURE 5 | Examples of profiles of *in situ* measured [PAR-CTD **(a–f)** and PAR-Sat **(a–c)**, the latter available only for measurements performed during the calibration exercise in June 2019] and AC-S-derived PAR [PAR-Kirk **(a–f)** and PAR-Lee **(a–f)**] for selected sampling stations.

relationship to K_o estimates. While K_d-Kirk presented a slope close to 1 for its correlation with K_o, it showed a systematic underestimation. K_d-Lee estimates were overall closer to the 1:1 line and presented the lowest RMSE in comparison to K_d-Kirk, but the slope between K_d-Lee and K_o was less than one (**Table 1** and **Figure 7**). The underestimation of K_d by the Kirk equation could be due to a lower zenith angle than assumed in Equation (2). We computed that K_d-Kirk is, on average, 1.29 times lower than K_d-CTD, which can be translated into a difference in zenith angle of 53°, that is in agreement with the values for

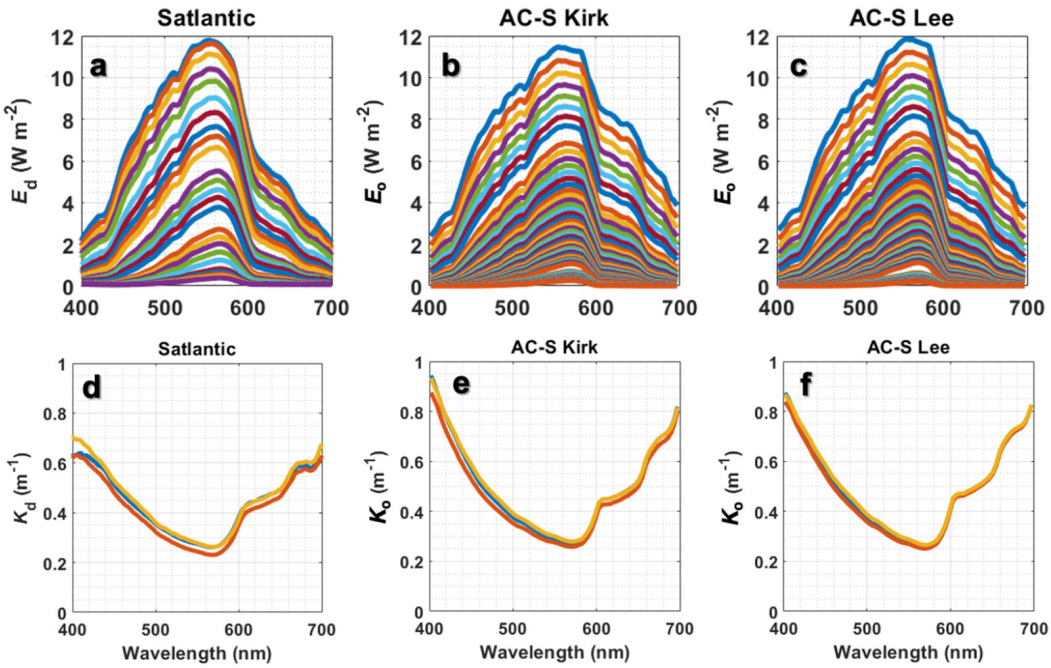

FIGURE 6 | Examples of *E* spectra over depth measured *in situ* with the free-falling Satlantic optical profiler **(a)** and estimated with Kirk's **(b)** and Lee's **(c)** methods. Examples of spectrally resolved *K* estimated from Satlantic measurements **(d)** and obtained with Kirk's **(e)** and Lee's **(f)** methods. All the examples displayed in this figure are from the same visited station on Jun. 13th, 2019. Colors in the top panels **(a–c)** represent different sampling depths, with the top lines indicating close-to-the-surface measurements and the bottom lines indicating measurements performed close to the bottom.

TABLE 1 | Mean, range, and information regarding the correlation (regression, *r*, *p*-value and RMSE) between the referred parameter and K_o for K_o, K_d-Kirk, K_d-Kirk adjusted (K_d-Kirk adj) and K_d-Lee.

Parameter	Mean (m^{-1})	Range (m^{-1})	Regression against K_d-CTD	*r*	*p*-value	RMSE (m^{-1})
K_o	0.36	0.21–0.62	–	–	–	–
K_d-Kirk	0.30	0.20–0.52	$y = 0.93x + 0.05$	0.84	<0.001	0.28
K_d-Kirk adj	0.39	0.25–0.69	$y = 1.02x + 0.02$	0.71	<0.001	0.16
K_d-Lee	0.39	0.27–0.65	$y = 0.87x + 0.05$	0.78	<0.001	0.18

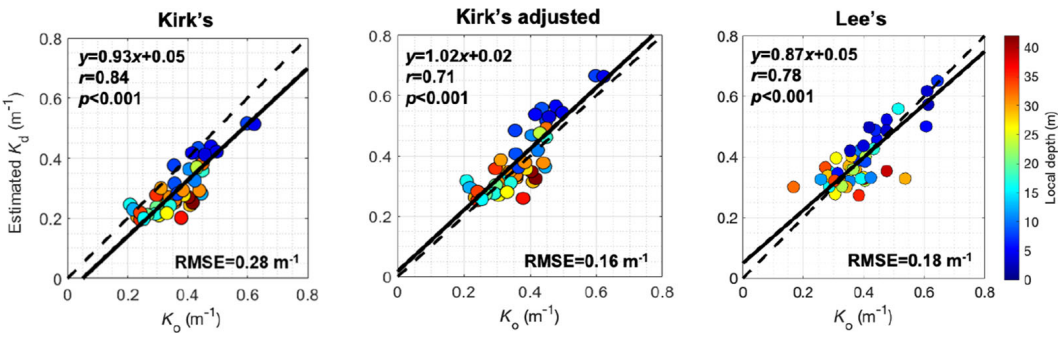

FIGURE 7 | Scatter plots between the reference (K_o) and K_d-Kirk (**Left**), and K_d-Kirk adjusted (**Center**) and K_d-Lee (**Right**) with local sampling depth as color-code.

the region (see discussion). We applied the computed correction factor of 1.29 to K_d-Kirk and observed an improvement in both slope (1.02) and RMSE (0.16 m^{-1}) (**Figure 7**). We have calculated the residuals for the correlation between estimated K_d vs. measured K_o for each method, and the residuals were correlated to environmental variables [e.g., local depth and surface temperature, salinity, a(440) and fluorescence]. There was no significant correlation observed, except for local depth that was inversely correlated to K_d-Kirk ($r = -0.36$; $p < 0.05$) and K_d-Kirk-adjusted ($r = -0.51$; $p < 0.01$).

DISCUSSION

The underwater light field in this study, described as profiles of PAR-values, was determined by two approaches: from *in situ* radiometric measurements (PAR-CTD and PAR-Sat), and from AC-S measurements (PAR-Kirk and PAR-Lee). PAR-CTD is widely used as the standard for estimating light attenuation in biological limnology and oceanography. The method has also been used in the Danish environmental monitoring program for decades and is therefore essential that new techniques are validated against this, as consistent time series are critical in environmental monitoring (Hanneke et al., 2015). In addition, the spectral shape of AC-S-derived $K_d(\lambda)$ was evaluated based on measurements with the Satlantic profiler. However, although the method here employed provides spectrally resolved information, we want to stress that our main objective to is to establish a comparison of K_o(PAR) and K_d(PAR) derived from AC-S measurements.

The measurements of $K_d(\lambda)$ with the Satlantic instrument show a good agreement with the modeled spectra for $K_d(\lambda)$ based on AC-S measurements (**Figure 6**). From 460 to 640 nm the deviation was on average 0.02 m^{-1} and positive, except from 530 to 590 nm for K_d-Lee. However, for each end of the spectra where $K_d(\lambda)$ values were high, the deviation was much higher, up to 0.3 m^{-1}. We hypothesize that the cause of this deviation lay in the Satlantic measurements and not in the modeling of $K_d(\lambda)$ from AC-S data. At depth, the ratio between irradiance at different wavelength becomes very large, e.g., 5×10^4 at the depth of 1% PAR between irradiance at 400 and 574 nm. The Satlantic instrument, as all spectral radiometers, has a limited ability to separate light at different wavelengths (straylight) so a spillover from wavelengths with low K_d (high irradiance at depth) to wavelengths with high K_d (low irradiance at depth) will occur. Such a spillover will cause an underestimation of K_d at both ends of the PAR spectrum at depth, as the observed irradiance at depth will be increasingly affected by irradiance from the middle of the spectrum. Such effects have been observed for other underwater spectroradiometers, e.g., with Li-Cor^{-1}800 underwater spectroradiometer (Markager, unpubl. results). Thus, even though the K_d spectra estimated from direct determined irradiance with the Satlantic instrument appear to be direct measurements, they might also be prone to errors. This shows the relevance and strength of the modeled $K_d(\lambda)$-values based on AC-S measurements, as they represented an alternative approach.

As PAR-meters are instruments that passively measure light, their measurements have limitations in terms of sensitivity and light availability. This is especially critical in temperate regions that have long periods with low solar angle and short day light length during winter. Combined with high attenuation in the water column, the irradiance in the first meters of water column is often close to or below the sensitivity of the instrument. This makes it challenging to do efficient environmental monitoring with radiometric-based measurements. Apart from the influence of the solar zenith angle on the performance of radiometers, surface effects from light refraction by waves-focusing and eventual shadows of the vessel may also affect radiometric measurements, particularly close to the surface, where the light attenuation tends to be the highest (Kirk, 1994; Markager and Vincent, 2000; You et al., 2010). We observed those effects in a few PAR-CTD profiles (see example in **Figure 5**) from shallow and highly turbidity stations, where, although resembling the overall exponential curve shape, a noisy profile was observed. Such noisy features in PAR-CTD profiles have been demonstrated to compromise the overall measurements, especially when those will be used for estimating the K_o (Markager and Vincent, 2000). Due to the abovementioned operational limitations, several of the PAR-CTD measurements (ca. 30%) did not pass the quality control and were discarded. Thus, to deal with the limitations associated to radiometric measurements often experienced in shallow temperate environments as the Danish waters, we propose the AC-S based alternative and IOP-based model to retrieve the underwater light field. The approach allows for monitoring light attenuation regardless of the solar conditions and even at night, thus increasing the sampling yield per unit effort (vessel time at sea).

Our estimations of K_d(PAR) were reliable and in agreement with values observed for Danish waters (Lund-Hansen, 2004), thus denoting the efficiency of the proposed approach to retrieve underwater light conditions. Such efficiency in applying IOP measurements to retrieve K_d at specific wavelengths has already been reported in the literature (Simon and Shanmugam, 2013; Alikas et al., 2015; Rose et al., 2019), however, to our knowledge, there is no previous study focusing on retrieving K_d(PAR) from a spectrally-resolved, semi-analytical model based on IOP measurements. We showed that the two methods employed in this study, K_d-Kirk and K_d-Lee, were in good agreement with K_o estimations. The K_d-Kirk approach presented the slope closest to 1 (0.93) for its correlation with K_o compared to 0.87 for the Lee model. Yet, K_d-Lee estimates presented the lowest RMSE (see **Figure 7**). The better agreement for the estimates obtained with K_d-Lee might be related to the fact that K_d-Lee takes into account the solar angle, which is considerably low in Denmark (latitude ∼55°N), especially during winter. Similar results were found by a study conducted in lakes and coastal waters in the Baltic Sea (Alikas et al., 2015), where they found Lee's method to provide better estimates compared to Kirk's method. Those authors, however, have used another extended equation for Kirk's method (Kirk, 1994):

$$K_d(\lambda) = \mu_0^{-1}[a^2 + (g_1 \times \mu_0 - g_2)a \times b]^{0.5} \quad (5)$$

where g_1 and g_2 are constants provided in Kirk (1994) and μ_0 is the cosine of the refracted solar beam just beneath the surface and was estimated as 0.88 for coastal waters in the Baltic Sea (Alikas et al., 2015). We have employed the same equation and constants to our data, however, the resulting K_d(PAR) estimates were poor in comparison to the ones obtained with (Equation 1). Therefore, we decided to present only the results obtained with (Equation 1).

Although K_d-Lee model showed the best agreement to the CTD-PAR based estimates based on the lowest RMSE-value, that method requires the measurement of $b_b(\lambda)$ that is not always available and, in our case, was retrieved from the AC-S measurements. Also, the slope was significantly different from

one whereas the K_d-Kirk model showed a slope close to one (0.93 for the original model and 1.02 for the adjusted model, **Figure 7**).

As mentioned above, we have estimated the difference between the K_d-Kirk values and K_o to a constant offset of 29%. A likely explanation for this difference is the actual zenith angle for the photons traveling down through the water. The zenith angle is affected by the combination of sun angle, cloud cover, wave conditions, refraction and the scattering of light in the water column. The latter is incorporated in Equation (1), but the others are variable and likely different from the conditions for which Kirk determined the constant in Equation (1) (Kirk, 1994). An increase of 29% for K_d will correspond to a difference in zenith angle from, e.g., ca. 35° (which is the angle observed in the region from where Kirk has derived his equation) to ca. 53° for our measurements. The zenith angle for the sun at 56° N is from 33 to 79°, but the average angle for the total irradiance is variable as mentioned above. As that actual zenith angle is variable, we conclude that applying a factor of 1.29 to the results from Equation (1) will bring the estimates in agreement with the measured values for K_o. We applied the computed correction factor of 1.29 to K_d-Kirk and observed a significant improvement in RMSE (0.16 m^{-1}) and a slope of 1.02 (see **Figure 6**). However, that factor might hold true particularly for the sampled seasons, as the solar zenith angle varies significantly over the year, particularly at high latitudes but also over the day at all latitudes. Further investigation of this subject would be helpful but since it is difficult to estimate the actual zenith angle, e.g., due to varying cloud cover and sea state, it will not help for the practical assessment of K_d estimations from AC-S measurements. At least one full annual sampling cycle would be required to establish reasonable correction factors over the seasonal cycle.

The aim of this study is to develop a method for calculating light attenuation from AC-S measurements and compare with the standard procedure. However, the comparison is hampered by the fact that the reference method has several shortcomings as outlined above. We believe that our methods (with a PAR sensor mounted on top of a CTD-frame and calculating the slope by linear regression on log-transformed data after a visual discarding of outliers) is close to the standard approach in biological limnology and oceanography. The exact protocol differ among investigators. Our irradiance data was measured with a scalar sensor and therefore, strictly speaking, we measure E_o and calculate K_o. However, as our PAR sensor was placed at the top of the frame and therefore, to some extent, shaded from upwelling irradiance. It can be argued, that this is not the ideal approach. However, placing the scalar sensor on a stick, or otherwise prevent shading from below, is not feasible in standard biological science but must of course be addressed in bio-optical research. Similarly, the application of a single exponential attenuation for PAR is not ideal, as Lambert-Beers law does not apply to broad band attenuation, but with our aim it is critical to evaluate the use of AC-S estimates vs. the standard method for estimating light attenuation. Despite of that, our K_d(PAR) estimates were highly correlated with the reference K_o(PAR), showing the strength of applying such an approach in environmental monitoring programs.

Whilst our IOP-based model generates robust underwater irradiance and K_d(PAR) estimates, the AC-S is a sensitive instrument that presents operational limitations, especially in shallow waters, as in our study. Such limitations are, e.g., related to the presence of bubbles in the system, primarily close to the surface, making the data unsuited to use and, thus, compromising the K_d(PAR) estimations. In this study, ˜20% of the total sampled stations have had their *a* and/or *c* measurements compromised most likely by the presence of bubbles in the system and were not considered. Finally, inelastic scattering, although likely to very low (Marshall and Smith, 1990), might be a source of error to our K_d(PAR) estimations. However, we have considered it to be negligible and have not accounted for it in our calculations. Finally, we acknowledge the existence of seasonal and inter-annual variability within the IOPs and underwater light field in the region and that our model may not represent the conditions considering different seasons or time scales. To account for these dynamic changes in optical and environmental properties, future efforts should consider high frequency sampling over a full annual cycle. Nevertheless, the strength of the IOP relationships across wavelengths (**Figure 6**) gives confidence that the suggested approach will work correctly also over seasons and correctly identify K_d(PAR) in different conditions, as shown in this study.

CONCLUSION

We have employed a spectrally resolved, semi-analytical model to reconstruct the underwater light field and estimate the diffuse attenuation coefficient of downwelling photosynthetically active radiation [K_d(PAR)] for shallow Danish waters from IOP measurements performed with an AC-S instrument in an environmental monitoring program. This study shows the synergistic benefits of using data from monitoring programs applied to scientific purposes, as both academia and environmental agencies gain from the development of new technologies that can be further employed to cope with limitations faced by traditional environmental programs. Our results showed that the model was capable of reconstructing the underwater light field, generating reliable PAR profiles, which agreed (in intensity and shape) with the reference measurements. PAR profiles retrieved from AC-S measurements were smoother than the reference measurements, thus, highlighting the effectiveness of the method. Such efficiency was translated in the determination of K_d(PAR) estimates that were reliable and in agreement with the reference, K_o(PAR). In addition, we showed that AC-S measurements have significant advantages when compared to the traditional PAR measurements. Those advantages are mostly related to the fact that AC-S measurements are not affected by fluctuations in light availability and solar zenith angle, which allows us to acquire data regardless of the solar irradiance (e.g., solar zenith angle and day length, allowing for sampling even during the night) and weather conditions (e.g., overcast situations). AC-S measurements are also efficient to retrieve the underwater light field in the surface layers, given that it is not affected by light refraction exerted by waves. Additionally, we have computed K_d(PAR) estimates from AC-S

measurements with two distinct methods (Equations 1 and 2) and both methods provided reliable estimates. However, at first sight Lee's method (Lee et al., 2005) had a better performance than Kirk's method (Kirk, 1994). We attribute this to the fact that Lee's model takes into account the variability in the solar angle, which is an important factor controlling light penetration in the water, especially in higher latitude environments. As Lee's method requires the direct measurement or estimation of $b_b(\lambda)$, here we proposed a simple way to correct K_d-Kirk for the solar zenith angle through the application of a correction factor. However, more investigation is necessary to evaluate the performance of such a factor, as the solar zenith angle significantly varies across the seasons and we have only sampled during two seasons. Finally, we acknowledge the existence of a suite of different methods that could be employed to the dataset here presented, and that this study could gain from the employment of radiative transfer modeling. However, at the same time it is worth it to highlight the importance of taking advantage of performing such a study with data provided by monitoring programs. Although with the monitoring program's sampling strategy might not be the ideal for further development of the model here presented, it provides a significant amount of information to the scientific community on top of contributing to the monitoring of the environment's health.

DATA AVAILABILITY STATEMENT

The datasets generated for this study are available upon request to the corresponding author.

AUTHOR CONTRIBUTIONS

SM and RG-A: conceptualization, formal analysis, methodology, visualization, and writing. RG-A: data curation and validation. SM: funding acquisition and project administration.

ACKNOWLEDGMENTS

We would like to thank to the Ministry of Environment and Food in Denmark for financial support to the project. We are also indebted to the dedicated crew of the monitoring vessel LIV-II and in particular to Lars Peter Jørgensen for organizing the measurements and the maintenance of the AC-S instrument. Finally, we would like to thank E. Therese Harvey (NIVA, Denmark) and Yangyang Liu (AWI, Germany) for discussions and their help with AC-S data processing.

REFERENCES

Alikas, K., Kratzer, S., Reinart, A., Kauer, T., and Paavel, B. (2015). Robust remote sensing algorithms to derive the diffuse attenuation coefficient for lakes and coastal waters. *Limnol. Oceanogr. Methods* 13, 402–415. doi: 10.1002/lom3.10033

Balsby, T. J. S., Carstensen, J., and Krause-Jensen, D. (2013). Sources of uncertainty in estimation of eelgrass depth limits. *Hydrobiologia* 704, 311–323. doi: 10.1007/s10750-012-1374-1378

Barnes, B. B., Hu, C., Cannizzaro, J. P., Craig, S. E., Hallock, P., Jones, D. L., et al. (2014). Estimation of diffuse attenuation of ultraviolet light in optically shallow Florida Keys waters from MODIS measurements. *Remote Sens. Environ.* 140, 519–532. doi: 10.1016/j.rse.2013.09.024

Bracchini, L., Dattilo, A. M., Hull, V., Loiselle, S. A., Tognazzi, A., and Rossi, C. (2009). Modelling Upwelling Irradiance using Secchi disk depth in lake ecosystems. *J. Limnol.* 68, 83–91.

Byun, D., Wang, X. H., Hart, D. E., and Zavatarelli, M. (2014). Review of PAR parameterizations in ocean ecosystem models. *Estuar. Coast. Shelf Sci.* 151, 318–323. doi: 10.1016/j.ecss.2014.05.006

Carstensen, J., Krause-Jensen, D., Markager, S., Timmermann, K., and Windolf, J. (2013). Water clarity and eelgrass responses to nitrogen reductions in the eutrophic Skive Fjord, Denmark. *Hydrobiologia* 704, 293–309. doi: 10.1007/s10750-012-1266-y

Cloern, J. (2001). Our evolving conceptual model of the coastal eutrophication problem. *Mar. Ecol. Prog. Ser.* 210, 223–253. doi: 10.3354/meps210223

Dalgaard, T., Hansen, B., Hasler, B., Hertel, O., Hutchings, N. J., Jacobsen, B. H., et al. (2014). Policies for agricultural nitrogen management—trends, challenges and prospects for improved efficiency in Denmark. *Environ. Res. Lett.* 9:115002. doi: 10.1088/1748-9326/9/11/115002

de Jonge, V. N., Elliott, M., and Brauer, V. S. (2006). Marine monitoring: its shortcomings and mismatch with the EU Water Framework Directive's objectives. *Mar. Pollut. Bull.* 53, 5–19. doi: 10.1016/j.marpolbul.2005.11.026

Devlin, M. J., Barry, J., Mills, D. K., Gowen, R. J., Foden, J., Sivyer, D., et al. (2009). Estimating the diffuse attenuation coefficient from optically active constituents in UK marine waters. *Estuar. Coast. Shelf Sci.* 82, 73–83. doi: 10.1016/j.ecss.2008.12.015

Dupont, N., and Aksnes, D. L. (2013). Centennial changes in water clarity of the Baltic Sea and the North Sea. *Estuar. Coast. Shelf Sci.* 131, 282–289. doi: 10.1016/j.ecss.2013.08.010

Fertig, B., Kennish, M. J., and Sakowicz, G. P. (2013). Changing eelgrass (*Zostera marina* L.) characteristics in a highly eutrophic temperate coastal lagoon. *Aquat. Bot.* 104, 70–79. doi: 10.1016/j.aquabot.2012.09.004

Fleming-Lehtinen, V., and Laamanen, M. (2012). Long-term changes in Secchi depth and the role of phytoplankton in explaining light attenuation in the Baltic Sea. *Estuar. Coast. Shelf Sci.* 10, 1–10. doi: 10.1016/j.ecss.2012.02.015

Friberg, N., Baattrup-Pedersen, A., Pedersen, M. L., and Skriver, J. (2005). The New Danish Stream Monitoring Programme (Novana) – Preparing Monitoring Activities For The Water Framework Directive Era. *Environ. Monit. Assess.* 111, 27–42. doi: 10.1007/s10661-005-8038-8033

Gonçalves-Araujo, R., Rabe, B., Peeken, I., and Bracher, A. (2018). High colored dissolved organic matter (CDOM) absorption in surface waters of the central-eastern Arctic Ocean: implications for biogeochemistry and ocean color algorithms. *PLoS One* 13:e0190838. doi: 10.1371/journal.pone.0190838

Gonçalves-Araujo, R., Röttgers, R., Haraguchi, L., and Brandini, F. P. (2019). Hydrography-driven variability of optically active constituents of water in the South Brazilian Bight: biogeochemical implications. *Front. Mar. Sci.* 6:716. doi: 10.3389/fmars.2019.00716

Hanneke, B.-B., Anne, S., Francisco, M.-R., Julia, W., Pamela, W., Lynda, M. M., et al. (2015). *The Chlorophyll Case Study in the JMP NS/CS Project. Document Produced as Part of the EU project: 'Towards Joint Monitoring for the North Sea and Celtic Sea'* (ENV/PP 2012/SEA). Available online at: https://archimer.ifremer.fr/doc/00398/50911/

Harvey, E. T., Walve, J., Andersson, A., Karlson, B., and Kratzer, S. (2019). The effect of optical properties on secchi depth and implications for eutrophication management. *Front. Mar. Sci.* 5:496. doi: 10.3389/fmars.2018.00496

Holding, J. M., Markager, S., Juul-Pedersen, T., Paulsen, M. L., Møller, E. F., Meire, L., et al. (2019). Seasonal and spatial patterns of primary production in a high-latitude fjord affected by Greenland Ice Sheet run-off. *Biogeosciences* 16, 3777–3792. doi: 10.5194/bg-16-3777-2019

IOCCG (2006). *IOCCG Report number 5: Remote Sensing of Inherent Optical Properties: Fundamentals, Tests of Algorithms, and Applications*. Monterey, CA: IOCCG.

Jamet, C., Loisel, H., and Dessailly, D. (2012). Retrieval of the spectral diffuse attenuation coefficient K d (λ) in open and coastal ocean waters using a neural network inversion. *J. Geophys. Res. Ocean.* 117, 1–14. doi: 10.1029/2012JC008076

Kirk, J. T. O. (1994). *Light and Photosynthesis in Aquatic Ecosystems*. 2nd Edn. Cambridge: Cambridge University Press.

Kirk, J. T. O. (2003). The vertical attenuation of irradiance as a function of the optical properties of the water. *Limnol. Oceanogr.* 48, 9–17. doi: 10.4319/lo.2003.48.1.0009

Kowalczuk, P., Meler, J., Kauko, H. M., Pavlov, A. K., Zabłocka, M., Peeken, I., et al. (2017). Bio-optical properties of Arctic drift ice and surface waters north of Svalbard from winter to spring. *J. Geophys. Res. Ocean.* 122, 4634–4660. doi: 10.1002/2016JC012589

Krause-Jensen, D., Markager, S., and Dalsgaard, T. (2012). Benthic and pelagic primary production in different nutrient regimes. *Estuar. Coasts* 35, 527–545. doi: 10.1007/s12237-011-9443-9441

Lee, Z.-P., Du, K.-P., and Arnone, R. (2005). A model for the diffuse attenuation coefficient of downwelling irradiance. *J. Geophys. Res.* 110:C02016. doi: 10.1029/2004JC002275

Lewis, M. R., Carr, M.-E., Feldmant, G. C., Esaias, W., and McClain, C. (1990). Influence of penetrating solar radiation on the heat budget of the equatorial Pacific Ocean. *Nature* 347, 543–545.

Loisel, H., Mériaux, X., Berthon, J.-F., and Poteau, A. (2007). Investigation of the optical backscattering to scattering ratio of marine particles in relation to their biogeochemical composition in the eastern English Channel and southern North Sea. *Limnol. Oceanogr.* 52, 739–752. doi: 10.4319/lo.2007.52.2.0739

Lund-Hansen, L. C. (2004). Diffuse attenuation coefficients Kd(PAR) at the estuarine North Sea–Baltic Sea transition: time-series, partitioning, absorption, and scattering. *Estuar. Coast. Shelf Sci.* 61, 251–259. doi: 10.1016/j.ecss.2004.05.004

Lyngsgaard, M. M., Markager, S., and Richardson, K. (2014). Changes in the vertical distribution of primary production in response to land-based nitrogen loading. *Limnol. Oceanogr.* 59, 1679–1690. doi: 10.4319/lo.2014.59.5.1679

Maar, M., Møller, E. F., Larsen, J., Madsen, K. S., Wan, Z., She, J., et al. (2011). Ecosystem modelling across a salinity gradient from the North Sea to the Baltic Sea. *Ecol. Modell.* 222, 1696–1711. doi: 10.1016/j.ecolmodel.2011.03.006

Markager, S., and Fossing, H. (2015). *Lyssvaekkelse (Technical description No. M06, Version 3)*. Available online at: http://bios.au.dk/fileadmin/bioscience/Fagdatacentre/MarintFagdatacenter/TekniskeAnvisninger2011_2015/TA_M06_Lyssvaekkelse_ver3.pdf

Markager, S., and Sand-Jensen, K. (1992). Light requirements and depth zonation of marine macroalgae. *Mar. Ecol. Prog. Ser.* 88, 83–92.

Markager, S., and Sand-Jensen, K. (1996). Implications of thallus thickness for growth-irradiance relationships of marine macroalgae. *Eur. J. Phycol.* 31, 79–87. doi: 10.1080/09670269600651231

Markager, S., and Vincent, W. F. (2000). Spectral light attenuation and the absorption of UV and blue light in natural waters. *Limnol. Oceanogr.* 45, 642–650. doi: 10.4319/lo.2000.45.3.0642

Marshall, B. R., and Smith, R. C. (1990). Raman scattering and in-water ocean optical properties. *Appl. Opt.* 29:71. doi: 10.1364/AO.29.000071

Middelboe, A. L., and Markager, S. (1997). Depth limits and minimum light requirements of freshwater macrophytes. *Freshw. Biol.* 37, 553–568. doi: 10.1046/j.1365-2427.1997.00183.x

Morel, A. (1974). "Optical properties of pure water and pure seawater," in *Optical Aspects of Oceanography*, eds N. G. Jerlov and E. Steeman Nielsen (London: Academic), 1–24.

Morel, A. (1988). Optical modeling of the upper ocean in relation to its biogenous matter content (case I waters). *J. Geophys. Res.* 93, 10749–10768. doi: 10.1029/JC093iC09p10749

Murray, C., Markager, S., Stedmon, C. A., Juul-Pedersen, T., Sejr, M. K., and Bruhn, A. (2015). The influence of glacial melt water on bio-optical properties in two contrasting Greenlandic fjords. *Estuar. Coast. Shelf Sci.* 163, 72–83. doi: 10.1016/j.ecss.2015.05.041

Murray, C. J. (2015). Light attenuation in natural waters. *Appl. Opt.* 22, 649-650.

Murray, C. J., Müller-Karulis, B., Carstensen, J., Conley, D. J., Gustafsson, B. G., and Andersen, J. H. (2019). Past, present and future eutrophication status of the Baltic Sea. *Front. Mar. Sci.* 6:2. doi: 10.3389/fmars.2019.00002

Neumann, T., Siegel, H., and Gerth, M. (2015). A new radiation model for Baltic Sea ecosystem modelling. *J. Mar. Syst.* 152, 83–91. doi: 10.1016/j.jmarsys.2015.08.001

Nielsen, S. L., Sand-Jensen, K., Borum, J., and Geertz-Hansen, O. (2002). Depth colonization of eelgrass (Zostera marina) and macroalgae as determined by water transparency in Danish coastal waters. *Estuaries* 25, 1025–1032. doi: 10.1007/BF02691349

Orth, R. J., Marion, S. R., Moore, K. A., and Wilcox, D. J. (2010). Eelgrass (*Zostera marina* L.) in the Chesapeake Bay region of mid-atlantic coast of the USA: challenges in conservation and restoration. *Estuar. Coasts* 33, 139–150. doi: 10.1007/s12237-009-9234-9230

Pedersen, T. M., Sand-Jensen, K., Markager, S., and Nielsen, S. L. (2014). Optical changes in a eutrophic estuary during reduced nutrient loadings. *Estuar. Coasts* 37, 880–892. doi: 10.1007/s12237-013-9732-y

Pierson, D. C., Kratzer, S., Strömbeck, N., and Håkansson, B. (2008). Relationship between the attenuation of downwelling irradiance at 490 nm with the attenuation of PAR (400 nm–700 nm) in the Baltic Sea. *Remote Sens. Environ.* 112, 668–680. doi: 10.1016/j.rse.2007.06.009

Pope, R. M., and Fry, E. S. (1997). Absorption spectrum (380–700 nm) of pure water. II Integrating cavity measurements. *Appl. Opt.* 36:8710. doi: 10.1364/AO.36.008710

Prieur, L., and Sathyendranath, S. (1981). An optical classification of coastal and oceanic waters based on the specific spectral absorption curves of phytoplankton pigments, dissolved organic matter, and other particulate materials1. *Limnol. Oceanogr.* 26, 671–689. doi: 10.4319/lo.1981.26.4.0671

Riemann, B., Carstensen, J., Dahl, K., Fossing, H., Hansen, J. W., Jakobsen, H. H., et al. (2016). Recovery of Danish coastal ecosystems after reductions in nutrient loading: a holistic ecosystem approach. *Estuar. Coasts* 39, 82–97. doi: 10.1007/s12237-015-9980-9980

Rose, K. C., Neale, P. J., Tzortziou, M., Gallegos, C. L., and Jordan, T. E. (2019). Patterns of spectral, spatial, and long-term variability in light attenuation in an optically complex sub-estuary. *Limnol. Oceanogr.* 64, S257–S272. doi: 10.1002/lno.11005

Simon, A., and Shanmugam, P. (2013). A new model for the vertical spectral diffuse attenuation coefficient of downwelling irradiance in turbid coastal waters: validation with in situ measurements. *Opt. Express* 21:30082. doi: 10.1364/OE.21.030082

Simon, A., and Shanmugam, P. (2016). Estimation of the spectral diffuse attenuation coefficient of downwelling irradiance in inland and coastal waters from hyperspectral remote sensing data: validation with experimental data. *Int. J. Appl. Earth Obs. Geoinf.* 49, 117–125. doi: 10.1016/j.jag.2016.02.003

Soppa, M. A., Pefanis, V., Hellmann, S., Losa, S. N., Hölemann, J., Martynov, F., et al. (2019). Assessing the influence of water constituents on the radiative heating of laptev sea shelf waters. *Front. Mar. Sci.* 6:221. doi: 10.3389/fmars.2019.00221

Sullivan, J. M., Twardowski, M. S., Zaneveld, J. R. V., Moore, C. M., Barnard, A. H., Donaghay, P. L., et al. (2006). Hyperspectral temperature and salt dependencies of absorption by water and heavy water in the 400-750 nm spectral range. *Appl. Opt.* 45:5294. doi: 10.1364/AO.45.005294

Thimijan, R. W., and Heins, R. D. (1983). Photometric, radiometric, and quantum light units of measure: a review of procedures for interconversion. *Hortic. Sci.* 18, 818–822.

Wang, M., Son, S., and Harding, L. W. (2009). Retrieval of diffuse attenuation coefficient in the Chesapeake Bay and turbid ocean regions for satellite ocean color applications. *J. Geophys. Res.* 114:C10011. doi: 10.1029/2009JC005286

You, Y., Stramski, D., Darecki, M., and Kattawar, G. W. (2010). Modeling of wave-induced irradiance fluctuations at near-surface depths in the ocean: a comparison with measurements. *Appl. Opt.* 49:1041. doi: 10.1364/AO.49.001041

Zaneveld, J. R. V., Kitchen, J. C., and Moore, C. C. (1994). "Scattering error correction of reflecting-tube absorption meters," in *Proceedings of the Volume 2258, Ocean Optics XII*, ed. J. S. Jaffe Bergen, 44–55. doi: 10.1117/12.190095

Zhang, X., Hu, L., and He, M.-X. (2009). Scattering by pure seawater: effect of salinity. *Opt. Express* 17:5698. doi: 10.1364/OE.17.005698

Zhang, Y., Liu, X., Yin, Y., Wang, M., and Qin, B. (2012a). A simple optical model to estimate diffuse attenuation coefficient of photosynthetically active radiation in an extremely turbid lake from surface reflectance. *Opt. Express* 20:20482. doi: 10.1364/OE.20.020482

Zhang, Y., Liu, X., Yin, Y., Wang, M., and Qin, B. (2012b). Predicting the light attenuation coefficient through Secchi disk depth and beam attenuation coefficient in a large, shallow, freshwater lake. *Hydrobiologia* 693, 29–37. doi: 10.1007/s10750-012-1084-1082

Conflict of Interest: The authors declare that the research was conducted in the absence of any commercial or financial relationships that could be construed as a potential conflict of interest.

frontiers in Environmental Science

ORIGINAL RESEARCH
published: 17 June 2020
doi: 10.3389/fenvs.2020.00073

Habitat-Mediated Responses of Zooplankton to Decreasing Light in Two Temperate Lakes Undergoing Long-Term Browning

Craig E. Williamson, Erin P. Overholt, Rachel M. Pilla and Keiko W. Wilkins*

Global Change Limnology Laboratory, Department of Biology, Miami University, Oxford, OH, United States

OPEN ACCESS

Edited by:
Maren Striebel,
University of Oldenburg, Germany

Reviewed by:
Patrick Kelly,
Rhodes College, United States
Tedy Ozersky,
University of Minnesota Duluth, United States

***Correspondence:**
Craig E. Williamson
craig.williamson@miamioh.edu

Specialty section:
This article was submitted to Freshwater Science, a section of the journal Frontiers in Environmental Science

Received: *03 February 2020*
Accepted: *15 May 2020*
Published: *17 June 2020*

Citation:
Williamson CE, Overholt EP, Pilla RM and Wilkins KW (2020) Habitat-Mediated Responses of Zooplankton to Decreasing Light in Two Temperate Lakes Undergoing Long-Term Browning. Front. Environ. Sci. 8:73. doi: 10.3389/fenvs.2020.00073

Increases in dissolved organic matter and the consequent "browning" of some lakes in recent decades are reducing water transparency to both ultraviolet and photosynthetically active radiation with important, but poorly understood ecosystem-level consequences for zooplankton grazers. The prevailing resource-based unimodal hypothesis posits that nutrients in dissolved organic matter stimulate primary production in clear-water lakes, while shading by dissolved organic matter inhibits primary production in browner lakes, with zooplankton responses following the patterns of their food resources. Support for this hypothesis derives primarily from short-term experiments, space-for-time analyses, and modeling studies. Here we use three decades of long-term monitoring data from two temperate lakes to assess zooplankton responses to changes in not only resources (chlorophyll) as drivers of change, but also light-related habitat variables (ultraviolet and photosynthetically active radiation, surface and deep-water temperatures, deep-water dissolved oxygen, and pH). The study lakes include one clear-water lake and one browner lake, both of which have experienced long-term browning. Given that zooplankton depth distribution and body size can vary with water transparency, color, and temperature, we test for responses in not only overall zooplankton abundance, but also in vertical distribution and body size. We also examine the ability of the relationship between short-term interannual variation in the driver vs. response variables to predict long-term zooplankton trends. The primary responses of zooplankton were strong changes in abundance that varied with taxon and life history stage in response to habitat variables rather than food resources. Only two groups showed vertical distribution responses, and they trended toward deeper distributions with browning. There was no significant change in body size ratio. The directionality of the response of zooplankton abundance to interannual variability in the driver variables was consistent with those observed in the long-term trends for 33 of 80 comparisons (41%), though only three of those (4%) had statistically significant short-term interannual variability relationships. We conclude that habitat-related changes

associated with browning in lakes have important consequences for zooplankton community structure with stronger effects in clear-water lakes than in browner lakes, and that even at the whole-lake scale short-term data are generally not adequate to predict long-term responses.

Keywords: light, ultraviolet radiation, dissolved organic matter, lake browning, zooplankton, habitat, long-term trends, interannual variability

INTRODUCTION

Water clarity is changing in lakes worldwide due to anthropogenic and natural environmental factors ranging from lake ontogeny following glacial recession (Engstrom et al., 2000; Williamson et al., 2001; Sommaruga, 2015) to increases in eutrophication and browning that are related to extreme precipitation events, changes in land use, and other anthropogenic activities (Kritzberg and Ekström, 2012; Williamson et al., 2016, 2017; Kritzberg, 2017; Rose et al., 2017; Leech et al., 2018). One of the most widespread changes in water clarity is the browning of lakes due to increases in the quantity and quality (color) of terrestrially-derived dissolved organic matter (DOM, often measured as concentration of dissolved organic carbon, DOC) (Monteith et al., 2007; SanClements et al., 2012; Kritzberg, 2017; Leach et al., 2019). This browning is expected to continue into the future with climate change-related increases in precipitation and extreme storm events (Larsen et al., 2011; de Wit et al., 2016; Weyhenmeyer et al., 2016).

Two largely light-driven hypotheses, resource-, vs. habitat-based, have been used to explain changes in zooplankton consumers in response to browning (**Figure 1**). The resource-based, unimodal hypothesis argues that during browning, basal resources are the primary driver of changes in phytoplankton (Ask et al., 2009; Seekell et al., 2015a,b), zooplankton (Jones et al., 2012; Kelly et al., 2014, 2016), and fish (Finstad et al., 2014). According to this hypothesis, in clear-water lakes with low DOM (generally $< \sim 5\,mg\,C\,L^{-1}$), increases in DOM introduce nutrients that stimulate increases in primary production and consequently zooplankton production, while in lakes above this threshold the effects of DOM shading of PAR reduce primary production and consequently zooplankton production. Support for this hypothesis derives from short-term experiments, space-for-time analyses, and modeling (Solomon et al., 2015).

While nutrients and light control primary production in the resource-based hypothesis, in the habitat-based hypothesis, light alters key vertical habitat characteristics such as temperature, oxygen, and the potential for UVR damage. In addition to the direct reductions of UVR and PAR, declines in water transparency to PAR result in warmer surface waters, cooler temperatures and depleted dissolved oxygen in deep waters, and pH also increases, all of which are typical of lakes undergoing browning in northeastern North America and northern Europe (Monteith et al., 2007; Williamson et al., 2015; Strock et al., 2017). One study found that benthic consumers are more influenced by habitat changes such as oxygen depletion than by changes in resources in lakes spanning a range of DOC concentrations (Craig et al., 2015). Similarly, an analysis of ∼20 years of data on a suite of 28 Adirondack lakes that have been undergoing browning reported that changes in pelagic primary producers were more related to changes in light than to nutrients, and the responses of phytoplankton and zooplankton to browning differed from each other, reflecting a trophic decoupling rather than a resource-based response of the zooplankton directly to changes in phytoplankton (Leach et al., 2019). These studies extend earlier work that has shown the importance of light limitation of primary and secondary production with increasing DOM (Karlsson et al., 2009; Kelly et al., 2014; Thrane et al., 2014).

While it is widely recognized that browning decreases both photosynthetically active (PAR) and ultraviolet (UVR) radiation in lakes (Carpenter et al., 1998; Finstad et al., 2014; Kelly et al., 2014; Seekell et al., 2015a), the effects of decreasing UVR are rarely considered due to the lack of available instrumentation and data. Yet decreases in UVR exposure can be very pronounced during browning due to the selective absorption of shorter wavelength UVR by terrestrially-derived DOM. In seepage lakes with minimal riverine inputs, DOM is the primary regulator of water transparency to UVR, and also to PAR (Morris et al., 1995). In addition, the non-linear relationship between DOC concentration and the compensation depth (1% of subsurface PAR, the depth above which there is net photosynthesis, and below which there is net respiration) or equivalent 1% depth to which UVR penetrates (Williamson et al., 1996) causes clear, low DOC lakes to experience much stronger changes in their underwater light environment during browning than lakes with initially higher DOC concentrations (Snucins and Gunn, 2000; Read and Rose, 2013; Williamson et al., 2015). Thus in clear-water lakes even small increases in DOM strongly reduce the underwater UVR exposure levels (Williamson et al., 1996), with consequences that have the potential to alter zooplankton nutrition (Nova et al., 2019), predation (Williamson et al., 1999; Boeing et al., 2004; Leech et al., 2009; Lindholm et al., 2016), parasite loads (Overholt et al., 2012; Williamson et al., 2017), behavior (Overholt et al., 2016; Wolf and Heuschele, 2018), and vertical distribution in the water column (Leech and Williamson, 2001; Cooke et al., 2008; Fischer et al., 2015; Leach et al., 2015; Urmy et al., 2016). Here we have a unique, long-term database that includes not only well-resolved changes in PAR during browning, but also changes in UVR. This enables us to test whether substantial decreases in both PAR and UVR are, in fact, related to changes in zooplankton distribution and abundance.

Our core objective here is to investigate the effects of changes in the underwater light environment, including UVR as well as PAR, on zooplankton consumers in lakes undergoing browning. We use long-term data from Lake Giles and Lake Lacawac, two browning temperate lakes in northeastern Pennsylvania, USA,

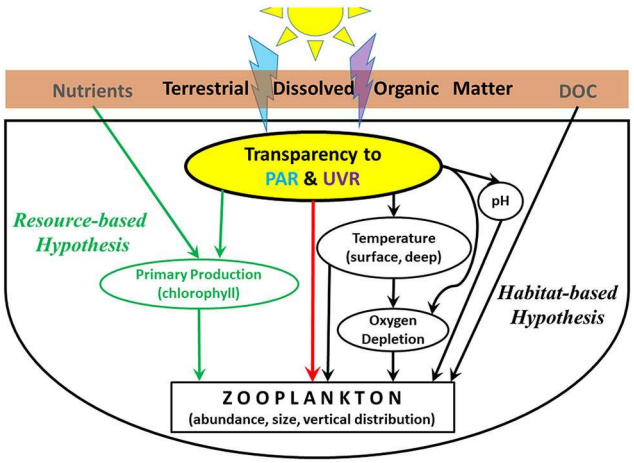

FIGURE 1 | Conceptual model of how DOM alters the underwater light environment to influence not only resources relevant to the resource-based hypothesis (green), but also many aspects of the pelagic habitat for zooplankton (black). Direct effects of PAR and UVR (e.g., vertical migration, DNA damage) are shown in red.

to test the importance of light-related drivers on zooplankton, and assess the relative importance of resource-based vs. habitat-based responses in the pelagic zone of lakes (**Figure 1**). Giles and Lacawac are both seepage lakes that have experienced long-term changes in their underwater light environments, with Giles responding more strongly to browning than Lacawac due to its initially very low DOC concentrations (Williamson et al., 2015). Here, we extend this prior study by (1) adding 5 years to the long-term data set, (2) analyzing the zooplankton data with higher taxonomic and life stage resolution, as well as with additional metrics including body size and vertical distribution since these variables have been shown to vary with water transparency, water temperature, and water color, and (3) relating changes in zooplankton to both the interannual variability (IAV) and the long-term trends (LTT) in light-related driver variables, following the approach of Leach et al. (2019). Importantly we examine whether using IAV can provide critical early insights into population- and ecosystem-level responses of zooplankton to both abiotic and biotic forcing over the long term. While short-term studies provide valuable insights into changes in lake structure and function in response to disturbance or extreme events, their ability to predict long-term responses of consumers is less certain.

METHODS

Sampling Methods

Lakes Giles and Lacawac are two small lakes in northeastern Pennsylvania, USA with surface areas of 48.0 and 21.4 hectares, maximum depths of 24 and 13 m, and mean depths of 10.1 and 5.2 m, respectively. Water samples were collected for pH, DOC, chlorophyll, and nutrient analyses from the epilimnion of both lakes using a Van Dorn sampler. Data from June, July and August were averaged to provide a single value for each year from 1988 to 2019. For measurements of DOC concentration, samples were filtered through a pre-ashed 0.7 μm glass fiber filter and analyzed with a TOC analyzer using a high temperature oxidation method. Water samples were analyzed for pH using an Orion pH meter, calibrated at 4.00 and 7.00 using commercial pH buffers. For measurements of total phosphorus, unfiltered samples were acidified using H_2SO_4, digested with a potassium persulfate solution, and analyzed using the molybdenum blue method. For measurements of soluble reactive phosphorus (SRP), samples were filtered through an A/E glass fiber filter (1 μm), acidified with H_2SO_4 and analyzed using the molybdenum blue method. Chlorophyll samples were filtered onto 1.0 μm A/E filters and immediately frozen. Extraction methods for chlorophyll varied among years, but followed standard methodologies as detailed in Williamson et al. (2015). Using a YSI temperature-oxygen meter (1988–1992) or a submersible temperature and UVR-PAR radiometer (1993–2019), epilimnetic temperature was measured at a depth of 2 m in both lakes, while hypolimnetic temperature was measured at depths of 18 m (Giles) and 10 m (Lacawac). The YSI temperature-oxygen meter was also used to measure dissolved oxygen (all years) at 1 m or greater resolution. The deep-water percent saturation of dissolved oxygen (20 m in Giles, 11 m in Lacawac) was calculated from dissolved oxygen concentration and water temperature using the "rMR" R package (Moulton, 2018). Light profiles were collected using submersible radiometers to measure attenuation of UVR (μW cm^{-2} nm^{-1} at 320 nm, with full width at half maximum bandwidth = 8 nm) and PAR (μmol $m^{-2}s^{-1}$ 400–700 nm). The radiometers used included Biospherical Instruments (BSI, San Diego, California) PUV radiometers (PAR and UVR; 1993–2003) and BSI BIC radiometers with a deck cell (PAR and UVR; 2003–2019). The depth to which 1% of subsurface irradiance penetrated was derived from the vertical profile data for PAR and UVR using the diffuse attenuation coefficient, K_d, calculated as the slope of the log-linear relationship between irradiance and depth (Williamson et al., 1996).

Zooplankton were collected according to the methods detailed in Williamson et al. (2015), and daytime densities from June, July, and August were averaged to provide a single annual value. Briefly, net tows with a closing bongo net (side-by-side Wisconsin-style 48 μm and standard 202 μm mesh nets) encompassed the full water column at the deepest point in each lake. Most often zooplankton samples were collected separately from the epilimnion and the meta-hypolimnion using the net's closing feature. These two strata were distinguished based on thermal profiles where the bottom of the epilimnion was defined as where temperature change was >1°C per m depth. For long-term trend analysis, samples from all depths were combined using depth-weighted densities to provide a single water column value. *Daphnia* from either a 48 μm or a 202 μm net were counted in a Bogorov chamber. Comparison of *Daphnia* abundance using samples from the 48 and 202 μm counts showed no difference in estimates of abundance. Calanoid and cyclopoid copepods as well as rotifers were collected with a 48 μm mesh net and counted in a Sedgewick-Rafter chamber. Copepod adults and copepodids (juveniles) were separated into cyclopoids or

calanoids. Cyclopoid and calanoid nauplii were counted together as nauplii and not differentiated. Total calanoids and total cyclopoids included adults and copepodids of the respective taxon, but not nauplii. The proportion of zooplankton in the epilimnion was estimated by dividing the proportion of a given zooplankton taxon collected in the epilimnion by the proportion of the depth of the water column that comprised the epilimnion. A value near 0.5 indicates an approximately even distribution of the zooplankton taxon between the epilimnion vs. deeper depths (metalimnion plus hypolimnion), while a larger value (e.g., nearer to 1) indicates a more epilimnetically-distributed taxon, and a smaller value (e.g., nearer to 0) indicates a more deeply distributed taxon. Zooplankton body size ratios (large: small) were calculated as the sum of all *Daphnia* and adult cyclopoid and calanoid copepods divided by the sum of all rotifers and nauplii.

Statistical Analysis

Following the data collection and preparation described above, the eight primary driver variables incorporated into the analyses had a median of 27 years of data out of a maximum of 32 (1988 through 2019), with a minimum of 19 years of data to a maximum of 32 years of data (**Supplementary Table 1**). The zooplankton response variables tended to have fewer years of data, with a median of 17 years of data, a minimum of 12 and a maximum of 20 (**Supplementary Table 1**). A non-parametric Mann-Kendall test was used to determine if there were statistically significant trends over time for each driver and zooplankton response variable for each lake using the full set of annually-averaged data with $\alpha = 0.05$, and Sen's slope was calculated to determine the direction and rate of change over time, using the "trend" R package (Pohlert, 2018). Mann-Kendall non-parametric trend tests and Sen's slope estimator have relaxed assumptions of normality and linearity compared to parametric tests, allow missing data points, and are robust to outliers and data gaps (Gilbert, 1987). Interannual variability correlations were conducted following the methods of Leach et al. (2019). Briefly, the first derivative of each variable was taken over time. Data gaps >1 year were not included in the subsequent correlations. Non-parametric Spearman rank correlations were conducted on the first derivative data for each pair of driver and zooplankton response variables independently for each lake. The resulting correlation coefficient (ρ) for IAV was compared to the pair of LTT to determine if there were consistent patterns at the interannual vs. long-term time scales. Consistent patterns included when long-term Sen's slope trends for the pair of abiotic and zooplankton LTT responses had the same sign (+/+ or −/−) and a positive ρ for IAV, or when long-term Sen's slope trends for the pair had opposing signs (+/−) and a negative ρ for IAV. If any given pair of driver and response variables had a significant LTT with a consistent directional pairing of LTT slopes and IAV ρ, it was considered to have some predictive power to estimate LTT from IAV. If these conditions were met and the IAV ρ was statistically significant ($\alpha = 0.05$), it was considered to have stronger predictive power (a higher level of confidence that IAV can predict LTT). All figures were created using the "ggplot2" R package (Wickham, 2016), and all analyses were completed in R version 3.6.2 (R Core Team, 2019).

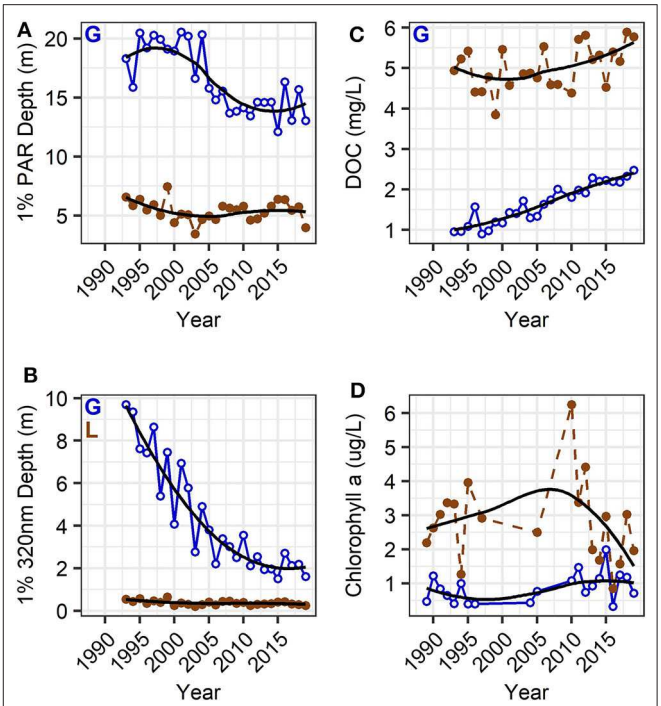

FIGURE 2 | Long-term summer average (June, July, August) trends of PAR **(A)** and 320 nm UVR radiation **(B)**, DOC **(C)**, and chlorophyll *a* **(D)** in Lake Giles (blue, open circles with solid line), and Lake Lacawac (brown, filled circles with dashed line). There was an abrupt change in PAR in Lake Giles following a strong variation in 2003–2004 that provided contrasting underwater PAR environments in the periods before 2003 and after 2004. Trends of change in UVR were much more gradual, and not as strong in Lacawac. Letters indicate statistically significant long-term trends in Giles ("G") and in Lacawac ("L"; Mann-Kendall non-parametric trend test, $p < 0.05$). Black trend lines are LOESS smoothed lines.

RESULTS

Adding 5 years to our previous data set shows that over the past three decades the LTT in compensation depth (1% PAR depth) in Lake Giles consisted of a decrease from 20 m or more to <15 m on average (**Figure 2A**). The 1% 320 nm UVR depth shallowed from close to 10 m to around 2.5 m (**Figure 2B**). Water clarity was high from 1993 to 2002, highly variable from 2003 to 2004, and substantially lower from 2005 to 2019 (**Figure 2A**). Lacawac had decreases in both PAR and UVR penetration that were much less pronounced than those in Giles, with only the trends in UVR being statistically significant (**Figure 2**, **Supplementary Table 1**).

There have been strong and significant increases in the LTT in DOC concentration in Lake Giles (**Figure 2C**), where DOC has more than doubled from ∼0.9 to 2.5 mg C L^{-1} over three decades. Increases in DOC were much less pronounced in Lacawac and not statistically significant (**Figure 2C**). While DOC has increased, chlorophyll has been highly variable with no consistent change over time in either lake (**Figure 2D**). Even

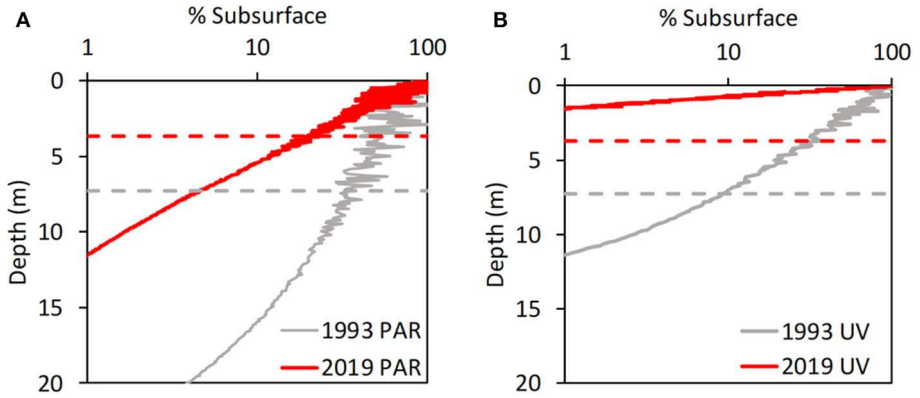

FIGURE 3 | Vertical profiles of PAR **(A)** and 320 nm UVR **(B)** in Lake Giles relative to the depth of the mixed layer (dashed lines) in 1993 and 2019. Note the strong shallowing of the compensation depth (1% of subsurface) for PAR, which influences the balance of photosynthesis and respiration, and thus the depth of light limitation of photosynthesis as well as oxygen depletion in the deeper waters. There is also a strong reduction in UVR and PAR exposure levels in the mixed layer.

at deeper depths, where we've observed a deep chlorophyll maximum in the past, the only significant trend was a decrease in chlorophyll in the hypolimnion of Lake Giles with browning (**Supplementary Table 1**). Similar tests on the 10–12 years of nutrient data indicated no significant change in total or soluble reactive phosphorus (**Supplementary Table 1**). The DOC: TP ratio did show a significant increase in Lake Giles, but not in Lacawac, consistent with a significant increase in DOC in Giles but not Lacawac, and no trend in TP in either lake (**Supplementary Table 1**).

In contrast to the lack of change in chlorophyll and nutrients, there were critical light-driven changes in habitat variables during browning, especially in Lake Giles. Lower water transparency reduced both sunlight penetration and surface mixed layer depth. For example, early in the study period (1993) in Lake Giles the compensation depth (1% PAR) extended to the bottom of the lake, supporting net photosynthesis throughout the water column. In contrast, after nearly three decades of browning (2019) the 1% PAR depth reached only about half as deep as in 1993 (**Figure 3A**). Similarly, in 1993, potentially damaging 320 nm UVR was 10% of the subsurface irradiance or greater throughout the surface mixed layer (**Figure 3B**), but by 2019, the mixed layer itself was only about half as deep, while the 1% UVR depth decreased by more than four-fold (**Figure 3B**). Corresponding to the strong decreases in PAR in Giles between 2002 and 2005 were particularly strong decreases in deep-water temperature and dissolved oxygen, as well as increases in surface water temperature and pH (**Figures 2A**, **4**). These primarily light-driven responses led to important ecosystem-level consequences including a significant decrease in chlorophyll in the hypolimnion (**Supplementary Table 1**), the onset of oxygen depletion in the hypolimnion (**Figure 4C**) and a refuge from damaging UVR exposure in the deeper portions of the warmer surface waters (**Figure 3B**). Lacawac showed a variable but significant decline in hypolimnetic temperature but no trends in surface temperature, dissolved oxygen, or pH (**Figure 4**).

Zooplankton LTT showed a diversity of changes in abundance, some changes in their daytime vertical distribution, but no changes in the community body size ratio (**Supplementary Table 1**). Similar to the changes in habitat variables, zooplankton responses were stronger in Giles than in Lacawac. Zooplankton were generally most abundant in the deeper waters, or distributed approximately evenly throughout the water column in both lakes (**Table 1**). Only the rotifer *Keratella* was distinctly epilimnetic (**Table 1**), and only two groups showed statistically significant changes in their vertical distribution (**Figure 5**). *Daphnia* in Lacawac showed a statistically significant but highly variable decrease in their proportion in the epilimnion ($p = 0.034$, **Figure 5A**, **Supplementary Table 1**), and nauplii in Giles showed a stronger and more consistent decrease in their proportion in the epilimnion ($p = 0.004$, **Figure 5B**, **Supplementary Table 1**). Copepods, cladocerans, and rotifers all exhibited significant decreasing (calanoids, *Daphnia*, *Gastropus, Polyarthra*) or increasing (cyclopoids, *Kellicottia*) LTT in abundance in Lake Giles (**Figure 6**). In Lacawac, abundance changes were only observed in *Gastropus,* which also declined (**Figure 6G**), and in cyclopoid copepod adults, which increased significantly (**Figure 6D**). The rotifer *Keratella* showed no significant LTT in abundance in either lake (**Supplementary Table 1**).

Of the 80 pairings that compared zooplankton responses to each potential driver variable on both an interannual vs. long-term basis, 33 (41%) showed consistent IAV and LTT responses (e.g., both positive, both negative, or both opposite). Only three (4%) of the total showed consistent IAV and LTT responses that were also statistically significant, all in Giles (**Figure 7**). Two of these three strong relationships involved light as a driver variable (one UVR and one PAR), while one involved pH (**Figure 7**). Chlorophyll *a*, an estimate of resource availability, was the only variable with no explanatory power, and no consistent relationships between IAV and LTT, due primarily to the lack of any significant LTT.

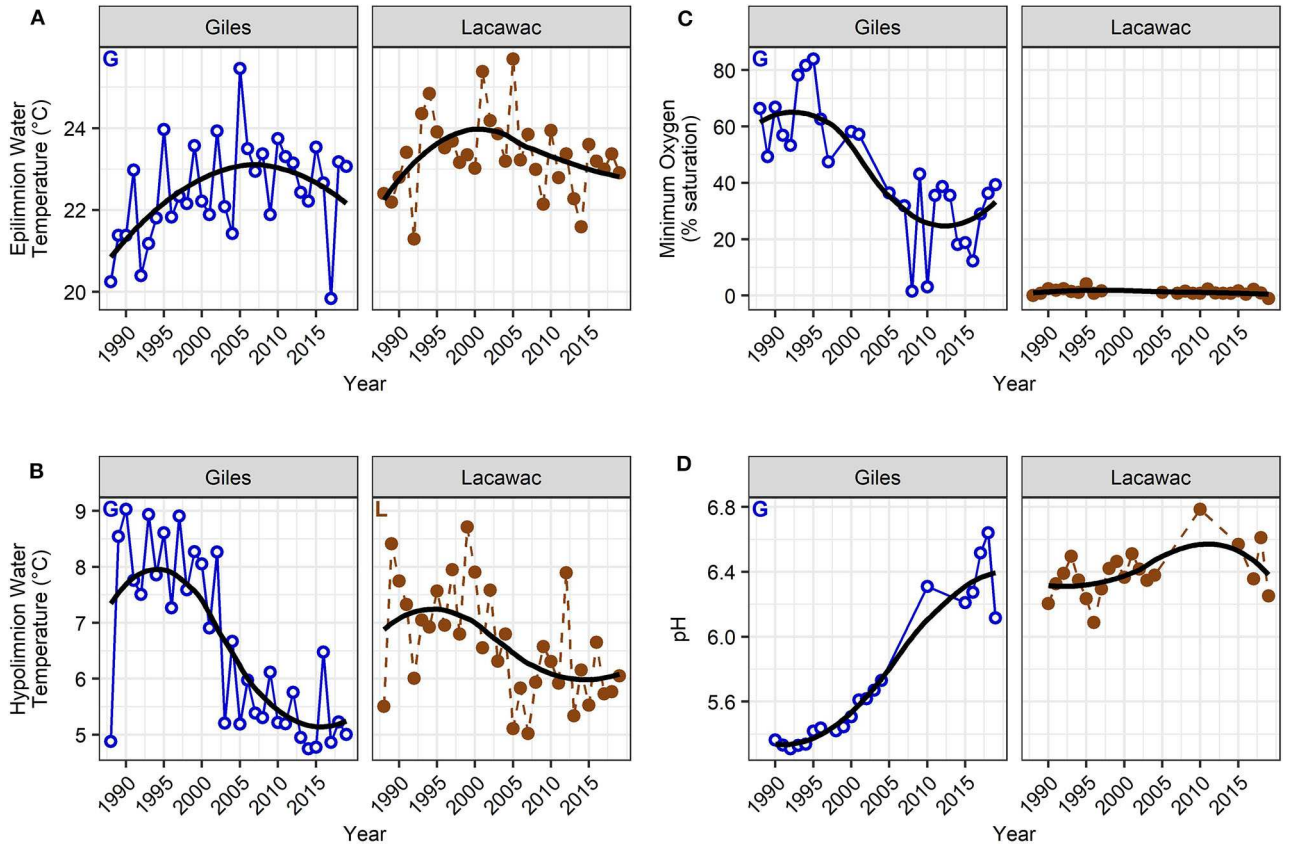

FIGURE 4 | Long-term summer average (June, July, August) changes in light-related habitat characteristics in Lake Giles (blue, open circles with solid line), and Lake Lacawac (brown, filled circles with dashed line). The strong change in PAR (**Figure 2**) is the most likely factor leading to the warming epilimnion **(A)**, cooling hypolimnion **(B)**, and decrease in deep-water dissolved oxygen **(C)** (Pilla et al., 2018). The increases in pH **(D)**, statistically significant only in Lake Giles, are most likely due to decreases in acid deposition in the region during the study period (Williamson et al., 2015). Letters indicate statistically significant long-term trends in Giles ("G") and in Lacawac ("L"; Mann-Kendall non-parametric trend test, $p < 0.05$). Black trend lines are LOESS smoothed lines.

DISCUSSION

Browning has induced strong changes in the underwater light environment in lakes that have in turn altered pelagic habitats with important consequences for zooplankton consumers. The light-related changes in habitat and responses by zooplankton observed here were much stronger than any changes in basal resources (i.e., chlorophyll), and also much more prevalent in clear-water Lake Giles than in browner Lake Lacawac. The resource-based hypothesis argues that nutrients in terrestrially-derived DOM are responsible for increases in primary production in clear-water lakes, while in browner lakes shading plays a more important role, and leads to a decrease in primary production. This leads to a unimodal relationship where in clear-water lakes such as our Lake Giles, and possibly more intermediate productivity Lake Lacawac, one would predict that as DOC concentration increases, nutrients and thus chlorophyll would also increase. Yet phosphorus did not change in either of the study lakes, and the only significant trend in chlorophyll was a decrease in the hypolimnion of Lake Giles with browning, which is the opposite of what would be expected according to the resource-based hypothesis. Chlorophyll is only a proxy for food resources, and the chlorophyll per unit biomass can increase at lower light levels. The fact that chlorophyll exhibited no increases even with browning-related reductions in light is thus also in contrast to the predictions of the resource-based hypothesis. Another possible, often mentioned but rarely tested, resource-based control of primary production at low levels of DOM is photoinhibition by UVR (Carpenter et al., 1998; Finstad et al., 2014; Kelly et al., 2014; Seekell et al., 2015a). Photoinhibition, which has been demonstrated *in situ* in Giles (Moeller, 1994), should be reduced with increases in DOM, leading to increases in primary production. However, the lack of any significant increases in chlorophyll or nutrients suggest that UVR effects on basal resources are also not the most likely explanation for the observed changes in zooplankton in these two lakes. Changes in vertical habitat gradients were more important.

We observed LTT in both abiotic driver variables and zooplankton responses. In only 4% of the cases, however, were LTT trends highly predictable from IAV, making it challenging to use short-term data to predict long-term responses. The ability to assess LTT based on short-term experiments or IAV

TABLE 1 | Primary depth inhabited by zooplankton estimated as the proportion of individuals of each taxon found in the epilimnion.

Taxon	Lake	Primary depth	Proportion in Epi.	
			Median	Quartiles
Calanoids	Giles	All	0.30	0.19–0.40
	Lacawac	Deep	0.06	0.02–0.13
Cyclopoids	Giles	Deep	0.01	0.00–0.03
	Lacawac	Deep	0.11	0.08–0.29
Nauplii	Giles	Deep	0.09	0.04–0.14
	Lacawac	Deep	0.11	0.05–0.15
Daphnia	Giles	Deep	0.11	0.04–0.18
	Lacawac	Deep	0.12	0.04–0.23
Gastropus	Giles	All	0.24	0.04–0.33
	Lacawac	All	0.27	0.07–0.54
Kellicottia	Giles	Deep	0.03	0.02–0.05
	Lacawac	Deep	0.03	0.01–0.05
Polyarthra	Giles	All	0.28	0.22–0.47
	Lacawac	All	0.43	0.20–0.52
Keratella	Giles	Epilimnion	0.62	0.46–0.73
	Lacawac	Epilimnion	0.66	0.51–0.73

Medians and 25 and 75% quartiles are given for all sampling dates.

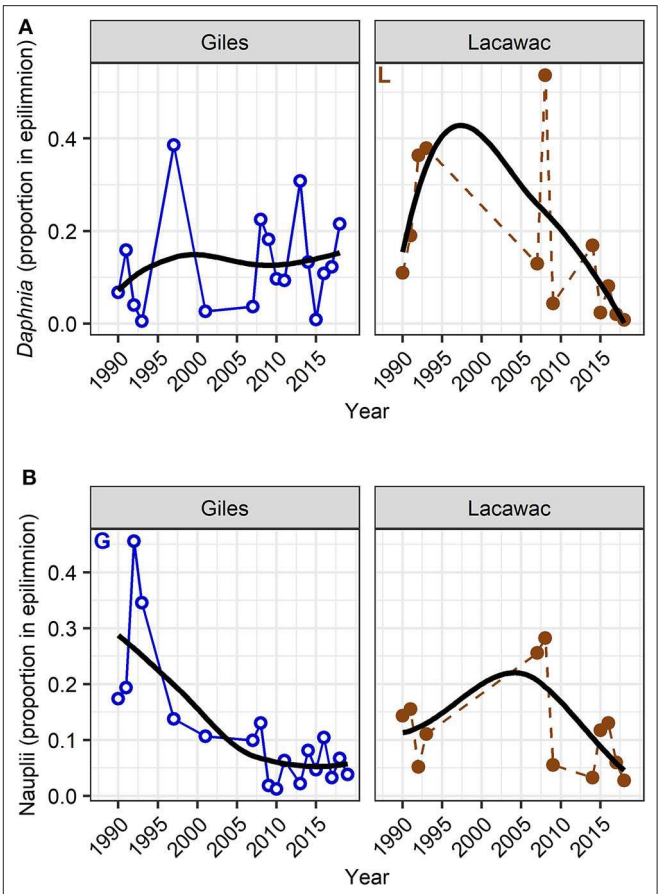

FIGURE 5 | Long-term summer average (June, July, August) changes in the vertical distribution (relative proportion in the epilimnion) of *Daphnia* **(A)** and copepod nauplii **(B)** in Lake Giles (blue, open circles with solid line), and Lake Lacawac (brown, filled circles with dashed line). Letters indicate statistically significant long-term trends in Giles ("G") and in Lacawac ("L"; Mann-Kendall non-parametric trend test, $p < 0.05$). Black trend lines are LOESS smoothed lines.

in whole lakes could provide early warning signals that enable implementation of management options to avoid the most severe changes in ecosystems well before they occur (Pace et al., 2015). Analyses that use a single or subset of only a few extreme years (e.g., heat waves or precipitation extremes) provide a convenient natural manipulation that promotes insights into how environmental change can alter lake ecosystem structure and function. For example, a single extremely warm year during a heat wave in Europe showed much stronger thermal stratification of the water column and deep-water oxygen depletion than normal (Jankowski et al., 2006). Comparison of 86 small Canadian lakes in one cool and two very warm years showed changes in thermal structure that were strongest in the clearer lakes (Snucins and Gunn, 2000). A study of 84 lakes in northeastern North America showed that an extreme wet year can lead to higher DOC concentrations and short-term browning, while an extreme dry year can lead to higher sulfate concentrations and acidification (Strock et al., 2016). Whole-lake manipulations can provide a similar short-term snapshot of how lake ecosystems respond to short-term changes (Christensen et al., 1996), though longer-term changes may not be detectable for many decades (Carpenter and Pace, 2018). The presence of so few consistent relationships between zooplankton responses and potential drivers at these two different time scales of IAV and LTT for the majority of our analyses (59%), however, suggests caution is needed before extrapolating LTT from short-term experiments or data, even at the whole-lake scale.

We did observe both direct and indirect effects of a changing light environment on pelagic habitats during browning, and they are likely related to regional increases in precipitation in addition to decreases in acid deposition. While there has been no significant LTT in air temperature or solar radiation in this region during the study period, there has been an increase in average precipitation with a shift to a wetter regime between 2001 and 2004 (Pilla et al., 2018), a period of particularly rapid change in light attenuation. In addition to the increases in DOC concentration documented here, there has been a precipitation-related increase in the color (DOC-specific UVR absorbance) of the DOM (Williamson et al., 2014). Thus, the changes in the underwater light environment observed here are a result of not only the observed increases in DOC concentration, but also increases in color.

Our unique long-term UVR database enabled us to examine the role of UVR-related changes and responses during browning. UVR has the potential to have direct negative effects on zooplankton. A recent meta-analysis on the negative effects of UVR on a wide variety of freshwater organisms ranging from phytoplankton and zooplankton to amphibians and fish, showed the greatest negative effects on zooplankton (Peng et al., 2016).

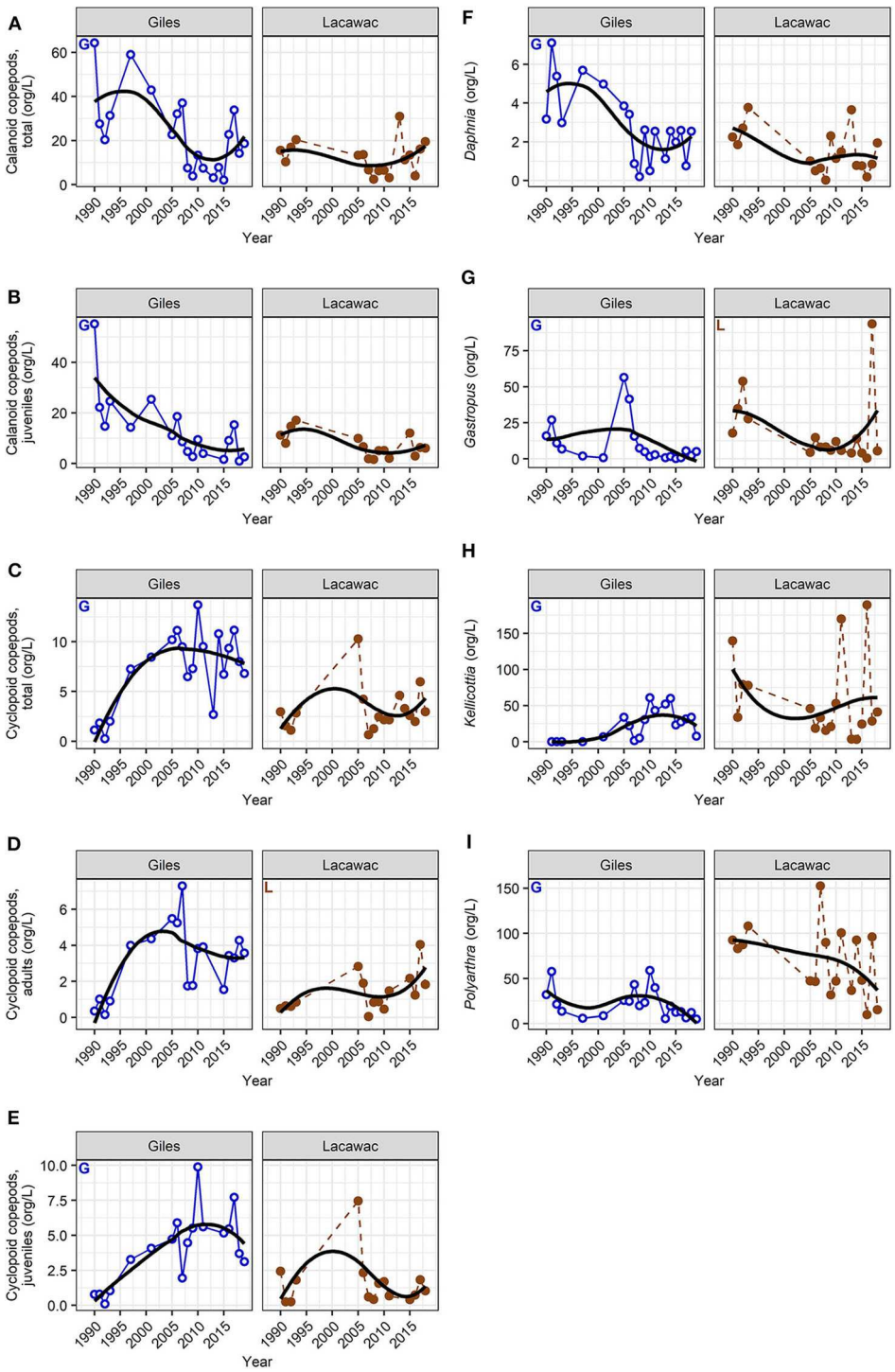

FIGURE 6 | Long-term summer average (June, July, August) changes in zooplankton abundance **(A–I)** in Lake Giles (blue, open circles with solid line), and Lake Lacawac (brown, filled circles with dashed line). Letters indicate statistically significant long-term trends in Giles ("G") and in Lacawac ("L"; Mann-Kendall non-parametric trend test, $p < 0.05$). Black trend lines are LOESS smoothed lines.

High exposure levels of >10% of surface 320 nm UVR, such as those observed historically in Lake Giles (**Figures 2B**, **3**), have been related to the elimination of all zooplankton species in shallow montane lakes in Argentina, with the exception of one very highly pigmented copepod (Marinone et al., 2006). This high UVR exposure level has been experimentally demonstrated to

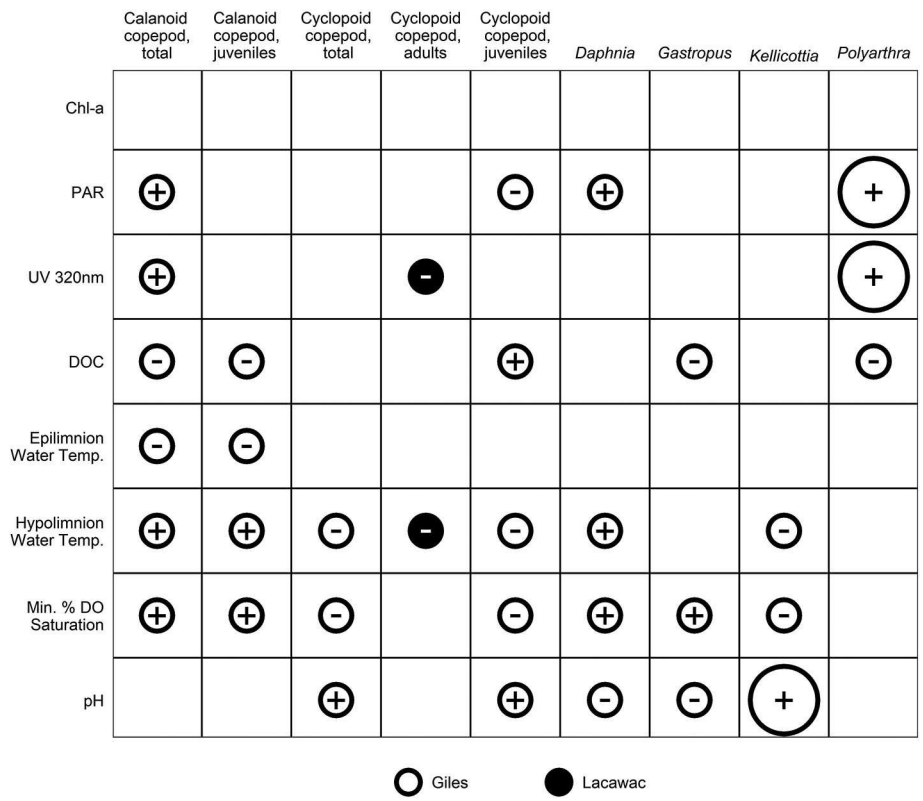

FIGURE 7 | Relationships between IAV and LTT of driver variables vs. zooplankton response variables. Rows are potential driver variables related to the resource-based or habitat-based hypotheses. Columns are zooplankton abundance response variables that had a significant long-term trend in either Giles or Lacawac. Small circles indicate when both the respective driver variable and zooplankton response variable LTT were statistically significant (Mann-Kendall non-parametric trend test, $p < 0.05$), and the direction of the interannual Spearman correlation was consistent with that of the LTT for the same lake (open white circles = Giles, filled black circles = Lacawac). Large points follow the same pattern, but indicate when the interannual Spearman correlation was consistent with that of the LTT, and also statistically significant (Spearman rank correlation, $p < 0.05$), suggesting a higher degree of confidence in predicting LTT from IAV data. Signs indicate the positive (+) or negative (–) nature of the relationship between the driver and response variables.

lead to high mortality rates of a range of not only zooplankton (Williamson et al., 1994, 1999), but also early life history stages of fish (Williamson et al., 1999; Huff et al., 2004; Olson et al., 2006, 2008). However, the decreases in *Daphnia, Polyarthra*, and *Gastropus* during a period of decreasing UVR exposure in the surface waters are not consistent with a direct UVR-damage hypothesis (Leech and Williamson, 2000; Persaud and Williamson, 2005). Similarly, zooplankton may also have historically been squeezed between UVR in the surface waters, and deeper-dwelling tactile invertebrate predators (Boeing et al., 2004), but we would expect a release from this squeeze with declining UVR, which contrasts with the observed declines in abundance of zooplankton grazers. Zooplankton have a wide variety of mechanisms to reduce UVR damage ranging from behavioral avoidance to the production of photoprotective compounds and photoenzymatic repair, though these protections come at some cost (Rautio and Tartarotti, 2010). While few zooplankton inhabited the surface waters of either of our lakes (**Table 1**), no increases in abundance in the epilimnion were observed with the decreases in UVR over time as might be expected if direct UVR damage was an important driver. Furthermore, the rotifer *Keratella* was the most epilimnetically-distributed of all of the species, and is also known to be one of the most UVR-tolerant zooplankton species in Giles (Williamson et al., 1994). *Keratella* showed no significant LTT in abundance and no change in vertical distribution with browning in either lake. In spite of the strong declines in surface UVR, it was the deep-water taxa such as cyclopoids and *Kellicottia* that showed the greatest increases over time, though they were not exposed directly to high levels of UVR at the depths where they were found. In contrast, calanoid copepods from Lake Giles are attracted to (Overholt et al., 2016) or benefit from (Cooke and Williamson, 2006) exposure to UVR. This is consistent with declines in calanoid copepods observed with concurrent declines in UVR exposure in Giles. In both Giles and Lacawac multiple single or interacting habitat-related factors are likely more important to the response of zooplankton than is direct exposure to UVR damage.

There is a strong interplay between reductions in water transparency to PAR, increases in surface water temperatures, and decreases in deep-water temperatures and oxygen. For example, a multi-lake modeling study, which included Giles,

showed that in lakes where both transparency and mixed layer depth were decreasing, the overall exposure to UVR and PAR in the mixed layer decreased, whereas in lakes where only the mixed layer depth decreased, average exposure increased (Neale and Smyth, 2019). Coupling these changes in light-related habitat variables to what is known about the ecology of zooplankton has the potential to add insights to the changes in zooplankton abundance and depth distribution presented here. Physiological tolerances to temperature and low oxygen involving cyclopoid copepods provide a good example of the importance of these complex interactions. *Cyclops scutifer* is the dominant cyclopoid in Giles, and it has shown some of the strongest increases with browning of any of the zooplankton taxa (**Figures 6C,E**). This may be related to several factors. First, *C. scutifer* is a cold stenotherm that inhabits deep waters during warmer seasons (Elgmork, 1967; Johnson et al., 2007). The rotifer *Kellicottia* can increase under colder conditions as well (Persaud and Williamson, 2005). One potential threat to cold stenotherms is being squeezed between two suboptimal habitats with warming surface waters, and oxygen-depleted deeper waters (Doubek et al., 2018), both of which have been observed in Lake Giles (**Figures 4A,C**). However, the deep waters of Giles have been cooling (**Figure 4B**), and oxygen depletion has not yet reached a state of anoxia as it has in Lacawac (**Figure 4C**). Therefore, the increase in optimal deep, cold-water habitat may actually be contributing to the increase in both *Kellicottia* and *C. scutifer*. The deeper depth distribution of nauplii with browning in Giles (**Figure 5B**) is most likely related to a shift from calanoid nauplii to cyclopoid nauplii as hypolimnetic cyclopoids increased in abundance and the calanoids declined (**Figure 6**, **Table 1**). Some cyclopoids such as *Mesocyclops edax* can tolerate anoxic conditions for at least short periods of time, and even use anoxic waters as a refuge from fish predation (Williamson and Magnien, 1982). *M. edax* is the species that is most abundant in the deeper hypoxic to anoxic waters of Lacawac (**Figure 4C**, **Table 1**). If hypoxia continues to intensify in Giles in the future, we may see a shift to this more anoxia-tolerant species.

While recovery from acidification and an increase in pH are characteristic of browning in lakes (Evans et al., 2006; Monteith et al., 2007; Williamson et al., 2015; Strock et al., 2016), short-term experiments that manipulate DOM from the microcosm to the whole-lake level as well as comparative space-for-time studies of browning have rarely considered changes in pH. Yet there is good evidence that zooplankton species composition varies with pH. A comparative space-for-time study of 20 lakes in northeastern North America showed a loss of biodiversity with a decrease in pH (Confer et al., 1983). While *Leptodiaptomus minutus* was found in acidified lakes, other zooplankton species such as *Daphnia* and cyclopoid copepods were rarely if ever found at a pH below 5. A comparative study of 32 lakes in Glacier Bay, Alaska, with a pH range from 5 to 8 found *Cyclops scutifer* and rotifers to be most abundant in lakes with a higher pH (Olson et al., 1995). During an experimental whole-lake basin acidification experiment, *Gastropus stylifer* was found to be most abundant at the most acidic pH of 4.7, while *Kellicottia longispina* was found at greater abundances at the two higher pH values of 5.2 and 5.6 (Frost et al., 1998). These patterns are consistent with the observed increases over time in cyclopoid copepods in Giles and Lacawac (**Figures 6C,E**) as well as *Kellicottia* in Giles (**Figures 6H**, **7**) where pH has also been increasing, though not significantly in Lacawac (**Figure 4D**). Increases in pH likely also contributed to the increases in fish that have been observed in these study lakes (Williamson et al., 2015), as fish tend to increase above a pH of around 5 in lakes recovering from acid deposition (Baldigo et al., 2016).

A third hypothesis that may contribute to changes in zooplankton communities during browning that has received less attention, but for which good evidence is accumulating, is predation. The three most important zooplanktivorous predators in our study lakes are cyclopoid copepods, larvae of the phantom midge *Chaoborus*, and young-of-year fish. Only our data on cyclopoid predators was sufficient to incorporate into the full analysis here, though we also have very limited data on young-of-year fish. Below we discuss how predation by both tactile invertebrates as well as visual predators has the potential to be an important indirect effect of browning on zooplankton.

Prior experimental work suggests that predation regimes will shift from being dominated by visual predators to domination by tactile invertebrate predators with increases in DOM (Wissel et al., 2003a). While the increase in abundance of cyclopoids in Giles is consistent with this prior experimental work, we also observed an increase in visual predators in our lakes (Williamson et al., 2015). As discussed above, these increases in cyclopoids and young-of-year fish may be due at least in part to the mitigating effects of recovery from acid deposition and a higher pH. This highlights the importance of browning-related factors other than resources or light alone in mediating the observed changes in zooplankton, including indirect effects such as predation.

The effects of predatory cyclopoids on zooplankton are most likely to be on smaller zooplankton species, and the rotifers in particular. Rotifers are an important food source for many cyclopoid copepods (Williamson, 1983, 1984). Cyclopoid copepod predators in lakes with warming surface waters (as observed in our lakes) can also benefit from increased availability of rotifers as food (Zhang et al., 2018). The changes that we observed in rotifer species are consistent with increases in cyclopoid predation. For example, the spined rotifers *Keratella* and *Kellicottia* are well-protected against cyclopoid predation (**Figure 8**), and either did not change in abundance, or increased, respectively (**Figure 6H**). In contrast, the soft-bodied rotifers *Gastropus* and *Polyarthra*, which are poorly defended against cyclopoid predators (Gilbert and Williamson, 1978; **Figure 8**), declined (**Figures 6G,I**).

Larvae of the phantom midge *Chaoborus* are some of the most important invertebrate predators of *Daphnia* in lakes (Riessen et al., 2012). *Chaoborus* are, however, highly heterogeneous in their horizontal distribution and migrate into the sediments during the day. Thus, adequate sampling requires multi-station sampling at night (Wissel et al., 2003b), something which was beyond our capacity in this long-term study. There is evidence, however, that *Chaoborus* abundance

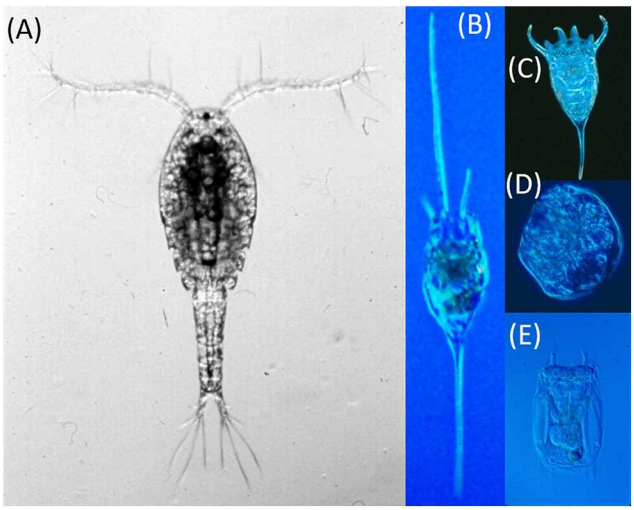

FIGURE 8 | Photographs showing a cyclopoid copepod (*Mesocyclops edax*) **(A)** and differential defenses of rotifers against cyclopoid predation including the spined rotifers *Kellicottia* **(B)** and *Keratella* **(C)** that either increased or did not change in abundance, respectively, and the soft-bodied rotifers *Gastropus* **(D)** and *Polyarthra* **(E)** that showed significant declines. Size of rotifers magnified relative to the copepod to show detail.

is positively correlated with DOM (Wissel et al., 2003a,b), and thus an increase in *Chaoborus* with browning would be expected. A recent paper has provided evidence that the refuge from UVR due to increased DOM enables *Chaoborus* in shallow arctic ponds to decimate their zooplankton prey (Lindholm et al., 2016). Thus, increases in *Chaoborus* are one possible explanation for the observed decline in *Daphnia* in Giles.

Changes in the underwater light environment can also influence visual predation by fish on larger zooplankton such as *Daphnia*. While increasing DOM can induce light limitation that reduces predation by bluegill (*Lepomis macrochirus*) and largemouth bass (*Micropterus salmoides*) (Weidel et al., 2017), there are more factors influencing predators than just visible light limitation during long-term lake browning. For example, bluegill and largemouth bass are two of the dominant fish predators in our lakes, yet sampling of young-of-year fish early and later during the process of browning has shown dramatic increases in fish abundance in both of our lakes, with an increase in catch-per-unit effort of young-of-year fish from 0 and 1.6 in 1991 in Giles and Lacawac respectively, to 5.0 and 5.5 in 2014 (Williamson et al., 2015). Early life history stages of planktivorous fish have historically been highly susceptible to UVR damage in Lake Giles (Williamson et al., 1997, 1999; Huff et al., 2004), and have increased in the past three decades as UVR exposure levels have declined (Williamson et al., 2015). This increase in fish may also contribute to the observed increase in cyclopoids because cyclopoids are known to be less susceptible to visual predators than are cladocerans, and thus are more abundant in lakes with fish (Johnson et al., 2010). The hypolimnetic nature of the cyclopoids in our lakes (**Table 1**) would additionally make them less susceptible to visual predators like young-of-year fish that primarily inhabit the warmer surface waters. These patterns support a stronger habitat-driven rather than resource-driven effect of browning when the predation changes and taxon-specific and life history stage-specific changes in zooplankton are considered.

Although the patterns of change in zooplankton observed during browning in this study are not consistent with the resource-based unimodal hypothesis, this does not mean that resources are not important. The key message is that habitat changes resulting from decreasing light penetration are also important, and zooplankton consumers are responding to more than simply resources during long-term browning. These responses are also often taxon- or life history stage-specific, even for a single driver variable (e.g., compare across rows in **Figure 7**). Pronounced changes in the underwater light environment, which are particularly strong in clear-water lakes, alter vertical habitat gradients in UVR, PAR, temperature, and dissolved oxygen in ways that have important consequences for zooplankton physiology, habitat availability, and trophic interactions, including predation. Recovery from acidification and corresponding increases in pH, an integral part of browning in many lakes, may also interact with changes in the light environment in ways that alter not only total zooplankton abundance, but also their vertical distribution, trophic structure, and hence community structure. The limitations in predicting long-term trends from short-term data highlight the value of long-term data on the underwater light environment to accurately characterize changes in zooplankton communities in lakes undergoing browning.

DATA AVAILABILITY STATEMENT

The datasets analyzed for this study can be found in the Environmental Data Initiative (EDI, Williamson, 2019). The raw zooplankton data supporting the conclusions of this article are available upon request from the authors, and are in the process of being added to the EDI.

AUTHOR CONTRIBUTIONS

CW was involved in and supervised the long-term data collection and analysis, conceived of the study, and wrote the manuscript with input from, and sections written by EO, RP, and KW. EO, RP, and KW were also involved in the long-term data collection and analysis, with RP leading the statistical analysis. EO was the primary one to oversee quality control and archiving of data. All authors contributed to the manuscript revision, as well as read, and approved the submitted version.

FUNDING

Long-term data collection was supported by grants from the Andrew W. Mellon Foundation, Geraldine R. Dodge Foundation, and numerous National Science Foundation grants, including

most recently NSF DEB LTREB 1754276. Data analysis, synthesis, and publication was supported by NSF DEB OPUS 1950170. We also thank the Miami University College of Arts and Sciences and the Ohio Eminent Scholar in Ecosystem Ecology fund.

ACKNOWLEDGMENTS

We thank Beth Mette and Eric Johnson for assistance in developing the database, Thomas Fisher for his statistical advice, and the students and colleagues, too numerous to mention by name, who assisted in the long-term data collection through the decades.

SUPPLEMENTARY MATERIAL

The Supplementary Material for this article can be found online at: https://www.frontiersin.org/articles/10.3389/fenvs.2020.00073/full#supplementary-material

REFERENCES

Ask, J., Karlsson, J., Persson, L., Ask, P., Bystrom, P., and Jansson, M. (2009). Terrestrial organic matter and light penetration: effects on bacterial and primary production in lakes. *Limnol. Oceanogr.* 54, 2034–2040. doi: 10.4319/lo.2009.54.6.2034

Baldigo, B. P., Roy, K. M., and Driscoll, C. T. (2016). Response of fish assemblages to declining acidic deposition in Adirondack Mountain lakes, 1984-2012, *Atmosp. Environ.* 146, 223–235. doi: 10.1016/j.atmosenv.2016.06.049

Boeing, W. J., Leech, D. M., Williamson, C. E., Cooke, S. L., and Torres, L. (2004). Damaging UV radiation and invertebrate predation: conflicting selective pressures for zooplankton vertical distribution in the water column of low DOC lakes. *Oecologia* 138, 603–612. doi: 10.1007/s00442-003-1468-0

Carpenter, S. R., Cole, J. J., Kitchell, J. F., and Pace, M. L. (1998). Impact of dissolved organic carbon, phosphorus, and grazing on phytoplankton biomass and production in experimental lakes. *Limnol. Oceanogr.* 43, 73–80. doi: 10.4319/lo.1998.43.1.0073

Carpenter, S. R., and Pace, M. L. (2018). Synthesis of a 33-yr series of whole-lake experiments: effects of nutrients, grazers, and precipitation-driven water color on chlorophyll. *Limnol. Oceanogr. Lett.* 3, 419–427. doi: 10.1002/lol2.10094

Christensen, D. L., Carpenter, S. R., Cottingham, K. L., Knight, S. E., LeBouton, J. P., Schindler, D. E., et al. (1996). Pelagic responses to changes in dissolved organic carbon following division of a seepage lake. *Limnol Oceanogr.* 41, 553–559. doi: 10.4319/lo.1996.41.3.0553

Confer, J. L., Kaaret, T., and Likens, G. E. (1983). Zooplankton diversity and biomass in recently acidified lakes. *Can. J. Fish. Aquatic Sci.* 40, 36–42. doi: 10.1139/f83-006

Cooke, S. L., and Williamson, C. E. (2006). Positive effects of UV radiation on a calanoid copepod in a transparent lake: do competition, predation or food availability play a role? *J. Plankton Res.* 28, 171–179. doi: 10.1093/plankt/fbi108

Cooke, S. L., Williamson, C. E., Leech, D. M., Boeing, W. J., and Torres, L. (2008). Effects of temperature and ultraviolet radiation on diel vertical migration of freshwater crustacean zooplankton. *Can. J. Fish. Aquatic Sci.* 65, 1144–1152. doi: 10.1139/F08-039

Craig, N., Jones, S. E., Weidel, B. C., and Solomon, C. T. (2015). Habitat, not resource availability, limits consumer production in lake ecosystems. *Limnol. Oceanogr.* 60, 2079–2089. doi: 10.1002/lno.10153

de Wit, H. A., Valinia, S., Weyhenmeyer, G. A., Futter, M. N., Kortelainen, P., Austnes, K., et al. (2016). Current browning of surface waters will be further promoted by wetter climate. *Environ. Sci. Technol. Lett.* 3, 430–435. doi: 10.1021/acs.estlett.6b00396

Doubek, J. P., Campbell, K. L., Doubek, K. M., Hamre, K. D., Lofton, M. E., Mcclure, R. P., et al. (2018). The effects of hypolimnetic anoxia on the diel vertical migration of freshwater crustacean zooplankton. *Ecosphere* 9:e02332. doi: 10.1002/ecs2.2332

Elgmork, K. (1967). On distribution and ecology of *Cyclops scutifer* Sars in New England (Copepoda Crustacea). *Ecology* 48, 967–971. doi: 10.2307/1934542

Engstrom, D. R., Fritz, S. C., Almendinger, J. E., and Juggins, S. (2000). Chemical and biological trends during lake evolution in recently deglaciated terrain. *Nature* 408, 161–166. doi: 10.1038/35041500

Evans, C. D., Chapman, P. J., Clark, J. M., Monteith, D. T., and Cresser, M. S. (2006). Alternative explanations for rising dissolved organic carbon export from organic soils. *Glob. Change Biol.* 12, 2044–2053. doi: 10.1111/j.1365-2486.2006.01241.x

Finstad, A. G., Helland, I. P., Ugedal, O., Hesthagen, T., and Hessen, D. O. (2014). Unimodal response of fish yield to dissolved organic carbon. *Ecol. Lett.* 17, 36–43. doi: 10.1111/ele.12201

Fischer, J. M., Olson, M. H., Theodore, N., Williamson, C. E., Rose, K. C., and Hwang, J. (2015). Diel vertical migration of copepods in mountain lakes: the changing role of ultraviolet radiation across a transparency gradient. *Limnol. Oceanogr.* 60, 252–262. doi: 10.1002/lno.10019

Frost, T. M., Montz, P. K., Gonzalez, M. J., Sanderson, B. L., and Arnott, S. E. (1998). Rotifer responses to increased acidity: long-term patterns during the experimental manipulation of Little Rock Lake. *Hydrobiologia* 387, 141–152. doi: 10.1023/A:1017055307027

Gilbert, J. J., and Williamson, C. E. (1978). Predator-prey behavoir and its effect on rotifer survival in associations of *Mesocyclops edax, Asplanchna girodi, Polyarthra vulgaris*, and *Keratella cochlearis*. *Oecologia* 37, 13–22. doi: 10.1007/BF00349987

Gilbert, R. O. (1987). *Statistical Methods for Environmental Pollution Monitoring*. New York, NY: Wiley.

Huff, D. D., Grad, G., and Williamson, C. E. (2004). Environmental constraints on spawning depth of yellow perch: The roles of low temperatures and high solar ultraviolet radiation. *Trans. Am. Fish. Soc.* 133, 718–726. doi: 10.1577/T03-048.1

Jankowski, T., Livingstone, D. M., Buhrer, H., Forster, R., and Niederhauser, P. (2006). Consequences of the 2003 European heat wave for lake temperature profiles, thermal stability, and hypolimnetic oxygen depletion: Implications for a warmer world. *Limnol. Oceanogr.* 51, 815–819. doi: 10.4319/lo.2006.51.2.0815

Johnson, C. R., Luecke, C., Whalen, S. C., and Evans, M. A. (2010). Direct and indirect effects of fish on pelagic nitrogen and phosphorus availability in oligotrophic Arctic Alaskan lakes. *Can. J. Fish. Aquatic Sci.* 67, 1635–1648. doi: 10.1139/F10-085

Johnson, C. R., O'Brien, W. J., and MacIntyre, S. (2007). Vertical and temporal distribution of two copepod species, *Cyclops scutfier* and *Diaptomus pribilofensis*, in 24 h arctic daylight. *J. Plankton Res.* 29, 275–289. doi: 10.1093/plankt/fbm014

Jones, S. E., Solomon, C. T., and Weidel, B. (2012). Subsidy or subtraction: how do terrestrial inputs influence consumer production in lakes? *Freshw. Rev.* 5, 37–49. doi: 10.1608/FRJ-5.1.475

Karlsson, J., Bystrom, P., Ask, J., Ask, P., Persson, L., and Jansson, M. (2009). Light limitation of nutrient-poor lake ecosystems. *Nature* 460, 506–509. doi: 10.1038/nature08179

Kelly, P. T., Craig, N., Solomon, C. T., Weidel, B. C., Zwart, J. A., and Jones, S. E. (2016). Experimental whole-lake increase of dissolved organic carbon concentration produces unexpected increase in crustacean zooplankton density. *Glob. Change Biol.* 22, 2766–2775. doi: 10.1111/gcb.13260

Kelly, P. T., Solomon, C. T., Weidel, B. C., and Jones, S. E. (2014). Terrestrial carbon is a resource, but not a subsidy, for lake zooplankton. *Ecology* 95, 1236–1242. doi: 10.1890/13-1586.1

Kritzberg, E. S. (2017). Centennial-long trends of lake browning show major effect of afforestation. *Limnol. Oceanogr. Lett.* 2, 105–112. doi: 10.1002/lol2.10041

Kritzberg, E. S., and Ekström, S. M. (2012). Increasing iron concentrations in surface waters - a factor behind brownification? *Biogeosciences* 9, 1465–1478. doi: 10.5194/bg-9-1465-2012

Larsen, S., Andersen, T., and Hessen, D. (2011). Climate change predicted to cause severe increase of organic carbon in lakes. *Glob. Change Biol.* 17, 1186–1192. doi: 10.1111/j.1365-2486.2010.02257.x

Leach, T. H., Williamson, C. E., Theodore, N., Fischer, J. M., and Olson, M. H. (2015). The role of ultraviolet radiation in the diel vertical migration of zooplankton: an experimental test of the transparency-regulator hypothesis. *J. Plankton Res.* 37, 886–896. doi: 10.1093/plankt/fbv061

Leach, T. H., Winslow, L. A., Hayes, N. M., and Rose, K. C. (2019). Decoupled trophic responses to long-term recovery from acidification and associated browning in lakes. *Glob. Change Biol.* 25, 1779–1792. doi: 10.1111/gcb.14580

Leech, D. M., Boeing, W. J., Cooke, S. L., Williamson, C. E., and Torres, L. (2009). UV-enhanced fish predation and the differential migration of zooplankton in response to UV radiation and fish. *Limnol. Oceanogr.* 54, 1152–1161. doi: 10.4319/lo.2009.54.4.1152

Leech, D. M., Pollard, A. I., Labou, S. G., and Hampton, S. E. (2018). Fewer blue lakes and more murky lakes across the continental U.S.: implications for planktonic food webs. *Limnol. Oceanogr.* 63, 2661–2680. doi: 10.1002/lno.10967

Leech, D. M., and Williamson, C. E. (2000). Is tolerance to UV radiation in zooplankton related to body size, taxon, or lake transparency? *Ecol. Appl.* 10, 1530–1540. doi: 10.1890/1051-0761(2000)010[1530:ITTURI]2.0.CO;2

Leech, D. M., and Williamson, C. E. (2001). *In situ* exposure to ultraviolet radiation alters the depth distribution of *Daphnia*. *Limnol. Oceanogr.* 46, 416–420. doi: 10.4319/lo.2001.46.2.0416

Lindholm, M., Wolf, R., Finstad, A., and Hessen, D. O. (2016). Water browning mediates predatory decimation of the arctic fairy shrimp *Branchinecta paludosa*. *Freshw. Biol.* 61, 340–347. doi: 10.1111/fwb.12712

Marinone, M. C., Marque, S. M., Suárez, D. A., del Carmen Diéguez, M., Pérez, P., De Los Ríos, P., et al. (2006). UV radiation as a potential driving force for zooplankton community structure in Patagonian Lakes. *Photochem. Photobiol.* 82, 962–971. doi: 10.1562/2005-09-09-RA-680

Moeller, R. E. (1994). Contribution of ultraviolet radiation (UV-A, UV-B) to photoinhibition of epilimnetic phytoplankton in lakes of differing UV transparency. *Archiv fur Hydrobiologie Beihefte Ergebnisse der Limnologie* 43, 157–170.

Monteith, D. T., Stoddard, J. L., Evans, C. D., de Wit, H. A., Forsius, M., Høgåsen, T., et al. (2007). Dissolved organic carbon trends resulting from changes in atmospheric deposition chemistry. *Nature* 450, 537–541. doi: 10.1038/nature06316

Morris, D. P., Zagarese, H., Williamson, C. E., Balseiro, E. G., Hargreaves, B. R., Modenutti, B., et al. (1995). The attenuation of solar UV radiation in lakes and the role of dissolved organic carbon. *Limnol. Oceanogr.* 40, 1381–1391. doi: 10.4319/lo.1995.40.8.1381

Moulton, T. L. (2018). *rMR: Importing Data from Loligo Systems Software, Calculating Metabolic Rates and Critical Tensions.* R Package Version 1.1.0. Available online at: https://CRAN.R-project.org/package=rMR (accessed January 21, 2018).

Neale, P., and Smyth, R. (2019). "Are warmer waters, brighter waters? An examination of the irradiance environment of lakes and oceans in a changing climate," *in Aquatic Ecosystems in a Changing Climate,* eds D. Häder and K. Gao *(Boca Raton, FL: CRC Press, Taylor & Francis Group)*, 89–115. doi: 10.1201/9780429436130-6

Nova, C. C., Bozelli, R. L., Spitzy, A., and Muller-Navarra, D. (2019). Living in a browning environment: effects on *Daphnia*'s growth and fatty acid pattern. *Limnol. Oceanogr.* 64, 18–31. doi: 10.1002/lno.11016

Olson, M. H., Adams-Deutsch, T., Cassels, K. J., Oliver, A. E., and Mitchell, D. L. (2008). Patterns of ultraviolet radiation exposure in bluegill nests over the course of the spawning season. *Trans. Am. Fish. Soc.* 137, 1446–1454. doi: 10.1577/T07-213.1

Olson, M. H., Colip, M. R., Gerlach, J. S., and Mitchell, D. L. (2006). Quantifying ultraviolet radiation mortality risk in bluegill larvae: effects of nest location. *Ecol. Appl.* 16, 328–338. doi: 10.1890/05-0287

Olson, O. G., Engstrom, D. R., and Fritz, S. C. (1995). "Long-term changes in zooplankton community structure inferred from a chronosequence of lakes in Glacier Bay National Park, Alaska," in *Proceedings of the Third Glacier Bay Science Symposium,* ed D. R. Engstrom (Fort Collins, CO: National Park Service), 154–163.

Overholt, E. P., Hall, S. H., Williamson, C. E., Meikle, C. K., Duffy, M. A., and Cáceres, C. E. (2012). Solar radiation decreases parasitism in *Daphnia*. *Ecol. Lett.* 15, 47–54. doi: 10.1111/j.1461-0248.2011.01707.x

Overholt, E. P., Rose, K. C., Williamson, C. E., Fischer, J., and Cabrol, N. (2016). Behavioral responses of freshwater calanoid copepods to the presence of ultraviolet radiation: avoidance and attraction. *J. Plankton Res.* 38, 16–26. doi: 10.1093/plankt/fbv113

Pace, M. L., Carpenter, S. R., and Cole, J. J. (2015). With and without warning: managing ecosystems in a changing world. *Front. Ecol. Environ.* 13, 460–467. doi: 10.1890/150003

Peng, S., Liao, H., Zhou, T., and Peng, S. (2016). Effects of UVB radiation on freshwater biota: a meta-analysis. *Glob. Ecol. Biogeogr.* 26, 500–510. doi: 10.1111/geb.12552

Persaud, A. D., and Williamson, C. E. (2005). Ultraviolet and temperature effects on planktonic rotifers and crustaceans in northern temperate lakes. *Freshw. Biol.* 50, 467–476. doi: 10.1111/j.1365-2427.2005.01334.x

Pilla, R. M., Williamson, C. E., Zhang, J., Smyth, R. L., Lenters, J. D., Brentrup, J. A., et al. (2018). Browning-related decreases in water transparency lead to long-term increases in surface water temperature and thermal stratification in two small lakes. *J. Geophys. Res. Biogeosci.* 123, 1651–1665. doi: 10.1029/2017JG004321

Pohlert, T. (2018). *trend: Non-Parametric Trend Tests and Change-Point Detection.* R Package Version 1.1.1. Available online at: https://CRAN.R-project.org/package=trend (accessed January 13, 2020).

R Core Team (2019). *R: A Language and Environment for Statistical Computing*. Vienna: R Foundation for Statistical Computing. Available online at: https://www.R-project.org/ (accessed December 12, 2019).

Rautio, M., and Tartarotti, B. (2010). UV radiation and freshwater zooplankton: damage, protection and recovery. *Freshw. Rev.* 3, 105–131. doi: 10.1608/FRJ-3.2.157

Read, J., and Rose, K. C. (2013). Physical responses of small temperate lakes to variation in dissolved organic carbon concentrations. *Limnol. Oceanogr.* 58, 921–931. doi: 10.4319/lo.2013.58.3.0921

Riessen, H. P., Linley, R. D., Altshuler, I., Rabus, M., Sollradl, T., Clausen-Schaumann, H., et al. (2012). Changes in water chemistry can disable plankton prey defenses, *Proc. Natl Acad. Sci. U.S.A.* 109, 15377–15382. doi: 10.1073/pnas.1209938109

Rose, K. C., Greb, S. R., Diebel, M., and Turner, M. G. (2017). Annual precipitation regulates spatial and temporal drivers of lake water clarity. *Ecol. Appl.* 27, 632–643. doi: 10.1002/eap.1471

SanClements, M. D., Oelsner, G. P., McKnight, D. M., Stoddard, J. L., and Nelson, S. J. (2012). New insights into the source of decadal increases of dissolved organic matter in acid-sensitive lakes of the Northeastern United States. *Environ. Sci. Technol.* 46, 3212–3219. doi: 10.1021/es204321x

Seekell, D. A., Lapierre, J.-F., Ask, J., Bergstroem, A.-K., Deininger, A., Rodriguez, P., et al. (2015a). The influence of dissolved organic carbon on primary production in northern lakes. *Limnol. Oceanogr.* 60, 1276–1285. doi: 10.1002/lno.10096

Seekell, D. A., Lapierre, J.-F., and Karlsson, J. (2015b). Trade-offs between light and nutrient availability across gradients of dissolved organic carbon concentration in Swedish lakes: implications for patterns in primary production. *Can. J. Fish. Aquatic Sci.* 72, 1663–1671. doi: 10.1139/cjfas-2015-0187

Snucins, E., and Gunn, J. (2000). Interannual variation in the thermal structure of clear and colored lakes. *Limnol. Oceanogr.* 45, 1639–1646. doi: 10.4319/lo.2000.45.7.1639

Solomon, C. T., Jones, S. E., Weidel, B. C., Buffam, I., Fork, M. L., Karlsson, J., et al. (2015). Ecosystem consequences of changing inputs of terrestrial dissolved organic matter to lakes: current knowledge and future challenges. *Ecosystems* 18, 376–389. doi: 10.1007/s10021-015-9848-y

Sommaruga, R. (2015). When glaciers and ice sheets melt: consequences for planktonic organisms. *J. Plankton Res.* 37, 509–518. doi: 10.1093/plankt/fbv027

Strock, K. E., Saros, J. E., Nelson, S. J., Birkel, S. D., Kahl, J. S., and McDowell, W. H. (2016). Extreme weather years drive episodic changes in lake chemistry: implications for recovery from sulfate deposition and long-term trends in dissolved organic carbon. *Biogeochemistry* 127, 353–365. doi: 10.1007/s10533-016-0185-9

Strock, K. E., Theodore, N., Gawley, W. G., Ellsworth, A. C., and Saros, J. E. (2017). Increasing dissolved organic carbon concentrations in northern boreal lakes: implications for lake water transparency and thermal structure. *J. Geophys. Res. Biogeosci.* 122, 1022–1035. doi: 10.1002/2017JG003767

Thrane, J.-E., Hessen, D. O., and Andersen, T. (2014). The absorption of light in lakes: negative impact of dissolved organic carbon on primary productivity. *Ecosystems* 17, 1040–1052. doi: 10.1007/s10021-014-9776-2

Urmy, S., Williamson, C. E., Leach, T. H., Schladow, S. G., Overholt, E., and Warren, J. D. (2016). Vertical redistribution of zooplankton in an oligotrophic lake associated with reduction in ultraviolet radiation by wildfire smoke. *Geophys. Res. Lett.* 43, 3746–3753. doi: 10.1002/2016GL068533

Weidel, B. C., Baglini, K., Jones, S. E., Kelly, P. T., Solomon, C. T., and Zwart, J. A. (2017). Light climate and dissolved organic carbon concentration influence species-specific changes in fish zooplanktivory. *Inland Waters* 7, 210–217. doi: 10.1080/20442041.2017.1329121

Weyhenmeyer, G. A., Müller, R. A., Norman, M., and Tranvik, L. J. (2016). Sensitivity of freshwaters to browning in response to future climate change. *Clim. Change* 134, 225–239. doi: 10.1007/s10584-015-1514-z

Wickham, H. (2016). *ggplot2: Elegant Graphics for Data Analysis. New York, NY*: Springer-Verlag. doi: 10.1007/978-3-319-24277-4_9

Williamson, C.E., Brentrup, J. A., Zhang, J., Renwick, W. H., Hargreaves, B. R., and Knoll, L. B., et al. (2014). Lakes as sensors in the landscape: optical metrics as scalable sentinel responses to climate change. *Limnol. Oceanogr.* 59, 840–850. doi: 10.4319/lo.2014.59.3.0840

Williamson, C. E. (1983). Invertebrate predation on planktonic rotifers. *Hydrobiologia* 104, 385–396. doi: 10.1007/BF00045996

Williamson, C. E. (1984). Laboratory and field experiments on the feeding ecology of the freshwater cyclopoid copepod, *Mesocyclops edax*. *Freshw. Biol.* 14, 575–585. doi: 10.1111/j.1365-2427.1984.tb00177.x

Williamson, C. E. (2019). *Three Decades of Limnological Data from Lakes in the Pocono Mountains Region, Pennsylvania, USA, 1988-2018. Environmental Data Initiative (EDI)*. doi: 10.6073/pasta/834c813f123c8faf3d59477e54bfc3ce

Williamson, C. E., Hargreaves, B. R., Orr, P. S., and Lovera, P. A. (1999). Does UV play a role in changes in predation and zooplankton community structure in acidified lakes? *Limnol. Oceanogr.* 44, 774–783. doi: 10.4319/lo.1999.44.3_part_2.0774

Williamson, C. E., Madronich, S., Lal, A., Zepp, R. E., Lucas, R. M., Overholt, E. P., et al. (2017). Climate change-induced increases in precipitation are reducing the potential for solar ultraviolet radiation to inactivate pathogens in surface waters. *Sci. Rep.* 7:13033. doi: 10.1038/s41598-017-13392-2

Williamson, C. E., and Magnien, R. E. (1982). Diel vertical migration in *Mesocyclops edax*: implications for predation rate estimates. *J. Plankton Res.* 4, 329–339. doi: 10.1093/plankt/4.2.329

Williamson, C. E., Metzgar, S. L., Lovera, P. A., and Moeller, R. E. (1997). Solar ultraviolet radiation and the spawning habitat of yellow perch, *Perca flavescens*. *Ecol. Appl.* 7, 1017–1023. doi: 10.1890/1051-0761(1997)007[1017:SURATS]2.0.CO;2

Williamson, C. E., Olson, O. G., Lott, S. E., Walker, N. D., Engstrom, D. R., and Hargreaves, B. R. (2001). Ultraviolet radiation and zooplankton community structure following deglaciation in Glacier Bay, Alaska. *Ecology* 82, 1748–1760. doi: 10.1890/0012-9658(2001)082[1748:URAZCS]2.0.CO;2

Williamson, C. E., Overholt, E. P., Brentrup, J. A., Pilla, R. M., Leach, T. H., Schladow, S. G., et al. (2016). Sentinel responses to droughts, wildfires, and floods: effects of UV radiation on lakes and their ecosystem services. *Front. Ecol. Environ.* 14, 102–109. doi: 10.1002/fee.1228

Williamson, C. E., Overholt, E. P., Pilla, R. M., Leach, T. H., Brentrup, J. A., Knoll, L. B., et al. (2015). Ecological consequences of long-term browning in lakes. *Sci. Rep.* 5:18666. doi: 10.1038/srep18666

Williamson, C. E., Stemberger, R. S., Morris, D. P., Frost, T. M., and Paulsen, S. G. (1996). Ultraviolet radiation in North American lakes: attenuation estimates from DOC measurements and implications for plankton communities. *Limnol. Oceanogr.* 41, 1024–1034. doi: 10.4319/lo.1996.41.5.1024

Williamson, C. E., Zagarese, H., Schulze, P., Hargreaves, B., and Seva, J. (1994). The impact of short-term exposure to UV-B radiation on zooplankton communities in north temperate lakes. *J. Plankton Res.* 16, 205–218. doi: 10.1093/plankt/16.3.205

Wissel, B., Boeing, W. J., and Ramcharan, C. W. (2003a). Effects of water color on predation regimes and zooplankton assemblages in freshwater lakes. *Limnol. Oceanogr.* 48, 1965–1976. doi: 10.4319/lo.2003.48.5.1965

Wissel, B., Yan, N. D., and Ramcharan, C. W. (2003b). Predation and refugia: implications for *Chaoborus* abundance and species composition. *Freshw. Biol.* 48, 1421–1431. doi: 10.1046/j.1365-2427.2003.01100.x

Wolf, R., and Heuschele, J. (2018). Water browning influences the behavioral effects of ultraviolet radiation on zooplankton. *Front. Ecol. Evol.* 6:26. doi: 10.3389/fevo.2018.00026

Zhang, H., Urrutia-Cordero, P., He, L., Geng, H., Chaguaceda, F., Xu, J., et al. (2018). Life-history traits buffer against heat wave effects on predator-prey dynamics in zooplankton. *Glob. Change Biol.* 24, 4747–4757. doi: 10.1111/gcb.14371

Conflict of Interest: The authors declare that the research was conducted in the absence of any commercial or financial relationships that could be construed as a potential conflict of interest.

frontiers in Marine Science

ORIGINAL RESEARCH
published: 30 June 2020
doi: 10.3389/fmars.2020.00512

An Empirically Derived Trimodal Parameterization of Underwater Light in Complex Coastal Waters – A Case Study in the North Sea

Jochen Wollschläger[1], Beke Tietjen[1], Daniela Voß[1] and Oliver Zielinski[1,2]*

[1] Institute for Chemistry and Biology of the Marine Environment, University Oldenburg, Oldenburg, Germany, [2] German Research Center for Artificial Intelligence (DFKI), Oldenburg, Germany

OPEN ACCESS

Edited by:
Christian Grenz, UMR 7294 Institut Méditerranéen d'Océanographie (MIO), France

Reviewed by:
Alexey K. Pavlov, Institute of Oceanology, PAN, Poland
Cecile Dupouy, UMR 7294 Institut Méditerranéen d'Océanographie (MIO), France

****Correspondence:***
Jochen Wollschläger
jochen.wollschlaeger@uol.de; jochen.wollschlaeger@uni-oldenburg.de

Specialty section:
This article was submitted to Marine Ecosystem Ecology, a section of the journal Frontiers in Marine Science

Received: *10 March 2020*
Accepted: *04 June 2020*
Published: *30 June 2020*

Citation:
Wollschläger J, Tietjen B, Voß D and Zielinski O (2020) An Empirically Derived Trimodal Parameterization of Underwater Light in Complex Coastal Waters – A Case Study in the North Sea. Front. Mar. Sci. 7:512. doi: 10.3389/fmars.2020.00512

As an essential parameter for all kinds of aquatic life, light influences life cycles and the behavior of various marine organisms. However, its primary role is that of a driver for photosynthesis and thus primary production, forming the basis of the marine food web. As a simplification when dealing with light, a common measure (e.g., used in biogeochemical models) is the photosynthetically active radiation (PAR), which integrates the spectral distribution of photon flux between 400 and 700 nm into a single value. While passing through the water column, light is attenuated by the water itself and its optically active substances (OAS) [e.g., phytoplankton, chromophoric dissolved organic matter (CDOM), and non-algal particles], summarized in the diffuse attenuation coefficient of downwelling radiation (K_d). Existing parameterizations for light attenuation in models often consider only phytoplankton as parameter, which is not sufficient for coastal areas where the contributions of CDOM and suspended mineral particles can be substantial. Furthermore, they mostly ignore the spectral variability of K_d by attenuating PAR with only a single coefficient. For this reason, this study proposes a parameterization of K_d that involves all relevant OAS and that attenuates PAR in three bands (trimodal approach). For this, the hyperspectral underwater light field was examined on three expeditions in different areas of the North Sea and along the British and Irish coasts. The derived K_d spectra were stepwise decomposed in the contributions of the different OAS and used in combination with direct OAS measurements to derive substance specific attenuation coefficients for the three bands. For comparison, also a monomodal and a spectral parameterization were developed. Evaluation showed that the trimodal approach was almost as accurate as the full spectral approach, while requiring only marginally more computational performance as the classical monomodal approach. Being therefore an excellent compromise between these factors, it can act as a valuable, yet computational affordable addition to biogeochemical models in order to improve their performance in coastal waters.

Keywords: underwater light field, PAR, modeling, optically active substances, chlorophyll, suspended matter, CDOM, North Sea

INTRODUCTION

Light is a parameter essential for aquatic life. It transfers heat to the upper water column, eventually leading to stratification, by that shaping the abiotic conditions for a considerable period of the year. Furthermore, light also influences life cycles and behavior of various organisms (McFarland, 1986). However, its most fundamental role is that of a resource that drives photosynthesis and thus primary production, essentially fueling the whole food web. For photosynthesis, the part of the electromagnetic spectrum is of importance that covers the range of 400–700 nm, as this is the region where the various photosynthetic pigments have their absorption maxima. Since for photosynthetic electron transport each photon, when absorbed (regardless of its wavelength and thus energy), is of equal efficiency, the biological relevant light is commonly summarized as photosynthetically active radiation (PAR), which is the integrated number of photons from 400 to 700 nm (in photons m^{-2} s^{-1}; for a list of abbreviations used in this study see **Table 1**).

When light enters the water column, it is subject to scattering and absorption (summarized as attenuation), which lead to a reduction of PAR with depth. This reduction can be described by an exponential function (e.g., Kirk, 2011):

$$PAR\,(z) = PAR\left(0^{-}\right)^{*} \exp -K_d\,(PAR)^{*}\,z\,(0)^{*} \exp -K^{*}_{d\,PAR} z$$

Here, z is the depth in which the light availability is going to be calculated, PAR(0^-) is the light just below the surface, and K_d (PAR) is the diffuse attenuation coefficient of PAR (in m^{-1}). K_d (PAR) depends on the degree by which the downwelling light is absorbed and scattered by the water itself, but also by the optically active substances (OAS) that are present therein (Mobley, 1994; Kirk, 2011; Zielinski, 2013). In the photosynthetic relevant part of the light spectrum, these constituents are mainly phytoplankton with its various pigments, especially chlorophyll-a (chl-a), but also chromophoric dissolved organic matter (CDOM), as well as non-algal particles like detritus and inorganic suspended particulate matter (iSPM). K_d (PAR) can be thought of being composed of the diffuse attenuation coefficients of water and these OAS. However, the attenuating properties of these substances are not equal over the range of PAR: Pure water attenuates predominantly at wavelengths >600 nm, while the absorption of all OAS generally increases toward the shorter wavelengths (but in various intensity). Scattering of CDOM is negligible compared to its absorption, although due to the small size of the molecules (per definition <0.2 μm), the scattering efficiency of the shorter wavelengths is higher. The scattering properties of larger particles like phytoplankton cells and iSPM are less wavelength depended, but their contribution to light attenuation can be high, especially in coastal areas (Kirk, 2011). Thus, an accurate representation of light attenuation with depth requires the use of a spectrally resolved attenuation coefficient [K_d (λ)], which can be obtained by taking hyperspectral measurements of the downwelling irradiance [E_d (λ)] in various depths (Lee et al., 2005; Kirk, 2011). Spectral light availability in dependence of waters OAS can be modeled by using radiative transfer equations, as implemented in software like HydroLight-EcoLight (Mobley, 1994).

Nevertheless, for many applications like calculating photosynthetic rates or primary productivity, only the

TABLE 1 | List of regularly used abbreviations.

Parameter	Unit	Definition
a_{cdom}	m^{-1}	Absorption coefficient of chromophoric dissolved organic matter
a_p	m^{-1}	Absorption coefficient of particles
CDOM	–	Chromophoric dissolved organic matter
Chl-a	μg L^{-1}	Chlorophyll-a
CTD	–	Conductivity, temperature, depth
E_d	W m^{-2}	Downwelling irradiance
E_s	W m^{-2}	Irradiance, above the sea surface
iSPM	mg L^{-1}	Inorganic suspended particulate matter
IOP –	Inherent optical properties	
K_d	m^{-1}	Diffuse attenuation coefficient
K_d*	m^{-1} (unit OAS)$^{-1}$	Substance specific diffuse attenuation coefficient
K_{dap}	m^{-1}	Diffuse absorption coefficient of particles
K_{dbp}	m^{-1}	Diffuse particle scattering coefficient
K_{dcdom}	m^{-1}	Diffuse attenuation coefficient of CDOM
K_{diSPM}	m^{-1}	Diffuse attenuation coefficient of inorganic suspended particulate matter
K_{dOAS}	m^{-1}	Diffuse attenuation coefficient of optically active substances
K_{dp}	m^{-1}	Diffuse particle attenuation coefficient
K_{dphyt}	m^{-1}	Diffuse attenuation coefficient of phytoplankton pigments
K_{dwater}	m^{-1}	Diffuse attenuation coefficient of water
OAS	–	Optically active substance
PAR	μmol photons m^{-2} s^{-1}	Photosynthetically active radiation
SD	m	Secchi depth
z	m	Depth, specific
λ	nm	Light wavelength, specific

bulk parameter PAR is used. Although it has been shown that the use of spectral light data significantly alters the result of ecosystem models (Mobley et al., 2015), there are a couple of reasons for using spectrally integrated, thus PAR-based approaches. This includes on the one hand the sparsity of available spectral data and the greater effort in evaluating a spectral model (Thewes et al., 2020), but also the increase in computational effort. Although the latter point will probably become less important with technological progress, to date it is still a limiting factor, both with respect to time and costs.

A common way of expressing vertical light attenuation in biogeochemical models is to parameterize K_d (PAR) with OAS that are part of the model (e.g., Fasham et al., 1990; Kühn and Radach, 1997; Zielinski et al., 2002). However, in many cases, only chl-a as representative of phytoplankton biomass is considered, what potentially limits the use of these parameterizations in coastal waters, where constituents like CDOM and iSPM contribute largely to light attenuation and also do not necessarily co-vary with phytoplankton abundance (case II waters; Morel and Prieur, 1977; Mobley, 1994). Furthermore, unweighted attenuation of PAR completely ignores the spectral dependence of the attenuation properties of the different OAS. In attempting to overcome this issue while still considering computational efficiency, bi- and multimodal parameterizations have been developed (Paulson and Simpson, 1977; Morel, 1988; Zielinski et al., 2002; Dutkiewicz et al., 2015), which have shown to be advantageous. In such approaches, the PAR spectrum is divided into two or more spectral bands, either equally spaced or driven by considerations related to the attenuation properties of the OAS. Then, for each band, a separate K_d is parameterized using the OAS of relevance. When subsequently modeling the attenuation of PAR with depth, its scalar surface value is proportionally divided according to the size of the spectral bands, and the K_d values are applied separately.

In this study, the results of underwater light field and water constituent measurements made along onshore-offshore transects in a coastal environment (North Sea) are shown. The collected data were used to parameterize the attenuation of PAR in a novel trimodal approach in order to obtain a sufficiently accurate, but still computational affordable representation of light attenuation in coastal waters for modeling purposes. The trimodal parameterization includes chl-a, iSPM, and also salinity as proxy for CDOM (Bowers et al., 2004), taking into account the typical V-shape of spectral K_d (λ) in coastal areas. In the mid-part of the spectrum usually the minimum of K_d (λ) is observed, which determines the visible transparency of the water as determined by Secchi disk measurement (Lee et al., 2015). This potential connection between modern model calculations and historical Secchi disk data was a further rationale for choosing the trimodal approach. Modeled PAR profiles using the trimodal approach are compared to measured data, but also to the profiles modeled with a monomodal and a spectral parameterization approach. Finally, strengths and weaknesses of the chosen approach are discussed.

MATERIALS AND METHODS

Research Area

The research area covers the southern and central North Sea as well as parts of the British and Irish coasts. Data were collected on discrete stations during three cruises with the research vessel "Heincke" (Knust et al., 2017; HE503: February/March 2018, HE516: July/August 2018, and HE527: March 2019; hereafter denoted as Winter, Summer, and Spring cruise). Thus, a wide range of different conditions is represented in the dataset used for this study. **Figure 1** shows the position of the stations which were considered for data analysis. Taking into account the different sampling depths, the total number of observations were n = 31/219/75 (Winter/Summer/Spring). However, not all parameters were available at each station, therefore the actual number of observations varies between the analyses.

Measurements of Underwater Light Field

Hyperspectral profiles of the underwater light field were taken in the range of 346–800 nm using a free falling profiling instrument (HyperPro II, Seabird Scientific, United States). It is equipped with a planar (cosine) radiometer for measuring downwelling irradiance E_d (λ) and a radiance-type radiometer with a field-of-view of 8.5° for measuring upwelling radiance L_u (λ). Furthermore, a reference irradiance sensor (identical to the E_d sensor) was attached to the upper deck of the ship to measure the available light above the sea surface E_s (λ). For this study, only data covering the range of PAR (400–700 nm) were considered. The HyperPro II has further mounted sensors for measuring conductivity, temperature, and pressure, as well as an ECO Puck (Seabird Scientific, United States) with channels for chlorophyll fluorescence (excitation 470 nm and emission 695 nm), CDOM fluorescence (excitation 370 nm and emission 460 nm), and backscattering (at 700 nm). The deployment of the profiler followed the protocols given in Holinde and Zielinski (2016) and Mascarenhas et al. (2017): Per station, at least three profiles were taken. Before starting the measurements, the ship was positioned with the stern to the sun to avoid ship shadow on the profile area and the reference sensor. The profiler's pressure sensor was tared on deck with the instrument being in an upright position. The profiler was deployed by its own drift in approximately 30 m distance to the ship, before it was lowered in free-falling mode with a speed of approx. 0.5 m/s. Profiles were taken as deep as possible, but at least to the depth which is reached by 1% of surface (above water) PAR. Data obtained during an instrument tilt $>10°$ was omitted from the dataset.

In order to account for changes in ambient light during the profile, E_d (λ) was normalized to E_s (λ) measured by the reference sensor (Mueller et al., 2003). Quality control was performed per wavelength according to the procedure suggested by Organelli et al. (2016) for radiometric data obtained from ARGO-floats. Profiles were extrapolated to the surface using the logarithm of the data points with the highest quality (flag 1) and a 2nd order polynomial fit. E_d (λ) data was smoothed spectrally using a moving median (window size: 7 nm) and subsequently, PAR was calculated by converting energy spectra of E_d (λ) (W/m^2 s)

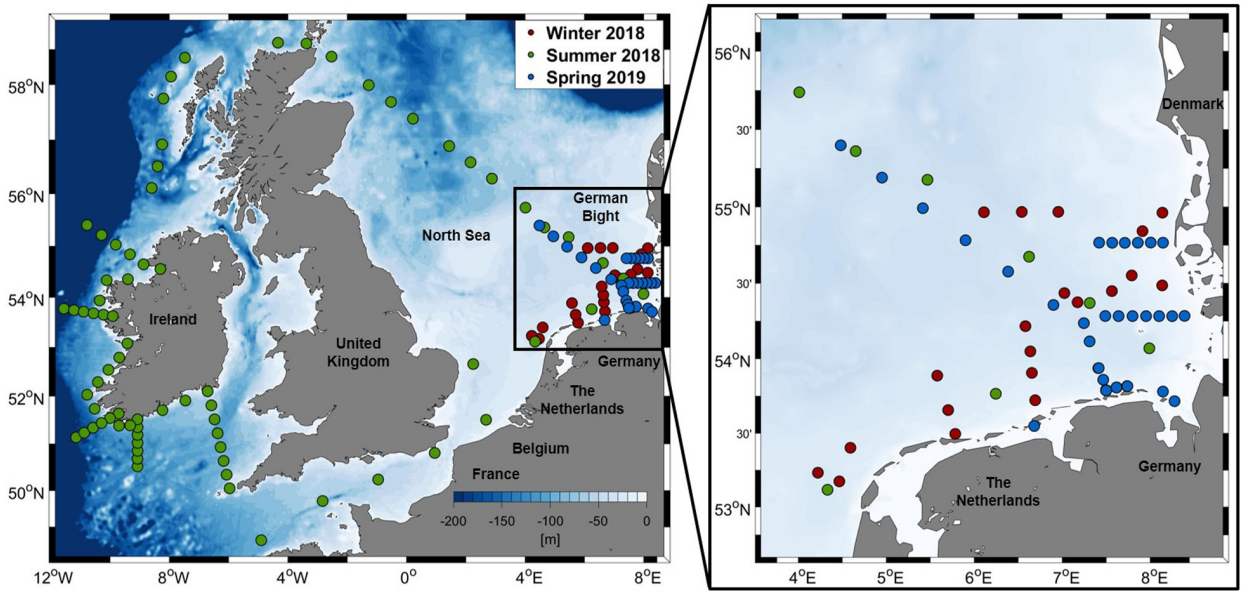

FIGURE 1 | Area of research with sampling stations, categorized by cruise **(left)**, close-up of the German Bight area **(right)**.

in photon flux density spectra (μmol photons/m^2 s) and integrate the spectrum from 400 to 700 nm. Profiles of K_d (λ) and K_d (PAR) were calculated as local slopes from the E_d (λ) and PAR profiles, respectively (Smith and Baker, 1984, 1986), using a half interval of 1 m. E_d (λ) and K_d (λ) from the obtained profiles were inspected manually for the respective sampling depths (see below), the most reasonable spectrum was used in the parameterization.

Additionally, Secchi depth (SD) was measured as indicator for water transparency. For this, a white disk of 30 cm diameter was lowered into the water up to the point where it was no longer visible. This depth was noted as SD.

Determination of Optically Active Substances and Absorption Coefficient Spectra

In order to link the light field measurements with the IOPs and OAS, water samples were taken at the stations using a carousel water sampler equipped with a CTD system (SBE911plus, Seabird Scientific, United States) including sensors for conductivity, temperature, pressure, oxygen, chl-a fluorescence (ECO-FL, excitation 470 nm, emission 695 nm, Seabird Scientific, United States), and beam transmission (C-Star, 650 nm, Seabird Scientific, United States). Up to three depths were sampled: The first sampling depth was 4–5 m, the second the depth in which a potential chlorophyll maximum occurred, and the third was the bottom depth. Not all depths were sampled on each station (e.g., in case the water column was thoroughly mixed); the decision was made based on the online data of the CTD sensors.

The sampled water was processed directly on board. For chlorophyll-a determination, aliquots of 0.2–10 L (depending on concentration of particulate matter) were filtered on pre-wetted glass fiber filters (47 mm diameter, pore size approximately 0.7 μm; Whatman, United Kingdom) and were subsequently frozen and stored at −80°C. Pigment extraction was done within 6 months after the cruise in 90% acetone-water solution with overnight incubation at 4°C. Additionally, extracts from empty filters were prepared as blanks. Extracts were centrifuged for 10 min at 3,020 × g and the fluorescence of the supernatant was determined at 665 nm before and after acidification of the samples using a pre-calibrated TD-700 laboratory fluorometer (Turner Designs, San Jose, CA, United States). On the basis of these measurements, chl-a concentration was calculated according to Arar and Collins (1997), taking into account the results from the blank filters. For SPM determination, pre-washed, pre-combusted, and pre-weighted filters of the same type as for chl-a analysis were used. After wetting the filter with purified water to prevent the accumulation of salt on the rim as much as possible, aliquots of 0.2–17 L sample water were filtered. After filtration, the filter was rinsed with purified water (>50 mL) to avoid salt remains. Subsequently, the filters were frozen and stored at −25°C, and SPM concentration was determined gravimetrically in the laboratory directly after the cruise. In order to obtain the concentration of iSPM afterward, the organic fraction was removed by combusting the filters at 450°C for 8 h, and the gravimetric analysis was repeated.

Water samples were further analyzed onboard with a custom-built PSICAM (Kirk, 1997; Röttgers et al., 2005) in order to obtain the total, particulate, and CDOM absorption coefficients hyperspectrally and free of scattering errors in a range of 400–700 nm. The specifications of the PSICAM used are described in Wollschläger et al. (2019). The measurement procedure was identically with that described in Röttgers and Doerffer (2007), while the calibration was made using a solid standard instead of the nigrosin solution (Wollschläger et al., 2019). Total spectral absorption coefficients a (λ) were determined by measuring an

unfiltered water sample (approximately 450 mL), while CDOM spectral absorption coefficients [a_{cdom} (λ)] was determined after filtration of the sample through a 0.2 μm membrane filter (Whatman, United States. The difference between the two measurements is considered the particulate absorption a_p (λ). The CDOM absorption at 440 nm [a_{cdom} (440)] was initially used as a proxy for CDOM concentration, however, for the parameterization the complete spectrum was used.

Per station, depth profiles of chl-a and iSPM were generated by correlating the laboratory data with the corresponding *in situ* chl-a fluorescence and beam transmission data. In order to have a positive correlation between beam transmission and iSPM concentration, the beam transmission was inverted to attenuance (1-transmission) and expressed in percent. CDOM profiles were created by correlations between different parts of a_{cdom} (λ) and practical salinity (calculated from CTD temperature and conductivity), as in coastal areas, the main sources of CDOM are riverine input and terrestrial runoff. All *in situ* data have been smoothed moderately in advance to remove spikes using a cubic smoothing spline, following the recommendations given in the MATLAB documentation for the "csaps.m" function, which was used for this purpose. Afterward, the profiles have been checked for reasonability by manual inspection.

Decomposition of K_d Spectra

In this study, it is assumed that K_d (λ) is linearly composed of the absorption and scattering contributions of phytoplankton (represented by chl-*a* concentration), CDOM (represented by salinity), iSPM, and water.

$$K_d(\lambda) = K_{d\ water}(\lambda) + K_{d\ cdom}(\lambda) + K_{d\ phyt}(\lambda) + K_{d\ iSPM}(\lambda)$$

We are aware that this is only a simplification as shown recently by Lee et al. (2018), however, this approach was chosen in order to keep the model as simple as possible. For the parameterization of K_d (λ) using the mentioned variables, it is necessary to establish substance-specific diffuse attenuation coefficient values (K_d*) for the selected spectral regions. For this, K_d (λ) measured at the stations have to be decomposed with respect to the contributions of the single OAS. The procedure relies on measurements of the absorption coefficients, as K_d (λ) is a function of the inherent optical properties absorption (*a*) and backscatter (b_b), with $a >> b_b$ (Mobley, 1994). It is described in the following, a visual summary is given in **Figure 2**.

As the water attenuation spectrum is known from literature (Morel and Maritorena, 2001), it can be subtracted from K_d (λ) to obtain the attenuation coefficient spectrum of the OAS [$K_{d\ OAS}$ (λ) = K_d (λ) − $K_{d\ water}$ (λ)]. $K_{d\ OAS}$ (λ) has to be subsequently divided in $K_{d\ cdom}$ (λ), $K_{d\ phyt}$ (λ), and $K_{d\ iSPM}$ (λ). Because CDOM is nearly dissolved in water, its attenuation can be thought of being largely driven by its absorption properties. Thus, a_{cdom} (λ) determined by PSICAM measurements can be assumed to be identical with $K_{d\ cdom}$ (λ). Its subtraction from $K_{d\ OAS}$ (λ) gives the diffuse particle attenuation coefficient $K_{d\ p}$ (λ) composed of the absorption and scattering properties of phytoplankton cells and iSPM [$K_{d\ p}$ (λ) = $K_{d\ OAS}$ (λ) − $K_{d\ cdom}$ (λ)]. The contribution of detritus is neglected at this point, as it is small compared to that of the other components. The particle absorption coefficients a_p (λ) have been directly measured with the PSICAM, and under the assumption that they are identical with the diffuse particle absorption coefficients $K_{d\ ap}$ (λ), they are subtracted from $K_{d\ p}$ (λ) to obtain $K_{d\ bp}$ (λ), the diffuse particle scattering coefficient [$K_{d\ bp}$ (λ) = $K_{d\ p}$ (λ) − $K_{d\ ap}$ (λ)]. Theoretically, $K_{d\ bp}$ (λ) summarizes the scattering of phytoplankton and iSPM, but the scattering in coastal waters is usually much stronger determined by iSPM due to its higher refractive index (Kirk, 2011). For this reason, and as we have no means to decompose $K_{d\ bp}$ (λ) further, it is regarded to be completely related to iSPM for our purposes. Similar to the diffuse particle scattering coefficient, the diffuse absorption coefficient $K_{d\ ap}$ (λ) is also composed of the contributions of phytoplankton and iSPM. The latter can become significant, especially in coastal areas with high sediment loads. For the decomposition of $K_{d\ ap}$ (λ) in the iSPM and phytoplankton part, respectively, the phytoplankton absorption is assumed to be largely driven by the phytoplankton pigments, neglecting contributions of non-pigmented phytoplankton parts (e.g., cell walls). Since phytoplankton pigment absorption is close to zero at wavelengths >700 nm (Babin and Stramski, 2002; Röttgers et al., 2007; Clementson and Wojtasiewicz, 2019), any absorption that is still visible at this wavelength can be thought to be related to iSPM. Because the absorption of inorganic matter increased exponentially toward the shorter wavelengths, a full iSPM absorption spectrum can be extrapolated based on a_p(700) as well as the equation and the mean slope provided by Bowers and Binding (2006). The constructed iSPM absorption coefficient spectrum is then added to the scattering part of $K_{d\ bp}$ (λ) to obtain $K_{d\ iSPM}$ (λ) [$K_{d\ iSPM}$ (λ) = $K_{d\ bp}$ (λ) + $K_{d\ ap(iSPM)}$ (λ)]. What remains is the diffuse attenuation coefficient of the phytoplankton pigments $K_{d\ phyt}$ (λ).

The derived spectra of $K_{d\ cdom}$ (λ), $K_{d\ iSPM}$ (λ), and $K_{d\ phyt}$ (λ) are subsequently related to the respective OAS (in case of CDOM with the proxy parameter salinity) by linear regression, in order to obtain the K_d* values required for the model formulation (see section "Deriving Substance-Specific K_d Values for the Different Optically Active Substances").

RESULTS AND DISCUSSION

Diffuse Attenuation Coefficient Spectra

K_d (λ) has been calculated from E_d (λ) profiles obtained during the three cruises. The values ranged from 0.04 to 1.95 m^{-1}, with considerable spectral variability (**Figure 3**, left panel). Generally, the values increased toward the blue and the red part of the spectrum, with minima in the range of 480 to 580 nm (**Figure 3**, right panel). The increase toward the shorter wavelengths was smaller for most of the stations from the summer cruise. Despite the quality control and smoothing of E_d (λ) before K_d (λ) calculation, some of the spectra still show artifacts or noise, especially in the red above 650 nm, and to a lesser degree also in the blue below 450 nm. Furthermore, not all spectra extend over

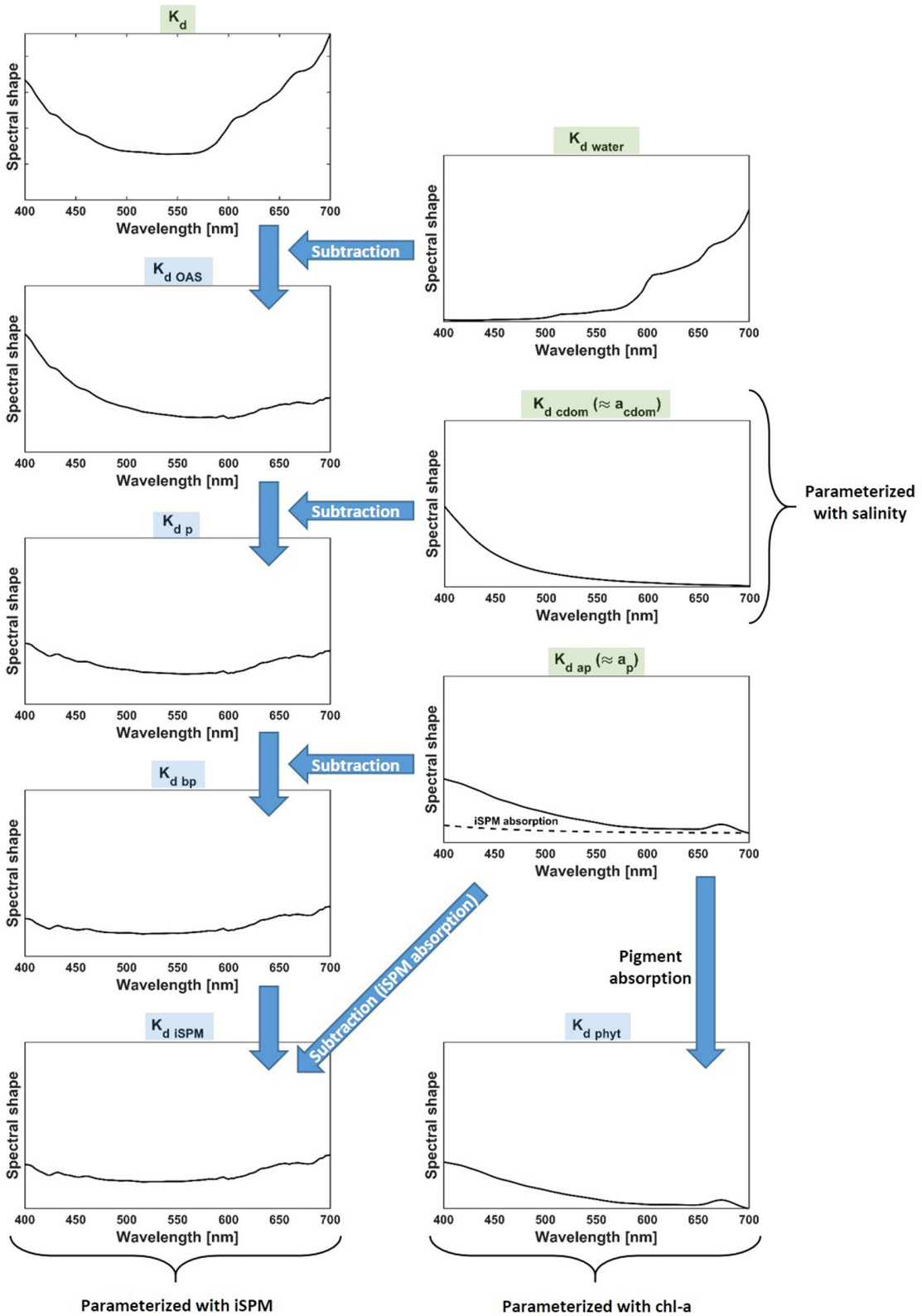

FIGURE 2 | Decomposition of K_d (λ) in spectra associated to the various optically active constituents [$K_{d\ water}$ (λ), $K_{d\ cdom}$ (λ), $K_{d\ phyt}$ (λ), and $K_{d\ iSPM}$ (λ)]. The arrows indicate which parameter has been taken into account for deriving the respective decomposition step. Parameters highlighted in green originate from measurements, while the parameters highlighted in blue are derived from the decomposition.

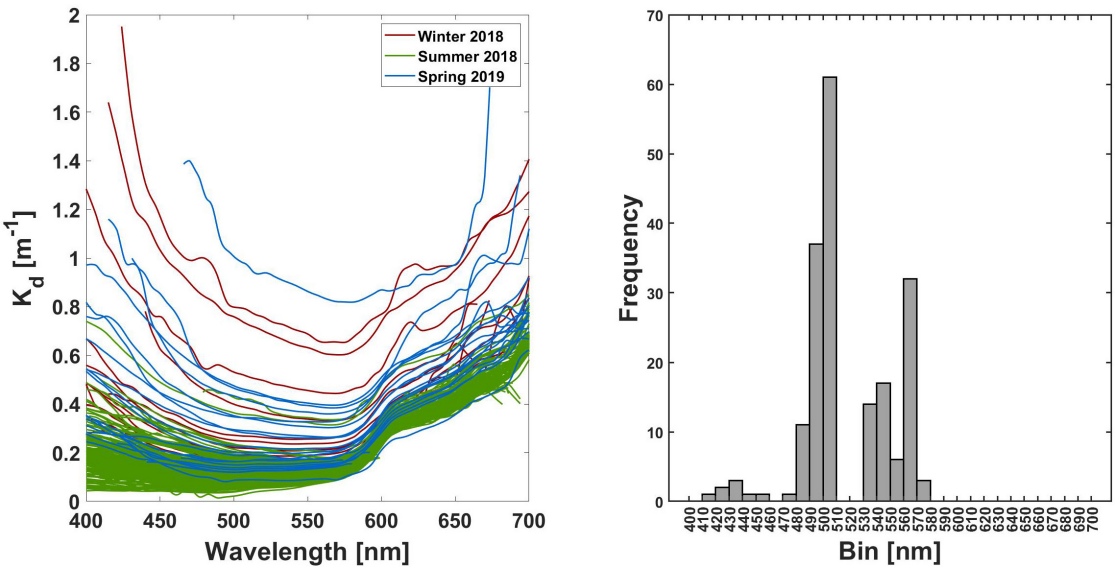

FIGURE 3 | Overview of K_d (λ). Spectra obtained at the sampling sites **(left)**. Histogram of K_d (λ) minimum wavelength distribution **(right)**.

the full range of PAR, as extremely noisy data did not pass the quality control. In the red spectral region light is already rapidly attenuated in the first few meters by the water itself. Therefore it is generally difficult to obtain reliable light field measurements in this region (Mueller et al., 2003), an effect that is increased by the presence of other light absorbing compounds. Similarly, as in coastal areas the concentration of OAS is commonly high compared to the open ocean, this effect can also be seen in the blue region, where the OAS dominate attenuation. However, as for the parameterization the median of a certain spectral range is used, the impact of artifacts or even incomplete spectra on the final result becomes smaller.

Relationships Between Optically Active Substances and *in situ* Proxies

Directly, the OAS were determined only at stations in various depths by discrete sampling. However, for modeling PAR profiles based on these substances and the established substance-specific attenuation coefficients (see section "Assessment of the Model Approaches"), depth-resolved OAS data is necessary. For this reason, the discrete measurements were correlated with the values of the *in situ* proxies in the respective depth (chl-a fluorescence for chl-a, beam attenuance for iSPM, and salinity for CDOM). The obtained coefficients allow a conversion of the proxy data profiles into OAS profiles. For chl-a and CDOM, linear regressions were used, while for iSPM, a more accurate representation was a polynomial fit of second order. Data were analyzed together but also separated by cruise (**Figure 4**). Potential outliers have been identified by analyzing the residuals of the linear regressions from the individual cruises. If the residual of a certain data point was outside of the residual mean ± 2 times their standard deviation, the data point was considered as being an outlier. For the sake of showing the complete dataset, they are displayed in **Figure 4** as crosses, but were not taken into account for the final regressions.

Chl-a concentrations were found to be 0.16 to 20.6 μg/L over all cruises, with considerably narrower ranges in Winter and Summer 2018 (**Figure 4**, upper panels). There were reasonable linear correlations with *in situ* chl-a fluorescence for all three cruises as well as for the combined dataset, with R^2 values ranging from 0.71 to 0.96. The offset (c0) in the data was similar, what was to be expected as the instrument used was identical and checked, but not recalibrated between the cruises. Interestingly, the slope (c1) was considerably higher in Summer 2018 than in the two other cruises, and also in the combined dataset. This indicates a real change in the ratio of chl-a to *in situ* chl-a fluorescence, which can occur due to differences in community composition, light acclimatization, and nutritional status of the phytoplankton (Kiefer, 1973; Soohoo et al., 1986; Cunningham, 1996). All these factors can vary with both season and location, and in fact, both the time and the study area of the Summer cruise were considerably different from the others. In contrast, the timing of the Winter and Spring cruise was similar, and so was the slope of the linear regression.

Regarding CDOM, here given as a_{cdom} (440) ranging from 0.01 to 0.61 m^{-1}, the results for the linear regressions were quite similar in all three cruises: CDOM was inversely related to salinity with a slope ranging between −0.046 and −0.053, while the offset was between 1.674 and 1.889 with R^2 between 0.66 and 0.98. This inverse relationship is to be expected under conservative mixing conditions when the dominant source of CDOM is riverine input and runoff from land (Liss, 1976; Stedmon and Markager, 2003; Bowers et al., 2004). In this form, it is a typical feature of European coastal waters and would have to be validated for other coastal regions. Furthermore, the slope of this relation can vary according to the optical properties of the CDOM, which are in turn influenced by, e.g., its chemical

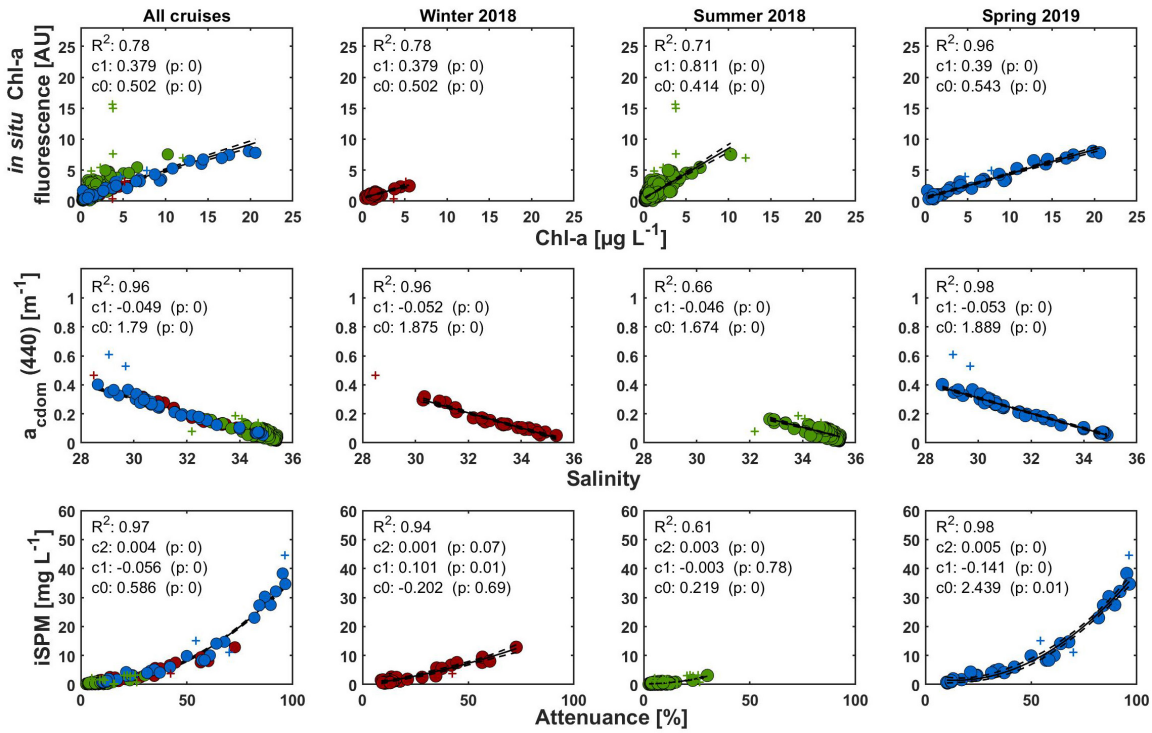

FIGURE 4 | Correlations between optically active substances and their respective *in situ* proxies. Data points considered as outliers (see text) are displayed as crosses and are not included in the fit represented by the solid line. The dashed lines give its 95% confidence interval. AU means that chl-a fluorescence is given in arbitrary units.

composition and degradation processes (Helms et al., 2008 and references therein). Thus, it is to a certain extent region-specific. In more offshore regions, other processes than conservative mixing (e.g., autochthonous production by phytoplankton) start to determine CDOM distribution, what weakens the relationship between salinity and CDOM. In this context, the strikingly higher variability and the less negative slope of the Summer cruise (**Figure 4**) compared to the others might be explainable with a higher number of offshore stations, and a general shift in research area (compare **Figure 1**). However, as the correlation applied to the pooled data indicates, salinity is still a sufficient proxy for CDOM absorption the investigated area. Of course, the relationship shown in **Figure 3** is only an example, because as CDOM absorption is a spectral parameter, its relationship to salinity varies with wavelength. Fits between salinity and other a_{cdom} (λ) wavelengths were of similar quality with R^2 values in the range of 0.75 to 0.96, but with different slopes and offsets (data not shown). Therefore, it is not accurate to use only a selected wavelength to convert salinity into CDOM, as its influence on light attenuation varies over the spectrum. Therefore, salinity was directly parameterized as a representative of CDOM in the different approaches (see section " Deriving Substance-Specific K_d Values for the Different Optically Active Substances").

Concentrations of iSPM varied between 0.02 and 40.52 mg L^{-1}. Highest concentration was obtained in the southern German Bight near the barrier islands and the Elbe estuary, while they were lowest off the continental shelf west of Ireland. Like the correlation of CDOM and salinity, the correlation for iSPM and beam attenuance was more variable in the Summer cruise than in the Winter and Spring cruise (R^2 of 0.59 compared to 0.94 and 0.98, respectively). This might also be caused by a more variable particle composition due to the more heterogeneous study area, but maybe also because of a smaller data range covered.

As a consequence of the variability between the cruises, the conversion of *in situ* data into OAS was done with the cruise specific coefficients, not with the coefficients obtained for the pooled dataset.

Deriving Substance-Specific K_d Values for the Different Optically Active Substances

In order to parameterize K_d (λ) on the basis of OAS concentration, it was decomposed in $K_{d\ water}$ (λ), $K_{d\ cdom}$ (λ), $K_{d\ phyt}$ (λ), and $K_{d\ iSPM}$ (λ) as described above (see section "Decomposition of K_d Spectra"). Subsequently, the median was taken (i) from the complete spectra (monomodal approach), (ii) from three spectral bands (trimodal approach), or (iii) the data were used in 1 nm resolution (spectral approach). The median was used instead of the mean, since it leads to a parameterization that provided model results more closely to the measured data, as has been found in the later assessment (not shown). The substance-specific K_d values (K_d*) for all

approaches were derived by applying linear fits to correlations of the median or spectral K_d data with chl-a concentration, salinity (directly parameterized as a proxy of CDOM), and iSPM concentration, respectively.

As the trimodal approach is the focus of this study, the results of these fits (**Figure 5**, **Table 2**) will be discussed in more detail. Nevertheless, the coefficients of the monomodal approach are given in **Table 3**, while that of the spectral approach are given in the **Supplementary Material**. With exception of $K_{d\ cdom}$, all fits were performed without intercept, assuming no contribution to K_d when the respective OAS is not present. This is justified, because calculations including an intercept showed that it was low in all cases and not statistically significant ($p > 0.05$, data not shown). K_d* of the OAS was considered to be the slope of the respective fit ($p < 0.05$ in all cases).

The range of the bands in the trimodal approach was not determined arbitrary, but was based on the spectral shape of K_d (λ). As shown in **Figure 3**, the majority of the spectra had their minimum value between 481 and 580 nm, which justifies this wavelength range to be defined as a spectral band (K_d II). On that basis, K_d I is the band covering the shorter wavelengths (400–480 nm), while K_d III covers the longer wavelengths (581–700 nm). Although the bands have been derived from this specific dataset, they are probably suitable also for other coastal environments. Due to sampling in different seasons and at different locations, a certain variability in K_d (λ) is already included in the data and thus considered in the definition of spectral band II (and thus the other two bands). Even if the optical properties defining the spectral shape of K_d (λ) might change to a certain extent with region, the general characteristic of having a minimum in the greenish wavelengths should persist.

It can be seen that K_d*(I) > K_d*(II) > K_d*(III) for all OAS with the exception of iSPM, where K_d* in spectral band III is as high as in band I. Normally, it would be expected of $K_{d\ iSPM}$ (λ) to decrease slowly with increasing wavelength, because this is the shape of the iSPM absorption coefficient spectrum, while the scatter spectrum is uniform over the wavelengths or has (due to Rayleigh scattering) also an decrease toward the longer wavelengths. However, as it is exemplarily shown in **Figure 2**, the $K_{d\ iSPM}$ (λ) spectrum that results from the decomposition of total K_d (λ) increases again toward the longer wavelengths, what is consistent with the observed higher K_d*$_{iSPM}$ in band III compared band II. This results probably from the fact that the simple addition (or in this case: subtraction) of the K_d (λ) contributions of the OAS are only an approximation, which is not fully consistent with radiative transfer theory (Lee et al., 2018). As demonstrated in the named publication, there are especially differences toward the red part of the spectrum, what fits to the observations made. Another source of discrepancy could be that K_d (λ) measurements and water sampling for the absorption coefficient measurements have not been performed at exactly the same location or time. The profiler was deployed approximately 30 m away from the ship, and the light profiles were taken approximately 45 min after the start of the CTD. However, this might have contributed to general variability in the data, but not to deviations specifically in the red part of the spectrum. But in general, a major part of all uncertainties associated with the measurements and the decomposition procedure are summarized in the $K_{d\ iSPM}$ (λ) parameter, as it is the last one that is derived in the course of the decomposition. Nevertheless, as light in spectral region III is anyway attenuated rapidly with depth due to the water itself ($K_{d\ water}$ (III): 0.31 m^{-1}) and, in coastal areas, due to high iSPM concentration, the slight overestimation of K_d*$_{iSPM}$ (III) can be considered of minor importance.

The relationship of salinity and $K_{d\ cdom}$ (I/II/III) becomes more variable in the high-saline regions (**Figure 5**, upper panels). Especially data points belonging to the Summer 2018 cruise are often located above the linear fit established for the whole dataset. This might indicate an increasing contribution of autochthonous production of CDOM by phytoplankton that weakens the conservative relationship between CDOM and salinity valid in the more coastal (less saline) waters. This has implications for the performance of the trimodal model approach with the proposed coefficients in these areas. However, the effect should be comparably small, as in spectral band I, where the impact of CDOM (and thus K_d*$_{cdom}$) is the highest, the variability in the high saline waters is still comparably small. Although the variability becomes higher in spectral bands II and III, its effect on the performance of the parameterization should be still low, as the coefficients itself are much smaller than in band I.

Compared to the other OAS, the relationship between chl-a and $K_{d\ phyt}$ (I/II/III) is the most variable. As K_d*$_{phyt}$ is basically identical with the chlorophyll-specific absorption coefficient (see the description of the decomposition procedure), also its sources of variability are the same. First of all, $K_{d\ phyt}$ (λ) is not only determined by chl-a, but is influenced by the occurrence of other photosynthetic and photoprotective pigments, as well as with the pigment packaging effect (Morel and Bricaud, 1981; Bricaud et al., 1995, 2004; Kirk, 2011). Thus, factors like phytoplankton taxonomical composition (spatial differences and seasonal succession) and light acclimatization contribute to the variability of K_d*$_{phyt}$ (I/II/III). For this reason, the highest uncertainty in the parameterization is probably associated with the values of K_d*$_{phyt}$ (I/II/III). In general, although the coefficients in this study have been derived from a dataset that already contains a certain regional and seasonal variability, the inclusion of additional data from other coastal areas would be beneficial to assess their general validity.

Assessment of the Model Approaches

In order to evaluate the performance of the monomodal, trimodal, and spectral approach to describe the attenuation of PAR with depth, a comparison between modeled and measured PAR profiles was made. For the trimodal approach, the modeled PAR profiles were calculated for each station from surface to the maximum depth of the measurements according to:

$$PAR(z) = PAR(0^-)^*[0.27\exp(-K_d(I)^*z) + 0.36\exp(-K_d(II)^*z) + 0.37\exp(-K_d(III)^*z)]$$

The factors 0.27, 0.36, and 0.37 represent the proportions of the three spectral bands to total PAR. They were derived by normalizing E_d (λ, 0^-) of all stations to the mean of E_d (λ, 0^-)

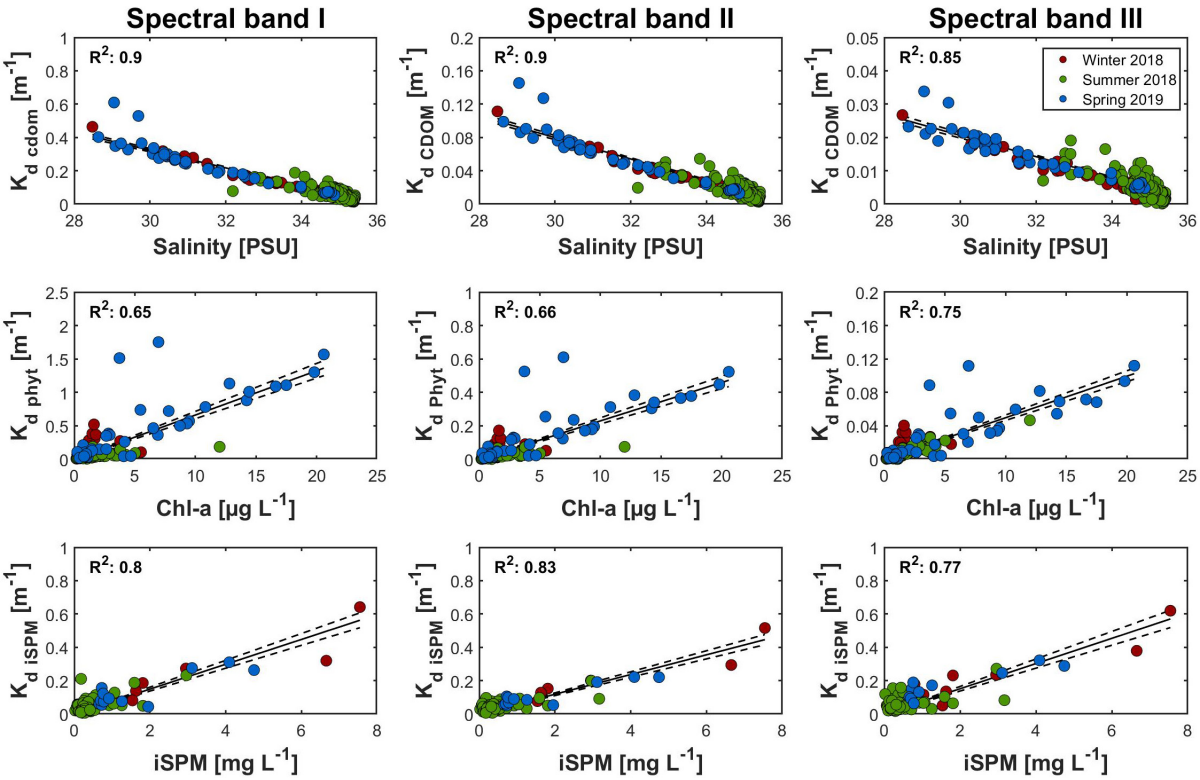

FIGURE 5 | Linear fits between the optically active constituents (CDOM represented by salinity) and their median K_d values in the three spectral bands. The solid line represents the linear fit, while the dashed lines give its 95% confidence interval.

TABLE 2 | Summary of the substance-specific diffuse attenuation coefficients (K_d*) for different OAS in the trimodal approach.

	Band I (400–480 nm)		Band II (481–580 nm)		Band III (580–700 nm)	
Optically active substance	**c1 [K_d* (I)]**	**c0 [Offset (I)]**	**c1 [K_d* (II)]**	**c0 [Offset (II)]**	**c1 [K_d* (III)]**	**c0 [Offset (III)]**
CDOM [m^{-1} PSU^{-1}]/[m^{-1}]	−0.053	1.918	−0.013	0.466	−0.003	0.116
Phytoplankton (L m^{-1} μg^{-1})	0.066	–	0.023	–	0.005	–
iSPM (L m^{-1} mg^{-1})	0.075	–	0.059	–	0.076	–

All coefficients are statistically significant at $p < 0.05$. Note that the c1 coefficients for CDOM are negative due to the inverse relationship of a_{cdom} (λ) and salinity.

over the whole dataset. Subsequently, these normalized spectra were integrated over the complete spectral range (giving PAR) as well as over the wavelengths constituting the spectral bands (giving the fraction of PAR that corresponds to the size of the respective band). The proportion of each integrated band to the total integrated spectrum was calculated for each station, and the median values were included in the equation above. In order to calculate PAR in a given depth, PAR(0^-) was partitioned proportionally to the size of the bands using these factors, and the bands were attenuated independently of each other down to that depth, before the values are finally summarized into PAR. The K_d profiles of the bands were calculated using the respective substance-specific coefficients (**Table 2**) and the *in situ* data acquired with the CTD. Chl-a fluorescence and beam attenuance have been converted in chl-a and iSPM concentration profiles for that purpose (see section "Relationships Between Optically Active Substances and *in situ* Proxies").

TABLE 3 | Summary of the substance-specific diffuse attenuation coefficients (K_d*) for different OAS in the monomodal approach.

K_d*$_{cdom}$ (m^{-1} PSU^{-1})	CDOM offset (m^{-1})	K_d*$_{phyt}$ (L m^{-1} μg^{-1})	K_d*$_{iSPM}$ (L m^{-1} mg^{-1})
−0.01	0.363	0.017	0.065

All coefficients are statistically significant at $p < 0.05$. Note that the c1 coefficients for CDOM are negative due to the inverse relationship of a_{cdom} (λ) and salinity.

$$K_d = \left(K^*_{d\ water} z\right) + \left(K^*_{d\ cdom} \int_0^z Salinity\left(z'\right) dz' + Salinity\ Offset\right) + \left(K^*_{d\ phyt} \int_0^z Chl-a\left(z'\right) dz'\right) + \left(K^*_{d\ iSPM} \int_0^z iSPM\left(z'\right) dz'\right)$$

For clarity, the designation of the bands (I/II/III) have been omitted in the equation above.

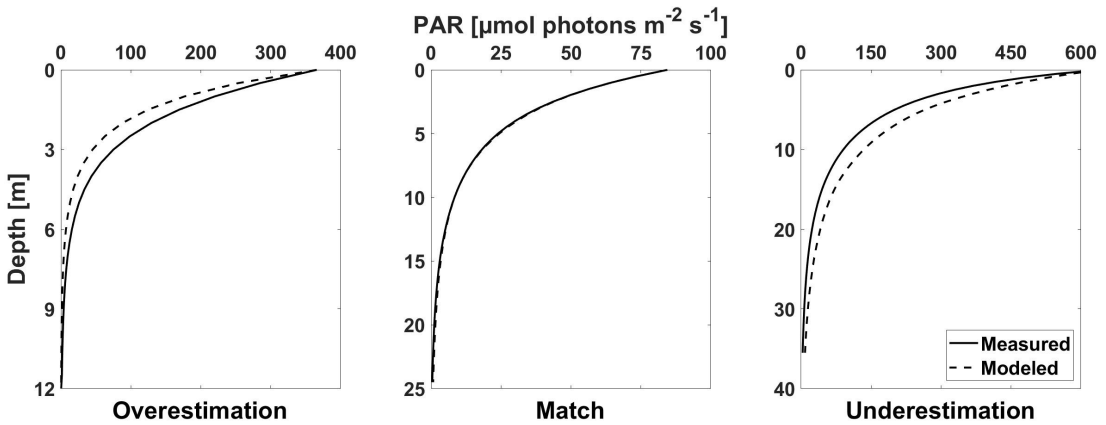

FIGURE 6 | Examples of measured and modeled PAR profiles at selected stations. Overestimation of available PAR by the trimodal approach **(left)**, match of model and measurements **(center)**, and underestimation **(right)**.

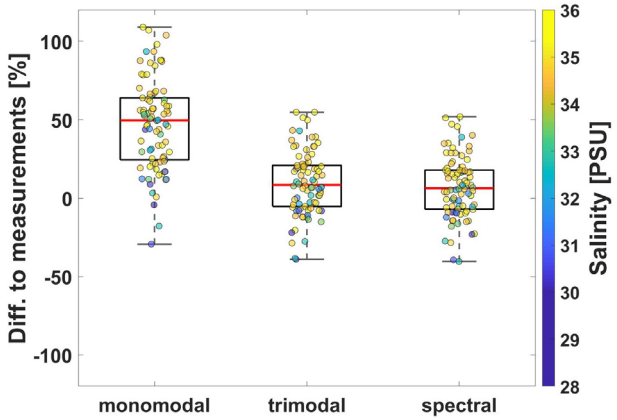

FIGURE 7 | Boxplot of the differences between depth-integrated modeled and measured PAR as percentage of the measurements. The data points give the differences for the individual stations, colored according to the respective median salinity.

The modeling of PAR profiles with the monomodal and spectral approach have been performed in a similar manner. However, for the monomodal approach no partitioning of PAR(0^-) was performed and only one K_d profile valid for the whole spectrum was calculated using OAS concentrations and OAS-specific K_d^* (**Table 3**). For the spectral approach, PAR(0^-) was partitioned in 301 bands (corresponding to a resolution of 1 nm) using a factor of 0.0033, and K_d profiles were calculated individually for each wavelength (for wavelength-specific K_d^* values see **Supplementary Material**).

Examples of typical measured and modeled PAR profiles are illustrated in **Figure 6**, showing overestimation, match, and underestimation of PAR by the model. In order to quantify these differences, both profiles were integrated over the investigated water column at all stations, basically obtaining two scalar values representing the measured and estimated amount of light present per station. The difference between model results and measurements were then expressed as percentage of the measurements. Thus, for example, a perfect match at a given station would result in a value of 0%, while ±10% means a 10% over- or underestimation of integrated PAR over the water column by the model data.

When comparing the three approaches in this respect, it can be seen that the trimodal approach performs similar to the spectral approach, while the monomodal approach overestimated the available light much more. The median differences to the measurements were 50, 8, and 6% for the monomodal, trimodal, and spectral approach, respectively (**Figure 7**). In addition, also the spread in the differences was considerably higher in the monomodal (−30 to 110%) than in the other approaches (approximately −40 to 50%). Thus, while K_d (PAR) is on average estimated correctly by the spectral and trimodal approach, it is systematically underestimated by the monomodal approach. Obviously, taking the median of K_d (λ) from the different OAS during the parameterization lead to K_d^* values that were too low to model light attenuation with depth correctly. The spread of the data in the boxplots (thus the variability in the differences) is related on the one hand to the variability of the OAS specific attenuation coefficients (**Figure 5** for the trimodal approach). They describe only an average attenuation of a specific concentration of a substance (represented by the slope of the fit). However, at a specific site, the properties of the OAS might deviate from this average. On the other hand, it has to be taken into consideration that not only the quality of the K_d^* values and thus the parameterization is responsible for any differences observed between measured and modeled PAR, but also the quality of the available OAS data. For an ideal evaluation of the model performance, direct measurements of OAS (pigment concentration and gravimetry of suspended matter) in high vertical resolution would be desirable. In practice, this would require an unrealistic high effort for a suitable number of profiles. Thus, the common way is to measure (optical) proxies which are then converted into OAS concentrations, as done in this study. However, this transfers any variability between the optical proxy and its OAS in the evaluation of the model performance,

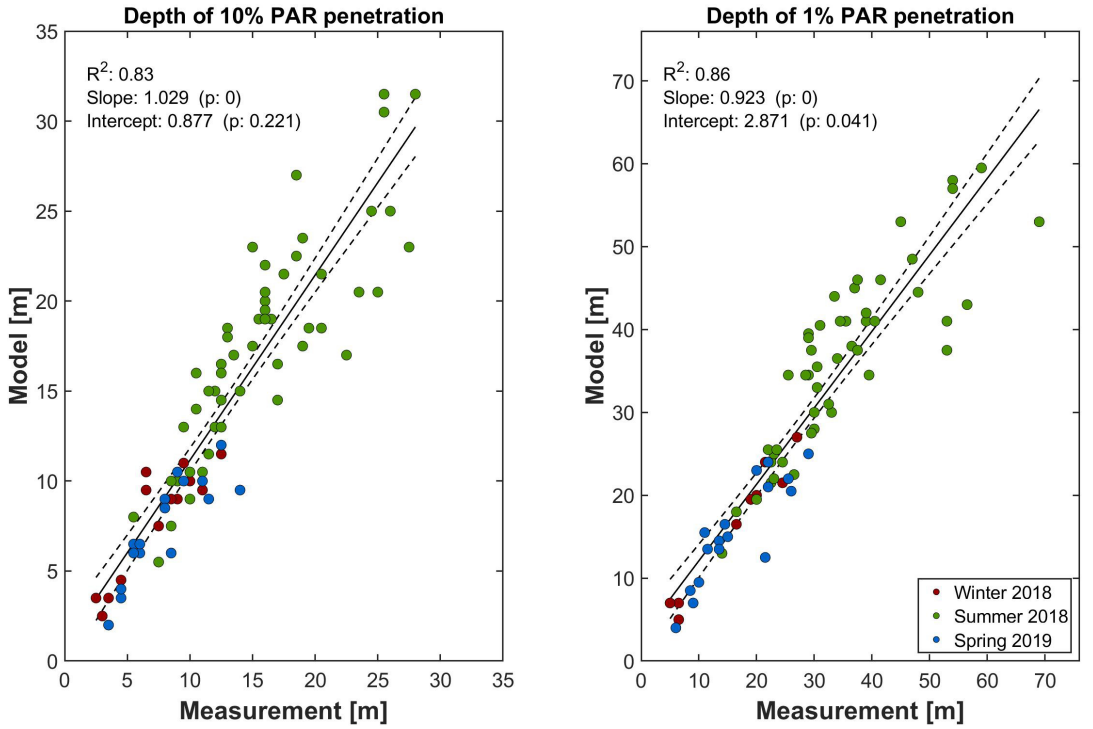

FIGURE 8 | Comparison of penetration depths from PAR derived from *in situ* and modeled profiles (trimodal approach). The solid line represents the linear fit, while the dashed lines give its 95% confidence interval.

e.g., changes in the relation between chl-a fluorescence to chl-a due to vertical changes in phytoplankton composition or due to non-photochemical quenching. Thus, the assessment made here primarily compares the approaches with each other, and the performance of the modeling approaches might be even better than implied by our evaluations.

In terms of computational effort, the monomodal approach required only 12% the time of the spectral approach, while the trimodal approach was only marginally slower with 13%. Although these values can only be a rough estimate, since the computational effort always depend on the hardware used and the efficiency of the code, this finding indicates that the trimodal approach is an excellent compromise between computational efficiency and accuracy regarding PAR attenuation with depth.

This is also supported by the fact that despite the differences in depth-integrated PAR, the PAR profiles derived with the trimodal approach reproduced well common measures of water transparency, like the center and the lower limit of the euphotic zone, which correspond to the depths were 10 and 1% of surface PAR are available to photosynthetic organisms (Kirk, 2011; **Figure 8**). For both penetration depths, linear correlations between measured and modeled data showed high R^2 values (0.83 and 0.86), and the slope of the fit was near the 1:1 line in both cases. This was comparable to regressions using data obtained from the spectral model (**Table 4**). Also the 10 and 1% PAR penetration depths derived from the monomodal model showed a strong linear correlation to the measured depths (R^2 of 0.8 for both depths). The slopes deviated more from the 1:1 line than that from the trimodal and spectral dataset, but the main difference was a statistically significant ($p < 0.05$) offset of 3.9 m (10% depth) and 7.4 m (1% depth). This would lead to high errors in estimating water transparency, especially in shallow coastal areas.

Derivation of Secchi Depth From K_d (II)

A special feature of the trimodal parameterization approach is the fact that the second spectral range [K_d (II)] covers basically the wavelengths where the majority of the measured K_d spectra had their minimum (**Figure 3**). As the SD can be estimated by $1/K_d$ (λ_{min}) (Lee et al., 2015), in this study it was also tested to use K_d (II) for this purpose. As K_d (λ_{min}) was on average approximately 6% smaller than K_d (II) (calculation not shown), K_d (II) has been multiplied by 0.94 before calculating SD. The modeled SD were then compared to those measured at the cruise stations (**Figure 9**). There was a reasonably robust linear relationship between the data modeled on the basis of K_d (II) and the measured SD data ($R^2 = 0.65$, left panel). However, in contrast to the results shown in Lee et al. (2015), the modeled values were almost 50% higher than the observations. This was apparently not an effect from using K_d (II) for SD calculation, as the correlation with SD data modeled with the real K_d (λ_{min}) yielded almost identical results (data not shown). However, when only a data range of 0–10 m is considered, the slope of the linear regression is much closer to the 1:1 line. Although this could indicate inaccuracies in K_d (II) values derived with the OAS-specific K_d* coefficients in clearer waters, this is probably not the case, since the estimations of 10 and 1% light penetration depths (**Figure 8**)

TABLE 4 | Results of linear fits between observed and modeled PAR penetration depths for the different parameterization approaches.

	10% depth			1% depth		
Parameterization approach	R^2	**Slope (c1)**	**Offset (c0) (m^{-1})**	R^2	**Slope (c1)**	**Offset (c0) (m^{-1})**
Monomodal	0.8	1.048	3.905	0.8	0.881	7.44
Trimodal	0.83	1.029	0.877*	0.86	0.923	2.871
Spectral	0.84	1.023	0.744*	0.86	0.937	2.152*

*Values marked with * are not statistically significant on the 0.05 level.*

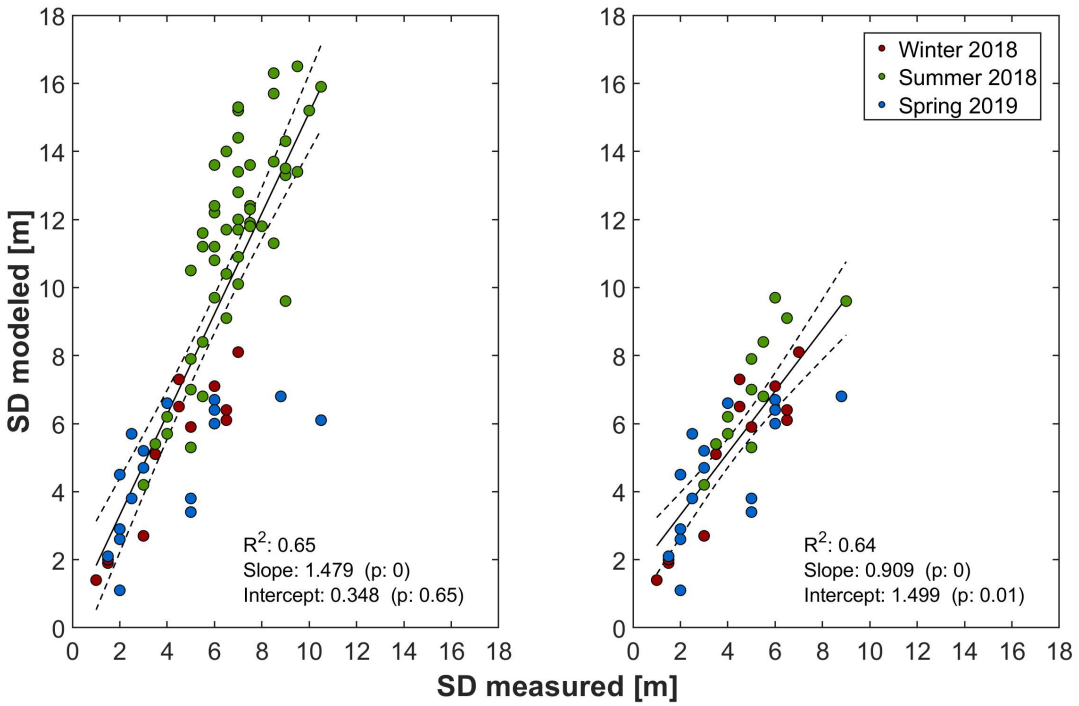

FIGURE 9 | Correlation of observed Secchi depths and those derived from K_d in spectral region II **(left)**. Same correlation considering only values up to 10 m depth **(right)**. The solid line represents the linear fit, while the dashed lines give its 95% confidence interval.

do not show similar deviations at these stations. Therefore, it is more likely that there was a bias in the SD field measurements in these optically deeper waters. As SD measurements are by their nature subjective, errors can occur easily, especially when the measurements are performed near the ship under suboptimal conditions (moderate to high waves or currents that drag the disk below the vessel). Nevertheless, even if the deviations were a result of the modeling process, the correlations provided in **Figure 9** would provide a mean to correct for that.

Practical Implementation of the Trimodal Parameterization in Numerical Models

The implementation of the trimodal parameterization in an existing coastal model could be made comparably straightforward. Of course, the first prerequisite would be that the model provides the variables used in the parameterization to describe PAR attenuation (chl-a, salinity, and iSPM), or that they could be derived from other variables of the model. If this is the case, the old parameterization could be replaced with the trimodal approach, including the coefficients shown in **Table 2**. Ideally, their validity for the area of interest should be checked beforehand as they could vary due to regional and temporal differences in the properties of the OAS, as discussed before. Subsequently, PAR has to be parted proportionally to the size of the spectral bands, and each band has to be attenuated independently with depth, as stressed in section "Assessment of the Model Approaches." Practically, this is realized in a stepwise process using the K_d (I/II/III) value calculated for this depth and the light that is transferred from the layer above as input.

The use of the trimodal parameterization in models covering both costal and open ocean waters would require additional modifications, a crucial point would be the smooth transition between case II waters, where attenuation by the different OAS vary independently, and case I waters, where they vary with phytoplankton abundance. Assuming that the trimodal approach is used for the whole area of the model, and that

there is no jump between different PAR parameterizations, the calculations would be made like described above and in section "Assessment of the Model Approaches." The attenuation due to iSPM (mostly suspended sediment), would become less anyway in the three bands toward the open ocean areas since the model would probably not provide much suspended sediments in these (usually deeper) areas. Otherwise, the suspended sediment component would have turned off in water to be considered case I, as suggested by Thewes et al. (2020). Similarly, also $K_{d\ cdom}$ (which reflects the contribution of terrestrial CDOM to PAR attenuation) would become smaller, reflecting that in the more saline open ocean waters this OAS is not relevant anymore. However, according to **Figure 5**, $K_{d\ cdom}$ would become negative at salinity >35.5, resulting in increasing (instead of decreasing) PAR with depth in the open ocean. To avoid this artifact, the model should set negative $K_{d\ cdom}$ values to zero. The most crucial part is probably related to ${K_d}^*_{phyt}$: due to differences in taxonomical composition, size, and the increasing importance of autochthonous CDOM, its values are probably different between the coastal and open ocean areas. In order to include such a shift in the parameterization, ${K_d}^*_{phyt}$ could be related to a parameter that describes the water mass or the coastal distance (e.g., salinity or bathymetry). However, this is probably not straightforward and would require additional studies specifically dedicated to this problem (including more measurements under open ocean conditions).

CONCLUSION

In contrast to the open ocean, where the optical properties are predominantly determined by the phytoplankton present, coastal waters are optically more complex. CDOM and non-algal particles play a more important role, and their contribution vary independently of phytoplankton abundance. However, when it comes to vertical attenuation of light (or more specific, of PAR) that is important for the calculation of primary productivity and phytoplankton growth, many biogeochemical models use parameterizations that do not account for this complexity. Furthermore, also the spectral variability in the light attenuation by different OAS is often ignored by, e.g., using mean values calculated over the whole spectrum as attenuation coefficients.

In this study, a trimodal parameterization has been developed that divides surface PAR in three parts which sizes correspond to the sizes of three spectral bands. These bands have been selected according to the spectral shape of K_d (λ) spectra measured in the field. In the first band, all OAS contribute similar to attenuation, while that of water is negligible. The second band is that where K_d had its minimum, and the third band is dominated by attenuation of water and iSPM, while contributions of CDOM and phytoplankton (chl-a) are negligible. PAR in each band is attenuated independently by using band- and substance-specific attenuation coefficients (${K_d}^*$) and profiles of OAS concentrations. This parameterization was compared in terms of accuracy in light attenuation and computational effort with a classical monomodal parameterization (that includes, however, in addition to chl-a also contributions of CDOM and iSPM to light attenuation), and a full spectral parameterization with 1 nm resolution. Although the ${K_d}^*$ values in this study have been derived from a dataset that contains already a certain degree of spatial and seasonal heterogeneity, it has to be kept in mind that they can change due to changes in the OAS' optical properties. Thus, they can be considered as a reasonable first estimate, but should be validated with additional field data, especially when the parameterization would be used in other coastal areas.

However, PAR profiles have been modeled for all approaches and were compared to field measurements of PAR. It has been found that the trimodal approach for the investigated research area of the North Sea provided an estimation of light attenuation that is of similar accuracy as a spectral approach, by being simultaneously of similar efficiency as a classical monomodal approach. Furthermore, as a special feature, the use of the trimodal approach allows the estimation of SDs that are of similar quality than those based on spectral K_d. This offers the possibility of adding SD with low effort as an output to biogeochemical models, and therefore relate model scenarios to historical observations of SD data. In summary, this makes the trimodal approach an ideal parameterization of light attenuation for biogeochemical models with many nodes, facilitating improved light prediction and primary production estimation on wide temporal and spatial scales.

DATA AVAILABILITY STATEMENT

The data used in this study are available on request from the authors. Unprocessed data from the free falling profiler as well as quality controlled CTD data from all cruises are available on PANGAEA (Badewien and Wisotzki, 2018, 2019; Krock and Wisotzki, 2018; Wollschläger et al., 2020a,b,c).

AUTHOR CONTRIBUTIONS

JW and OZ conceptualized the study. BT, DV, and JW performed the field investigations. BT and JW analyzed the data. All authors were involved in the interpretation of the results. DV, JW, and OZ wrote the manuscript. All authors contributed to the article and approved the submitted version.

FUNDING

This work was supported by the project "Coastal Ocean Darkening," funded by the German Lower Saxony Ministry for Science and Culture [VWZN3175]. DFKI acknowledges financial support by the MWK through "Niedersachsen Vorab" [ZN3480].

ACKNOWLEDGMENTS

Thanks goes to Rohan Henkel and Kathrin Dietrich who helped with the deployments of the instruments and with the laboratory analyses. We would like to thank also Daniel Thewes for giving his comments regarding the implementation of the parameterizations in models. As well, many thanks go to the crew

of the research vessel "Heincke" for their help on the cruises AWI_HE503_00, AWI_HE516_00, and AWI_HE527_00 where the data for this study has been gathered. Finally, we would like to thank the reviewers of this manuscript who helped to improve its quality by their comments.

SUPPLEMENTARY MATERIAL

The Supplementary Material for this article can be found online at: https://www.frontiersin.org/articles/10.3389/fmars.2020.00512/full#supplementary-material

REFERENCES

Arar, E. J., and Collins, G. B. (1997). *Method 445.0: In Vitro Determination of Chlorophyll a and Pheophytin a in Marine and Freshwater Algae by Fluorescence*. Ohio: National Exposure Research Laboratory.

Babin, M., and Stramski, D. (2002). Light absorption by aquatic particles in the near-infrared spectral region. *Limnol. Oceanogr.* 47, 911–915. doi: 10.4319/lo.2002.47.3.0911

Badewien, T. H., and Wisotzki, A. (2018). *Physical Oceanography During HEINCKE cruise HE503*. Bremerhaven: Alfred Wegener Institute.

Badewien, T. H., and Wisotzki, A. (2019). *Physical Oceanography During HEINCKE cruise HE527*. Bremerhaven: Alfred Wegener Institute.

Bowers, D. G., and Binding, C. E. (2006). The optical properties of mineral suspended particles: A review and synthesis. *Estuar. Coast. Shelf Sci.* 67, 219–230. doi: 10.1016/j.ecss.2005.11.010

Bowers, D. G., Evans, D., Thomas, D. N., Ellis, K., and Williams, P. J. L. B. (2004). Interpreting the colour of an estuary. *Estuar. Coast. Shelf Sci.* 59, 13–20. doi: 10.1016/j.ecss.2003.06.001

Bricaud, A., Babin, M., Morel, A., and Claustre, H. (1995). Variability in the chlorophyll-specific absorption coefficients of natural phytoplankton: Analysis and parameterization. *J. Geophys. Res.* 100, 13321–13332.

Bricaud, A., Claustre, H., Ras, J., and Oubelkheir, K. (2004). Natural variability of phytoplanktonic absorption in oceanic waters: Influence of the size structure of algal populations. *J. Geophys. Res. Ocean.* 109:CI1010.

Clementson, L. A., and Wojtasiewicz, B. (2019). Dataset on the absorption characteristics of extracted phytoplankton pigments. *Data Br.* 24:103875. doi: 10.1016/j.dib.2019.103875

Cunningham, A. (1996). Variability of in-vivo chlorophyll fluorescence and its implications for instrument development in bio optical oceanography. *Sci. Mar.* 60, 309–315.

Dutkiewicz, S., Hickman, A. E., Jahn, O., Gregg, W. W., Mouw, C. B., and Follows, M. J. (2015). Capturing optically important constituents and properties in a marine biogeochemical and ecosystem model. *Biogeosciences* 12, 4447–4481. doi: 10.5194/bg-12-4447-2015

Fasham, M. J. R., Ducklow, H. W., and McKelvie, S. M. (1990). Modeling plankton dynamics in oceanic mixed systems. *J. Mar. Res.* 48, 591–639. doi: 10.1357/002224090784984678

Helms, J. R., Stubbins, A., Ritchie, J. D., Minor, E. C., Kieber, D. J., and Mopper, K. (2008). Absorption spectral slopes and slope ratios as indicators of molecular weight, source, and photobleaching of chromophoric dissolved organic matter. *Limnol. Oceanogr.* 53, 955–969. doi: 10.4319/lo.2008.53.3.0955

Holinde, L., and Zielinski, O. (2016). Bio-optical characterization and light availability parameterization in Uummannaq Fjord and Vaigat-Disko Bay (West Greenland). *Ocean Sci.* 12, 117–128. doi: 10.5194/os-12-117-2016

Kiefer, D. A. (1973). Chlorophyll a fluorescence in marine centric diatoms: Responses of chloroplasts to light and nutrient stress. *Mar. Biol.* 23, 39–46. doi: 10.1007/bf00394110

Kirk, J. T. (1997). Point-source integrating-cavity absorption meter: theoretical principles and numerical modeling. *Appl. Opt.* 36, 6123–6128.

Kirk, J. T. O. (2011). *Light & Photosynthesis in Aquatic Ecosystems*, 3rd Edn. New York, NY: Cambridge University Press.

Knust, R., Nixdorf, U., and Hirsekorn, M. (2017). Research Vessel HEINCKE Operated by the Alfred-Wegener-Institute. *J. Large-Scale Res. Facil. JLSRF* 3, 1–8.

Krock, B., and Wisotzki, A. (2018). *Physical Oceanography During HEINCKE cruise HE516*. Bremerhaven: Alfred Wegener Institute.

Kühn, W., and Radach, G. (1997). A one-dimensional physical-biological model study of the pelagic nitrogen cycling during the spring bloom in the northern North Sea (FLEX '76). *J. Mar. Res.* 55, 687–734. doi: 10.1357/0022240973224229

Lee, Z., Shang, S., and Stavn, R. (2018). AOPs are not additive: on the biogeo-optical modeling of the diffuse attenuation coefficient. *Front. Mar. Sci.* 5:8. doi: 10.3389/fmars.2018.00008

Lee, Z.-P., Du, K.-P., and Arnone, R. (2005). A model for the diffuse attenuation coefficient of downwelling irradiance. *J. Geophys. Res.* 110:C02016.

Lee, Z. P., Shang, S., Hu, C., Du, K., Weidemann, A., Hou, W., et al. (2015). Secchi disk depth: A new theory and mechanistic model for underwater visibility. *Remote Sens. Environ.* 169, 139–149. doi: 10.1016/j.rse.2015.08.002

Liss, P. S. (1976). "Conservative and non-conservative behavior of dissolved constituents during estuarine mixing," in *Estuarine Chemistry*, eds J. D. Burton and P. S. Liss (London: Academic Press), 93–130.

Mascarenhas, V. J., Voß, D., Wollschläger, J., and Zielinski, O. (2017). Fjord light regime: Bio-optical variability, absorption budget, and hyperspectral light availability in Sognefjord and Trondheimsfjord, Norway. *J. Geophys. Res. Ocean.* 122.

McFarland, W. N. (1986). Light in the sea - correlations with behaviors of fishes and invertebrates. *Integr. Comp. Biol.* 26, 389–401. doi: 10.1093/icb/26.2.389

Mobley, C. D. (1994). *Light and Water: Radiative Transfer in Natural Waters*. Cambridge, MA: Academic press.

Mobley, C. D., Chai, F., Xiu, P., and Sundman, L. K. (2015). Impact of improved light calculations on predicted phytoplankton growth and heating in an idealized upwelling-downwelling channel geometry. *J. Geophys. Res. Ocean.* 120, 875–892. doi: 10.1002/2014jc010588

Morel, A. (1988). Optical modelling of upper ocean in relation to its Biogenic Matter content (case 1 waters). *J. Geophys. Res.* 93, 10749–10769.

Morel, A., and Bricaud, A. (1981). Theoretical Results Concerning Light-Absorption in a Discrete Medium, and Application To Specific Absorption of Phytoplankton. *Deep. Res. Part A Oceanogr. Res. Pap.* 28, 1375–1393. doi: 10.1016/0198-0149(81)90039-x

Morel, A., and Maritorena, S. (2001). Bio-optical properties of oceanic waters: A reappraisal. *J. Geophys. Res. Ocean.* 106, 7163–7180. doi: 10.1029/2000jc000319

Morel, A., and Prieur, L. (1977). Analysis of variations in ocean color. *Limnol. Oceanogr.* 22, 709–722. doi: 10.4319/lo.1977.22.4.0709

Mueller, J. L., Fargion, G. S., Mcclain, C. R., Morel, A., Frouin, R., Davis, C., et al. (2003). *Ocean Optics Protocols For Satellite Ocean Color Sensor Validation, Revision 4, Volume III?: Radiometric Measurements and Data Analysis Protocols NASA / TM-2003- Ocean Optics Protocols For Satellite Ocean Color Sensor Validation, Revision 4, Volume II. Ocean Color web page III*. Washington, DC: NASA, 84.

Organelli, E., Claustre, H., Bricaud, A., Schmechtig, C., Poteau, A., Xing, X., et al. (2016). A novel near-real-time quality-control procedure for radiometric profiles measured by bio-argo floats: Protocols and performances. *J. Atmos. Ocean. Technol.* 33, 937–951. doi: 10.1175/jtech-d-15-0193.1

Paulson, C. A., and Simpson, J. J. (1977). Irradiance Measurements in the Upper Ocean. *J. Phys. Oceanogr.* 7, 952–956. doi: 10.1175/1520-0485(1977)007<0952:imituo>2.0.co;2

Röttgers, R., and Doerffer, R. (2007). Measurements of optical absorption by chromophoric dissolved organic matter using a point-source integrating-cavity absorption meter. *Limnol. Oceanogr. Methods* 5, 126–135. doi: 10.4319/lom.2007.5.126

Röttgers, R., Häse, C., and Doerffer, R. (2007). Determination of the particulate absorption of microalgae using a point-source integrating-cavity absorption meter. *Limnol. Oceanogr. Methods* 5, 1–12. doi: 10.4319/lom.2007.5.1

Röttgers, R., Schönfeld, W., Kipp, P.-R., and Doerffer, R. (2005). Practical test of a point-source integrating cavity absorption meter: the performance of different collector assemblies. *Appl. Opt.* 44, 5549–5560.

Smith, R. C., and Baker, K. S. (1984). "The analysis of ocean optical data," in *Ocean Optics VII*, ed. M. A. Blizard (Washington, DC: SPIE), 119–126.

Smith, R. C., and Baker, K. S. (1986). "Analysis of ocean optical data II," in *Ocean Optics VIII*, ed. M. A. Blizard (Washington, DC: SPIE), 95–107.

Soohoo, J. B., Kiefer, D. A., Collins, D. J., and Mcdermid, I. S. (1986). In vivo fluorescence excitation and absorption spectra of marine phytoplankton: I. Taxonomic characteristics and responses to photoadaptation. *J. Plankton Res.* 8, 197–214. doi: 10.1093/plankt/8.1.197

Stedmon, C. A., and Markager, S. (2003). Behaviour of the optical properties of coloured dissolved organic matter under conservative mixing. *Estuar. Coast. Shelf Sci.* 57, 973–979. doi: 10.1016/s0272-7714(03)00003-9

Thewes, D., Stanev, E. V., and Zielinski, O. (2020). Sensitivity of a 3D Shelf Sea Ecosystem Model to Parameterizations of the Underwater Light Field. *Front. Mar. Sci.* 6:816. doi: 10.3389/fmars.2019.00816

Wollschläger, J., Henkel, R., Voß, D., and Zielinski, O. (2020a). *Hyperspectral Underwater Light Field Measured During the Cruise HE503 with RV HEINCKE*. Bremerhaven: Alfred Wegener Institute.

Wollschläger, J., Henkel, R., Voß, D., and Zielinski, O. (2020b). *Hyperspectral Underwater Light Field Measured During the cruise HE527 with RV HEINCKE*. Bremerhaven: Alfred Wegener Institute.

Wollschläger, J., Henkel, R., Voß, D., and Zielinski, O. (2020c). *Hyperspectral Underwater Light Field Measured during the cruise HE516 with RV HEINCKE*. Bremerhaven: Alfred Wegener Institute.

Wollschläger, J., Röttgers, R., Petersen, W., and Zielinski, O. (2019). Stick or Dye: Evaluating a Solid Standard Calibration Approach for Point-Source Integrating Cavity Absorption Meters (PSICAM). *Front. Mar. Sci.* 5:534. doi: 10.3389/fmars.2018.00534

Zielinski, O. (2013). *Subsea Optics: An Introduction, Subsea Optics and Imaging*. Sawston: Woodhead Publishing Limited.

Zielinski, O., Llinás, O., Oschlies, A., and Reuter, R. (2002). Underwater light field and its effect on a one-dimensional ecosystem model at station ESTOC, north of the Canary Islands. *Deep. Res. Part II Top. Stud. Oceanogr.* 49, 3529–3542. doi: 10.1016/s0967-0645(02)00096-6

Conflict of Interest: The authors declare that the research was conducted in the absence of any commercial or financial relationships that could be construed as a potential conflict of interest.

frontiers in Environmental Science

ORIGINAL RESEARCH
published: 30 July 2020
doi: 10.3389/fenvs.2020.00111

Filling in the Flyover Zone: High Phosphorus in Midwestern (USA) Reservoirs Results in High Phytoplankton Biomass but Not High Primary Productivity

*Erin L. Petty, Daniel V. Obrecht and Rebecca L. North**

MU Limnology Laboratory, School of Natural Resources, College of Food, Agriculture, and Natural Resources, University of Missouri, Columbia, MO, United States

OPEN ACCESS

Edited by:
Sergi Sabater, University of Girona, Spain

Reviewed by:
Guillaume Grosbois, Swedish University of Agricultural Sciences, Sweden
Davi Gasparini Fernandes Cunha, Universidade de São Paulo São Carlos, Brazil

****Correspondence:***
Rebecca L. North
northr@missouri.edu

Specialty section:
This article was submitted to Freshwater Science, a section of the journal Frontiers in Environmental Science

Received: *06 March 2020*
Accepted: *26 June 2020*
Published: *30 July 2020*

Citation:
Petty EL, Obrecht DV and North RL (2020) Filling in the Flyover Zone: High Phosphorus in Midwestern (USA) Reservoirs Results in High Phytoplankton Biomass but Not High Primary Productivity. Front. Environ. Sci. 8:111. doi: 10.3389/fenvs.2020.00111

In lakes and reservoirs, climate change increases surface water temperatures, promotes thermal stability, and decreases hypolimnetic oxygen. Increased anthropogenic land-use and precipitation enhance nutrient and sediment supply. Together, these effects alter the light and nutrient dynamics constraining phytoplankton biomass and productivity. Given that lake and reservoir processes differ, and that globally, reservoir numbers are increasing to meet water demands, reservoir-centric studies remain underrepresented. In the agricultural Midwest (United States), ubiquitous reservoirs experience eutrophy and hypolimnetic anoxia. Here, we explore influences of eutrophication and land-use on the proximate light and nutrient status of phytoplankton communities in 32 Missouri reservoirs. Light and nutrient status indicators include mixed layer irradiance, phosphorus (P) and nitrogen (N) stoichiometry/debts, photosynthetic efficiency, and photosynthetic-irradiance parameters. Contributing to the ongoing P vs. N and P management debate, we evaluate if phytoplankton biomass and productivity are constrained by light, P, N, or a combination thereof, across gradients of trophic status and land-use during two contrasting wet and dry summers. Despite agricultural prevalence, P-deficiency is more prominent than either N- or light-deficiency. In 2018, ∼46% of samples were P-deficient with ∼36% indicating neither light nor nutrient deficiency. Gross primary productivity per unit chlorophyll-*a* (GPP^B) demonstrates negative relationships with nutrients, biomass, and turbidity, and positive relationships with light availability. GPP^B is highest in oligotrophic reservoirs where light utilization efficiency is also highest. Overall, phytoplankton biomass and productivity appear constrained by P and light, respectively. If Midwestern reservoirs are precursors of future inland waters affected by climate change and eutrophication, our crystal ball indicates that both P and light will be important regulators of phytoplankton dynamics and subsequent water quality.

Keywords: nitrogen, phosphorus, trophic status, eutrophication, phytoplankton, climate change, nutrients, light

INTRODUCTION

Inland freshwaters, such as lakes and reservoirs, are viewed as valuable and sensitive sentinels of climatic change (Williamson et al., 2009a). Climate forcing is primarily driven by altered patterns of incident solar radiation, air temperature, and precipitation (Williamson et al., 2009b). In response to increasing air temperatures, there is global evidence that lakes are warming (Schmid et al., 2014; O'Reilly et al., 2015). While exact responses vary across systems (O'Reilly et al., 2015; Woolway and Merchant, 2017), long-term incremental increases in global air temperatures are promoting earlier, stronger, and extended stratification in many inland surface waters (Woolway and Merchant, 2019). Climate-induced alterations to vertical mixing and stratification are also expected to change in-lake productivity (O'Reilly et al., 2003; O'Beirne et al., 2017), impacting light and nutrient dynamics (Verburg and Hecky, 2009; Williamson et al., 2009b).

Climate and anthropogenic activity mutually contribute to intensify freshwater eutrophication (Jeppesen et al., 2010). Watershed land-use and regional precipitation patterns affect the supply of nutrients and sediment transported to- and transformed within- lakes and reservoirs (Hayes et al., 2015). Agriculture and urbanization have drastically increased proportions of the bioavailable macronutrients, phosphorus (P) and nitrogen (N), on the landscape and within aquatic ecosystems (Bennett et al., 2001; Galloway et al., 2008; Howarth et al., 2012). Watersheds dominated by cropland agriculture typically export nutrients and sediment to lakes and reservoirs at higher rates and concentrations than do undisturbed and/or forested watersheds (Knowlton and Jones, 1995; Knoll et al., 2003). In the central US, more intense rainfall events as a result of climate-induced changes in precipitation are expected to enhance episodic pulses of nutrients and sediment in surface runoff. These interactions influence aquatic light conditions and increase the quantity of P and N available to phytoplankton communities in lakes and reservoirs (Paerl and Scott, 2010).

Variations in light availability as well as P and N supply can impact the light and nutrient status of phytoplankton communities where a balance of light and nutrients is needed for photosynthesis, nutrient uptake, and assimilation. As such, deficiencies in light and/or nutrients play a key role in controlling phytoplankton community structure, growth, and productivity (Titman, 1976). The relative importance of P and N as controls in freshwater ecosystems, however, has been contested for decades (Schindler, 1977; Elser et al., 1990; Schindler et al., 2008; Paerl et al., 2016). The traditional paradigm designates P as the single primary macronutrient controlling phytoplankton growth and productivity in temperate freshwater lakes (Schindler, 1974, 1977; Guildford and Hecky, 2000), but there is evidence that N, too, has a role to play (Morris and Lewis, 1988; Elser et al., 1990; Lewis and Wurtsbaugh, 2008; Abell et al., 2010). Numerous inland studies even offer evidence of simultaneous control by P and N (Elser et al., 2007; North et al., 2007; Sterner, 2008; Rowland et al., 2019) and/or light (Millard et al., 1996; Guildford et al., 2000; Knowlton and Jones, 2000; Dubourg et al., 2015).

Lakes and reservoirs were once considered synonymous (Hutchinson, 1957). Contemporary limnology, however, has shown that even though they possess many shared characteristics, reservoir processes sometimes differ from those of natural lakes (Kimmel and Groeger, 1984; Hayes et al., 2017). For example, reservoirs tend to have larger watersheds with greater contributions of nutrients and sediment that promote increased productivity and reduced water clarity (Hayes et al., 2017). Reservoir-centric studies, however, are underrepresented relative to natural lake studies. As global reservoir and dam construction intensify to meet growing water demands (Zarfl et al., 2015), it may become increasingly important that we equally understand the processes of both lakes and reservoirs, particularly as they relate to climate change and eutrophication. Being the primary lentic habitat in the central US (Thornton, 1990), ubiquitous Midwestern reservoirs may serve as climate analogs for future aquatic ecosystems. High eutrophication rates in the agriculturally dominated Midwest (Mitsch et al., 2001; Jones et al., 2008a) make these reservoirs precursors of future surface water quality, as ∼94% of reservoirs in the study region are classified as mesotrophic, eutrophic, or hypertrophic (Jones et al., 2008b). Moreover, since Midwestern reservoirs regularly experience hypolimnetic anoxia during summer stratification (Jones et al., 2011), they may also forewarn how future light and nutrient dynamics will affect phytoplankton biomass and primary productivity.

Here, we explore influences of climate, eutrophication, and land-use on the proximate light and nutrient status of phytoplankton communities in 32 Midwestern reservoirs. By evaluating general indicators of water quality and proximate physiological deficiencies in the phytoplankton communities, we determine if chlorophyll-*a* (chl*a*), as a proxy for phytoplankton biomass, and primary productivity are constrained by light, P, N, or a combination thereof. We explore these constraints across gradients of trophic status and land-use, which reflect gradients in nutrient concentrations as well as ambient light environments, during the climatically contrasting summers of 2017 (wet) and 2018 (dry). Decades of previous work on Midwestern reservoirs utilized Liebig's Law of the Minimum (Von Liebig, 1840) to identify important empirical relationships between concentrations of chl*a*, and P ($r^2 = 0.83$) and N ($r^2 = 0.78$; Jones et al., 2008b). Our study applies the concept of Blackman limitation (Blackman, 1905), or rate limitation, to describe the condition(s) by which phytoplankton growth, productivity, and photosynthetic responses are constrained by resource availability. We describe limitation in terms of proximate deficiency (Tyrrell, 1999), which considers the phytoplankton communities' instantaneous responses to nutrients and/or light. We also invoke the term co-deficiency to describe simultaneous constraint by more than one resource (Saito et al., 2008), whether that be by light and a nutrient or by multiple nutrients (Healey, 1985). Building off previously elucidated relationships (Jones et al., 2008b), we predict that light and both P and N will serve as proximate controls of phytoplankton communities regardless of climatic year. Light deficiency will occur in eutrophic and hypertrophic reservoirs and nutrient deficiency in oligotrophic reservoirs; culminating in the highest phytoplankton biomass and productivity in hypertrophic reservoirs.

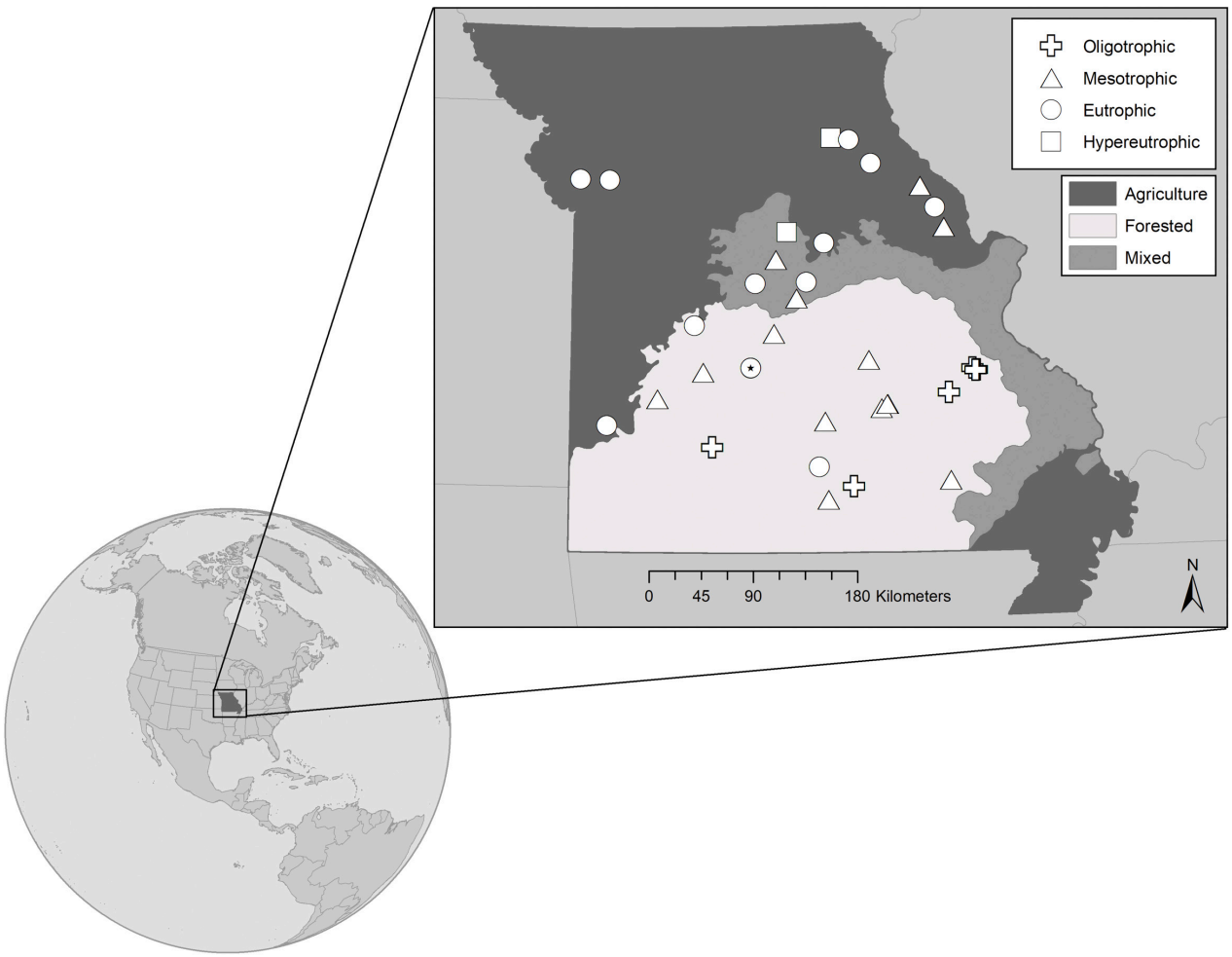

FIGURE 1 | Map showing the 32 reservoir study sites located in Missouri, United States. Sites represent the trophic gradient demonstrated by reservoirs throughout the state from very low (~0.10 μmol L^{-1}) to very high (~4.40 μmol L^{-1}) epilimnetic total phosphorus concentrations. Symbols distinguish trophic status, where ✣, △, ○, □ represent oligo-, meso-, eu-, and hyper- trophic, respectively. All are warm monomictic, except for polymictic Niangua which is denoted as a eutrophic circle with a filled dot (*) in the center. Shading indicates the dominant land-use that has been generalized for each of the state's major physiographic regions, with the north dominated by agriculture, the south largely forested, and mixed land cover in-between. Land-use specific to each reservoir's watershed has been classified separately.

MATERIALS AND METHODS

Study Site Description

We sampled 32 mid-continental, mid-latitude manmade reservoirs in the summers of 2017 and 2018. The reservoirs are located across Missouri, a Midwestern state in the central US (**Figure 1**). Missouri is characterized by five main physiographic regions (Thom and Wilson, 1980), which correspond to a gradient in dominant land-use. Our study reservoirs span four of the five physiographic regions, representing the land-use and resultant trophic status gradients (Jones et al., 2008a,b), where five of the reservoirs are oligo-, 13 meso-, 12 eu-, and 2 hyper- trophic. Trophic classification is based on average total phosphorus (TP) concentrations during the 2-year summer sampling window (criteria from Jones et al., 2008b). The reservoirs were chosen to represent a range in nutrient concentrations, underwater light conditions, phytoplankton biomass, reservoir morphology, and watershed land-use. All are warm monomictic, except for Lake Niangua, which is a shallow (6.1 m maximum depth), polymictic reservoir (**Supplementary Table 1**).

Watershed land-use/land-cover (LULC) data was derived from the 2016 National Land Cover Database, a product of the Multi-Resolution Land Characteristics Consortium (Yang et al., 2018)[1]. We selected watershed boundaries of interest from the Missouri 2019 Lake Numeric Nutrient Criteria Watersheds dataset developed by the Missouri Department of Natural Resources (MDNR)[2]. Watersheds not included in this dataset were manually digitized using flow direction and

[1]www.mrlc.gov

[2]http://msdisweb.missouri.edu

flow accumulation grids generated from 10-m resolution digital elevation models in ESRI ArcGIS 10.5. We zonally tabulated LULC for each watershed in ArcGIS, and calculated LULC as percent developed, barren, forest, rangeland, wetland, and agriculture which also contained pasture and cropland subclasses. Watersheds were categorically generalized as either agriculture (pasture or cropland), forest, or mixed based on the dominant (>50%) LULC. When a watershed contained >50% agriculture, the watershed was specified as either ag-pasture or ag-crop to denote the subclass with the higher contribution. A mixed classification was assigned to watersheds with no single LULC greater than 50%. Barren (0–2%), rangeland (0–10%), wetland (0–3%), and developed (0–10%, except for four watersheds with 22–44%) were considered minor contributions to overall LULC and were not included as unique LULC categories.

Each year, we sampled the reservoirs 3–4 times between mid-May and mid-September during a period of established thermal stratification. Throughout these months, the climate across Missouri was characterized by the Palmer Drought Severity Index (PDSI) to be mid-range to very moist for 2017 (statewide monthly average range for April through September: −0.88 to 2.36) and mid-range to severe-drought for 2018 (statewide monthly average range for April through September −2.07 to 0.55; NOAA, 2019). Indicators of water quality and nutrient status were assessed on 29 reservoirs in 2017, followed by a more in-depth collection of water chemistry as well as physiological measurements on 27 reservoirs in 2018. Most of the reservoirs (n = 24) were sampled in both years, allowing us to explore the influence of climate (i.e., wet vs. dry) on phytoplankton light and nutrient status (**Table 1**).

Field Sampling

Sampling occurred at maximum water depth near the dam of each reservoir. Secchi transparency depths were recorded. Photosynthetically active radiation (PAR) profiles were collected in 0.25-m increments using a cosine corrected underwater quantum sensor (LI-192, Li-Cor Biosciences, Lincoln, Nebraska, United States). The vertical attenuation coefficient (K_d) was calculated from the PAR profiles using the linear regression of the natural logarithm of irradiance to depth (Kirk, 2011). A Yellow Springs Instruments (Yellow Springs, Ohio, United States) EXO3 multi-parameter sonde was deployed to collect depth profiles (0.001 m resolution) of temperature (0.001°C resolution with an accuracy of ± 0.01°C) and dissolved oxygen (DO) measured with an optical sensor (0.01 mg L^{-1} resolution with an accuracy of ±0.1 mg L^{-1}). Integrated epilimnetic whole water samples were collected via peristaltic pump from the surface to one meter above the thermocline, where the thermocline was defined in the field by vertical temperature gradients ≥1.0°C m^{-1}. Discrete hypolimnetic whole water samples were collected via Van Dorn sampler from one meter off bottom. During isothermal conditions (e.g., polymictic Lake Niangua), a single integrated sample was taken from the surface to one meter off bottom via peristaltic pump. All water samples were collected into acid-washed high-density polyethylene (HDPE) containers, placed in coolers, and returned to the University of Missouri Limnology Laboratory within 12-h of collection where they were then processed.

Laboratory Analyses and Data Processing

Physical Parameters

Maximum depth (Z_{max}) was based on records of dam height provided by MDNR. Water column mixing depth (Z_{mix}) was determined using the "rLakeAnalyzer" R-package (Winslow et al., 2019) and reported as the depth from surface to the top of the metalimnion. Based on sampling date and latitude, daily incident irradiance was modeled in 1 min increments and scaled to PAR (μmol photons m^{-2} s^{-1}) using the "phytotools" R-package (Silsbe and Malkin, 2015). We then calculated mean daily (24-h) incident irradiance ($\bar{E}_0$), assuming cloud-free conditions. Following Guildford et al. (2000), we derived mean daily mixed layer irradiance ($\bar{E}_{24}$) from K_d, Z_{mix}, and $\bar{E}_0$:

$$\bar{E}_{24} = \bar{E}_0 \times (1 - \exp(-1 \times K_d \times Z_{mix})) \times (K_d \times Z_{mix})^{-1} \quad (1)$$

where $\bar{E}_{24}$ describes the amount of light experienced in the mixed layer by suspended phytoplankton over a 24-h period.

Chemical Parameters

Water samples were processed and analyzed for TP and total N (TN), total dissolved P (TDP) and N (TDN), dissolved reactive P (DRP), ammonium (NH_4^+), nitrate (NO_3^-), dissolved organic carbon (DOC), particulate N (PN), and particulate P (PP). TP and TN were pipetted directly into glass test tubes and refrigerated until analysis. All dissolved nutrient samples were filtered through glass-fiber filters (GFF, 0.7 μm pore). Filters for DOC filtrate were pre-combusted at 550°C for 4 h. Filtrate for TDP and TDN were refrigerated in glass test tubes, while DRP, NH_4^+, NO_3^- and DOC samples were stored frozen in acid-washed HDPE bottles. PN and PP were captured on pre-combusted GFF filters (0.7 μm pore), dried, and stored with desiccant.

All P samples were analyzed spectrophotometrically using an ascorbic acid colorimetric method (APHA, 2017; 4500-P E). TP, TDP, and DRP were analyzed in triplicate; PP in duplicate. TP, TDP, and PP were digested prior to analysis following an ammonium peroxydisulfate method (APHA, 2017; 4500-P B). Detection limits for all P analyses are 0.03 μmol L^{-1}.

TN and TDN were analyzed in triplicate using the second derivative spectroscopy method (Crumpton et al., 1992). NH_4^+ and NO_3^- were analyzed in duplicate on a Lachat QuikChem Flow Injection Analyzer (Hach, Loveland, Colorado, United States) using a Lachat method for NH_4^+ (10-107-06-1-K) and a slightly modified Lachat method for NO_3^- (10-107-04-1-B/C). Detection limits were 2.50 μmol L^{-1} for TN and TDN, 0.71 μmol L^{-1} for NH_4^+, and 0.36 μmol L^{-1} for NO_3^-. Dissolved organic nitrogen (DON) was calculated by difference from TDN, NH_4^+, and NO_3^-. PN was analyzed at the UC Davis Stable Isotope Facility using an Elementar Vario EL Cube or Micro Cube elemental analyzer (Elementar Analysensysteme GmbH, Hanau, Germany) interfaced to a PDZ Europa 20-20 isotope ratio mass spectrometer (Sercon Ltd., Cheshire, United Kingdom) with a detection limit of 0.7 μmol N.

TABLE 1 | Definitions, abbreviations, and units describing physical, chemical, and biological parameters.

	Defined parameter	Abbreviation	Unit
Physical	Maximum depth	Z_{max}	meters
	Mixing depth	Z_{mix}	meters
	Secchi disk depth	Secchi	meters
	Photosynthetically active radiation	PAR	μmol photons m^{-2} sec^{-1}
	Vertical light attenuation coefficient	K_d	$meters^{-1}$
	Mean daily incident irradiance	$\bar{E}_0$	μmol photons m^{-2} sec^{-1}
	Mean daily mixed layer irradiance	$\bar{E}_{24}$	μmol photons m^{-2} sec^{-1}
Chemical	Total phosphorus	TP	μmol L^{-1}
	Total dissolved phosphorus	TDP	μmol L^{-1}
	Dissolved reactive phosphorus	DRP	μmol L^{-1}
	Particulate phosphorus	PP	μmol L^{-1}
	Total nitrogen	TN	μmol L^{-1}
	Total dissolved nitrogen	TDN	μmol L^{-1}
	Ammonium	NH_4^+	μmol L^{-1}
	Nitrate	NO_3^-	μmol L^{-1}
	Dissolved organic nitrogen	DON	μmol L^{-1}
	Particulate nitrogen	PN	μmol L^{-1}
	Dissolved organic carbon	DOC	μmol L^{-1}
	Total suspended solids	TSS	μg L^{-1}
	Particulate organic matter	POM	μg L^{-1}
	Particulate inorganic matter	PIM	μg L^{-1}
Biological	Chlorophyll-*a*	chl*a*	μg L^{-1}
	Particulate organic carbon	POC	μmol L^{-1}
	Areal pigment absorption coefficient	a_ϕ	m^{-2} mg $chla^{-1}$
Nutrient status	Particulate organic carbon to chlorophyll-*a* ratio	POC:chl*a*	μmol C μg $chla^{-1}$
	Total nitrogen to total phosphorus ratio	TN:TP	Molar ratio
	Particulate organic carbon to particulate phosphorus ratio	POC:PP	Molar ratio
	Particulate nitrogen to particulate phosphorus ratio	PN:PP	Molar ratio
	Particulate organic carbon to particulate nitrogen ratio	POC:PN	Molar ratio
	Indicator of phosphorus uptake	P debt	μmol P μg $chla^{-1}$
	Indicator of ammonium uptake	NH_4^+-debt	μmol N μg $chla^{-1}$
	Indicator of nitrate uptake	NO_3^--debt	μmol N μg $chla^{-1}$
P-E parameters	Maximum quantum yield of PSII for photochemistry	ϕ_{PSII}	Unitless
	Light utilization efficiency (light limited slope of P-E curve)	α	Photons reemitted photons $absorbed^{-1}$/μmol photons m^{-2} sec^{-1}
	Light utilization efficiency normalized to chlorophyll-*a*	α^B	Photons reemitted photons $absorbed^{-1}$/μmol photons (mg $chla^{-1}$) m sec^{-1}
	Light saturation parameter	E_k	μmol photons m^{-2} sec^{-1}
	Light saturation parameter normalized to chlorophyll-*a*	$E_k{}^B$	μmol photons (mg $chla^{-1}$) m sec^{-1}
	Maximum relative electron transport rate through PSII	$rETR_{max}$	Photons reemitted photons $absorbed^{-1}$
	Light-deficiency threshold	$\bar{E}_{24}/E_k$	Unitless
	Daily gross primary productivity rate	GPP	mmol O_2 m^{-2} day^{-1}
	Daily gross primary productivity rate normalized to chl-*a*	GPP^B	mmol O_2 (mg $chla^{-1}$) m day^{-1}

We analyzed DOC in duplicate following a combustion-infrared method (APHA, 2017; 5310 B) with a Shimadzu total organic carbon analyzer (TOC-VCPH, Shimadzu Scientific Instruments, Columbia, Maryland, United States). The detection limit for DOC was 16.7 μmol L^{-1}.

Seston was collected on Whatman 934-AH filters (1.5 μm pore) in duplicate and analyzed for total suspended solids (TSS) using a standard tared-weight method (APHA, 2017; 2540-D E) with a detection limit of 0.1 mg L^{-1}. Dried (105°C) and weighed filters were placed in a muffle furnace at 550°C for 20 min to burn off particulate organic matter (POM). Filters were weighed again to determine particulate inorganic matter (PIM). POM was calculated by difference from TSS and PIM.

Biological Parameters

Chl*a* concentrations (proxy for phytoplankton biomass) were measured on whole water samples filtered onto 0.7 μm GFF filters which were immediately frozen and stored with desiccant. After ethanol extraction and pheophytin acid-correction, chl*a* was analyzed on a Turner Design fluorometer (TD700, San

Jose, California, United States; Knowlton, 1984; Sartory and Grobbelaar, 1984). The detection limit was 0.09 $\mu g\ L^{-1}$.

Particulate organic carbon (POC) samples were collected on pre-combusted GFF filters (0.7 μm pore). Inorganic carbonates were removed from samples following a modified fumigation method based on Brodie et al. (2011) wherein filters were continuously subjected to concentrated 37% hydrochloric acid fumes for 4 h. After fumigation, samples were dried at 55–60°C and stored with desiccant. POC was analyzed at the UC Davis Stable Isotope Facility using an Elementar Vario EL Cube or Micro Cube elemental analyzer (Elementar Analysensysteme GmbH, Hanau, Germany) interfaced to a PDZ Europa 20-20 isotope ratio mass spectrometer (Sercon Ltd., Cheshire, United Kingdom) with a detection limit of 1.7 μmol C.

The quantitative filter technique (Tassan and Ferrari, 1995) was used to determine the areal pigment absorption coefficient (a_ϕ), which provides an estimate of cross-sectional light absorption via chl*a* for photochemistry and photosynthesis. We passed whole water samples through GFF filters (pore size 0.7 μm) that were immediately placed in foil-wrapped petri dishes to limit light exposure and frozen. Absorbance was measured before and after depigmentation via sodium hypochlorite solution (4–5% active chlorine) on a scanning spectrophotometer (Agilent Cary60 UV/VIS, Santa Clara, California, United States) in 1 nm increments from wavelengths 350–750 nm. We calculated a_ϕ based on Silsbe et al. (2012):

$$a_\phi = 2.303 \times (A_P - A_{NAP}) \times \beta^{-1} \times (V_f/A_f)^{-1} \quad (2)$$

where A_P and A_{NAP} are sestonic absorption before and after depigmentation, respectively; β, equaling 2, is the path-length amplification factor adjusting for absorption differences between filter and water; V_f/A_f is the ratio of filter volume to circumferential area of filtered particulates.

Light and Nutrient Status Indicators

Phytoplankton light and nutrient status were assessed using a suite of deficiency indicators, which included $\bar{E}_{24}$; $\bar{E}_{24}/E_k$; POC:chl*a*; P-, NH_4^+-N, and NO_3^--N debts; stoichiometric nutrient ratios (TN:TP, POC:PP, PN:PP, POC:PN); and photosynthetic efficiency experiments. These indicators have previously established, literature-supported thresholds for estimating proximate deficiencies of light, P, and N (**Table 2**; Healey and Hendzel, 1979; Guildford and Hecky, 2000). Thresholds based on the work of Healey and Hendzel (1979) were applied to measurements of P and NH_4^+-N debt, as well as to POC:PP, PN:PP, POC:PN, and POC:chl*a*. These thresholds were developed on laboratory culture experiments (Healey and Hendzel, 1979), but have been successfully applied across a diverse range of lake systems worldwide (e.g., Guildford et al., 2000; North et al., 2008; Dubourg et al., 2015).

Light deficiency

Our light deficiency thresholds ($\bar{E}_{24}$, $\bar{E}_{24}/E_k$) were developed on a turbid Canadian reservoir where the onset of P-deficiency occurred when $\bar{E}_{24}$ was between 41.7 and 58.3 $\mu mol\ photon\ m^{-2}\ s^{-1}$ (Hecky and Guildford, 1984). Knowlton and Jones (1996), who focused on the turbid Missouri reservoir- Mark Twain, as well as Millard et al. (1996) who worked on Lake Ontario, suggested that co-limitation by light and nutrients could occur at irradiances ≤69.4 $\mu mol\ photon\ m^{-2}\ s^{-1}$. This irradiance threshold has been supported in other applications of shallow, turbid inland waters (Schallenberg and Burns, 2004). We have, therefore, adopted a $\bar{E}_{24}$ threshold of 69.4 $\mu mol\ photon\ m^{-2}\ s^{-1}$ to represent moderate light-deficiency and the Hecky and Guildford (1984) threshold of 41.7 to represent extreme light-deficiency (**Table 2**).

We also applied the ratio of $\bar{E}_{24}/E_k$ to assess light-deficiency, where $\bar{E}_{24}$ represents mean daily mixed layer irradiance and E_k, the LC-derived light saturation parameter (details below). The threshold for $\bar{E}_{24}/E_k$ light-deficiency is one (**Table 2**). When $\bar{E}_{24} > E_k$, there is theoretically enough light for photosynthesis. Alternatively, when $\bar{E}_{24} < E_k$, phytoplankton may experience light-deficient conditions (Hecky and Guildford, 1984).

Nutrient deficiency

Nutrient debt experiments based on Healey (1977) were conducted to assess nutrient deficiency. In the laboratory, one L subsamples of epilimnetic whole water were placed in acid-washed cubitainers and spiked with ∼5 μM of KH_2PO_4, NH_4Cl, or KNO_3. The four treatments (control receiving no nutrient addition, +P, $+NH_4^+$, $+NO_3^-$) were incubated in an environmental chamber for 18–24 h under darkened conditions (0.001–0.008 $\mu mol\ photons\ m^{-2}\ s^{-1}$) at average ambient epilimnetic water temperatures (23–30°C). Samples for DRP, NH_4^+, and NO_3^- were collected from the +P, $+NH_4^+$, and $+NO_3^-$ treatments, respectively, before and after incubation. DRP, NH_4^+, and NO_3^- samples were also collected from each control treatment. P debt, NH_4^+-N debt, and NO_3^--N debt, as indicators of nutrient uptake, were calculated as the change in nutrient concentration per unit of chl*a* before and after incubation.

We complemented the Healey and Hendzel (1979) nutrient debts with additional photosynthetic efficiency experiments.

TABLE 2 | Established light and nutrient status indicator thresholds that were applied to the reservoir phytoplankton communities to assess deficiency.

Limiting factor	Indicator	Deficient	Moderately deficient	Extremely deficient
Light	$\bar{E}_{24}/E_k$	<1		
	$\bar{E}_{24}$		<69.4	<41.7
P	P debt	>0.075		
	POC:PP		>129	>258
	PN:PP	>22		
	TN:TP	>50		
N	NH_4^+-N debt	>0.15		
	POC:PN		>8.3	>14.6
	TN:TP	<20		
N or P	POC:chl*a*		>4.2	>8.3
	TN:TP	20–50		

*Most indicator values are from Guildford and Hecky (2000); $\bar{E}_{24}$ and E_k are based on Hecky and Guildford (1984) and Knowlton and Jones (2000); and P debt, POC:PP, NH_4^+-N debt, POC:PN, and POC:chla on Healey and Hendzel (1979). See **Table 1** for parameter definitions, abbreviations, and units.*

These experiments assess phytoplankton physiological response to nutrient additions and provide additional evidence of nutrient deficiency. Nutrient additions and incubations followed the same protocol as the debt experiments described above. Following incubation, maximum quantum yields of photosystem II (ϕ_{PSII}) of each treatment was measured as described below. Significant increases in ϕ_{PSII} from control to nutrient addition treatment suggested deficiency of that nutrient.

P-E Parameters

We measured ϕ_{PSII} and rapid light curves (LC) to evaluate the phytoplanktons' capability to absorb and utilize light energy for photosynthesis via PSII. We used the empirical optimum value of ∼0.65 (Kromkamp et al., 2008) to assess overall phytoplankton stress. Following a 30-min dark adaptation period, both ϕ_{PSII} and LCs were measured from whole water samples in triplicate with a Water-Pulse Amplitude Modulated (Water-PAM) Fluorometer (Heinz Walz GmbH, Effeltrich, Germany) interfaced to WinControl software (version 3.26). We corrected for non-algal background fluorescence with sample filtrate that had been passed through a 0.2 μm pore GFF filter. LCs were measured in nine 1-min intervals wherein light intensity steadily increased from 21 to 1,420 μmol photons m^{-2} s^{-1}. Photosynthetic-irradiance (P-E) parameters describing light utilization efficiency (α) and light saturation (E_k) were derived by fitting each LC to a normalized irradiance model (Webb et al., 1974) in the "phytotools" R-package (Silsbe and Malkin, 2015). The maximum relative electron transport rate through PSII ($rETR_{max}$) was then calculated as the product of α and E_k. For comparison across systems, α and E_k were normalized to chl*a* (α^B, $E_k{}^B$).

Gross Primary Productivity

Areal rates of gross primary productivity (GPP) of the phytoplankton communities were estimated based on the Fee (1990) primary production model. With the "phytoprod" function of the "phytotools" R-package (Silsbe and Malkin, 2015), we calculated GPP from α, E_k, chl*a*, a_ϕ, K_d, and $\bar{E}_0$. Final units of mol O_2 m^{-2} day^{-1} were reached by multiplying the "phytoprod" output by the molecular weight of O_2 as well as the quantum yield of O_2 evolution, which we assume is 0.25 mol O_2 [mol e^-]$^{-1}$. For comparison across systems, GPP was normalized to chl*a* (GPP^B).

Statistical Analyses

All data were assessed for normality using the Shapiro-Wilk test ($p < 0.05$). If we accepted the null hypothesis of the Shapiro-Wilk test ($p < 0.05$), data were transformed accordingly (e.g., common log, square root, reciprocal), whenever possible, to achieve normality prior to any statistical analysis. If we rejected the null hypothesis of the Shapiro-Wilk test ($p > 0.05$), data were assumed normal and no transformations applied.

To explore relationships between continuous parametric variables, we used Pearson's correlation coefficients (r). To assess differences across temporal gradients (between years and/or sampling events), as well as across the trophic and land-use gradient for each reservoir, we ran linear mixed effect (LME) models with the "nlme" R-package (Pinheiro et al., 2020). For parameters collected in both 2017 and 2018, we used the following model structure:

$$Y_i = \beta_0 + \beta_1\ \text{Year} + \beta_2\ \text{SamplingEvent} + \beta_3\ \text{Year} * \text{SamplingEvent} + \beta_4\ \text{TrophicStatus} + \beta_5\ \text{LandUse} + \text{Reservoir} + \varepsilon_i$$

where Y_i was the normally distributed parameter Y at reservoir *i*, while Year (2017, 2018), SamplingEvent (1–4), TrophicStatus (oligotrophic to hypertrophic), and LandUse (forested, mixed, ag-pasture/crop) were fixed effects. Reservoir was a random effect that created a new baseline for each sampling location. Random effects and the residual error were assumed to be drawn from a normal distribution. A simplified model lacking Year and the interaction term (Year*SamplingEvent) was applied for parameters collected in a single year. Each LME was subjected to an analysis of variance (ANOVA). If the ANOVA identified statistically significant effects in the LME ($p < 0.05$), we conducted a Tukey's Honest Significant Difference *post-hoc* test to compare factor levels for significance. All *post-hoc* results are indicated by lowercase letters on figures and in tables, unless otherwise noted. Different lowercase letters indicate significant differences between factor levels. Letters are ordered alphabetically and indicate trend direction where, for example, "a" represents the lowest and "d" represents the highest mean.

To assess significant differences across sampling events, trophic status, and watershed land-use for the nutrient debt experiments, we conducted non-parametric Kruskal-Wallis one-way ANOVAs. If an ANOVA tested significant ($p < 0.05$), a Dunn's multiple comparisons *post-hoc* test was implemented to identify significant differences between factor levels. We also used one-way ANOVAs to test for significant differences among treatments for each ϕ_{PSII} experiment. If significant ($p < 0.05$), a 2-sided Dunnett-test (pairwise comparison) was conducted to identify significant positive responses to nutrient additions of P, NH_4^+, NO_3^-, and P+NH_4^+ relative to untreated control treatments.

RESULTS

Northern Missouri is 58% agriculture while the south is 61% forested (**Figure 1** and **Supplementary Table 1**). TP concentrations are correlated with forest ($p < 0.001$, $r = -0.65$), ag-crop ($p < 0.001$, $r = 0.65$), and ag-pasture ($p < 0.001$, $r = 0.31$) percent land-cover. As percent forest increases, we observe lower TP and more oligo- and meso- trophic systems. Alternatively, as percent agriculture increases, we observe higher TP and more eu- and hyper- trophic systems.

Physical Parameters

Missouri reservoirs are relatively shallow systems where Z_{max} ranges from 4.6 to 49.1 m (**Table 3**), with 63% of our study reservoirs <20 m and only 9% >40 m. Mean Z_{mix} was ∼27–30% of the water column in oligo-, meso-, and eu- trophic reservoirs, and 51% in hypertrophic reservoirs (**Tables 3**, **4**). There is a negative correlation between Z_{max} and trophic status ($p < 0.001$, $r = -0.47$), wherein shallower reservoirs are hypertrophic and deeper reservoirs are oligotrophic. Similarly, Z_{mix} was significantly shallower in hypertrophic than oligotrophic systems

TABLE 3 | Morphology and watershed land-use describing the 32 reservoirs sampled during the 2-year study window.

		Oligotrophic *n* = 5	Mesotrophic *n* = 13	Eutrophic *n* = 12	Hypertrophic *n* = 2
Morphology	Z_{max} (m)	25.1 (10.1–33.5)	19.5 (4.6–49.1)	17.2 (6.1–38.4)	6.8 (5.1–8.5)
	Surface area (ha)	109 (16–286)	2,759 (2–20,774)	2,716 (9–21,778)	11 (6–17)
	Watershed area (ha)	1,824 (139–5,069)	70,495 (28–464,073)	265,905 (90–2,397,033)	130 (58–202)
Land-use	% Forest	61 (42–97)	63 (32–89)	33 (13–58)	6 (1–12)
	% Pasture	20 (1–49)	27 (2–58)	40 (27–70)	28 (28–28)
	% Crop	0 (0–0)	2 (0–14)	17 (0–44)	53 (36–70)

*Shown are the arithmetic means and ranges (minimum-maximum) of n samples grouped along the trophic gradient. See **Table 1** for parameter definitions, abbreviations, and units.*

(**Table 5**). Hypolimnetic anoxia is common in Missouri reservoirs during summer stratification (Jones et al., 2011). We observed this in both summers, wherein every warm monomictic reservoir (n = 31) experienced hypolimnetic anoxia with DO concentrations < 0.5 mg L^{-1}. Across these 31 reservoirs, water columns were 27–87% anoxic, with the mean water column ∼65% anoxic.

The light environment in the reservoirs differed significantly from 2017 to 2018, although Z_{mix} did not. Water clarity was highest in oligotrophic reservoirs during the drier sampling year (2018). Across all reservoirs, Secchi depths were significantly deeper and K_ds were significantly smaller during the drier year (**Table 5**). In oligotrophic systems, Secchi depths were ∼6–7× deeper and K_ds were ∼73–82% smaller than in hypertrophic systems. Compared to 2017, TSS in 2018 was 25% lower in oligo- and ∼10% lower in meso- and eu- trophic reservoirs. These relationships fall apart in hypertrophic systems where we saw no significant differences ($p > 0.05$) in Secchi, K_d, nor TSS from 2017 to 2018 (**Table 4**).

Light Deficiency

Light deficiency was not prominent during the summers of 2017 and 2018. Across both years, $\bar{E}_{24}$ trophic means ranged from 65.9 to 227.3 μmol photons m^{-2} s^{-1} and while there were no significant differences between trophic status nor wet and dry years, $\bar{E}_{24}$ was lower during the wetter year and decreased from oligo- to hyper- trophic (**Figure 2**). Only 6% (2017) and 3% (2018) of individual samples were below the 41.7 μmol photons m^{-2} s^{-1} threshold for extreme light-deficiency (**Table 2** and **Figure 2**). No reservoir below the extreme light-deficiency threshold in 2017 fell below it again in 2018. Only the mean $\bar{E}_{24}$ for the 2017 hypertrophic reservoirs (65.9 μmol photons m^{-2} s^{-1}) was below the 69.4 μmol photons m^{-2} s^{-1} moderate threshold for light-deficiency (**Table 4** and **Figure 2**). Approximately 27% of all sampling events were less than the moderate threshold in 2017 compared to ∼19% in 2018 (**Figure 2**). Of the eight reservoirs below the threshold in 2017, nine also fell below during at least one sampling event in 2018. We found significant differences between $\bar{E}_{24}$ and sampling event, as well as land-use. $\bar{E}_{24}$ was significantly higher during the May/June sampling event, and in forested watersheds, than during the August/September sampling event or in ag-pasture watersheds (**Table 5**).

Relative to the light saturation parameter (E_k), the ratio of $\bar{E}_{24}/E_k$ indicates that light-deficiency dominated in these systems. Summer means for $\bar{E}_{24}/E_k$ across the trophic groupings ranged from 0.28 to 0.80 and were below the light-deficiency threshold of one (**Table 4**). Only calculated for the reservoirs sampled in 2018, it indicates that the demand for light exceeded the supply (ratio < 1) for 92% of sampling events; 75% in oligo-, 91% in meso-, 97% in eu-, and 100% in hyper- trophic reservoirs. All 29 of the reservoirs, regardless of trophic status, were light-deficient by this metric at least once during the 2018 season. All sampling events that were below the $\bar{E}_{24}$ moderate deficiency threshold in 2018 were also deemed light deficient by the $\bar{E}_{24}/E_k$ threshold. We found no evidence of photoacclimation (MacIntyre et al., 2002) as indicated by positive, significant relationships between POC and chl*a* in 2017 ($p < 0.001$, $r = 0.78$) and 2018 ($p < 0.001$, $r = 0.90$). Peak POC:chl*a* ratios occurred above the light threshold, when $\bar{E}_{24}$ was ∼50–150 μmol photons m^{-2} sec^{-1}, indicating nutrient deficiency.

Chemical and Biological Parameters

Nutrient concentrations were positively related to trophic status for most forms of P and N (TDP, DRP, PP, TN, TDN, DON, PN). Trophic mean concentrations of TP and DOC were higher during the wetter than the drier year (**Table 5**), except for in hypertrophic reservoirs where the relationship weakened (**Table 4**). Similarly, trophic mean particulate nutrient concentrations (i.e., PP, PN, POC) were also significantly higher during the wetter year (**Table 5**), barring the hypertrophic reservoirs.

From oligo- to hyper- trophic, mean epilimnetic TP concentrations ranged from 0.23 to 3.21 μmol L^{-1}. Across the trophic gradient, TP largely consisted of PP wherein TP was ∼70–80% PP (**Table 4**). Mean epilimnetic TDP and DRP concentrations generally increased with increasing trophic status. Across the trophic gradient, mean epilimnetic DRP constituted ∼20–50% of mean epilimnetic TDP, with oligo- and hyper-trophic reservoirs at the lower and upper end of that range, respectively (**Tables 3**, **6**).

Mean epilimnetic TN concentrations ranged from 21.35 in oligotrophic to 95.25 μmol L^{-1} in hypertrophic reservoirs. With dissolved N comprising the majority of TN in most reservoirs, PN constituted ∼30–39% of TN in oligo-, meso-, and eu- trophic and 61% of TN in hypertrophic reservoirs. DON represented the largest fraction of epilimnetic TDN, with NO_3^- + NH_4^+ accounting for 3–18% of epilimnetic TDN (**Table 4**). In 2018, mean epilimnetic NO_3^- was 1.75 μmol L^{-1}, while NH_4^+ was 0.89 μmol L^{-1} (**Table 6**). The majority of epilimnetic NH_4^+ (68%) and NO_3^- (79%) were below detection. In ag-crop

TABLE 4 | Limnological parameters for the 32 reservoirs sampled during the 2-year sample window. Shown are arithmetic means and ranges (minimum-maximum) of *n* samples grouped along the trophic gradient.

	Oligotrophic		Mesotrophic		Eutrophic		Hypertrophic	
	2017 ***n* = 20**	**2018** ***n* = 16**	**2017** ***n* = 50**	**2018** ***n* = 38**	**2017** ***n* = 34**	**2018** ***n* = 41**	**2017** ***n* = 8**	**2018** ***n* = 8**
Physical								
Secchi	3.43[16] (1.77–7.57)	3.69 (1.67–5.40)	1.78 (0.76–6.2)	1.78 (0.94–2.90)	0.71[31] (0.29–1.95)	1.08 (0.18–2.25)	0.56 (0.35–0.88)	0.52 (0.31–0.98)
K_d	0.72 (0.36–1.32)	0.50 (0.27–0.96)	1.35 (0.58–3.08)	1.08[37] (0.44–1.77)	2.19 (1.23–5.08)	1.71[40] (0.78–8.50)	2.70[7] (1.61–3.55)	2.81 (1.34–4.07)
Z_{mix}	7.52 (3.89–15.9)	6.16 (4.00–8.45)	5.41[49] (0.03–25.08)	6.43 (2.62–23.43)	4.43[33] (0.04–11.31)	5.26 (0.09–12.24)	3.87 (2.69–4.47)	3.06 (1.94–3.82)
$\bar{E}_0$	678.70 (631.60–699.60)	671.10 (616.40–698.30)	658.50 (514.00–699.60)	644.90 (477.20–698.40)	660.10 (581.90–701.40)	657.20 (477.60–696.70)	663.00 (598.20–693.20)	659.90 (575.40–695.30)
$\bar{E}_{24}$	154.90 (54.90–268.80)	227.30 (110.10–422.20)	156.90[49] (25.90–690.60)	132.70[37] (53.30–291.20)	107.80[33] (37.90–649.20)	108.40[40] (13.00–629.90)	65.90[7] (51.40–127.10)	88.30 (41.40–135.70)
Chemical								
TP	0.24 (0.10–0.50)	0.22 (0.10–0.30)	0.58 (0.30–1.20)	0.54 (0.20–1.40)	1.65 (0.80–4.40)	1.31 (0.50–3.40)	3.09 (2.10–3.90)	3.34 (2.40–3.70)
DRP	–	0.06[15] (0.03–0.11)	–	0.07[37] (0.03*–0.15)	–	0.11[38] (0.04–0.77)	–	0.15[7] (0.10–0.18)
PP	0.18[7] (0.03–0.46)	0.13[15] (0.03–0.44)	0.47[45] (0.14–1.29)	0.36 (0.15–0.86)	1.40[31] (0.48–7.25)	0.97[39] (0.21–2.04)	2.46 (1.55–3.24)	2.64[7] (1.74–2.95)
TN	20.88 (16.57–26.68)	21.93 (13.59–29.44)	29.96 (8.83–43.51)	32.88 (18.21–50.67)	66.46 (30.11–141.31)	59.82 (36.65–122.80)	94.71 (75.65–116.16)	84.76[7] (37.48–116.47)
PN	8.01[7] (5.53–16.99)	4.64[15] (2.11–11.48)	11.28[43] (4.13–41.12)	10.02[37] (4.10–21.39)	26.96[31] (12.26–56.83)	22.91[39] (5.91–51.41)	43.68 (5.47–69.51)	66.08[7] (43.58–92.11)
DOC	293.3[6] (238.0–342.4)	244.2[15] (197.5–307.7)	379.5[42] (51.5–559.7)	394.86 (185.6–608.5)	490.1[28] (98.12–733.0)	445.6[39] (72.6–672.2)	509.5[4] (430.9–580.93)	601.1[4] (525.8–774.0)
TSS	2.00[19] (1.10–3.30)	1.50 (0.80–4.10)	3.20[48] (1.10–6.80)	2.90 (1.20–8.20)	9.00[32] (3.20–22.10)	8.00 (1.90–76.50)	12.20 (8.10–20.00)	15.00 (6.70–23.60)
PIM	0.80 (0.20–1.70)	0.70 (0.20–1.60)	1.00 (0.10–2.70)	0.80 (0.20–4.50)	4.00 (0.70–18.50)	3.90 (0.30–67.00)	4.50 (0.70–11.80)	3.10 (0.60–7.40)
POM	1.20[19] (0.60–2.20)	0.80 (0.40–2.50)	2.20[48] (0.60–5.40)	2.10 (0.70–4.50)	5.40[32] (2.40–16.50)	4.10 (1.20–9.90)	7.70 (5.00–9.90)	12.00 (6.10–16.20)
Biological								
chl*a*	2.90 (0.90–9.60)	2.50 (1.00–12.40)	7.40 (1.00–19.30)	8.70 (1.00–22.70)	27.00 (5.40–125.70)	18.80 (2.20–54.80)	48.10 (18.60–71.10)	69.70 (46.00–99.60)
POC	68.54[7] (39.2–113.26)	38.56[15] (20.36–98.61)	89.66[44] (33.00–24.22)	82.66 (29.56–188.69)	204.05[31] (87.30–461.89)	160.41[39] (38.61–360.6)	284.82 (31.69–423.65)	474.48[7] (259.95–616.25)
Nutrient status								
POC:chl*a*	22.74[7] (10.24–55.32)	18.42[15] (7.93–27.16)	16.49[44] (2.75–67.47)	13.63 (3.56–57.93)	11.26[31] (1.81–32.59)	13.42[39] (4.74–139.39)	6.22 (1.30–11.08)	7.32[7] (4.68–10.05)
TN:TP	98.47 (48.79–195.54)	113.66 (69.15–169.22)	54.39 (30.34–109.55)	65.30 (20.72–114.23)	44.18 (14.54–97.98)	50.54 (19.00–103.38)	31.56 (23.38–46.54)	26.06[7] (10.21–40.40)
POC:PN	9.09[7] (6.45–15.1)	8.43[15] (6.60–10.64)	8.42[43] (1.92–14.42)	8.42[37] (5.41–12.02)	7.77[31] (6.28–11.72)	7.23[39] (3.97–10.23)	6.58 (5.79–8.65)	7.30[7] (5.62–8.75)
POC:PP	823.81[7] (179.25–3003.98)	370.49[15] (186.43–926.99)	248.37[44] (48.78–1659.53)	234.88 (122.37–458.26)	172.68[31] (63.71–474.79)	174.53[39] (83.93–286.41)	121.54 (11.18–184.72)	178.46[7] (140.64–216.36)
PN:PP	82.35[7] (27.8–281.44)	43.21[15] (19.68–87.08)	29.98[43] (6.67–132.24)	27.75[37] (18.39–51.94)	22.30[31] (7.84–59.92)	24.48[39] (13.22–58.28)	18.14 (1.93–26.22)	25.03[7] (17.01–32.34)
P debt	–	0.23[15] (0.03–0.55)	–	0.15[37] (0.00–0.40)	–	0.08[36] (0.01–0.27)	–	0.03[6] (0.02–0.07)
NH_4^+-N debt	–	0.14[12] (0.00–0.58)	–	0.04[36] (0.00–0.23)	–	0.05[37] (0.00–0.25)	–	0.03[6] (0.00–0.07)

(Continued)

TABLE 4 | Continued

	Oligotrophic		Mesotrophic		Eutrophic		Hypertrophic	
	2017 *n* = 20	2018 *n* = 16	2017 *n* = 50	2018 *n* = 38	2017 *n* = 34	2018 *n* = 41	2017 *n* = 8	2018 *n* = 8
NO_3^--N debt	–	0.04^{15} (0.00–0.10)	–	0.03^{37} (0.00–0.23)	–	0.03^{38} (0.00–0.11)	–	0.03^{7} (0.00–0.12)
$+NH_4^+ \phi_{PSII}$	–	0.36^{11} (0.21–0.55)	–	0.38^{34} (0.20–0.58)	–	0.36^{38} (0.20–0.63)	–	0.34^{7} (0.28–0.45)
$+NO_3^- \phi_{PSII}$	–	0.36^{11} (0.20–0.56)	–	0.39^{34} (0.17–0.60)	–	0.37^{38} (0.21–0.57)	–	0.34^{7} (0.22–0.47)
P-E parameters								
ϕ_{PSII}	–	0.48^{11} (0.33–0.56)	–	0.50^{35} (0.34–0.66)	–	0.48^{38} (0.38–0.63)	–	0.44^{7} (0.38–0.53)
α	–	0.52^{12} (0.38–0.62)	–	0.52^{35} (0.39–0.66)	–	0.50^{38} (0.35–0.88)	–	0.47^{7} (0.40–0.53)
α^B	–	0.32^{12} (0.03–0.59)	–	0.12^{35} (0.02–0.44)	–	0.06^{38} (0.01–0.40)	–	0.01^{7} (0.00–0.01)
E_k	–	278.20^{12} (171.92–405.89)	–	261.41^{35} (92.68–422.17)	–	311.35^{38} (97.65–491.34)	–	319.55^{7} (183.93–395.53)
E_k^B	–	160.97^{12} (32.62–273.39)	–	66.13^{35} (6.84–305.46)	–	30.02^{38} (6.28–173.84)	–	5.13^{7} (1.85–7.12)
$rETR_{max}$	–	140.32^{12} (73.91–216.69)	–	135.79^{35} (54.96–279.71)	–	152.71^{38} (66.58–265.65)	–	151.74^{7} (72.63–201.13)
$\bar{E}_{24}/E_k$	–	0.80^{12} (0.33–1.40)	–	0.54^{34} (0.19–1.17)	–	0.38^{37} (0.11–2.49)	–	0.28^{6} (0.19–0.40)
GPP	–	668.00^{12} (89.93–1,628.73)	–	701.47^{31} (33.36–2,668.00)	–	681.86^{36} (38.86–1,820.05)	–	607.42^{5} (458.47–768.31)
GPP^B	–	429.01^{12} (39.62–1,661.97)	–	134.54^{31} (9.83–630.11)	–	63.83^{36} (5.34–430.61)	–	9.79^{5} (4.60–13.82)

*Numbers in superscript indicate n values that differed from those reported in the column headers. An asterisk (*) is used when values are below detection limit. See **Table 1** for parameter definitions, abbreviations, and units. See **Table 6** for epilimnetic dissolved nutrient concentrations (TDP, TDN, NO_3^-, NH_4^+, DON).*

watersheds, NO_3^- was higher than NH_4^+ concentrations, whereas in forested, mixed, and ag-pasture reservoirs, NH_4^+ was higher than NO_3^-. Hypertrophic reservoirs also have more NH_4^+ relative to NO_3^- compared to oligo-, meso-, and eutrophic reservoirs.

Mean hypolimnetic TDP, TDN, NO_3^-, and NH_4^+ were consistently higher than epilimnetic concentrations across the trophic gradient. Hypolimnetic DRP was not measured due to interference with presumably high iron concentrations. Mean hypolimnetic TDP was 1.2–1.7× higher than epilimnetic concentrations in oligo- and hyper- trophic systems, and 5.3–5.8× higher in meso- and eu- trophic systems. Hypolimnetic NO_3^- was 2–2.5× higher than epilimnetic NO_3^- in eu- and hyper- trophic systems, and 13–15 x higher than epilimnetic NO_3^- in meso- and oligo- trophic systems. In contrast, hypolimnetic NH_4^+ was 32 (oligo-), 88 (meso-), 90 (eu-), and 78 (hyper- trophic)× higher than epilimnetic NH_4^+ concentrations. Hypolimnions contained ∼2, 14, 8, and 277× more NH_4^+ than NO_3^- in oligo-, meso-, eu-, and hyper- trophic systems, respectively (**Table 6**). TSS was dominated by POM (∼60–69% in 2017 and 51–80% in 2018; **Table 4**). PIM only exceeded POM in ∼15% of samples each year.

Both chl*a* and POC serve as proxies for phytoplankton biomass. There were increasingly higher chl*a* concentrations with increasing trophic status (**Table 4** and **Figure 3A**) and higher chl*a* trophic means in the wetter year. Reservoirs of forested and ag-pasture watersheds had the lowest and highest chl*a* concentrations, respectively (**Table 5**).

Nutrient Status

Physiological indicators suggest that P-deficiency is prevalent in Missouri reservoirs (**Figure 4**). TN:TP ratios favored P-deficiency in both years (**Table 4**) with only 2% of samples indicating N-deficiency. TN:TP ratios were significantly higher in the drier year (2018) than the wetter year (2017; **Tables 3**, **5**). Exceedance of the P-deficiency thresholds occurred in 83% of POC:PP and 65% of PN:PP samples (**Tables 2, 4** and **Figures** 4A,B) with no significant differences between wet and dry years (**Table 5**). P debt results also support P-deficiency, with 7% of the samples exceeding the threshold in 2018 (**Table 4** and **Figure 4C**). Only 11% of ϕ_{PSII} P-addition experiments exhibited positive increases in ϕ_{PSII} relative to the controls (**Figure 4D** and **Supplementary Table 2**).

TABLE 5 | Linear mixed effect (LME) model output for physical, chemical, biological, nutrient status, and photosynthesis-irradiance (P-E) parameters.

				Year		Sampling event				Trophic status				Land-use			
	Fixed effect	***F*-value**	***p*-value**	**2017**	**2018**	**1**	**2**	**3**	**4**	**O**	**M**	**E**	**H**	**F**	**Mix**	**Ag-P**	**Ag-C**
Physical																	
Secchi[a]	Year	$F_{1,172} = 8.287$	**0.005**	a	b												
	Sampling event	$F_{3,172} = 1.892$	0.133														
	Trophic status	$F_{3,25} = 22.117$	**<0.001**							c	b	a	a				
	Land-use	$F_{3,25} = 0.601$	0.621														
	Sampling Event:Year	$F_{3,172} = 2.069$	0.106														
K_d[a]	Year	$F_{1,175} = 21.735$	**<0.001**	b	a												
	Sampling event	$F_{3,175} = 1.731$	0.162														
	Trophic status	$F_{3,25} = 13.527$	**<0.001**							a	b	c	c				
	Land-use	$F_{3,25} = 1.482$	0.244														
	Sampling Event:Year	$F_{3,175} = 1.855$	0.139														
Z_{mix}[a]	Year	$F_{1,179} = 1.088$	0.298														
	Sampling event	$F_{3,179} = 1.131$	0.289														
	Trophic status	$F_{3,25} = 3.580$	**0.028**							b	ab	a	ab				
	Land-use	$F_{3,25} = 4.763$	**0.009**											b	ab	a	ab
	Sampling Event:Year	$F_{3,179} = 1.129$	0.289														
$\bar{E}_{24}$[a]	Year	$F_{1,174} = 0.582$	0.447														
	Sampling event	$F_{3,174} = 3.133$	**0.027**			b	ab	ab	a								
	Trophic status	$F_{3,25} = 1.467$	0.248														
	Land-use	$F_{3,25} = 5.838$	**0.004**											b	ab	a	ab
	Sampling Event:Year	$F_{3,174} = 0.365$	0.778														
Chemical																	
TP[a]	Year	$F_{1,183} = 14.270$	**<0.001**	b	a												
	Sampling event	$F_{3,183} = 1.602$	0.191														
	Trophic status	$F_{3,25} = 40.841$	**<0.001**							a	b	c	d				
	Land-use	$F_{3,25} = 1.835$	0.167														
	Sampling Event:Year	$F_{3,174} = 1.380$	0.251														
TDP[b]	Sampling event	$F_{3,67} = 2.569$	0.062														
	Trophic status	$F_{3,20} = 22.863$	**<0.001**							a	b	c	d				
	Land-use	$F_{3,20} = 1.044$	0.395														
DRP[b]	Sampling event	$F_{3,67} = 1.465$	0.232														
	Trophic status	$F_{3,20} = 5.799$	**0.005**							a	a	b	b				
	Land-use	$F_{3,20} = 1.754$	0.188														
PP[a]	Year	$F_{1,154} = 11.651$	**<0.001**	b	a												
	Sampling event	$F_{3,154} = 0.470$	0.704														
	Trophic status	$F_{3,25} = 60.346$	**<0.001**							a	b	c	d				
	Land-use	$F_{3,25} = 3.128$	**0.044**											a	b	ab	a
	Sampling Event:Year	$F_{3,154} = 1.478$	0.223														
TN[a]	Year	$F_{1,182} = 1.234$	0.268														
	Sampling event	$F_{3,182} = 2.245$	0.085														
	Trophic status	$F_{3,25} = 11.605$	**<0.001**							a	b	c	c				
	Land-use	$F_{3,25} = 0.635$	0.599														
	Sampling Event:Year	$F_{3,182} = 0.623$	0.601														
TDN[b]	Sampling event	$F_{3,67} = 2.193$	0.097														
	Trophic status	$F_{3,20} = 6.939$	**0.002**							a	b	c	bc				
	Land-use	$F_{3,20} = 1.462$	0.255														
DON[b]	Sampling event	$F_{3,66} = 0.918$	0.437														
	Trophic status	$F_{3,20} = 3.381$	**0.039**							a	ab	b	b				
	Land-use	$F_{3,20} = 0.147$	0.930														
PN[a]	Year	$F_{1,151} = 5.658$	**0.019**	b	a												
	Sampling event	$F_{3,151} = 0.155$	0.926							a	b	c	d				

(Continued)

TABLE 5 | Continued

				Year		Sampling event				Trophic status				Land-use			
	Fixed effect	***F*-value**	***p*-value**	**2017**	**2018**	**1**	**2**	**3**	**4**	**O**	**M**	**E**	**H**	**F**	**Mix**	**Ag-P**	**Ag-C**
	Trophic status	$F_{3,25}$ = 27.069	**<0.001**														
	Land-use	$F_{3,25}$ = 2.582	0.076														
	Sampling Event:Year	$F_{3,151}$ = 0.825	0.482														
DOC[a]	Year	$F_{1,140}$ = 7.363	**0.008**	b	a												
	Sampling event	$F_{3,140}$ = 19.803	**<0.001**			c	b	b	a								
	Trophic status	$F_{3,25}$ = 2.689	0.068														
	Land-use	$F_{3,25}$ = 0.450	0.720														
	Sampling Event:Year	$F_{3,140}$ = 6.250	**<0.001**														
TSS[a]	Year	$F_{1,178}$ = 15.762	**<0.001**	a	b												
	Sampling event	$F_{3,178}$ = 0.567	0.638														
	Trophic status	$F_{3,25}$ = 23.365	**<0.001**							a	b	c	d				
	Land-use	$F_{3,25}$ = 1.698	0.193														
	Sampling Event:Year	$F_{3,178}$ = 1.241	0.297														
POM[a]	Year	$F_{1,178}$ = 13.543	**<0.001**	a	b												
	Sampling event	$F_{3,178}$ = 0.474	0.701														
	Trophic status	$F_{3,25}$ = 31.500	**<0.001**							a	b	c	d				
	Land-use	$F_{3,25}$ = 4.562	**0.011**											a	b	ab	ab
	Sampling Event:Year	$F_{3,178}$ = 1.311	0.272														
PIM[a]	Year	$F_{1,183}$ = 10.712	**0.001**	a	b												
	Sampling event	$F_{3,183}$ = 2.219	0.088														
	Trophic status	$F_{3,25}$ = 5.672	**0.004**							a	ab	b	bc				
	Land-use	$F_{3,25}$ = 0.158	0.923														
	Sampling Event:Year	$F_{3,183}$ = 1.309	0.273														
Biological																	
chla[a]	Year	$F_{1,179}$ = 16.404	**<0.001**	a	b												
	Sampling event	$F_{3,179}$ = 0.544	0.653														
	Trophic status	$F_{3,25}$ = 17.166	**<0.001**							a	b	c	d				
	Land-use	$F_{3,25}$ = 4.161	**0.016**											a	ab	b	ab
	Sampling Event:Year	$F_{3,179}$ = 5.102	**0.002**														
POC[a]	Year	$F_{1,153}$ = 6.292	**0.013**	b	a												
	Sampling event	$F_{3,153}$ = 0.189	0.904														
	Trophic status	$F_{3,25}$ = 25.598	**<0.001**							a	b	c	d				
	Land-use	$F_{3,25}$ = 2.591	0.075														
	Sampling Event:Year	$F_{3,153}$ = 1.095	0.353														
Nutrient status																	
POC:chla[a]	Year	$F_{1,153}$ = 4.902	**0.028**	b	a												
	Sampling event	$F_{3,153}$ = 0.661	0.577														
	Trophic status	$F_{3,25}$ = 2.676	0.069														
	Land-use	$F_{3,25}$ = 2.890	0.055														
	Sampling Event:Year	$F_{3,153}$ = 2.550	0.058														
TN:TP[a]	Year	$F_{1,182}$ = 11.241	**0.001**	a	b												
	Sampling event	$F_{3,182}$ = 0.162	0.922														
	Trophic status	$F_{3,25}$ = 17.907	**<0.001**							c	b	b	a				
	Land-use	$F_{3,25}$ = 2.971	0.051														
	Sampling Event:Year	$F_{3,182}$ = 0.924	0.431														
POC:PN[a]	Year	$F_{1,151}$ = 0.029	0.865														
	Sampling event	$F_{3,151}$ = 0.688	0.561														
	Trophic status	$F_{3,25}$ = 0.822	0.494														
	Land-use	$F_{3,25}$ = 0.467	0.708														
	Sampling Event:Year	$F_{3,151}$ = 0.215	0.886														

(Continued)

TABLE 5 | Continued

				Year		Sampling event				Trophic status				Land-use			
	Fixed effect	***F*-value**	***p*-value**	**2017**	**2018**	**1**	**2**	**3**	**4**	**O**	**M**	**E**	**H**	**F**	**Mix**	**Ag-P**	**Ag-C**
POC:PP[a]	Year	$F_{1,152}$ = 1.561	0.214														
	Sampling event	$F_{3,152}$ = 1.031	0.381														
	Trophic status	$F_{3,25}$ = 8.747	**<0.001**							c	b	a	a				
	Land-use	$F_{3,25}$ = 0.322	0.809														
	Sampling Event:Year	$F_{3,152}$ = 0.082	0.970														
PN:PP[a]	Year	$F_{1,151}$ = 1.436	0.233														
	Sampling event	$F_{3,151}$ = 1.047	0.374														
	Trophic status	$F_{3,25}$ = 9.289	**<0.001**							b	a	a	a				
	Land-use	$F_{3,25}$ = 0.760	0.527														
	Sampling Event:Year	$F_{3,151}$ = 0.147	0.931														
P-E parameters																	
ϕ_{PSII}[b]	Sampling event	$F_{1,61}$ = 1.901	0.133														
	Trophic status	$F_{3,20}$ = 0.330	0.803														
	Land-use	$F_{3,20}$ = 4.296	**0.017**											b	ab	a	ab
E_k[b]	Sampling event	$F_{3,61}$ = 4.447	**0.007**			b	ab	a	ab								
	Trophic status	$F_{3,20}$ = 0.638	0.599														
	Land-use	$F_{3,20}$ = 1.387	0.276														
E_k[Bb]	Sampling event	$F_{3,62}$ = 11.340	**<0.001**			b	a	a	a								
	Trophic status	$F_{3,20}$ = 12.713	**<0.001**							c	b	b	a				
	Land-use	$F_{3,20}$ = 1.981	0.149														
α[b]	Sampling event	$F_{3,61}$ = 2.873	**0.043**			b	ab	ab	a								
	Trophic status	$F_{3,20}$ = 0.379	0.769														
	Land-use	$F_{3,20}$ = 4.109	**0.020**											b	ab	a	ab
α[Bb]	Sampling event	$F_{3,62}$ = 8.045	**<0.001**			b	ab	a	a								
	Trophic status	$F_{3,20}$ = 17.186	**<0.001**							c	b	b	a				
	Land-use	$F_{3,20}$ = 5.697	**<0.001**											b	a	a	ab
$rETR_{max}$[b]	Sampling event	$F_{3,62}$ = 4.182	**0.009**			b	ab	a	ab								
	Trophic status	$F_{3,20}$ = 0.762	0.529														
	Land-use	$F_{3,20}$ = 0.144	0.932														
$\bar{E}_{24}/E_k$[b]	Sampling event	$F_{3,59}$ = 2.748	0.051														
	Trophic status	$F_{3,20}$ = 4.592	**0.013**							b	a	a	a				
	Land-use	$F_{3,20}$ = 6.032	**0.004**											b	a	a ab	
GPP[b]	Sampling event	$F_{3,54}$ = 0.702	0.555														
	Trophic status	$F_{3,20}$ = 0.724	0.550														
	Land-use	$F_{3,20}$ = 2.236	0.115														
GPP[Bb]	Sampling event	$F_{3,54}$ = 1.349	0.268														
	Trophic status	$F_{3,20}$ = 8.160	**0.001**							c	b	a	a				
	Land-use	$F_{3,20}$ = 0.290	0.832														

*Data were tested for the effects of year, sampling event, trophic status, and watershed land-use. LME analyses were coupled with ANOVA's (F- and p-values). When factors were significant (bolded, $p < 0.05$), a Tukey's Honest Significant Difference test was conducted, as indicated by the lowercase letters. Different lowercase letters indicate significant differences between factor levels. Letters are ordered alphabetically to indicate trend direction where "a" represents the lowest mean. Heading abbreviations are as follows: O, oligotrophic; M, mesotrophic; E, eutrophic; H, hypertrophic; F, forested; Mix, mixed; Ag-P, pasture; Ag-C, cropland. The superscript [a] indicates parameters collected in both 2017 and 2018, whereas the superscript [b] indicates parameters collected only in 2018. Interactions (Sampling Event:Year) were not included in the model for those parameters only collected in 2018. See **Table 1** for parameter definitions, abbreviations, and units.*

N-deficiency is not common in Missouri reservoirs (**Figure 5**). The POC:PN ratio, which was the only N-indicator applied in both years, showed no difference between 2017 and 2018 (**Table 5**) and only 35% of samples were above the N-deficiency threshold (**Table 2**, **Figure 5A**, and **Supplementary Table 2**). N debts and ϕ_{PSII} N-addition experiments provided little support for N-deficiency (**Tables 4**, **6**, **7**, **Figure 5**, and **Supplementary Table 2**).

Missouri reservoirs are primarily P-deficient. When plotted on a coordinate plane, the P debt and NH_4^+-N debt thresholds create four quadrants wherein we can estimate N-only deficiency (quadrant 1), NP co-deficiency (quadrant 2), P-only deficiency (quadrant 3) and sufficiency of both N and P (quadrant 4; **Figure 6**). None of the phytoplankton communities indicated N-only deficiency (quadrant 1) and only 8% fell in quadrant 2 suggesting NP co-deficiency. Most samples

TABLE 6 | Epilimnetic and hypolimnetic dissolved nutrient chemistry from the 27 reservoirs sampled during 2018 summer stratification.

	Oligotrophic *n* = 15		Mesotrophic *n* = 37		Eutrophic *n* = 38		Hypertrophic *n* = 7	
	Epi	***Hypo***	***Epi***	***Hypo***	***Epi***	***Hypo***	***Epi***	***Hypo***
TDP	0.11 (0.06–0.17)	0.13 (0.10–0.19)	0.20 (0.12–0.33)	1.05 (0.12–5.07)	0.37 (0.21–1.33)	2.15 (0.19–10.08)	0.74 (0.54–0.93)	1.23 (0.45–2.02)
TDN	16.42 (10.79–23.70)	38.31 (16.45–66.77)	25.98 (9.29–36.51)	61.28 (17.60–163.55)	38.83 (12.01–90.68)	100.23 (11.16–307.83)	57.20 (37.48–70.00)	116.02 (38.34–293.44)
NO_3^-	0.54 (0.18*–2.28)	8.12 (0.18*–31.52)	0.25 (0.18*–1.04)	3.33 (0.18*–30.06)	6.01 (0.18*–46.91)	11.29 (0.18*–80.25)	0.18* (0.18*–0.18*)	0.43 (0.18*–1.71)
NH_4^+	0.49 (0.36*–1.32)	15.78 (0.36*–53.08)	0.51 (0.36*–1.43)	44.81 (0.36*–224.82)	1.02 (0.36*–9.46)	91.41 (0.36*–415.98)	1.52 (0.36*–6.68)	119.19 (0.36*–397.92)
DON	15.39 (10.25–20.88)	15.56 (8.28–29.22)	25.22 (8.76–35.16)	20.54 (0.00–41.70)	31.80 (4.24–47.16)	20.60 (0.00–43.34)	53.89[6] (36.95–68.89)	35.49[5] (0.00–58.93)

Shown are the seasonal arithmetic means and ranges (minimums–maximums) of n samples grouped along the trophic gradient. Total dissolved phosphorus (TDP), total dissolved nitrogen (TDN), nitrate (NO_3^-), and ammonium (NH_4^+) were collected in the field. Dissolved organic Nitrogen (DON) was calculated by difference. Below detection limit is denoted by an asterisk (*); detection limits are 0.03 μmol L^{-1} for TDP; for 2.50 μmol L^{-1} TDN; 0.36 μmol L^{-1} for NO_3^-; and 0.71 μmol L^{-1} for NH_4^+. Numbers in superscript indicate n values that differed from those reported in the column headers. See ***Table 1*** *for parameter definitions, abbreviations, and units.*

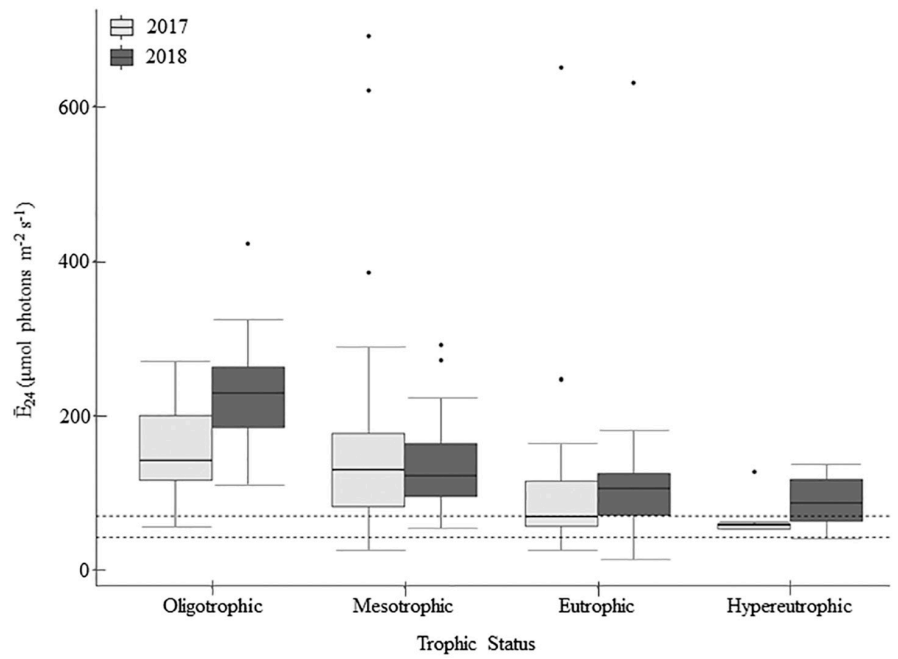

FIGURE 2 | Mean daily mixed layer irradiance ($\bar{E}_{24}$) across trophic status during the 2017 and 2018 sampling seasons (*n* = 213). Within the boxplots, the 50th percentile (median) is visualized with a solid horizontal line within each box. The 25th and 75th percentiles are represented by box hinges above and below the median line. On either end of the box, whiskers denote the smallest and largest values within 1.5× the interquartile range (IQR) and points indicate values beyond 1.5× the IQR. Dashed lines on the figure represent the light-deficiency thresholds, where values below the lines would be considered light deficient (**Table 2**).

indicated P-only deficiency (51%) or N and P sufficiency (41%; **Figure 6**).

Given that indicator values can vary due to influences of phytoplankton community composition and non-algal particulate matter (Hecky et al., 1993), multiple indicator implementation increases assessment strength, especially when observing agreement between ≥2 indicators (Hecky and Kilham, 1988). In 2017, POC:PP and PN:PP ratios were employed as our primary P status indicators with 100% agreement in favor of P-deficiency in oligotrophic reservoirs (**Supplementary Table 3**). In 2018, P-indicators were expanded to include P debt and P-addition ϕ_{PSII} experiments. All but one oligotrophic sample favored P-deficiency; 2% with complete agreement, and 73% with 3/4 indicator agreement. Overall agreement was much higher for N-indicators than P-indicators with all N-indicators agreeing 63–64% of the time for NH_4^+ and NO_3^- additions. We found 88% of indicator applications favored N-sufficiency for NH_4^+, while

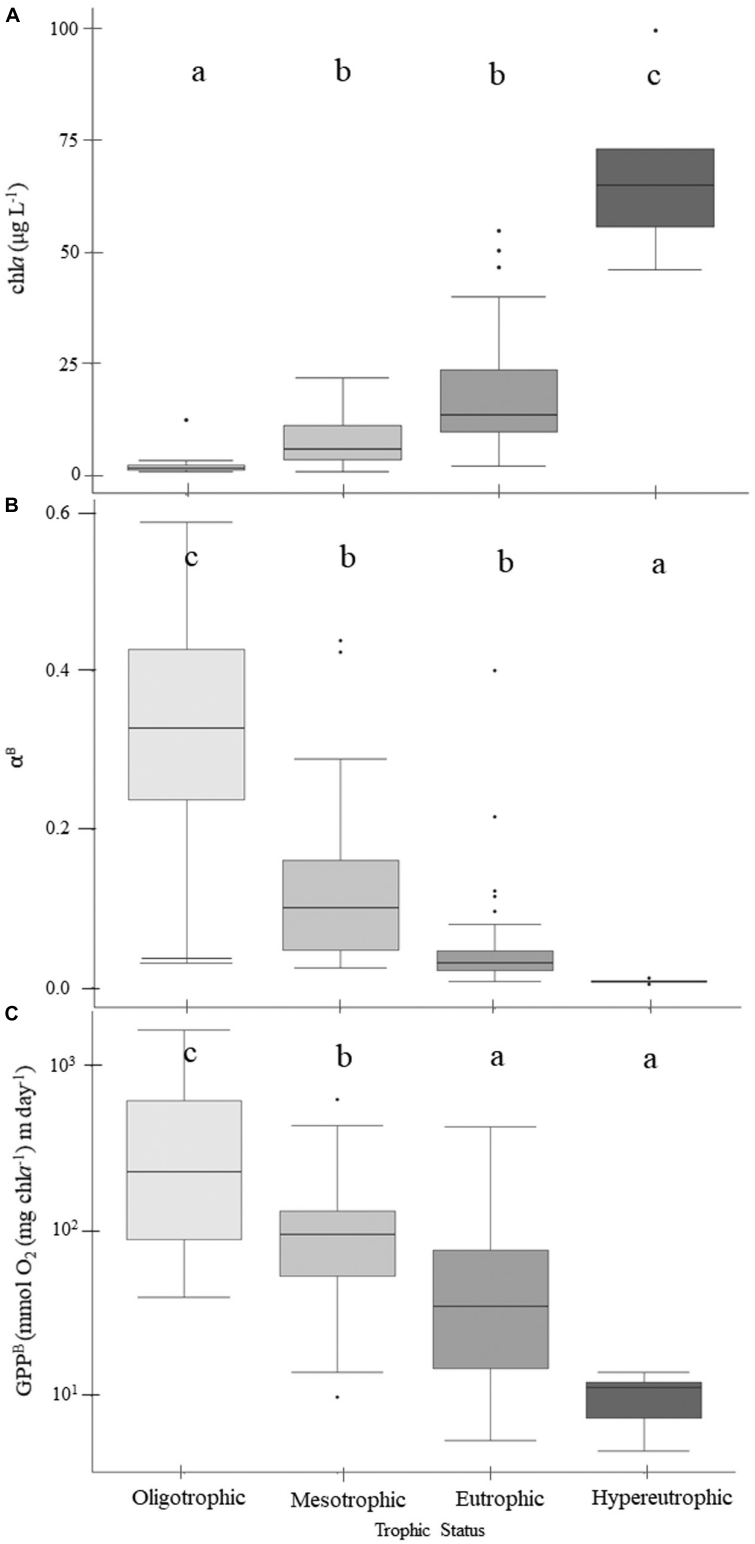

FIGURE 3 | Patterns of chlorophyll-*a* **(A)**, light utilization efficiency per unit of chlorophyll-*a* **(B)**, and gross primary production (GPP^B) rates normalized to chlorophyll-*a* **(C)** across the trophic gradient. Within the boxplots, the 50th percentile (median) is visualized with a solid horizontal line. The 25th and 75th percentiles are represented by box hinges above and below the median line. On either end of the box, whiskers denote the smallest and largest values within 1.5× the interquartile range (IQR) and points indicate values beyond 1.5× the IQR. Lowercase letters indicate results from multiple comparison *post-hoc* tests, where similar letters denote no significant differences between trophic states (**Table 5**).

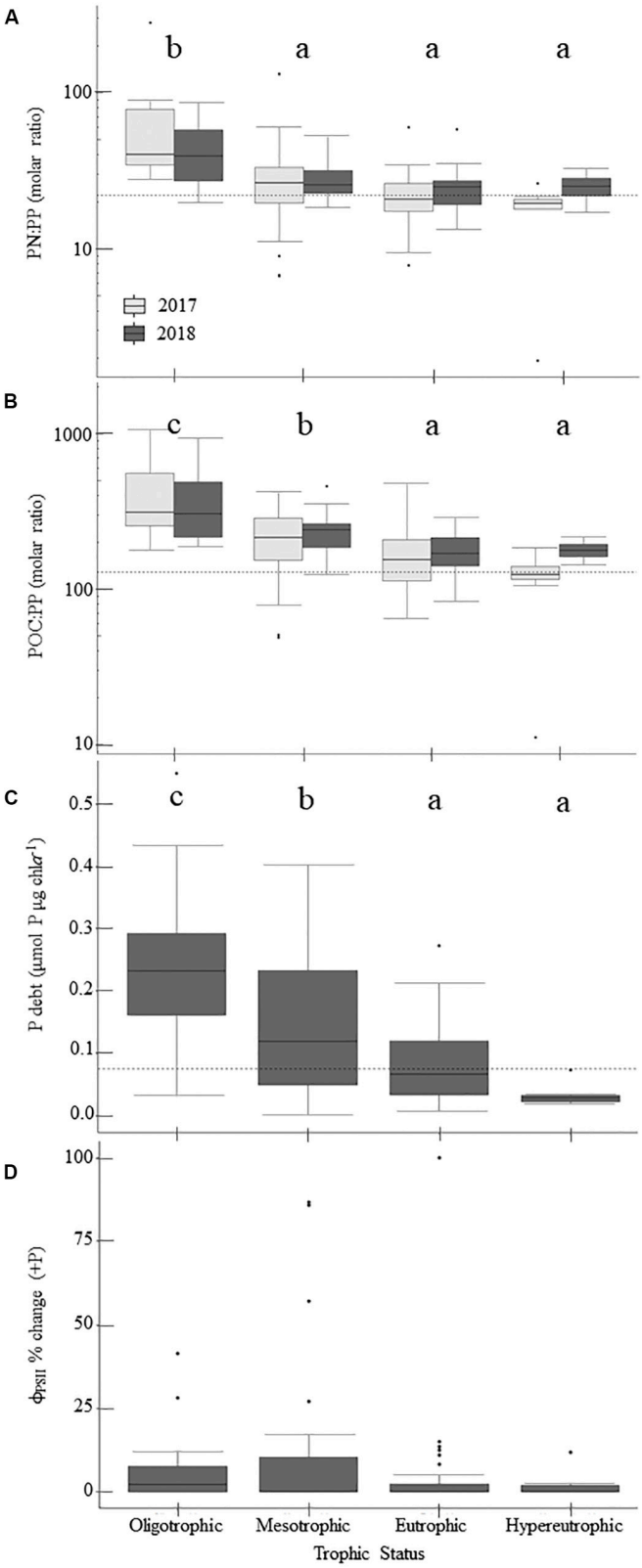

FIGURE 4 | Patterns in phosphorus-deficiency across the trophic gradient and 2-year sample period, if applicable, for parameters sampled in 2017 and 2018. Panels show particulate nitrogen to particulate phosphorus (PN:PP) ratios **(A)**, particulate organic carbon to particulate phosphorus (POC:PP) ratios **(B)**, phosphorus *(Continued)*

FIGURE 4 | Continued
debts (P debt; **C**), and percent change in ϕ_{PSII} relative to the control treatment following P-additions **(D)**. Dashed horizontal lines indicate phosphorus-deficiency thresholds where applicable. Values above those lines suggest phosphorus-deficiency (**Table 2**). Lowercase letters indicate results from multiple comparisons *post-hoc* tests, where similar letters denote no significant differences between trophic states (**Table 5**). Within the boxplots, the 50th percentile (median) is visualized with a solid horizontal line. The 25th and 75th percentiles are represented by box hinges above and below the median line. On either end of the box, whiskers denote the smallest and largest values within 1.5× the interquartile range (IQR) and points indicate values beyond 1.5× the IQR.

95% of applications favored N-sufficiency for NO_3^- additions (**Supplementary Table 3**).

Photosynthesis-Irradiance (P-E) Parameters

In 2018, ϕ_{PSII} ranged from 0.33 to 0.66 across the trophic gradient with a mean of 0.48 (**Table 4**). The ϕ_{PSII} in all but one sampling event fell below the empirical optimum value of ∼0.65, with only 8% of sampling events having values >0.60. Land-use had a significant effect on ϕ_{PSII}, where agricultural-pasture had the lowest mean ϕ_{PSII} and forested had the highest. There was no relationship with trophic status. We also found no relationship between trophic status and α, although a significant relationship did exist between α and land-use, as well as sampling event (**Table 5**). Phytoplankton in reservoirs of forested watersheds were the most efficient at utilizing light, whereas those in ag-pasture watersheds were the least efficient. Efficiency was highest in May/June and lowest in August/September. After normalization to chl*a*, α^B differed across trophic status with phytoplankton of oligotrophic reservoirs being more efficient than those of meso-, eu-, or hyper- trophic reservoirs (**Table 5** and **Figures 3A,B**). As with α, α^B demonstrated that efficiency was higher in May/June and in forested watersheds than in August/September or ag-pasture watersheds. Ranging from 92.68 to 491.34 with an average of 292.63 μmol photons m^{-2} s^{-1} (**Table 4**), there was no relationship between the light saturation parameter (E_k) and trophic status (**Table 5**). The maximum relative electron transport rate through photosystem II ($rETR_{max}$) ranged from 54.96 to 279.71 with an average of 145.14 (**Table 4**) and was also not related to trophic status (**Table 5**). Sampling event was related to both E_k and $rETR_{max}$ wherein both P-E parameters peaked in May/June and reached the lowest values by July/August. Per unit of chl*a*, however, $E_k{}^B$ was higher for phytoplankton in oligotrophic reservoirs compared to meso-, eu-, or hyper- trophic reservoirs. $E_k{}^B$ was also higher in May/June but was not related to land-use (**Table 5**).

Gross Primary Productivity

Ranging from 668 to 701 mmol O_2 m^{-2} day^{-1}, mean GPP rates were similar between oligo-, meso-, and eu- trophic reservoirs. Hypertrophic reservoirs demonstrated a lower mean GPP of 607 mmol O_2 m^{-2} day^{-1}. Across individual samples, GPP widely ranged from ∼33 to 2,668 (**Table 4**). There was no relationship between GPP and any chemical or biological parameters nor with trophic status (**Table 5**).

Rates of GPP normalized to chl*a* (GPP^B) were negatively related to trophic status, where GPP^B was highest in oligotrophic reservoirs and decreased with increasing eutrophy (p = 0.001; **Figure 3C**). While trophic mean GPP^B rates ranged from ∼10 to 430 mmol O_2 (mg Chla^{-1}) m day^{-1}, the mean GPP^B in oligotrophic reservoirs was ∼3, ∼7, and ∼44× higher than those in meso-, eu-, and hyper- trophic reservoirs, respectively (**Table 4** and **Figure 3C**). We found positive correlations between GPP^B and physical and P-E parameters, and negative correlations for chemical and biological parameters. Higher GPP^B rates correlated with higher light availability and P-E activity, and lower turbidity, nutrients, and proxies for phytoplankton biomass (**Supplementary Table 4**).

DISCUSSION

Missouri reservoirs have variable light availability, nutrient chemistry, proxies for phytoplankton biomass, and GPP rates across the trophic gradient and between the climatically contrasting summers of 2017 and 2018. P-deficiency was the predominant constraint on phytoplankton biomass with rare occurrences of N-deficiency. Light deficiency was observed ∼25% of the times sampled. Highest in oligotrophic reservoirs, mean GPP^B, $E_k{}^B$, and α^B decreased with increasing eutrophy. Productivity was constrained by light availability, induced through self-shading by phytoplankton communities.

Production:Biomass Ratios

The median chl*a* concentration in our study reservoirs is 9.3 μg L^{-1}, ranging from 0.9 to 125.7 μg L^{-1}. These concentrations are ∼1.5× higher than the median summer chl*a* (6 μg L^{-1}) measured in 2,239 lakes in the Midwest and Northeast United States (Oliver et al., 2017). A global study of 1,316 lakes ranging from tropical to polar, reported a median chl*a* concentration of 5.9 μg L^{-1} (Abell et al., 2012). Within this dataset, the low-temperate lakes had a median chl*a* of 13.2 μg L^{-1} (Abell et al., 2012), 1.4× higher than our Midwest reservoirs. Neither of these studies, however, differentiated between lakes and reservoirs; reservoirs tend to have higher phytoplankton biomass and productivity (Kimmel and Groeger, 1984).

Just as P is assumed to be the primary constraint on phytoplankton biomass (Schindler, 1974), a similar paradigm exists for lake productivity (Vollenweider, 1976). Global lake observations support the paradigm, showing strong positive relationships between GPP and TP (Hanson et al., 2003; Solomon et al., 2013). While most Missouri reservoirs are consistent with the P-paradigm for biomass accrual, their productivity diverges from the lake-centric model by GPP and GPP^B having, respectively, no relationship and a strongly negative relationship with TP (**Supplementary Table 4**). The ratio of production to biomass across our trophic gradient is high at low TP (oligotrophic) and low at high TP (hypertrophic). A negative relationship between GPP^B and TP has also been observed in seven Midwestern (Wisconsin) lakes (Lauster et al., 2006). There, GPP^B decreased with increasing eutrophy, wherein the median

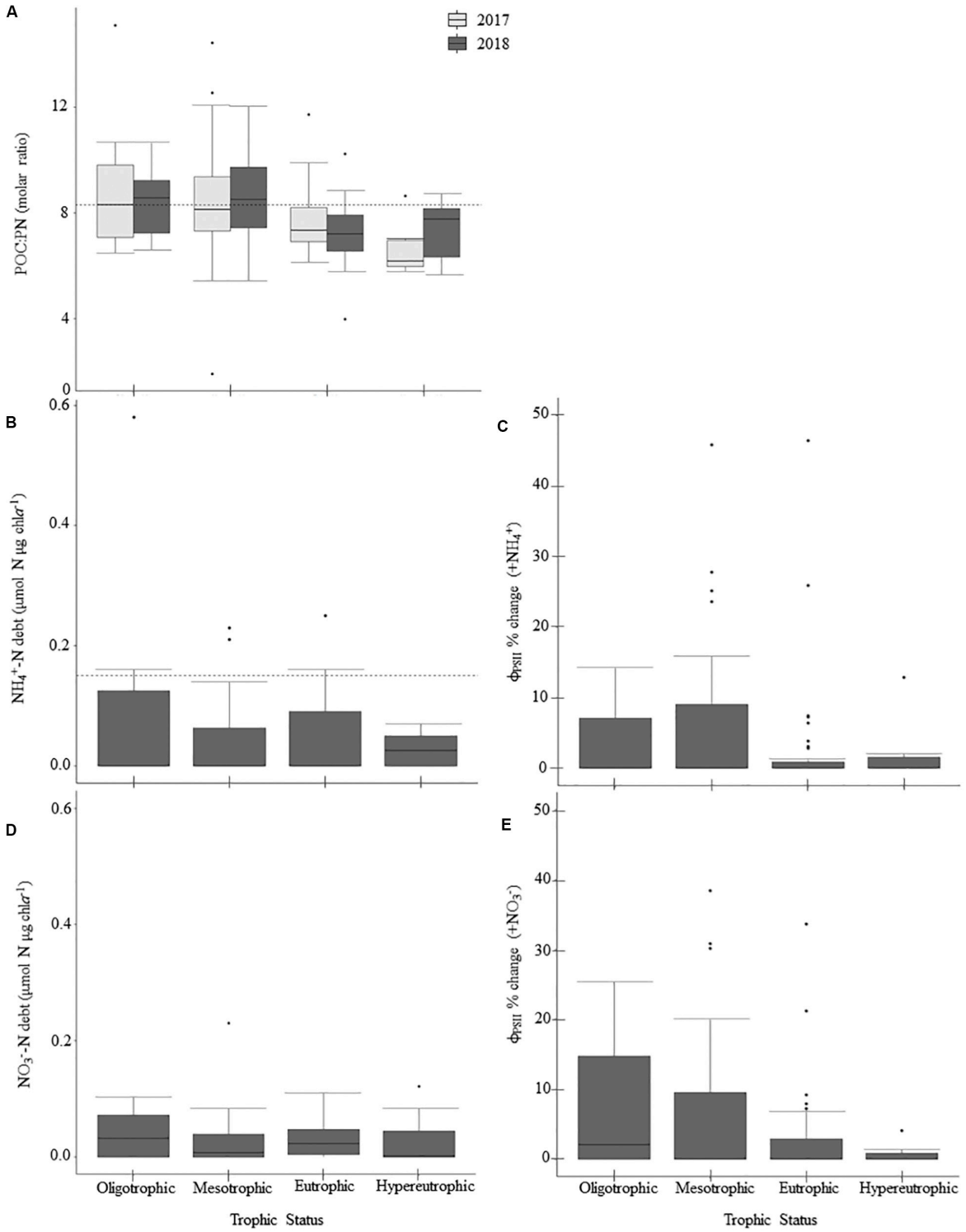

FIGURE 5 | Patterns in nitrogen-deficiency across the trophic gradient and 2-year sample period, if applicable, for parameters sampled in 2017 and 2018. Panels show particulate organic carbon to particulate nitrogen (POC:PN) ratios **(A)**, ammonium debts (NH_4^+-debt; **B**), percent change in ϕ_{PSII} relative to the control treatment following NH_4^+-additions **(C)**, nitrate debts (NO_3^--debt; **D**), and percent change in ϕ_{PSII} relative to the control treatment following NO_3^- additions **(E)**. Dashed horizontal lines indicate nitrogen-deficiency thresholds where applicable. Values above those lines suggest nitrogen-deficiency (**Table 2**). There were no significant differences between trophic states (**Table 5**). Within the boxplots, the 50th percentile (median) is visualized with a solid horizontal line. The 25th and 75th percentiles are represented by box hinges above and below the median line. On either end of the box, whiskers denote the smallest and largest values within 1.5× the interquartile range (IQR) and points indicate values beyond 1.5× the IQR.

TABLE 7 | A Kruskal Wallis ANOVA was conducted on the 2018 nutrient debts (P debt, NH_4^+-N debt, NO_3^--N debt) to test for the effects of sampling event, trophic status, and watershed land-use.

						Trophic status				Land-use			
	Factor	**Chi square**	***p*-value**	***n***	***df***	**O**	**M**	**E**	**H**	**F**	**Mix**	**Ag-P**	**Ag-C**
P debt	Sampling Event	3.084	0.380	94	3								
	Trophic Status	25.597	**<0.001**			c	b	a	a				
	Land-Use	6.299	0.100										
NH_4^+-N debt	Sampling Event	0.634	0.889	93	3								
	Trophic Status	3.461	0.326										
	Land-Use	9.552	**0.023**							a	ab	b	a
NO_3^--N debt	Sampling Event	7.434	0.059	97	3								
	Trophic Status	3.180	0.365										
	Land-Use	4.997	0.172										

When factors were significant (bolded, $p < 0.05$), a Dunn's Test of Multiple Comparisons was conducted, as indicated by the lowercase letters. Different lowercase letters indicate significant differences between factor levels. Letters are ordered alphabetically to indicate trend direction where "a" represents the lowest mean. Heading abbreviations are as follows: O, oligotrophic; M, mesotrophic; E, eutrophic; H, hypertrophic; F, forested; Mix, mixed; Ag-P, pasture; Ag-C, cropland.

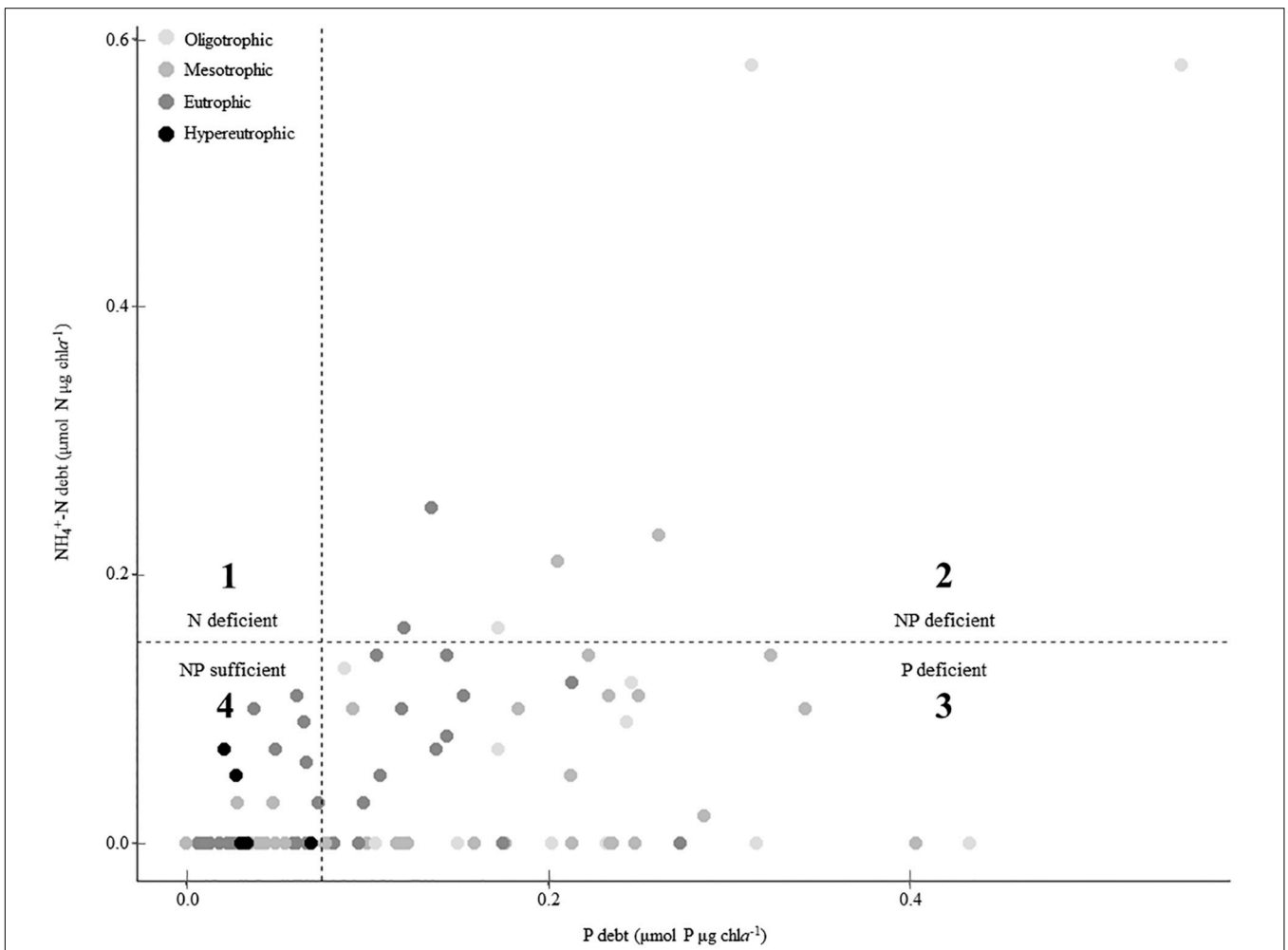

FIGURE 6 | Summary of nutrient deficiency across the trophic gradient according to phosphorus (P) and ammonium (NH_4^+) debts. Dashed lines indicate deficiency thresholds for P and NH_4^+-debts (**Table 2**). Values above these lines suggest deficiency, thus quadrants 1, 3, and 2 represent N-only deficiency, P-only deficiency, and NP co-deficiency, respectively. Quadrant 4 represents nutrient sufficiency in both P and N.

GPP^B, measured with light/dark bottle incubations, was 21.89, 8.39, 5.67, and 0.72 mmol O_2 (mg chla^{-1}) m day^{-1} for oligo-, meso-, eu-, and dys- trophic lakes, respectively (Lauster et al., 2006). They also reported a wide, albeit lower range in GPP (9–179 mmol O_2 m^{-2} day^{-1}) and GPP^B (1–320 mmol O_2 (mg chla^{-1}) m day^{-1}; Lauster et al., 2006). The wide range we observed in GPP (33–2,668 mmol O_2 m^{-2} day^{-1}) is also higher than a literature synthesis utilizing various GPP methods from a global assemblage of lakes (3–1,100 mmol O_2 m^{-2} day^{-1}, n = 72; Hoellein et al., 2013). Given the higher productivity expected from reservoirs (Kimmel and Groeger, 1984), our rates are more comparable to other temperate reservoirs, for which productivity studies are rare. Rates from 2 Canadian reservoirs-South Indian Lake and Lake Diefenbaker are still lower than what we report here. Two years after impoundment, productivity measured with ^{14}C uptake in South Indian Lake were 71 mmol O_2 m^{-2} day^{-1} for GPP and 17 mmol O_2 (mg chla^{-1}) m day^{-1} for GPP^B (Hecky and Guildford, 1984). In the oligo-mesotrophic reservoir, Lake Diefenbaker, fluorometrically derived GPP rates (11–746 mmol O_2 m^{-2} day^{-1}) overlapped the range of rates in our oligotrophic reservoirs, but its mean GPP was ∼6× smaller. Similar chl*a* averages between our reservoirs and Lake Diefenbaker (2.5 and 3.0 μg L^{-1}, respectively) shortened the gap between mean GPP^B rates, but Lake Diefenbaker rates were still ∼3× smaller than those of our oligotrophic reservoirs (Dubourg et al., 2015). Given that reservoir construction has increased by an order of magnitude in the past half century (Zarfl et al., 2015), it is important to consider these elevated reservoir rates in global carbon modeling exercises. The high GPP rates reported here in Midwest reservoirs will also have implications for reservoir ecological functioning and food webs.

Variances between reported productivity estimates may be attributed not only to intersystem differences, but also to methodological differences. We derived our estimates fluorometrically, as did others, but traditional methods rely on diel changes in O_2, light/dark bottle incubations and/or ^{14}C fixation. Fluorometric methods predict GPP 1.6× higher than actual C-fixation (Kromkamp et al., 2008). Fluorometrically derived P-E parameters can also vary with species composition of the phytoplankton (Campbell et al., 1998; Suggett et al., 2009). Cyanobacteria, in particular, are known to exhibit significantly lower ϕ_{PSII} than eukaryotes (Campbell et al., 1998). While the members of our present-day phytoplankton communities are unknown, it has been previously demonstrated that cyanobacterial abundance increases with trophic status in Missouri reservoirs (Jones et al., 2008b).

In north temperate lakes, productivity exhibits notable positive and negative interactions with $\bar{E}_{24}$ and turbidity, respectively (Staehr and Sand-Jensen, 2007; Torremorell et al., 2009; Staehr et al., 2010; Laas et al., 2012). Low productivity in turbid waters can be attributed to high PIM (Grobbelaar, 1989) or high POM, via the light-shade acclimation response (Kromkamp et al., 2008). Previous studies on Missouri reservoirs have shown that PIM typically dominates summer seston (29–87% of TSS; Jones and Knowlton, 1993; Knowlton and Jones, 1995, 2000). During our 2-year sampling window, TSS was dominated by POM in 85% of samples and the lowest GPP^B rates corresponded with the highest POM concentrations. We conclude that self-shading by phytoplankton induced light deficiencies which regulated primary productivity. Increased turbidity via elevated biomass accrual and self-shading were also evidenced by negative correlations of both GPP^B and α^B with chl*a* and K_d in a eutrophic lake in the Netherlands (Kromkamp et al., 2008).

Light-deficiency was most common in reservoirs from Missouri watersheds dominated by ag-crop, followed by ag-pasture. While agricultural land use enhances nutrient export to surface waters, row-crop agriculture is often associated with higher nutrient enrichment than low-intensity livestock production (Strayer et al., 2003). Although our high-nutrient systems had more PIM than did our low-nutrient systems, POM concentrations were notably higher than PIM concentrations in nearly all samples. Thus, when light-deficiency occurred, it was induced by self-shading rather than mineral turbidity.

The shallow mixing depths of Missouri reservoirs ensure that phytoplankton communities spend sufficient time in the euphotic zone, reflected in high $\bar{E}_{24}$ values and lack of evidence for photoacclimation. As with the GPP methodological issues, E_k derived from fluorometry is often higher than E_k from C-incorporation (Napoléon and Claquin, 2012). Nutrient deficiency, in particular, can perturb the relationship between electron transport rate and C, from which the fluorometric-E_k is derived (Napoléon et al., 2013). The $\bar{E}_{24}$:E_k ratio was originally applied using C-incorporation methods (Hecky and Guildford, 1984), therefore, using fluorometrically derived $\bar{E}_{24}$:E_k may overestimate the actual degree of light-deficiency. As a physiological measurement, ϕ_{PSII} is often used as a general indicator of phytoplankton stress, with values less than 0.65, as most of our samples were, indicative of light and/or nutrient deficiency (Kromkamp and Forster, 2003), hindering photosynthetic capacity (Kromkamp et al., 2008). Given that the lowest ϕ_{PSII} occurred in the highest-nutrient/lowest-light systems, the physiological stress likely does not reflect a lack of nutrients, but rather, light deficiency. If the phytoplankton were stressed due to nutrient deficiencies, we would have observed significant increases in ϕ_{PSII} post-nutrient additions.

The Role of Nutrients in Constraining Phytoplankton Biomass in an Agricultural State

Agriculture is prominent on the Missouri landscape, representing 41% of the land-use, therefore, we would expect P to be in ample supply in these surface waters. Yet, P-deficiency is prevalent. We observe high concentrations of the most bioavailable form of P, DRP, in eu- and hyper- trophic reservoirs within agricultural watersheds. Conservation tillage and surface broadcasting of fertilizer resulted in a 218% increase in concentrations of DRP in Lake Erie (Michalak et al., 2013), and similar practices in Pennsylvania caused DRP to increase 3–28× above background levels following fertilizer application (Kleinman et al., 2009). The prominence of P deficiency in Missouri reservoirs implies that additional inputs of P could result in increased phytoplankton biomass. Thus, implementation of beneficial management practices (BMPs) that would reduce DRP runoff are advised. Climate-induced increases in flow to

downstream reservoirs need to be countered with increased efforts for nutrient retention on the landscape (Sharpley et al., 2013). These land-based nutrient management efforts, however, may not yield an immediate improvement in water quality. Internal P loading rates are likely high in these reservoirs, as evidenced by high TDP concentrations in the hypolimnions during summer stratification. Extended stratification in a future climate (Woolway and Merchant, 2019) would further exacerbate internal P loading rates (North et al., 2014).

We recommend increased focus on mitigating non-point source P inputs, as it appears that these reservoirs are effective in N removal, resulting in low epilimnetic dissolved inorganic N concentrations, likely due to high rates of denitrification (Gooding and Baulch, 2017). Globally, increasing N-based fertilizer use is resulting in N concentrations in surface waters in excess of phytoplankton demand (Glibert et al., 2016). Despite these trends, studies in Kansas and Arkansas have demonstrated N to be a potentially important constraint on phytoplankton biomass (Dzialowski et al., 2005; Scott and Grantz, 2013). Our mean epilimnetic DON concentrations in reservoirs with row-crop agriculture watersheds were nearly double those in forested watersheds. Globally, urea fertilizer use has increased more than 100-fold in the last four decades (Glibert et al., 2006), and in the United States, nearly 90% of N-based fertilizer being applied is urea instead of ammonium nitrate (Paerl et al., 2016). Urea can exceed 40% of the DON pool (Glibert et al., 2006). Historical urea and DON concentrations are unknown for Missouri reservoirs, but previous publications indicate that 45% of the reservoirs had molar TN:TP ratios < 38 (Jones and Knowlton, 1993), indicating some N deficiency (Guildford and Hecky, 2000).

How Might Light and Nutrients Constrain Phytoplankton Dynamics in a Changing World?

The increase in rainfall intensity associated with climate change, accompanied by the pervasiveness of agriculture and urbanization, will contribute to greater proportions of bioavailable P and N reaching inland waters. Simultaneously, climatically induced stronger and longer-lasting thermal stratification (Woolway and Merchant, 2019) is anticipated to increase hypolimnetic oxygen depletion. Bottom-water anoxia stimulates internal loading, which amplifies hypolimnetic nutrient concentrations (North et al., 2014). Given that ∼94% of Missouri reservoirs are already meso-, eu-, or hyper- trophic and quickly develop hypolimnetic anoxia during summer stratification, these Midwestern systems represent potential climate analogs and precursors of the light and nutrient conditions impacting future reservoir phytoplankton dynamics. Although light-deficiency may be alleviated due to shallower mixing depths; most of these characteristically turbid systems will likely still have enough light to support phytoplankton growth, photosynthesis, and nutrient uptake.

CONCLUSION

Under current climatic and anthropogenic influences, both P and light play active roles in controlling phytoplankton biomass and primary productivity in Midwestern reservoirs. Phytoplankton biomass is predominantly constrained by P concentrations during the summer stratified season, despite the abundance of both P and N in the agriculturally dominant region. Although this conclusion aligns with the traditionally accepted P-paradigm for freshwater ecosystems, the demonstration of co-deficiency between light, P, and N should also be acknowledged, especially within the context of the P vs. N and P management debate (Schindler et al., 2008; Paerl et al., 2016). Primary productivity in Midwestern reservoirs contradicts the traditional P-paradigm for lake productivity. GPP^B was higher in low-nutrient reservoirs where light was in sufficient supply, and not shaded by high phytoplankton biomass. Here, we offer further evidence for the need to evaluate application of these paradigms to all systems across time and space, especially as we see shifts in climate patterns and anthropogenic activity that will ultimately alter the light and nutrient dynamics of future ecosystems.

DATA AVAILABILITY STATEMENT

The datasets generated for this study are available on request to the corresponding author.

AUTHOR CONTRIBUTIONS

EP designed the study under the direction and leadership of RN who conceived the original idea. EP collected the data by processing water samples, performing the experiments, and conducting laboratory and statistical analyses, performed calculations and modeled parameters described in the manuscript, designed figures, and wrote the manuscript in close consultation with RN. DO coordinated field sampling efforts, contributed data, and assisted in QA/QC of data. All authors contributed to the article and approved the submitted version.

ACKNOWLEDGMENTS

This work was made possible by the Missouri Department of Natural Resources, which generously funds the Missouri Statewide Lake Assessment Program coordinated by the University of Missouri (MU) Limnology Laboratory. We would like to thank the numerous MU Limnology Laboratory employees who contributed to sample collection and analysis. Specifically, thank you to Thomas Swenson, undergraduate research assistant; Carol Pollard and Clare Vanderwerken, laboratory technicians; Cody Kimbell and Matthew Sauer (2017) field rovers; and Madalyn Stoeker and Emily Phaup (2018) field rovers. Thank you to Dr. Greg Silsbe for his insight regarding the "phytotools" R-package, Dr. Christine Spinka for providing statistical consultation, Drs. Chung-ho Lin and Jacob Westhoff for generously sharing environmental chamber space for experiments, Dr. Patrick Neale for providing expert testimonial, and Dr. Alba Argerich for providing helpful comments to improve and clarify the writing of this manuscript. We thank Dr. John R. Jones for his title suggestion. We would also like to

acknowledge Dr. Joy Matthews and the University of California – Davis Stable Isotope Facility for their professional and timely analytical services. Analytical costs were, in part, supported by a Grant-In-Aid of Research from Sigma Xi, the Scientific Research Honor Society.

SUPPLEMENTARY MATERIAL

The Supplementary Material for this article can be found online at: https://www.frontiersin.org/articles/10.3389/fenvs.2020.00111/full#supplementary-material

REFERENCES

Abell, J. M., Özkundakci, D., and Hamilton, D. P. (2010). Nitrogen and phosphorus limitation of phytoplankton growth in New Zealand lakes: implications for eutrophication control. *Ecosystems* 13, 966–977. doi: 10.1007/s10021-010-9367-9

Abell, J. M., Özkundakci, D., Hamilton, D. P., and Jones, J. R. (2012). Latitudinal variation in nutrient stoichiometry and chlorophyll-nutrient relationships in lakes: A global study. *Fundam Appl. Limnol.* 181, 1–14. doi: 10.1127/1863-9135/2012/0272

APHA (2017). *Standard Methods for the Examination of Water and Wastewater*, 23 Edn, eds E. W. Rice, R. B. Baird, and A. D. Eaton (Washington, DC: American Public Health Association).

Bennett, E. M., Carpenter, S. R., and Caraco, N. F. (2001). Human impact on erodable phosphorus and eutrophication: a global perspective. *Bioscience* 51, 227–234.

Blackman, F. F. (1905). Optima and limiting factors. *Ann. Bot.* 19, 281–296. doi: 10.1093/oxfordjournals.aob.a089000

Brodie, C. R., Leng, M. J., Casford, J. S. L., Kendrick, C. P., Lloyd, J. M., Yongqiang, Z., et al. (2011). Evidence for bias in C and N concentrations and δ13C composition of terrestrial and aquatic organic materials due to pre-analysis acid preparation methods. *Chem. Geol.* 282, 67–83. doi: 10.1016/j.chemgeo.2011.01.007

Campbell, D., Hurry, V., Clarke, A. K., Gustafsson, P., and Oquist, G. (1998). Chlorophyll fluorescence analysis of cyanobacterial photosynthesis and acclimation. *Microbiol. Mol. Biol. Rev.* 62, 667–683. doi: 10.1128/mmbr.62.3.667-683.1998

Crumpton, W. G., Isenhart, T. M., and Mitchell, P. D. (1992). Nitrate and organic N analyses with second-derivative spectroscopy. *Limnol. Oceanogr.* 37, 907–913. doi: 10.4319/lo.1992.37.4.0907

Dubourg, P., North, R. L., Hunter, K., Vandergucht, D. M., Abirhire, O., Silsbe, G. M., et al. (2015). Light and nutrient co-limitation of phytoplankton communities in a large reservoir: lake Diefenbaker, Saskatchewan, Canada. *J. Great Lakes Res.* 41, 129–143. doi: 10.1016/j.jglr.2015.10.001

Dzialowski, A. R., Wang, S. H., Lim, N. C., Spotts, W. W., and Huggins, D. G. (2005). Nutrient limitation of phytoplankton growth in central plains reservoirs, USA. *J. Plankton Res.* 27, 587–595. doi: 10.1093/plankt/fbi034

Elser, J. J., Bracken, M. E. S., Cleland, E. E., Gruner, D. S., Harpole, W., Hillebrand, H., et al. (2007). Global analysis of nitrogen and phosphorus limitation of primary producers in freshwater, marine and terrestrial ecosystems. *Ecol. Lett.* 10, 1135–1142. doi: 10.1111/j.1461-0248.2007.01113.x

Elser, J. J., Marzolf, E. R., and Goldman, C. R. (1990). Phosphorus and nitrogen limitation of phytoplankton growth in the freshwaters of North America: a review and critique of experimental enrichments. *Can. J. Fish. Aquat. Sci.* 47, 1468–1477. doi: 10.1139/f90-165

Fee, E. J. (1990). Computer programs for calculating in situ phytoplankton photosynthesis. *Can. Tech. Rep. Fish. Aquat. Sci.* 1740, 1–27.

Galloway, J. N., Townsend, A. R., Erisman, J. W., Bekunda, M., Cai, Z., Freney, J. R., et al. (2008). Transformation of the nitrogen cycle: recent trends, questions, and potential solutions. *Science* 320, 889–892. doi: 10.1126/science.1136674

Glibert, P. M., Harrison, J., Heil, C., and Seitzinger, S. (2006). Escalating worldwide use of urea: a global change contributing to coastal eutrophication. *Biogeochemistry* 77, 441–463. doi: 10.1007/s10533-005-3070-5

Glibert, P. M., Wilkerson, F. P., Dugdale, R. C., Raven, J. A., Dupont, C. L., Leavitt, P. R., et al. (2016). Pluses and minuses of ammonium and nitrate uptake and assimilation by phytoplankton and implications for productivity and community composition, with emphasis on nitrogen-enriched conditions. *Limnol. Oceanogr.* 61, 165–197. doi: 10.1002/lno.10203

Gooding, R. M., and Baulch, H. M. (2017). Small reservoirs as a beneficial management practice for nitrogen removal. *J. Environ. Qual.* 46, 96–104. doi: 10.2134/jeq2016.07.0252

Grobbelaar, J. U. (1989). The contribution of phytoplankton productivity in turbid freshwaters to their trophic status. *Hydrobiologia* 173, 127–133. doi: 10.1007/BF00015522

Guildford, S. J., Bootsma, H. A., Fee, E. J., Hecky, R. E., and Patterson, G. (2000). Phytoplankton nutrient status and mean water column irradiance in lakes Malawi and Superior. *Aquat. Ecosyst. Heal Manag.* 3, 35–45. doi: 10.1080/14634980008656989

Guildford, S. J., and Hecky, R. E. (2000). Total nitrogen, total phosphorus, and nutrient limitation in lakes and oceans: is there a common relationship? *Limnol. Oceanogr.* 45, 1213–1223. doi: 10.4319/lo.2000.45.6.1213

Hanson, P. C., Bade, D. L., Carpenter, S. R., Kratz, T. K., and Long, W. (2003). Lake metabolism: relationships with dissolved organic carbon and phosphorus. *Limnol. Oceanogr.* 48, 1112–1119. doi: 10.4319/lo.2003.48.3.1112

Hayes, N. M., Deemer, B. R., Corman, J. R., Razavi, N. R., and Strock, K. E. (2017). Key differences between lakes and reservoirs modify climate signals: a case for a new conceptual model. *Limnol. Oceanogr. Lett.* 2, 47–62. doi: 10.1002/lol2.10036

Hayes, N. M., Vanni, M. J., Horgan, M. J., and Renwick, W. H. (2015). Climate and land use interactively affect lake phytoplankton nutrient limitation status. *Ecology* 96, 392–402. doi: 10.1890/13-1840.1

Healey, F. P. (1977). Ammonium and urea uptake by some freshwater algae. *Can. J. Bot.* 55, 61–69. doi: 10.1139/b77-013

Healey, F. P., and Hendzel, L. L. (1979). Indicators of phosphorus and nitrogen deficiency in five algae in culture. *J. Fish. Res. Board Canada* 36, 1364–1369. doi: 10.1139/f79-195

Healey, P. F. (1985). Interacting effects of light and nutrient limitation on the growth rate of *Synechococcus linearis* (Cyanophyceae). *J. Phycol.* 21, 134–146. doi: 10.1111/j.0022-3646.1985.00134.x

Hecky, R. E., Campbell, P., and Hendzel, L. L. (1993). The stoichiometry of carbon, nitrogen, and phosphorus in particulate matter of lakes and oceans. *Limnol. Oceanogr.* 38, 709–724. doi: 10.4319/lo.1993.38.4.0709

Hecky, R. E., and Guildford, S. J. (1984). Primary productivity of Southern Indian Lake before, during, and after impoundment and Churchill River diversion. *Can. J. Fish. Aquat. Sci.* 41, 591–604. doi: 10.1139/f84-072

Hecky, R. E., and Kilham, P. (1988). Nutrient limitation of phytoplankton in freshwater and marine environments: a review of recent evidence on the effects of enrichment. *Limnol. Oceanogr.* 33, 796–822. doi: 10.4319/lo.1988.33.4part2.0796

Hoellein, T. J., Bruesewitz, D. A., and Richardson, D. C. (2013). Revisiting Odum (1956): a synthesis of aquatic ecosystem metabolism. *Limnol. Oceanogr.* 58, 2089–2100. doi: 10.4319/lo.2013.58.6.2089

Howarth, R., Swaney, D., Billen, G., Garnier, J., Hong, B., Humborg, C., et al. (2012). Nitrogen fluxes from the landscape are controlled by net anthropogenic nitrogen inputs and by climate. *Front. Ecol. Environ.* 10:37–43. doi: 10.1890/100178

Hutchinson, G. E. (1957). *A Treatise on Limnology*. New York, NY: John Wiley & Sons, Inc.

Jeppesen, E., Moss, B., Bennion, H., Carvalho, L., Demeester, L., Feuchtmayr, H., et al. (2010). "Interaction of climate change and eutrophication," in *Climate Change Impacts on Freshwater Ecosystems*, eds M. Kernan, R. W. Battarbee, and B. Moss (Hoboken, NY: Blackwell Publishing Ltd), 119–151. doi: 10.1002/9781444327397.ch6

Jones, J. R., and Knowlton, M. F. (1993). Limnology of Missouri reservoirs: an analysis of regional patterns. *Lake Reserv. Manag.* 8, 17–30. doi: 10.1080/07438149309354455

Jones, J. R., Knowlton, M. F., and Obrecht, D. V. (2008a). Role of land cover and hydrology in determining nutrients in mid-continent reservoirs: implications

for nutrient criteria and management. *Lake Reserv. Manag.* 24, 1–9. doi: 10.1080/07438140809354045

Jones, J. R., Obrecht, D. V., Perkins, B. D., Knowlton, M. F., Thorpe, A. P., Watanabe, S., et al. (2008b). Nutrients, seston, and transparency of Missouri reservoirs and oxbow lakes: an analysis of regional limnology. *Lake Reserv. Manag.* 24, 155–180. doi: 10.1080/07438140809354058

Jones, J. R., Knowlton, M. F., Obrecht, D. V., and Graham, J. L. (2011). Temperature and oxygen in Missouri reservoirs. *Lake Reserv. Manag.* 27, 173–182. doi: 10.1080/07438141.2011.583713

Kimmel, B. L., and Groeger, A. W. (1984). Factors controlling primary production in lakes and reservoirs?: a perspective. *Lake Reserv. Manag.* 1, 277–281. doi: 10.1080/07438148409354524

Kirk, J. T. O. (2011). *Light and Photosynthesis in Aquatic Ecosystems*, 3rd Edn. New York, NY: Cambridge University Press, doi: 10.4319/lo.1987.32.1.0275

Kleinman, P., Buda, A. R., Saporito, L. S., Sharpley, A. N., and Bryant, R. B. (2009). Application of manure to no-till soils: phosphorus losses by sub-surface and surface pathways. *Nutr. Cycl. Agroecosyst.* 84, 215–227. doi: 10.1007/s10705-008-9238-3

Knoll, L. B., Vanni, M. J., and Renwick, W. H. (2003). Phytoplankton primary production and photosynthetic parameters in reservoirs along a gradient of watershed land use. *Limnol. Oceanogr.* 48, 608–617. doi: 10.4319/lo.2003.48.2.0608

Knowlton, M. F. (1984). Flow-through micocuvette for fluorometric determination of chlorophyll. *Water Resour. Bull.* 20, 795–799. doi: 10.1111/j.1752-1688.1973.tb05876.x

Knowlton, M. F., and Jones, J. R. (1995). Temporal and spatial dynamics of suspended sediment, nutrients, and algal biomass in Mark Twain Lake. *Missouri. Arch. Hydrobiol.* 135, 145–178.

Knowlton, M. F., and Jones, J. R. (1996). Experimental evidence of light and nutrient limitation of algal growth in a turbid midwest reservoir. *Arch. Hydrobiol.* 135, 321–335.

Knowlton, M. F., and Jones, J. R. (2000). Non-algal seston, light, nutrients, and chlorophyll in Missouri reservoirs. *J. Lake Reserv. Manag.* 16, 322–332. doi: 10.1080/07438140009354239

Kromkamp, J. C., Dijkman, N. A., Peene, J., Simis, S. G. H., and Gons, H. J. (2008). Estimating phytoplankton primary production in Lake IJsselmeer (The Netherlands) using variable fluorescence (PAM-FRRF) and C-uptake techniques. *Eur. J. Phycol.* 43, 327–344. doi: 10.1080/09670260802080895

Kromkamp, J. C., and Forster, R. M. (2003). The use of variable fluorescence measurements in aquatic ecosystems: differences between multiple and single turnover measuring protocols and suggested terminology. *Eur. J. Phycol.* 38, 103–112. doi: 10.1080/0967026031000094094

Laas, A., Noges, P., Koiv, T., and Noges, T. (2012). High-frequency metabolism study in a large and shallow temperate lake reveals seasonal switching between net autotrophy and net heterotrophy. *Hydrobiologia* 694, 57–74. doi: 10.1007/s10750-012-1131-z

Lauster, G. H., Hanson, P. C., and Kratz, T. K. (2006). Gross primary production and respiration differences among littoral and pelagic habitats in northern Wisconsin lakes. *Can. J. Fish. Aquat. Sci.* 63, 1130–1141. doi: 10.1139/F06-018

Lewis, W. M., and Wurtsbaugh, W. A. (2008). Control of lacustrine phytoplankton by nutrients: erosion of the phosphorus paradigm. *Int. Rev. Hydrobiol.* 93, 446–465. doi: 10.1002/iroh.200811065

MacIntyre, H. L., Kana, T. M., Anning, T., and Geider, R. J. (2002). Photoacclimation of photosynthesis irradiance response curves and photosynthetic pigments in microalgae and cyanobacteria. *J. Phycol.* 38, 17–38. doi: 10.1046/j.1529-8817.2002.00094.x

Michalak, A. M., Anderson, E. J., Beletsky, D., Boland, S., Bosch, N. S., Bridgeman, T. B., et al. (2013). Record-setting algal bloom in Lake Erie caused by agricultural and meteorological trends consistent with expected future conditions. *Proc. Natl. Acad. Sci. U.S.A.* 110, 6448–6452. doi: 10.1073/pnas.1216006110

Millard, E. S., Myles, D. D., Johannsson, O. E., and Ralph, K. M. (1996). Seasonal phosphorus deficiency of Lake Ontario phytoplankton at two index stations: light versus phosphorus limitation of growth. *Can. J. Fish. Aquat. Sci.* 53, 1112–1124. doi: 10.1139/cjfas-53-5-1112

Mitsch, W. J., Day, J. W., Gilliam, J. W., Groffman, P. M., and Hey, D. L. (2001). Reducing nitrogen loading to the Gulf of Mexico from the Mississippi River Basin: strategies to counter a persistent ecological problem. *Bioscience* 51, 373–388.

Morris, D. P., and Lewis, W. M. (1988). Phytoplankton nutrient limitation in Colorado mountain lakes. *Freshw. Biol.* 20, 315–327. doi: 10.1111/j.1365-2427.1988.tb00457.x

Napoléon, C., and Claquin, P. (2012). Multi-parametric relationships between PAM measurements and carbon incorporation, an in situ approach. *PLoS One* 7:1–12. doi: 10.1371/journal.pone.0040284

Napoléon, C., Raimbault, V., and Claquin, P. (2013). Influence of nutrient stress on the relationships between PAM measurements and carbon incorporation in four phytoplankton species. *PLoS One* 8:66423. doi: 10.1371/journal.pone.0066423

NOAA (2019). *Historical Palmer Drought Indices. Natl Ocean Atmos Adm*. Available online at: https://www.ncdc.noaa.gov/temp-and-precip/drought/historical-palmers (accessed August 5, 2019).

North, R. L., Guildford, S. J., Smith, R. E. H., Havens, S. M., and Twiss, M. R. (2007). Evidence for phosphorus, nitrogen, and iron colimitation of phytoplankton communities in Lake Erie. *Limnol. Oceanogr.* 52, 315–328. doi: 10.4319/lo.2007.52.1.0315

North, R. L., Guildford, S. J., Smith, R. E. H., Twiss, M. R., and Kling, H. J. (2008). Nitrogen, phosphorus, and iron colimitation of phytoplankton communities in the nearshore and offshore regions of the African Great Lakes. *Verh. Int. Verein Limnol.* 30, 259–264. doi: 10.1080/03680770.2008.11902122

North, R. P., North, R. L., Livingstone, D. M., Köster, O., and Kipfer, R. (2014). Long-term changes in hypoxia and soluble reactive phosphorus in the hypolimnion of a large temperate lake: Consequences of a climate regime shift. *Glob. Chang Biol.* 20, 811–823. doi: 10.1111/gcb.12371

O'Reilly, C. M., Rowley, R. J., Schneider, P., Lenters, J. D., Mcintyre, P. B., Kraemer, B. M., et al. (2015). Rapid and highly variable warming of lake surface waters around the globe. *Geophys. Res. Lett.* 42, 10773–10781. doi: 10.1002/2015GL066235

O'Beirne, M. D., Werne, J. P., Hecky, R. E., Johnson, T. C., Katsev, S., and Reavie, E. D. (2017). Anthropogenic climate change has altered primary productivity in Lake Superior. *Nat. Commun.* 8:15713. doi: 10.1038/ncomms15713

Oliver, S. K., Collins, S. M., Soranno, P. A., Wagner, T., Stanley, E. H., Jones, J. R., et al. (2017). Unexpected stasis in a changing world: Lake nutrient and chlorophyll trends since 1990. *Glob. Chang Biol.* 23, 5455–5467. doi: 10.1111/gcb.13810

O'Reilly, C. M., Alin, S. R., Piisnier, P. D., Cohen, A. S., and McKee, B. A. (2003). Climate change decreases aquatic ecosystem productivity of Lake Tanganyika, Africa. *Nature* 424, 766–768. doi: 10.1038/nature01833

Paerl, H. W., and Scott, J. T. (2010). Throwing fuel on the fire: synergistic effects of excessive nitrogen inputs and global warming on harmful algal blooms. *Environ. Sci. Technol.* 44, 7756–7758. doi: 10.1021/es102665e

Paerl, H. W., Scott, J. T., McCarthy, M. J., Newell, S. E., Gardner, W. S., Havens, K. E., et al. (2016). It takes two to tango: when and where dual nutrient (N & P) reductions are needed to protect lakes and downstream ecosystems. *Environ. Sci. Technol.* 50, 10805–10813. doi: 10.1021/acs.est.6b02575

Pinheiro, J., Bates, D., DebRoy, S., Sarkar, D., and R Core Team. (2020). *nlme: Linear and Nonlinear Mixed Effects Models*. Available online at: https://cran.r-project.org/package=nlme (accessed May 24, 2020).

Rowland, F. E., North, R. L., McEachern, P., Obrecht, D. V., Gurung, T. B., Jones, S. B., et al. (2019). Phytoplankton nutrient deficiencies vary with season in sub-tropical lakes of Nepal. *Hydrobiologia* 833, 157–172. doi: 10.1007/s10750-019-3897-8

Saito, M. A., Goepfert, T. J., and Ritt, J. T. (2008). Some thoughts on the concept of colimitation: three definitions and the importance of bioavailability. *Limnol. Oceanogr.* 53, 1–16.

Sartory, D. P., and Grobbelaar, J. U. (1984). Extraction of chlorophyll a from freshwater phytoplankton for spectrophotometric analysis. *Hydrobiologia* 114, 177–187. doi: 10.1007/BF00031869

Schallenberg, M., and Burns, C. W. (2004). Effects of sediment resuspension on phytoplankton production: teasing apart the influences of light, nutrients and algal entrainment. *Freshw. Biol.* 49, 143–159. doi: 10.1046/j.1365-2426.2003.01172.x

Schindler, D. W. (1974). Eutrophication and recovery in experimental lakes: implications for lake management. *Science* 184, 897–899. doi: 10.1126/science.184.4139.897

Schindler, D. W. (1977). Evolution of phosphorus limitation in lakes. *Science* 195, 260–262. doi: 10.1126/science.195.4275.260

Schindler, D. W., Hecky, R. E., Findlay, D. L., Stainton, M. P., Parker, B. R., Paterson, M. J., et al. (2008). Eutrophication of lakes cannot be controlled by reducing nitrogen input: results of a 37-year whole-ecosystem experiment. *Proc. Natl. Acad. Sci. U.S.A.* 105, 11254–11258. doi: 10.1073/pnas.0805108105

Schmid, M., Hunziker, S., and Wüest, A. (2014). Lake surface temperatures in a changing climate: a global sensitivity analysis. *Clim. Chang* 124, 301–315. doi: 10.1007/s10584-014-1087-2

Scott, J. T., and Grantz, E. M. (2013). N2 fixation exceeds internal nitrogen loading as a phytoplankton nutrient source in perpetually nitrogen-limited reservoirs. *Freshw. Sci.* 32, 849–861. doi: 10.1899/12-190.1

Sharpley, A., Jarvie, H. P., Buda, A., May, L., Spears, B., and Kleinman, P. (2013). Phosphorus legacy: overcoming the effects of past management practices to mitigate future water quality impairment. *J. Environ. Qual.* 42, 1308–1326. doi: 10.2134/jeq2013.03.0098

Silsbe, G. M., Hecky, R. E., and Smith, R. E. H. (2012). Improved estimation of carbon fixation rates from active flourometry using spectral fluorescence in light-limited environments. *Limnol. Oceanogr. Methods* 10, 736–751. doi: 10.4319/lom.2012.10.736

Silsbe, G. M., and Malkin, S. Y. (2015). *Phytotools: Phytoplankton Production Tools*. Available online at: https://cran.r-project.org/package=phytotools (accessed February 14, 2015).

Solomon, C. T., Bruesewitz, D. A., Richardson, D. C., Rose, K. C., Van de Bogert, M. C., Hanson, P. C., et al. (2013). Ecosystem respiration: drivers of daily variability and background respiration in lakes around the globe. *Limnol. Oceanogr.* 58, 849–866. doi: 10.4319/lo.2013.58.3.0849

Staehr, P., Sand-Jensen, K., Raun, A., Nielsson, B., and Kidmose, J. (2010). Drivers of metabolism and net heterotrophy in contrasting lakes. *Limnol. Oceangr.* 55, 817–830. doi: 10.4319/lo.2010.55.2.0817

Staehr, P. A., and Sand-Jensen, K. (2007). Temporal dynamics and regulation of lake metabolism. *Limnol. Oceanogr.* 52, 108–120. doi: 10.4319/lo.2007.52.1.0108

Sterner, R. W. (2008). On the phosphorus limitation paradigm for lakes. *Int. Rev. Hydrobiol.* 93, 433–445. doi: 10.1002/iroh.200811068

Strayer, D. L., Beighley, R. E., Thompson, L. C., Brooks, S., Nilsson, C., Pinay, G., et al. (2003). Effects of land cover on stream ecosystems: roles of empirical models and scaling issues. *Ecosystems* 6, 407–423. doi: 10.1007/s10021-002-0170-0

Suggett, D. J., Moore, C. M., Hickman, A. E., and Geider, R. J. (2009). Interpretation of fast repetition rate (FRR) fluorescence: signatures of phytoplankton community structure versus physiological state. *Mar. Ecol. Progr. Ser.* 9, 1–19. doi: 10.3354/meps07830

Tassan, S., and Ferrari, G. M. (1995). An alternative approach to absorption measurements of retained on filters aquatic particles. *Limnol. Oceanogr.* 40, 1358–1368. doi: 10.4319/lo.1995.40.8.1358

Thom, R. H., and Wilson, J. H. (1980). The natural divisions of Missouri. *Trans. Mo. Acad. Sci.* 4, 9–23.

Thornton, K. W. (1990). "Perspectives on reservoir limnology," in *Reservoir Limnology: Ecological Perspectives*, eds K. W. Thornton, B. L. Kimmel, and F. E. Payne (New York, NY: John Wiley & Sons, Inc), 1–14.

Titman, D. (1976). Ecological competition between algae: experimental confirmation of resource-based competition theory. *Science* 192, 463–465. doi: 10.1126/science.192.4238.463

Torremorell, A., Llames, M., Perez, G., Escaray, R., Bustingorry, J., and Zagarese, H. (2009). Annual patterns of phytoplankton density and primary production in a large, shallow lake: the central role of light. *Freshw. Biol.* 54, 437–449. doi: 10.1111/j.1365-2427.2008.02119.x

Tyrrell, T. (1999). The relative influences of nitrogen and phosphorus on oceanic primary production. *Nature* 400, 525–531. doi: 10.1038/22941

Verburg, P., and Hecky, R. E. (2009). The physics of the warming of Lake Tanganyika by climate change. *Limnol. Oceanogr.* 54, 2418–2430. doi: 10.4319/lo.2009.54.6_part_2.2418

Vollenweider, R. A. (1976). Advances in defining critical loading levels for phosphorus in lake eutrophication. *Mem. Ist. Ital. Idrobiol.* 33, 53–83.

Von Liebig, J. (1840). *Die Organische Chemie in ihrer Anwendung auf Agrikultur und Physiologie*. Braunschweig: Friedrich Vieweg.

Webb, W. L., Newton, M., and Starr, D. (1974). Carbon dioxide exchange of *Alnus rubra*. *Oecologia* 17, 281–291. doi: 10.1007/bf00345747

Williamson, C. E., Saros, J. E., and Schindler, D. W. (2009a). Climate change: sentinels of change. *Science* 323, 887–888. doi: 10.1126/science.1169443

Williamson, C. E., Saros, J. E., Vincent, W. F., and Smol, J. P. (2009b). Lakes and reservoirs as sentinels, integrators, and regulators of climate change. *Limnol. Oceanogr.* 54, 2273–2282. doi: 10.4319/lo.2009.54.6_part_2.2273

Winslow, L., Read, J., Woolway, R., Brentrup, J., Leach, T., Zwart, J., et al. (2019). *rLakeAnalyzer: Lake Physics Tools*. Available online: https://zenodo.org/record/1003169#.Ws82F9NubEY (accessed October 6, 2017).

Woolway, R. I., and Merchant, C. J. (2017). Amplified surface temperature response of cold, deep lakes to inter-annual air temperature variability. *Sci. Rep.* 7, 1–8. doi: 10.1038/s41598-017-04058-0

Woolway, R. I., and Merchant, C. J. (2019). Worldwide alteration of lake mixing regimes in response to climate change. *Nat. Geosci.* 12, 271–276. doi: 10.1038/s41561-019-0322-x

Yang, L., Jin, S., Danielson, P., Homer, C., Gass, L., Bender, S. M., et al. (2018). A new generation of the United States National Land Cover Database: requirements, research priorities, design, and implementation strategies. *ISPRS J. Photogramm. Remote Sens.* 146, 108–123. doi: 10.1016/j.isprsjprs.2018.09.006

Zarfl, C., Lumsdon, A. E., Berlekamp, J., Tydecks, L., and Tockner, K. (2015). A global boom in hydropower dam construction. *Aquat. Sci.* 77, 161–170. doi: 10.1007/s00027-014-0377-0

Conflict of Interest: The authors declare that the research was conducted in the absence of any commercial or financial relationships that could be construed as a potential conflict of interest.

frontiers in Marine Science

ORIGINAL RESEARCH
published: 08 October 2020
doi: 10.3389/fmars.2020.547829

Edited by:
Xosé Anxelu G. Morán, King Abdullah University of Science and Technology, Saudi Arabia

Reviewed by:
Tzong-Yueh Chen, National Taiwan Ocean University, Taiwan
Maria Ll. Calleja, Max Planck Institute for Chemistry, Germany

***Correspondence:**
Nur Ili Hamizah Mustaffa
iliehamizah@gmail.com;
nur.ili.hamizah.mustaffa@uol.de

†Present address:
Nur Ili Hamizah Mustaffa, Department of Earth Sciences and Environment, Faculty of Science and Technology, Universiti Kebangsaan Malaysia, Bangi, Malaysia
Alexandra Schlenker, Department of River Ecology, Helmholtz Centre for Environmental Research (UFZ), Magdeburg, Germany;
Institute for Hydrobiology, Technical University of Dresden, Dresden, Germany

Specialty section:
This article was submitted to Marine Ecosystem Ecology, a section of the journal Frontiers in Marine Science

Received: *31 March 2020*
Accepted: *15 September 2020*
Published: *08 October 2020*

Citation:
Mustaffa NIH, Kallajoki L, Biederbick J, Binder FI, Schlenker A and Striebel M (2020) Coastal Ocean Darkening Effects via Terrigenous DOM Addition on Plankton: An Indoor Mesocosm Experiment. Front. Mar. Sci. 7:547829. doi: 10.3389/fmars.2020.547829

Coastal Ocean Darkening Effects via Terrigenous DOM Addition on Plankton: An Indoor Mesocosm Experiment

Nur Ili Hamizah Mustaffa*†, Liisa Kallajoki, Johanna Biederbick, Franziska Isabell Binder, Alexandra Schlenker† and Maren Striebel

Institute for Chemistry and Biology of the Marine Environment, Carl von Ossietzky University of Oldenburg, Wilhelmshaven, Germany

Human activities, increasing precipitation, and changes in land run-off deliver a large input of allochthonous nutrients into coastal waters including terrigenous dissolved organic matter (tDOM). Increased subsidies of tDOM into the coastal water are expected to reduce light availability and thus might be one of the factors causing coastal ocean darkening. To investigate the effect of increased tDOM input and thus limitation in light availability on primary production as well as the transfer to higher trophic levels (zooplankton), we conducted a large-scale indoor mesocosm "Planktotrons" experiment with natural (pelagic and benthic) plankton communities from the North Sea. We simulated a coastal ocean system with daily light and tidal cycles for 35 days. The experimental treatments included a light gradient consisting of three levels of tDOM addition (i.e., low tDOM, medium tDOM, and high tDOM) and a control without tDOM addition. Results showed that tDOM addition reduced the light availability by 27% (low tDOM addition), 62% (medium tDOM addition) and 86% (high tDOM addition). Light reduction through tDOM addition negatively influenced phytoplankton biomass during the first half of the experiment (<18 days) mainly in the "medium tDOM" and "high tDOM" treatments. The tDOM addition changed the phytoplankton community composition, potentially due to adaptations to different light conditions. Neither phytobenthos biomass nor composition was significantly affected by tDOM addition, probably because the tidal cycle assured sufficient light availability during low tide. Overall, our results indicate that the tDOM addition negatively influenced phytoplankton biomass and composition via light availability and tDOM effects were also observed on the zooplankton level (biomass and C:N ratio). Our experiment demonstrates possible implications of coastal darkening under climate-driven environmental changes on primary producers and their interactions in the aquatic food web.

Keywords: phytoplankton, phytobenthos, terrigenous dissolved organic matter, coastal darkening, zooplankton, top-down, bottom-up, tidal cycle

INTRODUCTION

Ongoing and future predicted climate change will not only increase sea surface temperature but also cause intensified run-off into coastal ecosystems due to an increase in precipitation (Evans et al., 2006; Roulet and Moore, 2006; Monteith et al., 2007). Moreover, human activities, changes in land use, and changes in the frequency of short and heavy rainfall events can result in large pulses of soil and sediment into coastal systems (Nunes et al., 2009) consequently affecting the light climate by reducing the level of water clarity and depth of light penetration. Changes in light climate have strong implications for primary productivity and interactions in aquatic food webs. For instance, observations of the last 100 years show a global decrease in phytoplankton biomass with a decline of approximately 1% of the global median biomass per year (Boyce et al., 2010) while regional greening of the water column in the open ocean was reported (Wernand et al., 2013). However, these studies mostly exclude coastal regions even though they are the most productive ocean areas, hot spots for terrigenous dissolved organic matter (tDOM) cycling, and highly sensitive to abiotic changes and human activities. Indeed, previous studies reported a reduction in the light availability in coastal waters (Fleming-Lehtinen and Laamanen, 2012; Capuzzo et al., 2015) as well as bays (Kemp et al., 2005) and fjords (Aksnes et al., 2009) as a consequence of large nutrient inputs from land. Increasing terrestrial run-off, glacier melting, storms in coastal areas, and agriculture accompanied by tDOM input alters nutrient concentration in the water column and is expected to reduce light availability, a so-called (ocean) darkening (Aksnes et al., 2009). The negative effect of tDOM on water quality and ecosystem health is recognized (de Wit et al., 2016) and tDOM has been suggested to be included as a proxy in coastal monitoring programs and management policies (Deininger and Frigstad, 2019).

Terrigenous dissolved organic matter is a complex mixture of organic compounds that play an important role in marine biogeochemical cycling (Anderson et al., 2015; Carlson and Hansell, 2015). Chromophoric DOM (CDOM) is the light-adsorbing component of DOM, capable of absorbing the light in the range of visible and ultraviolet (UV) wavelengths (Coble, 2007). High concentrations of CDOM in the water column leads to brownification, decreases penetration of UV light and thus decreases the water transparency (Coble, 2007). The effect of tDOM addition has been predicted to affect primary production and community composition (Jones, 1992; Klug, 2002; Deininger et al., 2017b). Delivery of labile tDOM and inorganic nutrients through run-off can stimulate planktonic food webs (i.e., primary production and bacterial growth). For instance, increasing inorganic nutrients through terrestrial run-off provides excess nutrients to support fast-growing diatom species (Deininger et al., 2016; Paczkowska et al., 2020), and bacterial growth can be triggered by increasing dissolved organic nutrients (Kissman et al., 2013) and dissolved organic carbon (DOC) availability (Cole et al., 2011). However, excessive inorganic nutrient load can lead to harmful algal blooms, increase light attenuation (Klug, 2002), and decrease light availability in the water column thus leading to a tipping point where primary production decreases. On the other hand, bacteria production might be favored as tDOM provides a carbon food source and thus the system may shift from autotrophic toward heterotrophic production (Wikner and Andersson, 2012; Andersson et al., 2018). The lability of tDOM is influenced by heterotrophic bacterial utilization which may affect tDOM shading properties (Tranvik, 1988; Wikner and Andersson, 2012). Moreover, heterotrophic bacteria can also remineralize dissolved organic nitrogen (DON) and organic phosphorus (DOP), part of tDOM, to inorganic nutrients. Overall, this underlying process may affect phytoplankton production by shaping both light penetration and nutrient availability with consequences for the pelagic food structure and overall coastal productivity.

Phytoplankton and phytobenthos form the basis of aquatic food webs and act as an energy source for higher trophic levels, such as zooplankton and fish (Lefebure et al., 2013). Besides living in different habitats, phytoplankton, and phytobenthos are different in their taxonomic compositions which results in a difference in their photosynthetic and photo-protective strategies (Bonilla et al., 2005, 2009). It is known that high nutrient concentrations increase phytoplankton biomass which feeds back to an increase in light attenuation. If the light attenuation increases, phytoplankton biomass will affect the light intensity that reaches benthic microalgae and light becomes a limiting resource for phytobenthos (Hansson, 1988). The nutrient uptake of phytobenthos is generally subjected to boundary-layer kinetics, thus uptake velocities are considered lower as thus of phytoplankton (Riber and Wetzel, 1987). However, phytobenthos can utilize nutrients from the sediments and thus may reduce nutrient availability for phytoplankton (Blumenshine et al., 1997). The competition for nutrients between phytoplankton and phytobenthos link benthic and pelagic food webs at the primary trophic level (Vadeboncoeur et al., 2003). Therefore, it is essential to study the factors that influence this competition.

Furthermore, light or substrate availability through tDOM addition potentially affects food quantity and quality with consequences for zooplankton (Kissman et al., 2013; Lefebure et al., 2013). The addition of tDOM reduces light availability and thus lowers phytoplankton photosynthesis and carbon fixation rates while providing additional nutrients (if the DOM substrate can be utilized) resulting in decreasing carbon:nutrient ratios. This may result in a decrease of food quantity but increase food quality for zooplankton (Elser and Urabe, 1999). Bartels et al. (2012) demonstrated that the light reduction due to tDOM addition further decreases primary production and affects autotrophic resource availability for zooplankton. tDOM also has been shown to indirectly affect zooplankton biomass via enhanced bacterial production (Faithfull et al., 2012), consequently altering zooplankton grazing intensity and selectivity on phytoplankton (Kissman et al., 2013). Furthermore, Deininger et al. (2017a) observed that the inorganic nutrient-enriched system from DOC increases zooplankton growth by causing a marginal change in primary productivity to bacterial production ratio as well as phytoplankton food quality. Finally, the addition of

tDOM and the associated dissolved organic nutrient (labile substrate) addition have been shown to reduce zooplankton richness with a profound effect on biodiversity (Shurin et al., 2010). In higher trophic levels, reduction in light availability has also been documented to trigger pronounced restraints in photic habitat, reducing visibility for visual predators (Capuzzo et al., 2018).

Overall, the effects of tDOM addition on whole plankton communities can be various and the complex relations are poorly understood. Hence, this study aims to test these possible aspects of darkening in coastal systems by investigating the effect of tDOM addition on primary producers and the food web in a coastal system. We, therefore, hypothesize that:

H1: Increasing tDOM concentrations will reduce light availability. We expect that decreased light availability will reduce the total phytoplankton biomass. Furthermore, tDOM addition will shift the light spectrum due to the properties of CDOM and thus will cause a change in the phytoplankton species composition.

H2: In a light-limited system, we expect that the light reduction via tDOM addition will negatively affect the phytobenthos even more than the phytoplankton. As tDOM addition is accompanied by organic nutrient availability, i.e., dissolved organic molecules containing nitrogen (DON) and phosphorous (DOP) (Klug, 2002), it will stimulate pelagic phytoplankton growth (particularly in the nutrient-limited system) more than the phytobenthos growth. Additionally, we expect a significant interaction between phytoplankton and phytobenthos as both are affected by light and nutrient availability.

H3: The effects of tDOM addition via light and nutrients on phytoplankton will transfer to higher trophic levels, i.e., zooplankton. As we expect nutrient availability via tDOM addition will influence phytoplankton biomass, it is reasonable to expect that the food quantity will directly affect the zooplankton biomass and composition. In terms of stoichiometry, reduced light availability via tDOM addition will decrease the carbon:nitrogen (C:N) ratio of phytoplankton, increase food quality for zooplankton, and thus enhance zooplankton growth.

MATERIALS AND METHODS

Experimental Setup

The experiment was conducted in 12 fully controllable indoor-mesocosms, so-called Planktotrons (Gall et al., 2017), in August 2017 for 35 days. Tidal flat sediment (including benthos) was collected from the Jade Bay, Wilhelmshaven, Germany (53.512945 N, 8.144166 E). 50 L of wet sediment (height approximately 0.05 m) was added to each Planktotron and filled with 600 L of seawater containing plankton from the North Sea resulting in a 1.15-m water column. The temperature was constantly held at 18.9 ± 0.9°C for the whole duration of the experiment. We programmed a natural tidal cycle with two high tide and low tide occurrences per day, each lasting 6:15 h leading to a shift of 1 h per day. To achieve a low tide condition (0.10 m of seawater height), approximately 470 L of seawater was pumped out of the Planktotron (within 5 h) into a 500 L tidal-exchange container, respectively. After 6:15 h, the seawater was restored achieve high tide conditions (1.10 m of seawater height). A light:dark cycle was set for 18:6 h with two controllable LED lighting units (IT 2040 Evergrow). The lighting units were off during the night and then run for 1 h each at 60 μmol m^{-2} s^{-1} and 180 μmol m^{-2} s^{-1} light intensity respectively to simulate sunrise (light intensity measured as photon flux integrated over the range of the photosynthetic active radiation of 400–700 nm). During the day the lighting units ran at 300 μmol m^{-2} s^{-1} light intensity for 14 h. Sunset was simulated by applying 1 h of 180 μmol m^{-2} s^{-1} light intensity followed by 1 h of 60 μmol m^{-2} s^{-1} light intensity (**Supplementary Figure 1**). The average of light intensity (measured as lux) per day and the relative light intensity (%) using control treatment as reference during the first half of the experiment are in **Supplementary Figure 2**. Meanwhile, light intensity (measured as lux) directly above the sediment was measured with data loggers (HOBO UA-002-064 Pendant Datenlogger, Germany) during the whole experiment (**Supplementary Figure 3**).

The treatment was simulated through the addition of terrigenous dissolved organic matter (tDOM) that was extracted by alkaline extraction from commercial peat (Torfhumus Floragard®) (Riedel et al., 2012; Gall et al., 2017). The peat was filtered through a series of 3, 1, and 0.2 μm large-volume filter cartridges (Causa-filter system, Infiltec GmbH, Germany) to remove bacteria and other particles (Gall et al., 2017). We set up four levels consisting of control (without tDOM addition, ambient DOC concentrations of 322 μmolL^{-1}), "low tDOM," "medium tDOM" and "high tDOM" with the addition of 100, 150, and 350 μmol DOC L^{-1} resulting in a decrease in absorbance (at 254 nm, **Supplementary Figure 4**) of 27, 62, and 86%, respectively. Absorbance was measured from day 0 to day 35 and absorbance coefficient at wavelengths of 254 and 440 nm was calculated (**Figure 1**). To compensate the nutrient addition in terms of the limiting nutrient in the system (phosphorus), we amended corresponding amounts of phosphorus to the control, "low tDOM" and "medium tDOM" treatments (**Figure 2B**). Each treatment was replicated three times, resulting in a total of 12 units.

Sampling and Analyses

Samples were generally collected twice a week with a sampling bottle (2 L) from the surface of the tidal-exchange container during low tide condition (highest water column in the tidal-exchange container) after homogenizing the water column with a disc (Striebel et al., 2013). *In vivo* chlorophyll *a* concentration was measured daily using a hand-held fluorometer (AquaFluor, Turner Designs, United States) as a proxy for phytoplankton biomass using an external standard calibration. Samples for pigment concentrations, particulate organic carbon (POC), nitrate (PON), and phosphorous (POP) concentrations

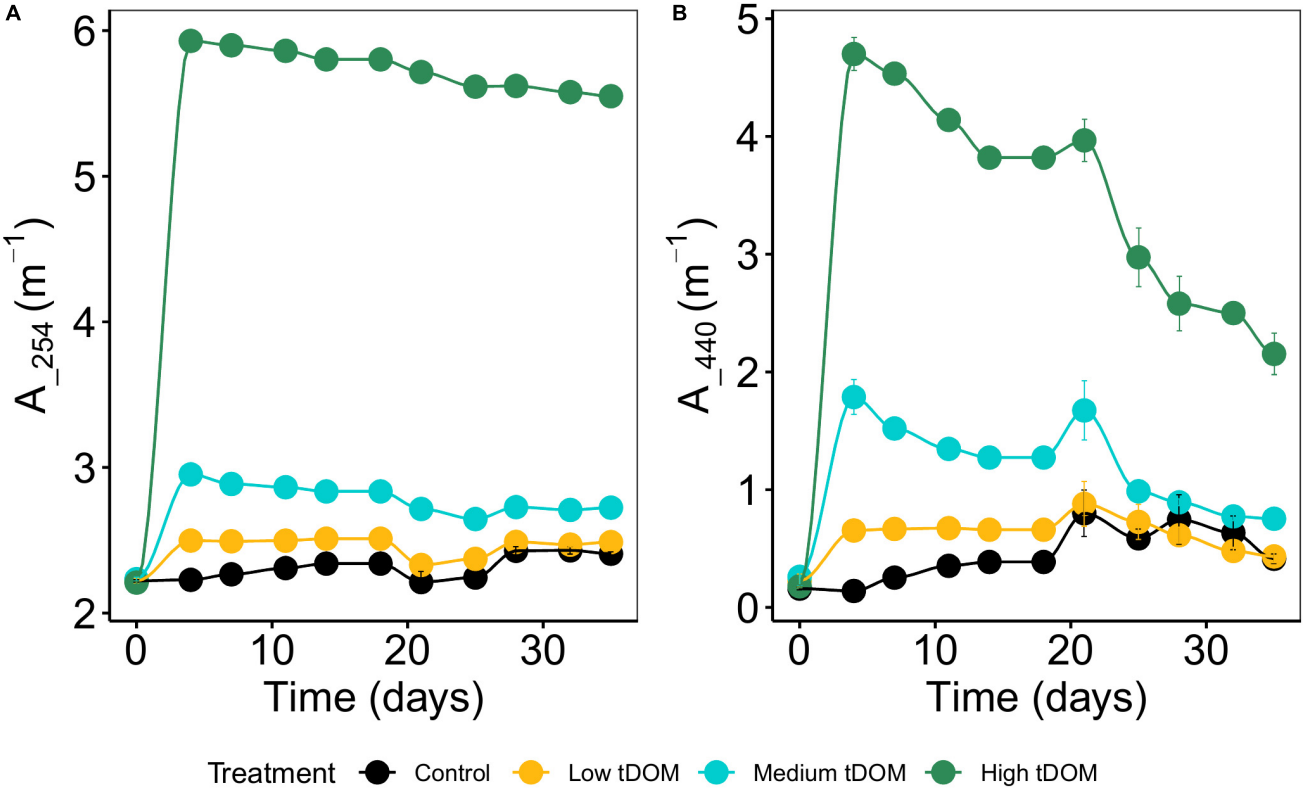

FIGURE 1 | Absorbance coefficient of tDOM **(A)** at 254 nm and **(B)** at 440 nm (shown as decadal (log 10) absorption coefficient) over 35 days of the experiments. Error bars represent standard deviation within treatment replicates. Colors represent tDOM addition: control (black), low tDOM (yellow), medium tDOM (blue), and high tDOM (green) treatments.

were collected twice a week, filtered onto acid-washed and pre-combusted GF/C filters (Whatman, United Kingdom), and stored at −80°C until analyses. Filters for POC and PON were oven-dried at 58°C, placed in tin capsules, and measured using an elemental analyzer (Thermo Fischer Scientific, Flash EA 1112, United States). Particulate organic phosphorus (POP, using the filter samples) and total phosphorus (TP, using unfiltered water samples) concentrations were determined spectrophotometrically using molybdate reaction after sulfuric acid digestion (Grasshoff et al., 1999). For soluble reactive phosphorus (SRP), dissolved nutrient (nitrate and nitrite), and dissolved silicate (Si), 10 mL of the filtrates were analyzed using a continuous flow analyzer (Skalar, Netherlands). Samples for DOC were filtered with double layer pre-combusted and acid-washed glass-fiber filters (Whatman GF/F). DOC samples were acidified to pH 2.0 with 32% HCl and analyzed by Shimadzu TOC-VCPH/CPN with TNM-1 Modul (TDN) ASI-V Autosampler. Filters for pigment analysis were stored at −80°C until analysis, treated with 10 mL of 90 vol% ethanol solution, sonicated on ice for 30 min (GT SONIC, Germany), and left in the dark at 4°C for 24 h for further extraction. The extract was measured at a wavelength range between 400 and 700 nm using a photometer (Aqua Mate Plus UV-VIS, Thermo Fischer Scientific, United States), and absorption values were converted into concentration ($\mu g\ L^{-1}$) using the spectral deconvolution method according to Thrane et al. (2015).

Phytobenthos and Zooplankton

Phytobenthos samples were taken during low tide from the Planktotrons using a self-made benthos stick (length: 1 m). The sampling was done by sticking the tip with the cylindrical opening (2.8 cm diameter, 3 cm height) into the sediment perpendicular to the sediment surface. By pulling the stick's plunger, suction was created that held the sample inside the tip and through pushing was transferred into a vial for storing. The inner part of the tip was then rinsed with water to ensure that all remaining phytobenthos was collected. Phytobenthos pigments were extracted using 20 mL of 90% ethanol solution similar to phytoplankton samples. Concentrations of pigment were related to the sampling area (cm^3) for phytobenthos. Zooplankton samples were collected from the tidal-exchange container during low tide condition (highest water column in the tidal-exchange container) by lowering and lifting a zooplankton net. Thus, 7 L of the water was filtered with a 100 μm plankton net, and the collected zooplankton sample was divided into subsamples for CN analysis, fixed with Lugol's iodine (1% final concentration), and counted

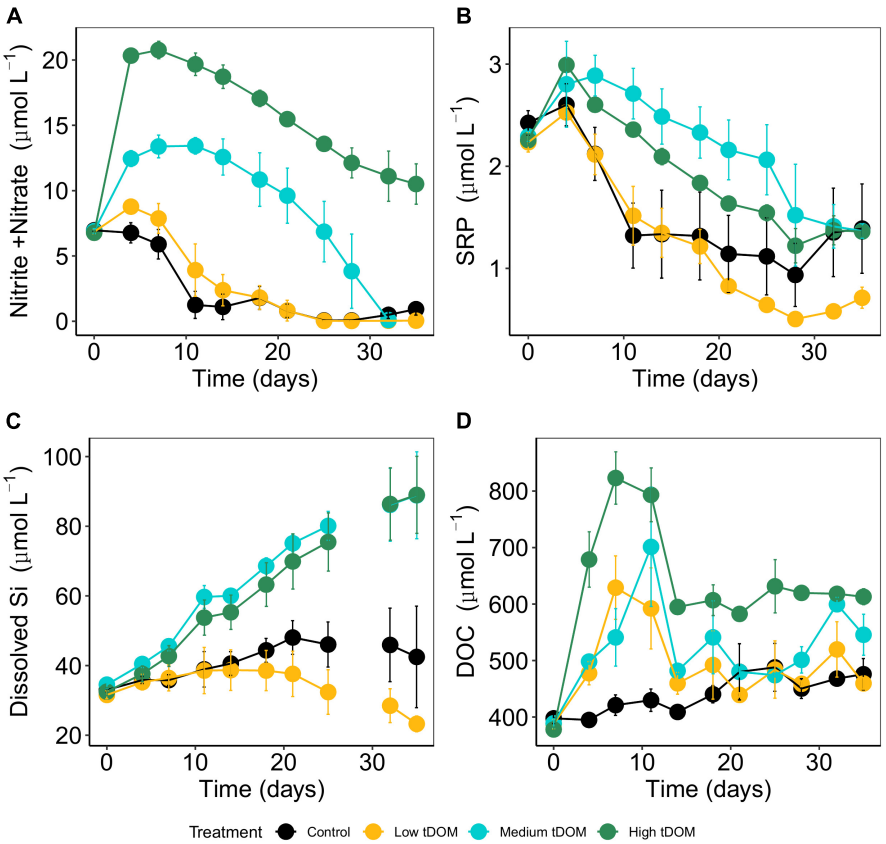

FIGURE 2 | Inorganic nutrient concentrations over 35 days of the experiments: **(A)** dissolved inorganic nitrogen (nitrate + nitrite), **(B)** soluble reactive phosphorus (SRP), and **(C)** dissolved silicate. Panel **(D)** represents the concentration of dissolved organic carbon (DOC). Error bars represent standard deviation. Color plots represent tDOM addition in the control (black), low tDOM (yellow), medium tDOM (blue), and high tDOM (green) treatments.

with a binocular (Zeiss®, Germany). At the beginning of the experiment the whole samples were counted, and from day 21 onward subsamples of only 30% (three times 10%) of the samples were counted.

Statistical Analyses

All statistical procedures and graphs were performed using R version 3.5.3 (R Core Team, 2019). Repeated measures ANOVA were used to test for treatment ("control," "low tDOM," "medium tDOM," and "high tDOM") and time ("day") effects as well as for interactive effects of treatment and time. *p*-values were obtained by pairwise analysis comparison of "tDOM addition" and "day" model (to account for interaction between tDOM addition and day). Resource use efficiency (RUE) is a proxy for ecosystem function to track the functional change in relation or reaction to species change (Ptacnik et al., 2008; Hodapp et al., 2019). RUE was defined as unit biomass production in chlorophyll *a* (µg L^{-1}) per unit TP (µg L^{-1}). Diagnostic pigments can be used as both qualitative and quantitative indicators of the respective phytoplankton group (Schlüter and Havskum, 1997). Therefore, phytoplankton and phytobenthos taxonomic pigment signatures (µg L^{-1} and µg cm^{-3}, respectively) were calculated based on pigment compositions according to Jeffrey et al. (2011) based on the following formulae:

$$\text{Diatom and Crysophytes} = \text{Fucoxanthin} + \text{Chlorophyll } c_1 + \text{Chlorophyll } c_2 \quad (1)$$

$$\text{Dinoflagellates and Cryptophytes} = \text{Peridinin} + \text{Alloxanthin} + \beta,\ \text{Cyptoxanthin} \quad (2)$$

$$\text{Chlorophytes} = \text{Chlorophyll } b + \text{Lutein} + \text{Neoxanthin} + \text{Violaxanthin} \quad (3)$$

$$\text{Cyanobacteria} = \text{Echinenone} + \text{Zeaxanthin} \quad (4)$$

RESULTS

tDOM Effects on Phytoplankton Growth and Community Composition

Adding tDOM to the respective treatments increased the light absorption coefficient (determined for 254 and 440 nm,

Figure 1) and thus, decreased the available light intensity by 27% in "low tDOM," 61% in "medium tDOM," and 86% in "high tDOM" compared to the control treatment (see also **Supplementary Figures 2**, **3**). DIN concentrations (nitrate and nitrite), SRP, and DOC increased in all treatments with tDOM addition and were higher in the "medium tDOM" and "high tDOM" treatments but generally decreased over time (**Table 1** and **Figure 2**). Si concentrations increased over time in the "medium tDOM" and "high tDOM" treatments but not in the "low tDOM" treatment and control (**Figure 2** and **Table 1**).

Phytoplankton biomass (here as chlorophyll *a* concentration) was significantly affected by tDOM addition and this effect changes over time (treatment × time interaction, **Table 1** and **Figure 3A**). While chlorophyll *a* concentrations were highest in the control and the "low tDOM" treatment in the first half of the experiment (days 4–11, see **Table 2** for comparison of treatments), chlorophyll *a* concentrations were higher in the "medium tDOM" treatment in the second half (days 28–35) while the "high tDOM" treatment generally showed the lowest chlorophyll *a* concentrations (**Figure 3A** and **Table 2**).

Treatment effects could also be observed for RUE (**Table 1**), whereby the "high tDOM" showed the lowest RUE (**Figure 3B**). In general, the RUE increased during the experiment (**Table 1**, significant effect of time) except for the last 2 days. In terms of stoichiometry, the C:N ratios decreased significantly over time (**Table 1** and **Figure 3C**) and were lower in the control (**Table 1** and **Figure 3C**). Meanwhile, C:P and N:P ratios (**Figures 3D,E**) were higher in the "medium tDOM" and "high tDOM" treatments (especially in the first half of the experiment) and generally higher with higher tDOM addition (treatment effect, **Table 1** and **Figure 3**). Both ratios decreased over time but were highest on the last day (**Table 1** and **Figures 3D,E**).

The effect of tDOM addition and time were observed for all phytoplankton groups (**Table 1**). Initially, diatoms and chrysophytes were dominant based on the relative pigment amounts in all treatments (**Figure 4A**). Diatoms were negatively affected by tDOM addition (treatment effect, **Table 1**) and their relative amount decreased over time (effect of time, **Table 1** and **Figure 4**). By contrast, chlorophytes (**Figure 4C**) increased over time (effect of time, **Table 1**). While dinoflagellates and cryptophytes (**Figure 4B**) were lowest in the control, chlorophytes were lowest in the "high tDOM" treatment.

TABLE 1 | Summary of repeated measures ANOVA model, showing the effect of treatment (tDOM addition), time (using "day") and their interaction.

Parameter	Variable	Treatment		Time		Treatment × time		Residuals
		df	*F* (*p*)	df	*F* (*p*)	df	*F* (*p*)	
Dissolved nutrients	Nitrate + nitrite	3	**326.0 (<0.001)**	10	**28.0 (<0.001)**	29	**5.7 (<0.001)**	81
	SRP	3	**28.0 (<0.001)**	10	**21.3 (<0.001)**	30	1.1 (0.334)	87
	Si	3	**53.8 (<0.001)**	9	**11.5 (<0.001)**	27	**3.4 (<0.001)**	79
	DOC	3	**55.5 (<0.001)**	10	**12.5 (<0.001)**	30	**2.6 (<0.001)**	87
Phytoplankton	Chlorophyll *a*	3	**17.3 (<0.001)**	10	**73.4 (<0.001)**	30	**16.2 (<0.001**)	87
	Diatoms	3	**5.8 (<0.001)**	10	**5.6 (<0.001)**	30	**2.6 (<0.001)**	87
	Dinoflagellates	3	**2.7 (0.049)**	10	**5.06 (<0.001)**	30	1.3 (0.1935)	87
	Cyanobacteria	3	**2.9 (0.0407)**	10	**2.2 (0.0286)**	30	0.9 (0.6061)	87
	Chlorophytes	3	**7.8 (<0.001)**	10	**7.2 (<0.001)**	30	**1.6 (0.0423)**	87
	RUE	3	**3.2 (0.0267)**	10	**11.4 (<0.001)**	30	1.9 (0.0122)	80
	C:N	3	**7.2 (<0.001)**	10	10.6 **(<0.001)**	30	**3.2 (<0.001)**	87
	C:P	3	**18.7 (<0.001)**	10	**8.9 (<0.001)**	30	**1.95 (0.0093)**	83
	N:P	3	**9.9 (<0.001)**	10	**7.5 (<0.001)**	30	1.3 (0.148)	83
Phytobenthos	Chlorophyll *a*	3	1.3 (0.2846)	9	1.9 (0.0627)	27	0.9 (0.6465)	79
	Diatoms	3	1.2 (0.301)	9	**3.86 (<0.001)**	27	0.87 (0.6526)	79
	Dinoflagellates	3	0.6 (0.600)	9	**5.0 (<0.001)**	27	0.9 (0.621)	79
	Cyanobacteria	3	1.8 (1.563)	9	**2.7 (0.008)**	27	0.7 (0.8056)	79
	Chlorophytes	3	1.1 (0.353)	9	1.2 (0.296)	27	0.8 (0.687)	79
Zooplankton	Biomass	3	**2.8 (0.0428)**	10	**7.4 (<0.001)**	30	**3.6 (<0.001)**	87
	C:N	3	**38.5 (<0.001)**	10	**19.0 (<0.001)**	30	**5.1 (<0.001)**	86
	Calanoid	3	2.3 (0.0822)	9	**9.6 (<0.001)**	27	1.5 (0.0870)	79
	Cyclopoid	3	0.8 (0.4968)	9	**2.5 (0.0143)**	27	0.8 (0.7838)	79
	Harpacticoid	3	2.3 (0.0814)	9	**4.5 (<0.001)**	27	0.5 (0.9631)	79
	Nauplii	3	**4.3 (<0.01)**	9	**9.4 (<0.001)**	27	1.3 (9.2196)	79
	Copepodid	3	3.7 (0.0148)	9	**9.5 (<0.001)**	27	0.6 (0.9342)	79
	Polycheta	3	**4.9 (<0.01)**	9	**5.3 (<0.001)**	27	1.4 (0.1299)	79

The table gives F-values for each test and denotes the respective p-values. Significant effects are shown in bold.

TABLE 2 | ANOVA analyses conducted per day for Chl *a* concentrations testing for treatment effects.

Day	*F*	*p*	Treatment comparison	diff	*p* adj
0	1.4	0.313			
4	4.3	**0.014**			
			High tDOM – control	−1.63	**0.0110**
			Low tDOM – control	−0.63	0.3926
			Medium tDOM – control	−1.12	0.0686
			Low tDOM – high tDOM	0.99	0.1115
			Medium tDOM – high tDOM	0.50	0.5687
			Medium tDOM – low tDOM	−0.49	0.5883
7	17.1	**0.003**			
			High tDOM – control	−3.14	**0.0019**
			Low tDOM – control	−1.01	0.3159
			Medium tDOM – control	−2.24	**0.0144**
			Low tDOM – high tDOM	2.12	**0.0192**
			Medium tDOM – high tDOM	0.90	0.4085
			Medium tDOM – low tDOM	−1.23	0.1895
11	550.3	**0.004**			
			High tDOM – control	−17.31	**0.0049**
			Low tDOM – control	−6.09	0.3639
			Medium tDOM – control	−14.05	**0.0162**
			Low tDOM – high tDOM	11.22	**0.0494**
			Medium tDOM – high tDOM	3.26	0.7892
			Medium tDOM – low tDOM	−7.96	0.1824
14	162.1	0.221			
18	59.7	0.080			
21	78.9	0.130			
25	212.3	0.231			
28	689.1	**0.022**			
			High tDOM – control	−7.28	0.5339
			Low tDOM – control	−7.97	0.4641
			Medium tDOM – control	10.86	0.2361
			Low tDOM – high tDOM	−0.69	0.9991
			Medium tDOM – high tDOM	18.14	**0.0337**
			Medium tDOM – low tDOM	18.83	**0.0281**
32	2287.0	**0.029**			
			High tDOM – control	−1.59	0.9985
			Low tDOM – control	−1.83	0.9977
			Medium tDOM – control	30.70	0.0604
			Low tDOM – high tDOM	−0.24	1.0000
			Medium tDOM – high tDOM	32.29	**0.0483**
			Medium tDOM – low tDOM	32.53	**0.0467**
35	1135.1	**0.0073**			
			High tDOM – control	0.32	0.9999
			Low tDOM – control	−1.64	0.9898
			Medium tDOM – control	21.95	**0.0162**
			Low tDOM – high tDOM	−1.96	0.9829
			Medium tDOM – high tDOM	21.63	**0.0175**
			Medium tDOM – low tDOM	23.60	**0.0109**

Post hoc tests (TukeyHSD) were conducted if treatment effects were significant. df treatment = 3, df residuals = 8. For treatment comparisons difference in means (diff) and adjusted p-values are given and significant comparisons are shown in bold.

Cyanobacteria (**Figure 4D**) relative pigment concentrations were low in all treatments (<5%) and but were higher in the control treatment (**Figure 4D** and **Table 1**).

Phytoplankton – Phytobenthos Interaction

Phytoplankton biomass in all treatments was not significantly correlated with phytobenthos biomass which, could have indicated a direct interaction (**Supplementary Figure 5**). Neither phytobenthos biomass (**Figure 5**) nor its composition was significantly affected by tDOM addition (**Table 1**) but the effects of "time" were observed. The concentrations measured for benthic pigments were low in most samples and highly variable between replicates and over time (**Figure 6**).

tDOM Effect via Phytoplankton on Zooplankton

Zooplankton biomass (C μmol L^{-1}) and molar C:N ratios were affected by tDOM addition and time (**Table 1** and **Figure 7**). Zooplankton biomass was lowest in the "low tDOM" treatment while C:N ratios were lowest in the control and increased with higher tDOM addition (**Table 1** and **Figure 7**). In terms of zooplankton community composition, microscopic analysis revealed that the community consisted mainly of calanoid copepods, polychetes, and cyclopoid copepods, while the abundance of juvenile copepods (copepodites) remained low throughout the experiment (**Figure 8**). Copepod nauplii were highly abundant in all treatments during the whole experiment and showed a treatment effect (**Table 1**). Most zooplankton groups, except Nauplii and Polycheta (**Table 1**), did not show significant treatment effects, but their relative abundance changed over time (significant effect of time, **Table 1**). The copepodites significantly decreased in all treatments during the second half of the experiment (significant effect of time, **Table 1**). By the end of the experiment, calanoids copepods dominated in both the "low tDOM" and "high tDOM" treatments, meanwhile, nauplii larvae dominated in the "medium tDOM" and "high tDOM" treatments.

DISCUSSION

Effect of Different tDOM Concentrations (H1)

Light reduction was achieved by adding tDOM which reduced light availability between 27% and 86%. Results showed that phytoplankton biomass increased in all treatments during the experiment, while the biomass was slightly higher in the control and "low tDOM" treatments during the first half of the experiment and lowest in the "high tDOM" treatment. Reduced light availability due to tDOM addition in the "medium tDOM" and "high tDOM" treatments might have limited the phytoplankton growth via shading while the higher light availability, as well as the supply of directly bioavailable dissolved nutrients, might have favored phytoplankton growth in the control and "low tDOM" treatment. Klug (2002) suggested that the net effect on phytoplankton biomass depends on the concentration and availability of nutrients associated with tDOM as well as the physiological status of the phytoplankton community. Overall, our results are consistent with other

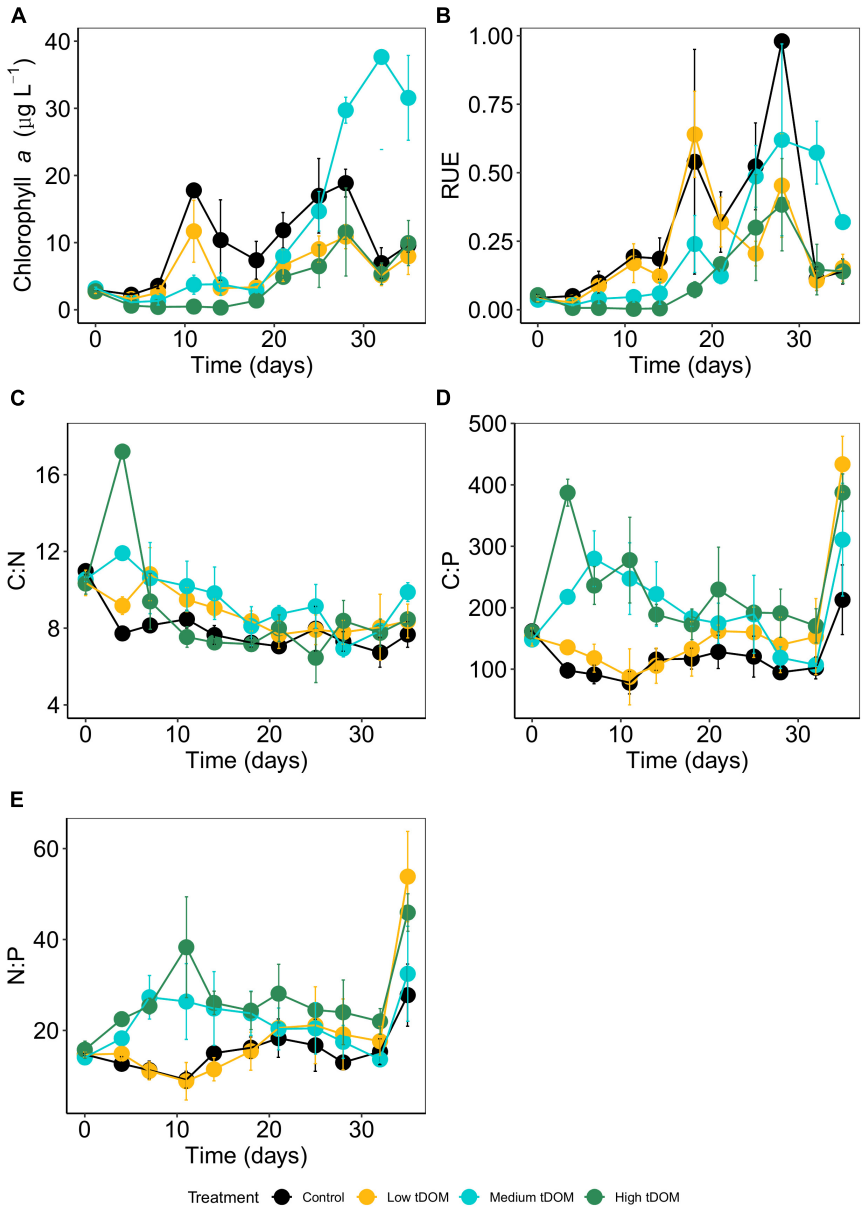

FIGURE 3 | Phytoplankton **(A)** biomass (Chl *a* in µg L^{-1}), **(B)** resource use efficiency (RUE), and molar particulate **(C)** C:N, **(D)** C:P, and **(E)** N:P ratios over 35 days of the experiments. Data are given as mean values with standard deviation. Colors indicate treatments: control (black), low tDOM addition (yellow), medium tDOM addition (blue), and high tDOM addition (green).

studies (Bartels et al., 2012; Gall et al., 2017) where different tDOM concentrations affected phytoplankton biomass over time and phytoplankton biomass was significantly lower in higher tDOM treatments (supporting H1) (Jones, 1992; Thrane et al., 2014). However, phytoplankton biomass in the "medium tDOM" treatment increased from day 18 until the end of the experiment, potentially due to the high dissolved nutrient concentration available in the "medium tDOM" and the comparably lower shading effect (**Figure 3**; Traving et al., 2017). In general, we conclude that the shading effect of tDOM was stronger during the first half (<18 days) of the experiment (supporting H1) and was reduced over time potentially due to degradation of tDOM in the water column as shown by decreased absorption coefficient in all tDOM treatments (**Figure 1B**). Degradation of tDOM in the water column could be due to microbial utilization and flocculation followed by sedimentation (Tranvik, 1998). Limited data on bacterial abundance is available in **Supplementary Figure 6**. Previous studies showed that tDOM addition can stimulate bacterial production especially when nutrients are scarce (Tranvik, 1998; Gall et al., 2017). Moreover, lability of tDOM changes through bacterial utilization and thus may affect tDOM shading properties

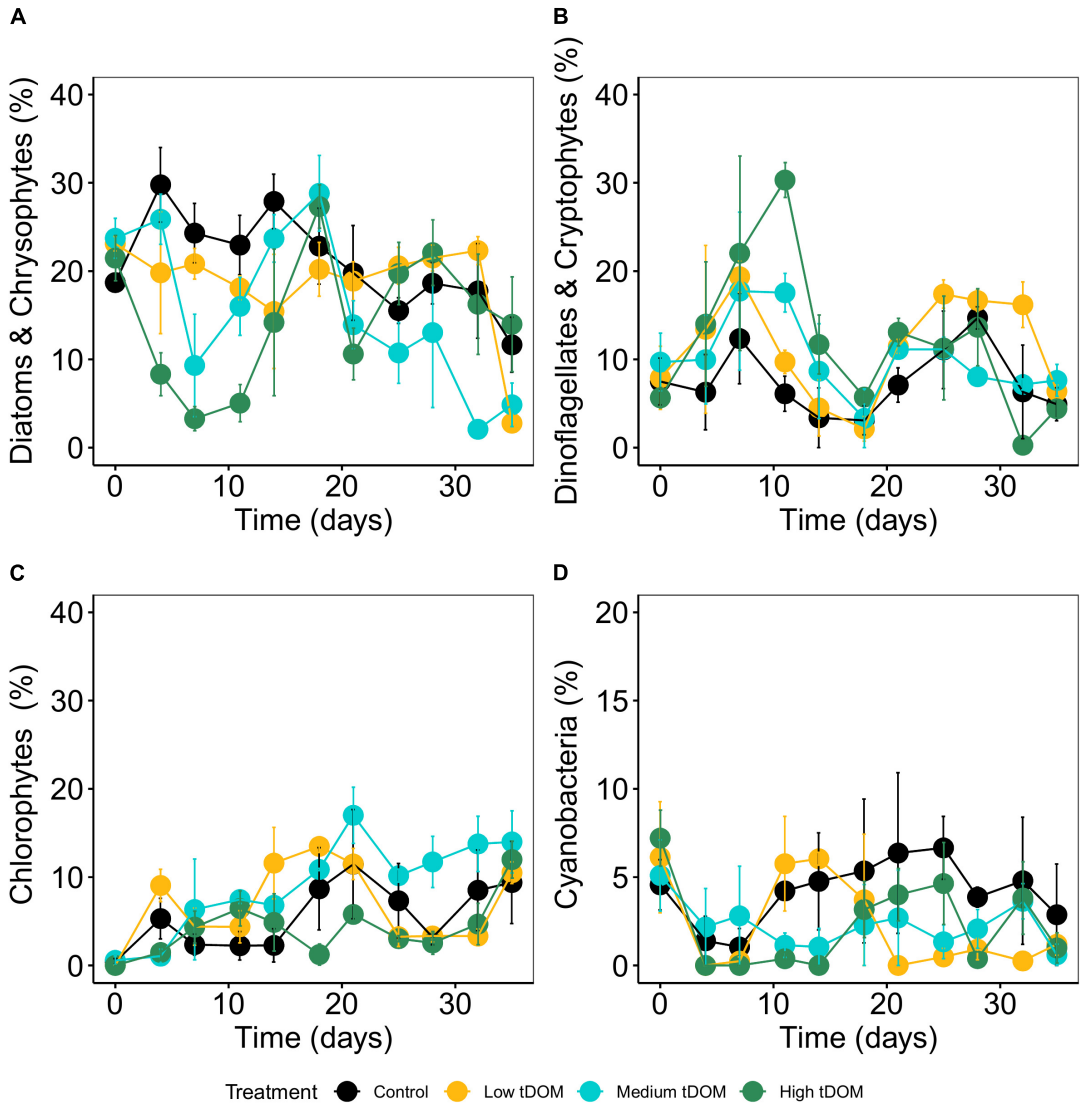

FIGURE 4 | Relative abundance of phytoplankton (%) specific pigment signature compositions over 35 days of the experiment. **(A)** Diatom and chrysophytes, **(B)** dinoflagellates and cryptophytes, **(C)** chlorophytes and **(D)** cyanobacteria. Error bars represent standard deviation. Color plots represent tDOM addition in the control (black), low tDOM (yellow), medium tDOM (blue), and high tDOM (green) treatments.

(Tranvik, 1988; Wikner and Andersson, 2012). In general, the presence of heterotrophic bacteria plays an important role in this process.

We found lower RUE in the "high tDOM" treatment during the first half of the experiment (significant effect treatment × time). The cellular and individual RUE are mainly characterized by the functional response of resource uptake to resource supply, dependent on an increase in uptake as well as luxury consumption and storage of resource supply (Hodapp et al., 2019). Therefore, increasing RUE indicates decreasing resource supply (Niu et al., 2011) as shown by the decrease in SRP concentration in our study. Our results are in agreement with previous studies that found increasing RUE was due to the decrease in nutrient availability (Bridgham et al., 1995). In contrast, Verbeek et al. (2018) showed that high nutrient availability led to an increase in RUE.

tDOM addition can change the water color to yellow or brown and potentially shift the light spectrum away from the blue wavelengths that are most useful to algae toward a predominance of yellow to red wavelengths (Suthers and Rissik, 2009) which in turn affects community composition. Changes in phytoplankton composition were observed in most treatments (treatment effects on all phytoplankton groups), especially over time. However, as these changes in community composition predominantly occurred over time, we could not clearly distinguish between "time" and "tDOM" effects. Thus, our finding generally supports the hypothesis (H1) that different tDOM concentrations could lead to shifts in species composition

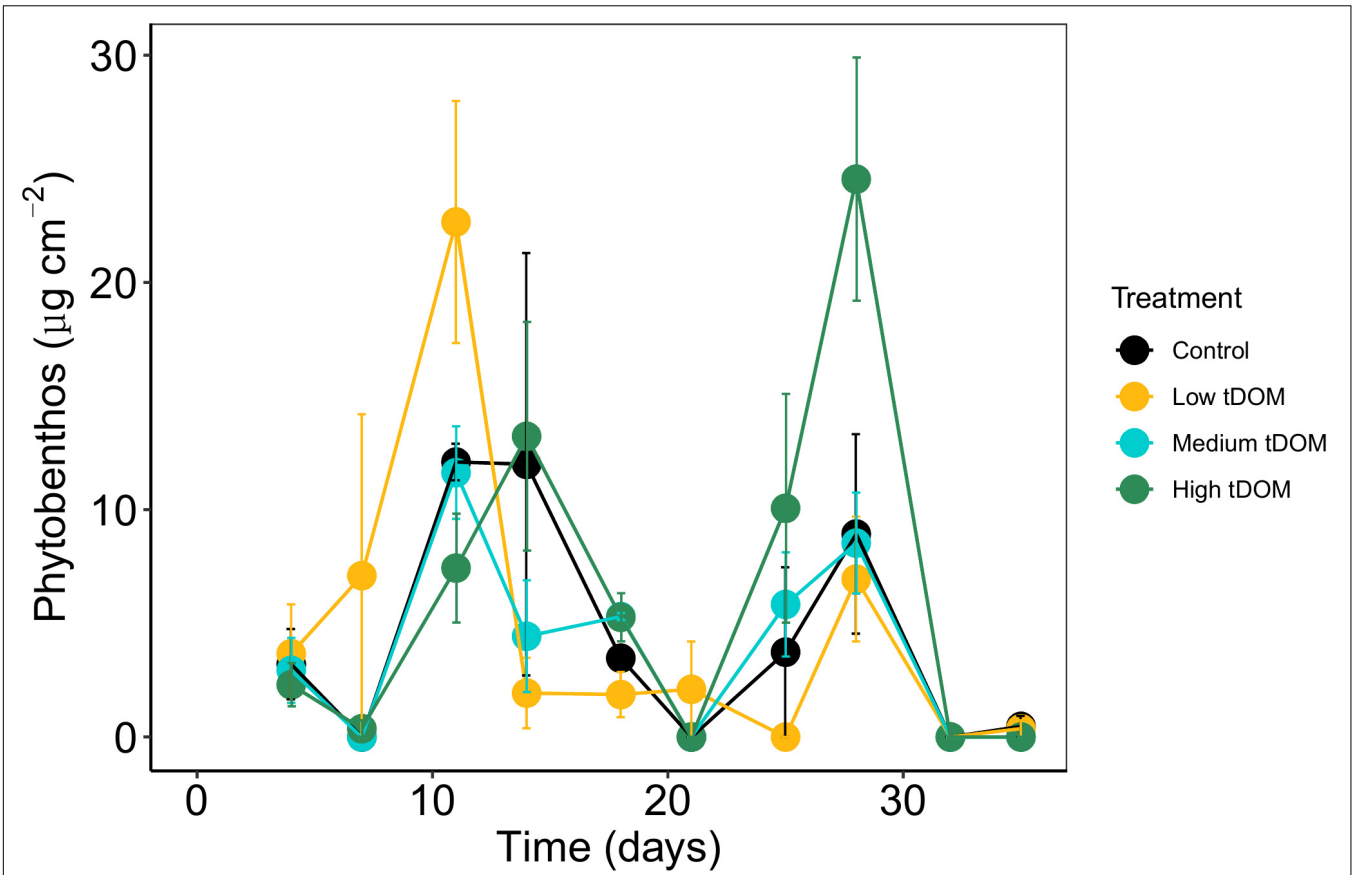

FIGURE 5 | Average of phytobenthos biomass (Chl *a* in µg cm^{-2}) over 35 days of the experiment. Error bars represent standard deviation. Color plots represent tDOM addition in the control (black), low tDOM (yellow), medium tDOM (blue), and high tDOM (green) treatments.

due to species-specific growth-irradiance curves and pigment composition (Kirk, 2011). While clear effects of tDOM on chrysophytes were observed by Lefebure et al. (2013), our results indicate an effect of tDOM on diatoms that is dependent on time (treatment × time). It is known that diatoms and dinoflagellates are able to adapt and grow at low light condition by increasing their content of Peridinin-Chlorophyll α-Proteins to maintain their cellular photosynthetic capacity (Prézelin, 1976; Falkowski and Owens, 1980) which might have occurred in this experiment. Chlorophytes showed an increase in the "medium tDOM" over time, particularly after half of the experiment (treatment × time interaction). However, our result is contrary to Deininger et al. (2016) as they observed a decreasing trend of chlorophytes concentration over time and the chlorophytes were not affected by nutrient enrichment through soil addition. This could be due to the different composition of soil than the tDOM used in our experiment. As for cyanobacteria, the concentration was relatively low during the whole experiment and tDOM addition tended to decrease their concentrations (highest amounts in control compared to other treatments). Lefebure et al. (2013) observed there was no significant effect of tDOM addition on cyanobacteria concentrations collected from the Baltic Sea. Thus, our results suggested that there is a potential of interactive effect between nutrients, light intensity, and spectrum that affect the species in a specific way and thus shifts the community composition. However, more detailed species-specific investigations are needed here.

Phytoplankton and Phytobenthos Interaction (H2)

Despite assuming that phytoplankton and phytobenthos would compete for light and nutrients and thus interactively affect each other, we did not find a significant correlation between phytoplankton and phytobenthos biomass to support their direct interaction (rejecting H2). The lack of interaction between phytoplankton and phytobenthos could be due to zooplankton species found in our study which are phytoplankton feeders. However, we only sampled the pelagic zooplankton and did not determine the benthic habitat for an herbivore to support this assumption. Another reason that there was no clear effect of tDOM addition via nutrient or light on phytobenthos biomass (rejecting H2) could be the tidal cycle during our experiment. We expected that phytobenthos biomass would be negatively affected as tDOM-contained water would increase the shading effect. However, by reducing the water column during low tide,

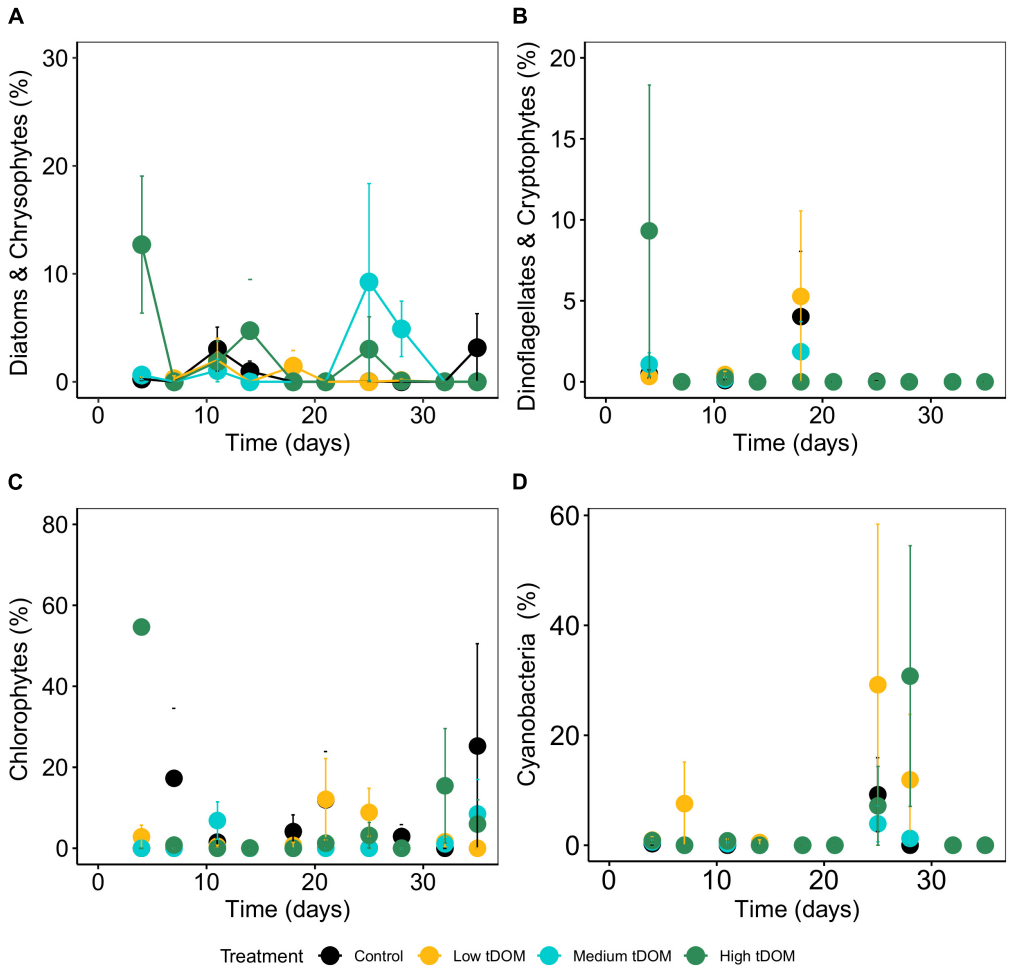

FIGURE 6 | Relative abundance of phytobenthos specific pigment signature composition (%) over 35 days of the experiment. **(A)** Diatom and chrysophytes, **(B)** dinoflagellates and cryptophytes, **(C)** chlorophytes and **(D)** cyanobacteria. Error bars represent standard deviation. Color plots represent tDOM addition in the control (black), low tDOM (yellow), medium tDOM (blue), and high tDOM (green) treatments.

light availability increased and might have been sufficient for phytobenthos. Furthermore, phytobenthos has been reported to be tolerant toward shading (Barranguet et al., 1998; Gattuso et al., 2006). Besides, the primary production of benthic algae in intertidal systems is also dependent on the coarse size of the sediment (Billerbeck et al., 2007). The missing significant correlation between phytoplankton and phytobenthos biomass could also be because their response toward nutrient and light changes are in different time scales. For instance, Bonilla et al. (2005) observed phytoplankton biomass increased by 19-fold after 2 weeks of the nutrient-enriched experiment, but phytobenthos biomass did not respond to nutrient enrichment at least over timescales of days to weeks.

Phytobenthos composition indicates the ecological status in the aquatic ecosystem. Bergamasco et al. (2003) showed that the hydrodynamics of the tidal current can stimulate benthic diatom production and affect the flux of nutrients from the sediment through resuspension of the topmost layer and consequent release of pore water. Benthic dinoflagellates and cryptophytes were rarely detected, probably due to their movement to the water column during low tide stimulation. Changes in the composition over time were not detected, and these data should be interpreted by keeping in mind the generally low and variable concentrations. It was suggested that the benthic cyanobacteria could have moved into the water column and become a part of phytoplankton when suspended by tidal currents (MacIntyre et al., 1996). Overall, the nutritional status of phytobenthos and phytoplankton showed different responses toward tDOM addition in terms of their biomass and community composition. The results imply that the phytobenthos and phytoplankton may have different strategies toward environmental changes, particularly in terms of nutrient and light changes. Regarding the complex system of coastal environments, more investigations are needed to explore the phytoplankton and phytobenthos interaction to further

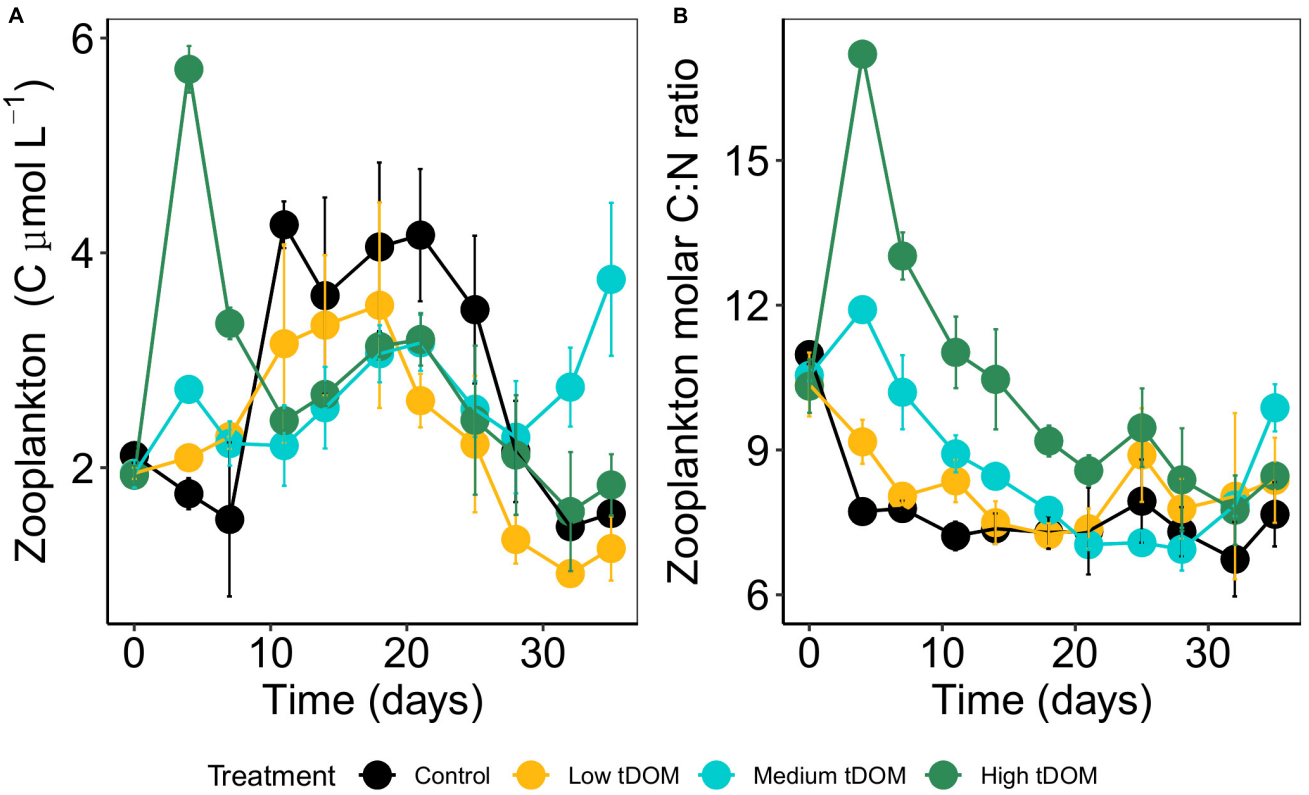

FIGURE 7 | (A) Average dry zooplankton biomass (C µmol L^{-1}) and **(B)** zooplankton C:N ratio over 35 days of the experiment. Error bars represent standard deviation. Color plots represent tDOM addition in the control (black), low tDOM (yellow), medium tDOM (blue), and high tDOM (green) treatments.

understand their response toward future eutrophication or coastal darkening.

The Effects of tDOM on Higher Trophic Levels (H3)

Changes in phytoplankton biomass consequently modify the zooplankton grazing intensities and selectivity on phytoplankton which in turn may alter phytoplankton species assemblages (Kissman et al., 2013). Similar to phytoplankton biomass, light availability reduction via tDOM addition significantly affected zooplankton biomass (supporting H3). This observation supports our hypothesis that changes in phytoplankton biomass with increasing tDOM concentration directly link to the next trophic level, and food availability appears to be an important factor for copepod abundance. For instance, the trend of phytoplankton biomass was similar to an increase of zooplankton biomass particularly during the first half of the experiment. This observation might be an effect of the bottom-up process due to the transfer of energy and nutrients from phytoplankton to zooplankton. The bottom-up effect should dominate if primary producers receive nutrient subsidies meanwhile top-down grazing processes dominate if high trophic levels received nutrient subsidies (Polis and Strong, 1996). Therefore, increasing food availability during the first half of the experiment may have increased the abundance of zooplankton. This result partly supports H3. In terms of phytoplankton quality as a food resource (here C:N, C:P, and N:P ratios), we observed a decrease in phytoplankton C:N ratios over time reflecting that more particulate N per phytoplankton biomass was available. Zooplankton C:N ratios increased with tDOM addition. tDOM addition resulted in higher phytoplankton C:P and N:P ratios in "medium tDOM" and "high tDOM" treatments, thus indicating lower amounts of P in relation to carbon biomass or N, respectively.

Lower phytoplankton biomass in the control, "low tDOM," and "high tDOM" treatments were measured after day 28 of the experiment, possibly due to increasing top-down grazing processes of zooplankton. This is supported by an increase in the relative abundance of larger zooplankton (e.g., calanoid copepods instead of smaller development stages) in those treatments. In contrast, increased phytoplankton biomass in the "medium tDOM" treatment after day 28 could be due to a delay (compared to other treatments) of calanoid grazing pressure (Sommer et al., 2003). Although phytoplankton composition changes with tDOM addition, zooplankton composition changed over time but was not directly affected by tDOM driven changes in food availability or quality. It could be that zooplankton composition would have needed more time to respond to the treatment or changes in food sources (Lebret et al., 2018).

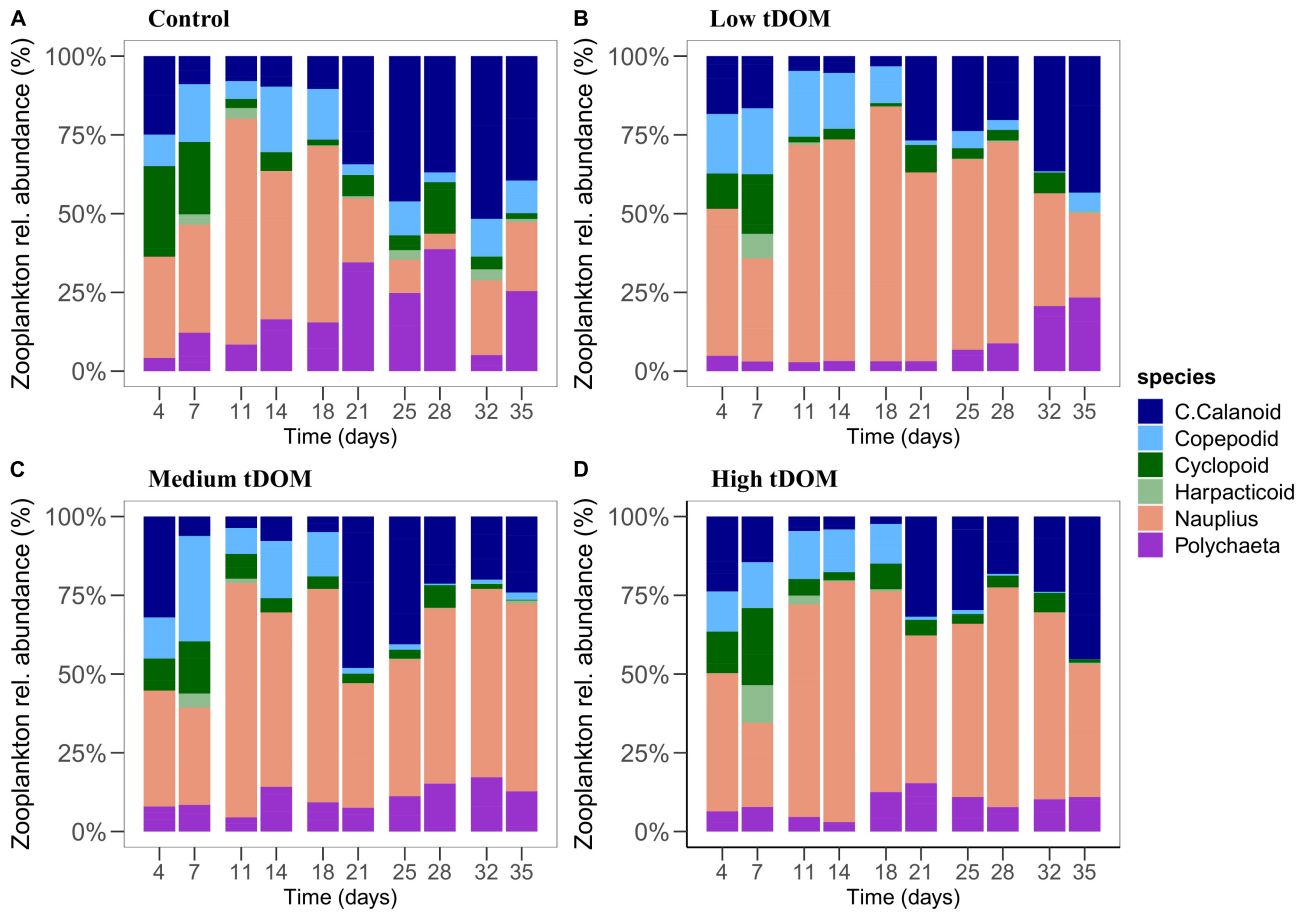

FIGURE 8 | Zooplankton relative abundance (%) of the different treatments over 35 days of the experiment. Panels **(A–D)** represent control, low tDOM, medium tDOM, and high tDOM treatments, respectively.

Overall, we found no clear effect of tDOM addition on zooplankton biomass but changes in zooplankton biomass and composition occurred over time. Given the increasing tDOM input into the water column particularly in the coastal system, our study does support previous observations (Kissman et al., 2013; Lefebure et al., 2013) where the effect of darkening showed strong implications for the higher trophic level. However, stronger effects on zooplankton might occur over longer periods than tested in our experiment or after multiple tDOM additions. As zooplankton constitutes an important connection to the next tropic levels, determining how energy will be transferred via zooplankton will provide further insights to how coastal darkening affects the coastal ecosystem functions.

CONCLUSION

Our study showed that the shading effect of tDOM addition limited the phytoplankton biomass due to enhanced light absorption by tDOM. Moreover, different tDOM concentrations resulted in differences in the community's composition potentially due to species-specific light demands and pigment composition. There was no significant treatment effect on the phytobenthos biomass and composition which might be a result of the tidal cycle allowing sufficient light penetration to the sediment surface during low tide. Although tDOM effects on phytoplankton and zooplankton were found, no direct bottom-up effect of tDOM addition via phytoplankton on zooplankton could be observed. With a predicted increase of tDOM input (concentrations and frequency) into the water column leading to further darkening of coastal waters, we propose that darkening of coastal waters will have negative effects on primary producer's biomass and composition with a consequence to the next trophic level, i.e., zooplankton. However, those tDOM effects are highly dependent on the characteristics of DOM itself (i.e., light attenuation properties, substrate lability, and bio-degradability). Furthermore, multiple disturbance effects via tDOM addition could have more severe and long-lasting effects on aquatic systems than just a single tDOM input as investigated in this study. This highlights the need for more experiments in order to assess the specific effects in each coastal ecosystem.

DATA AVAILABILITY STATEMENT

The raw data supporting the conclusions of this article will be made available by the authors, without undue reservation.

AUTHOR CONTRIBUTIONS

LK and MS designed the experiment in discussion with Oliver Zielinski. NIHM drafted the manuscript. MS, JB, FB, LK, and AS participated in the Planktotron experiment, samples collection, and laboratory analyses. NIHM and MS analyzed the data. All authors contributed significantly to the manuscript.

FUNDING

This research was funded by the Lower Saxony Ministry of Science and Culture (MWK) through the COD project (Coastal Ocean Darkening – Light availability in the past and future marine environment) (grant number VWZN3175).

SUPPLEMENTARY MATERIAL

The Supplementary Material for this article can be found online at: https://www.frontiersin.org/articles/10.3389/fmars.2020.547829/full#supplementary-material

REFERENCES

Aksnes, D. L., Dupont, N., Staby, A., Fiksen, Ø, Kaartvedt, S., and Aure, J. (2009). Coastal water darkening and implications for mesopelagic regime shifts in Norwegian fjords. *Mar. Ecol. Prog. Ser.* 387, 39–49. doi: 10.3354/meps08120

Anderson, T. R., Christian, J. R., and Flynn, K. J. (2015). "Chapter 15 - modeling DOM biogeochemistry," in *Biogeochemistry of Marine Dissolved Organic Matter (Second Edition)*, eds D. A. Hansell and C. A. Carlson (Boston: Academic Press), 635–667. doi: 10.1016/b978-0-12-405940-5.00015-7

Andersson, A., Brugel, S., Paczkowska, J., Rowe, O. F., Figueroa, D., Kratzer, S., et al. (2018). Influence of allochthonous dissolved organic matter on pelagic basal production in a northerly estuary. *Estuar. Coast. Shelf Sci.* 204, 225–235. doi: 10.1016/j.ecss.2018.02.032

Barranguet, C., Kromkamp, J., and Peene, J. (1998). Factors controlling primary production and photosynthetic characteristics of intertidal microphytobenthos. *Mar. Ecol. Prog. Ser.* 173, 117–126. doi: 10.3354/meps173117

Bartels, P., Cucherousset, J., Gudasz, C., Jansson, M., Karlsson, J., Persson, L., et al. (2012). Terrestrial subsidies to lake food webs: an experimental approach. *Oecologia* 168, 807–818. doi: 10.1007/s00442-011-2141-7

Bergamasco, A., De Nat, L., Flindt, M., and Amos, C. (2003). Interactions and feedbacks among phytobenthos, hydrodynamics, nutrient cycling and sediment transport in estuarine ecosystems. *Continent. Shelf Res.* 23, 1715–1741. doi: 10.1016/j.csr.2003.06.014

Billerbeck, M., Røy, H., Bosselmann, K., and Huettel, M. (2007). Benthic photosynthesis in submerged Wadden Sea intertidal flats. *Estuar. Coast. Shelf Sci.* 71, 704–716. doi: 10.1016/j.ecss.2006.09.019

Blumenshine, S., Vadeboncoeur, Y., Lodge, D., Cottingham, K., and Knight, S. (1997). Benthic-pelagic links: responses of benthos to water-column nutrient enrichment. *J. N. Am. Benthol. Soc.* 16, 466–479. doi: 10.2307/1468138

Bonilla, S., Rautio, M., and Vincent, W. F. (2009). Phytoplankton and phytobenthos pigment strategies: implications for algal survival in the changing Arctic. *Polar Biol.* 32, 1293–1303. doi: 10.1007/s00300-009-0626-1

Bonilla, S., Villeneuve, V., and Vincent, W. F. (2005). Benthic and planktonic algal communities in a high arctic lake: Pigment structure and contrasting responses to nutrient enrichment. *J. Phycol.* 41, 1120–1130. doi: 10.1111/j.1529-8817.2005.00154.x

Boyce, D. G., Lewis, M. R., and Worm, B. (2010). Global phytoplankton decline over the past century. *Nature* 466:591. doi: 10.1038/nature09268

Bridgham, S. D., Pastor, J., Mcclaugherty, C. A., and Richardson, C. J. (1995). Nutrient-use efficiency: a litterfall index, a model, and a test along a nutrient-availability gradient in North Carolina peatlands. *Am. Nat.* 145, 1–21. doi: 10.1086/285725

Capuzzo, E., Lynam, C. P., Barry, J., Stephens, D., Forster, R. M., Greenwood, N., et al. (2018). A decline in primary production in the North Sea over 25 years, associated with reductions in zooplankton abundance and fish stock recruitment. *Glob. Change Biol.* 24, e352–e364.

Capuzzo, E., Stephens, D., Silva, T., Barry, J., and Forster, R. M. (2015). Decrease in water clarity of the southern and central North Sea during the 20th century. *Glob. Change Biol.* 21, 2206–2214. doi: 10.1111/gcb.12854

Carlson, C. A., and Hansell, D. A. (2015). "Chapter 3 - DOM sources, sinks, reactivity, and budgets," in *Biogeochemistry of Marine Dissolved Organic Matter (Second Edition)*, eds D. A. Hansell and C. A. Carlson (Boston: Academic Press), 65–126. doi: 10.1016/b978-0-12-405940-5.00003-0

Coble, P. G. (2007). Marine optical biogeochemistry: the chemistry of ocean color. *Chem. Rev.* 107, 402–418. doi: 10.1021/cr0503502B

Cole, J. J., Carpenter, S. R., Kitchell, J., Pace, M. L., Solomon, C. T., and Weidel, B. (2011). Strong evidence for terrestrial support of zooplankton in small lakes based on stable isotopes of carbon, nitrogen, and hydrogen. *Proc. Natl. Acad. Sci. U.S.A.* 108, 1975–1980. doi: 10.1073/pnas.1012807108

de Wit, H. A., Valinia, S., Weyhenmeyer, G. A., Futter, M. N., Kortelainen, P., Austnes, K., et al. (2016). Current browning of surface waters will be further promoted by wetter climate. *Environ. Sci. Technol. Lett.* 3, 430–435. doi: 10.1021/acs.estlett.6b00396

Deininger, A., Faithfull, C. L., and Bergström, A.-K. (2017a). Nitrogen effects on the pelagic food web are modified by dissolved organic carbon. *Oecologia* 184, 901–916. doi: 10.1007/s00442-017-3921-5

Deininger, A., Faithfull, C. L., and Bergström, A. K. (2017b). Phytoplankton response to whole lake inorganic N fertilization along a gradient in dissolved organic carbon. *Ecology* 98, 982–994. doi: 10.1002/ecy.1758

Deininger, A., Faithfull, C. L., Lange, K., Bayer, T., Vidussi, F., and Liess, A. (2016). Simulated terrestrial runoff triggered a phytoplankton succession and changed seston stoichiometry in coastal lagoon mesocosms. *Mar. Environ. Res.* 119, 40–50. doi: 10.1016/j.marenvres.2016.05.001

Deininger, A., and Frigstad, H. (2019). Reevaluating the role of organic matter sources for coastal eutrophication, oligotrophication, and ecosystem health. *Front. Mar. Sci.* 6:210. doi: 10.3389/fmars.2019.00210

Elser, J. J., and Urabe, J. (1999). The stoichiometry of consumer-driven nutrient recycling: theory, observations, and consequences. *Ecology* 80, 735–751. doi: 10.1890/0012-9658(1999)080[0735:tsocdn]2.0.co;2

Evans, C. D., Chapman, P. J., Clark, J. M., Monteith, D. T., and Cresser, M. S. (2006). Alternative explanations for rising dissolved organic carbon export from organic soils. *Glob. Change Biol.* 12, 2044–2053. doi: 10.1111/j.1365-2486.2006.01241.x

Faithfull, C., Huss, M., Vrede, T., Karlsson, J., and Bergström, A.-K. (2012). Transfer of bacterial production based on labile carbon to higher trophic levels

in an oligotrophic pelagic system. *Can. J. Fish. Aquat. Sci.* 69, 85–93. doi: 10.1139/f2011-142

Falkowski, P. G., and Owens, T. G. (1980). Light—Shade Adaptation : two strategies in marine phytoplankton. *Plant Physiol.* 66, 592–595. doi: 10.1104/pp.66.4.592

Fleming-Lehtinen, V., and Laamanen, M. (2012). Long-term changes in Secchi depth and the role of phytoplankton in explaining light attenuation in the Baltic Sea. *Estuar. Coast. Shelf Sci.* 102, 1–10. doi: 10.1016/j.ecss.2012.02.015

Gall, A., Uebel, U., Ebensen, U., Hillebrand, H., Meier, S., Singer, G., et al. (2017). Planktotrons: a novel indoor mesocosm facility for aquatic biodiversity and food web research. *Limnol. Oceanogr. Methods* 15, 663–677. doi: 10.1002/lom3.10196

Gattuso, J. P., Gentili, B., Duarte, C. M., Kleypas, J. A., Middelburg, J. J., and Antoine, D. (2006). Light availability in the coastal ocean: impact on the distribution of benthic photosynthetic organisms and their contribution to primary production. *Biogeosciences* 3, 489–513. doi: 10.5194/bg-3-489-2006

Grasshoff, K., Kremling, K., and Ehrhardt, M. (1999). *Methods of Seawater Analysis*. Hoboken, NJ: John Wiley & Sons.

Hansson, L. A. (1988). Effects of competitive interactions on the biomass development of planktonic and periphytic algae in lakes 1. *Limnol. Oceanogr.* 33, 121–128. doi: 10.4319/lo.1988.33.1.0121

Hodapp, D., Hillebrand, H., and Striebel, M. (2019). "Unifying" the concept of resource use efficiency in ecology. *Front. Ecol. Evol.* 6:233. doi: 10.3389/fevo.2018.00233

Jeffrey, S. W., Wright, S. W., and Zapata, M. (2011). "Microalgal classes and their signature pigments," in *Phytoplankton Pigments: Characterization, Chemotaxonomy and Applications in Oceanography*, eds C. A. Llewellyn, E. S. Egeland, G. Johnsen, and S. Roy (Cambridge, MA: Cambridge University Press), 3–77. doi: 10.1017/cbo9780511732263.004

Jones, R. I. (1992). The influence of humic substances on lacustrine planktonic food chains. *Hydrobiologia* 229, 73–91. doi: 10.1007/bf00006992

Kemp, W. M., Boynton, W. R., Adolf, J. E., Boesch, D. F., Boicourt, W. C., Brush, G., et al. (2005). Eutrophication of Chesapeake Bay: historical trends and ecological interactions. *Mar. Ecol. Prog. Ser.* 303, 1–29. doi: 10.3354/meps303001

Kirk, J. T. (2011). *Light and Photosynthesis in Aquatic Ecosystems*. Cambridge, MA: Cambridge University Press.

Kissman, C. E., Williamson, C. E., Rose, K. C., and Saros, J. E. (2013). Response of phytoplankton in an alpine lake to inputs of dissolved organic matter through nutrient enrichment and trophic forcing. *Limnol. Oceanogr.* 58, 867–880. doi: 10.4319/lo.2013.58.3.0867

Klug, J. L. (2002). Positive and negative effects of allochthonous dissolved organic matter and inorganic nutrients on phytoplankton growth. *Can. J. Fish. Aquat. Sci.* 59, 85–95. doi: 10.1139/f01-194

Lebret, K., Langenheder, S., Colinas, N., Östman, Ö, and Lindström, E. S. (2018). Increased water colour affects freshwater plankton communities in a mesocosm study. *Aquat. Microb. Ecol.* 81, 1–17. doi: 10.3354/ame01858

Lefebure, R., Degerman, R., Andersson, A., Larsson, S., Eriksson, L. O., Båmstedt, U., et al. (2013). Impacts of elevated terrestrial nutrient loads and temperature on pelagic food-web efficiency and fish production. *Glob. Change Biol.* 19, 1358–1372. doi: 10.1111/gcb.12134

MacIntyre, H. L., Geider, R. J., and Miller, D. C. (1996). Microphytobenthos: the ecological role of the "secret garden" of unvegetated, shallow-water marine habitats. I. Distribution, abundance and primary production. *Estuaries* 19, 186–201. doi: 10.2307/1352224

Monteith, D. T., Stoddard, J. L., Evans, C. D., De Wit, H. A., Forsius, M., Høgåsen, T., et al. (2007). Dissolved organic carbon trends resulting from changes in atmospheric deposition chemistry. *Nature* 450:537. doi: 10.1038/nature06316

Niu, S., Xing, X., Zhang, Z., Xia, J., Zhou, X., Song, B., et al. (2011). Water-use efficiency in response to climate change: from leaf to ecosystem in a temperate steppe. *Glob. Change Biol.* 17, 1073–1082. doi: 10.1111/j.1365-2486.2010.02280.x

Nunes, J. P., Seixas, J., Keizer, J. J., and Ferreira, A. J. D. (2009). Sensitivity of runoff and soil erosion to climate change in two Mediterranean watersheds. Part I: model parameterization and evaluation. *Hydrol. Process.* 23, 1202–1211. doi: 10.1002/hyp.7247

Paczkowska, J., Brugel, S., Rowe, O., Lefébure, R., Brutemark, A., and Andersson, A. (2020). Response of coastal phytoplankton to high inflows of terrestrial matter. *Front. Mar. Sci.* 7:80. doi: 10.3389/fmars.2020.00080

Polis, G. A., and Strong, D. R. (1996). Food web complexity and community dynamics. *Am. Nat.* 147, 813–846. doi: 10.1086/285880

Prézelin, B. B. (1976). The role of peridinin-chlorophyll a-proteins in the photosynthetic light adaption of the marine dinoflagellate, *Glenodinium* sp. *Planta* 130, 225–233. doi: 10.1007/bf00387826

Ptacnik, R., Solimini, A. G., Andersen, T., Tamminen, T., Brettum, P., Lepistö, L., et al. (2008). Diversity predicts stability and resource use efficiency in natural phytoplankton communities. *Proc. Natl. Acad. Sci. U.S.A.* 105, 5134–5138. doi: 10.1073/pnas.0708328105

R Core Team (2019). *R: A languagE and Environmental Statistical Computing*. Vienna: R Foundation for Statistical Computing.

Riber, H. H., and Wetzel, R. G. (1987). Boundary-layer and internal diffusion effects on phosphorus fluxes in lake periphyton1. *Limnol. Oceanogr.* 32, 1181–1194. doi: 10.4319/lo.1987.32.6.1181

Riedel, T., Biester, H., and Dittmar, T. (2012). Molecular fractionation of dissolved organic matter with metal salts. *Environ. Sci. Technol.* 46, 4419–4426. doi: 10.1021/es203901u

Roulet, N., and Moore, T. R. (2006). Browning the waters. *Nature* 444, 283–284. doi: 10.1038/444283a

Schlüter, L., and Havskum, H. (1997). Phytoplankton pigments in relation to carbon content in phytoplankton communities. *Mar. Ecol. Prog. Ser.* 155, 55–65. doi: 10.3354/meps155055

Shurin, J. B., Winder, M., Adrian, R., Keller, W., Matthews, B., Paterson, A. M., et al. (2010). Environmental stability and lake zooplankton diversity – contrasting effects of chemical and thermal variability. *Ecol. Lett.* 13, 453–463. doi: 10.1111/j.1461-0248.2009.01438.x

Sommer, U., Sommer, F., Santer, B., Zöllner, E., Jürgens, K., Jamieson, C., et al. (2003). Daphnia versus copepod impact on summer phytoplankton: functional compensation at both trophic levels. *Oecologia* 135, 639–647. doi: 10.1007/s00442-003-1214-7

Striebel, M., Kirchmaier, L., and Hingsamer, P. (2013). Different mixing techniques in experimental mesocosms—does mixing affect plankton biomass and community composition? *Limnol. Oceanogr. Methods* 11, 176–186. doi: 10.4319/lom.2013.11.176

Suthers, I. M., and Rissik, D. (2009). *Plankton : A Guide to Their Ecology and Monitoring for Water Quality*. Collingwood: CSIRO.

Thrane, J.-E., Hessen, D. O., and Andersen, T. (2014). The absorption of light in lakes: negative impact of dissolved organic carbon on primary productivity. *Ecosystems* 17, 1040–1052. doi: 10.1007/s10021-014-9776-2

Thrane, J.-E., Kyle, M., Striebel, M., Haande, S., Grung, M., Rohrlack, T., et al. (2015). Spectrophotometric analysis of pigments: a critical assessment of a high-throughput method for analysis of algal pigment mixtures by spectral deconvolution. *PLoS One* 10:e0137645. doi: 10.1371/journal.pone.0137645

Tranvik, L. J. (1988). Availability of dissolved organic carbon for planktonic bacteria in oligotrophic lakes of differing humic content. *Microb. Ecol.* 16, 311–322. doi: 10.1007/bf02011702

Tranvik, L. J. (1998). "Degradation of dissolved organic matter in humic waters by bacteria," in *Aquatic Humic Substances*, eds D.O. Hessen and L. J. Tranvik (Berlin: Springer), 259–283. doi: 10.1007/978-3-662-03736-2_11

Traving, S. J., Rowe, O., Jakobsen, N. M., Sørensen, H., Dinasquet, J., Stedmon, C. A., et al. (2017). The effect of increased loads of dissolved organic matter on estuarine microbial community composition and function. *Front. Microbiol.* 8:351. doi: 10.3389/fmicb.2017.00351

Vadeboncoeur, Y., Jeppesen, E., Zanden, M. J. V., Schierup, H.-H., Christoffersen, K., and Lodge, D. M. (2003). From Greenland to green lakes: cultural eutrophication and the loss of benthic pathways in lakes. *Limnol. Oceanogr.* 48, 1408–1418. doi: 10.4319/lo.2003.48.4.1408

Verbeek, L., Gall, A., Hillebrand, H., and Striebel, M. (2018). Warming and oligotrophication cause shifts in freshwater phytoplankton communities. *Glob. Change Biol.* 24, 4532–4543. doi: 10.1111/gcb.14337

Wernand, M. R., Hommersom, A., and Van Der Woerd, H. J. (2013). MERIS-based ocean colour classification with the discrete Forel–Ule scale. *Ocean Sci.* 9, 477–487. doi: 10.5194/os-9-477-2013

Wikner, J., and Andersson, A. (2012). Increased freshwater discharge shifts the trophic balance in the coastal zone of the northern Baltic Sea. *Glob. Change Biol.* 18, 2509–2519. doi: 10.1111/j.1365-2486.2012.02718.x

Conflict of Interest: The authors declare that the research was conducted in the absence of any commercial or financial relationships that could be construed as a potential conflict of interest.

frontiers in Environmental Science

ORIGINAL RESEARCH
published: 09 October 2020
doi: 10.3389/fenvs.2020.540607

Phytoplankton Community Response to Changes in Light: Can Glacial Rock Flour Be Used to Control Cyanobacterial Blooms?

Jacob A. Gaskill[1], Ted D. Harris[2] and Rebecca L. North[1]*

[1] School of Natural Resources, University of Missouri, Columbia, MO, United States, [2] Kansas Biological Survey, University of Kansas, Lawrence, KS, United States

Cyanobacterial harmful algal blooms are one of the most prominent threats to water quality in freshwater ecosystems and are expected to become more common as the climate continues to change. While traditional strategies to manage algal blooms have focused on controlling nutrients, manipulating light as a way to reduce cyanobacteria is less frequently explored. Here, we propose the addition of glacial rock flour (GRF), a fine particulate that floats on the water's surface and remains suspended in the water column, to reduce light availability and in turn, phytoplankton biomass dominated by cyanobacteria. To determine if a sustained reduction in light could lower cyanobacteria biomass and microcystin concentrations, we applied GRF to large-scale (11 kL) mesocosm tanks for 9 consecutive days. Mesocosm tanks were amended by adding nitrogen and phosphorus to generate chlorophyte- and cyanophyte- dominated experimental tanks. To assess how the phytoplankton community was impacted in each tank, we measured photosynthetic irradiance parameters, the maximum quantum yield of photosystem II, gross primary productivity (GPP), phytoplankton biovolume, and phytoplankton community composition before and after the addition of GRF. GRF effectively reduced cyanophyte biovolume by 78% in the cyanophyte-dominated tanks, despite no significant change in total phytoplankton community biovolume. Cyanophytes were replaced by cryptophytes, which increased by 106% in the chlorophyte-dominated tanks and by 240% in the cyanophyte-dominated tanks. The change in photosynthetic irradiance parameters and GPP after the addition of GRF was not significantly different between any of the treatment or control groups, suggesting that either the cyanophytes will likely recover if light availability increases, or that the new cryptophyte-dominated community was well suited to a reduced light environment. Cyanobacterial blooms are expected to increase in frequency and magnitude as climate change progresses, but our study suggests that light manipulation may be a useful in-lake management strategy for controlling these blooms and warrants further investigation.

Keywords: algal blooms, climate change, functional traits, geoengineering, mesocosm tanks

OPEN ACCESS

Edited by:
Bas Ibelings,
Université de Genève, Switzerland

Reviewed by:
Guillaume Grosbois,
Swedish University of Agricultural Sciences, Sweden
Simone Jaqueline Cardoso,
Juiz de Fora Federal University, Brazil

****Correspondence:***
Jacob A. Gaskill
jagcgz@mail.missouri.edu

Specialty section:
This article was submitted to Freshwater Science, a section of the journal Frontiers in Environmental Science

Received: *05 March 2020*
Accepted: *08 September 2020*
Published: *09 October 2020*

Citation:
Gaskill JA, Harris TD and North RL (2020) Phytoplankton Community Response to Changes in Light: Can Glacial Rock Flour Be Used to Control Cyanobacterial Blooms? Front. Environ. Sci. 8:540607. doi: 10.3389/fenvs.2020.540607

INTRODUCTION

Cyanobacterial harmful algal blooms often occur in lakes and reservoirs with high nutrient concentrations (Heisler et al., 2008). These blooms are increasing in frequency and magnitude across the globe and are a threat to aquatic resources (Brooks et al., 2016). Cyanobacteria are of poor nutritional food quality compared to other phytoplankton taxa for zooplankton grazers, which rely on foods high in polyunsaturated fatty acids, and can cause inefficiencies in trophic transfers (Brett et al., 2009; Grosbois et al., 2017). Some cyanobacteria produce secondary metabolites, the most common of which is the cyanotoxin microcystin, that are toxic to animals and have been identified as potentially carcinogenic to humans (Grosse et al., 2006). Cyanotoxins have caused livestock (Van Halderen et al., 1995), pet (Backer et al., 2013), and wildlife (Miller et al., 2010) mortality and in extreme instances can result in human fatalities (Carmichael et al., 2001). Given the human and animal health hazard posed by cyanobacterial blooms, water body advisories and closures are common during bloom events, which can strain local economies during cyanobacterial outbreaks (Dodds et al., 2009).

Light is a critical resource for all phytoplankton. Phytoplankton use stored sugars and starches or rely on mixotrophy to temporarily survive in the absence of light (Lee, 2008), but prolonged light limitation can result in cell death or cause the cell to enter a resting phase (Bellinger and Sigee, 2010). Light requirements vary among individual taxa, and many cyanobacteria can be superior competitors at both low and high light intensities (Yang and Jin, 2008). Cyanobacteria are tolerant of reduced light conditions because of low maintenance energy requirements and their ability to maintain higher growth rates at lower light levels than many other phytoplankton (Van Liere and Mur, 1980). This tolerance allows them to persist deeper in the water column underneath other phytoplankton groups until conditions become favorable (Chorus and Bartram, 1999). Light also influences the ability of buoyancy regulating cyanobacteria to position themselves at a favorable depth in the water column. Low light levels induce gas vacuole production, giving the cell positive buoyancy (Deacon and Walsby, 1990), while high light intensities increase photosynthetic rates, allowing cells to store dense carbohydrate ballasts (Wallace and Hamilton, 2000). Cyanobacteria are also superior competitors under high light conditions due to their ability to withstand high levels of UV radiation (Paerl et al., 1983; Sinha and Häder, 2008). The ability to withstand variable light intensities may be allowing cyanobacteria to adapt to a changing climate more favorably compared to eukaryotic algae.

Cyanobacteria are anticipated to benefit from climate-induced environmental changes. Warmer water temperatures will favor cyanobacteria, many of which have peak growth rates at temperatures between 25 and 34°C (Robarts and Zohary, 1987; but see Lürling et al., 2013). Warming waters will result in earlier and stronger thermal stratification, which will benefit buoyancy regulating taxa (Paerl and Huisman, 2009). Projected climate change scenarios indicate that some states will experience more severe droughts while others will have higher rates of precipitation (U.S. Environmental Protection Agency, 2016). Extended droughts can increase the salinity of surface waters, which may favor cyanobacteria over other phytoplankton taxa (Paerl and Paul, 2012; Lehman et al., 2013). Higher rates of precipitation will result in increased nutrient runoff from the landscape, potentially leading to an increase in cyanobacterial blooms (Paerl and Paul, 2012). These impending climatic changes emphasize the need for a reliable method to mitigate cyanobacterial blooms.

A commonality among cyanobacterial management strategies is to reduce water column nutrient availability. Each management strategy has tradeoffs and no single strategy has been successful at controlling all types of cyanobacterial blooms (Ibelings et al., 2016). For example, beneficial management practices (BMPs) are often used to reduce external nutrient loading and subsequent cyanobacteria biomass (Sharpley et al., 2000). While BMPs can be effective, it can take several decades before noticeable improvements to water quality are observed (Osgood, 2017). Another strategy to control cyanobacterial blooms is to lower in-lake phosphorus (P) concentrations. Commercially available solid-phase P sorbents can reduce available P, and in turn cyanobacterial biomass, but these reductions are not permanent unless external nutrient loading is also reduced (Mackay et al., 2014). Where it is not always practical to reduce nutrient availability, other approaches could provide a more realistic way to reduce cyanobacterial blooms. One strategy is to negate the advantage that buoyancy regulation provides some taxa with approaches such as artificial mixing or lake flushing (Visser et al., 2016).

When nutrient reduction methods are not feasible, light reduction management strategies may help mitigate cyanobacterial blooms. To the best of our knowledge, the only management strategy designed to control algal growth by altering the light environment is the application of artificial dye products. These dyes come in a variety of colors, but all are designed to absorb incoming photosynthetically active radiation (PAR), thus reducing the amount available for aquatic photosynthesizers. These dyes are touted as environmentally friendly and published research shows they have no effect on fish, crayfish, nor tadpoles (Spencer, 1984; Bristow et al., 1996; Bartson et al., 2018), but can reduce zooplankton diversity (Suski et al., 2018). The main drawback to these dyes is that they are designed to control rooted macrophytes and have limited effectiveness in controlling cyanophyta, bacillariophyta, euglenophyta, or chlorophyta biomass (Ludwig et al., 2008). In this study, we designed an experiment to test the efficacy of an alternative way to reduce light availability through the addition of glacial rock flour (GRF).

Glacial rock flour is defined broadly as the fine particulate derived from glacial erosion and occurs naturally as the erosional silt- and clay-sized particles formed from a glacier passing over bedrock (Rampe et al., 2017). No standards exist to characterize it by size class or composition because GRF is composed of minerals reflecting the local geology in a lake catchment (Chanudet and Filella, 2009). As the glacier melts, either from seasonal receding (Casassa et al., 2009) or climate change (Moore et al., 2009), GRF runs off into the lake, often via a tributary. In glacial lakes, GRF attenuates 63% of the

total water column PAR (Rose et al., 2014). Lakes that receive glacial meltwater have reduced primary productivity due to the decreased light availability, though mixotrophic phytoplankton are less sensitive to this change in light than those who rely solely on photosynthesis (Slemmons et al., 2013; Sommaruga and Kandolf, 2014).

We conducted an experiment where we reduced light through the addition of GRF with the objective of decreasing cyanophyta biomass and microcystin concentrations. Phytoplankton growth was stimulated in mesocosm tanks with amendments of P, nitrogen (N), or a combination of both to produce phytoplankton communities dominated by either chlorophytes or cyanophytes. The light environment in experimental tanks was manipulated through the addition of GRF. We hypothesize that cyanophyte biovolume and microcystin concentrations would be impacted by GRF additions, and that this change would be reflected in the physiology and primary productivity of the phytoplankton community. Our results have important implications for the future management of our changing water bodies.

MATERIALS AND METHODS

Experimental Design and Sample Collection

This experiment was conducted at the University of Kansas field station in Lawrence, KS, United States (39.049674°N, 95.190777°W) in closed bottom, fiberglass mesocosm tanks. Each was filled to a volume of 11,000 L and depth of 1.25 m. To insulate from fluctuations in air temperatures, mesocosm tanks were kept in a ∼1,300 m^2 shallow pond and were surrounded with ∼1 m of water (**Figure 1**). The insulation pond was surrounded by low vegetation, mainly grasses and wildflowers that were mowed periodically throughout the summer (**Supplementary Figure 1**). The closest trees were over 100 m away from the mesocosm tank set. Tanks were positioned within 50 cm of each other and were accessed via anchored walkways. On July 23, 2018, we filled each tank with 10,840 L of water from an on-site storage impoundment, then inoculated each tank with 160 L of surface water from a nearby reservoir (Milford Lake, KS, United States) with a well-documented history of cyanobacterial harmful algal blooms (Harris et al., 2020). For 8 consecutive weeks prior to the beginning of our experiment, 20 of the 23 mesocosm tanks received weekly N and P amendments. Treatments were designed to result in tanks with N- or P- deficient conditions for phytoplankton growth. Three tanks were maintained as ambient control tanks and received no nutrient nor GRF additions (**Table 1**). Each tank was randomly assigned a nutrient amendment, or in the case of the controls, no nutrient amendment.

A preliminary experiment was conducted on 6 of the 20 amended tanks to assess the quantity of GRF required to achieve the greatest reduction in light. We compared light conditions in tanks that received zero (n = 3), 5 (n = 2), 10 (n = 2), and 20 (n = 2) kg of GRF and determined that adding more than 5 kg of GRF did not result in any additional reduction in light based on no significant difference in PAR among tanks that received the 3 doses of GRF (Kruskal-Wallis p = 0.2551, df = 3, χ^2 = 18.01). We chose 5 kg of GRF as the optimum quantity to add in our subsequent experiment (**Supplementary Figure 2**). The 6 tanks that received GRF during this preliminary experiment were then removed from the experiment described below.

The GRF used was commercially available from Vital Earth's®. Its elemental composition was determined in triplicate by Activation Laboratories Ltd. (ActLabs, Ancaster, ON) via lithium metaborate/tetraborate fusion followed by aqueous phase analyses using inductively coupled plasma (ICP)–optical emission spectrometry (OES) and ICP–mass spectrometry (MS) for major and trace elements, respectively (**Supplementary Table 1**). We determined GRF sediment particle fractionation using a hydrometer (Gee and Bauder, 1979). Sediment particles were measured in the following size fractions: 0.5 – 2 mm (sand), 0.002 – 0.05 mm (silt), and < 0.002 mm (clay). GRF was 18.3% sand, 70.7% silt, and 11.2% clay. We did not explicitly test for any biota associated with the GRF.

Algal communities were created by weekly nutrient amendments by adding different forms of nutrients so that algal communities would vary (**Table 1**). We kept tanks that received the same nutrient forms together, even if a single tank in the group was not dominated by the same phytoplankton. We included 1 tank in the chlorophyte-dominated group where chlorophytes only comprised 9.2% of the total biovolume (Tank #3, **Supplementary Table 2**). Cryptophytes were the dominant taxa in this tank on day 0 (71.2%), but we decided to include it with the other tanks that received the same nutrient amendments because we do not believe excluding it would have changed our results. If this tank were excluded, cryptophyte biovolume would have increased in the 5 remaining chlorophyte-dominated tanks by 111.0% between day 0 and day 9, compared to an increase of 105.7% if the tank were included. In 1 of the cyanophyte-dominated tanks as well, cyanophytes were not the dominant taxa on day 0, comprising only 14.3% (Tank #11, **Supplementary Table 2**). We included this tank for the same reasons. When it was included, cryptophytes increased by 240.0% between day 0 and day 9. When this tank was excluded, they increased by 408.0%. Ultimately, we considered phytoplankton dominance to be the taxa with the highest biovolume, averaged across all tanks within the group. On day 0, 6 of the 17 tanks were included in the chlorophyte-dominated group (biovolume mean and range = 1.51, 0.06 – 3.11 mm^3 L^{-1}; % of total phytoplankton biovolume mean and range = 51.4, 9.2 – 89.4%) and 8 were included in the cyanophyte-dominated group (biovolume mean and range = 28.17, 0.98 – 71.87 mm^3 L^{-1}; % of total biovolume mean and range = 71.3, 14.3 – 92.0%). *Oocystis* was the most prevalent phytoplankton in chlorophyte-dominated tanks, comprising a mean 35.4% of total phytoplankton biovolume (range = 0 – 86.9%), while *Aphanizomenon*, which comprised a mean 22.8% total phytoplankton biovolume (range = 0 – 49.4%), was the most prevalent phytoplankton in cyanophyte-dominated tanks (**Table 2** and **Supplementary Table 2**). Control tanks (n = 3) were also dominated by chlorophytes (biovolume mean and range = 3.17, 0.28 – 8.08 mm^3 L^{-1}; % of total biovolume mean and range = 52.3, 25.1 – 82.0%) when the experiment

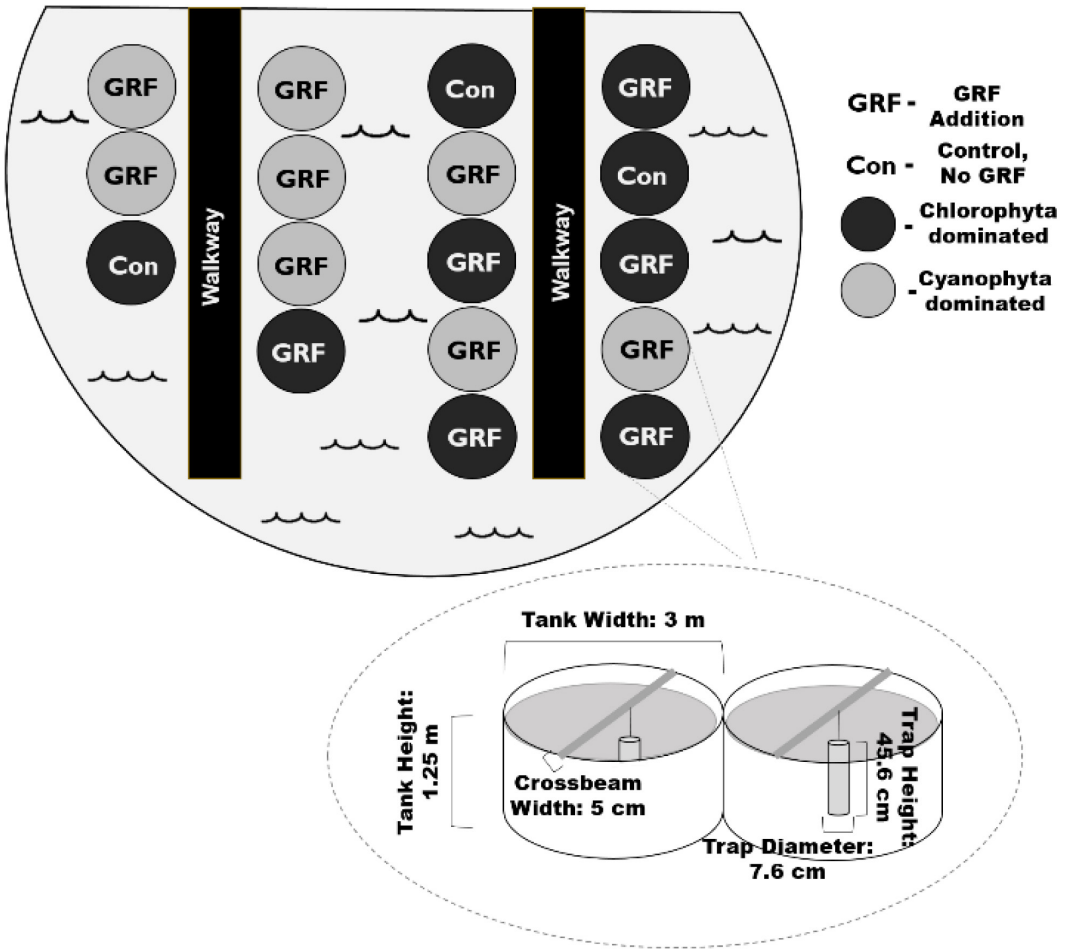

FIGURE 1 | Birds-eye view of mesocosm tank set-up. We added glacial rock flour (GRF) to 14 of the 17 mesocosm tanks used in this experiment. Phytoplankton communities were dominated by either chlorophytes or cyanophytes (n = 8) at the beginning of the experiment. Of the 9 chlorophyte dominated tanks, a subset (n = 3) did not receive any nutrient nor GRF amendments and were treated as a control (Con). The remaining chlorophyte dominated tanks (n = 6) received daily GRF additions. Tanks were kept in a ∼1300 m^2 shallow pond that was ∼1 m deep to insulate for changes in air temperatures. The pond was surrounded by low vegetation. Mesocosm tanks were ∼3 m across, 1.25 m high, and had a volume of 11,000 L. Crossbeams were placed across each mesocosm. Sediment traps were suspended from each crossbeam.

began, particularly from the genus *Tetraedron*, which comprised a mean 26.2% of total phytoplankton biovolume (range = 0 – 78.5%, **Table 2** and **Supplementary Table 2**). We added GRF to each of the chlorophyte- and cyanophyte-dominated treatment tanks, exclusive of the 3 control tanks. For 9 consecutive mornings between 9:00–10:30 AM (CST), we distributed 5 kg of GRF evenly across the surface of each tank with a sifter. GRF was allowed to float on the tank surface, although some mixed into the water column over the next 24 h. PAR measurements were taken in the air above the water surface, just below the water's surface, 0.5, and 1 m below the surface in each tank using a cosine Li-Cor underwater quantum sensor (LI-192). To account for changes in PAR from the time we measured the first tank to the time that we measured the last, we corrected each underwater PAR measurement by dividing it by the air PAR measurement we made above the water's surface. We report this value as the PAR ratio (0.5 m water/air reading). To ensure that a reduction in light was maintained throughout the entire day, light was measured one hour after GRF addition on all experimental days, 4 h after GRF addition on days 0, 5, 6, and 7, and 6 h after GRF addition on day 4. PAR measurements from just below the surface, 0.5, and 1 m below the surface, were used to determine the light attenuation coefficient (K_d) in all tanks from the natural logarithm of irradiance versus depth (Kirk, 1994). Temperature profiles were collected from just below the surface, 0.5, and 1 m below the surface using a Yellow Springs Instrument EXO3, which is accurate to ± 0.01°C.

We collected water samples from each tank on days 0 and 9 with a PVC integrated sampler with a check valve from the surface to a depth of 1.0 m to avoid collecting or resuspending any material that had settled to the tank bottom. We then filtered water samples onto pre-combusted, 1.2 μm, GF/C filters for total suspended solids (TSS), which were frozen until analysis. Integrated whole water for total

TABLE 1 | Experimental design to promote phytoplankton growth through nutrient amendments.

Nutrient forms added	Amount N and/or P added (moles)	Experimental group	ln(TN:TP) (molar ratio)
$NH_4Cl + K_2HPO_4$ (n = 3)	3.08N + 2.20P	cyanophyte-dominated	3.73
$NaNO_3 + K_2HPO_4$ (n = 3)	3.08N + 2.20P	cyanophyte-dominated	3.12
K_2HPO_4 (n = 2)	2.20	cyanophyte-dominated	3.29
NH_4Cl (n = 3)	3.08	chlorophyte-dominated	4.52
$NaNO_3$ (n = 3)	3.08	chlorophyte-dominated	4.95
None (n = 3)	0	control	4.61

Nitrogen (N) and/or phosphorus (P) were added to 11,000 L mesocosm tanks to create bloom conditions and induce nutrient deficiency. A total of 3.08 moles of N was added as ammonium chloride (NH_4Cl) or sodium nitrate ($NaNO_3$), and 2.20 moles of P was added as dipotassium phosphate (K_2HPO_4). Control tanks did not receive nutrient amendments and were dominated by chlorophytes at the beginning of the experiment. The ln(TN:TP) molar ratio is from day 0 of the experiment. Sample size (n) refers to the number of mesocosm tanks that received each nutrient form.

TABLE 2 | Top 3 dominant phytoplankton genera on day 0 and day 9.

	Dominant Algal Genus on Day 0			Dominant Algal Genus on Day 9		
Experimental Group	**Functional Group**	**Genus**	**% Comp.**	**Functional Group**	**Genus**	**% Comp.**
Control	Chlorophyta	*Tetraedron*	26.2	Chlorophyta	*Tetraedron*	23.4
	Chlorophyta	*Scenedesmus*	13.8	Chlorophyta	*Scenedesmus*	12.5
	Cryptophyta & Dinoflagellates	*Cryptomonas*	13.6	Cryptophyta & Dinoflagellates	*Plagioselmis*	12.0
Chlorophyte-Dominated	Chlorophyta	*Oocystis*	35.4	Cryptophyta & Dinoflagellates	*Cryptomonas*	32.2
	Cryptophyta & Dinoflagellates	*Cryptomonas*	9.6	Chrysophyta	*Chrysochromulina*	14.7
	Chrysophyta	*Chrysochromulina*	7.3	Chlorophyta	*Oocystis*	10.7
Cyanophyte-Dominated	Potentially Toxigenic Cyanophyta	*Aphanizomenon*	22.8	Cryptophyta & Dinoflagellates	*Cryptomonas*	37.1
	Potentially Toxigenic Cyanophyta	*Dolichospermum*	22.1	Potentially Toxigenic Cyanophyta	*Aphanizomenon*	13.8
	Non-toxin Producing Cyanophyta	*Pseudanabaena*	13.3	Chlorophyta	*Scenedesmus*	9.8

*Percent composition (% Comp.) was calculated for each genera as the percent of total phytoplankton biovolume in each tank. The mean percent composition of all tanks within each group is reported for control (n = 3), chlorophyte- (n = 6), and cyanophyte-dominated (n = 8) mesocosm tanks. Lowest taxonomic identification was down to genus (**Supplementary Table 2**).*

P (TP) and total N (TN) analyses were stored in glass digestion test tubes. Filtrate from 0.7 μm glass fiber filters (GFF) was also stored in glass digestion test tubes within 30 h of collection to measure total dissolved P (TDP) and total dissolved N (TDN). Filtrate from 0.45 μm nitrocellulose membrane filters was frozen for nitrate (NO_3^-) and ammonium (NH_4^+) analysis. Dissolved organic carbon (DOC) samples were stored frozen as filtrate from pre-combusted, 0.7 μm GFF filters. A subset of the integrated water sample was immediately frozen at −20°C in amber, HDPE bottles for microcystin analysis. Samples for phytoplankton identification and enumeration were collected by taking a subset of the integrated water sample and preserving it with 1% Lugols solution in amber vials. Within 30 h of collection, water filtered onto 0.7 μm GF/F filters were frozen until they were analyzed for chlorophyll-*a* (chl-*a*) and the phytoplankton pigment absorption coefficient (α_ϕ). Whole water for P–E parameters, gross primary production (GPP), and the maximum quantum yield of photosystem II (ϕ_{PSII}) were stored in the dark prior to running on the Water-Pulse Amplitude Modulated fluorometer (PAM, Heinz Walz GmbH) within 30 h of collection.

We collected samples for zooplankton identification and enumeration throughout the entire water column of each tank (1.25 m deep) using a 243 μm Wisconsin net (diameter = 200 mm) raised at approximately one-third of a meter per second. Zooplankton samples were immediately preserved with 4% formalin for enumeration.

We used sediment traps, positioned 0.5 m below the water's surface, to determine sedimentation rates in each tank. Sediment traps were constructed from PVC with a 7.6 cm diameter and 6:1 height to aspect ratio (Bloesch and Burns, 1980). On each sampling date, the entire 2 L sediment trap was emptied into a HDPE collection bottle and homogenized by inverting 3 times. A portion of homogenized water was retained on pre-combusted, 1.2 μm, GF/C filters and later analyzed for TSS.

Laboratory Analyses

We measured TSS from both whole water integrated samples and sediment traps using standard methods (Section 2540 D

and E; APHA 2017). Pre-weighed filters with retained material were dried at 105°C for 30 min and then weighed. Filters were then incinerated at 550°C for 20 min to burn off organic material before being weighed again. This loss-on-ignition analysis allowed us to differentiate TSS by subtracting the mass left after incineration, which is particulate inorganic matter (PIM), from the total filter mass before incineration, which is TSS. The difference is particulate organic matter (POM). TSS had a detection limit of 0.1 mg L^{-1}. We determined sedimentation rates from the TSS measured in our sediment traps using (Kalff, 2002):

$$\text{Sedimentation Rate} = \frac{\text{Subsample Dry Weight } (\text{mg}) \times \text{Total Sample Vol. } (\text{cm}^3)}{10 \times \text{Subsample Vol. } (\text{cm}^3) \times \text{Trap Area } (\text{cm}^2) \times \text{Period (day)}}$$

Total sample volume was always 2000 cm^3, sediment trap area was 45.6 cm^2, and the period that traps were deployed was 9 days.

Mean daily mixed layer irradiance ($\bar{E}_{24}$) is a measure of the amount of light phytoplankton in the mixed layer are exposed to over 24 h. It was calculated using the formula:

$$\bar{E}_{24} = \bar{E}_0 \times (1 - \exp(-1 \times K_d \times Z_{mix})) \times (K_d \times Z_{mix})^{-1}$$

Incident irradiance, $\bar{E}_0$, was calculated as the 24 h mean of PAR measurements taken at an onsite meteorological station (Natural Resources Conservation Service, site Ku-Nesa[1]) on day 0 (9/24/18) and day 9 (10/2/18). Mixing depth within each tank, Z_{mix}, was calculated from temperature profiles using the rLakeAnalyzer package (Winslow et al., 2017). Profiles were taken one hour after GRF addition on all experimental days, 4 h after GRF addition on days 0, 5, 6, and 7, and 6 h after GRF addition on day 4. Occasionally, tanks would temporarily stratify in the afternoon between the water's surface and 0.5 m. Tanks were isothermal every morning, indicating that even if a tank did stratify at the end of the previous day, it mixed during the night. We used the maximum depth of each tank, 1.25 m, as the value for Z_{mix} when calculating $\bar{E}_{24}$.

Total P and TDP were measured spectrophotometrically using the ascorbic acid colorimetric method (Section 4500-P E; APHA, 2017) with a detection limit of 0.03 μmol L^{-1}. TN and TDN were measured with the second derivative spectroscopy procedure (Crumpton et al., 1992) with a detection limit of 2.50 μmol L^{-1}. Total and total dissolved P and N samples were measured in triplicate. NO_3^-, which was measured in duplicate on a Lachat QuikChem Flow Injection Analyzer (Lachat Method 10-107-04-1-B/C), had a detection limit of 0.36 μmol L^{-1}. This method reports NO_3^- as NO_3^- plus nitrite (NO_2^-) based on the assumption that environmental NO_2^- concentrations are minimal. We measured NH_4^+ in duplicate on a Lachat QuikChem Flow Injection Analyzer (Lachat Method 10-107-06-1-K) based on the Berthelot reaction with a limit of detection of 0.71 μmol L^{-1}. We report NH_4^+ as NH_3 plus NH_4^+. We measured DOC in duplicate using a Shimadzu total organic C analyzer with the high-temperature combustion method (Section 5310B; APHA, 2017), with a limit of detection of 16.7 μmol L^{-1}. Intracellular microcystin was extracted via 3 freeze-thaw cycles from whole water samples, which were then filtered through 0.45 μm GFFs. We measured total microcystin, both the intracellular microcystin previously released from freeze-thaw cycles and the extracellular microcystin present in the water, using indirect competitive ELISA (Enzyme Linked Immunosorbent Assay) kits from Abraxis LLC, which have a limit of detection of 0.15 μg L^{-1}. Chl-*a* concentrations were quantified fluorometrically with a Turner Design Fluorometer (TD-700) after ethanol extraction and phaeophytin acid-correction (Knowlton, 1984; Sartory and Grobbelaar, 1986). The chl-*a* detection limit was 0.09 μg L^{-1}.

Phytoplankton were identified to genus (**Supplementary Table 2**) by BSA Environmental Services Inc. (Guiry and Guiry, 2020), and enumerated using the Ütermohl method (Lund et al., 1958). Phytoplankton were allowed to settle for at least 20 h in a dark enclosure protected from vibrations and temperature changes prior to enumeration (Burkholder and Wetzel, 1989). Cell biovolume estimates are based on measurements from 10 cells in each taxon and were calculated using the formula of Hillebrand et al. (1999) for solid geometric shapes that most closely match cell shape. All enumerations were conducted using a LEICA DMiL inverted microscope at 800 × and 1260 × magnification, depending on the size of the dominant taxa, particulates, and variation in the range of taxon sizes. Heterocyte abundance was calculated for all phytoplankton samples. It is beneficial to group phytoplankton into functional groups when trying to understand ecological function (Salmaso et al., 2015). For example, both cryptophytes and dinoflagellates have 2 flagella, are known to participate in diel vertical migrations to take advantage of both the nutrient-rich hypolimnion and light-replete surface waters, and can supplement metabolic requirements with mixotrophy (Raven and Richardson, 1984; Lee, 2008). We classified phytoplankton by the following 6 taxonomic groups: (1) potentially toxigenic cyanophyta (Chapman and Foss, 2019), (2) non-toxin producing cyanophyta, (3) chlorophyta, (4) euglenophyta, (5) cryptophyta and dinoflagellates, and (6) chrysophyta, including chrysophytes, bacillariophyta, ochrophytes, and haptophytes (**Supplementary Table 3**).

We assessed phytoplankton physiology, including ϕ_{PSII}, P–E parameters (alpha normalized to chl-*a* [α^B], the light saturation threshold normalized to chl-*a* [$E_k{}^B$], and the maximum relative electron transport rate [$rETR_{MAX}$]), and gross primary productivity normalized to chl-*a* (GPP^B) following the procedures outlined in Petty et al. (2020). Within 30 h of collection, we measured ϕ_{PSII} in triplicate with a Water-PAM fluorometer on whole, integrated water that had been dark adapted for 30 min. Water samples were corrected for background fluorescence with 0.2 μm PTFE sample water filtrate. We also used the Water-PAM to perform rapid light curves. For each light curve, the light limited slope (α) and light saturation threshold (E_k) were defined as ϕ_{PSII} fit against

[1]https://wcc.sc.egov.usda.gov/nwcc/site?sitenum=2147

irradiance to a light intensity (E) using the normalized version of Webb et al. (1974):

$$\alpha \times E_k \times (1 - e(-E \times E_k)) \times E^{-1}$$

where $rETR_{MAX}$ was the product of α and E_k. We divided $\bar{E}_{24}$ by E_k to assess light deficiency within each tank. When this ratio is above 1, light availability is greater than phytoplankton light saturation and light does not limit photosynthesis. Below 1, phytoplankton do not receive enough light to reach saturation and may experience light deficiency (Hecky and Guildford, 1984). The areal pigment absorption coefficient (α_ϕ), a factor in our calculation of GPP^B, was quantified using the quantitative filter technique by measuring absorbance at 350 – 750 with a scanning spectrophotometer (Agilent Cary60 UV/VIS) before and after depigmentation with a sodium hypochlorite solution (4.00 – 4.99% available chlorine). a_ϕ was then calculated using:

$$a_\phi = 2.303 \times (A_P - A_{NAP}) \times \beta^{-1} \times (V_f/A_f)^{-1}$$

where A_P is absorption before and A_{NAP} is absorption after depigmentation, β is the path-length amplification factor to adjust for differences in absorption between water and filter, and V_f/A_f is the ratio of volume of water filtered to the filter area (Silsbe et al., 2012). We determined GPP using the R package phytotools (Silsbe and Malkin, 2015). This package is based on the primary production model of Fee (1990) and incorporates chl-*a*, P–E parameters, a_ϕ, K_d, and $\bar{E}_0$.

Zooplankton were enumerated by the Central Plains Center for Bioassessment to the following taxonomic groups: cladocerans, adult copepods, and copepod nauplii (Thorp and Covich, 2001). Before being photographed, samples were switched from the 4% fixation preservative from the field to 80% ethanol. Images of each zooplankton were taken using a Motic Plus 2.0 digital camera at 10 × magnification (87.7 pixels mm^{-1}) using Image-J software (National Institutes of Health, Bethesda, MD, United States). All abundance calculations of each zooplankton taxa assumed 100% net filtering efficiency.

Statistical Analyses

A Shapiro–Wilk test was used to test for normality and a Levene's test to assess homoscedasticity. The alpha value for all statistical tests was set at 0.05. All statistical analyses were performed in Program R (R Core Team, 2019) and all figures were created using the ggplot2 package (Wickham, 2009).

We tested for a significant difference in K_d and the PAR ratio (0.5 m water/air reading) between tanks that received GRF and the control tanks that did not receive GRF. We took the mean of control (n = 3) and GRF (n = 14) tanks. Neither parameter was normally distributed, even after transformation, so we used a Kruskal–Wallis test to look for significant differences at one, 4, and 6 h after GRF addition and a Dunn's *post hoc* test to identify where significant differences existed.

Unless stated otherwise, statistical analyses were performed on the change in each parameter between days 0 and 9. We calculated this change by subtracting the value for each parameter on day 9 from the value for that parameter on day 0 (i.e., day 9 - day 0). Positive values indicate an increase in the parameter on day 9, while negative values indicate a decrease. We used a One-Way Analysis of Variance (ANOVA) to test whether the change in each parameter was significantly different between the control (n = 3), chlorophyte-dominated (n = 6), and cyanophyte-dominated (n = 8) tanks. In instances where a parameter was not normally distributed, even after transformation, we used a Kruskal–Wallis test. When a significant difference did exist, we used a Tukey *post hoc* to identify significant differences for parameters that followed a parametric distribution, and a Dunn's test on parameters that did not follow a normal distribution. For tanks where the microcystin concentrations were below the limit of detection, we used the limit of detection, 0.15 μg L^{-1}, for statistical analyses. We compared chl-*a* concentrations and phytoplankton biovolume to assess photoacclimation. Neither chl-*a* nor biovolume were normally distributed, even after transformation, so we used the non-parametric Spearman's Rank correlation to assess the relationship between these 2 variables.

RESULTS

Physical Parameters

We assessed water clarity by measuring K_d and the PAR ratio (0.5 m water/air reading) in each tank. K_d was significantly higher (Kruskal–Wallis $p < 0.0001$, df = 1, $\chi^2 = 118.84$) and the PAR ratio (Kruskal–Wallis $p < 0.0001$, df = 1, $\chi^2 = 112.18$) was significantly lower in tanks that received GRF. The PAR ratio was significantly lower one hour after GRF addition than 4 (Kruskal–Wallis $p < 0.0001$, df = 2, $\chi^2 = 26.46$) or 6 hours (Kruskal–Wallis $p = 0.0002$, df = 2, $\chi^2 = 26.46$), but not significantly different between 4 and 6 h (Kruskal–Wallis $p = 0.1709$, df = 2, $\chi^2 = 26.46$; **Figure 2**). In tanks that received GRF, K_d was significantly higher one hour after GRF addition than 4 (Kruskal–Wallis $p < 0.0001$, df = 2, $\chi^2 = 37.10$) or 6 (Kruskal–Wallis $p < 0.0001$, df = 2, $\chi^2 = 37.10$) hours, but not significantly different between 4 and 6 h (Kruskal–Wallis $p = 0.2347$, df = 2, $\chi^2 = 37.10$; **Figure 2**). K_d was ∼3 × higher in tanks that received GRF compared to the control tanks (**Figure 2**). Tanks that received GRF had PAR ratios 86.4, 60.4, and 67.7% lower, and mean K_ds 80.5, 73.6, and 68.8% higher, compared to control tanks for one, 4, and 6 h after GRF application, respectively.

Water temperatures remained below 25°C throughout the experiment (**Table 3**). The change in temperature over the course of the experiment was not significantly different between control, chlorophyte-, and cyanophyte- dominated tanks (**Table 4** and **Supplementary Figure 3**).

Mean TSS sedimentation rates were 0.1 g m^{-2} day^{-1} (range = below detection limit [BDL] – 0.1 g m^{-2} day^{-1}) in control, 1.9 g m^{-2} day^{-1} (range = 0.8 – 2.9 g m^{-2} day^{-1}) in chlorophyte-dominated, and 2.3 g m^{-2} day^{-1} (range = 1.0 – 3.4 g m^{-2} day^{-1}) in cyanophyte-dominated tanks. Mean PIM sedimentation rates were BDL (range = BDL – 0.1 g m^{-2} day^{-1}) in control, 1.9 g m^{-2} day^{-1} (range = 0.8 – 2.8 g m^{-2} day^{-1}) in chlorophyte-dominated, and 2.2 g m^{-2} day^{-1} (range = BDL – 0.1 g m^{-2} day^{-1}) in cyanophyte-dominated tanks. Mean POM

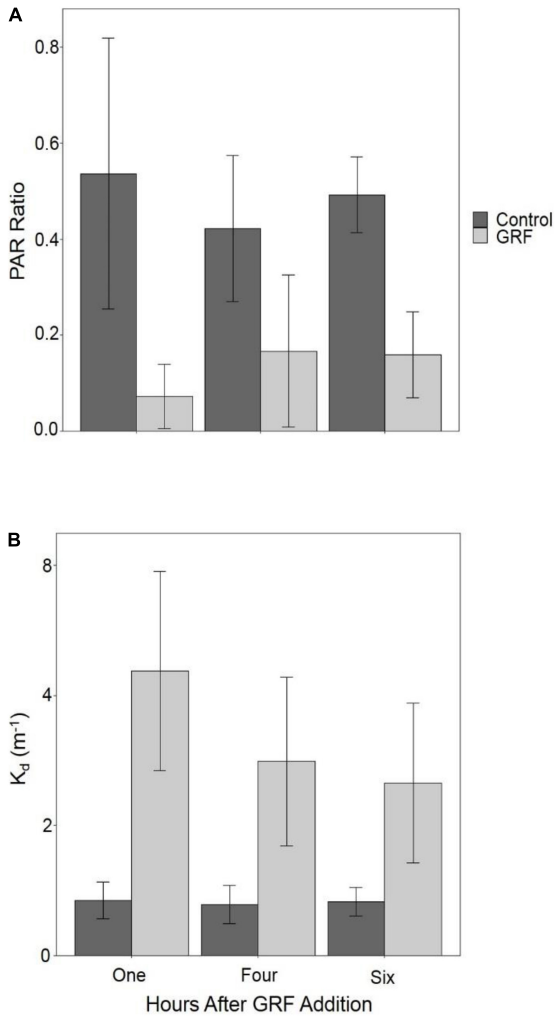

FIGURE 2 | Comparison of the light environment between tanks that received glacial rock flour (GRF) and tanks that did not receive GRF. PAR ratio (0.5 m water/air reading; **(A)** and vertical light attenuation coefficient (K_d; **B**) were measured in all tanks after GRF was added to all (n = 14) but the control tanks (n = 3). Both the PAR ratio and K_d were measured one hour after GRF addition every day of the experiment, 4 hours after addition on days 0, 5, 6, and 7, and 6 h after addition on day 4. The light ratio was determined by dividing photosynthetically active radiation (PAR) measurements made at 0.5 m depth by PAR measurements from above the water's surface in the air. Among GRF tanks, the light ratio was significantly lower one hour after GRF addition than 4 (Kruskal–Wallis $p < 0.0001$, df = 2, $\chi^2 = 26.46$) or 6 h (Kruskal–Wallis $p = 0.0002$, df = 2, $\chi^2 = 26.46$), but not significantly different between 4 and 6 hours (Kruskal-Wallis $p = 0.1709$, df = 2, $\chi^2 = 26.46$; **Figure 2**). K_d was significantly higher one hour after GRF addition (Kruskal–Wallis $p < 0.0001$, df = 2, $\chi^2 = 37.10$), but not 4 nor 6 hours after addition (Kruskal–Wallis $p = 0.2347$, df = 2, $\chi^2 = 37.10$). For each time, the light ratio was significantly lower (Kruskal–Wallis $p < 0.0001$, df = 1, $\chi^2 = 75.99$) in tanks that received GRF compared to control tanks that did not. For each time, K_d was significantly higher (Kruskal–Wallis $p < 0.0001$, df = 1, $\chi^2 = 87.88$) in tanks that received GRF compared to control tanks that did not.

sedimentation rates were always BDL in control and 0.1 g m^{-2} day^{-1} (range = BDL – 0.1 g m^{-2} day^{-1}) in both chlorophyte- and cyanophyte-dominated tanks (**Table 3**).

Between days 0 and 9, $\bar{E}_{24}$ increased from 106.67 to 115.45 μmol photons m^{-2} s^{-1} in control, and from 57.14 to 64.36 μmol photons m^{-2} s^{-1} in cyanophyte-dominated tanks. $\bar{E}_{24}$ decreased from 114.16 to 110.66 μmol photons m^{-2} s^{-1} in chlorophyte-dominated tanks (**Table 3** and **Supplementary Figure 3**). The change in $\bar{E}_{24}$ throughout the experiment was not significantly different between the control, chlorophyte-, and cyanophyte- dominated tanks (**Table 4**). The $\bar{E}_{24}$ values we observed throughout the experiment were above the light deficiency threshold of 41.7 μmol photons m^{-2} s^{-1} (Hecky and Guildford, 1984) in all tanks.

Water Chemistry

We report all water chemistry parameters as the mean of control, chlorophyte-, and cyanophyte- dominated mesocosm tanks (**Table 3**). To determine the influence of GRF on water chemistry, we examined the change in each parameter between day 9 and day 0 and tested to see if this change was different between the control, chlorophyte-, and cyanophyte- dominated tanks, but in most cases it was not (**Tables 3**, **4**). The change in water column TSS, PIM, and POM was not significantly different between any of the experimental groups. TSS increased from 0.8 to 3.1 mg L^{-1}, from 1.5 to 7.3 mg L^{-1}, and from 4.5 to 20.2 mg L^{-1} in the control, chlorophyte-, and cyanophyte-dominated tanks, respectively. PIM decreased from 0.4 to 0.3 mg L^{-1} in the control, but increased from 1.0 to 5.5 mg L^{-1} and from 2.2 to 10.5 mg L^{-1} in the chlorophyte- and cyanophyte-dominated tanks, respectively. POM increased in the control and cyanophyte-dominated tanks from 0.9 to 2.8 mg L^{-1} and from 6.6 to 9.7 mg L^{-1}, respectively, but decreased in the chlorophyte-dominated tanks from 2.9 to 1.8 mg L^{-1} (**Table 3** and **Supplementary Figure 3**).

TP concentrations decreased from 0.74 to 0.67 μmol L^{-1} in the control and from 5.89 to 3.85 μmol L^{-1} in the cyanophyte-dominated tanks. All cyanophyte-dominated tanks received P amendments for 8 weeks prior to the beginning of the experiment (**Table 1**). The change in TP concentrations was not significantly different between the control and chlorophyte-dominated, nor the control and cyanophyte-dominated tanks (**Table 4**). TP concentrations were unchanged over the course of the experiment in the chlorophyte-dominated tanks (mean = 0.57 μmol L^{-1}; **Table 3** and **Supplementary Figure 4**). The change in TP concentrations between days 9 and 0 in the cyanophyte-dominated tanks was significantly greater than the change between days 9 and 0 in the chlorophyte-dominated tanks.

The change in TN concentrations between days 9 and 0 was not significantly different between the control, chlorophyte-, and cyanophyte- dominated tanks (**Table 4**). TN concentrations were stable in the control and chlorophyte-dominated, but decreased from 163.06 to 153.54 μmol L^{-1} in the cyanophyte-dominated tanks (**Table 3** and **Supplementary Figure 4**).

The TN:TP molar ratio can serve as an indicator of phytoplankton nutrient deficiency. We report the natural log (ln) of the TN:TP ratio as this transformation reduces bias inherent with calculating the mean of a ratio (Isles, 2020). If the ln(TN:TP)

TABLE 3 | Water quality and phytoplankton physiology parameters. Control (Con), chlorophyte- (Chloro), and cyanophyte- (Cyano) dominated mesocosm tanks prior to glacial rock flour addition (day 0) and at the end of the experiment (day 9).

	Day 0 Mean ± Std Dev			Day 9 Mean ± Std Dev		
	Con ***n = 3***	**Chloro** ***n = 6***	**Cyano** ***n = 8***	**Con** ***n = 3****	**Chloro** ***n = 6***	**Cyano** ***n = 8***†
Physical Parameters						
Temperature (°C)	21.1 ± 0.1	21.2 ± 0.1	20.8 ± 0.1	18.6 ± 0.1	18.6 ± 0.2	18.4 ± 0.1
Total Suspended Solids, TSS ($mg\ L^{-1}$)	0.8 ± 0.6	1.5 ± 0.6	4.5 ± 1.7	3.1 ± 1.2	7.3 ± 2.2	20.2 ± 7.7
Particulate Inorganic Matter, PIM ($mg\ L^{-1}$)	0.4 ± 0.3	1.0 ± 0.5	2.2 ± 0.6	0.3 ± 0.2	5.5 ± 1.8	10.5 ± 5.2
Particulate Organic Matter, POM ($mg\ L^{-1}$)	0.9 ± 1.0	2.9 ± 2.4	6.6 ± 6.7	2.8 ± 1.2	1.8 ± 0.7	9.7 ± 5.2
TSS Sedimentation Rate ($g\ m^{-2}\ day^{-1}$)	n/a	n/a	n/a	0.1 ± 0.0	1.9 ± 0.8	2.3 ± 0.9
PIM Sedimentation Rate ($g\ m^{-2}\ day^{-1}$)	n/a	n/a	n/a	0.0 ± 0.0	1.9 ± 0.8	2.2 ± 0.9
POM Sedimentation Rate ($g\ m^{-2}\ day^{-1}$)	n/a	n/a	n/a	0.0 ± 0.0	0.1 ± 0.0	0.1 ± 0.0
Mean daily mixed layer irradiance, $\bar{E}_{24}$ ($\mu mol\ photons\ m^{-2}\ s^{-1}$)	106.67 ± 11.64	114.16 ± 10.69	57.14 ± 19.64	115.45 ± 9.55	110.66 ± 14.07	64.36 ± 22.67
Chemical Parameters						
Total Nitrogen:Total Phosphorus, ln(TN:TP) (molar ratio)	4.61 ± 0.39	4.74 ± 0.40	3.39 ± 0.40	4.67 ± 0.33	4.70 ± 0.28	3.72 ± 0.22
Total Phosphorus, TP ($\mu mol\ L^{-1}$)	0.74 ± 0.42	0.57 ± 0.18	5.89 ± 2.05	0.67 ± 0.34	0.56 ± 0.09	3.85 ± 1.53
Total Dissolved Phosphorus, TDP ($\mu mol\ L^{-1}$)	0.25 ± 0.10	0.16 ± 0.01	1.52 ± 1.61	0.23 ± 0.04	0.18 ± 0.03	1.27 ± 0.58
Total Nitrogen, TN ($\mu mol\ L^{-1}$)	65.43 ± 9.25	62.09 ± 5.63	163.06 ± 35.41	64.45 ± 9.58	61.68 ± 7.83	153.54 ± 46.67
Total Dissolved Nitrogen, TDN ($\mu mol\ L^{-1}$)	49.92 ± 4.12	53.71 ± 6.82	93.20 ± 22.17	51.80 ± 4.74	55.88 ± 8.83	91.16 ± 23.28
Nitrate, NO_3^- ($\mu mol\ L^{-1}$)	BDL	3.94 ± 5.53	1.75 ± 2.51	BDL	2.78 ± 2.05	0.45 ± 0.21
Ammonium, NH_4^+ ($\mu mol\ L^{-1}$)	1.51 ± 0.12	3.49 ± 1.64	8.53 ± 14.26	1.83 ± 0.32	3.03 ± 1.19	12.17 ± 10.91
Dissolved Organic Carbon, DOC ($\mu mol\ L^{-1}$)	1009.25 ± 236.88	1015.00 ± 256.75	1032.98 ± 157.96	1063.20 ± 248.10	1030.73 ± 261.91	1081.02 ± 147.70
Microcystin ($\mu g\ L^{-1}$)	0.17 ± 0.03	0.16 ± 0.01	0.70 ± 0.93	0.19 ± 0.04	0.19 ± 0.06	0.87 ± 1.27
Biological Parameters						
Total Phytoplankton Biovolume ($mm^3\ L^{-1}$)	4.43 ± 3.87	2.55 ± 1.38	35.31 ± 28.91	2.64 ± 1.21	2.56 ± 1.41	28.13 ± 37.08
Potentially Toxigenic Cyanophyta Biovolume ($mm^3\ L^{-1}$)	0.12 ± 0.16	0.02 ± 0.02	17.94 ± 16.60	0.14 ± 0.20	0.00 ± 0.01	4.27 ± 6.65
Non-toxin Producing Cyanophyta Biovolume ($mm^3\ L^{-1}$)	0.19 ± 0.18	0.17 ± 0.17	10.23 ± 11.60	0.06 ± 0.03	0.13 ± 0.14	2.34 ± 2.24
Chlorophyta Biovolume ($mm^3\ L^{-1}$)	3.17 ± 3.49	1.51 ± 1.13	2.08 ± 1.30	1.56 ± 1.49	0.57 ± 0.32	1.46 ± 1.62
Euglenophyta Biovolume ($mm^3\ L^{-1}$)	0 ± 0	0 ± 0	0 ± 0	0 ± 0	0.01 ± 0.01	0.07 ± 0.18
Cryptophyta + Dinoflagellate Biovolume ($mm^3\ L^{-1}$)	0.41 ± 0.30	0.54 ± 0.55	3.75 ± 5.12	0.61 ± 0.46	1.10 ± 0.82	19.50 ± 36.49
Chrysophyta (including Chrysophytes, Bacillariophytes, Ochrophytes, and Haptophytes) Biovolume ($mm^3\ L^{-1}$)	0.54 ± 0.37	0.32 ± 0.30	1.31 ± 2.47	0.26 ± 0.23	0.75 ± 1.10	0.49 ± 0.82
Chlorophyll-*a,* Chl-*a* ($\mu g\ L^{-1}$)	3.54 ± 1.21	2.97 ± 2.30	48.70 ± 39.85	2.09 ± 1.07	1.53 ± 1.02	63.52 ± 79.94

(Continued)

TABLE 3 | Continued

	Day 0 Mean ± Std Dev			Day 9 Mean ± Std Dev		
	Con ***n* = 3**	**Chloro** ***n* = 6**	**Cyano** ***n* = 8**	**Con** ***n* = 3***	**Chloro** ***n* = 6**	**Cyano** ***n* = 8†**
Maximum Quantum Yield of Photosystem II, ϕ_{PSII} (unitless)	0.57 ± 0.11	0.61 ± 0.11	0.34 ± 0.15	0.53 ± 0.03	0.56 ± 0.02	0.48 ± 0.13
Light saturation threshold normalized for Chl-*a*, $E_k{}^B$ (μmol photons [μg Chl-a^{-1}] m s^{-1})	153.23 ± 177.98	428.24 ± 728.62	80.90 ± 174.58	377.22 ± 430.44	388.69 ± 360.81	32.34 ± 33.67
Alpha normalized for Chl-*a*, α^B	0.21 ± 0.10	0.48 ± 0.53	0.07 ± 0.14	0.58 ± 0.54	0.65 ± 0.43	0.05 ± 0.06
Maximum relative electron transport rate, $rETR_{MAX}$ (photons reemitted photons absorbed^{-1})	315.69 ± 359.98	175.63 ± 150.92	136.12 ± 47.95	291.40 ± 265.33	222.69 ± 138.22	197.21 ± 46.31
Light deficiency parameter, $\tilde{E}_{24}/E_k$	0.85 ± 0.70	0.55 ± 0.28	0.20 ± 0.15	0.45 ± 0.21	0.43 ± 0.20	0.18 ± 0.07
Gross Primary Productivity normalized to Chl-*a*, GPP^B (mmol O_2 [μg Chl-a^{-1}] m day^{-1})	25.9 ± 13.0	15.4 ± 13.7	15.2 ± 9.5	33.3*	18.2 ± 15.5	22.8 ± 12.3
Total Zooplankton Abundance (Individuals L^{-1})	70.85 ± 57.89	79.56 ± 51.45	211.84 ± 149.78	111.87 ± 90.99	31.78 ± 17.90	126.04 ± 95.11
Adult Copepod Abundance (Individuals L^{-1})	14.82 ± 9.13	17.36 ± 9.66	89.05 ± 82.69	16.00 ± 3.75	12.73 ± 9.92	59.59 ± 74.25
Copepod Nauplii Abundance (Individuals L^{-1})	26.73 ± 25.39	31.46 ± 39.62	63.54 ± 54.43	16.59 ± 6.57	12.75 ± 8.20	39.01 ± 55.49
Cladoceran Abundance (Individuals L^{-1})	29.30 ± 23.47	30.75 ± 28.30	59.25 ± 75.82	79.27 ± 80.83	6.30 ± 3.28	27.43 ± 36.79

*Mean and standard deviation (std dev) are reported. "BDL" indicates that all tanks in a group were below the detection limit as stated in the Methods. Sediment traps were collected only on day 9, so it is not applicable (n/a) to report day 0 sedimentation rates.*There was only one control tank for day 9 GPP^B †There were only 7 cyanophyte dominated tanks for day 9 DOC.*

molar ratio exceeds 3.91, then the phytoplankton community is P-deficient, and if it is lower than 3.00 then the phytoplankton community is N-deficient (Guildford and Hecky, 2000). Between 3.00 and 3.91, it could be N, P, or some other factor restricting growth (Guildford and Hecky, 2000). The mean ln(TN:TP) molar ratios for control and chlorophyte-dominated tanks on day 0 were 4.61 (range = 4.07 – 4.96) and 4.74 (range = 4.30 – 5.47), respectively, indicating P-deficient conditions (**Tables 1**, **3**; Guildford and Hecky, 2000). Cyanophyte-dominated tanks had a mean ln(TN:TP) molar ratio of 3.39 (range = 2.74 – 4.23) on day 0 (**Tables 1**, **3** and **Supplementary Figure 4**). This value was between P-deficient and N-deficient conditions, suggesting that these tanks could have been either N or P deficient. Alternatively, cyanophyte-dominated tanks could have been growth-limited by other factors such as light (Guildford and Hecky, 2000). Heterocytes were only present in the cyanophyte-dominated tanks. They were identified in 6 tanks on day 0 and only 4 tanks on day 9 in low densities (mean = 5,850, range = 27 – 13,800 cells L^{-1}). The change in the ln(TN:TP) ratio between days 9 and 0 was not significantly different between the control, chlorophyte- and cyanophyte- dominated tanks (**Table 4**).

The change in TDN, TDP, $NO_3{}^-$, and $NH_4{}^+$ concentrations were not significantly different between any of the experimental groups (**Table 4**). TDN and TDP concentrations were stable in all tanks throughout the experiment, though a notable deviation was the decrease in TDP from 1.52 to 1.27 μmol L^{-1} in the cyanophyte-dominated tanks (**Table 3**). $NO_3{}^-$ concentrations were never above the limit of detection in control, and decreased from 3.94 to 2.78 μmol L^{-1} and from 1.75 to 0.45 μmol L^{-1} in chlorophyte- and cyanophyte-dominated tanks, respectively (**Table 3**). $NH_4{}^+$ concentrations increased from 1.51 to 1.83 μmol L^{-1} and from 8.53 to 12.17 μmol L^{-1} in the control and cyanophyte-dominated tanks, respectively, but decreased from 3.49 to 3.03 μmol L^{-1} in the chlorophyte-dominated tanks (**Table 3** and **Supplementary Figure 4**).

Over the course of the experiment, DOC concentrations increased from 1009.25 to 1063.20 μmol L^{-1} in the control, from 1015.00 to 1030.73 μmol L^{-1} in the chlorophyte-dominated, and from 1032.98 to 1081.02 μmol L^{-1} in the cyanophyte-dominated tanks (**Table 3** and **Supplementary Figure 4**). The difference between day 9 and day 0 DOC concentrations in the cyanophyta-dominated tanks were significantly larger than in the chlorophyte-dominated tanks (**Table 4**), but there was no significant difference between the control and neither the chlorophyte- nor cyanophyte-dominated tanks (**Table 4**).

Microcystin concentrations ranged from BDL to 4.04 μg L^{-1} (**Table 3**). Over this 9-day experiment, they increased from 0.17 to 0.19 μg L^{-1} in the control, from 0.16 to 0.19 μg L^{-1} in the chlorophyte-dominated, and from 0.70 to 0.87 μg L^{-1} in the cyanophyte-dominated tanks (**Table 3**). The change in microcystin concentrations between days 9 and 0 was not significantly different among any of the experimental groups (**Table 4** and **Supplementary Figure 3**).

Phytoplankton Community Biovolume

Photoacclimation is photosynthesizer's physiological response to changes in light and displays as an increase or decrease in chl-*a* concentrations relative to phytoplankton biomass (Falkowski and LaRoche, 1991). To check if photoacclimation was occurring in the experimental tanks to which we added GRF, we examined

TABLE 4 | Statistical analyses for each parameter.

	Test	*p*	Test Statistic	*Post Hoc*		
				Con	Chloro	Cyano
Physical Parameters						
Temperature	ANOVA	$p = 0.08$	$F_{2,14} = 3.05$			
Total Suspended Solids, TSS	KW	$p = 0.97$	$\chi^2 = 0.07$ df = 2			
Particulate Inorganic Matter, PIM	KW	$p = 0.43$	$\chi^2 = 1.67$ df = 2			
Particulate Organic Matter, POM	ANOVA	$p = 0.93$	$F_{2,14} = 0.08$			
Mean daily mixed layer irradiance, $\bar{E}_{24}$	ANOVA	$p = 0.61$	$F_{2,14} = 0.52$			
Chemical Parameters						
Total Nitrogen:Total Phosphorus, ln(TN:TP)	ANOVA	$p = 0.10$	$\chi^2 = 2.10$ df = 2			
Total Phosphorus, TP	KW	$p = 0.03$	$\chi^2 = 7.16$ df = 2	ab	a	b
Total Dissolved Phosphorus, TDP	KW	$p = 0.87$	$\chi^2 = 0.23$ df = 2			
Total Nitrogen, TN	KW	$p = 0.27$	$\chi^2 = 2.63$ df = 2			
Total Dissolved Nitrogen, TDN	ANOVA	$p = 0.90$	$F_{2,14} = 0.11$			
Nitrate, NO_3^-	KW	$p = 0.45$	$\chi^2 = 1.58$ df = 2			
Ammonium, NH_4^+	KW	$p = 0.20$	$\chi^2 = 3.18$ df = 2			
Dissolved Organic Carbon, DOC	ANOVA	$p = 0.05$	$F_{2,13} = 3.92$	ab	a	b
Microcystin	KW	$p = 0.12$	$\chi^2 = 4.26$ df = 2			
Biological Parameters						
Total Phytoplankton Biovolume	KW	$p = 0.20$	$\chi^2 = 3.18$ df = 2			
Potentially Toxigenic Cyanophyta Biovolume	KW	$p = 0.01$	$\chi^2 = 12.61$ df = 2	a	a	b
Non-toxin Producing Cyanophyta Biovolume	KW	$p = 0.78$	$\chi^2 = 0.51$ df = 2			
Chlorophyta Biovolume	KW	$p = 0.99$	$\chi^2 = 0.02$ df = 2			
Euglenophyta Biovolume	KW	$p = 0.79$	$\chi^2 = 0.47$ df = 2			
Cryptophyta + Dinoflagellate Biovolume	KW	$p = 0.74$	$\chi^2 = 0.60$ df = 2			
Chrysophyta (including Chrysophytes, Bacillariophytes, Ochrophytes, and Haptophytes) Biovolume	KW	$p = 0.11$	$\chi^2 = 4.46$ df = 2			
Chlorophyll-*a,* Chl-*a*	KW	$p = 0.44$	$\chi^2 = 1.64$ df = 2			
Maximum Quantum Yield of Photosystem II, ϕ_{PSII}	ANOVA	$p = 0.06$	$F_{2,14} = 3.43$			
Light saturation threshold normalized for Chl-*a*, $E_k{}^B$	ANOVA	$p = 0.26$	$F_{2,14} = 1.50$			
Alpha normalized for Chl-*a*, α^B	ANOVA	$p = 0.71$	$F_{2,14} = 0.36$			
Maximum relative electron transport rate, $rETR_{MAX}$	ANOVA	$p = 0.28$	$F_{2,14} = 1.40$			

(Continued)

TABLE 4 | Continued

	Test	*p*	Test Statistic	*Post Hoc*		
				Con	Chloro	Cyano
Light deficiency parameter, $\bar{E}_{24}/E_k$	ANOVA	$p = 0.70$	$F_{2,14} = 0.36$			
Gross Primary Productivity normalized for Chl-*a*, GPP^B	ANOVA	$p = 0.16$	$F_{2,9} = 2.26$			
Total Zooplankton Abundance	ANOVA	$p = 0.45$	$F_{2,14} = 0.85$			
Adult Copepod Abundance	KW	$p = 0.51$	$\chi^2 = 1.35$ df = 2			
Copepod Nauplii Abundance	KW	$p = 0.88$	$\chi^2 = 0.27$ df = 2			
Cladoceran Abundance	ANOVA	$p = 0.06$	$F_{2,14} = 3.42$			

Analyses were evaluated on the difference between day 9 and day 0 (i.e., day 9 - day 0). We used a one-way analysis of variance (ANOVA) when the parameter followed a normal distribution, or when a normal distribution resulted from a transformation. A Kruskal–Wallis test (KW) was used when the data did not follow a normal distribution. Statistically significant differences between groups ($p < 0.05$) are denoted by different letters, while same letters indicate that no significant difference exists. Post Hoc tests were used to identify when the change in each parameter was different between control (Con), chlorophyte- (Chloro), and cyanophyte- (Cyano) dominated mesocosm tanks. A Tukey post hoc test was used to identify significant differences for parameters that followed a parametric distribution while Dunn's test was used on non-parametric parameters.

the relationship between chl-*a* concentrations and phytoplankton biovolume. There was a significant positive correlation between these parameters prior to GRF addition (day 0; Spearman's Rank, $p = 0.0023$, rho = 0.76, $n = 14$) and on day 9 (Spearman's Rank, $p = 0.0038$, rho = 0.74, $n = 14$), indicating that the phytoplankton did not exhibit photoacclimation. Chl-*a* concentrations decreased from 3.54 to 2.09 $\mu g\ L^{-1}$ and from 2.97 to 1.53 $\mu g\ L^{-1}$ in the control and chlorophyte-dominated, respectively, but increased from 48.7 to 63.52 $\mu g\ L^{-1}$ in the cyanophyte-dominated tanks (**Table 3** and **Supplementary Figure 5**). The change in chl-*a* concentrations and phytoplankton biovolume between days 9 and 0 was not significantly different between the control, chlorophyte- and cyanophyte- dominated tanks (**Table 4**). Total phytoplankton biovolume decreased from 4.43 to 2.64 $mm^3\ L^{-1}$ and from 35.31 to 28.13 $mm^3\ L^{-1}$ in the control and cyanophyte-dominated tanks, respectively. Total phytoplankton biovolume remained unchanged in the chlorophyte-dominated tanks (mean = 2.55 $mm^3\ L^{-1}$; **Table 3**). Within all tanks, dinoflagellates comprised only 23.0, 13.3, and 0.1%, respectively, of the cryptophyte and dinoflagellate functional group. Throughout the rest of this study, we refer to the group containing cryptophytes and dinoflagellates as the cryptophyte functional group.

Within the chlorophyte- and cyanophyte-dominated tanks, declines in cyanophytes (49.4 and 77.9%, respectively) were compensated by an increase in cryptophytes (105.7 and 240%, respectively; **Figure 3**). Much of this cryptophyte increase can be attributed to the genus *Cryptomonas*, which comprised 32.2 and 37.1% of total phytoplankton biovolume on day 9 in chlorophyte- and cyanophyte-dominated tanks, respectively (**Table 2** and **Supplementary Table 2**). The change in potentially toxigenic cyanophyta biovolume was significantly different in the cyanophyte-dominated tanks compared to the control and chlorophyte-dominated tanks (**Table 4**). Potentially toxigenic cyanophytes increased by 16.7% in control, and declined by 100 and 76.2% in chlorophyte and cyanophyte-dominated tanks, respectively. All cyanobacteria (potentially toxigenic taxa and non-toxin producing taxa combined) declined by 22.8, 49.4, and 77.9% in the control, chlorophyte- and cyanophyte-dominated tanks, respectively, between days 9 and 0. While the change in biovolume from days 9 to 0 of all other taxonomic groups was not significantly different between experimental tanks, cryptophytes increased by 18.8, 105.7, and 240.0% in the control, chlorophyte- and cyanophyte-dominated tanks, respectively.

Phytoplankton Physiology and Gross Primary Productivity

Phytoplankton samples with ϕ_{PSII} values below 0.65 can indicate that the communities are physiologically stressed due to light, nutrients, or some combination thereof (Kromkamp et al., 2008). At no point on days 0 nor 9 did ϕ_{PSII} exceed the empirical optimum threshold of ∼0.65 in any tank (**Table 3** and **Supplementary Figure 6**). ϕ_{PSII} decreased from 0.57 to 0.53 and from 0.61 to 0.56 in the control and chlorophyte-dominated tanks, respectively, but increased from 0.34 to 0.48 in the cyanophyte-dominated tanks (**Table 3** and **Supplementary Figure 6**). We observed no significant difference in the change in ϕ_{PSII} between the control, chlorophyte-, and cyanophyte-dominated tanks.

Additional indicators of phytoplankton physiology also remained largely unchanged after the addition of GRF (**Table 4**). The light utilization efficiency parameter (α^B) increased from 0.51 to 0.58 and from 0.48 to 0.65 in the control and chlorophyte-dominated tanks, respectively, but decreased from 0.07 to 0.05 in the cyanophyte-dominated tanks. The light saturation parameter ($E_k{}^B$) increased from 153.23 to 377.22 μmol photons (μg Chl-a^{-1}) m s^{-1} in the control, but decreased in both the chlorophyte- and cyanophyte-dominated tanks from 428.24 to 388.69 and from 80.90 to 32.34 μmol photons (μg Chl-a^{-1}) m s^{-1}, respectively (**Table 3**). $rETR_{MAX}$ decreased from 315.69 to 291.40 in the control, but increased from 175.63 to 222.69 and from 136.12 to 197.21

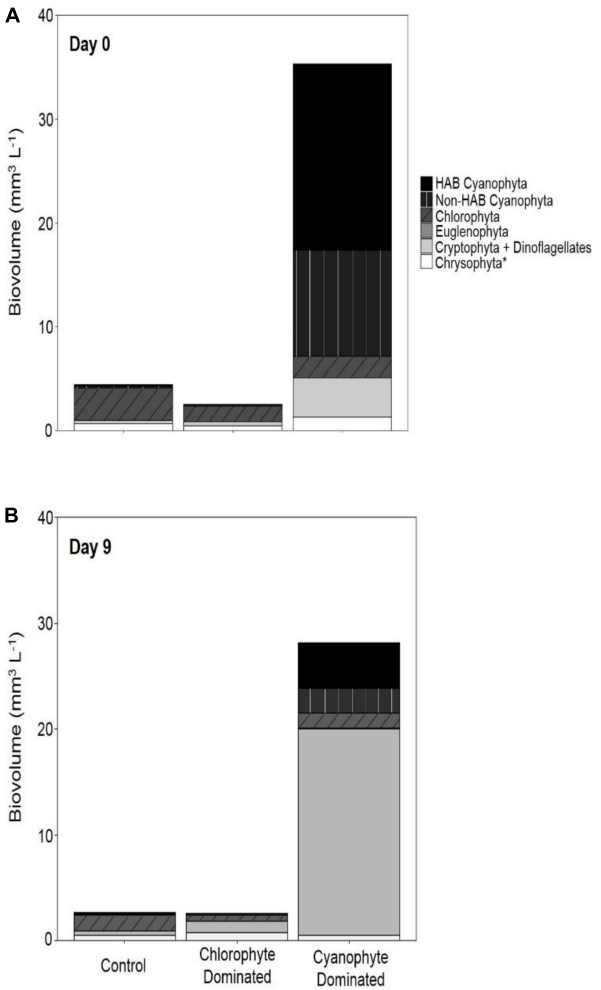

FIGURE 3 | Phytoplankton biovolume categorized by functional group. Biovolume for day 0 **(A)** and day 9 **(B)** for control tanks, tanks dominated by chlorophytes at the beginning of the experiment, and tanks dominated by cyanophytes at the beginning of the experiment. The chrysophyta* group includes chrysophyta, bacillariophyta, haptophyta, and ochrophyta.

photons reemitted photons absorbed^{-1} in the chlorophyte- and cyanophyte- dominated tanks, respectively (**Table 3**). The light deficiency parameter ($\bar{E}_{24}/E_k$) decreased in control, chlorophyte-, and cyanophyte-dominated tanks from 0.85 to 0.45, 0.55 to 0.43, and from 0.20 to 0.18, respectively (**Table 3** and **Supplementary Figure 6**). We observed no significant difference in the change in α^B, $E_k{}^B$, $rETR_{MAX}$, nor $\bar{E}_{24}/E_k$, between the control, chlorophyte- and cyanophyte-dominated tanks.

Gross primary productivity normalized to chl-*a* (GPP^B) increased from 25.9 to 33.3, from 15.4 to 18.2, and from 15.2 to 22.8 mmol O_2 (μg Chl-a^{-1}) m day^{-1} in the control, chlorophyte- and cyanophyte- dominated tanks, respectively (**Table 3** and **Supplementary Figure 6**). We did not observe a significant difference in the change in GPP^B between any of the tanks (**Table 4**).

Zooplankton

To evaluate whether zooplankton dynamics were influenced by GRF addition and/or if grazing was impacting phytoplankton populations differently between tanks and over the course of the experiment, we compared total zooplankton, cladoceran, and copepod abundance between days 0 and 9 (**Supplementary Table 4** and **Figure 4**). Copepods were separated into adults and nauplii. Between days 9 and 0, the change in total zooplankton, cladoceran, adult copepod, and copepod nauplii abundance was not significantly different in any of the tanks (**Table 4**). While not significant (**Table 3** and **Supplementary Figure 7**), total zooplankton abundance increased from 70.85 to 111.87 in control, but decreased from 79.56 to 31.78 and from 211.84 to 126.04 in chlorophyte- and cyanophyte-dominated tanks, respectively. Adult copepod abundance increased from 14.82 to 16.00 individuals L^{-1} in the control, but decreased from 17.36 to 12.73 and from 89.05 to 59.59 individuals L^{-1} in chlorophyte- and cyanophyte- dominated tanks, respectively. Copepod nauplii abundance decreased from 26.73 to 16.59 in control, from 31.46 to 12.75 in chlorophyte-dominated, and from 63.54 to 39.01 individuals L^{-1} in cyanophyte-dominated tanks. Cladocerans increased from 29.30 to 79.27 in control tanks, but decreased from 30.75 to 6.30 and from 59.25 to 27.43 individuals L^{-1}

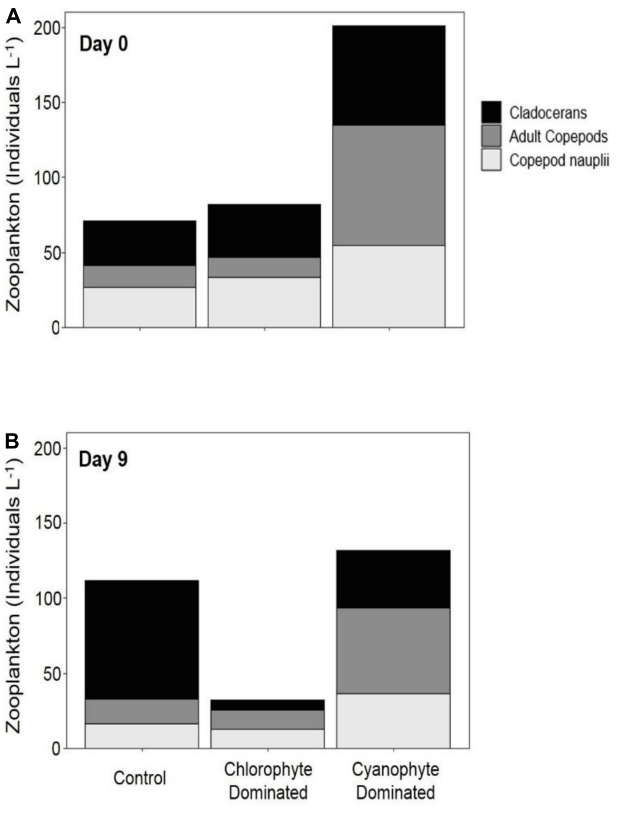

FIGURE 4 | Zooplankton abundance in mesocosm tanks. Abundance was measured on day 0 **(A)** and day 9 **(B)** for control tanks, tanks dominated by chlorophytes at the beginning of the experiment, and tanks dominated by cyanophytes at the beginning of the experiment.

in chlorophyte- and cyanophyte- dominated tanks, respectively (**Table 3** and **Supplementary Figure 7**).

DISCUSSION

Light availability throughout the water column was significantly reduced in all mesocosm tanks that received GRF relative to the control tanks. This reduction in light was maintained throughout the 9-day experiment and resulted in a 77.9% decline in cyanophyte biovolume in tanks dominated by cyanophytes. While total phytoplankton biovolume did not change after the addition of GRF, cryptophytes increased by 240.0% in cyanophyta-dominated tanks. In the chlorophyte-dominated tanks, cyanophytes decreased by 49.4% while cryptophytes increased by 105.7%. Changes in cyanophytes and cryptophytes were less in the control tanks where cyanophytes decreased by 22.8% and cryptophytes increased by 18.8% between days 0 and 9.

How Did the GRF Addition Affect Physical, Chemical, and Biological Parameters in the Mesocosm Tanks?

The addition of GRF to mesocosm tanks significantly reduced PAR by half and maintained this relatively low light level throughout the 9-day experiment. PIM concentrations increased by ∼80% from day 0 to day 9 in the chlorophyte- and cyanophyte-dominated tanks that received GRF. POM decreased by 37.9% in chlorophyte-dominated tanks and increased by only 32.0% in cyanophyte-dominated tanks between day 0 and day 9, suggesting that the reduction in light is due to increases in suspended inorganic particles derived from the GRF. In tanks that received GRF, the mean K_d value was 3.77 m^{-1}. This was higher than what occurs in many glacially fed, natural lakes. Glacially fed lakes in New Zealand, Chile, and Canada have mean K_ds of 0.96 m^{-1} and a maximum of 2.28 m^{-1} (Rose et al., 2014). Lakes in the US Rocky Mountains do not exceed K_d of 0.30 m^{-1} (Slemmons and Saros, 2012) and K_d in glacially fed Mascardi Lake in Argentina is often between 0.40 and 0.75 m^{-1} (Modenutti et al., 2000; Hylander et al., 2011). Our K_d values are likely higher than those that occur in water bodies, due to the smaller scale of our experiment, the lack of flow in our mesocosm tanks, and the higher rate of GRF addition. In natural systems, GRF inputs are relatively constant due to consistent tributary inflows creating horizontal gradients in turbidity as particles fall out of suspension with increasing distance from tributary inflows (Laspoumaderes et al., 2013).

Our experimental approach was to manipulate light while maintaining nutrient concentrations. We wanted to ensure that the GRF additions were not adding or precipitating nutrients in the experimental tanks. TN, TDN, NO_3^-, NH_4^+, and TDP concentrations remained largely unchanged throughout this 9-day experiment. The change in TP from days 9 to 0 was significantly different in the chlorophyte-dominated tanks compared to the cyanophyte-dominated tanks, but not compared to the control tanks. If the addition of GRF precipitated P from the water column, we would have expected to see a decline in TP in all of the GRF tanks, including both the chlorophyte- and cyanophyte- dominated tanks. This was not the case as TP only declined by 0.01 μmol L^{-1} in the chlorophyte-dominated tanks. We believe the decrease in cyanophyta and increase in cryptophyta can be attributed to reduced light and not an increase in P deficiency because we also saw no significant change in the ln(TN:TP) molar ratio in any of the tanks.

Microcystin concentrations were low throughout the experiment but increased in all tanks between days 0 and 9. The decline in cyanophyta in the chlorophyte- and cyanophyte-dominated tanks could explain the increase in microcystin concentrations. As cyanobacterial cells lyse, they can release intracellular microcystin into the water column (Greenfield et al., 2014). Microcystin concentrations never exceeded 4.04 μg L^{-1} on day 9 and increases in microcystin between days 0 and 9 were never more than 0.17 μg L^{-1}, despite the declines we observed in cyanophyta. Non-toxic strains of the cyanobacterium *Microcystis* outcompete toxic strains at low light levels (Kardinaal et al., 2007), which could be why we did not see a greater increase in microcystin concentrations following the addition of GRF.

We anticipated that increased turbidity resulting from GRF additions would negatively impact zooplankton abundance and diversity, especially for filter-feeding cladocerans (Sommaruga, 2015). High concentrations of suspended particles can make it difficult for filter-feeding cladocerans to obtain food and they are often absent from lakes with high GRF inputs (Barouillet et al., 2019). Copepods are able to survive higher turbidities than other zooplankton (Sommaruga, 2015). We observed a decline in cladoceran, adult copepod, and copepod nauplii abundance in the chlorophyte- and cyanophyte- dominated tanks. The decline in cladocerans could be the result of an increase in fine particulates, which interferes with their ability to filter organic particles out of the water (Sommaruga, 2015; Barouillet et al., 2019). In our experiment, cladocerans declined in tanks that received GRF, but increased in the control tanks. A longer study period is necessary to properly evaluate whether the decline in zooplankton we observed is a direct result of GRF application, or simply natural variation in the population. Our 9-day experiment was not long enough to see a dramatic change in the zooplankton community life cycle as cladocerans can live for 15 – 50 days depending on species (Sarma et al., 2002), and lay new egg clutches every 3 – 7 days (Dodson and Frey, 1991). It is not uncommon for many copepods to live up to a year (Allan, 1976), and it can take a month before nauplii reach sexual maturity (Gilbert and Williamson, 1983). The additional time it would take for at least one generation of zooplankton to be born likely explains why we did not see a significant change in zooplankton abundance by day 9 of our experiment. Our findings suggest that additional work is needed over a longer time period to better understand how the addition of GRF impacts zooplankton communities.

The dominant cyanophyte in cyanophyte-dominated tanks at the beginning of the experiment was *Aphanizomenon*. While *Aphanizomenon* has been shown to persist at light levels as low as 50 μmol photons m^{-2} s^{-1} in culture, its highest growth rates occur above 150 μmol photons m^{-2} s^{-1} (Hadas et al., 2002; Üveges et al., 2012) and it is often outcompeted in reduced light environments (Huisman et al., 1999). *Cryptomonas,* the most common cryptophyte on day 9, can dominate algal communities

when light levels are as low as 15 μmol photons m^{-2} s^{-1} (Lizotte and Priscu, 1992). The reduced light environment created from GRF addition could have enabled *Cryptomonas* to replace *Aphanizomenon* as the most prevalent genera.

The switch from a cyanophyte-dominated community to one where cryptophytes are the dominant taxon is efficient and beneficial for trophic interactions. Cyanophytes create inefficient trophic transfers due to their low composition of polyunsaturated fatty acids (Brett et al., 2009). Zooplankton meet most of their polyunsaturated fatty acid requirements from eukaryotic phytoplankton and are not able to survive long periods when these fatty acids are unavailable (Grosbois et al., 2017). Cyanophytes can be too large for many gape-limited grazers to consume, either because they form mucilaginous colonies or long filaments (Haney, 1987). The production of cyanotoxins can also be detrimental to grazers, though the magnitude of these effects are debated (Rohrlack et al., 2001; Paes et al., 2016). Conversely, cryptophytes are highly nutritious and are an important component of aquatic food webs (Stemberger and Gilbert, 1985; Sarnelle, 1993). Thus, the switch from cyanophyte- to cryptophyte-dominated phytoplankton communities likely provided a net benefit to the treated mesocosms by creating a highly edible phytoplankton community for primary consumers.

Which Functional Traits Enabled Cryptophytes to Replace Cyanophytes?

Both cryptophytes and cyanophytes can tolerate low light, but in our study, cryptophytes replaced cyanophytes when GRF was added. Cryptophytes, especially of the genus *Cryptomonas*, are better suited to sustained periods of reduced light availability and are often the dominant phytoplankton in permanently ice-covered lakes (Gervais, 1998). *Cryptomonas* was the most common cryptophyte we observed on day 9 in tanks that were originally dominated by cyanophytes on day 0 (**Supplementary Table 2**). Cryptophytes can position themselves at favorable light intensities using their 2 flagella, and many are mixotrophs that can supplement their metabolic (Porter, 1988) and nutrient (Urabe et al., 2000) requirements with heterotrophy. This is consistent with existing projections that protists, like cryptophytes, sometimes use phagotrophy to survive and outcompete phototrophs at low irradiance levels (Jones, 2000; Schwaderer et al., 2011). The ability to acquire energy through both heterotrophy and autotrophy provides mixotrophs with a competitive advantage (Tittle et al., 2003). Some models even suggest a positive relationship between mixotrophy and primary productivity (Hammer and Pitchford, 2005; Stoecker et al., 2017) because mixotrophs can use phagotrophy to relieve nutrient stress, enabling them to be productive in nutrient-deficient conditions (Jost et al., 2004). None of our tanks were nutrient sufficient (Guildford and Hecky, 2000). Phagotrophy might explain why GPP^B increased in all of them, albeit at low rates. Our maximum increases of 7.6 mmol O_2 [μg Chl-a^{-1}] m day^{-1} are consistent with low increases in GPP for phagocytic phytoplankton (Hammer and Pitchford, 2005).

The increase in GPP^B over the course of the experiment also suggests that the new cryptophyte-dominated community used light more efficiently than the previous chlorophyte- or cyanophyte- dominated communities. Phycobiliproteins, secondary pigments present in both cyanophytes and cryptophytes, can lead to an inverse relationship between α^B and PAR that is contrary to the positive relationship observed in other phytoplankton groups (MacIntyre et al., 2002; Overkamp et al., 2014). This could explain why α^B in the chlorophyte-dominated tanks, which switched from a chlorophyte- to a cryptophyte-dominated community increased, and why α^B in the cyanophyte-dominated tanks did not change. Cyanophyta can have E_k values between 150.82 and 783.30 μmol photons m^{-2} s^{-1} (Zhang et al., 2011), while cryptophytes under ice cover have been between 15 and 45 μmol photons m^{-2} s^{-1} (Lizotte and Priscu, 1992). Our cyanophyte-dominated tanks experienced a 2.5-fold decrease in $E_K{}^B$ from day 0 to 9, suggesting that the shift to dominance by cryptophytes impacted P–E parameters.

Eukaryotic phytoplankton are physiologically stressed at ϕ_{PSII} values below 0.65, while cyanophyta thresholds are lower, typically between 0.4 and 0.6 (Campbell et al., 1998; Kromkamp et al., 2008). In our cyanophyte-dominated tanks, ϕ_{PSII} increased from 0.34 to 0.48 over the course of the experiment, corresponding with a decline in prokaryotic cyanophyta and an increase in eukaryotic cryptophytes. The control and chlorophyte tanks remained dominated by eukaryotes throughout the experiment and exhibited little change in ϕ_{PSII}. Phytoplankton communities in all tanks were physiologically stressed throughout the experiment.

What Implications Do Our Findings Have for the Nutrient Load Hypothesis?

Our findings provide important insights for the nutrient load hypothesis (Brauer et al., 2012), which predicts phytoplankton dominance based on nutrient concentrations and light availability. It postulates that in low-nutrient environments, the ln(TN:TP) ratio will determine phytoplankton composition while in high-nutrient systems, absolute nutrient concentrations explain which species dominate (Brauer et al., 2012). Increased nutrient enrichment leads to an increase in algal biomass, which in turn reduces light availability through self-shading. Thus, when absolute nutrient concentrations are high, light becomes the single limiting resource. This hypothesis assumes that cyanophyta are superior competitors for light and will dominate the community unless light limitation is reached, at which point total phytoplankton biomass is expected to decline (Brauer et al., 2012). Our results suggest the assumption that cyanophytes will be sole "winners" in this scenario should be revised to include phytoplankton functional traits (**Figure 5**). These functional traits could enable certain taxa to thrive in the reduced light environment created by bloom formation and self-shading.

The nutrient load hypothesis does consider some functional traits for cyanophyta such as their ability to fix atmospheric N_2 or regulate their buoyancy with gas vacuoles. In our experiment, heterocystous N_2 fixation rates were insubstantial given the low (mean = 5,850 cells L^{-1}) number enumerated. The ln(TN:TP) ratios were lowest in the cyanophyte-dominated tanks, but were always between the N- and P- deficiency thresholds where it

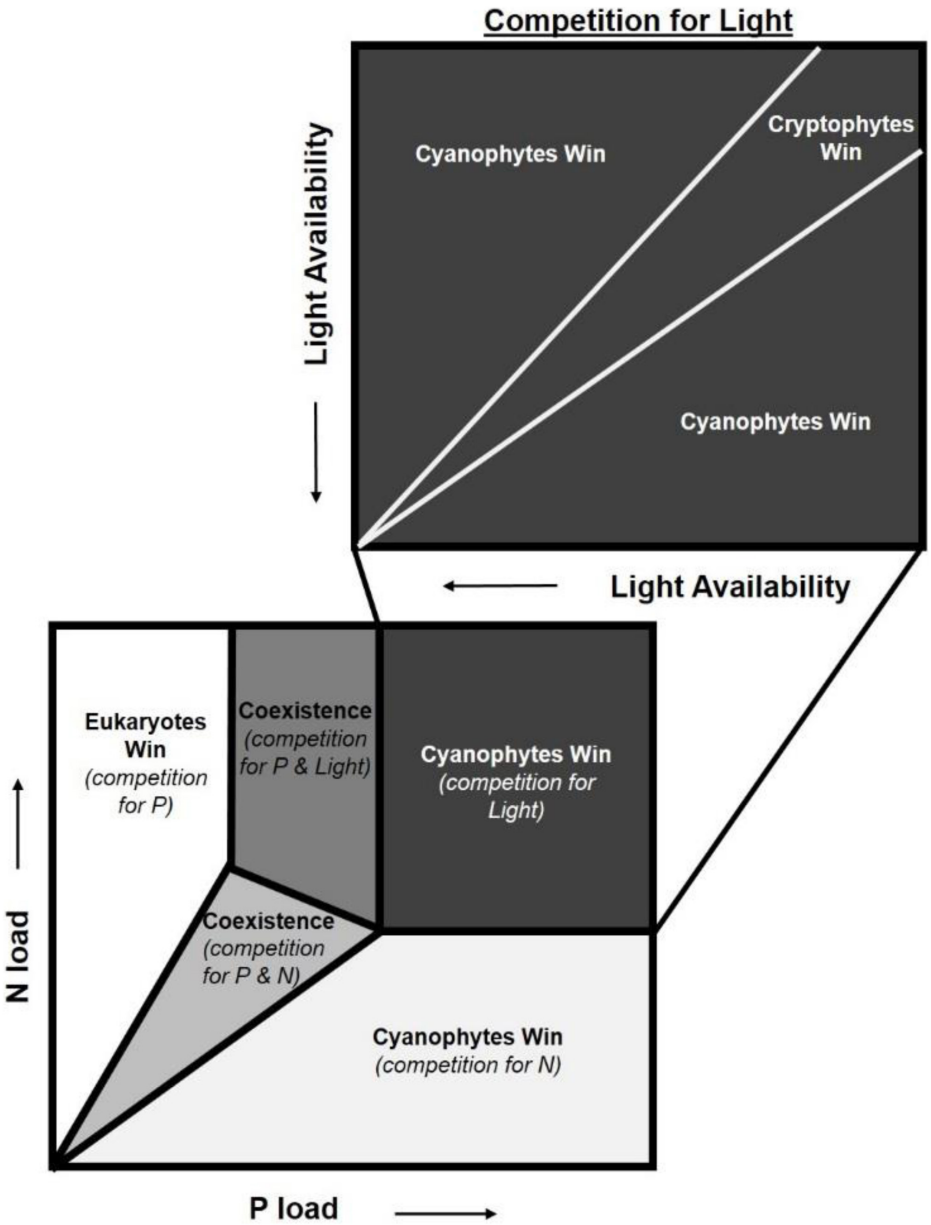

FIGURE 5 | Adaptation of the nutrient load hypothesis from Brauer et al. (2012). This hypothesis predicts which phytoplankton dominate based on competition for nitrogen (N), phosphorus (P), and light. The nutrient load hypothesis is based on the assumption that cyanobacteria are superior competitors for light and are able to dominate when N and P concentrations are high (Brauer et al., 2012). We add an additional box to highlight the nuance that functional traits can add to competition for these resources, specifically light. While cyanobacteria often dominate when light is the limiting resource, our findings suggest that cryptophytes can outcompete cyanobacteria under specific light levels due to functional traits.

can be N, P, or something else that limits growth (Guildford and Hecky, 2000). This, along with the increase in NH_4^+ concentrations observed from days 0 to 9, suggest that the cyanophyte-dominated tanks were not N-deficient. Functional traits for other phytoplankton groups, such as mixotrophy or flagella, both of which might enable other phytoplankton to dominate in low light environments, are not considered (Brauer et al., 2012). Contrary to predictions from the nutrient load hypothesis (Brauer et al., 2012), cyanophyta were not the dominant taxa at the end of our experiment. Cryptophytes were, suggesting that at high nutrient concentrations, functional traits add nuance to competition for light not previously considered.

While cyanobacteria often dominate when light is the limiting resource, our findings suggest that cryptophytes can outcompete cyanobacteria under low light levels. In Lake Peipsi, Estonia/Russia, cyanobacteria are replaced by cryptophytes shortly after the formation of ice and its associated reduction in light availability (Blank et al., 2009). Further experimentation is

required to quantify the thresholds where this shift from nutrient stoichiometry to functional traits occurs, but the importance of functional traits in determining phytoplankton community composition should not be overlooked.

How Does GRF Compare to Other Geoengineering Strategies?

One of the challenges faced by lake managers and drinking water treatment plant operators is mitigating or controlling harmful algal blooms. In 2014, a toxic cyanobacterial bloom in Lake Erie cost the Toledo drinking water plant ∼$4 million and had a total economic impact of ∼$65 million (Bingham et al., 2015). Reductions in external nutrient loading can successfully lower cyanobacterial biomass, but it usually takes years after government regulations have been enacted before declines in biomass are observed (Osgood, 2017). Sometimes, managers need to reduce phytoplankton biomass over a much shorter time scale if, for example, the resource is being used for drinking water. In other instances, it might not always be feasible to reduce external nutrient loading, such as in water bodies with watersheds dominated by agriculture or urban areas. In these situations, alternative geoengineering strategies can be used. Solid-phase P sorbents may be the most common geoengineering approach. These materials are clays enriched with aluminum (Gibbs et al., 2010), iron (Zamparas et al., 2012), or lanthanum (Haghseresht et al., 2009) and work by binding to any soluble reactive P they contact as they sink through the water column.

One benefit of GRF over other geoengineering techniques is its effectiveness on a short timescale. We saw a 49.4 and 77.6% decline in cyanobacteria in chlorophyte- and cyanophyte-dominated tanks, respectively, after 9 days. This decline occurred more quickly than the several months to a year phytoplankton biomass declines after the addition of solid-phase P sorbents (Epe et al., 2017; Wagner et al., 2017). Re-application of solid-phase P sorbents can be required in as short as a couple of years to as long as a decade, depending on lake morphology, nutrient inputs, inorganic particle inputs, and sedimentation rates (Lürling and van Oosterhout, 2012; Mackay et al., 2014; Wagner et al., 2017). Another benefit of GRF is that it results in a decrease in cyanobacteria, but not total phytoplankton biovolume, while solid-phase P sorbents are typically associated with a decline in total phytoplankton biomass (Epe et al., 2017). Maintaining phytoplankton biomass is important in systems where fish yield is a concern (Downing and Plante, 1993).

A consideration to using GRF is that it adds inorganic particles into the water, a concern in reservoirs with limited storage capacity (deNoyelles and Kastens, 2016). Of the 14 tanks that received GRF, the highest TSS sedimentation rate was 3.4 g m^{-2} day^{-1}. This rate is well within the range of natural sedimentation and is lower than some rates found in the North American Midwest. Sedimentation rates in Iowa lakes can range from 11.6 to as high as 203.0 g m^{-2} day^{-1} during the summer (Canfield et al., 1982). We added GRF based on tank surface area at a rate of 0.68 kg m^{-2} day^{-1}. For the average small impoundment of 0.027 km^2 (Downing et al., 2006), this would come to 18,360 kg day^{-1}. At this application rate, it would cost $16,579 USD per day, based on the $0.90 USD per kg price at which we purchased GRF. Such a high application rate and cost likely makes GRF an untenable management strategy in large systems.

Another consideration to the use of GRF is that it must be applied more frequently than most other geoengineering techniques, at least initially. Frequent GRF additions may not be required if the phytoplankton community shifts to an alternative stable state. The alternative stable state hypothesis posits that ecosystems maintain resilience and do not experience state change until a dramatic disturbance shifts the ecosystem to a different state with its own resilience (Scheffer et al., 2001; Carpenter and Brock, 2006). We were able to shift a cyanophyte- dominated phytoplankton community to dominance by cryptophytes in 9 days but we did not continue the experiment long enough to see if an alternate stable state was achieved, nor the time point at which further GRF additions would be unnecessary. In Shidou Reservoir, China, cyanophyta made up ∼100% of the phytoplankton biovolume before an abrupt reduction in the human population within the watershed shifted the phytoplankton community to dominance by chlorophytes (Yang et al., 2017). This shift was sustained for ∼3 years, during which time cyanophytes made up less than 20% of phytoplankton biomass, before a climatic disturbance event shifted the community back to dominance by cyanophytes (Yang et al., 2017). Additional experimentation should investigate long-term trends in the phytoplankton community to determine if GRF application is able to shift the phytoplankton community to an alternative stable state.

The effects of GRF to higher trophic levels will be important when determining whether it should be used in cyanoHAB management. The reduction in light availability from GRF additions could reduce the foraging efficiency of visual predators (Miner and Stein, 1996; Vogel and Beauchamp, 1999). GRF also increases the amount of suspended inorganic particles, which can have a negative impact on fish by damaging gills (Lake and Hinch, 1999) or reducing the filtering efficiency of filter-feeders (Sommaruga, 2015). These effects to biota might not be substantial if short periods of GRF application result in a shift to an alternate stable state. In addition to aquatic biota, the extraction of GRF might impact the terrestrial environment. Commercial GRF is mined from terminal moraines located in the northwestern United States and southwestern Canada, and is sold as a soil amendment for micronutrients. Additional studies should evaluate the long-term effects of GRF addition to higher trophic levels and on the terrestrial environment before its adoption as a widespread management strategy.

CONCLUSION

We demonstrate that GRF application reduces light availability, resulting in a decline in cyanophytes and replacement by cryptophytes. Our findings provide valuable insights to the nutrient load hypothesis (Brauer et al., 2012), suggesting that cryptophytes might outcompete cyanophytes for light when

nutrients are abundant. Further iterations of this hypothesis should consider incorporating functional traits into predictionsof phytoplankton community composition. Before GRF can be advocated as a harmful algal bloom management strategy, further investigation is needed to determine whether an alternative stable state was reached after cryptophytes became the dominant taxa. Regardless, we believe that manipulating light is an important and overlooked strategy for algal bloom management. As the effects of climate change become more pronounced, algal blooms will continue to increase in frequency and magnitude (Paerl and Paul, 2012), and it will become even more important for lake managers to have a variety of techniques to address this challenge.

DATA AVAILABILITY STATEMENT

All datasets generated for this study are available upon request.

AUTHOR CONTRIBUTIONS

RN conceived the idea of using GRF to control cyanobacteria. JG, RN, and TH planned the experiment, which was conducted by JG and TH. Statistical and laboratory analyses were performed by JG, except for phytoplankton and zooplankton counts which were contracted to external labs. JG wrote the manuscript with input from RN and TH. All authors contributed to the article and approved the submitted version.

FUNDING

This research was funded through internal funds from the School of Natural Resources and the Richard Wallace MU Faculty Incentive Grant, University of Missouri, and through the Kansas Water Resource Institute.

ACKNOWLEDGMENTS

Thank you to Steven Baker, Amy Burgin, Scott Campbell, Jerry deNoyelles, Emily Kinzinger, Josh Hagerty, Josh Horne, Regina Klepikow, Dan Obrecht, Carol Pollard, Amy Shields, Tony Thorpe, Laura Webb, and Clare Vanderwerken for all of your help in both the field and lab. This project would not have been possible without your hard work, positive attitudes, and generosity with your time. We are grateful. Thank you also to LeeAnn Bennett for graciously enumerating zooplankton, Thomas Anderson for assistance with statistical analyses, and to members of the School of Natural Resources Writing Workshop, whose suggestions greatly improved the quality and clarity of this manuscript.

SUPPLEMENTARY MATERIAL

The Supplementary Material for this article can be found online at: https://www.frontiersin.org/articles/10.3389/fenvs.2020.540607/full#supplementary-material

REFERENCES

Allan, J. D. (1976). Life history patterns in zooplankton. *Am. Nat.* 110, 165–180. doi: 10.1086/283056

APHA (2017). *Standard Methods for the Examination of Water and Wastewater*, 23rd Edn, eds R. B. Baird, A. D. Eaton, and E. W. Rice (Washington, DC: American Public Health Association).

Backer, L. C., Landsberg, J. H., Miller, M., Keel, K., and Taylor, T. K. (2013). Canine cyanotoxin poisonings in the United States (1920s–2012): review of suspected and confirmed cases from three data sources. *Toxins* 5, 1597–1628. doi: 10.3390/toxins5091597

Barouillet, C., Cumming, B. F., Laird, K. R., Perrin, C. J., and Selbie, D. T. (2019). Influence of glacial flour on the primary and secondary production of sockeye salmon nursery lakes: a comparative modern and paleolimnological study. *Can. J. Fish. Aquat. Sci.* 76, 2303–2314. doi: 10.1139/cjfas-2018-0372

Bartson, S., Ogilvie, J., Petroff, A. J., Smith, G. R., and Rettig, J. E. (2018). Effect of pond dye on the response of Southern Leopard Frog tadpoles (*Lithobates sphenocephalus*) to Western Mosquitofish (*Gambusia affinis*) cues. *Basic Appl. Herpetol.* 32, 71–76.

Bellinger, E. G., and Sigee, D. C. (2010). *Freshwater Algae: Identification and Use as Bioindicators*. Chichester: John Wiley & Sons, Ltd.

Bingham, M., Sinha, S. K., and Lupi, F. (2015). *Economic benefits of reducing harmful algal blooms in Lake Erie*. Gainesville, FL: Environmental Consulting and Technology Inc.

Blank, K., Haberman, J., Haldna, M., and Laugaste, R. (2009). Effect of winter conditions on spring nutrient concentrations and plankton in a large shallow Lake Peipsi (Estonia/Russia). *Aquat. Ecol.* 43, 745–753. doi: 10.1007/s10452-009-9283-2

Bloesch, J., and Burns, N. M. (1980). A critical review on sedimentation trap technique. *Schweiz. Z. Hydrol.* 42, 15–55. doi: 10.1007/bf02502505

Brauer, V. S., Stomp, M., and Huisman, J. (2012). The nutrient-load hypothesis: patterns of resource limitation and community structure driven by competition for nutrients and light. *Am. Nat.* 179, 721–740. doi: 10.1086/665650

Brett, M. T., Kainz, M. J., Taipale, S. J., and Seshan, H. (2009). Phytoplankton, not allochthonous carbon, sustains herbivorous zooplankton production. *Proc. Natl. Acad. Sci. U.S.A.* 106, 21197–21201. doi: 10.1073/pnas.0904129106

Bristow, B. T., Summerfelt, R. C., and Clayton, R. D. (1996). Comparative performance of intensively cultured larval walleye in clear, turbid, and colored water. *Prog. Fish Cult.* 58, 1–10. doi: 10.1577/1548-8640(1996)058<0001:cpoicl>2.3.co;2

Brooks, B. W., Lazorchak, J. M., Howard, M. D. A., Johnson, M. V., Morton, S. L., Perkins, D. A. K., et al. (2016). Are harmful algal blooms becoming the greatest inland water quality threat to public health and aquatic ecosystems? *Environ. Toxicol. Chem.* 35, 6–13. doi: 10.1002/etc.3220

Burkholder, J. M., and Wetzel, R. G. (1989). Epiphytic microalgae on natural substrata in a hardwater lake: seasonal dynamics of community structure, biomass and ATP content. *Arch. Hydrobiol.* 83, 1–56.

Campbell, D., Hurry, V., Clarke, A. K., Gustafsson, P., and ?quist, G. (1998). Chlorophyll fluorescence analysis of cyanobacterial photosynthesis and acclimation. *Microbiol. Mol. Biol. Rev.* 62, 667–683. doi: 10.1128/mmbr.62.3.667-683.1998

Canfield, D. E., Jones, J. R., and Bachmann, R. W. (1982). Sedimentary losses of phosphorus in some natural and artificial Iowa lakes. *Hydrobiologia* 87, 65–76. doi: 10.1007/bf00016663

Carmichael, W. W., Azevedo, S. M., An, J. S., Molica, R. J., Jochimsen, E. M., Lau, S., et al. (2001). Human fatalities from cyanobacteria: chemical and biological evidence for cyanotoxins. *Environ. Health Perspect.* 109, 663–668. doi: 10.1289/ehp.01109663

Carpenter, S. R., and Brock, W. A. (2006). Rising variance: a leading indicator of ecological transition. *Ecol. Lett.* 9, 311–318. doi: 10.1111/j.1461-0248.2005.00877.x

Casassa, G., Lüpez, P., Pouyaud, B., and Escobar, F. (2009). Detection of changes in glacial run-off in alpine basins: examples from North America, the Alps, central Asia and the Andes. *Hydrol. Process* 23, 31–41. doi: 10.1002/hyp.7194

Chanudet, V., and Filella, M. (2009). Size and composition of inorganic colloids in a peri-alpine, glacial flour-rich lake. *Geochim. Cosmochim. Acta* 72, 1466–1479. doi: 10.1016/j.gca.2008.01.002

Chapman, A., and Foss, A. (2019). *Potentially Toxigenic (PTOX) Cyanobacteria List*. Palatka, FL: GreenWater Laboratories.

Chorus, I., and Bartram, J. (1999). *Toxic Cyanobacteria in Water: A Guide to their Public Health Consequences, Monitoring and Management*. London: E & FN Spon.

Crumpton, W. G., Isehart, T. M., and Mitchell, P. D. (1992). Nitrate and organic N analyses with second derivative spectroscopy. *Limnol. Oceanogr.* 37, 907–913. doi: 10.4319/lo.1992.37.4.0907

Deacon, C., and Walsby, A. E. (1990). Gas vesicle formation in the dark, and in the light of different irradiances, by the cyanobacterium *Microcystis* sp. *Br. Phycol. J.* 25, 133–139. doi: 10.1080/00071619000650121

deNoyelles, F., and Kastens, J. H. (2016). Reservoir sedimentation challenges Kansas. *Trans. Kans. Acad. Sci.* 119, 69–81. doi: 10.1660/062.119.0110

Dodds, W. K., Bouska, W. W., Eitzmann, J. L., Pilger, T. J., Pitts, K. L., Riley, A. J., et al. (2009). Eutrophication of U.S. freshwaters: analysis of potential economic damages. *Envir. Sci. Technol.* 43, 12–19. doi: 10.1021/es801217q

Dodson, S. I., and Frey, D. G. (1991). "Cladocera and other Banchiopoda," in *Ecology and Classification of North American Freshwater Invertebrates*, eds J. H. Thorp and A. P. Covich (Londong: Academic Press), 723–763.

Downing, J. A., and Plante, C. (1993). Production of fish populations in lakes. *Can. J. Fish. Aquat. Sci.* 50, 110–120. doi: 10.1139/f93-013

Downing, J. A., Prairie, Y. T., Cole, J. J., Duarte, C. M., Tranvik, L. J., Striegl, R. G., et al. (2006). The global abundance and size distribution of lakes, ponds, and impoundments. *Limnol. Oceanogr.* 51, 2388–2397. doi: 10.4319/lo.2006.51.5.2388

Epe, T. S., Finsterle, K., and Yasseri, S. (2017). Nine years of phosphorus management with lanthanum modified bentonite (Phoslock in a eutrophic, shallow swimming lake in Germany). *Lake Reserv. Manage.* 33, 119–129. doi: 10.1080/10402381.2016.1263693

Falkowski, P. G., and LaRoche, J. (1991). Acclimation to spectral irradiance in algae. *J. Phycol.* 27, 8–14. doi: 10.1111/j.0022-3646.1991.00008.x

Fee, E. J. (1990). Computer programs for calculating in-situ phytoplankton photosynthesis. *Can. Tech. Rep. Fish. Aquat. Sci.* 1740, 1–27.

Gee, G. W., and Bauder, J. W. (1979). Particle size analysis by hydrometer: a simplified method for routine textural analysis and a sensitivity test of measurement parameters. *Soil Sci. Soc. Am. J.* 43, 1004–1007. doi: 10.2136/sssaj1979.03615995004300050038x

Gervais, F. (1998). Ecology of cryptophytes coexisting near a freshwater chemocline. *Freshw. Biol.* 39, 61–78. doi: 10.1046/j.1365-2427.1998.00260.x

Gibbs, M. M., Hickey, C. W., and ?zkundakci, D. (2010). Sustainability assessment and comparison of efficacy of four P-inactivation agents for managing internal phosphorus loads in lakes: sediment incubations. *Hydrobiologia* 658, 253–275. doi: 10.1007/s10750-010-0477-3

Gilbert, J. J., and Williamson, C. E. (1983). Sexual dimorphism in zooplankton (Copepoda, Cladocera, and Rotifera). *Annu. Rev. Ecol. Syst.* 14, 1–33. doi: 10.1146/annurev.es.14.110183.000245

Greenfield, D. I., Duquette, A., Goodson, A., Keppler, C. J., Williams, S. H., Brock, L. M., et al. (2014). The effects of three chemical algaecides on cell numbers and toxin content of the cyanobacteria *Microcystis aeruginosa* and *Anabaenopsis* sp. *Environ. Manage.* 54, 1110–1120. doi: 10.1007/s00267-014-0339-2

Grosbois, G., Mariash, H., Schneider, T., and Rautio, M. (2017). Under-ice availability of phytoplankton lipids is key to freshwater zooplankton winter survival. *Sci. Rep.* 7:11543. doi: 10.1038/s41598-017-10956-0

Grosse, Y., Baan, R., Straif, K., Secretan, B., Ghissassi, F. E., and Cogliano, V. (2006). Carcinogenicity of nitrate, nitrite, and cyanobacterial peptide toxins. *Lancet Oncol.* 7, 628–629. doi: 10.1016/s1470-2045(06)70789-6

Guildford, S. J., and Hecky, R. E. (2000). Total nitrogen, total phosphorus, and nutrient limitation in lakes and oceans: is there a common relationship? *Limnol. Oceanogr.* 45, 1213–1223. doi: 10.4319/lo.2000.45.6.1213

Guiry, M. D., and Guiry, G. M. (2020). *AlgaeBase*. Galway: National University of Ireland.

Hadas, O., Pinkas, R., Malinsky-Rushansky, N., Shalev-Alon, G., Delphine, E., Berner, T., et al. (2002). Physiological variables determined under laboratory conditions may explain the bloom of *Aphanizomenon ovalisporum* in Lake Kinneret. *Eur. J. Phycol.* 37, 259–267. doi: 10.1017/s0967026202003645

Haghseresht, F., Wang, S., and Do, D. (2009). A novel lanthanum-modified bentonite, Phoslock§, for phosphate removal from wastewaters. *Appl. Clay Sci.* 46, 369–375. doi: 10.1016/j.clay.2009.09.009

Hammer, A. C., and Pitchford, J. W. (2005). The role of mixotrophy in plankton bloom dynamics, and the consequences for productivity. *ICES J. Mar. Sci.* 5, 833–840. doi: 10.1016/j.icesjms.2005.03.001

Haney, J. F. (1987). Field studies on zooplankton-cyanobacteria interactions. *N. Z. J. Mar. Freshw.* 21, 467–475. doi: 10.1080/00288330.1987.9516242

Harris, T., Yun, J., Baker, D. S., Kastens, J., Sturm, B., Leavitt, P., et al. (2020). *Phytoplankton and Water Quality in Milford Reservoir: Results of Paleolimnological Sediment Core and Historical Data Analyses. Kansas Biological Survey Report No.* 197. Lawrence: University of Kansas.

Hecky, R. E., and Guildford, S. J. (1984). Primary productivity of Southern Indian Lake before, during, and after impoundment and Churchill River diversion. *Can. J. Fish. Aquat. Sci.* 41, 591–604. doi: 10.1139/f84-072

Heisler, J., Glibert, P. M., Burkholder, J. M., Anderson, D. M., Cochlan, W., Dennison, W. C., et al. (2008). Eutrophication and harmful algal blooms: a scientific consensus. *Harmful Algae* 8, 3–13. doi: 10.1016/j.hal.2008.08.006

Hillebrand, H., Dürselen, C. D., Kirschtel, D., Pollingher, U., and Zohary, T. (1999). Biovolume calculation for pelagic and benthic microalgae. *J. Phycol.* 35, 403–424. doi: 10.1046/j.1529-8817.1999.3520403.x

Huisman, J., Jonker, R. R., Zonneveld, C., and Weissing, F. J. (1999). Competition for light between phytoplankton species: experimental tests of mechanistic theory. *Ecology* 80, 211–222. doi: 10.1890/0012-9658(1999)080[0211:cflbps]2.0.co;2

Hylander, S., Jephson, T., Lebret, K., Einem, J., Fagerberg, T., Balseiro, E., et al. (2011). Climate-induced input of turbid glacial meltwater affects vertical distribution and community composition of phyto- and zooplankton. *J. Plankton Res.* 33, 1239–1248. doi: 10.1093/plankt/fbr025

Ibelings, B. W., Bormans, M., Fastner, J., and Visser, P. M. (2016). CYANOCOST special issue on cyanobacterial blooms: synopsis – a critical review of the management options for their prevention, control and mitigation. *Aquat. Ecol.* 50, 595–605. doi: 10.1007/s10452-016-9596-x

Isles, P. D. F. (2020). The misuse of ratios in ecological stoichiometry. *Ecology*. doi: 10.1002/ecy.3153 [Epub ahead of print].

Jones, R. I. (2000). Mixotrophy in planktonic protists: an overview. *Freshw. Biol.* 45, 219–226. doi: 10.1046/j.1365-2427.2000.00672.x

Jost, C., Lawrence, C. A., Campolongo, F., van de Bund, W., Hill, S., and DeAngelis, D. L. (2004). The effects of mixotrophy on the stability and dynamics of a simple planktonic food web model. *Thor. Popul. Biol.* 66, 37–51. doi: 10.1016/j.tpb.2004.02.001

Kalff, J. (2002). *Limnology: Inland Water Ecosystems*. Upper Saddle River, NJ: Prentice Hall.

Kardinaal, W. E. A., Tonk, L., Janse, I., Hol, S., Slot, P., Huisman, J., et al. (2007). Competition for light between toxic and nontoxic strains of the harmful cyanobacterium *Microcystis*. *Appl. Environ. Microbiol.* 73, 2939–2946. doi: 10.1128/aem.02892-06

Kirk, J. T. (1994). *Light and Photosynthesis in Aquatic Ecosystems*. Oxford: Oxford University Press.

Knowlton, M. F. (1984). Flow-through microcuvette for fluorometric determination of chlorophyll. *Water Resour. Bull.* 20, 795–799. doi: 10.1111/j.1752-1688.1984.tb04763.x

Kromkamp, J. C., Dijkman, N. A., Peene, J., Simms, S. G. H., and Gons, H. J. (2008). Estimating phytoplankton primary production in Lake Ijsselmeer (The Netherlands) using variable fluorescence (PAM-FRRF) and C-uptake technique. *Eur. J. Phycol.* 43, 327–344. doi: 10.1080/09670260802080895

Lake, R. G., and Hinch, S. G. (1999). Acute effects of suspended sediment angularity on juvenile coho salmon (*Oncorhynchus kisutch*). *Can. J. Fish. Aquat. Sci.* 56, 862–867. doi: 10.1139/f99-024

Laspoumaderes, C., Modenutti, B., Souza, M. S., Navarro, M. B., Cuassolo, F., and Balseiro, E. (2013). Glacier melting and stoichiometric implications for lake community structure: zooplankton species distributions across a natural light gradient. *Glob. Change Biol.* 19, 316–326. doi: 10.1111/gcb.12040

Lee, R. E. (2008). *Phycology*. Cambridge: Cambridge University Press.

Lehman, P. W., Marr, K., Boyer, G. L., Acuna, S., and Teh, S. J. (2013). Long-term and causal factors associated with *Microcystis* abundance and toxicity in San Francisco Estuary and implication for climate change impacts. *Hydrobiologia* 718, 141–158. doi: 10.1007/s10750-013-1612-8

Lizotte, M. P., and Priscu, J. C. (1992). Photosynthesis–Irradiance relationships in phytoplankton from the physically stable water column of a perennially ice-covered lake (Lake Bonney, Antarctica). *J. Phycol.* 28, 179–185. doi: 10.1111/j.0022-3646.1992.00179.x

Ludwig, G. R., Perschbacher, P., and Edziyie, R. (2008). The effect of the dye Aquashade§on water quality, phytoplankton, zooplankton, and sunshine bass, *Morone chrysops x M-saxatilis*, fingerling production in fertilized culture ponds. *J. World Aquacult. Soc.* 41, 40–48. doi: 10.1111/j.1749-7345.2009.00331.x

Lund, J. W. G., Kipling, C., and LeCren, E. D. (1958). The inverted microscope method of estimating algal numbers and the statistical basis of estimates by counting. *Hydrobiologia* 11, 143–170. doi: 10.1007/bf00007865

Lürling, M., Eshetu, F., Faassen, E. J., Kosten, S., and Husza, V. L. M. (2013). Comparison of cyanobacterial and green algal growth rates at different temperatures. *Freshw. Biol.* 58, 552–559. doi: 10.1111/j.1365-2427.2012.02866.x

Lürling, M., and van Oosterhout, F. (2012). Case study on the efficacy of a lanthanum-enriched clay (Phoslock§) in controlling eutrophication in Lake Het Groene Eiland (The Netherlands). *Hydrobiologia* 710, 253–263. doi: 10.1007/s10750-012-1141-x

MacIntyre, H. L., Kana, T. M., Anning, T., and Geider, R. J. (2002). Photoacclimation of photosynthesis irradiance response curves and photosynthetic pigments in microalgae and cyanobacteria. *J. Phycol.* 38, 17–38. doi: 10.1046/j.1529-8817.2002.00094.x

Mackay, E. B., Maberly, S. C., Pan, G., Reitzel, K., Bruere, A., Corker, N., et al. (2014). Geoengineering in lakes: welcome attraction or fatal distraction? *Inland Waters* 4, 349–356. doi: 10.5268/iw-4.4.769

Miller, M. A., Kudela, R. M., Mekebri, A., Crane, D., Oates, S. C., Tinker, M. T., et al. (2010). Evidence for a novel marine harmful algal bloom: cyanotoxin (microcystin) transfer from land to sea otters. *PLoS One* 5:e12576. doi: 10.1371/journal.pone.0012576

Miner, J. G., and Stein, R. A. (1996). Detection of predators and habitat choice by small bluegills: effect of turbidity and alternative prey. *Trans. Am. Fish. Soc.* 125, 97–103. doi: 10.1577/1548-8659(1996)125<0097:dopahc>2.3.co;2

Modenutti, B., Pérez, G., Balseiro, E., and Queimalinos, C. (2000). The relationship between light attenuation, chlorophyll a and total suspended solids in a Southern Andes glacial lake. *Verh. Int. Ver. Limnol.* 27, 1–4. doi: 10.1080/07438141.2011.554962

Moore, R. D., Fleming, S. W., Menounos, B., Wheate, R., Fountain, A., Stahl, K., et al. (2009). Glacier change in western North America: influences on hydrology, geomorphic hazards and water quality. *Hydrol. Process.* 23, 42–61. doi: 10.1002/hyp.7162

Osgood, R. A. (2017). Inadequacy of best management practices for restoring eutrophic lakes in the United States: guidance for policy and practice. *Inland Waters* 7, 401–407. doi: 10.1080/20442041.2017.1368881

Overkamp, K. E., Gasper, R., Kock, K., Herrmann, C., Hofmann, E., and Frankenberg-Dinkel, N. (2014). Insights into the biosynthesis and assembly of cryptophycean phycobiliproteins. *J. Biol. Chem.* 289, 26691–26707. doi: 10.1074/jbc.m114.591131

Paerl, H. W., and Huisman, J. (2009). Climate change: a catalyst for global expansion of harmful cyanobacterial blooms. *Environ. Microbiol. Rep.* 1, 27–37. doi: 10.1111/j.1758-2229.2008.00004.x

Paerl, H. W., and Paul, V. J. (2012). Climate change: links to global expansion of harmful cyanobacteria. *Water Res.* 46, 1349–1363. doi: 10.1016/j.watres.2011.08.002

Paerl, H. W., Tucker, J., and Bland, P. T. (1983). Carotenoid enhancement and its role in maintaining blue-green algal (*Microcystis aeruginosa*) surface blooms. *Limnol. Oceanogr.* 28, 847–857. doi: 10.4319/lo.1983.28.5.0847

Paes, T. A. S. V., Costa, I. A. S., Silva, A. P. C., and Eskinazi-Sant'Anna, E. M. (2016). Can microcystins affect zooplankton structure community in tropical eutrophic reservoirs? *Braz. J. Biol.* 76, 450–460. doi: 10.1590/1519-6984.21014

Petty, E. L., Obrecht, D. V., and North, R. L. (2020). Filling in the flyover zone: high phosphorus in midwestern (USA) reservoirs results in high phytoplankton biomass but not high primary productivity. *Front. Environ. Sci.* 8:111. doi: 10.3389/fenvs.2020.00111

Porter, K. G. (1988). Phagotrophic phytoflagellates in microbial food webs. *Hydrobiologia* 159, 89–97. doi: 10.1007/bf00007370

R Core Team (2019). *R: A Language and Environment for Statistical Computing*. Vienna: R Foundation for Statistical Computing.

Rampe, E. B., Horgan, B., Scudder, N., Smith, R. J., and Rutledge, A. M. (2017). *Mineralogy of Rock Flour in Glaciated Volcanic Terrains: An Analog for a Cold and Icy Early Mars. NASA Technical Report JSC-CN-38727*. Washington, DC: NASA.

Raven, J. A., and Richardson, K. (1984). Dinophyte flagella: a cost-benefit analysis. *New Phytol.* 98, 259–276. doi: 10.1111/j.1469-8137.1984.tb02736.x

Robarts, R. D., and Zohary, T. (1987). Temperature effects on photosynthetic capacity, respiration, and growth rates of bloom-forming cyanobacteria. *N. Z. J. Mar. Freshw. Res.* 21, 391–399. doi: 10.1080/00288330.1987.9516235

Rohrlack, T., Dittmann, E., Börner, T., and Christoffersen, K. (2001). Effects of cell-bound microcystins on survival and feeding of *Daphnia* spp. *Appl. Environ. Microbiol.* 67, 3523–3529. doi: 10.1128/aem.67.8.3523-3529.2001

Rose, K. C., Hamilton, D. P., Williamson, C. E., McBride, C. G., Fischer, J. M., Olson, M. H., et al. (2014). Light attenuation characteristics of glacially-fed lakes. *J. Geophys. Res. Biogeosci.* 119, 1446–1457. doi: 10.1002/2014jg002674

Salmaso, N., Naselli-Flores, L., and Padisák, J. (2015). Functional classifications and their applications in phytoplankton ecology. *Freshw. Biol.* 60, 603–619. doi: 10.1111/fwb.12520

Sarma, S. S. S., Nandini, S., and Gulati, R. D. (2002). Cost of reproduction in selected species of zooplankton (rotifers and cladocerans). *Hydrobiologia* 481, 89–99.

Sarnelle, O. (1993). Herbivore effects on phytoplankton succession in a eutrophic lake. *Ecol. Monogr.* 63, 129–149. doi: 10.2307/2937177

Sartory, D. P., and Grobbelaar, J. U. (1986). Extraction of chlorophyll-*a* from freshwater phytoplankton for spectrophotometric analysis. *Hydrobiologia* 114, 117–187.

Scheffer, M., Carpenter, S., Foley, J. M., Folke, C., and Walker, B. (2001). Catastrophic shifts in ecosystems. *Nature* 413, 591–596. doi: 10.1038/35098000

Schwaderer, A. S., Yoshiyama, K., Pinto, P., Swenson, N. G., Klausmeier, C. A., and Litchman, E. (2011). Eco-evolutionary differences in light utilization traits and distributions of freshwater phytoplankton. *Limnol. Oceanogr.* 56, 589–598. doi: 10.4319/lo.2011.56.2.0589

Sharpley, A., Foy, B., and Withers, P. (2000). Practical and innovative measures for the control of agricultural phosphorus losses to water: an overview. *J. Environ. Qual.* 29, 1–9. doi: 10.2134/jeq2000.00472425002900010001x

Silsbe, G. M., Hecky, R. E., and Smith, R. E. H. (2012). Improved estimation of carbon fixation rates from active flourometry using spectral fluorescence in light-limited environments. *Limnol. Oceanogr. Methods* 10, 736–751. doi: 10.4319/lom.2012.10.736

Silsbe, G. M., and Malkin, S. Y. (2015). *phytotools: Phytoplankton Production Tools. R package version 1.0*. Available online at: https://CRAN.R-project.org/package=phytotools (accessed March 1, 2020).

Sinha, R. P., and Häder, D. P. (2008). UV-protectants in cyanobacteria. *Plant Sci.* 174, 278–289. doi: 10.1016/j.plantsci.2007.12.004

Slemmons, K. E. H., and Saros, J. E. (2012). Implications of nitrogen-rich glacial meltwater for phytoplankton diversity and productivity in alpine lakes. *Limnol. Oceanogr.* 57, 1651–1663. doi: 10.4319/lo.2012.57.6.1651

Slemmons, K. E. H., Saros, J. E., and Simon, K. (2013). The influence of glacial meltwater on alpine aquatic ecosystems: a review. *Environ. Sci. Proc. Imp.* 15, 1794–1806. doi: 10.1039/c3em00243h

Sommaruga, R. (2015). When glaciers and ice sheets melt: consequences for planktonic organisms. *J. Plankton Res.* 37, 509–518. doi: 10.1093/plankt/fbv027

Sommaruga, R., and Kandolf, G. (2014). Negative consequences of glacial turbidity for the survival of freshwater planktonic heterotrophic flagellates. *Sci. Rep.* 4:4113. doi: 10.1038/srep04113

Spencer, D. F. (1984). Oxygen consumption by the crayfish *Orconectes propinquus* (Girard) exposed to Aquashade. *Bull. Environ. Contam. Toxicol.* 33, 373–378. doi: 10.1007/bf01625557

Stemberger, R. S., and Gilbert, J. J. (1985). Body size, food concentration, and population growth in planktonic rotifers. *Ecology* 66, 1151–1159. doi: 10.2307/1939167

Stoecker, D. K., Hansen, P. J., Caron, D. A., and Mitra, A. (2017). Mixotrophy in the marine plankton. *Annu. Rev. Mar. Sci.* 9, 311–335. doi: 10.1146/annurev-marine-010816-060617

Suski, J. G., Swan, C. M., Salice, C. J., and Wahl, C. F. (2018). Effects of pond management on biodiversity patterns and community structure of zooplankton in urban environments. *Sci. Total. Environ.* 619, 1441–1450. doi: 10.1016/j.scitotenv.2017.11.153

Thorp, J. H., and Covich, A. P. (2001). *Ecology and Classification of North American Freshwater Invertebrates*. San Diego, CA: Academic Press.

Tittle, J., Bissinger, V., Zipple, B., Gaedke, U., Bell, E., Lorke, A., et al. (2003). Mixotrophs combine resource use to outcompete specialists: implications for aquatic food webs. *Proc. Natl. Acad. Sci. U.S.A.* 100, 12776–12781. doi: 10.1073/pnas.2130696100

U.S. Environmental Protection Agency (2016). *Climate Change Indicators in the United States, 2016*, Fourth Edn. Washington, DC: U.S. Environmental Protection Agency.

Urabe, J., Gurung, T. B., Yoshida, T., Sekino, T., and Nakanishi, M. (2000). Diel changes in phagotrophy by *Cryptomonas* in Lake Biwa. *Limnol. Oceanogr.* 45, 1558–1563. doi: 10.4319/lo.2000.45.7.1558

Üveges, V., Tapolczai, K., Krienitz, L., and Padisák, J. (2012). Photosynthetic characteristics and physiological plasticity of an *Aphanizomenon flos-aquae* (Cyanobacteria, Nostocaceae) winter bloom in a dep oligo-mesotrophic lake (Lake Stechlin, Germany). *Hydrobiologia* 698, 263–272. doi: 10.1007/978-94-007-5790-5_20

Van Halderen, A., Harding, W. R., Wessels, J. C., Schneider, D. J., Heine, E. W. P., Van Der Merwe, J., et al. (1995). Cyanobacterial (blue-green algae) poisoning of livestock in the Western Cape Province of South Africa. *J. S. Afr. Vet. Assoc.* 66, 260–264.

Van Liere, L., and Mur, L. R. (1980). "Occurrence of *Oscillatoria Agardhii* and some related species, a survey," in *Hypertrophic Ecosystems: Developments in Hydrobiology*, Vol. 2, eds J. Barica and L. R. Mur (Dordrecht: Springer), 66–77.

Visser, P. M., Ibelings, B. W., Bormans, M., and Huisman, J. (2016). Artificial mixing to control cyanobacterial blooms: a review. *Aquat. Ecol.* 50, 423–441. doi: 10.1007/s10452-015-9537-0

Vogel, J. L., and Beauchamp, D. A. (1999). Effects of light, prey size, and turbidity on reaction distances of lake trout (*Salvelinus namaycush*) to salmonid prey. *Can. J. Fish. Aquat. Sci.* 56, 1293–1297. doi: 10.1139/f99-071

Wagner, K. J., Meringolo, D., Mitchell, D. F., Moran, E., and Smith, S. (2017). Aluminum treatments to control internal phosphorus loading in lakes on Cape Cod, Massachusetts. *Lake Reserv. Manage.* 33, 171–186. doi: 10.1080/10402381.2017.1308449

Wallace, B. B., and Hamilton, D. P. (2000). Simulation of water-bloom formation in the cyanobacterium *Microcystis aeruginosa*. *J. Plankton Res.* 22, 1127–1138. doi: 10.1093/plankt/22.6.1127

Webb, W. L., Newton, M., and Starr, D. (1974). Carbon dioxide exchange of *Alnus rubra*: a mathematical model. *Oecologia* 17, 281–291. doi: 10.1007/bf00345747

Wickham, H. (2009). *ggplot2: Elegant Graphics for Data Analysis*. New York, NY: Springer.

Winslow, L., Read, J., Woolway, R., Brentrup, J., Leach, T., Zward, J., et al. (2017). *rLakeAnalyzer: Lake Physics Tools*. Available online at: https://cran.r-project.org/package=rLakeAnalyzer (accessed March 1, 2020).

Yang, J. R., Lv, H., Isabwe, A., Liu, L., Yu, X., Chen, H., et al. (2017). Disturbance-induced phytoplankton regime shifts and recovery of cyanobacteria dominance in two subtropical reservoirs. *Water Res.* 120, 52–63. doi: 10.1016/j.watres.2017.04.062

Yang, S., and Jin, X. (2008). Critical light intensities for *Microcystis aeruginosa, Scenedesmus quadricauda* and *Cytoclotella* sp. and competitive growth patterns under different light:N:P ratios. *J. Freshw. Ecol.* 23, 387–396. doi: 10.1080/02705060.2008.9664215

Zamparas, M., Gianni, A., Stathi, P., Deligiannakis, Y., and Zacharias, I. (2012). Removal of phosphate from natural waters using innovative modified bentonites. *Appl. Clay Sci.* 62, 101–106. doi: 10.1016/j.clay.2012.04.020

Zhang, M., Shi, X., Yu, Y., and Kong, F. (2011). The acclimative changes in photochemistry after colony formation of the cyanobacteria *Microcystis aeruginosa*. *J. Phycol.* 47, 524–532. doi: 10.1111/j.1529-8817.2011.00987.x

Conflict of Interest: The authors declare that the research was conducted in the absence of any commercial or financial relationships that could be construed as a potential conflict of interest.

frontiers in Environmental Science

ORIGINAL RESEARCH
published: 16 December 2020
doi: 10.3389/fenvs.2020.539733

Phytoplankton Community Responses to Interactions Between Light Intensity, Light Variations, and Phosphorus Supply

Vanessa Marzetz[1,2]*, *Elly Spijkerman*[1], *Maren Striebel*[3] and *Alexander Wacker*[2]

[1] Ecology and Ecosystem Modeling, Institute of Biochemistry and Biology, University of Potsdam, Potsdam, Germany, [2] Animal Ecology, Zoological Institute and Museum, University of Greifswald, Greifswald, Germany, [3] Plankton Ecology, Institute for Chemistry and Biology of the Marine Environment, University of Oldenburg, Wilhelmshaven, Germany

In a changing world, phytoplankton communities face a large variety of challenges including altered light regimes. These alterations are caused by more pronounced stratification due to rising temperatures, enhanced eutrophication, and browning of lakes. Community responses toward these effects can emerge as alterations in physiology, biomass, biochemical composition, or diversity. In this study, we addressed the combined effects of changes in light and nutrient conditions on community responses. In particular, we investigated how light intensity and variability under two nutrient conditions influence (1) fast responses such as adjustments in photosynthesis, (2) intermediate responses such as pigment adaptation and (3) slow responses such as changes in community biomass and species composition. Therefore, we exposed communities consisting of five phytoplankton species belonging to different taxonomic groups to two constant and two variable light intensity treatments combined with two levels of phosphorus supply. The tested phytoplankton communities exhibited increased fast reactions of photosynthetic processes to light variability and light intensity. The adjustment of their light harvesting mechanisms via community pigment composition was not affected by light intensity, variability, or nutrient supply. However, pigment specific effects of light intensity, light variability, and nutrient supply on the proportion of the respective pigments were detected. Biomass was positively affected by higher light intensity and nutrient concentrations while the direction of the effect of variability was modulated by light intensity. Light variability had a negative impact on biomass at low, but a positive impact at high light intensity. The effects on community composition were species specific. Generally, the proportion of green algae was higher under high light intensity, whereas the cyanobacterium performed better under low light conditions. In addition to that, the diatom and the cryptophyte performed better with high nutrient supply while the green algae as well as the cyanobacterium performed better at low nutrient conditions. This shows that light intensity, light variability, and nutrient supply interactively affect communities. Furthermore, the responses are highly species and pigment specific, thus to clarify the effects of climate change a deeper understanding of the effects of light variability and species interactions within communities is important.

Keywords: phytoplankton communities, light variability, photosynthetic rate, climate change, resource competition, light intensity (irradiance), pigment composition, nutrient supply

OPEN ACCESS

Edited by:
Patrick J. Neale, Smithsonian Environmental Research Center (SI), United States

Reviewed by:
Jan Köhler, Leibniz-Institute of Freshwater Ecology and Inland Fisheries (IGB), Germany
Elena Litchman, Michigan State University, United States

***Correspondence:**
Vanessa Marzetz
marzetz@uni-potsdam.de

Specialty section:
This article was submitted to Freshwater Science, a section of the journal Frontiers in Environmental Science

Received: *02 March 2020*
Accepted: *25 November 2020*
Published: *16 December 2020*

Citation:
Marzetz V, Spijkerman E, Striebel M and Wacker A (2020) Phytoplankton Community Responses to Interactions Between Light Intensity, Light Variations, and Phosphorus Supply. Front. Environ. Sci. 8:539733. doi: 10.3389/fenvs.2020.539733

INTRODUCTION

In a world of climate change, phytoplankton communities face a large variety of challenges due to manifold changes. Rising temperatures, e.g., directly influence many physical and physiological processes (Hatt, 1983; Connelly et al., 2009; Gross-Wittke et al., 2010; Warren et al., 2012; Pachepsky et al., 2014; Havens et al., 2015; Huang and Chou, 2017). Besides these direct temperature effects on organisms, increasing temperature leads to a phenological shift, i.e., spring starts earlier and summer lasts longer (Stine et al., 2009). Temperate regions are strongly influenced by seasonality and thus are particularly affected by rising temperatures. Rising temperatures lead to shorter or no ice coverage and distinctly altered mixing regimes and periods, such as decreased length of spring vertical mixing followed by increased duration of summer stratification (Vincent, 2009; Wagner et al., 2013; IGB Dossier, 2018). Climate change is also accompanied by more common weather extremes, increased precipitation, and storm events. Higher precipitation is linked to increased terrestrial run-off, thus external inputs of light absorbing dissolved organic material as well as nutrients into lakes (de Wit et al., 2016; Deininger and Frigstad, 2019). More frequent storm events and changes in temperatures will affect the turbidity and biomass production and thus also the light availability. All these manifold changes influence light availability and heterogeneity. The heterogeneity in light conditions in aquatic systems may cause shifts in phytoplankton growth rates (Litchman, 1998), photosynthesis rates (Piccinin, 1976; Marra, 1978; Grobbelaar et al., 1992; Kroon et al., 1992), respiration rates (Beardall et al., 1994; Litchman, 1998), and biochemical composition (Gibson and Foy, 1988; Kroon et al., 1992; Ibelings et al., 1994). All these responses occur on different time scales, e.g., adjusting the electron transport rate (photosynthesis) within milliseconds, whereas building complex biochemical molecules can take several hours. Further, light fluctuations can occur not just seasonally and daily, but in shorter time scales, such as waves that focus light or clouds that shade the water. On one hand, even the shortest light fluctuations influence phytoplankton, as photosynthesis can react very rapidly to light changes (Dromgoole, 1988; Flameling and Kromkamp, 1997; Garcia-Mendoza et al., 2002; Dimier et al., 2009). On the other hand, slower fluctuations affect phytoplankton communities in their composition and diversity (Flöder et al., 2002; Flöder and Burns, 2005) and growth rates (Köhler et al., 2018). In phytoplankton composition changes with the annual succession of a lake, e.g., diatoms dominate in spring, green algae in summer (Salmaso, 2003). Nevertheless, individual species respond very specifically to light intensities and variability (Litchman, 2000; Garcia-Mendoza et al., 2002; Shatwell et al., 2012) and show distinct light reaction curves (unpublished Data). These species-specific responses to variability of resource availability in general evolved due to interspecific competition in a community leading to niche partitioning and coexistence (Litchman and Klausmeier, 2001). Competition, adaptation to different light intensities, and the resulting dominance of one species compared to other species might hold a positive effect for the inferior species. For example, a dominating species that can cope with high light intensities might reduce light stress for low light adapted species due to shading. In addition to light adaptation, species have different physiological properties, e.g., size and differential nutrient acquisition rates (Huisman and Weissing, 1995; Dickman et al., 2006; Kerimoglu et al., 2012). Competition within communities is driven by all these factors and thus low light adapted species might not be outcompeted by the high light specialist, if they are able to use nutrients in a more efficient way Thus, within a community different mechanisms can become relevant e.g., physiological plasticity for various light acclimation mechanisms. This could (if possible) be distinguished from the effects caused by phenotypic plasticity of individual species within a community and from the effects caused by species sorting. Competition always influences both, i.e., the physiological processes within the community, which can arise from interactions between light and/or nutrient acquisition. Here we addressed the combined interactions to understand the fundamental implications of all these effects in concert and to examine their relative effects. As different species in communities have a variety of traits, e.g., in utilizing nutrients or light, the species in communities will have different reactions and therefore may overall compensate for environmental variability. This compensation possibly takes place at different temporal scales, as e.g., photosynthesis is a fast response and biomass production a slow response. We hypothesize that (1) photosynthesis at shorter time scales, as well as, (2) pigment concentrations at intermediate time scales change due to light intensity, fluctuations, and nutrients. (3) Communities exposed to fluctuating light show similar slow responses as communities that were constantly exposed to the same mean light intensity. Finally, we hypothesize that (4) light intensity and fluctuations have a larger impact on a community than nutrient (Phosphorus, P) supply.

To test these hypotheses, we carried out laboratory experiments with communities consisting of five phytoplankton species, which were exposed to constant and variable light conditions at different intensities. We evaluated the electron transport rate as measure for the fast photosynthesis response to light changes, phytoplankton pigments concentrations as measure for light response at intermediate time scale, and phytoplankton biomass and community compositions as measure of long-term responses to different light intensities and fluctuations. To test if the nutrient availability influences these phytoplankton responses to light changes, we ran the experiment at high and low nutrient supply.

MATERIALS AND METHODS

Phytoplankton Cultures

Five freshwater phytoplankton species were used in this experiment. They were chosen based on taxonomic affiliation and specific traits such as differences in pigment composition, nutrient use, and size.

In detail we used the Cyanophyceae *Synechococcus elongatus* Nägeli (Syn, SAG 89.79), the Chlorophyceae *Acutodesmus obliquus* (Turpin) Hegewald et Hanagata (Acu, SAG 276-3a), the Bacillariophyceae *Stephanodiscus hantzschii*

GRUNOW (Ste, University of Constance), the Cryptophyceae *Cryptomonas ovata* EHRENBERG (Cry, SAG 979-3), and the Eustigmatophyceae *Nannochloropsis limnetica* KRIENITZ, HEPPERLE, STICH, WEILER, (Nan, SAG 18.99).

Every phytoplankton species was pre-cultured either in high P-supply (50 μmol P · L^{-1}, in the form of K_2HPO_4) or low P-supply (5 μmol P · L^{-1}) modified Woods Hole MBL medium (Nichols, 1973). To avoid a limitation by potassium in the cultures with a low P-supply, the final concentration of potassium was adjusted to 100 μmol · L^{-1} using potassium chloride. These P-supplies represent commonly found conditions in natural lakes.

Experimental Set Up

Different species pre-grown as monocultures under controlled laboratory conditions were combined to multi-species communities which were exposed to different P (high and low) and light conditions (constant and variable). Aliquots of the pre-cultures were used to inoculate the experimental phytoplankton communities with equal carbon (C) shares of each species. A total biomass concentration of 1.67 mg C · L^{-1} and 0.67 mg C · L^{-1} was established for cultures with high and low P-supply, respectively. Carbon concentrations were estimated using previously determined carbon-light equations based on the extinction at 800 nm (OD_{800}). All experimental phytoplankton cultures were diluted once a day by exchanging 20 mL of the culture with fresh medium. If variable light conditions were applied as treatments (see below) cultures were diluted at the end of their low light phase and then placed into the high light chamber (0.067 d^{-1}). The cultures were grown in triplicates, at 20°C in 500 mL Erlenmeyer flasks filled with a total volume of 300 mL.

Light treatments consisted of two different light intensities and light conditions (constant and variable). In general, light intensities and light condition treatments in this experiment were chosen based on the common light-optimum curve, going with increasing light intensities from below the compensation point (photosynthesis equals compensation) over a light optimum (highest growth/ photosynthesis) to light inhibition (decrease due to photo damage). The constant light intensities represent possible optimum and near inhibiting light intensities for some of the species (Gervais, 1997; Litchman, 2000). The variable treatments had the same mean light intensity as the constant light treatment, but the cultures were exposed to a combination of light intensities that were either near compensation point and optimum or optimum and inhibiting. The constant light intensities with a regular 12/12 h light/dark cycle were set to 105 or 195 μmol photons · m^{-2} · s^{-1} using different numbers of fluorescent tubes (FLUORA L30W / 77 and LUMILUX L30W / 830, warm white, Osram AG, München, Germany) and distances to the flasks. Additional darkening foils (neutral density foil filters, Lee Filters, Hampshire, England) were used if necessary. The light intensity was verified with a spherical light sensor (LI-1400 data logger; LI-COR Environmental GmbH, Bad Homburg, Germany, equipped with a 4π quantum sensor). Additionally, two variable light conditions were set up, in which phytoplankton communities were irradiated with the same average light intensities as communities exposed to constant light intensities. They were exposed to 3 h lower light intensity, 6 h higher light intensity, and again 3 h of the lower light intensity, which was each shifted by 90 μmol photons · m^{-2} · s^{-1} in one direction or the other from the mean light intensity. This cycle was followed by 12 h darkness (**Supplementary Figure 1**). Consequently, the variability range of the light intensity from low to high light in both variable light treatments was the same, but the mean light intensity was different. The cultures with a high P-supply were harvested after 6 days, whereas the cultures with a low P-supply after 8 days of exponential growth (**Supplementary Figure 2**). This way a large change in treatment light intensity due to high cell densities was avoided. Additionally low P-supply cultures were expected to grow slower and therefore needed more time to obtain sufficient biomass.

Rapid Light Reaction Curves

Rapid light reaction curves of each sample were recorded a day before harvesting using the Phytoplankton Analyzer (PhytoPAM, Walz GmbH, Effeltrich, Germany). For the variable treated cultures samples were taken at the end of the first low light intensity phase. 1.6 mL culture was placed in an all clear glass cuvette. The quantum yield as a reaction to ten different actinic light intensities (8, 32, 64, 128, 192, 256, 320, 384, 448, and 512 μmol photons · m^{-2} · s^{-1}, with an exposure time of 20 s) was recorded. It represents a ratio of emitted and absorbed photons, which indicates photosynthetic efficiency. The electron transport rate (ETR), as an indicator for photosynthetic activity, was calculated from the product of the quantum yield, given by the PhytoPAM, and the amount of light emitted to the algae and the constants of 0.84 and 0.5 as optical cross section and light absorption coefficients, respectively (Consalvey et al., 2005; Kromkamp et al., 2008).

The ETR values were fitted against actinic light intensities of the PhytoPAM to interpolate the values for the specific experimental light intensities (**Supplementary Figure 3**) using the software package R version 3.4.4 (R Development Core Team, 2010). Although, the actinic light does not equal the experimental light conditions completely, due to different bandwidth, we assume the error to be quite similar, as we have used the interpolation for both light intensities in the same way. The ETR value was taken from the curve fit at the growth light intensity. Therefore, it represents the ETR activity of the community at the growth light intensity. The quantum yield of the cultures at growth light intensity was linearly interpolated based on the two light intensities that were higher and lower than the growth light intensity.

Chemical Analysis

Each phytoplankton culture was analyzed at the end of the experiment (harvesting) for particulate organic carbon (C) and pigments. For carbon analysis, aliquots of the algal suspensions were filtered onto 25 mm precombusted glass fiber filters (GF /F, Whatman, Dassel, Germany), dried at 50°C for 48 h and analyzed using an elemental analyzer (Euro EA 3000, HEKAtech GmbH, Wegberg, Germany). For pigment analysis, aliquots of the phytoplankton cultures were filtered onto 25 mm glass

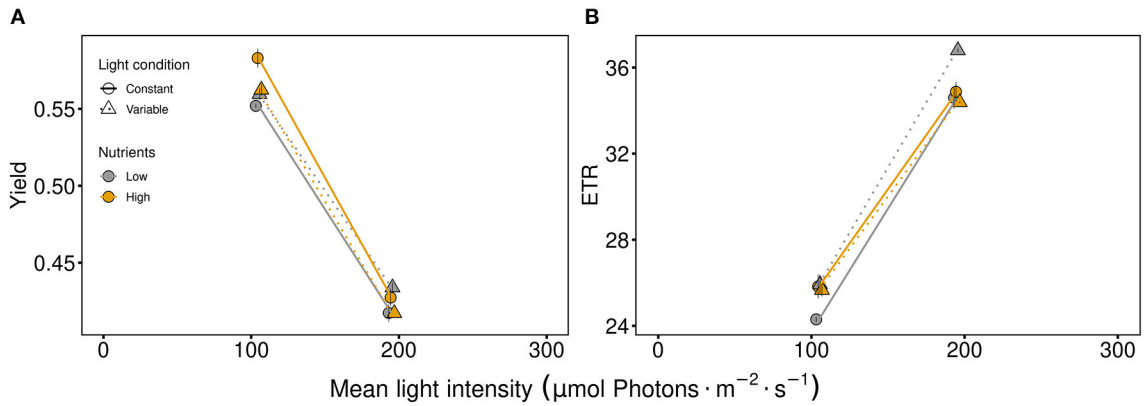

FIGURE 1 | Photosynthetic parameters of the communities: **(A)** the quantum yield indicating photosynthetic efficiency and **(B)** the electron transport rate (ETR) as a measure of photosynthetic activity. Communities were either cultivated under variable (triangles, dashed line) or constant (circles, solid line) light conditions. Mean values are shown for high (orange symbols and lines) and low (gray symbols and lines) nutrient supply and are displayed with ± standard error.

fiber filters (GF/F, Whatman), immediately frozen in liquid nitrogen and stored at −80°C. Pigments were extracted in the dark with 90 vol% ethanol on ice in an ultrasonic bath for 30 min and stored at 4°C overnight. Spectral scans were recorded in a 96 well-plate (Polystyrol, F-bottom type, Boettger, Bodenmais, Germany) in technical triplicates at a spectral absorbance between 300 and 800 nm in 1 nm steps (Synergy H1, BioTek Instruments, Winooski, VT, USA). These scans were fitted with a modified Gauss-peak-spectra analysis in R (R Development Core Team, 2010) according to Thrane et al. (2015). For further evaluation pigments were chosen or grouped according to Roy et al. (2011), which resulted in the following pigment parameters and sum parameters: chlorophyll a, b, c, chlorophyll decomposition products, and xanthophylls. These specific pigments were related to the total detected pigment content (called total pigment content hereafter), which resulted in proportions of pigments and pigment groups.

Community Composition

Phytoplankton species distribution in the communities, cell numbers, and biovolume of the phytoplankton cultures were determined, as during growth species experienced competition and therefore the community composition was expected to be unequal compared to the inoculation. For this, samples from the harvesting day were fixed with Lugol's iodine solution and phytoplankton cells were counted using an inverted light microscope (Thalheim Spezial Optik, Pulsnitz, Germany). The cyanobacterium was counted by epifluorescence microscopy (Axioskop 2, Carl Zeiss, Jena, Germany) under blue light (excitation: BP 450–490 nm; emission: BP 515–565 nm) after staining with acridin-orange (Merck, Darmstadt, Germany). Sizes of phytoplankton cells were measured and converted into biovolume according to Hillebrand et al. (1999). The community composition was calculated based on the cell numbers and biovolume.

Data Analysis

Effects of nutrient availability (high and low P-supply), average light intensity (105 or 195 µmol photons · m^{-2} · s^{-1}), and light condition (constant or variable) on electron transport rate (ETR), pigment composition, biomass (Carbon concentration; C), and species composition were tested using three-way ANOVA.

All statistical analyses were carried out using the statistical software package R (R Development Core Team, 2010).

RESULTS

Different light intensities, light conditions, and nutrient supplies resulted in distinct responses at different temporal scales. Thereby, photosynthetic activity, pigment composition, and biomass and species composition reflect fast, intermediate, and slow responses.

The fast responding quantum yield and electron transport rate (ETR), used as indicator for photosynthetic efficiency and activity, respectively, were strongly affected by light intensity (**Figure 1**, **Table 1**). On one hand, the photosynthetic efficiency decreased at high light intensities (**Figure 1A**, **Table 1**). On the other hand, high light intensity and variability favored higher photosynthetic activity (**Figure 1B**, **Table 1**). Under low nutrient conditions, the quantum yield and the ETR were higher at variable light conditions at both light intensities (105 µmol photons · m^{-2} · s^{-1} and 195 µmol photons · m^{-2} · s^{-1}) compared to constant light conditions (**Figure 1**, **Table 1**). Thus, the effect of nutrient concentrations differed between light levels and light conditions (indicated by the significant interaction of light intensity and nutrients as well as light conditions and nutrients, **Figure 1**).

No significant effect due to any factor was seen at the intermediate response, while the total pigment per carbon (**Figure 2A**) tended to be lower at high light intensities. Considering specific pigments (examined as the proportion of total pigments), significant adjustments in pigments were observed (**Figure 2**, **Table 1**). Light conditions (variability) had

TABLE 1 | ANOVA table for all factors (light intensity, light condition, and nutrient condition) including interactive effects conducted for all response variables.

Factor			Yield		ETR	
	dfN	dfD	*F*	*p*	*F*	*p*
Intensity	1	16	2083	**<0.001**	1413	**<0.001**
Condition	1	16	8.72	0.773	9.36	**0.007**
Nutrients	1	16	0.07	0.096	0.70	0.415
Intensity*condition	1	16	0.08	0.154	0.07	0.803
Intensity*nutrients	1	16	9.40	**0.008**	10.75	**0.005**
Condition*nutrients	1	16	16.66	**<0.001**	18.79	**0.001**
Intensity*condition*nutrients	1	16	0.02	0.881	0.77	0.394

Factor			Total pigm mg C		Log Chl a		Log Chl b		Log Chl c		Log Chl decom.		Log Xan	
	dfN	dfD	*F*	*p*	*F*	*p*	*F*	*p*	*F*	*p*	*F*	*p*	*F*	*p*
Intensity	1	16	2.64	0.124	0.38	0.545	6.41	**0.022**	22.15	**<0.001**	1.99	0.178	15.09	**0.001**
Condition	1	16	0.60	0.448	4.70	**0.046**	0.11	0.749	1.52	0.236	7.75	**0.013**	1.06	0.318
Nutrients	1	16	0.004	0.952	1.12	0.305	79.98	**<0.001**	817.1	**<0.001**	1.41	0.252	48.04	**<0.001**
Intensity*condition	1	16	0.002	0.961	3.20	0.093	0.57	0.461	3.16	0.094	0.61	0.445	6.47	**0.022**
Intensity*nutrients	1	16	0.46	0.509	0.62	0.444	0.09	0.774	31.36	**<0.001**	0.03	0.874	1.94	0.183
Condition*nutrients	1	16	0.07	0.791	0.07	0.800	6.58	**0.021**	0.11	0.741	0.07	0.790	8.64	**0.010**
Intensity*condition*nutrients	1	16	0.25	0.622	0.34	0.570	0.35	0.562	0.78	0.390	1.79	0.199	5.28	0.035

Factor			Biomass		Log Syn		Log Acu		Log Ste		Log Cry		Log Nan	
	dfN	dfD	*F*	*p*	*F*	*p*	*F*	*p*	*F*	*p*	*F*	*p*	*F*	*p*
Intensity	1	16	42.22	**<0.001**	1.96	0.18	1.05	0.32	15.25	**0.001**	2.72	0.119	0.57	0.461
Condition	1	16	0.08	0.777	0.02	0.889	0.04	0.844	1.57	0.229	8.50	**0.01**	0.25	0.624
Nutrients	1	16	58.50	**<0.001**	26.21	**<0.001**	6.66	**0.02**	183.9	**<0.001**	121.1	**<0.001**	1.72	0.208
Intensity*condition	1	16	13.50	**0.002**	3.40	0.084	0.46	0.505	0.06	0.804	0.50	0.491	0.06	0.806
Intensity*nutrients	1	16	1.06	0.319	1.15	0.299	1.48	0.242	0.05	0.828	0.28	0.605	0.37	0.55
Condition*nutrients	1	16	1.70	0.211	0.007	0.937	0.22	0.648	2.21	0.157	0.43	0.524	0.07	0.794
Intensity*condition*nutrients	1	16	1.04	0.324	0.008	0.93	1.10	0.309	2.00	0.176	0.35	0.561	2.62	0.125

Significant results are shown in bold numbers. Total pigments per mg C represent the sum of the detected pigments in the community based on the community biomass in mg C. Yield, species and pigment proportions were log-transformed before analysis. Yield was not homogenous. Log Acu and Chl c data were not homogeneous and normally distributed. Acronyms are ETR, electron transport rate; total pigm. mg C, total pigment per mg C; Chl, chlorophyll; Chl decom., chlorophyll decomposition products; Xan, xanthophylls; Syn, Synechococcus elongatus; Acu, Acutodesmus obliquus; Ste, Stephanodiscus hantzschii; Cry, Cryptomonas ovata; Nan, Nannochloropsis limnetica.

a significant effect on chlorophyll *a* proportion (**Table 1**), resulting in a lower proportion of chlorophyll *a* under variable light conditions (**Figure 2B**). Chlorophyll *b* proportions were significantly higher under low P-supply and even higher at higher light intensity (**Figure 2C**). Light variability had a positive effect on the proportion of chlorophyll *b* under limiting nutrient conditions while the effect of light variability was negative (compared to constant conditions) under high nutrient conditions (indicated by the significant interaction term of light conditions and nutrients, **Table 1**). Chlorophyll *c* proportions strongly differed between nutrient levels (main effect for nutrients, **Table 1**) and under low nutrient conditions chlorophyll *c* proportions were almost zero (**Figure 2D**). High light intensity resulted in lower proportions of chlorophyll *c* compared to low light intensity under high nutrient conditions (light intensity and nutrient interaction, **Table 1**). Chlorophyll decomposition products were higher under variable light conditions, especially if the light intensity was high (**Figure 2E**, **Table 1**). This mirrors chlorophyll *a*, which was lowest under variable high light conditions. The proportion of xanthophyll was generally higher with high nutrient supply (**Figure 2F**, **Table 1**). While variable light conditions resulted in higher xanthophyll proportions with high nutrient supply, xanthophyll proportions were lower at variable light conditions when exposed to low nutrient concentrations (significant light conditions and nutrient interactive effect, **Table 1**).

Biomass was significantly higher at higher light intensity and with higher nutrient supply (**Figure 3A**, **Table 1**). The effect of light conditions was dependent on the light intensity. At low light intensity the constant light condition treatments were higher while at high light intensity the fluctuating light condition treatments obtained higher biomass (indicated by the light intensity and condition interactive effect, **Figure 3A** and **Table 1**). The effects of light intensity, light and nutrient

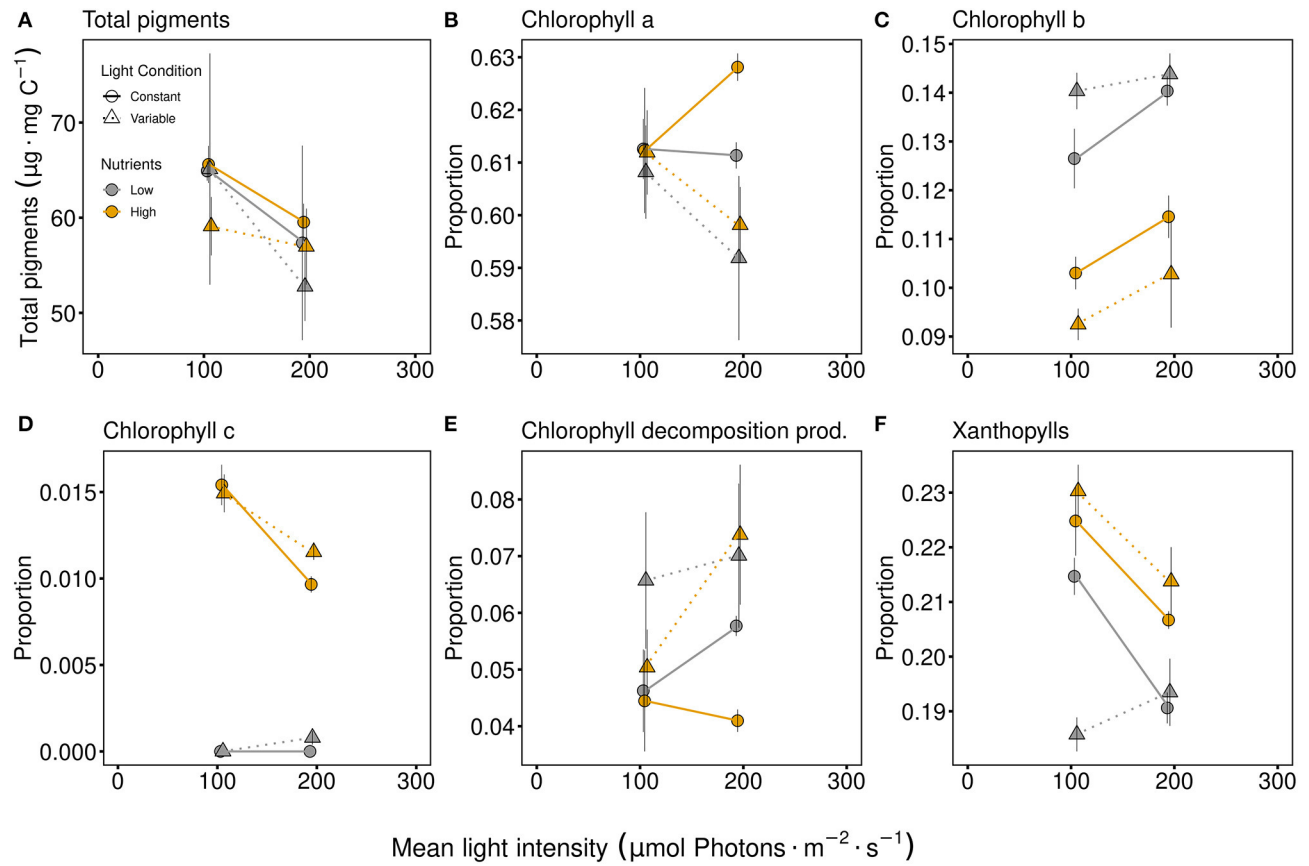

FIGURE 2 | Total pigment content [µg Pigments per mg carbon; **(A)**] and proportions of specific chlorophylls **(B–D)**, as well as chlorophyll decomposition products [Chlorophyll decomposition prod., **(E)**] and xanthophylls **(F)**. Communities were either cultivated under variable (triangles, dashed line) or constant (circles, solid line) light conditions. Mean values are shown for high (orange symbols and lines) and low (gray symbols and lines) nutrient supply and are displayed with ± standard error. Pigment proportions in more detail are shown in **Supplementary Figure 5**.

conditions in the community differed between the species. In general, *Acutodesmus obliquus* was the dominant species in all treatments (**Figure 3C**). While *Synechococcus elongatus* and *Acutodesmus obliquus* were present in higher proportions with low nutrient conditions (**Figure 3** and **Table 1**), *Stephanodiscus hantzschii* and *Cryptomonas ovata* had higher proportions under high nutrient conditions (**Figure 3** and **Table 1**) and *Nannochloropsis limnetica* exhibited no effect from the three factors at all (**Table 1**). Besides the nutrient effect, *Stephanodiscus hantzschii* was also affected by light intensity, obtaining higher proportions under low light conditions (**Figure 3D**, **Table 1**). The proportion of *Cryptomonas ovata* differed significantly due to light conditions, thus higher proportions were obtained under constant light conditions (**Figure 3E**, **Table 1**).

DISCUSSION

Photosynthesis as a fast response to light was highly influenced by light intensity and light condition. Although, there was no direct nutrient effect on the quantum yield or the ETR, the significant interaction terms (**Table 1**) indicated that nutrient supply affected photosynthetic efficiency and activity differently under different light intensities and conditions. This could indicate that under constant light conditions a low supply in nutrients reduces the photosynthetic efficiency and activity compared to fluctuating conditions. In other words, when nutrient supply was low, in addition to a constant light stress the community experienced nutrient stress as well. In this case variability causes light stress relief and resulted in higher short-time photosynthetic rates. This double stress effect is possibly related to the observation that light energy cannot be used for biomass production when nutrients are lacking (Burson et al., 2018). From monocultures, it has been suggested that variability increased maximum photosynthesis and efficiency as photosynthesis was optimized in fluctuating light (Flameling and Kromkamp, 1997; Talmy et al., 2013).

The total pigment content was not affected by the three factors at intermediate time scales (**Figure 2A**). However, the factors led to different reactions in specific pigment groups. As pigments are affected by both light intensity (Garcia-Mendoza et al., 2002; Dimier et al., 2009) and variability (Flameling and Kromkamp, 1997) their proportions would generally be expected to show large differences between variable and constant light regimes. Beside the factor of irradiance (Johnsen et al., 1994; Goericke

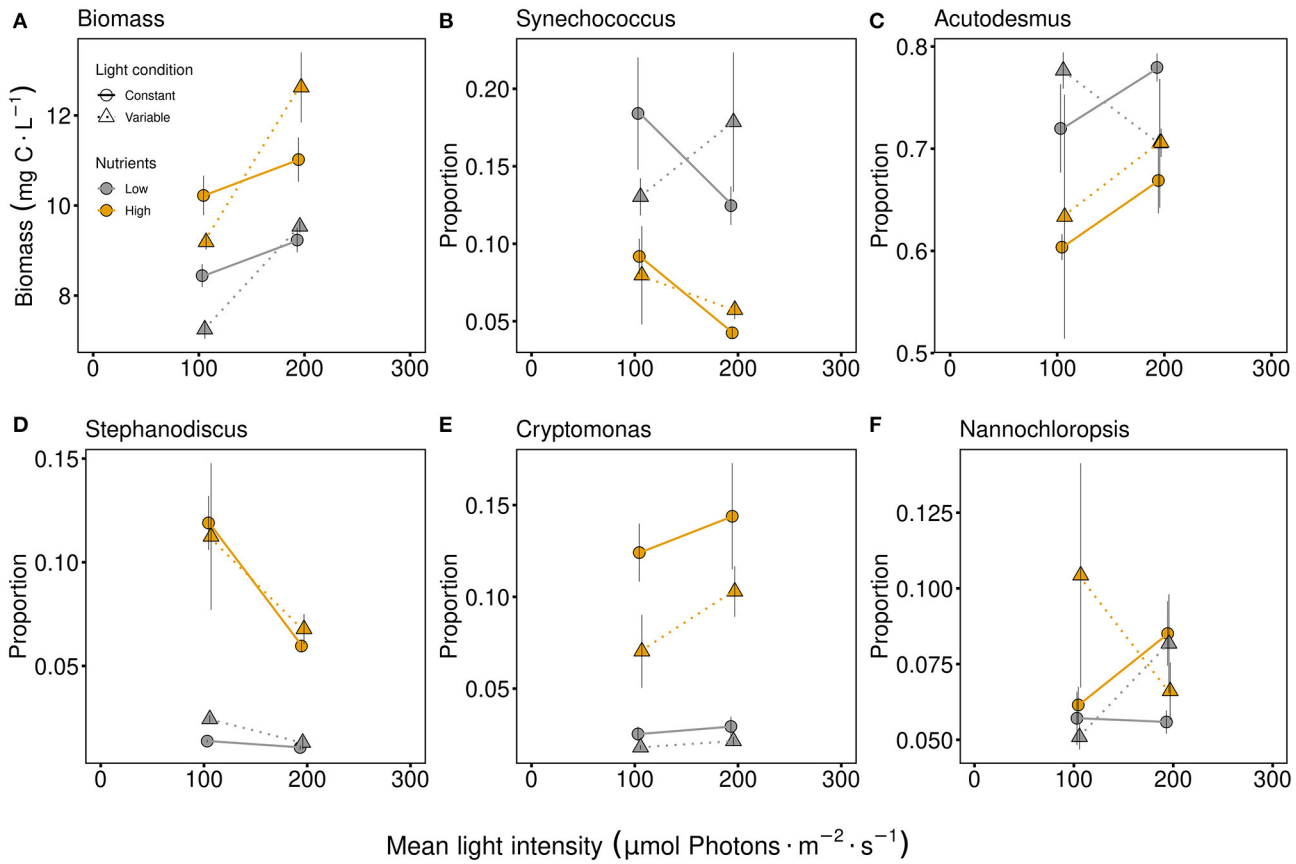

FIGURE 3 | Total biomass [mg carbon per liter; **(A)**] and proportions of specific species in the community after six or eight days of interspecific competition and acclimation to light and P conditions. The genus names of *Synechococcus elongatus* **(B)**, *Acutodesmus obliquus* **(C)**, *Stephanodiscus hantzschii* **(D)**, *Cryptomonas ovata* **(E)**, and *Nannochloropsis limnetica* **(F)** are used in the figure titles. Communities were either cultivated under variable (triangles, dashed line) or constant (circles, solid line) light conditions. Mean values are shown for high (orange symbols and lines) and low (gray symbols and lines) nutrient supply and are displayed with ± standard error. Additional barplots of the species proportion are given in **Supplementary Figure 4**.

and Montoya, 1998; Schlüter et al., 2000; Henriksen, 2002), the pigment composition of phytoplankton can be additionally affected by day length (Sakshaug and Andresen, 1986), diurnal cycle (Tukaj et al., 2003), or nutrient status (Goericke and Montoya, 1998; Henriksen, 2002). The proportion of the main light harvesting component chlorophyll *a* was neither affected by light intensity nor nutrient supply and was only affected by light condition (variability). While the proportion of chlorophyll *a* tended to decrease at high light intensity with fluctuating light conditions, the chlorophyll decomposition products increased. This appears to contradict to the photosynthesis results, as chlorophyll decomposition products can be seen as an indicator for light stress. Due to light stress phytoplankton decrease their concentration of chlorophyll *a* with high light intensities to protect the photosynthetic machinery against oxygen radical formation (Richardson et al., 1983). Possibly, light variability can be considered stress at high light intensities and stress relief at the lower light intensities. Therefore, the light variability can be relief or stress depending on where the range of the variability lies: at an already higher range, variability can cause stress, as they are varying over high light intensities, whereas at a lower range phytoplankton is receiving periods where the light intensity is much lower than the possible optimum. Another mechanism to increase light harvesting or decrease light stress is the regulation of xanthophylls. For green algae, an up-regulation of the xanthophyll cycle at high light intensities is a mechanisms to redirect excess light energy away from the photosynthetic reaction centers (Garcia-Mendoza et al., 2002; Lavaud et al., 2007; Dimier et al., 2009). In this experiment, the communities generally produced higher xanthophyll proportions at lower light intensities. Besides possible increased light harvesting, this partly can be explained by the higher proportion of the cyanobacterium in these treatments, rather than changes in the xanthophyll cycle. In the xanthophyll cycle the total concentration of xanthophyll would not change, as e.g., diadinoxanthin would change to diatoxanthin, but the overall quantity remains the same. The nutrient supply affected chlorophyll *b* and chlorophyll *c* differently. When nutrients were low, communities did not

contain chlorophyll *c*, but more chlorophyll *b*, suggesting that under low nutrient supply the chlorophyll *b* containing green algae had a competitive advantage as opposed to the chlorophyll *c* containing diatom and cryptophyte. This can be confirmed by considering that the nutrient condition affected mainly the community composition. There the green algae generally dominates and is particularly successful at low nutrient supply. Besides nutrient supply, light intensity differently affected chlorophyll *b* and *c*, chlorophyll *b* was higher at high light while chlorophyll *c* was higher at low light intensity. Since we investigated communities, it is difficult to differentiate between regulation of chlorophyll *a* and *b* due to light or species composition, as both can affect them. Chlorophyll *c* can only be related to species composition, which possibly explains the higher proportion in the lower light, as *Stephanodiscus hantzschii* has a higher proportion in the lower compared to the higher light intensity.

In the slow response of community biomass and composition, we suggest here that phytoplankton communities consisting of different taxonomical groups and associated with different physiological traits were able to compensate for light variability by adjusting their light harvesting mechanisms on the intermediate temporal scale. Communities exposed to constant and fluctuating light conditions behaved predominantly similar in several measures. This was especially prominent for the more slowly changing overall biomass and community composition. There mainly nutrient conditions, and rarely light intensity (for biomass and proportion of the diatom) or condition (only proportion of the cryptophyte) had a large impact, contrastingly to the fast reacting process of photosynthesis. We assume that the effects of variability were compensated by different traits of specific taxonomic groups and species, testing monocultures in addition to the community could strengthen this assumption. For example, significantly distinct light requirements can be found in different algal classes (Gibson and Foy, 1982; Richardson et al., 1983; Kana and Glibert, 1987; Huisman and Weissing, 1995; Gervais, 1997; Flameling and Kromkamp, 1998; Litchman, 2000; Schwaderer et al., 2011; Wacker et al., 2015). Different taxonomic groups differ in their antenna organization and pigment composition, which leads to differences in light utilization efficiencies (Kunath et al., 2012). Yet, neither light intensity nor condition strongly affected the community composition in our current experiment. Only *Stephanodiscus hantzschii* and *Cryptomonas ovata* decreased in their proportion due to light intensity and condition, respectively. Here, light fluctuated in shorter intervals of 3 h low light, 6 h high light, and 3 h low light followed by 12 h darkness. Larger interval lengths of several days have been shown to positively influence stable co-existence (Litchman and Klausmeier, 2001) and species diversity of a phytoplankton community (Flöder et al., 2002; Litchman et al., 2015). However, even shorter intervals (20 min) have been shown to allow stable coexistence and even showed that light acquisition traits can be changed, indicating high plasticity of cyanobacteria (Guislain et al., 2019). However, interval length as well as the average irradiance has been shown to influence growth (Litchman, 2000), partially because algae show a high degree of acclimation to light (Dimier et al., 2009). With respect to the overall biomass, this was also valid here, since biomass increased with higher light intensity and was additionally positively affected by light variability. At the lower mean light intensity the biomass of the communities experiencing variability decreased compared to ones grown in constant light, which can be due to light varying over an irradiance range of limiting to saturating light intensities (Litchman, 2000) and a general lower growth efficiency caused by light variation (Köhler et al., 2018). On one hand, fluctuating over a higher mean light intensity could be advantageous for the algae, while being temporarily relieved from the inhibiting light intensity they were able to recover from light stress, which would explain the increase in biomass due to fluctuations. On the other hand varying over lower light intensities can have caused some species to be below their light compensation point (Gervais, 1997; Litchman, 2000), resulting the light period effectively available for growth to be shortened. Therefore, the requirements of single species matter, which influence nutrient and light competitive abilities of communities (Huisman and Weissing, 1995).

In our experiment, the interplay between nutrient supply and light as a resource was additionally dependent on the light condition, i.e., if constant or fluctuating. As phytoplankton communities are subjected to temporal light variations ranging from seconds to hours or days that are overlaid on the diurnal cycle of light (Steele, 1985; Grobbelaar, 1989) the interplay of these factors is of high importance at all temporal scales. In surface mixed layers, the light environment of phytoplankton is modified and the cells may be rapidly moved across a large light gradient from very high intensities to darkness (MacIntyre et al., 2000; Dimier et al., 2009; Köhler et al., 2018). These rapid changes modify photosynthesis of the community, but over several days, pigment and biomass production could remain at an intermediate level, especially because different species are complementary in their light use. Thus, the effect of light variability could be seen in two different ways: (1) Communities do have the capability of compensating and therefore maintain similar values in species composition (except for the cryptophyte) and biomass to the constant counterpart and (2) variability is possibly even needed to sustain diverse communities due to niche partitioning.

Changes in light variability, light intensity, and nutrients are expected to become more and more important as lakes are affected by climate change. Climate change effects such as increasing mean temperature leads to a phenological shift (Stine et al., 2009) and results in changed mixing regimes and periods (Wagner et al., 2013; Selmeczy et al., 2019). In addition to these indirect effects on light and nutrient conditions, shifts in precipitation and more extreme weather events causes direct changes in light and nutrient regimes (IBG ed., Vincent, 2009). Many studies have shown effects of one or two factors influencing single species (Gibson and Foy, 1982; Dimier et al., 2009) or communities (Marra, 1978; Köhler et al., 2018) while investigating either photosynthesis (Flameling and Kromkamp, 1997; Garcia-Mendoza et al., 2002), growth (Litchman, 2000; Burson et al., 2018), or diversity (Flöder et al., 2002). Our approach demonstrates that better knowledge on the effects of variability and intensity of light coupled with nutrient supply is

important to understand the effect on community physiology, biomass, and composition.

DATA AVAILABILITY STATEMENT

The datasets generated for this study are available on request to the corresponding author.

AUTHOR CONTRIBUTIONS

VM and AW designed the experiment and wrote the first draft and all authors contributed substantially to later versions of the manuscript. VM performed the experiment. VM and MS did the chemical/biochemical analysis. All authors analyzed the data.

FUNDING

This study was supported by the German Research Foundation (WA2445/10-1) and the Open Access Publishing Fond of the University of Potsdam.

ACKNOWLEDGMENTS

We thank Silvia Heim, Sabine Hergt, and Caroline Maik for experimental assistance, Svenja Schälicke for comments on the manuscript, and Aaron Katz for English corrections.

SUPPLEMENTARY MATERIAL

The Supplementary Material for this article can be found online at: https://www.frontiersin.org/articles/10.3389/fenvs.2020.539733/full#supplementary-material

REFERENCES

Beardall, J., Burger-Wiersma, T., Rijkeboer, M., Sukenik, A., Lemoalle, J., Dubinsky, Z., et al. (1994). Studies on enhanced post-illumination respiration in microalgae. *J. Plankton Res.* 16, 1401–1410. doi: 10.1093/plankt/16.10.1401

Burson, A., Stomp, M., Greenwell, E., Grosse, J., and Huisman, J. (2018). Competition for nutrients and light: testing advances in resource competition with a natural phytoplankton community. *Ecology* 99, 1108–1118. doi: 10.1002/ecy.2187

Connelly, S. J., Moeller, R. E., Sanchez, G., and Mitchell, D. L. (2009). Temperature effects on survival and DNA repair in four freshwater cladoceran Daphnia species exposed to UV radiation. *Photochem. Photobiol.* 85, 144–152. doi: 10.1111/j.1751-1097.2008.00408.x

Consalvey, M., Perkins, R. G., Paterson, D. M., and Underwood, G. J. C. (2005). Pam Fluorescence: a beginners guide for benthic diatomists. *Diatom Res.* 20, 1–22. doi: 10.1080/0269249X.2005.9705619

de Wit, H. A., Valinia, S., Weyhenmeyer, G. A., Futter, M. N., Kortelainen, P., Austnes, K., et al. (2016). Current browning of surface waters will be further promoted by wetter climate. *Environ. Sci. Technol. Lett.* 3, 430–435. doi: 10.1021/acs.estlett.6b00396

Deininger, A., and Frigstad, H. (2019). Reevaluating the role of organic matter sources for coastal eutrophication, oligotrophication, and ecosystem health. *Front. Mar. Sci.* 6:144. doi: 10.3389/fmars.2019.00210

Dickman, E. M., Vanni, M. J., and Horgan, M. J. (2006). Interactive effects of light and nutrients on phytoplankton stoichiometry. *Oecologia* 149, 676–689. doi: 10.1007/s00442-006-0473-5

Dimier, C., Brunet, C., Geider, R., and Raven, J. (2009). Growth and photoregulation dynamics of the picoeukaryote Pelagomonas calceolata in fluctuating light. *Limnol. Oceanogr.* 54, 823–836. doi: 10.4319/lo.2009.54.3.0823

Dromgoole, F. I. (1988). Light fluctuations and the photosynthesis of marine algae. II. Photosynthetic response to frequency, phase ratio and amplitude. *Funct. Ecol.* 2, 211–219. doi: 10.2307/2389697

Flameling, I. A., and Kromkamp, J. (1997). Photoacclimation of Scenedesmus protuberans (Chlorophycea) to fluctuating irradiances simulating vertical mixing. *J. Plankton Res.* 19, 1011–1024. doi: 10.1093/plankt/19.8.1011

Flameling, I. A., and Kromkamp, J. (1998). Light dependence of quantum yields for PSII charge separation and oxygen evolution in eucaryotic algae. *Limnol. Oceanogr.* 43, 284–297. doi: 10.4319/lo.1998.43.2.0284

Flöder, S., and Burns, C. W. (2005). The influence of fluctuating light on diversity and species number of nutrient-limited phytoplankton. *J. Phycol.* 41, 950–956. doi: 10.1111/j.1529-8817.2005.00124.x

Flöder, S., Urabe, J., and Kawabata, Z. I. (2002). The influence of fluctuating light intensities on species composition and diversity of natural phytoplankton communities. *Oecologia* 133, 395–401. doi: 10.1007/s00442-002-1048-8

Garcia-Mendoza, E., Matthijs, H. C. P., Schubert, H., and Mur, L. R. (2002). Non-photochemical quenching of chlorophyll fluorescence in Chlorella fusca acclimated to constant and dynamic light conditions. *Photosyn Res.* 74, 303–315. doi: 10.1023/A:1021230601077

Gervais, F. (1997). Light-dependent growth, dark survival, and glucose uptake by Cryptophytes isolated from a freshwater chemocline. *J. Phycol.* 33, 18–25. doi: 10.1111/j.0022-3646.1997.00018.x

Gibson, C. E., and Foy, R. H. (1982). Photosynthetic characteristics of planktonic blue-green algae: the response of twenty strains grown under high and low light. *Br. Phycol. J.* 17, 169–182. doi: 10.1080/00071618200650171

Gibson, C. E., and Foy, R. H. (1988). "The significance of growth rate and storage products for the ecology of Melosira italica ssp. subarctica in Lough Neagh," in *Algae and The Aquatic Environment*, ed F. E. Round (Bristol: Biopress), 88–106.

Goericke, R., and Montoya, J. P. (1998). Estimating the contribution of microalgal taxa to chlorophyll a in the field-variations of pigment ratios under nutrient- and light-limited growth. *Mar. Ecol. Prog. Ser.* 169, 97–112. doi: 10.3354/meps169097

Grobbelaar, J. U. (1989). Do light/dark cycles of medium frequency enhance phytoplankton productivity? *J. Appl. Phycol.* 1, 333–340. doi: 10.1007/BF00003470

Grobbelaar, J. U., Kroon, B. M. A., Burger-Wiersma, T., and Mur, L. R. (1992). Influence of medium frequency light/dark cycles of equal duration on the photosynthesis and respiration of Chlorella pyrenoidosa. *Hydrobiologia* 238, 53–62. doi: 10.1007/BF00048773

Gross-Wittke, A., Gunkel, G., and Hoffmann, A. (2010). Temperature effects on bank filtration: redox conditions and physical-chemical parameters of pore water at Lake Tegel, Berlin, Germany. *J. Wat. Clim. Chan* 1, 55–66. doi: 10.2166/wcc.2010.005

Guislain, A., Beisner, B. E., and Köhler, J. (2019). Variation in species light acquisition traits under fluctuating light regimes: implications for non-equilibrium coexistence. *Oikos* 128, 716–728. doi: 10.1111/oik.05297

Hatt, H. (1983). Effect of temperature on the activity of the amino acid receptors in the crayfish walking leg. *J. Comp. Physiol.* 152, 405–409. doi: 10.1007/BF00606245

Havens, K. E., Pinto-Coelho, R. M., Beklioglu, M., Christoffersen, K. S., Jeppesen, E., Lauridsen, T. L., et al. (2015). Temperature effects on body size of freshwater crustacean zooplankton from Greenland to the tropics. *Hydrobiologia* 743, 27–35. doi: 10.1007/s10750-014-2000-8

Henriksen, P. (2002). Effects of nutrient-limitation and irradiance on marine phytoplankton pigments. *J. Plankton Res.* 24, 835–858. doi: 10.1093/plankt/24.9.835

Hillebrand, H., Dürselen, C. D., Kirschtel, D., Pollingher, U., and Zohary, T. (1999). Biovolume calculation for pelagic and benthic microalgae. *J. Phycol.* 35, 403–424. doi: 10.1046/j.1529-8817.1999.3520403.x

Huang, W.-P., and Chou, L.-S. (2017). Temperature effects on life history traits of two sympatric branchiopods from an ephemeral wetland. *PLoS ONE* 12:e0179449. doi: 10.1371/journal.pone.0179449

Huisman, J., and Weissing, F. J. (1995). Competition for nutrients and light in a mixed water column: a theoretical analysis. *Am. Nat.* 146, 536–564. doi: 10.1086/285814

Ibelings, B. W., Kroon, B. M. A., and Mur, L. R. (1994). Acclimation of photosystem II in a cyanobacterium and a eukaryotic green alga to high and fluctuating photosynthetic photon flux densities, simulating light regimes induced by mixing in lakes. *New Phytol.* 128, 407–424. doi: 10.1111/j.1469-8137.1994.tb02987.x

IGB Dossier (2018). *Lakes Under Climate Change Diagnosis and Prognosis From Long- Term Research*. Berlin: Leibniz-Institute of Freshwater Ecology and Inland Fisheries. doi: 10.4126/FRL01-006410415

Johnsen, G., Samset, O., Granskog, L., and Sakshaug, E. (1994). In vivo absorption characteristics in 10 classes of bloom-forming phytoplankton: taxonomic characteristics and responses to photoadaptation by means of discriminant and HPLC analysis. *Mar. Ecol. Prog. Ser.* 105, 149–157. doi: 10.3354/meps105149

Kana, T. M., and Glibert, P. M. (1987). Effect of irradiances up to 2000 μE m−2 s−1 on marine Synechococcus WH7803—II. Photosynthetic responses and mechanisms. *Deep Sea Res. Part I Oceanogr. Res. Pap.* 34, 497–516. doi: 10.1016/0198-0149(87)90002-1

Kerimoglu, O., Straile, D., and Peeters, F. (2012). Role of phytoplankton cell size on the competition for nutrients and light in incompletely mixed systems. *J. Theor. Biol.* 300, 330–343. doi: 10.1016/j.jtbi.2012.01.044

Köhler, J., Wang, L., Guislain, A., and Shatwell, T. (2018). Influence of vertical mixing on light-dependency of phytoplankton growth. *Limnol. Oceanogr.* 63, 1156–1167. doi: 10.1002/lno.10761

Kromkamp, J. C., Dijkman, N. A., Peene, J., Simis, S. G. H., and Gons, H. J. (2008). Estimating phytoplankton primary production in Lake IJsselmeer (The Netherlands) using variable fluorescence (PAM-FRRF) and C-uptake techniques. *Eur. J. Phycol.* 43, 327–344. doi: 10.1080/09670260802080895

Kroon, B. M. A., Burger-Wiersma, T., Visser, P. M., and Mur, L. R. (1992). The effect of dynamic light regimes on Chlorella II. Minimum quantum requirement and photosynthesis-irradiance parameters. *Hydrobiologia* 238, 79–88. doi: 10.1007/BF00048776

Kunath, C., Jakob, T., and Wilhelm, C. (2012). Different phycobilin antenna organisations affect the balance between light use and growth rate in the cyanobacterium Microcystis aeruginosa and in the cryptophyte Cryptomonas ovata. *Photosyn. Res.* 111, 173–183. doi: 10.1007/s11120-011-9715-4

Lavaud, J., Strzepek, R. F., and Kroth, P. G. (2007). Photoprotection capacity differs among diatoms: Possible consequences on the spatial distribution of diatoms related to fluctuations in the underwater light climate. *Limnol. Oceanogr.* 52, 1188–1194. doi: 10.4319/lo.2007.52.3.1188

Litchman, E. (1998). Population and community responses of phytoplankton to fluctuating light. *Oecologia* 117, 247–257. doi: 10.1007/s004420050655

Litchman, E. (2000). Growth rates of phytoplankton under fluctuating light. *Freshw. Biol.* 44, 223–235. doi: 10.1046/j.1365-2427.2000.00559.x

Litchman, E., and Klausmeier, C. A. (2001). Competition of phytoplankton under fluctuating light. *Am. Nat.* 157, 170–187. doi: 10.1086/318628

Litchman, E., Klausmeier, C. A., and Bossard, P. (2015). Phytoplankton nutrient competition under dynamic light regimes. *Limnol. Oceanogr.* 49, 1457–1462. doi: 10.4319/lo.2004.49.4_part_2.1457

MacIntyre, H. L., Kana, T. M., and Geider, R. J. (2000). The effect of water motion on short-term rates of photosynthesis by marine phytoplankton. *Trends Plant Sci.* 5, 12–17. doi: 10.1016/S1360-1385(99)01504-6

Marra, J. (1978). Phytoplankton photosynthetic response to vertical movement in a mixed layer. *Mar. Biol.* 46, 203–208. doi: 10.1007/BF00390681

Nichols, H. W. (1973). "Culture methods and growth measurements," in *Handbook of Phycological Methods*. Culture Methods and Growth Measurements, ed J. R. Stein (Cambridge: Cambridge University Press), 7–24.

Pachepsky, Y. A., Blaustein, R. A., Whelan, G., and Shelton, D. R. (2014). Comparing temperature effects on *Escherichia coli*, Salmonella, and Enterococcus survival in surface waters. *Lett. Appl. Microbiol.* 59, 278–283. doi: 10.1111/lam.12272

Piccinin, B. B. (1976). *Photosynthesis by natural phytoplankton populations and its interrelationship with light and temperature*. (Master thesis). McMaster University, Hamilton, Ontario, Canada.

R Development Core Team. (2010). *R: A Language and Environment for Statistical Computing*. Vienna, Austria: R Foundation for Statistical Computing. Available online at: http://www.r-project.org

Richardson, K., Beardall, J., and Raven, J. A. (1983). Adaption of unicellular algae to irradiance: an analysis of strategies. *New Phytol.* 93, 157–191. doi: 10.1111/j.1469-8137.1983.tb03422.x

Roy, S., Llewellyn, C. A., Egeland, E. S., and Johnsen, G. (2011). *Phytoplankton Pigments: Characterization, Chemotaxonomy and Applications in Oceanography*. Cambridge: Cambridge University Press. doi: 10.1017/CBO9780511732263

Sakshaug, E., and Andresen, K. (1986). Effect of light regime upon growth rate and chemical composition of a clone of Skeletonema costatum from the Trondheimsfjord, Norway. *J. Plankton Res.* 8, 619–637. doi: 10.1093/plankt/8.4.619

Salmaso, N. (2003). Life strategies, dominance patterns and mechanisms promoting species coexistence in phytoplankton communities along complex environmental gradients. *Hydrobiologia* 502, 13–36. doi: 10.1023/B:HYDR.0000004267.64870.85

Schlüter, L., Møhlenberg, F., Havskum, H., and Larsen, S. (2000). The use of phytoplankton pigments for identifying and quantifying phytoplankton groups in coastal areas:testing the influence of light and nutrients on pigment/chlorophyll a ratios. *Mar. Ecol. Prog. Ser.* 192, 49–63. doi: 10.3354/meps192049

Schwaderer, A. S., Yoshiyama, K., Tezanos Pinto, P., Swenson, N. G., Klausmeier, C. A., and Litchman, E. (2011). Eco-evolutionary differences in light utilization traits and distributions of freshwater phytoplankton. *Limnol. Oceanogr.* 56, 589–598. doi: 10.4319/lo.2011.56.2.0589

Selmeczy, G. B., Abonyi, A., Krienitz, L., Kasprzak, P., Casper, P., Telcs, A., et al. (2019). Old sins have long shadows: climate change weakens efficiency of trophic coupling of phyto- and zooplankton in a deep oligo-mesotrophic lowland lake (Stechlin, Germany)—a causality analysis. *Hydrobiologia* 831, 101–117. doi: 10.1007/s10750-018-3793-7

Shatwell, T., Nicklisch, A., and Köhler, J. (2012). Temperature and photoperiod effects on phytoplankton growing under simulated mixed layer light fluctuations. *Limnol. Oceanogr.* 57, 541–553. doi: 10.4319/lo.2012.57.2.0541

Steele, J. H. (1985). A comparison of terrestrial and marine ecological systems. *Nature* 313, 355–358. doi: 10.1038/313355a0

Stine, A. R., Huybers, P., and Fung, I. Y. (2009). Changes in the phase of the annual cycle of surface temperature. *Nature* 457, 435–440. doi: 10.1038/nature07675

Talmy, D., Blackford, J., Hardman-Mountford, N. J., Dumbrell, A. J., and Geider, R. J. (2013). An optimality model of photoadaptation in contrasting aquatic light regimes. *Limnol. Oceanogr* 58, 1802–1818. doi: 10.4319/lo.2013.58.5.1802

Thrane, J. E., Kyle, M., Striebel, M., Haande, S., Grung, M., Rohrlack, T., et al. (2015). Spectrophotometric analysis of pigments: a critical assessment of a high-throughput method for analysis of algal pigment mixtures by spectral deconvolution. *PLoS ONE* 10:e0137645. doi: 10.1371/journal.pone.0137645

Tukaj, Z., Matusiak-Mikulin, K., Lewandowska, J., and Szurkowski, J. (2003). Changes in the pigment patterns and the photosynthetic activity during a light-induced cell cycle of the green alga Scenedesmus armatus. *Plant Physiol. Biochem.* 41, 337–344. doi: 10.1016/S0981-9428(03)00028-7

Vincent, W. F. (2009). "*Effects of Climate Change on Lakes*," in *Encyclopedia of Inland Waters*, G. E. Likens (Amsterdam: Elsevier), 55–60. doi: 10.1016/B978-012370626-3.00233-7

Wacker, A., Piepho, M., and Spijkerman, E. (2015). Photosynthetic and fatty acid acclimation of four phytoplankton species in response to light intensity and phosphorus availability. *Eur. J. Phycol.* 50, 288–300. doi: 10.1080/09670262.2015.1050068

Wagner, A., Hülsmann, S., Horn, W., Schiller, T., Schulze, T., Volkmann, S., et al. (2013). Food-web-mediated effects of climate warming: consequences for the seasonal Daphnia dynamics. *Freshw. Biol.* 58, 573–587. doi: 10.1111/j.1365-2427.2012.02809.x

Warren, D. R., Robinson, J. M., Josephson, D. C., Sheldon, D. R., and Kraft, C. E. (2012). Elevated summer temperatures delay spawning and reduce redd construction for resident brook trout (Salvelinus fontinalis). *Glob. Chang. Biol.* 18, 1804–1811. doi: 10.1111/j.1365-2486.2012.02670.x

Conflict of Interest: The authors declare that the research was conducted in the absence of any commercial or financial relationships that could be construed as a potential conflict of interest.

The handling editor is currently organizing a Research Topic with one of the author MS, and confirms the absence of any other collaboration.

Advantages of publishing in Frontiers

OPEN ACCESS
Articles are free to read for greatest visibility and readership

FAST PUBLICATION
Around 90 days from submission to decision

HIGH QUALITY PEER-REVIEW
Rigorous, collaborative, and constructive peer-review

TRANSPARENT PEER-REVIEW
Editors and reviewers acknowledged by name on published articles

Frontiers
Avenue du Tribunal-Fédéral 34
1005 Lausanne | Switzerland

Visit us: www.frontiersin.org
Contact us: frontiersin.org/about/contact

REPRODUCIBILITY OF RESEARCH
Support open data and methods to enhance research reproducibility

DIGITAL PUBLISHING
Articles designed for optimal readership across devices

FOLLOW US
@frontiersin

IMPACT METRICS
Advanced article metrics track visibility across digital media

EXTENSIVE PROMOTION
Marketing and promotion of impactful research

LOOP RESEARCH NETWORK
Our network increases your article's readership